PHOTOGRAPH THIS SHEET

AD A084869

DTIC ACCESSION NUMBER

II

LEVEL

I

INVENTORY

JTCG/MD WP #12
Army, Navy, Air Force
"Aircraft/Stores Compatibility Symposium Proceedings" Volume I
2-4 Sept. 1975

DOCUMENT IDENTIFICATION

DISTRIBUTION STATEMENT A
Approved for public release;
Distribution Unlimited

DISTRIBUTION STATEMENT

ACCESSION FOR	
NTIS GRA&I	☒
DTIC TAB	☐
UNANNOUNCED	☐
JUSTIFICATION	
BY	
DISTRIBUTION /	
AVAILABILITY CODES	
DIST	AVAIL AND/OR SPECIAL
A	

DISTRIBUTION STAMP

DTIC
ELECTE
S JUN 2 1980 D
D

DATE ACCESSIONED

DATE RECEIVED IN DTIC

PHOTOGRAPH THIS SHEET AND RETURN TO DTIC-DDA-2

DTIC FORM 70A OCT 79

DOCUMENT PROCESSING SHEET

Best
Available
Copy

AIRCRAFT/STORES COMPATIBILITY SYMPOSIUM PROCEEDINGS

2 - 4 SEPTEMBER 1975

VOLUME I

SPONSORED BY

NAVAL AIR SYSTEMS COMMAND

PROCEEDINGS COMPILED BY

JTCG/MD WP #12

FOREWORD

This publication contains the technical papers presented at the Aircraft/Stores Compatibility Symposium, held at Stouffer's National Center Hotel, Arlington, Virginia on 2-4 September 1975.

The purpose of the symposium was to bring together engineers, technicians, and others interested in aircraft/stores compatibility to learn of the latest developments in that field. Representatives of industry and governments throughout the world were in attendance. It is most important that the adverse effects of stores and suspension equipment on aircraft be minimized. The same is true for the reverse, the effects of aircraft on stores. Only if the designers in both fields interchange requirements, development information, and problems, can optimum designers in both fields interchange requirements, development information, and problems, can optimum design be achieved.

The symposium committee expresses its deep appreciation to all who contributed to the success of the endeavor; those who wrote and presented papers; the session chairmen; and the attendees. Special thanks are extended to Carolyn M. Steeper, Robert P. Phelan, Fred S. Pierce, and Harry P. Lehman for their dedicated efforts in connection with the arrangements and day-to-day workings of the symposium. The committee is also most grateful to Vice Admiral Kent L. Lee, U.S.N., Commander of the Naval Air Systems Command, for acting as official sponsor of the symposium.

PRECEDING PAGE BLANK-NOT FILMED

Publication of this document does not constitute approval of the technical papers' findings or conclusions by the Naval Air Systems Command, the Joint Commands, or the JTCG/MD. It is published only for the exchange of information, data and ideas relating to aircraft/stores compatibility.

Wm. P. STEEPER
Chairman
Aircraft/Stores Compatibility
Working Party No. 12
JTCG/MD

ABSTRACT

These proceedings contain the technical papers presented at the Aircraft/Stores Compatibility Symposium held at Stouffer's National Center Hotel, Arlington, Virginia on 2-4 September 1975, which was sponsored by the Naval Air Systems Command and hosted by Working Party No. 12 for Aircraft/Stores Compatibility of the Joint Technical Coordinating Group for Munitions Development (JTCG/MD). The purpose of the symposium was to bring together engineers and others concerned with aircraft/stores compatibility to exchange ideas and information related to that field. Technical papers were presented in five sessions: General, Aero-Structures, Store Separation, Bomb/Racks Interface, and Experimental. Each paper in the proceedings has its own abstract, presentation of data, conclusions, and associated photographs, charts, and diagrams. This compilation should prove to be of value to both aircraft and stores/suspension equipment designers and engineers to keep them abreast of the latest experiences in the field, thereby enabling them to produce better products.

SYMPOSIUM COMMITTEE

Mr. W. P. Steeper Chairman	Navy Material Command
Mr. C. S. Epstein	Air Force Systems Command
Mr. J. C. Phillip	Air Force Logistics Command

PAPER SELECTION

Mr. C. S. Epstein	Air Force System Command
Mr. W. P. Steeper	Navy Material Command

SESSION CHAIRMEN

GENERAL	Mr. W. R. Burris, NAVMAT/NAVAIR HQ
AERO-STRUCTURES	Mr. W. P. Steeper, NAVMAT/NAVAIRHQ
STORE SEPARATION BOMB RACKS/INTERFACE	Mr. C. S. Epstein, AFSC/AFATL Mr. H. L. Washmuth, PACMISTESTCEN Mr. L. S. Johnson, Sandia Corp.
EXPERIMENTAL	Mr. R. E. Smith, NAVWEARCEN

PROCEEDINGS

Mr. W. P. Steeper — NAVAIR HQ

SPONSOR

Commander, Naval Air Systems Command

PRECEDING PAGE BLANK-NOT FILMED

TABLE OF CONTENTS

VOLUME 1		PAGE
	FOREWORD	iii
	ABSTRACT	v
	TABLE OF CONTENTS	vii
PAPERS		
#1	THE USE OF THEORETICAL AERODYNAMIC TECHNIQUES FOR DESIGN AND ANALYSIS OF EXTERNAL STORE SHAPES L. D. Smith Vought Systems Division	1
#2	AIRCRAFT/STORES COMPATIBILITY ANALYSIS AND FLIGHT TESTING C. S. Epstein Air Force Armament Laboratory	21
#3	THEORETICAL ANALYSIS AND EXPERIMENTAL MEASUREMENTS OF SEPARATION DISTURBANCES IN WEAPON DELIVERY SYSTEMS J. S. Ausman Litton Systems, Inc	53
#4	SYSTEMS SAFETY J. C. Phillip Sacramento ALC	87
#5	Paper withdrawn	
#6	PREDICTION TECHNIQUE TO DETERMINE EFFECTS OF EXTERNAL STORES ON AIRCRAFT PERFORMANCE R. D. Dyer Air Force Flight Dynamics Laboratory R. D. Gallagher Vought Systems Division	103
#7	THE REDUCTION OF THE INSTALLED DRAG OF MULTIPLE STORE CARRIERS A. B. Haines Aircraft Research Association, Ltd.	141

PRECEDING PAGE BLANK-NOT FILMED

#8 AN EXTENSION OF THE FACES TECHNIQUE FOR RAPID WING STORE FLUTTER CLEARANCE 165
M. A. Ferman and W. H. Unger
McDonnell Douglas Corp.

#9 EXTERNAL STORE AIRLOADS PREDICTION TECHNIQUE 195
A. R. Rudnicki and E. G. Waggoner
Vought Systems Division

#10 FUTURE NAVY WEAPONS SUSPENSION REQUIREMENTS 231
T. E. Milhous
Naval Air Development Center

#11 HYDRAULIC CONSTANT RECOIL PROGRAM 241
P. E. Townsend
Rock Island Arsenal

#12 BOMB RACK SUSPENSION HOOK 259
E. Turissini
Naval Avionics Facility, Indianapolis
L. D. Seal
Dayton T. Brown, Inc.

#13 EJECTION RELEASE OF AERODYNAMICALLY UNSTABLE STORES 271
S. J. Jendras
McDonnell Douglas Corp.

#14 ON THE FEASIBILITY OF INCLUDING THE EFFECTS OF STORE SEPARATION IN FREE-FALL WEAPON BALLISTICS 309
L. Devan
Naval Surface Weapons Center

#15 F-14/PHOENIX MISSILE SEPARATION PROGRAM 337
C. J. Dragowitz and R. J. Johnson
Grumman Aerospace Corp

#16 Paper withdrawn

#17 A TECHNIQUE FOR INVESTIGATING THE LAUNCH AND SEPARATION OF GUIDED WEAPONS 355
C. B. Mathews, Capt R. D. Cason
Lt P. G. McGirr, and Lt E. M. Carreras
Air Force Armament Laboratory

#18 LAUNCH TRANSIENT ANALYSIS: ELEMENT OF AIR LAUNCHED WEAPON CONFIGURATION DEVELOPMENT 411
T. G. Blose and R. M. Barnes
Rockwell International

#19 CHASE - THE OPTIMUM PHOTO ANALYSIS SYSTEM 461
Alan Aden
McDonnell Douglas Corp.

VOLUME 2

#20 THE 30-INCH NUCLEAR WEAPON EJECTOR FOR THE B-1 499
P. F. Peterson
Rockwell International

#21 EVALUATION OF N_2 POWERED, MECHANICALLY LINKED DUAL E-JECTOR SYSTEM 525
L. J. Holt and C. E. Panlaqui
Naval Weapons Center

#22 THE DEVELOPMENT OF A COMPACT HIGH STRENGTH EJECTOR RELEASE UNIT FOR THE MRCA 573
Byron Hiscock
Frazer - Nash Ltd.

#23 ADVANTAGES AND POSSIBLE DEVELOPMENTS OF RELEASE AND EJECTOR UNITS UTILIZING THE SADDLE STORE SUSPENSION SYSTEM 609
J. H. Hasquenoph and J. P. L. Lautour
Alkan and Co.

#24 ADVANCED FUZE FUNCTION CONTROL SET 625
A. E. Pertman
Naval Surface Weapons Center

#25 AIRCRAFT/STORES ELECTRICAL INTERFACE COMPTAIBILITY CONFORMATION 651
Capt J. F. Stuart
Air Force Armament Laboratory

#26 BRU-10 SIDEPLATE CORROSION STUDY 723
K. J. Trelewicz
Dayton T. Brown, Inc.

#27 AIRCRAFT/STORES INTERFACE MANUAL 733
H. L. Washmuth
Pacific Missile Test Center

#28 DIGITAL STORES MANAGEMENT SYSTEM 741
C. M. Connell
Air Force Armament Laboratory

#29 FIGHTER LAUNCHED ADVANCED MATERIALS EXPERIMENT (FLAME) UTILIZING AN F-4J AIRCRAFT AND A TWO STAGE PEDRO/RECRUIT ROCKET 767
Lt H. D. Wolcott and A. C. Cruce
Naval Air Test Center

#30 AERODYNAMIC CHARACTERISTICS OF OPEN WEAPON BAYS ON THE B-1 791
R. E. Little
Rockwell International

#31 INVESTIGATION OF MUTUAL WAKE INTERFERENCE BETWEEN RETARDED BOMBS 837
K. G. Smith
Hunting Engineering Ltd.

#32 THE EFFECTS OF MODEL STORE DISTORTION ON RELEASE DISTURBANCE 885
E. G. Cane
Royal Aircraft Establishment

#33 PRELIMINARY DESIGN OF AN OPERATIONAL F-4 CONFORMAL CARRIAGE 903
E. J. Zapel
The Boeing Aerospace Co.

#34 OBJECTIVES OF THE AGARD F. D. P. WORKING GROUP ON DRAG AND OTHER AERODYNAMIC EFFECTS OF EXTERNAL STORES 943
C. L. Bore
Hawker Siddeley Aviation, Ltd.

#35 FLIGHT TEST HEAT TRANSFER MEASUREMENTS ON A PYLON-MOUNTED STORE 955
R. K. Mathews
ARO, Inc
Maj J. C. Key, Jr
Air Force Armament Laboratory

#36 EVOLUTION OF THE PAVE PENNY GUNFIRE VIBRATION ENVIRONMENTAL QUALIFICATION TESTS 977
F. D. Robertson, Jr.
Martin Marietta Aerospace

THE USE OF THEORETICAL AERODYNAMIC TECHNIQUES FOR DESIGN AND ANALYSIS OF EXTERNAL STORE SHAPED (U)

(Article UNCLASSIFIED)

by

L. D. SMITH

Vought Systems Division
LTV Aerospace Corporation
Dallas, Texas 75222

ABSTRACT. (U) Shapes of external stores are often determined by considerations other than aerodynamic. The result is usually a mechanically well-designed store that often creates unnecessary drag, withstands its own buffet environment, but occasionally causes cracks in adjacent skins. The aerodynamicist is in part responsible because, in the absence of readily available tools to evaluate the shape, he must make arbitrary judgements.

This paper presents an example wherein the shape of an external store was determined using theoretical tools to consider not only the isolated store flow field, but the captive store flow field as well. The primary tool was three-dimensional potential flow; however, this technique was supported by use of two-dimensional potential flow and by boundary layer analysis. Also presented are flight test results for comparison with theoretical predictions. The success demonstrated in this example should show that theoretical tools are useful during preliminary and primary design and can have a positive impact on the selection of external store shapes. In fact, the complexity of the shape can be reduced by such a logical approach, thus reducing the potential for design and fabrication problems.

Approved for public release; distribution unlimited.

LIST OF FIGURES

1. A-7E with TRAM Pod
2. Geometric Constraints
3. Analysis of Candidate Fairings
4. Preprototype Pod General Arrangement
5. Flight Test Pressures – Upper and Lower Centerline
6. Flight Test Pressures – Inboard and Outboard Sides
7. Fluctuating Pressure – Lower Centerline
8. Comparison of Theory and Test for Angle of Attack – Upper and Lower Centerline
9. Comparison of Theory and Test for Angle of Attack – Z_{POD} 100
10. Comparison of Theory and Test for Sideslip – Upper and Lower Centerline
11. Comparison of Theory and Test for Sideslip – Z_{POD} 100

LIST OF SYMBOLS AND ABBREVIATIONS

α_F	Fuselage Angle of Attack, Degrees, Pod is oriented 3° nose down to the fuselage reference line
db	Decibels
$\mathcal{L}$	Centerline
C_p	Pressure Coefficient, $\frac{\text{Local Static Pressure} - \text{Ambient Pressure}}{\text{Dynamic Pressure}}$
FLIR	Forward Looking Infrared
g	Load Factor
H_i	Incompressible Flow Boundary Layer Form Factor
MN	Mach Number
TRAM	Target Recognition and Attack Multisensors
V_H	Maximum Aircraft Velocity in Level Flight
X_{POD}	Pod Station, Distance in Inches along the Pod Centerline (Z_{POD} 100)
Z_{POD}	Vertical Distance in Inches Perpendicular to Pod Centerline

1. INTRODUCTION

Past experience with external store shape selection has demonstrated an unhealthy attitude toward the aerodynamics of not only the stores but the parent aircraft/store combination as well. This disrespect coupled with the residual effect – a store shape once selected will last forever – has plagued performance-minded designers in recent years. A typical example of this situation is multiply-carried M-117 on the F-111.

A second-generation technique for store shape selection considered such lofty parameters as fineness ratio for bodies, aspect ratio for fins or wings, forebody shape, and boattail angle. In the final analysis, however, most of these criteria were ignored in favor of an old shell that was handy, through the residual effect, for the prototype article; and, when the program felt the press of budget and time, the old shell became a new store. This phenomenon has not always prevailed. Occasionally a good shape was defined, as in the case of the MK-80 series stores, but even the performance of these shapes are degraded by the residual effect of lugs, fuses, and swaybraces.

Several years ago, a new breed of external stores began to appear on aircraft bomb racks. These new stores rather than being deliverable ordnance were carried for airborne function. To support their function, these stores sprouted antenna, air turbines, cooling air inlets and exhausts, and windows. The complex shapes required to package these functioning stores require even more of the aerodynamicist's attention than do bombs, because, in addition to aircraft/store compatibility, i.e., lift, drag, and buffet; there is a store/function compatibility, i.e., boresight and internal environment, that must be addressed.

Today's tasks then become those of defining a new breed of old shells whose characteristics, compatibilities, and limitations are known and can be applied to fullest advantage. Favorable changes will not occur instantly but rather through a gradual process in which we all have a part.

This paper, hopefully, is one such example where equipment at hand, namely the computer and existing theoretical tools are teamed to define and analyze a shape for a functioning store that will have the smallest impact on the parent aircraft flow field and still meet the function criteria. It will be shown that the use of these tools also provides by-products of design simplification and timely design data that are as beneficial as the initial intent of shape analyzation.

The plan of this paper is as follows:

1. Introduction
2. Design Task
3. Theoretical Techniques
4. Flight Test Data
5. Comparison of Theoretical Results and Flight Test Data
6. Conclusions

2. DESIGN TASK

The parent aircraft in the design task was the A-7E which is a single-place, carrier-based, light attack aircraft with a 35^{0} swept wing mounted high on the fuselage. Each wing has three external store stations. It was the right-hand inboard store station that was selected to locate a pod containing a Forward Looking Infrared (FLIR) sensor. Figure 1 shows the A-7E aircraft with the pod installed on the right wing inboard store station. The FLIR, on the A-7E, is a part of a Target Recognition and Attack Multisensors system; thus, the pod is named the TRAM pod. The TRAM pod operating criteria required a maneuvering envelope of 0.5 g to 2.0 g out to V_H of the A-7E. Structurally, the pod was to be designed to the limits of the basic aircraft.

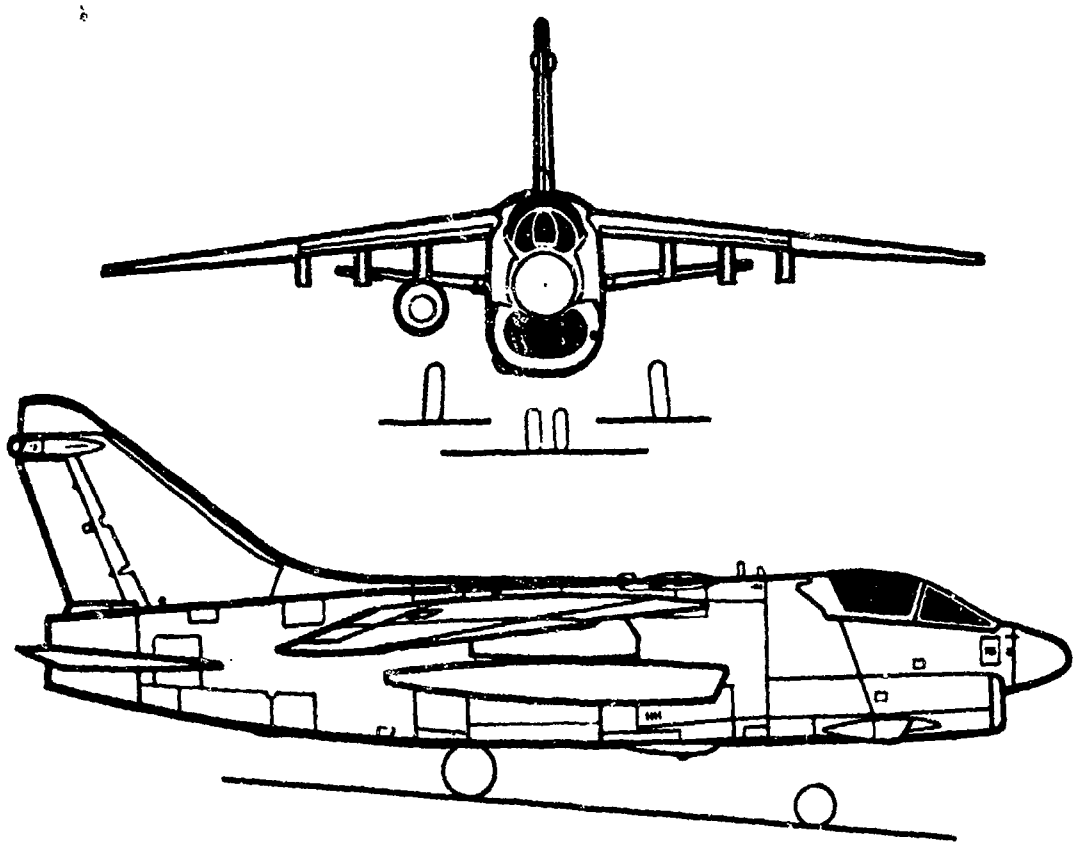


Figure 1 A-7E with TRAM Pod

The design task was to select a pod shape to contain a FLIR that would be compatible with the A-7 aircraft. Criteria for the FLIR required a forward field of view past the aircraft fuselage, which determined the forward location of a flat window and a stable line of sight, i.e., steady airflow around the pod at least within the aircraft Mach number and load factor regime where the FLIR is to function. Criteria for aircraft compatibility also required steady airflow near the pod, but in addition, included minimum drag and minimum mutual interference between the pod/pylon/wing and fuselage throughout the transonic Mach regime of the aircraft.

The TRAM pod is, for purposes of design, divided into three sections, nose, mid, and afterbody; with the FLIR sensor located in the nose and the attendant hardware in the pod mid section. It is the nose section which contains the FLIR window where the bulk of the aerodynamic design effort was concentrated. To meet the field of view criteria, the FLIR window required a twelve-inch diameter (front projection) flat glass canted 30^{o} to the vertical plane. A true view of the window therefore is an ellipse. The size of the attendant hardware to support the FLIR dictated the diameter of the mid section, twenty-one inches. The nose section then is a shape starting with a slanted, elliptically-shaped, flat face ending in a twenty-one inch diameter section. Figure 2 shows these geometric constraints. More specifically now, the aerodynamic design task was to define a fairing between these two end points that would permit steady flow up to Mach number = 0.9.

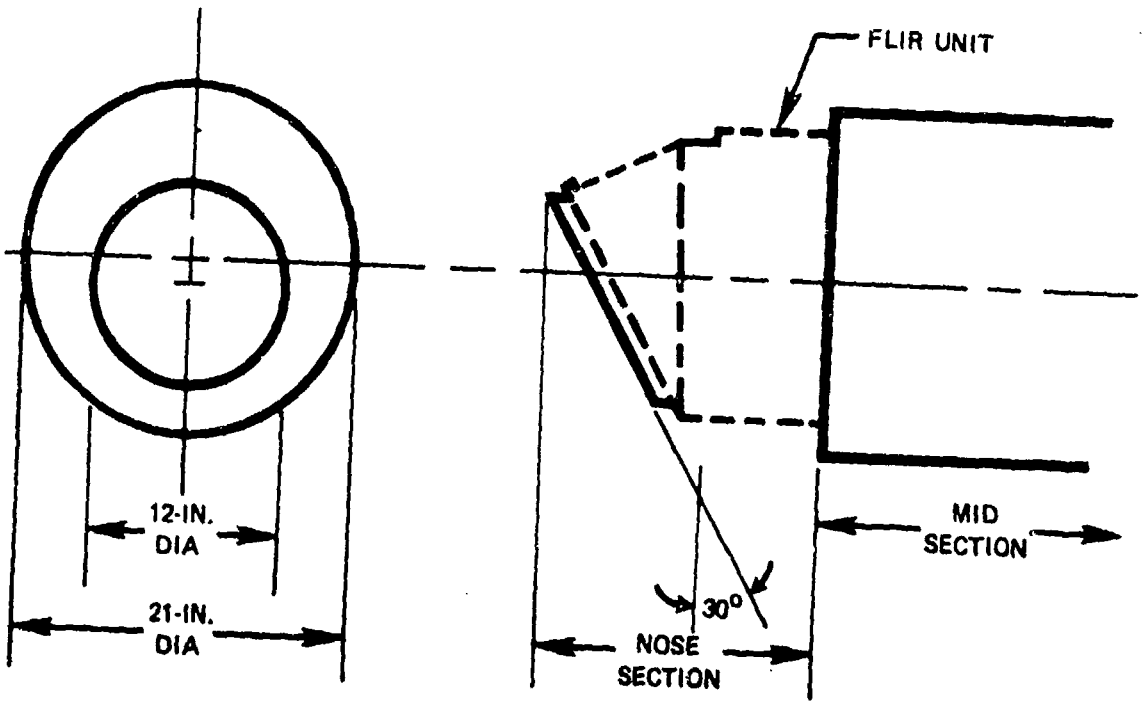


Figure 2 Geometric Constraints

3. THEORETICAL TECHNIQUES

Theoretical techniques to predict flow field behavior have been in existence for many years. During the last fifteen years, coincident with the availability of the large-capacity high-speed computer, theoretical techniques have become tools readily applicable to aerodynamic design. Unfortunately, these routines are so complex and the geometry definition so stringent that the aerodynamicist is reluctant to apply them as a working tool for daily design interface with other aerospace engineering disciplines. This situation was typified during the preliminary design phase of the TRAM pod when it became necessary to identify, at least in preliminary form, a fairing for the pod nose section.

The most appropriate theoretical tool available to evaluate the TRAM pod nose section fairing was a three-dimensional potential flow routine developed by Hess.[1] However, the development of the appropriate geometry for a large number of candidate fairings would have been too time consuming and the computer time costly for so many runs. This necessitated a paring of the numbers of candidate fairings to a more manageable task. This paring was accomplished using a computerized version of the Theodorsen[2] potential flow technique for two-dimensional wings to analyze eighty candidate fairings. Three of these candidate fairings were selected and then analyzed using the Hess program to predict local pressures and the McNally[3] routine to predict boundary layer separation. Figure 3 presents a profile view of the three fairings and the results of the Hess and McNally routines for each fairing. The final pod nose section fairing was selected using the criteria of external flow and internal area distribution. This final fairing was also analyzed using the Hess routine. The success of this procedure is demonstrated by the fact that preliminary air loads distributions generated by the Hess program were, after favorable comparison with flight test data, rereleased as final design airloads.

3.1 HESS ROUTINE

The principal theoretical tool used for this investigation was a three-dimensional finite element computer routine that solves the full incompressible potential flow equation. This routine developed by John L. Hess uses nonlinear boundary conditions, i.e., boundary conditions are satisfied on the surface of a lifting wing rather than in the plane of the wing. Bodies, like the pod and fuselage, are treated as nonlifting surfaces. The routine is intended to calculate flow properties for incompressible conditions; however, a modification has been included that accounts for first-order Mach effects. Still, the routine is limited to applications where subcritical flow is expected.

Two constraints prevent the application of this routine for the daily design task. One is cost which will be discussed later. The other is the time required for geometry definition. The routine requires the use of flat panels to represent the body surface, and pressures are calculated at the centroid of each of these panels. In representing the pod nose section, particular attention was paid to the region of the flat face and adjacent fairing because of the steep pressure gradient expected in that region. It is in this application that experience is required before confidence in the results can be achieved.

The initial investigations using this routine were made on three isolated bodies, each of which represents a family of candidate fairings. Figure 3 presents predicted pressure distributions over the nose section of the pod with these three candidate fairings. After the final fairing was selected, the isolated body geometry was married to the full geometry of the A-7E aircraft and the total flow field, pod/pylon/wing and body was analyzed.

---

[1]Hess, John L., "Calculation of Potential Flow About Arbitrary Three-Dimensional Lifting Bodies," McDonnell Douglas Rpt. No. MDC J5679-01, dated October 1972.

[2]Theodorsen, Theodore, "Theory of Wing Sections of Arbitrary Shape," NACA TR-411, dated 1932.

[3]McNally, William D., "Fortran Program for Calculating Compressible Laminar and Turbulent Boundary Layers in Arbitrary Pressure Gradients," NASA TN D-5681, dated May 1970.

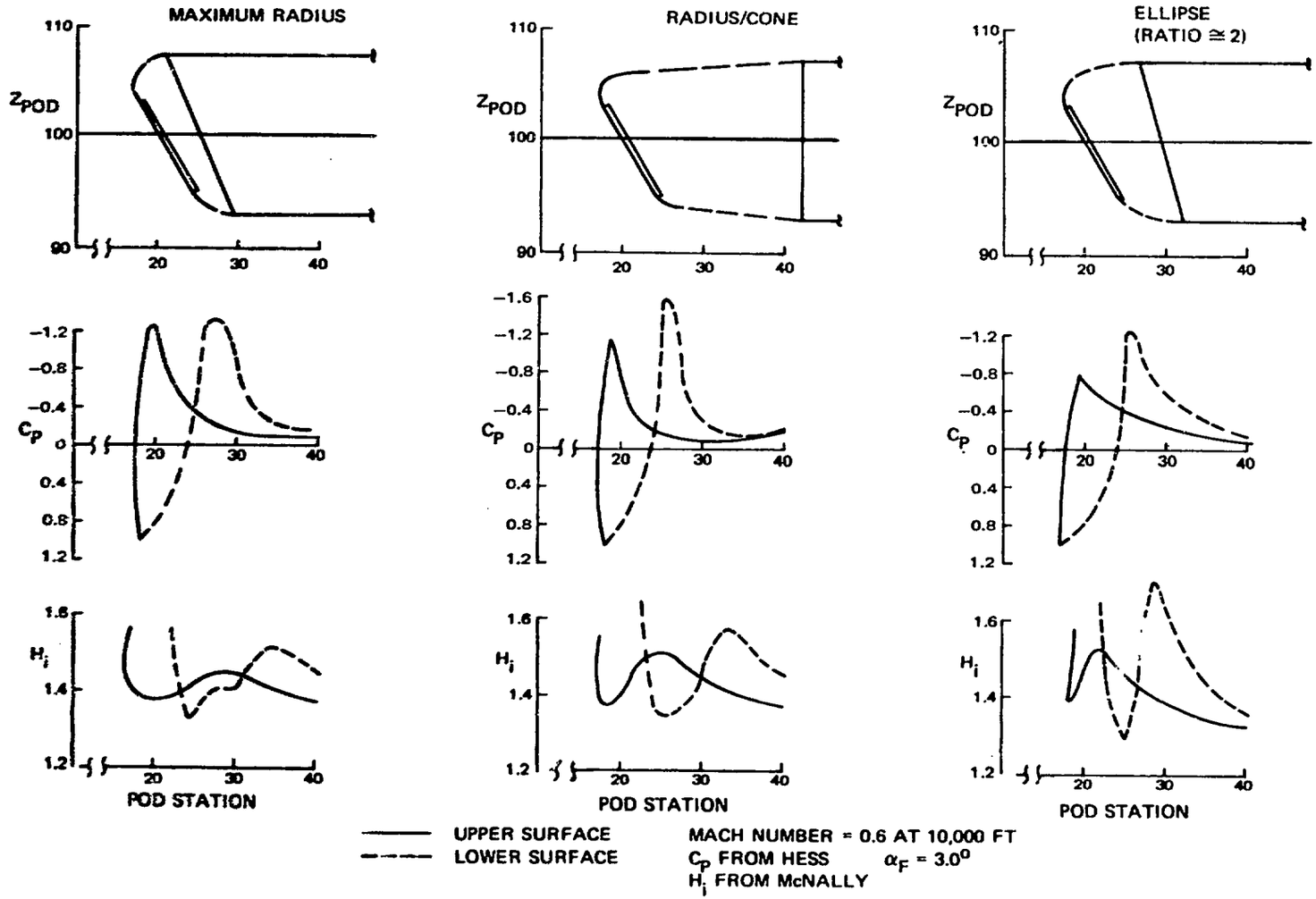


Figure 3 Analysis of Candidate Fairings

Computer solutions are normally considered to be a monetary short cut to wind tunnel testing. The calendar time saving of computer analysis over wind tunnel testing is fully recognized. Computer time is costly, however, and the dollar cost of the use of this equipment should be considered. The Hess routine in this investigation was used with two levels of geometry input, isolated pod and total aircraft plus pod. The computer time for each run on the CDC 6600 was 77 seconds for an isolated body, and 330 seconds for the aircraft/store configuration.

3.2 McNALLY BOUNDARY LAYER ANALYSIS

The Hess routine, being an inviscid technique, should not be expected to adequately predict pressures on the pod in the transonic flight regime where boundary layer development is so dependent upon viscosity. To evaluate the possible flow conditions around the face and fairing of the pod in this regime, a boundary analysis routine developed by McNally, which includes viscous effects, was used. This routine is a two-dimensional laminar and turbulent boundary layer technique that uses local geometry and pressure distributions to predict not only laminar-to-turbulent transition and separation, but to indicate, via a form factor, the relative quality of the local boundary layer. This form factor is the ratio of the local boundary layer displacement thickness to momentum thickness. The form factor normally rises to a value of 2.5 to 2.8 as the shear or friction coefficient at the surface approaches zero, thus boundary layer separation is predicted. Local flow with form factors less than 2.5 can be considered to be attached flow.

Figure 3 presents the results of a boundary layer analysis on the three candidate fairings for which pressures predicted by the Hess routine were available. In each case, the McNally routine did not predict boundary layer separation because the turbulent form factors are less than the criteria for separation.

Since the McNally routine uses existing geometry and pressure distributions, the boundary layer analysis is virtually a fallout of previous effort. Also, the computer time for the routine is low enough to encourage its general application. The McNally routine requires approximately 11 seconds of CDC 6600 time for each surface analyzed.

3.3 THEODORSEN TECHNIQUE

The Theodorsen technique is intended to analyze two-dimensional wings at zero Mach number. The theory is potential flow using a conformal mapping technique to predict velocity, and hence, pressure distributions on wings. The technique is normally very accurate near the wing leading edge provided the input geometry is very accurate. The key here is accurate geometry input. The geometry input from even large-scale sketches that are carefully read has a tendency to give erroneous results from the computerized version of this technique. Therefore, the input geometry was mathematically definable shapes, i.e., single radii, radius/cones, double radii (radius ogive profile), and various ratio ellipses. Variations of these fairings were applied as fairings to the shape representing the geometric constraints presented in Figure 2. A wedge afterbody or trailing edge was assumed to complete the two-dimensional wing geometry for this analysis.

The intent of this application was to calculate an upper surface peak pressure for each fairing (wing) and select that family of fairings that showed the least negative peak pressures. The results for the eighty fairings investigated showed the family of ellipses to have the lowest peak negative pressures.

In retrospect, the use of Theodorsen for this application is not recommended for several reasons. First, although inexpensive to run, less than two seconds of CDC 6600 computer time per run, there are more applicable two-dimensional techniques available to do this analysis. Second, the Theodorsen technique depends on accurate definition of leading edge radius which for this application is difficult to define, particularly if the stagnation point moves onto the flat face with increasing angle of attack. Finally, by way of defense, the application of Theodorsen, as inappropriate as it may be, is still more desirable than hand waving a temporary fairing that may become the final lines.

3.4 PROJECTION

In the past few years, large strides have been made towards the development of theoretical methods. It is the applicability of these powerful tools to the design task that must now be addressed, keeping in mind the requirement of timeliness. For example, the design task described in this paper would have been greatly simplified by the availability of an inverse method. In this case, the inverse method would, with the inputs of geometric constraints and flow parameters, define the best fairing available. These theoretical tools once available, and with confidence established, can be applied as needed throughout the design phase to identify and address potential problem areas.

One of the potential problems faced by all aerodynamicists is the fabrication of idealistic shapes. Optimum aerodynamic configurations tend to be compromised by other considerations when analytical methods are not responsive enough to evaluate penalties of the compromise. This situation is prevalent nowhere more than store design for several reasons. First, the presence of external stores connotates a draggy airplane and the discipline breaks down. Second, the aerodynamicist armed only with intuition is no match for a hard-nosed, practical designer who understands the problems of fabrication. The solution to this dilemma lies also in the realm of theoretical tools. The tools available, although applicable to irregular complex shapes, are easiest applied to simple, mathematically defined shapes. The timely availability of defined lines in three-dimensions backed by sound logic and loads distribution will stand the test with the designers. In addition, the implementation of these mathematically defined lines into hardware is far more likely to occur than is the more complex shapes.

4. FLIGHT TEST DATA

As a result of analytical studies, a pod nose section was designed which incorporated a family of elliptical fairings (ratio = 3 on the upper surface) such that every point on the fairing of the nose section was mathematically related to every other point. This shape was fabricated from molded fiberglas and married to a cylindrical extension of the mid section of a Sargent-Fletcher instrumentation pod. This preprototype pod, shown in Figure 4, was instrumented with static pressure orifices and fluctuating pressure pickups and flight tested aboard the A-7E aircraft. The purpose of the flight test was two-fold. First, to permit pilot evaluation of the aircraft with the pod installed, and second, to test for indications of separated flow that would degrade the line of sight of the FLIR sensor.

Flight test data taken at 10,000 feet has been selected for presentation in this section and for comparison with theoretical analysis in the following section. Data taken at 17,000 feet and 30,000 feet show the same relationships presented herein. In each case, static pressures were measured along the top and bottom centerline of the pod, and along the inboard and outboard maximum half-breadth of the pod at Z_{POD} 100. The fluctuating pressure transducers were located in these same planes and just downstream from the aft tangency point of the nose section.

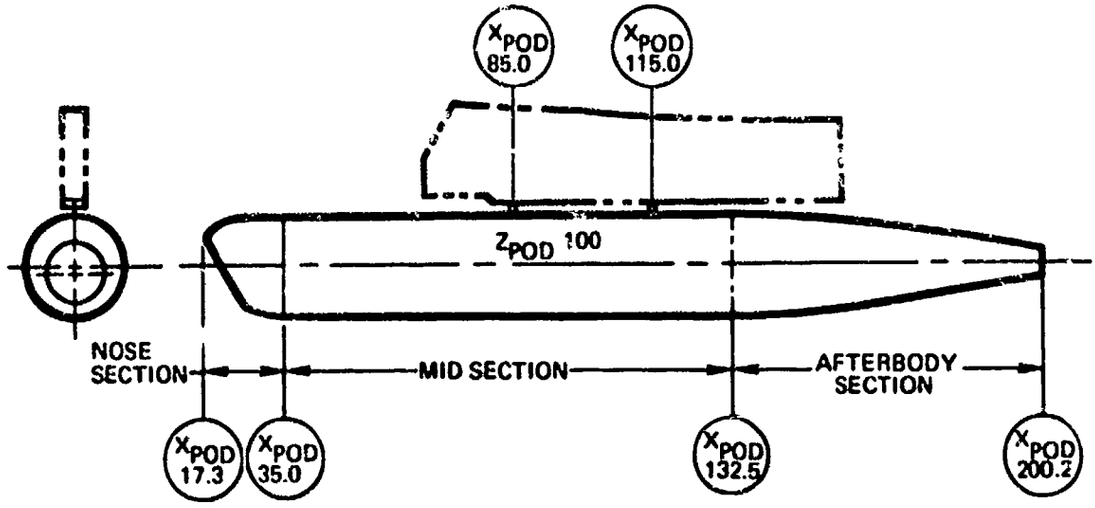


Figure 4 Preprototype Pod General Arrangement

Figure 5 presents a composite of the pod static pressures in the vertical plane for several Mach numbers. Figure 6 presents comparable data for the inboard and outboard sides along Z_{POD} 100. Each data set was taken in one g flight. As one would expect, there is a rapid expansion around the forward fairing followed by recovery and then re-expansion forward of the afterbody section. Local shocks appear likely as low as Mach number 0.725 to 0.75, particularly on the lower forward surface, but in each case large areas of separation did not occur. These same observations hold for the effects of angle of attack and sideslip

Data from a fluctuating pressure transducer located on the lower centerline of the pod are presented in Figure 7. Assuming that the divergence in overall sound pressure level is an indication of separated flow, it appears that separation started near Mach number 0.78 on the lower surface of the pod. The pressure data in Figures 5 and 6 tend to support this possibility, but indicate that the area of separation is small and that reattachment does occur. The pilot noted perceptible, but negligible, pod buffet between Mach numbers 0.90 to 0.95, and buffet-free flight above and below that Mach number band.

5. COMPARISON OF THEORETICAL RESULTS AND FLIGHT TEST DATA

A comparison of the results of theoretical analysis using the Hess routine and data obtained from flight testing the preprototype TRAM pod is presented in Figures 8 through 11. In general, the comparison shows excellent agreement, particularly if the data are to be used to determine design running airloads distributions. For purposes of flow field analysis, the agreement is good but may tend to be slightly misleading especially on the sides of the pod. In this area, the Hess routine predicts a more gentle adverse pressure gradient both downstream of the nose fairing and on the afterbody fairing.

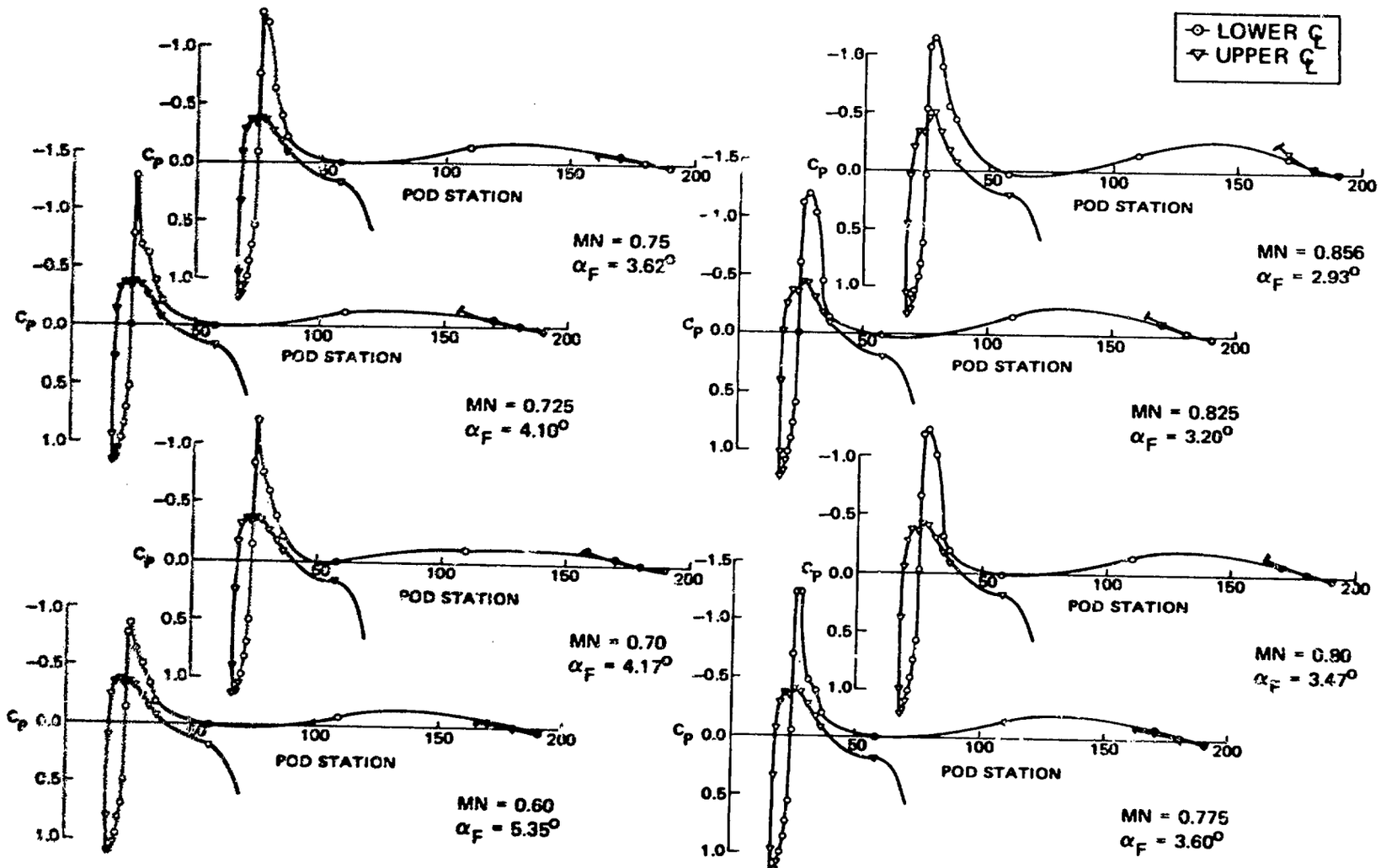


Figure 5 Flight Test Pressures – Upper and Lower Centerline

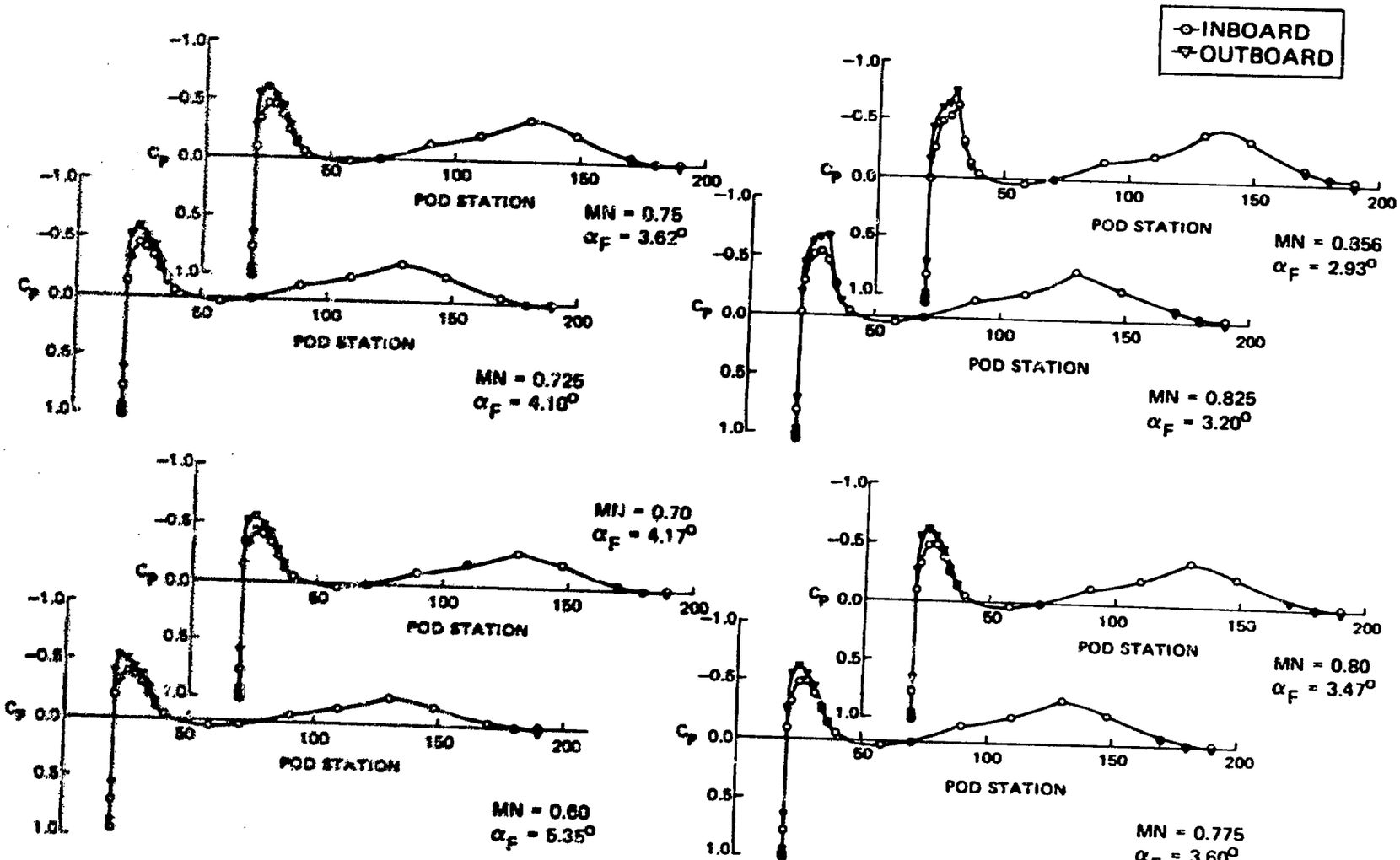


Figure 6 Flight Test Pressures – Inboard and Outboard Sides

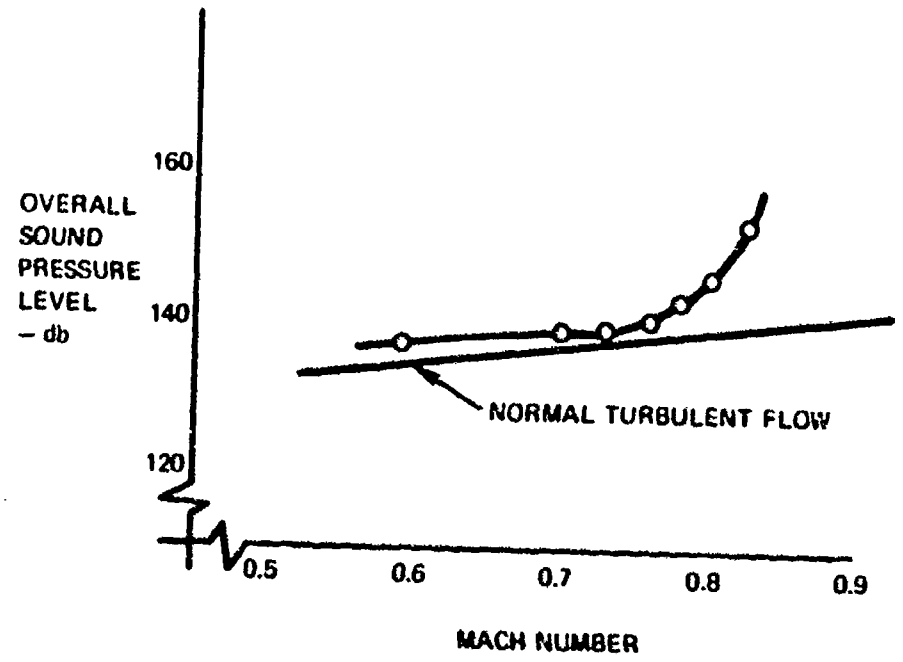


Figure 7 Fluctuating Pressure – Lower Centerline

Figures 8 and 9 present a comparison of the results as a function of angle of attack. The flight test data were taken at fuselage angles of attack, α_F, corresponding to load factors of approximately 0.5, 1.0, 1.5, and 2.0. The analytical results were run at a pod angle of attack of zero and 10^0, which corresponds to $\alpha_F = 2^0$ and 13^0 respectively. Predicted data for intermediate angles of attack were obtained through linear interpolation. Agreement of the two sets of pressure coefficients are particularly good for the lower surface of the pod nose section, both at the peak, and in the slope of the adverse gradient. For the upper nose section, the analytical predictions were high and the amount of recovery was low. On the sides of the pod, theory under predicted the magnitude of the peak, but the relation between inboard and outboard peak pressure at the nose section is the same for test and theory. This difference may be attributable to inadequate panel definition of the Hess routine. The increase in spanwise flow under the wing is evidenced in both data sets as angle of attack is increased.

Figures 10 and 11 present a comparison of the results as a function of sideslip. Flight test data were taken for approximately half-rudder sideslips both left and right. The Hess routine was run for 0 and $\pm 5^0$ sideslip at angles of attack of zero and 10^0, and linearly interpolated (or extrapolated) to obtain comparable sideslip angles and angle of attack. In this comparison as in Figures 8 and 9, the Hess routine predicted the delta from side to side but over predicted both the peak pressure and the gentleness of the adverse pressure gradient.

As a result of the agreement between the results of the Hess routine and flight test pressure data, the preliminary running airloads distributions released during the design phase were released as final design airloads. These loads, being generated in coefficient form, could be ratioed by dynamic pressure to represent both the shape and magnitude of the limit airloads on the pod.

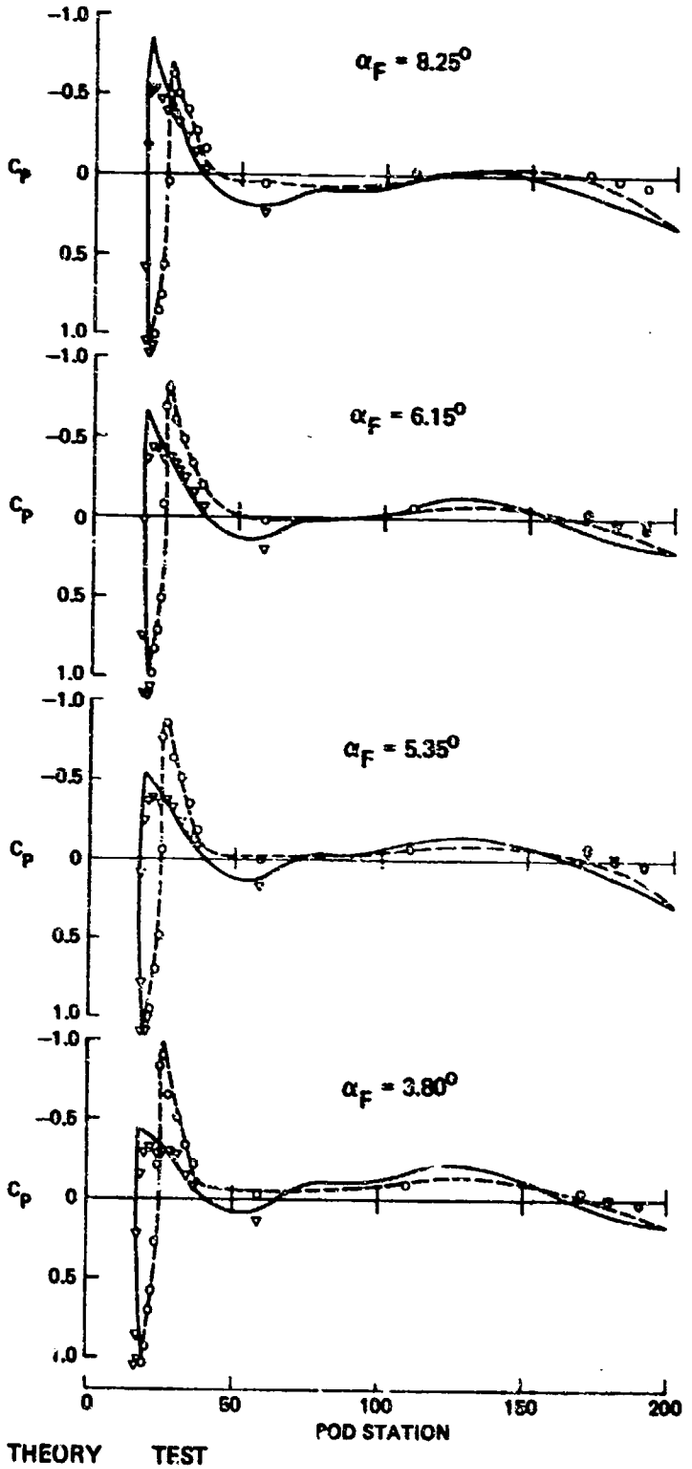


Figure 8 Comparison of Theory and Test for Angle of Attack – Upper and Lower Centerline

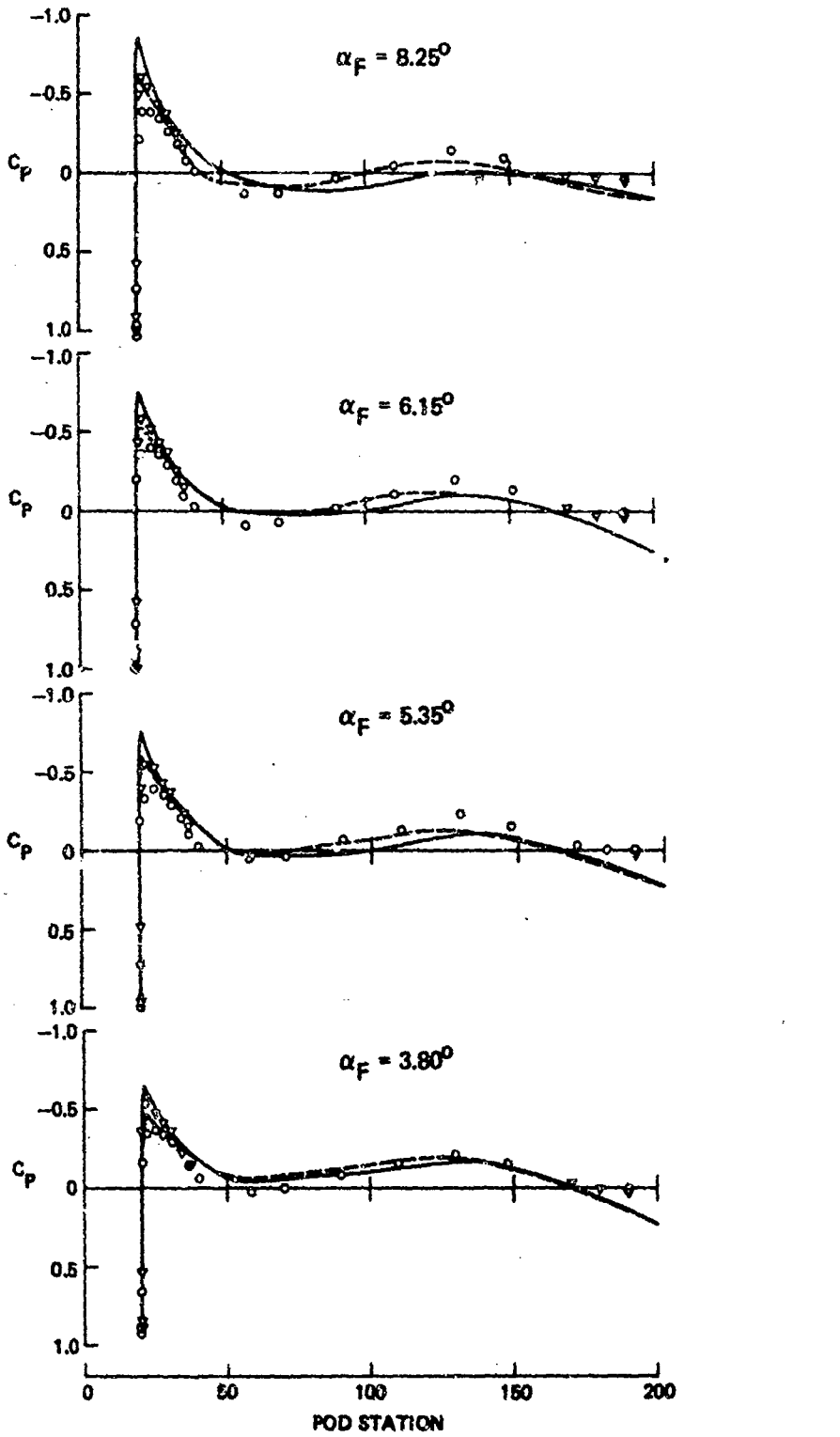


Figure 9 Comparison of Theory and Test for Angle of Attack – Z_{POD} 100

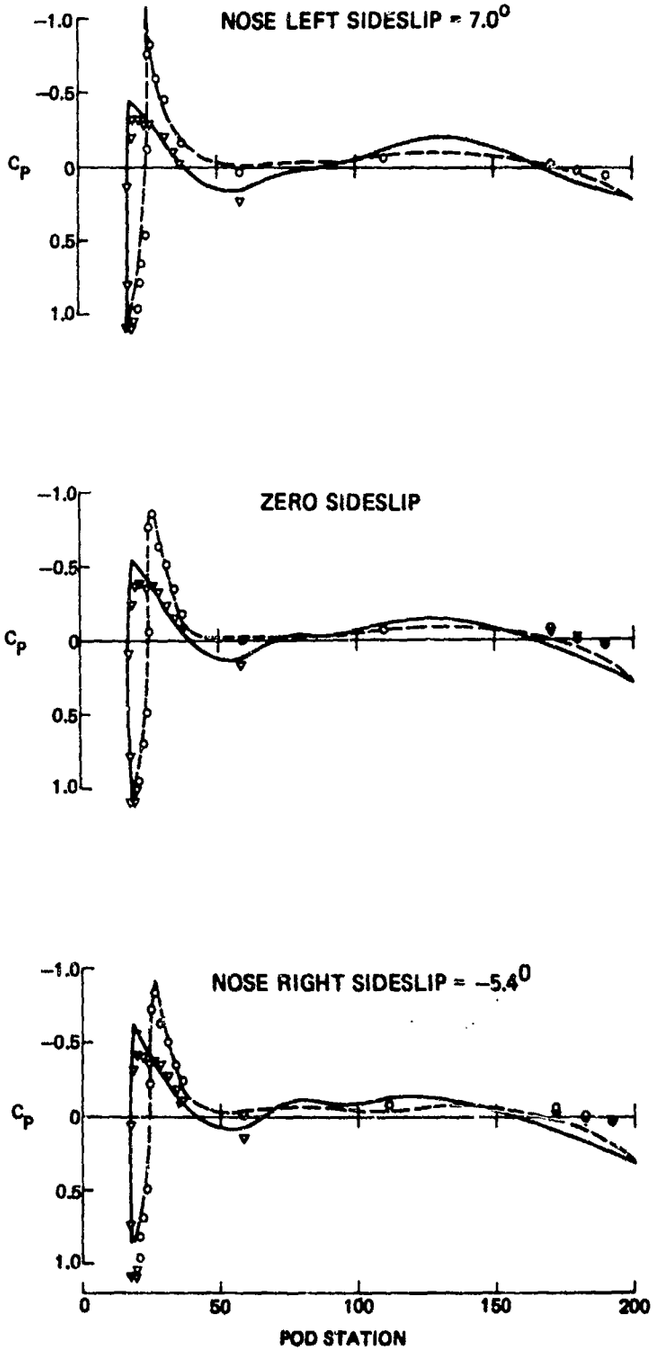


Figure 10 Comparison of Theory and Test for Sideslip – Upper and Lower Centerline

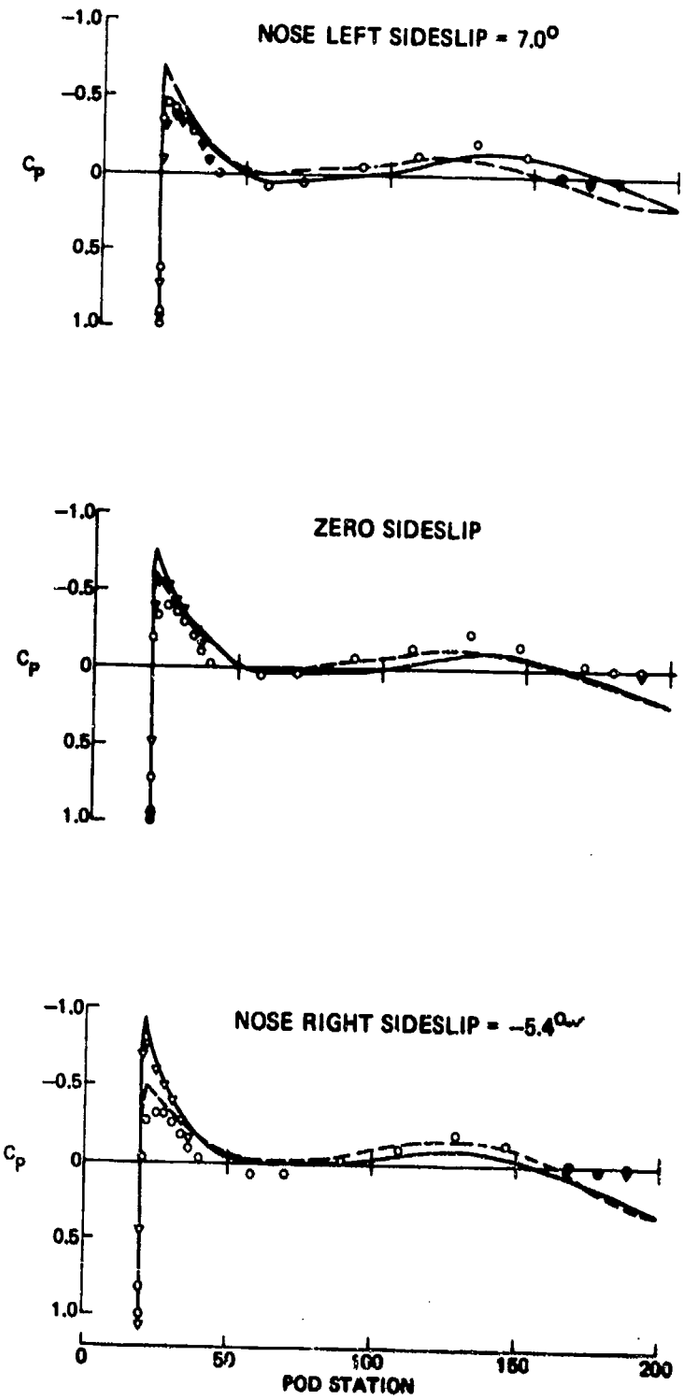


Figure 11 Comparison of Theory and Test for Sideslip – Z_{POD} 100

6. CONCLUSIONS

Theoretical tools in general and the Hess program in particular have been demonstrated by this paper to be useful in predicting the flow field around complex external store shapes up to those conditions where critical flow exists. Also identified are limitations other than those of theory. These are limitations of adaptability, usability, and confidence. Most, but not all, of these limitations will diminish with continued application of theoretical tools in the daily design environment. It is those techniques whose limitations do not diminish with usage that should be identified for improvement. These include:

1. The need for an inverse technique where the geometric constraings and desired flow conditions are identified, and the result is one or several shapes that satisfy the input criteria.

2. The need for a variable complexity technique where preliminary input yields preliminary results plus sufficient guidance for further application. This process can be continued in subroutine fashion until the need for final complex results is satisfied by final complex output.

It should be noted, however, that whatever progress is made in the field of aircraft/store compatibility, whether analytical or experimental, the very best configuration attainable for today's aircraft will be degraded by the sway braces and lugs with which they are mounted.

AUTOBIOGRAPHY

Lee D. Smith

Mr. Smith received his B.S. in aeronautical engineering from the University of Oklahoma in 1958. That year, he was employed at the Naval Air Development Center, Johnsville, Pennsylvania, where he performed design and analysis of airborne electro-mechanical devices including trajectory analysis of the aerodynamically retarded "miniature sonobuoy." In 1962, he joined LTV where he performed airloads tasks on the XC-142.

From 1964 to the present, Mr. Smith has been associated with the A-7 light attack aircraft. Initial responsibilities included wind tunnel testing and analysis of captive store loads, and store separation characteristics. Additional A-7-related assignments involved development of high and low speed wind tunnel flow visualization techniques, and techniques for determining buffet boundaries both through wind tunnel testing and flight testing. Since 1971, Mr. Smith has been responsible for all fluid mechanics tasks on A-7-related programs, including the TA-7C aircraft.

AIRCRAFT/STORES COMPATIBILITY ANALYSIS AND FLIGHT TESTING (U) (Article UNCLASSIFIED)

by

Charles S. Epstein
US Air Force Armament Laboratory (DLJC)
Eglin Air Force Base, Florida 32542

ABSTRACT. (U) In the past several years, the lack of a coordinated development program for aircraft and stores has resulted in many problems such as aircraft performance degradation, dangerous store separation, and reduced weapon delivery accuracy. The state-of-the-art in the field of aircraft/store compatibility testing is rapidly being expanded through new photographic, analytic, wind tunnel and computer techniques. This unique aerodynamic discipline concerns almost every military aircraft and involves the expenditure of large sums of money, yet is almost totally unknown and untreated in university degree programs. This paper will show how aircraft/store compatibility technology is being expanded and applied to problems of both present and future aircraft. An in-depth explanation of the latest analysis and flight test techniques will be given, including the unique marriage of the wind tunnel and the high-speed digital computer in the preflight analysis of data, and the photo-imaging technique of flight test data reduction.

Approved for public release; distribution unlimited.

INTRODUCTION

The compatibility with and separation of expendable stores from aircraft is a problem which has plagued engineers since the earliest days of flying. It gained early recognition in World War I. Since that time, regardless of the size or speed of the aircraft, or whether the stores were carried internally or externally, weapons compatibility and store separation have been continuous problems, despite the staggering advances in technology during the past fifty years. Not until the advent of high-speed jet aircraft, however, have the problems become of significant magnitude. The speed and complexities of modern fighter-bomber aircraft have made the solution of aircraft/store compatibility problems a necessity from both tactical and flight safety standpoints.

In the years following World War II, United States defense strategy emphasized the nuclear deterrent. In the early 1960's, the strategy suddenly shifted to limited conventional war while maintaining the massive nuclear retaliation capability. Almost overnight the "instant fighter-bomber aircraft" emerged. It was created by devising equipment to allow the already-existing nuclear strike aircraft to carry as many conventional bombs as possible. This hybrid aircraft was capable of enormous destruction — more than most heavy bombers of the past. To perform their assigned multiple missions, however, expensive and complex equipment was added — with accompanying weight. Added weight required added power, which itself required added weight. The end result of this spiral has been the appearance of today's multimillion dollar fighter bombers, some of which are large as World War II heavy bombers.

The emphasis in the past decade on conventional munitions has produced a large family of new weapons, each designed to provide a certain tactical effect, or to "kill" a particular target. They were, for budgetary and logistic reasons, usually required to fit and be employed on all current aircraft, rather than to mate with a specific aircraft. In the US today, because of the conflict in Southeast Asia, there are nearly 100 different conventional munitions in the inventory.

Although the development of US fighter aircraft over the past 30 years has been impressive, little attention has been given to the carriage of external stores in the aircraft design phase. Fighter aircraft today are still being designed around their "clean" aircraft performance, with stores added later on an "as much as possible" basis. The F-4, one of our

best tactical weapons delivery aircraft, was originally designed as a Navy long-range fleet interceptor. Many weapons suspension racks and other airborne armament equipment in use today were designed years ago to meet the crash requirement for a limited war capability. The multiple and triple ejector rack (MER, TER) concept was conceived over 10 years ago to pack as many bombs on an existing aircraft as possible. The pressing situation at the time did not permit in-depth examination of potential problems such as store separation. This situation has led to aircraft performance and stability problems, dangerous store separation, reduced weapon accuracy, and a monumental testing workload to certify weapons for use with each aircraft. One aircraft, such as the F-4 or A-7, has several external pylons, each capable of carrying different types of bomb racks (such as MER's or TER's). Each rack, in turn, can carry many different numbers and types of stores. With the nearly 100 types of stores currently in the inventory, the possible loadings on one aircraft can be as high as 6,000,000. To cope with the unacceptable large testing workload generated by this situation, the US Air Force created project "SEEK EAGLE" in which aircraft/store compatibility is recognized as a distinctly separate requirement and only certain stores are designated for certification on specific aircraft. To further reduce the scope of the problem, the tactical forces are asked to identify individual aircraft/store loading configurations they feel are necessary, and only those loadings are certified. Since 1966, the Armament Development and Test Center at Eglin AFB, Florida, has conducted over 800 aircraft/store compatibility tests involving over 85 types of stores and 18 different aircraft types.

STORE CERTIFICATION

Prior to further discussion, it is essential that certain terms be defined (these definitions, and others of value to the reader's understanding of this problem are contained in reference 1).

STORE

Any device intended for internal or external carriage and mounted on aircraft suspension and release equipment, whether or not the item is intended to be separated in flight from the aircraft. Stores include missiles, rockets, bombs, nuclear weapons, mines, torpedoes, pyrotechnic devices, detachable fuel and spray tanks, line-source disseminators, dispensers, pods (refueling, thrust augmentation, gun, electronic-countermeasures, camera, designator, etc.), targets, cargo drop containers, and drones.

AIRCRAFT/STORE COMPATIBILITY

The ability of an aircraft, stores, and related suspension equipment to coexist without unacceptable effects of one on the aerodynamic, structural, or functional characteristics of the others under all flight and ground conditions expected to be experienced by the aircraft/store combination. A particular store may be compatible with an aircraft in a specific configuration, although not necessarily so with all pylons (or stations) or under all conditions.

CERTIFICATION

The determination of the extent of specific aircraft/store compatibility and the formal publication of all information necessary for appropriate employment of a store on a specified aircraft (aircraft series) in the applicable technical manuals and flight operation manuals (or interim supplements or revisions thereto).

The determination of compatibility of a particular store with a specific aircraft is an involved process. On present day aircraft with multiple external store stations and multiple store carriage at many of these stations, loading configurations can lead to serious weight and balance, stability, structural, or flutter problems. Keeping track of the approved and the not approved (and reasons for non-approval) configurations is a monumental task for even one type aircraft. In determining the compatibility of a store with an aircraft, many areas must be examined and many tasks performed which cut across almost every engineering and testing discipline. Some of the most important of these are discussed below.

Pre-flight Analyses

These include the necessary tasks and analyses which must be performed prior to flight testing the store. First, the specific loading configurations of interest are identified and station loading capabilities and physical clearances are checked analytically. To accomplish this, two documents (MIL-STD-1289 and the "Aircraft/Stores Interface Manual") prepared by the Joint Technical Coordinating Group (JTCG/MD) Working Party for Aircraft/Stores Compatibility are of significant value. As principal Air Force Systems Command member of this committee, I had a major role in their preparation and subsequent publication (see references 2 and 3). Once physical compatibility has been confirmed, analysis is begun to determine if acceptable operational carriage and employment

envelopes can be established. Establishing a captive carriage envelope involves determining if any adverse stability and control, structural loading or flutter problems are caused by the carriage of the store on the aircraft. Similarly, establishing an employment envelope involves determining if any adverse store separation or jettison problems exist. Once these envelopes have been acceptably established, a flight test plan is then formulated which identifies the minimum flight test demonstration points that are required to clear the entire operational envelope. These analyses often require considerable amounts of electronic computer and wind tunnel test time and sometimes involve the conduct of ground vibration and other structural tests prior to allowing the store to be flown. We have the capability to perform these captive envelope analyses on the F-4 and will soon obtain this capability on the A-7.

Fit and Function Test

Prior to actually flying the store on the aircraft, a physical and electrical compatibility fit test is conducted. Procedures for accomplishing this test are contained in MIL-STD-1289 (Ref 2); however, in general, the store is fitted on the aircraft in the desired loading configuration (or configurations) to insure adequate clearances exist between all parts of the store, the aircraft, the ground, and other stores. If the store has electrical connections, the physical mating of all plugs as well as pin functions are checked. It is at this time also that procedures for loading the store on the aircraft are verified and that arming wire or lanyard hook-ups are determined.

Flutter Flight Tests

Prior to flying any aircraft/store configuration, a mathematical flutter analysis is made to determine whether any flutter modes will be encountered within the expected captive flight envelope for the configuration. Unfortunately, even though we have developed complex sophisticated aircraft analytical flutter models, this mathematical analysis often tells us only that a problem may exist. If this occurs, flights with a specially instrumented flutter aircraft must be performed to confirm or reject the analysis prior to proceeding further. Currently, the USAF has no flutter-instrumented aircraft in its inventory and, if such flights are required, they are contracted to the aircraft manufacturer. It should be stressed, however, that after some flight experience has been gained on a particular aircraft, it may be possible to develop an analytical flutter prediction capability

which, through tests, has shown a high enough degree of reliability to preclude further flight tests. We have almost attained such a capability within the Armament Laboratory for the F-4 and are in the process of gaining it on several other aircraft.

Captive Structural Integrity Flights

One discovery, very important to the field of aircraft/stores compatibility, was made as a direct result of US participation in the Southeast Asia conflict. Many times stores were loaded on aircraft in Vietnam and flown, but not dropped, due to lack of a target or other operational reasons and were still attached upon the aircraft's return to base. Stores sometimes made as many as three or four flights before being dropped. In addition, many missions to Northern Vietnam required one or more inflight refuelings enroute. In these cases, the store might be subjected to as much as two or three hours of maneuvering flight (some of it highly evasive) prior to being released. As a result, failures of the stores themselves were being experienced — fins cracked, fuzes failed, arming wires became loose, etc. To simulate these conditions in the initial aircraft/store compatibility testing, we initiated a specific captive flight test. This qualitative flight test, using uninstrumented aircraft, usually consists of two sorties for fighter type aircraft because of fuel requirements; however, some aircraft have the fuel capacity for accomplishing the specified profile in only one sortie. If two sorties are required, stores are not downloaded or otherwise disturbed between sorties so that an accumulative effect of maneuvering and vibration may be assessed. During these flights, the store (loaded on the aircraft in the desired operational configuration, including other stores such as fuel tanks if necessary) is subjected to various maneuvers (such as pushovers, pullups, stick pulses, rolling pullouts, etc.) at various speeds and load factors up to the maximum predicted allowable. The minimum total flight time for the two sorties should be the time equivalent of the aircraft's combat radius plus 50%. Of this total time, approximately 30 minutes should be performed at 0.9 Mach (or the maximum allowable airspeed, whichever is lower) at the lowest practical altitude commensurate with weather and safety of flight (500 to 1000 feet above sea level is recommended). A more thorough discussion and detailed instructions for this flight test may be found in Section 5 of Ref 1. Since initiation of these qualitative flight tests several years ago, we have found and corrected many structural deficiencies which otherwise might not have been found until the configuration was in use operationally.

Weapon Separation Tests

Separation testing involves releasing (employing) stores loaded on the aircraft in realistic operational configurations at various airspeeds, attitudes (level flight and dives) and release modes (single, pair, ripple) in sufficient quantity to demonstrate that an operational envelope may be cleared. These separations must demonstrate that the store can be safely released from the aircraft without excessive disturbances, store-to-aircraft or store-to-store collisions, and with sufficient repeatability to allow accurate delivery. Since this part of the flight test program presents the greatest cost and hazards to flight safety, preflight analyses should be used to the maximum extent to reduce the amount of actual flight testing required. To do this, the analyses must be verified early in the flight testing. In 1966, when we first began attacking aircraft/stores compatibility with a planned program, little constructive information or technology on store separation existed. The information that did exist was woefully fragmented in the engineering departments of many different aircraft manufacturers. Because of the rapid buildup of the conventional weapon inventory, there was a serious lack of manpower and facilities available (or able) to accomplish the necessary preflight analyses and wind tunnel tests prior to flight tests. For that reason, most flight tests were run in what is called the "brute force" method. Based on whatever information we had, an initial flight test point was determined analytically. Store releases were made at this point, and subsequently in increments of increasing (or decreasing) speed, usually 25 to 50 knots, until the maximum predicted envelope was demonstrated. Level flight was completed prior to dive angles. Single drops were made prior to ripple releases, and decisions to proceed to the next point were based exclusively on a qualitative analysis of this film. Today, however, as a result of experience and newly-developed technology, we are able to reduce the number of actual test flights on any given aircraft/store combination to about 1/4 of what they were in 1966. Today's methods involve the use of any of a number of newly-developed analytical and wind tunnel techniques to define the predicted safe separation envelope of the store. A minimum number of flight demonstration points are then selected from this analysis, and store releases are made at these points, while recording the stores' separation trajectory through the use of onboard high-speed motion picture cameras. This quantitative store separation data is then reduced utilizing processes such as photogrammetry or photo-imaging, and a direct comparison made between the flight test and predicted separation trajectories. Time, excessive safety hazards and cost have made the "brute force," or qualitative, method of flight testing prohibitive.

Bomb Ballistics

The near flow field of the aircraft and ejector rack characteristics of each type aircraft can materially affect the initial trajectory of a store immediately after release, thereby having a substantial effect on its impact point. Because of this, releasing a number of stores on an instrumented range may be required to establish accurate bombing tables.

Electromagnetic Compatibility (EMC)

EMC testing involves determining if any electrical or electronic equipment on the aircraft, other stores, ground support equipment, or enemy ground installations might produce an electrical potential in the weapon, causing an explosion, abnormal operation, or other undesirable side effect. It consists of testing for both electromagnetic interference (EMI) and for hazards of electromagnetic radiation to ordnance (HERO). Our office has the capability to perform EMC analyses on almost any type of store. The Armament Development and Test Center has the capability to perform HERO tests. EMI testing, on the other hand, requires extremely sophisticated and specialized test facilities, not available to us at Eglin AFB. We usually perform such tests at other Air Force and contractor facilities.

STORE SEPARATION ANALYSIS

Wind tunnels have been used for a number of years to determine aerodynamic loads acting on stores on or near an aircraft in flight. Initially, store models were mounted on the aircraft model and only total captive store loads were measured. As wind tunnel equipment was refined, later capabilities included a secondary store support sting which permitted the measurement of loads on the store as it was released from the aircraft. To obtain a store trajectory by this method, however, a large amount of experimental data had to be obtained and forces integrated using manual interpolation between points. Many hours of tedious calculations were required to determine a single store separation trajectory. The spectacular development of high-speed digital computers, however, has permitted important advances in the use of wind tunnels to study store separation problems. With their vast memory storage capacities, computers can store all the aerodynamic loads data and perform both the spatial interpolations and trajectory integrations in seconds. It has now become practical to use experimental data to evaluate the separation characteristics of specific stores over a wide range of flight conditions, rather than merely spot check theoretical predictions. Currently, the compatibility engineers in my office

CAPTIVE TRAJECTORY SYSTEM INSTALLATION

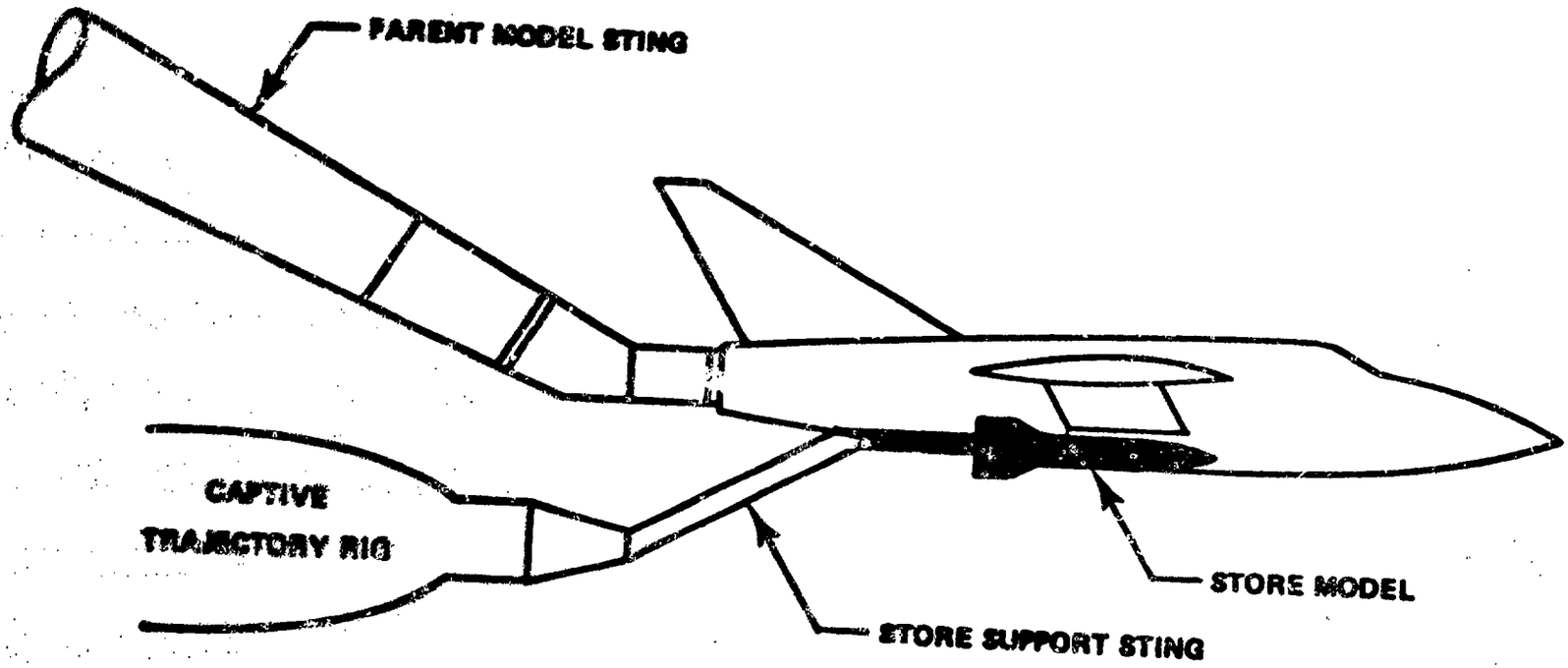


FIGURE 1

use four separate techniques for the preflight prediction of store separation trajectories. All of these techniques involve the unique marriage of the high-speed digital computer and the wind tunnel. None of the techniques is, in itself, the entire answer to store separation prediction. Each has its advantages and its weaknesses. Rather, the compatibility engineer must decide, in each case, which method most closely meets the needs of his particular situation. Each technique is discussed in detail below.

Captive Trajectory System (CTS) Testing

In recent years, the computer's speed has been utilized to perform store separation calculations "on-line" (while the wind tunnel is operating) utilizing separate stings for the aircraft and the store. (See Figure 1). This technique is referred to as Captive Trajectory System Testing. First attempts to accomplish this type of testing utilized an on-line analog computer. Later tunnels used digital computers, primarily because of their speed. The USAF's newest digital computer controlled wind tunnel with a CTS capability is located at the Arnold Engineering Development Center (AEDC), Tullahoma, Tennessee. This tunnel, the four-foot transonic tunnel known as 4T, is our primary analysis tool. The 4T tunnel is a closed-loop, continuous flow, variable density tunnel with a Mach range from 0.1 to 2.0. Two independently operated stings are used. The aircraft is mounted on its sting inverted (for ease of mechanical operation only), and the store to be released is mounted on a separate sting with its own internal balance. All stores in the specific loading configuration other than the one being separated are mounted rigidly to the aircraft model. This is a very important aspect since complex aerodynamic interference flow fields generated by today's multiple carriage of stores externally are virtually impossible to predict analytically. Interacting shock waves and pressure distributions affect the store during separation, and any perturbations caused by them generally determine whether or not the store separates cleanly. When the store is properly positioned on its sting as close as possible to its carriage point on the aircraft and desired tunnel flow conditions are established, control of the store model is given to the on-line computer. The computer measures the captive position loads and moves the store away a small distance, simulating initial separation. Forces acting on the store are again measured, examined by the computer, and a prediction made as to the next expected position of the store in its separation trajectory. The computer automatically activates a control system which then moves the store to the predicted new position. In making its predictions, the computer considers aircraft speed, attitude, and load factor, the bomb rack ejector forces (if any) and the aerodynamic flow

field around the aircraft and store. If, upon reaching a point, the measured store forces do not agree with the predictions, the computer automatically backs the store and obtains additional intermediate measurements. After tunnel conditions are stabilized and repetitive runs are begun, up to eight runs per hour can be made. One of the unique features of CTS is that the wind tunnel is of secondary importance — the computer being the dominant component. The computer is pre-programmed to solve the six-degree-of-freedom equations of motion with real time as the independent variable. During the runs, the tunnel operators are provided continuous TV pictures of the model, and the on-line computer, using a high-speed printer, prints out the separation trajectory data almost immediately. CTS testing is, compared with other wind tunnel methods, very fast. Low-cost reusable store models are utilized. Because all of the store mass parameters are input to the computer for its trajectory solution through the store internal balance, the models need only be shells with accurate outside shape, and no inertial or mass property simulation is required. Again, because of the computer's ability to manipulate mass and acceleration data in its solutions, CTS store separation testing can be accomplished at simulated aircraft dive angles — something which is unique to the CTS method. Data printed out from CTS runs are complete and may, therefore, be used with no further reduction or manipulation as the prediction of an actual store separation. Although the computer may be programmed to plot any particular parameter, or even to cross-plot several parameters, the usual output for our engineers is a complete tabulation of all data plus six selected plots. These plots are used directly in the preparation of a flight test plan and in the subsequent comparison of flight test and predicted separation trajectories.

Drop Model Testing

Another method of using wind tunnels for store separation simulation is called Drop Model Testing. This method has been in use for several years, and involves actually releasing store models in the tunnel from the aircraft model. Such store models must, of course, be extremely accurately scaled, both in aerodynamic and in dynamic mass properties. The store models are photographed during tunnel release with high-speed motion picture cameras from at least two directions, usually side and bottom. This film is then reduced frame-by-frame using a computer to define the spatial position of the store versus time. Two problems immediately face the engineer desiring to use the drop model method. First, since most external stores today are ejected from the aircraft, some method of accurately simulating the ejection force, and its point of application to the store, must be provided in the aircraft

model. Constructing such a device in the small-scale aircraft models used is no easy task. Quite often calibrated springs are used, with electrical burn-through bolts providing the release on command. Secondly, constructing the store models is extremely difficult, particularly for small-scale models, and moments of inertia may be impossible to simulate even when exotic metals such as tungsten or gold are used. Because of this, wind tunnel engineers have developed two basic sets of model scaling relationships, the so-called "light model" and "heavy model" methods (see Ref 4). Although a detailed description of these two methods of scaling is too lengthy to include here, suffice it to say that, with "light" model scaling, the angular motion of the store versus time seen in the movie film of the separation will be essentially correct, but the vertical distance versus time will be in error. When "heavy" model scaling is used, the vertical distance versus time will be essentially correct, but the angular motion will be in error (usually more motion will be seen in the tunnel than in actual flight). Some engineers use a hybrid method in which the "light" model laws are used to construct the store model, and the ejection velocity is intentionally increased by a calculated increment to offset the store model's mass deficiency. Drop model testing at high speeds is, compared with CTS, very slow. One run per hour is not uncommon. Also, the store models are expensive and, in most cases, not reusable. Because of the potential for the released store models to damage the tunnel equipment, this method is not available at many tunnels. Drop model testing is, however, most advantageous in investigating separation trajectories of low density, unstable stores such as empty dispensers, pods, napalm bombs and tanks. This type of store, because of its large angular excursions during separation, almost always causes abbreviated CTS runs due to contact of the store model with the aircraft or due to the sting's mechanical limit being reached. Drop model testing, on the other hand, produces complete trajectories -- even if the store impacts the aircraft. Multiple (or ripple) releases of stores may also be made in drop model testing, but only level flight releases are possible. Reduced data from drop model testing may also be used directly in the preparation of flight test plans and in the subsequent comparison of flight test with predicted separation trajectories.

Grid Testing Technique

Possibly the oldest of the still-used wind tunnel techniques is the Grid Method. In this method, the aircraft is mounted on one sting and the store to be investigated is mounted on a separate sting with its own internal balance, just as in the CTS method. Once tunnel flow conditions have

been stabilized, the store is moved to various discrete positions below the aircraft, and forces and moments acting on the store are measured. These points describe a three-dimensional box, or grid, below the point from which the store is to be separated. Grid runs are then made for each configuration of interest and at several different Mach numbers. Free-stream store aerodynamic data are also needed so that, if the data are not already available, these data may also be gathered on the same test by merely removing the aircraft model and performing pitch and yaw polar runs with the store still attached to its sting. Once the free-stream data and the forces and moments on the store with the flow field are obtained, they are input to a six-degree-of-freedom computer program which calculates the trajectory by combining the data into the equations of motion of the store. The grid technique is less expensive than CTS or drop model testing in that less actual wind tunnel test hours generally are used — particularly if store free-stream aerodynamic data are already available. Grid testing, however, does not produce complete store separation trajectories. Considerable data reduction and manipulation are required prior to being able to predict specific store separation trajectories in support of a flight test program. Once the wind tunnel test has been accomplished and the computer program checked out, an almost infinite number of store separation trajectories, run at any conceivable set of conditions, may be obtained quickly. An additional advantage is that if, during the flight test program, something unusual or unexpected occurs, the phenomenon may be investigated by changing various parameters in the computer input and attempting to identify the causative factor by duplicating the actual trajectory. Such fault analyses are not possible with the other wind tunnel techniques without additional tunnel testing.

Flow Field Angularity Technique

The three prediction methods discussed above, although dissimilar in their methods, all represent empirical approaches to the problem of store separation. Such empirical approaches measure the forces and moments on the store in the interference flow field, and are generally useful only for a specific store and a specific set of separation conditions. All are relatively expensive in that they consume considerable amounts of wind tunnel testing time for the given stores being investigated. If, later, it is desired to predict store separation trajectories for additional store types, the previously acquired wind tunnel data are of only minimal usefulness. Several engineers in the past few years have studied and proposed a number of purely theoretical approaches to the store separation problem utilizing potential flow theory, vortex lattice, or finite difference

techniques. Although much work has been performed in these areas, and some of it very encouraging, for the most part the resultant methods are highly complex and extremely time consuming and unusable for predicting the large amount of store separation trajectories necessary in a flight test. Because of this, the Air Force has developed a hybrid method called the Flow Angularity Technique, which combines the inexpensiveness of the theoretical analysis with the speed of the wind tunnel to provide an excellent prediction tool which is usable for a large variety of stores over a wide range of separation conditions. Because of its wide application, it is most useful when stores are initially being certified on an aircraft or when a large number of additional stores are added to the aircraft's certification list. It is essentially a one-time test in that, once accomplished, the data can be used to predict store separation trajectories on many new stores. The technique, developed by a young Air Force engineer in our office, is described in detail in references 5 and 6. However, the essential elements are as follows:

a. First, a wind tunnel test is run in which several stores of interest are loaded on the aircraft model in various configurations. While these stores are in the captive carriage position, the aircraft flow field below and beside the store is explored with a pressure probe to measure velocity vectors. The output from this test is a set of data showing the changes in angle of attack and angle of sideslip of the flow field caused by the immersion of the store into this flow (store interference effects).

b. Store interference aerodynamic coefficients are then calculated by using the store free-stream coefficients and the flow angularity values obtained empirically from the wind tunnel. A series of wind tunnel tests and analyses over the past few years has shown that the predominant factors affecting a store's separation behavior are the forces and moments on the store while in the captive carriage position. Tests have shown that these forces and moments can be represented effectively for most conventionally shaped stores by two forces — one on the nose-body and one on the tail. Total store aerodynamic interference coefficients are those caused by the nose-body plus those of the tail. These incremental coefficients are calculated using the flow angularity values obtained in the wind tunnel.

c. After calculating the store aerodynamic interference coefficients, a six-degree-of-freedom computer program is then used to solve the equations of motion of the store during separation. Again, as in the grid method, the wind tunnel does not supply complete store separation trajectory data. A computer program must be used to combine these empirical data

with analytical methods. Once the data have been acquired, however, and the computer program operational, large numbers of trajectories may be produced in a short time. Also, like the grid method, post-flight analysis of unusual occurrences can be made by varying the computer inputs. Unlike the grid method (which provides data only for the store being tested), the flow angularity technique provides data which can be used later in predicting separation trajectories of other type stores. It is, of course, cheaper than CTS or drop model testing, and more widely applicable than grid testing.

The flow angularity technique is now in constant use by our compatibility engineers for predicting store separation from the F-4 aircraft. We have also recently expanded its use to the F-15 and A-10. Flow field data have been collected this year for the A-7D, and the prediction program for the A-7D will be operational soon.

STORE SEPARATION FLIGHT TESTING

After the preflight analyses have been completed, and predicted safe carriage, jettison and separation envelopes have been developed for the particular store loading configuration, flight test demonstration points are selected and a test plan formulated. These demonstration points are held to an absolute minimum consistent with flight safety. If the store appears in the analyses to be relatively well behaved and insensitive to large changes in Mach number, airspeed or dive angle, as few as three points may be selected for demonstration.

Much emphasis in the past few years has rightfully been placed on the preflight analysis efforts of aircraft/stores compatibility due to the high cost and risk factors that accompany actual flight testing. However, no analytical or wind tunnel prediction technique can be effectively used to reduce flight testing without some method of correlating the predicted store trajectory to its actual inflight trajectory. Without a quantitative inflight store separation trajectory definition system, it can never be determined if the prediction techniques used are accurate. To do this, we require that the aircraft used to release the stores be equipped with several high speed, 16mm motion picture cameras, operating at 200 frames/second and having time annotation on each frame. The cameras are mounted to view the store release from at least two angles, one of which should be as close as possible to a side view. So that camera data will be of the highest quality, the cameras should be equipped with automatic exposure control, and wired such that when the pilot activates the stores release button, the cameras are immediately turned on but the stores release signal is delayed by 0.5 seconds. This delay in

release allows the cameras to reach full running speed prior to the photographing of the store release. The cameras then run for a preselected time (usually 3-5 seconds) and then automatically shut off. This relatively simple delay circuit installation has caused a significant increase of usable camera data since its initial use a few years ago. In addition to these data cameras, we also record aircraft conditions at time of stores release by means of a cockpit camera, an onboard data recording package tied into the aircraft instrument system, or (occasionally) by pilot,or flight crew readings of the cockpit instruments.

Once the store separation has been made, the quantitative photographic data must be reduced to a form similar to that of the predictions so that a direct comparison between predicted and inflight trajectories may be made. To do this, we currently employ two techniques; one, called "photogrammetry" developed by the Air Force at Eglin AFB, and the other called "photo-imaging", developed by US Navy engineers at the Naval Missile Center and Naval Weapons Center. Both provide excellent data but the photo-imaging technique is superior in its usefulness and considered to be state-of-the-art.

Photogrammetric Data Reduction

In this method, both the store being released and the aircraft pylon must be painted with a background color and a contrasting-color pattern of dots whose positions are accurately known with reference to some specific point (see Figure 2). Size and color of the spots is not fixed; they are optimized for accuracy and ease of film reading. However, a minimum number of dots must be visible at all times in the film. Onboard camera lenses are selected so that both the store being released and the part of the aircraft adjacent (pylon, for example) are visible on the film. After the release, each frame of the onboard-gathered movie film is processed through a film reader manually. These data, along with a series of geometric and physical constants, such as location of the reference dots with respect to a specific position, camera location and lens focal length, are input to a computer. The computer is programmed to solve the equations of motion and defines the store trajectory, printing out roll, pitch, and yaw angles and X, Y, and Z displacements of the store versus time. Although a two-camera solution would be preferable, we have found that a one-camera solution can be used most of the time, and will provide accuracies of about ± 2 inches for displacements and ± 2° for angular motions. The photogrammetric computer program requires starting estimates of store and camera orientation with respect to the aircraft. A final, iterated, solution

TYPICAL PAINTING PATTERN USED FOR PHOTOGRAMMETRIC DATA REDUCTION OF STORE SEPARATION

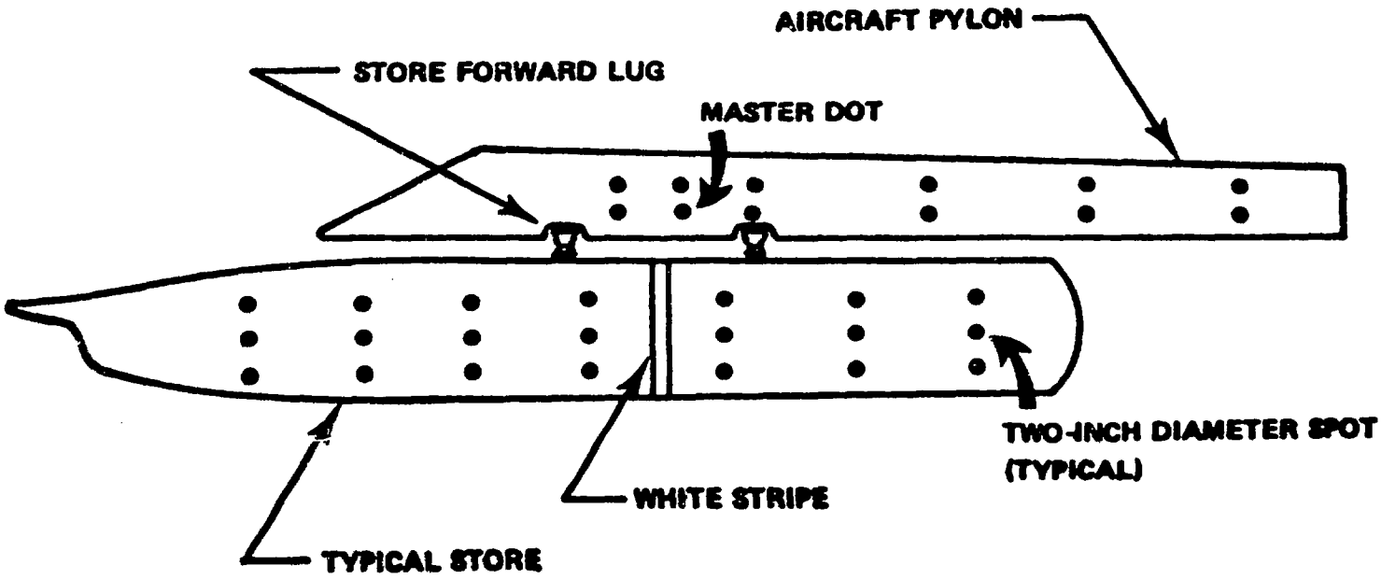


FIGURE 2

is then obtained which achieves convergence for even poor starting values. After the first frame, the program employs previous frame results as the estimate for the succeeding frame. Because of this, wing flexure and vibration are automatically eliminated. The computer is programmed to print out the trajectories in both a tabular and plotted format, so that a direct comparison may be made between predicted and inflight trajectories.

Photo-Imaging Data Reduction

This system utilizes an image matching technique to obtain spatial position and orientation of photographed objects with respect to recording cameras (see Figure 3). It consists of projecting each frame of the onboard flight-gathered data film through an optical system into a high resolution video camera and displaying the resulting image on a TV monitor located on an operator's console. Another high resolution video camera is positioned near the console to view an exact scale model of the store. This store model is mounted on a remotely-controlled six-degree-of-freedom model positioner mechanism. The video signal from this second TV camera is fed through a video mixer and the resulting image is simultaneously displayed on the same TV monitor as that from the data film. The operator can adjust the position and orientation of the store model through the use of a set of levers on the console. He adjusts the store model until the image of the store on the positioner is exactly superimposed on the image of the store from the data film (a process similar to using a camera range finder). Once the two images are exactly aligned and superimposed, the operator can press a single button which transfers the encoded frame count and position data to an IBM card. Each frame of the film is similarly reduced, until a card deck is generated. This deck is input to a computer program — just as in the photogrammetry process — to solve the spatial relationships. The output from the photo-imaging technique is a set of tabular data and selected plots which accurately define the store separation trajectory to compare directly with the predictions. This technique produces extremely accurate data (± 0.1 ft for displacements and ± 1.0° for angles) and has the added advantage of not requiring a complex painting scheme on the store and aircraft. Because of this, the cost of reducing the film data from a specific store separation is about one half that of the photogrammetric technique. A photo-imaging system now exists at three US Navy testing locations and we are attempting to have one installed at Eglin AFB. In the meantime, we are utilizing the Navy's system at the Naval Missile Center, Pt Mugu, CA, for reducing all the store separation flight test data for the A-10 and F-15 aircraft. A complete

SCHEMATIC REPRESENTATION OF PHOTO-IMAGING SYSTEM USED FOR FLIGHT TEST DATA REDUCTION OF STORE SEPARATIONS

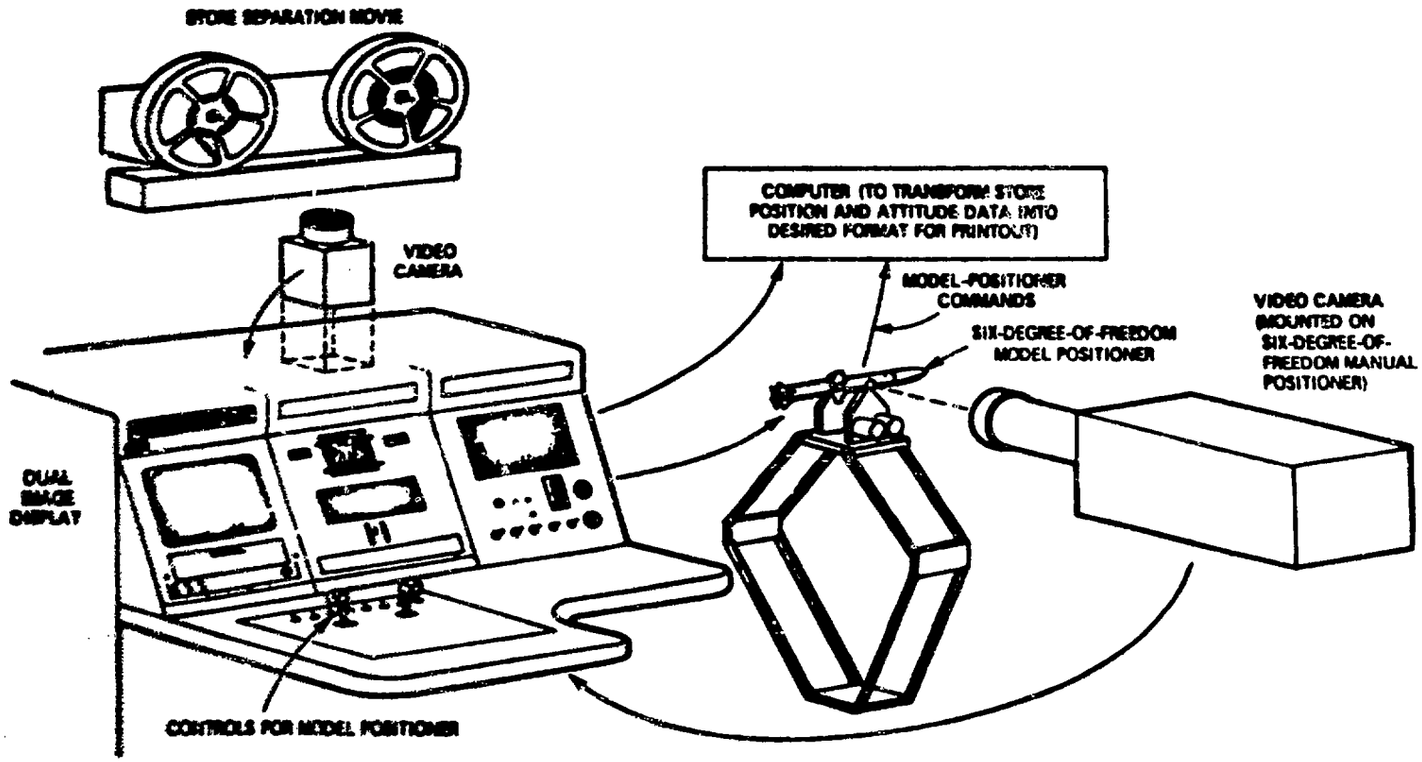


FIGURE 3

description of the photo-imaging system currently in use by the Navy at Pt Mugu can be found in reference 7.

Both of the methods described above provide accurate, useful quantitative data, both in a tabular and a plotted format. We have run comparisons of the two methods by inputting the same film strip of a particular store drop and comparing the output plots. No useful purpose could be served by presenting this comparison in this paper as a figure, as the data superimposed from both methods results in essentially the same line. This brings us to an important conclusion. We have examined several methods of reducing flight test data, the kinds described above, and others developed by various airframe contractors. All of them are inherently accurate enough to provide good, usable data. The degree of mathematical accuracy attained is not as important as how many of the error-causing factors are accounted for by the method, and (more importantly) whether the factors are compensated for or corrected. Data reduction accuracies of ± 2 or 3 inches and ± 2 or 3 degrees can be absolutely adequate, but not if the effect on store separation of wing flexibility, for instance, is not properly accounted for. Of all the error-causing factors, the ones which seem to be the most important (and most difficult to correct for) involve those connected with the camera optics. Errors caused by lens/camera alignment, calibration, internal manufacturing aberrations and uncertain optical centers are among the most important. Although great care must be exercised in developing a data reduction method which properly accounts for as many of the error-causing factors as is possible, equal care must be used in insuring that the method does not introduce other, larger errors through the human factor. A method which requires an inordinate amount of human input and manipulation of data prior to and during computer reduction is extremely liable to errors, particularly if no built-in-test features are incorporated.

CURRENT AIRCRAFT DESIGN PROBLEMS

I have already mentioned the many hundreds of aircraft/store compatibility tests performed at ADTC in the past few years. I have also described the methods employed to conduct those tests, and how we have continuously improved and refined our methods. This refinement has saved millions of dollars over the last few years ($16.5 million on the A-7D alone). All of these improvements, although representing large advances in technology, have only resulted in our being able to more efficiently and safely test items that already exist. The real promise in the development of aircraft/stores compatibility technology lies in our ability to apply this technology

to future aircraft and stores design. There is an old truism which says that a problem is easier avoided than solved. The aircraft that are on the drawing boards or in early infancy today are complex vehicles with amazing aerodynamic performance. Aircraft/store compatibility, if not treated adequately early in the design stage, will create enormously complex problems. There are five major problems facing today's aircraft designers which affect the overall problem of aircraft/stores compatibility.

Mission Definition

When a new aircraft is being designed, the procuring service gives the prospective contractors a stores list for which the aircraft should be capable of carriage and employment. More often than not, this list is not consistent with the real operational needs of the aircraft. For example, a recent Air Force air-superiority aircraft had a list of over 50 conventional munitions in its original specification. These weapons, some of which had already been cancelled, ranged from rocket pods and dispensers to a Korean War vintage 3000-lb general purpose bomb. Instructions are usually given to the contractors in such cases that carriage and employment of the weapons should be an "off-design" capability. In other words, the aircraft should be designed for its primary mission, and the service will accept whatever performance penalties are necessary in order to carry the stores. All too often, however, lurking in another part of the aircraft specification, is a requirement to carry the stores "throughout the aircraft's flight envelope," which is usually in excess of 6.0 g's. Such anomalies or oversights as these, of course, almost always lead to aircraft design points. Even though the contractor may privately doubt the wisdom of, say, carrying a Korean War type 3000-lb bomb on an air-superiority fighter up to six or seven "g's," he is also engaged in a fierce competition with other contractors for a lucrative contract. Often, then, he accepts the store requirements as valid and designs his aircraft to match them — including, in many cases, the additional structure necessary. Removing unrealistic stores from the list later does little good, because by that time the basic aircraft structure has already been designed.

Store Loading Configurations

The aircraft designer should know, in addition to which stores the service wants carried, how they want them carried. That is, how many of each store could be realistically used on a mission; how should they be carried (MER's, TER's, single pylon), and what stores are likely to be "mixed" with other

stores (rockets and bombs, or bombs and napalm) and in what desired quantities? Rarely, however is this done. As a result, the contractor usually analyzes his own design and advertises the loading configurations which maximize the numbers of the stores carried, regardless of the operational usefulness of such configurations. Even a conscientious attempt to develop usable operational configurations is wholly dependent on the contractor's familiarity with current stores and tactical air operations.

Store Mass Properties

Many of today's fighter-bomber or attack aircraft can carry a large number of weapons on a single loading. Flutter and structural analyses of the aircraft while carrying stores are dependent on knowing the physical or mass properties of all the stores. Unfortunately, these numbers are often not known accurately. During the development and test of a weapon, mass properties are usually determined and controlled. Once the weapon goes into production, however, the control is rapidly lost. Because weapons are bought in very large numbers, an enormous amount of money is involved. Those agencies engaged in weapons procurement are continually looking for ways to cut unit procurement cost. Unfortunately, this desire usually leads to a relaxation of inspection and quality control standards as well as design changes which cut costs. These factors both may cause mass property variations in the store. Manufacturing tolerances are almost nonexistent today because to impose them would make the weapon more expensive. Through a rather extensive survey over the past few years, we have determined that most stores can be described in their production mass properties with a ± 5% tolerance in weight, ± 0.5 in tolerance in center of gravity, and a ± 5% tolerance in moments of inertia. It is imperative that aircraft designers use these manufacturing tolerances in their calculations because weight or center-of-gravity variations of the magnitude we have measured in the past could cause flutter or structural analyses to be invalid. To further complicate the issue, there is no catalog, book, or central location which the contractor can use to obtain authorized store mass properties. My office has been appointed the central USAF source for this information, but we do not have the resources to continuously sample stores to insure that our data are valid. Rather, our high usage of the stores in tests provides us a random sampling, and if variations become apparent, more stores are measured utilizing a very accurate machine which we have at Eglin AFB.

Store Design Strength

The aircraft contractor, in order to insure that his aircraft can carry the specified stores throughout the required flight envelope, must analyze the structure of the aircraft and the store attachment provisions. To do this, he should know the failure strength of the stores and racks which are furnished to him by the government. To his surprise, when he asks the procuring service for this information, he is told it does not exist, or that only a small amount is available. Nearly all of today's stores are designed to the provisions of MIL-A-8591. However, this specification does not cover local store failures, and stores are rarely static tested to destruction to confirm their failure strength. As a result, almost all the aircraft contractor is told is that the specific store is currently certified on some other aircraft up to the limits shown in that aircraft's technical orders or manuals. In addition, suppose the contractor were told that a certain store would fail if it receives 5000 pounds of side load at the forward lug. With today's technology, and assuming multiple carriage of stores is employed, no one can accurately predict at what condition the required failure load would be produced on a particular store because of the complex aerodynamic interference flow field.

Rack Ejection Forces

After assuring that his aircraft can safely carry the required stores, the contractor must then determine if the stores will separate safely from the aircraft. The methods used to accomplish this determination have been covered previously. However, all of the analysis or wind tunnel techniques require (a) the store mass properties; and (b) the time history of the bomb rack ejector forces (including variations for different cartridges and rack orifice settings). Again, there are practically no reliable inflight-measured rack ejector force data available. Virtually all the available data were gathered by ejecting stores singly from a rigid ground testing structure. Rarely, if ever, were ejection forces or velocities measured for stores ejected in the ripple mode. Experience has shown us that ground test statically-derived values of ejection velocity are higher than those obtained inflight. For example, ground tests of a 500-lb store from a particular multiple ejector rack (MER) showed an ejection velocity of 8 to 10 ft/sec. Flight tests of this same combination showed only five to six ft/sec. Because of aircraft, pylon and rack flexibility, bombs ejected in the ripple mode can vary all the way from the maximum down to zero. Aside from being a dangerous situation,

variations such as these can mean that much of the store separation wind tunnel tests or analyses could be invalid, since store ejection force or velocity was a primary input.

APPLYING AIRCRAFT/STORE COMPATIBILITY TECHNOLOGY

Despite the difficult nature of the problems outlined above, there are several areas in the design of a new aircraft in which today's aircraft/store technology may be of great value. These areas are treated in detail in reference 1, but a discussion of some of the most important is given below.

Aircraft Flow Field

Early in the aircraft design stages, accurate determination of the aerodynamic flow field around the aircraft (both clean and with specific stores loaded) should be made. This analysis should be made in a parametric form so that good preflight analyses of new aircraft/store combinations may be made later. We have already obtained these flow field data on the F-4, F-15, A-10, and A-7 aircraft.

Environmental Studies

Thorough thermal, acoustic and aeroelastic analyses should also be made — with and without stores — as early as possible. We have flown empty instrumented dispenser munitions on an F-4 inboard station TER and measured sound levels of 170 db and vibrations inside the store of 60 g's. Navy flight tests a few years ago showed that shock waves from the aircraft wing, pylon or rack impinging on a store can act as heat ducts, increasing the rate of heat transfer by factors of five or ten. Also, most conventional munitions today are filled with explosives based on TNT (such as tritonal), which melts around 160°F. Although most engineers think of temperature problems as being associated with the supersonic flight regime where most current fighter aircraft cannot operate with stores attached, several studies have shown that severe overheat problems can be experienced subsonically. One such study, conducted in the United Kingdom on the F-4 aircraft showed that thermal problems can occur at lower subsonic speeds (see references 8 and 9). The current practice, generally used by the aircraft industry, of restricting the aircraft/store combination to the flight regime where the stagnation (or adiabatic wall) temperature does not exceed 160° is totally unrealistic, since it does not consider time or heat flux rate.

Aircraft Stability and Control

In the majority of cases, the handling qualities of a new aircraft are optimized on a clean aircraft with the degradation caused by external stores being treated on a set of predicted "worst case" conditions. Because of the inability to pre-pick the true worst cases, it is not unusual to discover an aircraft stability or control problem after a particular aircraft/store combination has been cleared for operational use. When this does occur, it can generally be traced back to that particular configuration being cleared, without flight test, by similarity to another configuration. We have found that every store should be flown in one or more configurations before release for operational use on that aircraft. The qualitative captive flights we use to evaluate aircraft handling qualities and structural integrity have already been described. These flights are not intended to replace our stability and control analyses that we generally make on the "worst case" basis — rather, our flight tests are intended to supplement the analyses. A few of the problem areas that we have identified with our flight testing are:

1. Most conventional munitions are designed for subsonic flight. Because of this, they do not materially affect the basic static directional stability of aircraft designed for supersonic flight. Weapons designed for supersonic flight, however, usually do affect the aircraft's directional stability.

2. Stores often noticeably affect Dutch roll and short period motion. Dutch roll damping is often improved by the presence of long slender, finned stores. This is very important in bomb delivery, since any degradation of aircraft longitudinal or directional stability makes target tracking more difficult.

3. Speed stability is rarely affected by conventional stores. This, however, has been shown to be untrue in the case of some of the new family of free-fall guided weapons which have very large fins and canards.

4. Stick force per "g" may vary considerably with airspeed, and a drastic change may occur rapidly, with little warning, over a relatively small airspeed regime.

5. Stores loaded considerably forward or aft of the aircraft center of gravity can cause severe aircraft control problems upon release. The sudden gross weight reduction, coupled with a c.g. and center of pressure shift, can cause large pitch excursions of the aircraft (pilots call it "g"-jump or instant "g"). In trying to overcome these excursions, the pilot may easily overstress the aircraft.

6. During dive delivery, releasing large, bulky stores from only one side of an aircraft while retaining a like store on the other side can cause severe control problems during pull-out when the high "g's" demand high angles of attack.

Store Structural Integrity

As previously explained, because of the store structural failures being experienced in Vietnam, we use qualitative captive flights to evaluate the structural integrity of both the store and the aircraft/store combination. Since initiation of these tests a few years ago, we have found many store structural deficiencies which were either corrected or the configuration was not certified. More importantly, there has not been one reported case of store failure on a configuration which we certified using the captive flight tests. It should be stressed that these failures can occur on only one specific aircraft type or in only one configuration.

Store Separation

Store separation problems are not necessarily accidental. Many times they are built into the store or aircraft design. I have divided some of the things we have learned in this area into aircraft design aspects and those of the store.

Aircraft Design - Such things as high wings, low horizontal tails, close pylon spacing, multiple carriage racks, flexible pylons and racks, and low store ejector forces are prime contributors to store separation problems. The flexible ejector rack with its low force and a single ejector piston located away from the store center of gravity is one of the biggest problems. High aircraft wings cause stores to remain in the disturbed aircraft flow field longer, and to be "sucked" in toward the fuselage centerline. Low horizontal tails present two major problems.

The first is that they are directly in the path of rearward dispensed stores and debris. The other problem is not so obvious. Stores which change shape immediately after release (such as the opening of a retarded bomb fin) radically affect the airflow behind the store. If this drastically disturbed air hits a low aircraft horizontal tail, very large aircraft pitch or roll excursions may occur. Balanced against these problems, however, is the low tail's superior control performance at high "g's" and high angle of attack. If all of these points are combined into a single aircraft design, the probability of store separation problems is very high.

Store Design - To minimize store separation problems, stores, ideally, should be both statically and dynamically stable. Usually, to insure good store separation, a store should have a positive static margin of at least one body diameter and a slenderness ratio (length to diameter) between eight and ten. Nose fairings should be two to three body diameters in length. Large diameter stores with short, or hemispherical nose fairings almost always exhibit severe store separation problems (absolutely blunt, or "bluff," stores, on the other hand, usually separate cleanly). The store c.g. should be "tuned" to the ejector rack. If the rack has only one ejector piston, the store c.g. should be just aft of that piston. If the rack has two pistons, the c.g. should be centered, generally. As a rule, the higher the store's mass and density, the better the separation. Moments of inertia should be kept at the maximum possible, particularly for dispensers which must be jettisoned empty. Guided weapons, because of their inherent maneuverability requirements, must be either unstable or marginally positively stable. If such weapons are to be released from an ejector rack (as opposed to fired from a rail launcher), they must retain some positive static stability in order to maintain safe store separation. Also, if the guided weapon contains an autopilot, this system should be inactive for the first one to two seconds after release so that autopilot failures cannot drive the control surfaces hard over and cause an aircraft/store collision. In such cases, the control surfaces should be locked into whatever attitude

necessary to enhance store separation. In contrast to aircraft-generated store separation problems, if the store design is the reason for poor store separation, this trend will likely be evident on more than one aircraft type.

SOLUTIONS TO THE PROBLEMS

There are many companies and government agencies involved with aircraft/stores compatibility, and these organizations all have theories and plans for solving the problem in the future. We cannot, however, escape the fact that, because of the already-designed or built aircraft and stores, the problems of aircraft/store compatibility will be with us into the 1980's. We cannot wait for a full, long range solution. Some interim measures must be adopted now.

The first step in reducing the problem should be to standardize store suspension equipment (bomb racks), the stores being used, and the testing techniques between all services — or at least between the Air Force and Navy, since the Army equipment and stores tend to be specialized for their use only. A maximum standardization of equipment and information would drastically cut overall testing requirements, logistic support and costs, while enhancing flight safety substantially. Programs should be initiated now to determine, and subsequently control, store production tolerances, design strengths, and mass properties.

Several years ago, the commanders of the Air Force's Systems Command and Logistic Command, the Navy's Material Command and the Army's Materiel Command (known collectively as the Joint Logistic Commanders, or JLC) convened a working group of civilian and military experts to look into the problems of aircraft/stores compatibility. This group, of which I am the principal member from AFSC, chartered under the aegis of the Joint Technical Coordinating Group for Air-Launched Non-Nuclear Ordnance (JTCG/ALNNO), became Working Party 12. The Working Party recognized quickly that the principal obstacle to overcome was the lack of directive documents in the field of aircraft/store compatibility, and set as its primary task the publishing of the necessary documents. The result of this effort has been a design manual for the aircraft, the store, and the rack designer (reference 1, a Military Standard which defines ground fit tests and store clearance requirements (reference 2), and a manual which depicts the interface now existing on all aircraft, to which stores must mate (reference 3). The group is now working on a document which will standardize, between

the Navy and Air Force, ground and flight testing techniques used for store certification purposes, and an addition to reference 3 which will give the geometric and mass properties of all currently-used stores. The group is also currently attempting to standardize data reduction of flight test film, using the Navy-developed photo-imaging technique. As an aside, the JTCG/ALNNO has recently been redesignated the JTCG/MD (Munitions Development).

All the efforts mentioned above will, of course, remove some of the more pressing problems associated with today's aircraft and stores. They will also lay the groundwork for future designers — something which these designers have never had before. However, all this could be compared to a doctor treating symptoms rather than curing a disease. The overall cure, in my opinion, lies in taking a radical departure from our present thinking. Our operational experiences in the past few years have shown us the utter futility of certifying stores to limits that are less than those which can be attained by the aircraft. A pilot inbound on a bombing run over hostile territory is concerned only with safely dropping his load and escaping. He is not going to worry about — or even remember — arbitrary flight limitations which tell him he must not drop his stores beyond certain parameters. Experience has shown that he will ignore such limits and push his aircraft to the maximum. But, it makes little sense to carry a load of bombs all the way to the enemy's heartland — dodging flak, interceptors, and SAM's all the while — and then have the bombs miss the target. This is not only a waste of munitions, it unnecessarily jeopardizes the lives of the flight crew.

Ideally, munitions and aircraft should be designed together as a weapons system. The weapons could then be optimized to exploit the capabilities of one aircraft. If cost and logistic factors outweigh the advantages of the ideal situation, as they frequently do, then the weapons should be designed for maximum effect and minimum impact on the carrying aircraft. These weapons should be large, carried singly (not on multiple racks), have terminal guidance of some sort (preferably several interchangable sets of different types), and be effective enough to destroy the desired target. Single carriage of large high-density stores also allows realistic supersonic carriage and release. If, for tactical reasons, smaller weapons carried in large numbers must be employed, then these weapons should be carried in new, more efficient ways than those currently in use — conformal (or tangent) carriage, for example.

In conclusion, I believe we have only scratched the surface of a large new area of technology in aircraft/stores compatibility. We must continue to go forward with a vigorous and aggressive approach to solving of problems associated with today's aircraft and stores, while at the same time using our knowledge to precipitate drastic changes in the design of new aircraft and stores as well as store carriage techniques. Although today's problems are large and important, we cannot allow our thirst for knowledge and zeal for an immediate solution to cause us to expend vast resources exploring in detail a problem which could best be eliminated through a rigorous and progressive design philosophy.

REFERENCES

1. Military Handbook - 244, A Guide to Aircraft/Stores Compatibility, Aug 1975, Sections 3 and 5.

2. Military Standard - 1289, Ground Fit and Compatibility Tests of Airborne Stores, Procedure for, Oct 1972.

3. Joint Technical Coordinating Group for Air-Launched Non-Nuclear Ordnance, Working Party for Aircraft/Stores Compatibility, Aircraft/Stores Interface Manual, Sep 1973, JTCG/ALNNO WP 12-1.

4. Reed, James F., and Curry, Warren H., Aircraft Separation Problems Associated with Nuclear Ordnance - A Survey, Nov 1969, Proceedings of Aircraft/Stores Compatibility Symposium, Volume VI, pages 6-374 through 6-399.

5. Korn, Stephen C., Lt, USAF, Use of the Flow Angularity Technique for Predicting Store Separation Trajectories, Aug 1972, Proceedings of the Aircraft/Stores Compatibility Symposium, AFFDL-TR-72-67, Volume 2, page 415.

6. Korn, Stephen C., Captain, USAF, Air Force Armament Laboratory, Validation and Expansion of the Flow Angularity Technique for Predicting Store Separation Trajectories, Sep 1972, AFATL-TR-72-184.

7. Cooper, Guy, and Kingery, Ron, Naval Missile Center Photo Data Analysis of Store Separation Films, Sep 73, Proceedings of Aircraft/Stores Compatibility Symposium, JTCG/ALNNO WP-12-2, Volume 2, pages 53 through 106.

8. Hunting Engineering Ltd (UK), Flight Limitations Required to Prevent Overheating of the Conventional Explosive 1000 lb Bomb During Carriage by the Phantom F4K and F4M, Apr 1966, Thermal Effects on Airborne Conventional Armament Stores and Equipment (TEACASE) Working Party, Paper No. 33(BR34134). SECRET - UNITED KINGDOM.

9. Hunting Engineering Ltd (UK), An Alternative Method of Deriving the Flight Limitations Required to Prevent Overheating of Stores, Oct 1967, Thermal Effects on Airborne Conventional Armament Stores and Equipment (TEACASE) Working Party, Working Note No. 47(BR34136). RESTRICTED-UNITED KINGDOM.

AUTOBIOGRAPHY

Mr. Epstein received his BS in Aeronautical Engineering from Georgia Institute of Technology in 1952. After serving several years in the Navy as both a shipboard officer and as a patrol plane (P-2) commander, he was employed in 1957 by General Dynamics/Ft Worth as a structural loads engineer. In 1961, he began work with the USAF at Eglin AFB, Fl. Since coming to Eglin, he has worked as a test modification design engineer and as a test design engineer in the Munitions Test Division. In 1969, he assumed duties as the Chief of the Aeromechanics Team in the Weapons Compatibility Branch where he was responsible for the wind tunnel testing, separation analysis test design, flight testing and other technical aspects related to aircraft/stores compatibility. Due to several internal reorganizations since 1969, Mr. Epstein is currently Chief of the Compatibility Engineering Team in the Aircraft Compatibility Branch. His duties, however, remain the same as those assumed in 1969. He is a member of the American Defense Preparedness Association, the principal member for AFSC to the JTCG/MD Working Party for Aircraft/ Stores Compatibility, and a member of two similar international working groups concerned with air armament standardization.

"THEORETICAL ANALYSIS AND EXPERIMENTAL MEASUREMENTS OF SEPARATION DISTURBANCES IN WEAPON DELIVERY SYSTEMS" (U)
(Article UNCLASSIFIED)

by
Dr. J. S. Ausman
Chief Scientist
Litton Industries Inc.,
Guidance and Control Systems Division
5500 Canoga Ave., Woodland Hills, Ca. 91364

ABSTRACT. (U) Previous theoretical and experimental work has identified separation disturbances to be the principle cause of bomb dispersion, at least for low drag bombs. This implies that appropriate compensation for separation disturbances in weapon delivery systems can reduce the bomb dispersion error in those systems to the extent that the separation disturbances are repeatable or systematic. The objective of this paper is to develop a practical method of compensating for the systematic portion of bomb dispersion as caused by separation disturbances.

The first step is to derive analytical relationships between initial angular disturbances of the bomb and the subsequent deflection of its ballistic trajectory away from the unperturbed, nominal trajectory. This analysis reveals that the principle deflection of the trajectory can be modeled as a "jump velocity", i. e., an additional ejection-like velocity imparted to the bomb at release. In general, this jump velocity has three components, a lateral component caused by initial yawing oscillations of the bomb, a normal component arising from initial

---

Approved for public release; distribution unlimited.

pitching oscillations, and a rearward component which accounts for induced drag resulting from both pitching and yawing oscillations.

Sample numerical calculations supported by physical reasoning indicate that initial angular rate disturbances deflect the bomb's trajectory far more than do initial angular offsets, even though the amplitude of the bomb's angular oscillation is the same in both cases. On this basis, one can neglect the initial angular offset effect and directly express the jump velocity components in terms of initial angular rates. In particular,

$$V_{j\theta} = -F\dot{\alpha}_{\psi o}$$
$$V_{j\psi} = F\dot{\alpha}_{\theta o} \qquad (0)$$

where F is a function of the bomb's physical characteristics (size, mass, and transverse moment of inertia) and aerodynamic coefficients (ratio of lift and moment coefficients); $V_{j\theta}$ and $V_{j\psi}$ are the lateral and normal components of jump velocity, respectively; and $\dot{\alpha}_{\psi o}$ and $\dot{\alpha}_{\theta o}$ are the initial yawing and pitching rates of the bomb.

There are two ways of measuring jump velocities. One is through cinematographic measurements of $\dot{\alpha}_{\psi o}$ and $\dot{\alpha}_{\theta o}$ followed by application of Eq. (0). The second method is to calculate the jump velocity required to make the predicted bomb impact match the actual bomb impact.

The impact point matching technique was used to analyze MK84 (2000 lb low drag bomb) releases from A6E and F111E aircraft. Table I summarizes the resulting jump velocity measurements.

TABLE I
JUMP VELOCITIES MEASURED FOR MK84 BOMBS RELEASED FROM F111E AND A6E AIRCRAFT

Aircraft	Wing Pylon Station	Jump Velocity	
		Direction	Magnitude (fps)
F111E	Outboard	Outward	1.0
A6E	Outboard	---	Zero
A6E	Inboard	Rearward	1.3

In addition, the outboard wing pylon stations on both the F111E and A6E aircraft were found to receive 20 percent less ejection velocity than normal, probably due to wing flexure and/or aircraft roll reaction. Residual dispersion of the MK84 bomb impact points after compensation for these systematic separation disturbances is less than one mil, CEP.

Approved for public release; distribution unlimited.

LIST OF FIGURES

Figure 1 Swerve Velocity Caused by Initial Yaw Rate and by Initial Yaw Angle-of-Attack

Figure 2 Cross-Range Miss Sensitivity to Yaw Oscillations as Predicted by Jump Velocity Theory and by 5DF Simulations of Ref. 5

Figure 3 Down-Range Miss Sensitivity to Yaw Oscillations as Predicted by Jump Velocity Theory and by 5DF Simulations of Ref. (5)

Figure 4 Down-Range Miss Sensitivity to Pitch Oscillations as Predicted by Jump Velocity Theory and by 5DF Simulations of Ref. (5)

Figure 5 MK 84 LDGP Bomb Impacts Relative to Impacts Predicted on Basis of Release Point Measurements Alone

Figure 6 MK 84 LDGP Bomb Impacts Relative to Predicted Impacts Corrected for Jump Velocity

LIST OF TABLES

Table I Jump Velocities Measured for MK 84 Bombs Released from F111E and A6E Aircraft

Table II Aerodynamic Coefficients for MK 81 - 84 Series of LDGP Bombs

Table III Physical Parameters for MK 81 - 84 Series of LDGP Bombs

Table IV Jump Velocity for MK 84 LDGP Bombs by Weapon Station

NOMENCLATURE

A	Maximum frontal area of bomb
C_{D2}	Induced drag coefficient
$C_{M\alpha}$	Slope of moment coefficient vs angle-of-attack
$C_{N\alpha}$	Slope of normal force coefficient vs angle-of-attack
$C_{Mq} + C_{M\dot{\alpha}}$	Pitch or yaw damping coefficient
d	Maximum diameter of bomb
I	Transverse moment of inertia
M	Mass of bomb
R_m	Down range miss distance
q	Dynamic pressure
T	Time constant for exponential decay of angular oscillations
t	Time after release
t_f	Time-of-fall
V	Velocity of bomb
V_E	Ejection velocity
V_θ	Swerving velocity
V_ψ	Heaving velocity
V_ϕ	Velocity component of bomb resulting from induced drag force
$V_{J\theta}$	Pitch axis component of jump velocity
$V_{J\psi}$	Yaw axis component of jump velocity
$V_{J\phi}$	Roll axis component of jump velocity

NOMENCLATURE (cont)

α	Total angle-of-attack
α_θ	Pitch angle-of-attack
α_ψ	Yaw angle-of-attack or side slip
$\partial R/\partial V_E$	Bomb range sensitivity to ejection velocity
ω	Frequency of angular oscillation
$\dot{(\ )}$	Time derivative of ( )
$\ddot{(\ )}$	Second derivative of ( ) with respect to time
$(\ )_o$	Initial value of ( ) at t = 0

INTRODUCTION

As more accurate sensors, faster airborne digital computers, and better software techniques continue to improve the accuracy of air-to-ground weapon delivery systems, bomb dispersion eventually becomes the dominant error source in such systems. Further improvement in accuracy beyond this point can only come through reduction or circumvention of bomb dispersion. Guided bombs are one example of the circumvention approach. However, the high cost of guided bombs still justifies exploration of the more direct solution, that of reducing bomb dispersion itself.

To reduce bomb dispersion, we must qualitatively understand its root causes, analyze them quantitatively to separate out the dominant effects, and develop practical methods of eliminating or compensating for these dominant effects. The final proof will be to test it out with actual bomb drops. This report follows the same general outline described above.

Nicolaides in Reference 1 identifies separation disturbances as the principal cause of bomb dispersion. In his treatise on missile flight and astrodynamics, he states, "The dispersion of rockets, bombs, projectiles, and other ballistic type missiles is a direct result of..... the random initial launching conditions". He proceeds to single out the dominant initial launching condition to be the initial angular velocity. In particular, he states, "...for the case of fin-stabilized missiles,... the effect of initial angle of attack ... is small, but ... the effect of initial angular velocity is large".

Reference 2 provides experimental corroboration for these statements and furthermore reveals the fact that a substantial portion of the observed bomb dispersion is systematic or repeatable in nature. In these tests, for example, the bombs released from the left wing consistently impacted to the left of their expected impact point, while the bombs released from the right wing consistently impacted to the right of their expected impact point.

Combining the experimental observation of the existence of a systematic component of bomb dispersion with the theoretical concept that bomb dispersion is caused by initial angular disturbances, we conclude that there must be systematic repeatable angular disturbances imparted to bombs at release or during their separation from the flow field surrounding the aircraft. These systematic separation disturbances may differ from weapon station to weapon station, but they are potentially compensable through calibration.

In addition, there will be random angular disturbances superimposed upon the repeatable motion. These random disturbances are not amenable to compensation by calibration and will remain as a residual source of bomb dispersion. They can be attacked through careful mechanical and aerodynamic design of the release and separation mechanism, but this is outside the scope of the present report.

The objective of this report is to develop a practical method of calibrating and compensating for the systematic component of bomb dispersion caused by repeatable separation disturbances. To this end let us first review the theoretical analysis of the physical process through which angular motion of a bomb causes it to deflect away from its nominal, unperturbed trajectory.

THEORETICAL ANALYSIS

In the interest of obtaining a practical solution to at least a portion of the bomb dispersion problem, the following treatment makes no pretense to retaining complete generality. Specifically, it is presumed that the bombs under discussion are fin-stabilized bombs having characteristics similar to those of the MK81-84 series of low drag bombs.

The theoretical analysis begins with a solution to the yawing and swerving equations of motion. The corresponding pitching and heaving solutions follow by analogy. Finally, a study of the induced drag caused by yawing and pitching motions completes the analysis.

YAWING AND SWERVING MOTION

Equation (1) is the differential equation for yawing motion. It equates the time rate of change of the yawing component of angular momentum to the aerodynamic moments acting about the yaw axis. There are two such moments, (1) a restoring moment proportional to the yaw angle-of-attack, and (2) a damping moment proportional to the angular rate of the bomb about its yaw axis. The coefficients of proportionality are in accordance with conventional aerodynamic usage (see References 1 and 3, for example)

YAWING MOMENT EQUATION

$$\underbrace{I\ddot{\alpha}_\psi}_{\substack{\text{Rate of Change}\\ \text{of Angular}\\ \text{Momentum}}} = \underbrace{-C_{M\alpha} Aqd\alpha_\psi}_{\substack{\text{Restoring}\\ \text{Moment}}} - \underbrace{\frac{C_{Mq} + C_{M\dot{\alpha}}}{2V} Aqd^2\dot{\alpha}_\psi}_{\text{Damping Moment}} \qquad (1)$$

Rearrangement of terms and division by I results in

$$\ddot{\alpha}_{\psi} + \frac{C_{Mq} + C_{M\dot{\alpha}}}{2IV} Aqd^2 \dot{\alpha}_{\psi} + \frac{C_{M\alpha} Aqd}{I} \alpha_{\psi} = 0 \qquad (2)$$

The three types of solutions to second-order differential equations of this form are well known. In the present case, the bombs have comparatively small damping, and the solution of interest is the so-called underdamped or damped sinusoidal response given by Eq. (3).

$$\alpha_{\psi} = e^{-t/T}\left[\alpha_{\psi_o} \cos \omega t + \frac{T\dot{\alpha}_{\psi_o} + \alpha_{\psi_o}}{\omega T} \sin \omega t\right] \qquad (3)$$

where

$$T \doteq \frac{4IV}{(C_{Mq} + C_{M\dot{\alpha}}) Aqd^2}$$

$$\omega = \sqrt{\frac{C_{M\alpha} Adq}{I} - \frac{1}{T^2}}$$

$$\alpha_{\psi_o} = \text{initial value of } \alpha_{\psi} \text{ at } t = 0$$

and

$$\dot{\alpha}_{\psi_o} = \text{initial value of } \dot{\alpha}_{\psi} \text{ at } t = 0$$

Substitution of Eq. (3) back into Eq. (2) will readily verify that Eq. (3) is a solution to the differential equation of motion, Eq. (2).

Next, let us consider the differential equation for swerving (cross-track) motion as shown in Eq. (4). It equates the rate of change of cross-track momentum to the swerving force generated by a yaw angle of attack.

SWERVING FORCE EQUATION

$$\underbrace{M\dot{V}_\theta}_{\substack{\text{Rate of Change}\\ \text{of Momentum}}} = \underbrace{-(C_{N\alpha} Aq)\,\alpha_\psi}_{\text{Swerving Force}} \tag{4}$$

Dividing Eq. (4) by M, substituting for α_ψ from Eq. (3), and integrating, we find the cross-track velocity to be

$$V_\theta = -\frac{C_{N\alpha} Aq}{M} \int_0^t e^{-t/T} \left(\alpha_{\psi_o} \cos \omega t + \frac{T\dot{\alpha}_{\psi_o} + \alpha_{\psi_o}}{\omega T} \sin \omega t \right) dt \tag{5}$$

Carrying out the indicated integration yields

$$V_\theta = -\left(\frac{C_{N\alpha} Aq}{M}\right)\left(\frac{T}{1 + \omega^2 T^2}\right) \left\{ \left[1 - (\cos \omega t - \omega T \sin \omega t)\, e^{-t/T}\right] \alpha_{\psi_o} \right.$$

$$\left. + \left[\omega T - (\sin \omega t + \omega T \cos \omega t)\, e^{-t/T}\right] \left(\frac{T\dot{\alpha}_{\psi_o} + \alpha_{\psi_o}}{\omega T} \right) \right\} \tag{6}$$

Equation (6) shows that the swerving velocity consists of (1) a constant cross track velocity plus (2) a transient oscillation which decays exponentially with time. Even after the oscillatory motion disappears, the constant velocity term remains, causing the bomb to continue to diverge from its nominal, zero cross-track velocity trajectory.

From a practical viewpoint, we can afford to neglect the oscillatory terms in Eq. (6) and concentrate on the constant terms. The basis for this simplification is that the oscillatory terms are significant with respect to the constant terms only for short time-of-fall trajectories, for which cases the trajectory deflection does not have time to build up to a serious extent anyway. For the long time-of-fall trajectories ($t >> T$), the constant velocity terms are sufficient to describe the predominant dispersion effects.

If one divides the constant velocity of divergence by the release velocity, one obtains an angular divergence which Nicolaides refers to as the "jump angle". Accordingly, let us call the divergence velocity itself a "jump velocity". The (cross-track) component of this jump velocity is then defined as

SWERVING COMPONENT OF JUMP VELOCITY

$$V_{J_\theta} = \lim_{t \to \infty} V_\theta = -\left(\frac{C_{N\alpha} A q}{M}\right) \frac{T}{1 + \omega^2 T^2} (2\alpha_{\psi_o} + T\dot{\alpha}_{\psi_o}) \qquad (7)$$

Next, let us evaluate the sensitivity coefficients of α_{ψ_o} and $\dot{\alpha}_{\psi_o}$ to determine their relative influence on cross-track dispersion.

NUMERICAL EVALUATION OF CROSS-TRACK JUMP VELOCITY

Tables II and III provide numerical values for the aerodynamic coefficients and for the physical properties of the MK81-84 series of low drag general purpose (LDGP) bombs. As a numerical example, let us compute the jump velocity coefficients for a MK 82 bomb released from 5000 ft altitude at 450 kt (760 fps or Mach number of 0.69). The dynamic pressure, q, under these release conditions is 667 lb/ft^2.

Substituting the appropriate numerical values for these release conditions into the definitions of T and ω which follow Eq. (3), we obtain the following.

TABLE II
AERODYNAMIC COEFFICIENTS FOR MK81-84 SERIES OF LDGP BOMBS

Mach No.	$C_{N\alpha}$ (per rad)	$C_{M\alpha}$ (per rad)	C_{D2} (per rad^2)	$(C_{Mq} + C_{M\dot{\alpha}})$ (per rad)
0.70	4.7	3.3	5.7	125
0.80	4.7	3.4	5.8	130
0.85	4.7	3.7	5.3	175
0.90	4.8	4.1	4.9	200
0.95	4.9	5.0	5.1	215
1.00	5.0	6.3	5.3	220
1.05	5.15	6.0	5.3	225
1.10	5.3	5.1	5.3	220
1.20	5.4	4.2	5.4	200

Notes: (1) $C_{N\alpha}$, $C_{M\alpha}$ and $C_{Mq} + C_{M\dot{\alpha}}$ data extracted from Ref. 3.
(2) C_{D2} data supplied by Mr. J. Roman of Naval Weapons Laboratory, Dahlgren, Va.

TABLE III
PHYSICAL PARAMETERS FOR MK81-84 SERIES OF LDGP BOMBS

Bomb Type	Weight Mg (lbs)	Maximum Diameter d (ft)	Frontal Area A (ft^2)	Transverse Moment of Inertia I(slug ft^2)
MK 81	274	0.750	0.442	14.6
MK 82	527	0.895	0.631	36.7*
MK 83	985	1.167	1.068	106
MK 84	1970	1.500	1.767	363

Note: All data extracted from Ref. 4 except the figure marked with * which comes from Ref. 5.

$$T = \frac{4IV}{(C_{Mq} + C_{M\dot{\alpha}})\, Aqd^2}$$

$$= \frac{4 \times 36.7 \text{ lb-sec}^2\text{-ft} \times 760 \text{ ft/sec}}{125 \times 0.631 \text{ ft}^2 \times 667 \text{ lb/ft}^2 \times (0.895)^2 \text{ ft}^2}$$

$$T = 2.65 \text{ sec} \tag{8}$$

$$\omega T = \sqrt{\frac{C_{M\alpha} AqdT^2}{I} - 1}$$

$$= \sqrt{\frac{3.3 \times 0.631 \text{ ft}^2 \times 667 \text{ lb/ft}^2 \times 0.895 \text{ ft} \times (2.65 \text{ sec})^2}{36.7 \text{ lb-sec}^2\text{-ft}} - 1}$$

$$\omega T = 15.4 \tag{9}$$

Similarly, the swerving acceleration per unit (radian) side slip angle is

$$\frac{C_{N\alpha}Aq}{M} = \frac{4.7 \times 0.631 \text{ ft}^2 \times 667 \text{ lb/ft}^2}{527 \text{ lb}/32.2 \text{ ft/sec}^2}$$

$$= 121 \text{ ft/sec}^2 \text{ per radian} \qquad (10)$$

Putting Eqs. (8), (9), and (10) together to compute the coefficient of α_{ψ_o} in Eq. (7), we have

$$2\frac{C_{N\alpha}Aq}{M}\left(\frac{T}{1+\omega^2T^2}\right) = 2 \times 121 \text{ ft/sec}^2 \times \frac{2.65 \text{ sec}}{1+(15.4)^2}$$

$$= 2.70 \text{ fps per radian}$$

$$= \underline{0.047 \text{ fps per degree}} \qquad (11)$$

Similarly, the coefficient of $\dot{\alpha}_{\psi_o}/\omega$ in Eq. (7) is

$$\left(\frac{C_{N\alpha}Aq}{M}\right)\frac{T}{1+\omega^2T^2}\,\omega T = 0.0235 \text{ fps per degree} \times 15.4$$

$$= \underline{0.362 \text{ fps per degree}} \qquad (12)$$

The reason for computing the coefficient of $\dot{\alpha}_{\psi_o}/\omega$ instead of the coefficient of $\dot{\alpha}_{\psi_o}$ is that $\dot{\alpha}_{\psi_o}/\omega$ is an approximation to the maximum amplitude of the first half cycle of the sinusoidal oscillation triggered by $\dot{\alpha}_{\psi_o}$. This allows a direct comparison between the effect, Eq. (11), of an initial angular offset and the effect, Eq. (12), of an initial angular rate, each causing the same amplitude of oscillatory motion.

A comparison of Eqs. (11) and (12) reveals the somewhat startling conclusion that the jump velocity caused by an initial yaw rate is an order of magnitude larger than the jump velocity caused by an initial side slip angle, <u>even though the yaw oscillations in both cases have about the same amplitude</u>! Figure 1 affords a physical explanation for this seemingly contradictory conclusion.

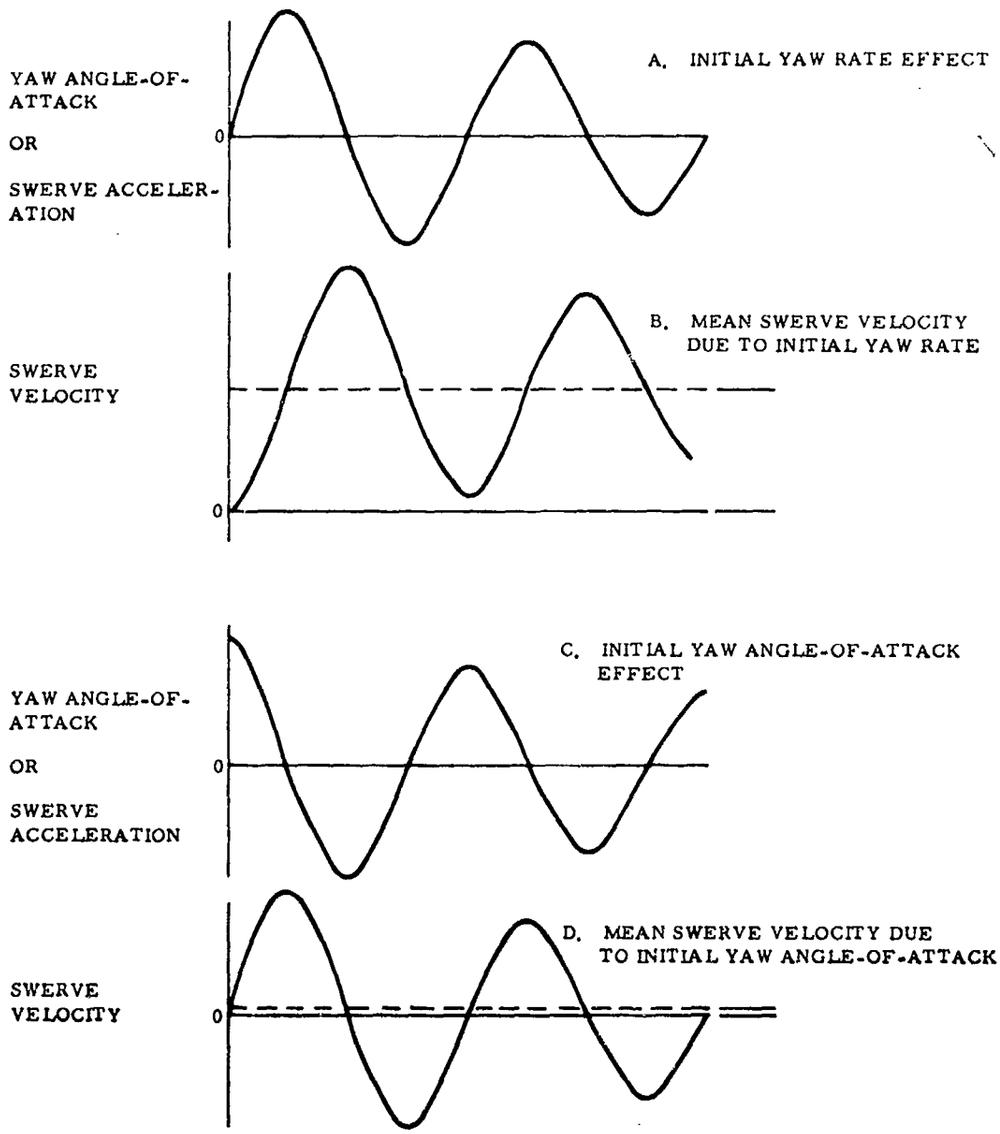


Figure 1. Swerve Velocity Caused by Initial Yaw Rate and by Initial Yaw Angle-of-Attack

Figure 1a and 1c both describe lightly damped oscillations in the yaw angle-of-attack, one (the damped sine wave of Fig. 1a) beginning with an initial yaw rate and the other (the damped cosine wave of Fig. 1c) beginning with an initial yaw angle. Because the aerodynamic swerving force is proportional to the yaw angle-of-attack, the swerving component of jump velocity is proportional to the integral of the yaw angle-of-attack curve.

In the case of an initial angular rate, the integral of the damped sine ωT curve of Fig. 1a is the damped $1 - \cos \omega t$ curve shown in Fig. 1b. Note that in this case, the swerve velocity is always of the same sign and has an average velocity approximately equal to one-half the peak swerve velocity. However, in the case of an initial angle-of-attack, the integral of the damped cosine curve of Fig. 1c is the damped sine wave of Fig. 1d which would have a mean value of zero except for the damping effect which causes the oscillations to be slightly asymmetrical.

The physical insight brought out by Fig. 1 reveals that even an undamped yaw oscillation started by an initial yaw rate would generate a jump velocity, whereas an undamped yaw oscillation started by an initial yaw angle-of-attack would not. The theoretical expression, Eq. (7), confirms this behavior for undamped ($T \to \infty$) oscillations.

The above discussion leads us to the conclusion that we can neglect the α_{ψ_0} effect in Eq. (7) and approximate the swerving component of jump velocity with

$$V_{J\theta} \approx -\left(\frac{C_{N\alpha} A q}{M}\right) \frac{T^2}{1 + \omega^2 T^2} \dot{\alpha}_{\psi_0} \tag{13}$$

We can simplify Eq. (13) even further by noting from the definitions of T and ω following Eq. (3) that

$$\frac{T^2}{1 + \omega^2 T^2} = \frac{I}{C_{M\dot{\alpha}} A q d} \tag{14}$$

with this substitution, Eq. (13) becomes

APPROXIMATE SWERVE JUMP VELOCITY

$$V_{J\theta} \approx -\frac{C_{N\alpha}}{C_{M\alpha}} \frac{I}{Md} \dot{\alpha}_{\psi_o} \tag{15}$$

Let us now proceed to analyze the heaving component of jump velocity caused by pitching oscillations of the bomb.

PITCHING AND HEAVING MOTION

Equation (16) is the differential equation for pitching motion. It equates the time rate of change of the pitching component of angular momentum to the aerodynamic restoring and damping moments acting about the pitch axis.

PITCHING MOMENT EQUATION

$$\underbrace{I\dot{\omega}_\theta}_{\substack{\text{Rate of Change} \\ \text{of Angular} \\ \text{Momentum}}} = \underbrace{-C_{M\alpha} Aqd\alpha_\theta}_{\text{Restoring Moment}} \underbrace{-\frac{C_{Mq} + C_{M\dot{\alpha}}}{2V} Aqd^2\dot{\alpha}_\theta}_{\text{Damping Moment}} \tag{16}$$

The heaving force equation, which equates the lift force generated by a pitch angle of attack to the rate of change of linear momentum along the yaw-axis, appears as Eq. (17).

HEAVING FORCE EQUATION

$$\underbrace{M\ddot{V}_\psi}_{\substack{\text{Rate of Change} \\ \text{of Momentum}}} = \underbrace{C_{N\alpha} Aq\alpha_\theta}_{\text{Heaving Force}} \tag{17}$$

Because Eqs. (16) and (17) have forms which are identical to those of Eqs. (1) and (4), respectively, we can anticipate their solution, Eq. (18), by its similarity to Eq. (7).

HEAVING COMPONENT OF JUMP VELOCITY

$$V_{J\psi} = \lim_{t \to \infty} V_{\psi} = \left(\frac{C_{N\alpha} Aq}{M} \right) \frac{T}{1 + \omega^2 T^2} \left(2\alpha_{\theta o} + T\dot{\alpha}_{\theta o} \right) \qquad (18)$$

The same numerical argument which allowed us to neglect the $\alpha_{\psi o}$ effect in Eq. (7) also applies to the $\alpha_{\theta o}$ term in Eq. (18). Accordingly, we can neglect the $\alpha_{\theta o}$ term and, with the aid of Eq. (14), reduce Eq. (18) to its approximate form given by Eq. (19).

APPROXIMATE HEAVE JUMP VELOCITY

$$V_{J\psi} \approx \frac{C_{N\alpha}}{C_{M\alpha}} \frac{I}{Md} \dot{\alpha}_{\theta o} \qquad (19)$$

With Eq. (13) and (19), we now have formulas for two components of jump velocity. The next section takes up the third component, the roll axis component.

INDUCED DRAG

Pitching and yawing oscillations of the bomb create an induced drag proportional to the square of the angle between the bomb's axis of symmetry and its direction of travel. Equation (20) is the mathematical representation of this behavior

INDUCED DRAG EQUATION

$$M\dot{V}_{\phi} = -(C_{D2} Aq)\, \alpha^2 \qquad (20)$$

where

$$\alpha^2 = \alpha_{\psi}^2 + \alpha_{\theta}^2$$

The induced drag is an additional drag force acting on the bomb, over and above the zero angle-of-attack drag force accounted for in the weapon delivery system's ballistic trajectory solution. This induced drag effect will cause a rearward divergence of the bomb from its expected flight path.

Let us first consider that portion of the induced drag caused by the yaw angle, α_{ψ}. From Eq. (3)

$$\alpha_\psi^2 = e^{-2t/T}\left[\alpha_{\psi_o}\cos\omega t + \frac{T\dot{\alpha}_{\psi_o} + \alpha_{\psi_o}}{\omega T}\sin\omega t\right]^2$$

$$= e^{-2t/T}\left[\alpha_{\psi_o}^2\cos^2\omega t + \left(\frac{T\dot{\alpha}_{\psi_o} + \alpha_{\psi_o}}{\omega T}\right)^2\sin^2\omega t + 2\left(\frac{T\dot{\alpha}_{\psi_o} + \alpha_{\psi_o}}{\omega T}\right)\alpha_{\psi_o}\sin\omega t\cos\omega t\right] \qquad (21)$$

Substituting Eq. (21) into Eq. (20) with α_θ temporarily set to zero, we have after dividing by M and integrating,

$$(V_{J\phi})_{\alpha_\theta=0} = \lim_{t\to\infty}(V_\phi)_{\alpha_\theta=0} = \lim_{t\to\infty} -\left(\frac{C_{D2}Aq}{M}\right)\int_0^t \alpha_\psi^2\,dt$$

$$= -\frac{C_{D2}Aq}{M}\frac{T}{4}\left[\left(1 + \frac{1}{1+\omega^2T^2}\right)\alpha_{\psi_o}^2 + \left(1 - \frac{1}{1+\omega^2T^2}\right)\left(\frac{T\dot{\alpha}_{\psi_o} + \alpha_{\psi_o}}{\omega T}\right)^2 + 2\left(\frac{\omega T}{1+\omega^2T^2}\right)\left(\frac{T\dot{\alpha}_{\psi_o} + \alpha_{\psi_o}}{\omega T}\right)\alpha_{\psi_o}\right] \qquad (22)$$

By applying the same approximation made to the other jump velocity components, namely that 1 is negligible with respect to ωT, we can simplify Eq. (22) to the following

$$(V_{J\phi})_{\alpha_\theta=0} \approx -\left(\frac{C_{D2}Aq}{M}\right)\frac{T}{4}\left(\alpha_{\psi_o}^2 + \frac{\dot{\alpha}_{\psi_o}^2}{\omega^2}\right) \qquad (23)$$

By analogy we can write for the part of the roll axis jump velocity due to α_θ,

$$(V_{J\phi})_{\alpha_\psi=0} \approx -\left(\frac{C_{D2}Aq}{M}\right)\frac{T}{4}\left(\alpha_{\theta_o}^2 + \frac{\dot{\alpha}_{\theta_o}^2}{\omega^2}\right) \tag{24}$$

Adding Eq. (23) and (24) to obtain the total roll axis jump velocity, we have

APPROXIMATE ROLL AXIS JUMP VELOCITY

$$V_{J\phi} \approx -\left(\frac{C_{D2}Aq}{M}\right)\frac{T}{4}\left(\alpha_o^2 + \frac{\dot{\alpha}_o^2}{\omega^2}\right) \tag{25}$$

where

$$\alpha_o^2 = \alpha_{\psi_o}^2 + \alpha_{\theta_o}^2$$

and

$$\dot{\alpha}_o^2 = \dot{\alpha}_{\psi_o}^2 + \dot{\alpha}_{\theta_o}^2$$

Note that, contrary to the situation in the swerving and heaving components of jump velocity, angular oscillations caused by initial angular offsets and initial angular rates are equally effective in producing roll axis jump velocity. This is understandable because induced drag depends only on the amplitude of the angular oscillations and not on their phase.

COMPARISON WITH PREVIOUS THEORETICAL RESULTS

The foregoing analysis shows that separation disturbances which cause pitching and yawing oscillations of the bomb create a trajectory divergence which can be characterized as a constant velocity. This is an important conclusion from the standpoint of our stated goal of finding a practical method of compensating for systematic separation disturbances, because it means that the weapon delivery system can model such disturbances simply as additional ejection velocities, albeit in three dimensions.

Later on we will apply this concept to some actual bomb drops to see if it can be used to reduce the amount of apparent bomb dispersion. First, let us compare the jump velocity formulas with previously published theoretical results.

As previously stated, Nicolaides in Ref. (1) stated that for fin-stabilized missiles, jump angle results mostly from initial angular rates rather than from initial angles-of-attack. The foregoing analysis supports this statement. Furthermore, the formula relating jump angle to initial angular rates in Ref. (1) is

FROM REF. 1

$$\text{Pitch Jump Angle} \approx \frac{I(C_{N\alpha}Aq)}{MV(C_{M\alpha}Aqd)}\dot{\alpha}_{\theta o} = \frac{IC_{N\alpha}}{MVC_{M\alpha}d}\dot{\alpha}_{\theta o} \qquad (26)$$

where the notation of Ref. (1) has been changed to correspond to the notation used herein.

A comparison of Eq. (26) with Eq. (19) shows that the pitch jump angle as defined by Nicolaides is equivalent to the jump velocity divided by the total velocity. Thus, the two formulas are completely reconcilable as regards the swerving and heaving components of jump velocity.

Reference (5) reports results of a 5 degree-of-freedom (5DF) computer simulation of bomb trajectories in which the bomb receives an initial angular disturbance. It will prove instructive to compare the simplified solutions afforded by Eq. (15), (19) and (24) with the more elaborate analysis included in that reference. One of the cases included in Ref. (5) is that of a MK 82 bomb released from 5000 ft altitude in level flight at 450 kts, a Mach number of 0.69. Figure 2 shows a plot of the cross-range miss distance vs the "maximum yaw angle for the first half oscillation", $\dot{\alpha}_{\psi o}/\omega$, as taken from Ref. (5).

For comparison, the swerve jump velocity calculated from Eq. (15) in terms of $\dot{\alpha}_{\psi o}/\omega$ is

$$V_{J\theta} \approx -\left(\frac{C_{N\alpha}}{C_{M\alpha}}\frac{I\omega}{Md}\right)\frac{\dot{\alpha}_{\psi o}}{\omega} \qquad (27)$$

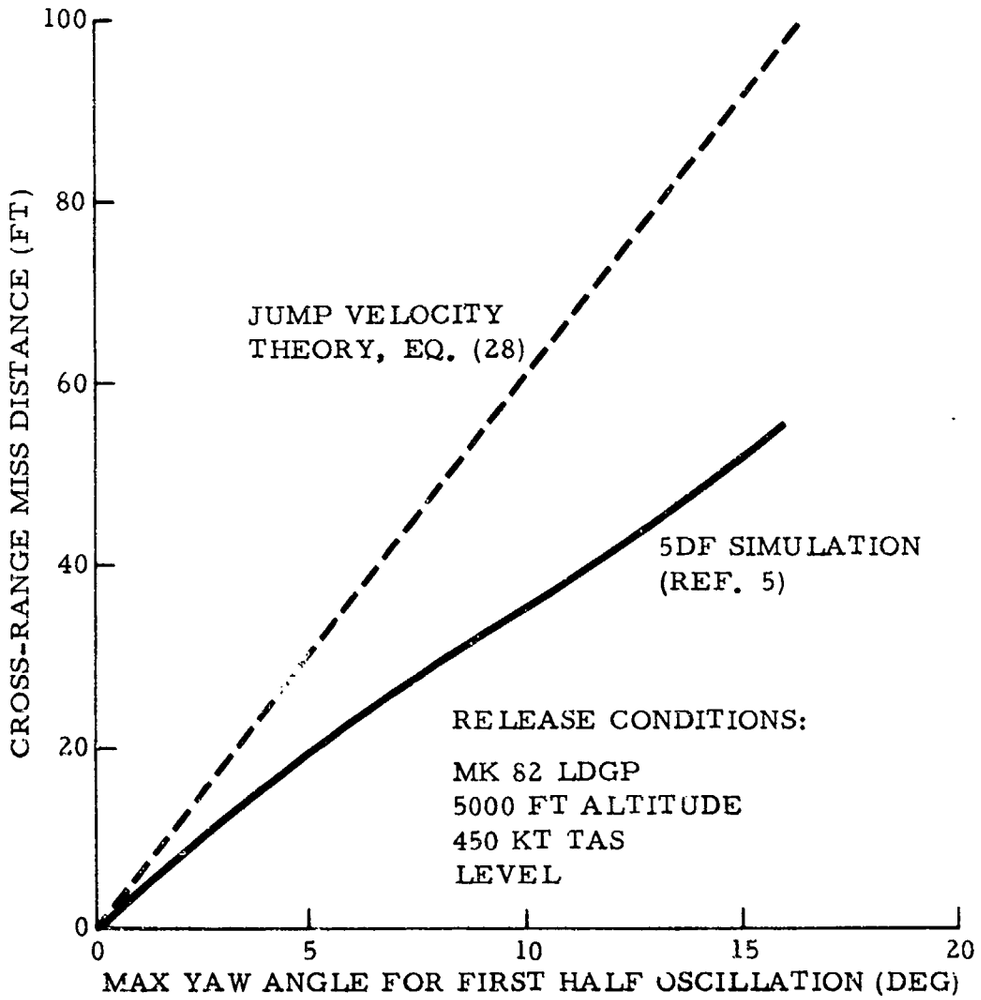


Figure 2. Cross-Range Miss Sensitivity to Yaw Oscillations as Predicted By Jump Velocity Theory and By 5DF Simulations of Ref. 5.

Substituting the appropriate values from Tables I and II and Eqs. (8) and (9), we compute

$$V_{J\theta} \approx -\frac{4.7 \times 36.7 \text{ lb-sec}^2\text{-ft} \times 15.4 \times 32.2 \text{ ft/sec}^2}{3.3 \times 527 \text{ lb} \times 0.895 \text{ ft} \times 2.65 \text{ sec}} \left(\frac{\dot{\alpha}_{\zeta_o}}{\omega}\right)$$

$$= -20.7 \text{ fps/radian} \left(\frac{\dot{\alpha}_{\zeta_o}}{\omega}\right) = -0.362 \text{ fps/deg} \left(\frac{\dot{\alpha}_{\zeta_o}}{\omega}\right) \quad (28)$$

In order to compare this figure with the corresponding miss distance plot of Ref. (5), we must multiply the swerve jump velocity of Eq. (28) by the time-of-fall, which is 16.8 seconds in this example. Figure 2 shows this result, 6.1 ft/deg, plotted as a straight, dashed line. The comparison shows Eq. (28) to be somewhat pessimistic relative to the 5DF simulation reported in Ref. (5).

Reference (5) also reports the downrange miss distance resulting from a yaw oscillation. Figure 3 displays this result along with the corresponding prediction based on Eq. (25) which is

$$R_m = V_{J\phi} t_f = -\left(\frac{C_{D2} Aq}{M}\right) \frac{T}{4} t_f \left(\frac{\dot{\alpha}_{\psi_o}}{\omega}\right)^2$$

$$= \frac{5.7 \times 0.631 \text{ ft}^2 \times 667 \text{ lb/ft}^2 \times 2.65 \text{ sec} \times 16.8 \text{ sec}}{527 \text{ lb}/32.2 \text{ ft/sec}^2 \times 4} \left(\frac{\dot{\alpha}_{\psi_o}}{\omega}\right)^2 \quad (29)$$

$$= -1,631 \text{ ft/(radian)}^2 \left(\frac{\dot{\alpha}_{\psi_o}}{\omega}\right)^2 = -0.497 \text{ ft/(deg)}^2 \left(\frac{\dot{\alpha}_{\psi_o}}{\omega}\right)^2$$

The parabola represented by Eq. (29) follows Ref. (5)'s simulation results but, again, is slightly pessimistic with respect to those results.

As one more comparison with the 5DF simulation results, we can compare the downrange miss sensitivities to pitch oscillations as reported in Ref. (5) and as computed from the jump velocity components of Eqs. (19) and (25). The 5DF simulation result appears in Fig. 4. For the level release example, the miss distance computed from the jump velocities is

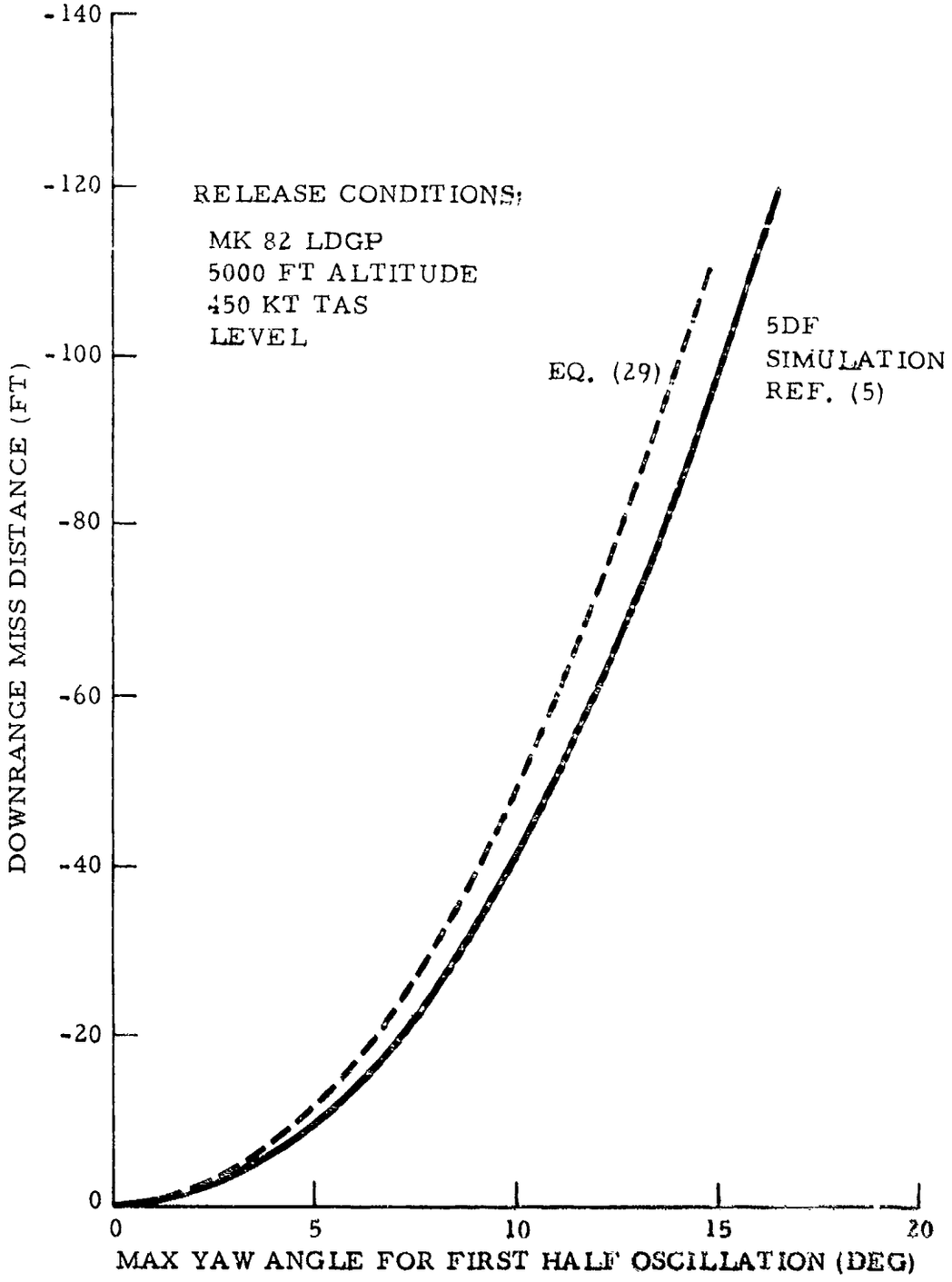


Figure 3. Down-Range Miss Sensitivity to Yaw Oscillations as Predicted by Jump Velocity Theory and by 5DF Simulation of Ref. (5).

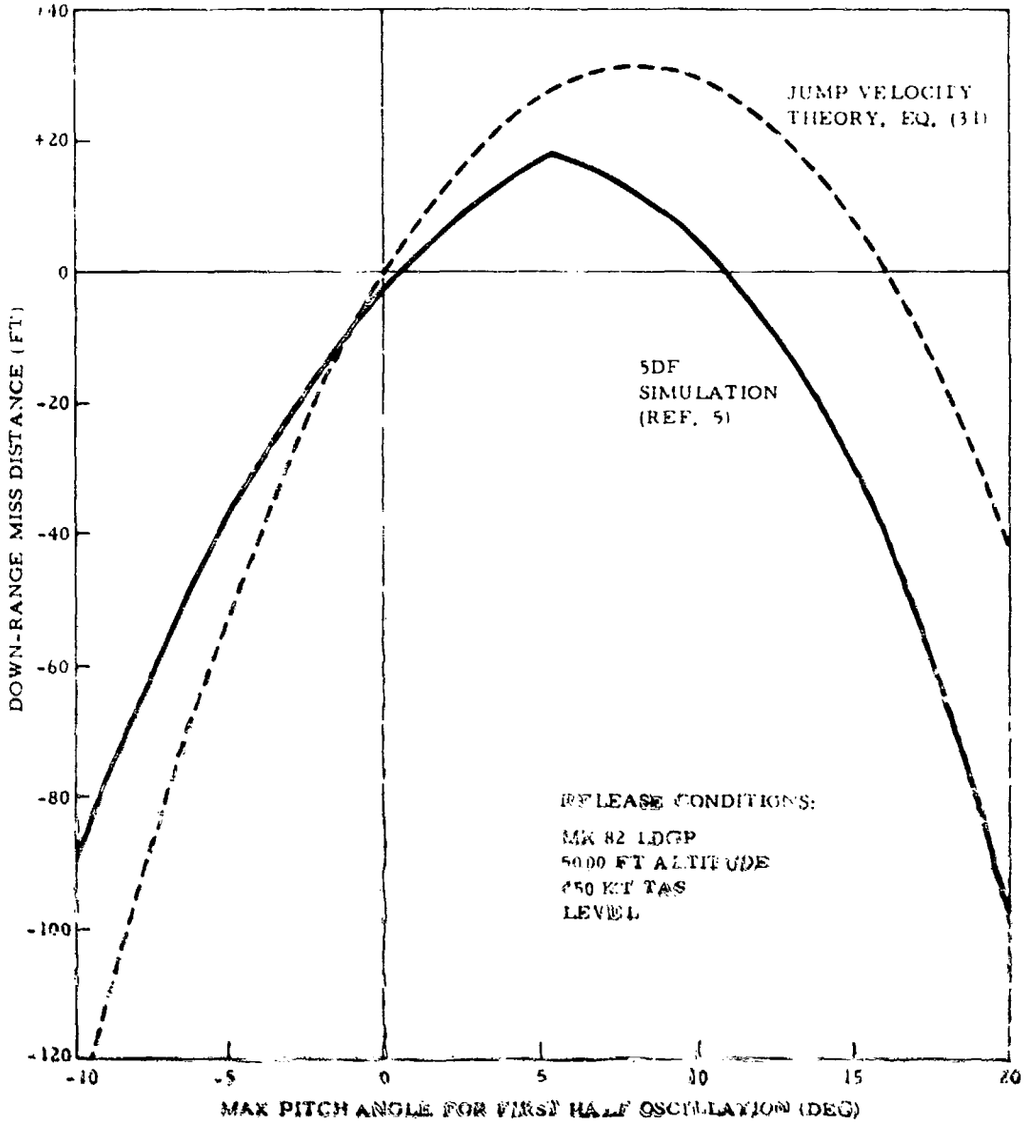


Figure 4. Down-Range Miss Sensitivity to Pitch Oscillations as Predicted by Jump Velocity Theory and by 5DF Simulations of Ref. (5).

$$R_m = V_{J\psi}\left(\frac{\partial R}{\partial V_E}\right) + V_{J\phi}t_f \tag{30}$$

where $\partial R/\partial V_E$ is the miss distance sensitivity to ejection velocity and is equal to 22 ft/fps (Ref. 5) for a 5000 ft, 450 kt, level delivery of a MK 82 bomb. Because the equations for computing $V_{J\psi}$ and $V_{J\phi}$ from $\dot{\alpha}_{\theta o}/\omega$ are numerically the same as for computing $V_{J\theta}$ and $V_{J\phi}$ from $\dot{\alpha}_{\psi o}/\omega$, we can utilize the numerical results of Eq. (28) and (29) directly in evaluating Eq. (30). Accordingly, numerical evaluation of Eq. (30) results in

$$R_m = 0.362 \text{ fps/deg} \times 22 \text{ ft/fps} \times\left(\frac{\dot{\alpha}_{\theta o}}{\omega}\right) - 0.497 \text{ ft/(deg)}^2\left(\frac{\dot{\alpha}_{\theta o}}{\omega}\right)^2$$

$$= 7.96 \text{ ft/deg}\left(\frac{\dot{\alpha}_{\theta o}}{\omega}\right) - 0.497 \text{ ft/(deg)}^2\left(\frac{\dot{\alpha}_{\theta o}}{\omega}\right)^2 \tag{31}$$

A plot of the parabola represented by Eq. (31) appears in Fig. 4 for direct comparison with the corresponding result published in Ref. (5). The two curves in Fig. 4 do have the same general characteristics, although they differ somewhat numerically, especially for large disturbances.

Considering the simplicity of the jump velocity concept in comparison with the more comprehensive 5DF simulation technique, the agreement displayed in Figs. 2, 3 and 4 is reasonably good, especially in the important region where angular disturbances are of the order of 5 deg or less. Certainly, the agreement justifies an attempt to apply the jump velocity concept to some actual bomb drops to see if it can successfully compensate for at least a portion of the apparant bomb dispersion.

APPLICATION TO ACTUAL BOMB DROPS

Having reached the conclusion that we can probably account for systematic separation disturbances by introducing an additional, 3-dimensional, jump velocity or pseudo-ejection velocity into the weapon delivery equations, the next question is, "How do we determine the jump velocity?" The direct way would be to instrument some bomb

drops with high speed cameras so as to measure the angular disturbances imparted during release and separation. This data in conjunction with Eqs. (15), (19), and (25) would suffice to determine mean values for the jump velocity components.

A second, more indirect method is to measure the release conditions accurately, predict the impact point of an unperturbed bomb, and then infer the jump velocity based on the actual impact relative to the predicted impact. Ideally, both methods should be used on the same bomb drops as a cross check, but the author knows of no such available test data.

The MK 84 bomb drop tests reported in Refs, (6), (7), and (8) provide the best set of available data for the impact point matching method. The reason is that the release point was instrumented very accurately with a bomb scoring pod carried by the aircraft, which measured release position and velocity (verified by cinetheodolite and laser tracker data), aircraft attitude, air speed, air density, and bomb lever arm effects caused by aircraft rolling or yawing at the moment of release. With all the major release conditions measured except for ejection velocity uncertainties and separation disturbances, the actual bomb impacts relative to the computed or predicted impact point should provide a good measure of the jump velocity.

Under the conditions of the tests reported in Refs. (6), (7) and (8) (MK 84 LDGP bombs released in level flight from 1500 and 5000 ft above ground level at 400 and 500 kt) the bomb scoring pod has a reported bomb impact prediction accuracy of about 12 ft (CEP), based on release point measurement accuracy alone. This means that the impact data from these tests should allow us to determine the horizontal components of jump velocity to a probable accuracy of 12 ft divided by the time-of-fall, which was about 18 sec for the 5000 ft drops and about 9 sec for the 1500 ft drops. Similarly, the probable accuracy of the vertical component of jump velocity obtainable from these test data is 12 ft divided by $\partial R/\partial V_E$, which was about 25 sec for the 500 kt drops and about 20 sec for the 400 kt drops. On this basis, we should expect to be able to measure jump velocities to probable accuracies between 0.7 and 1.3 fps for the horizontal components and between 0.5 and 0.6 fps for the vertical component.

Figure 5 shows the bomb impact pattern relative to the predicted impact for the 22 MK 84 bomb drops reported in Refs. (6), (7) and (8). For the purpose of this figure, all predictions are based on standard ejection velocities of 10 fps for the F111E and 15 fps for the A6E, with no jump velocities included. This differs from the original data wherein

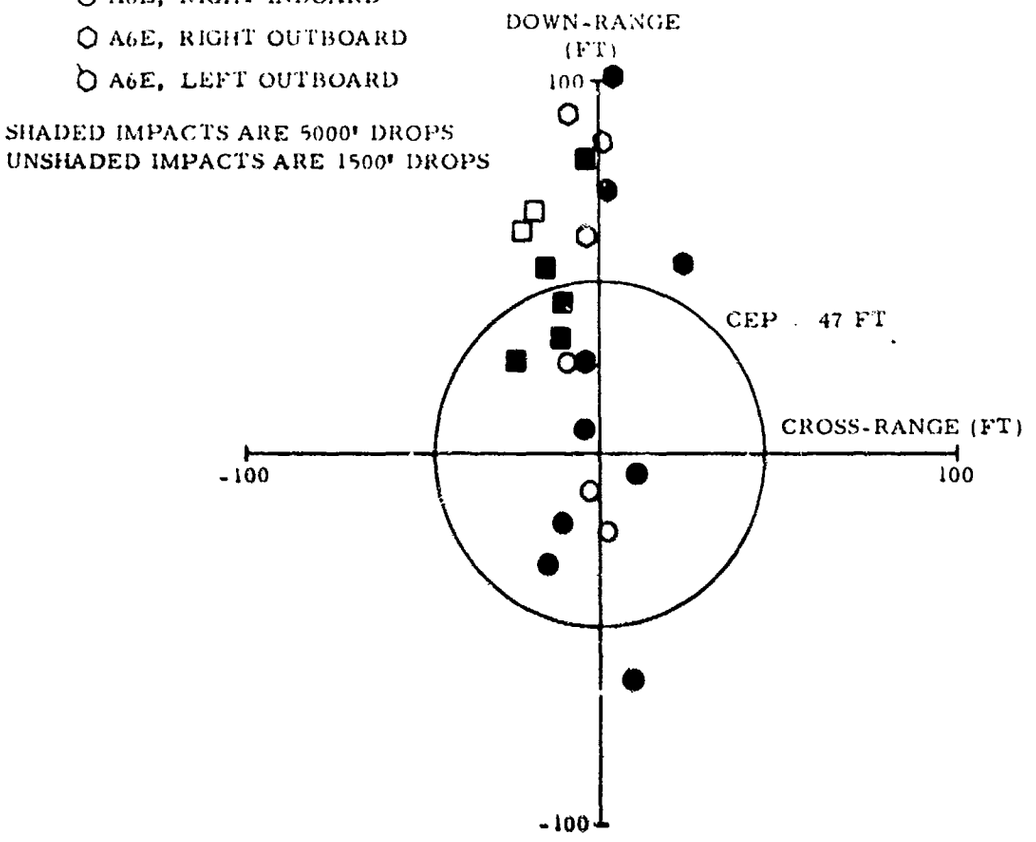


Figure 5. MK 84 LDGP Bomb Impacts Relative to Impacts Predicted On Basis of Release Point Measurements Alone.

the predicted points were modified by jump velocities which changed during the course of the test series as more and more bomb impact data was accumulated.

The shape of the symbols which mark each impact designate the weapon station. The shaded symbols signify the high altitude (5000 ft) releases; the open symbols signify the low altitude releases.

A perusal of the impact pattern for each weapon station reveals definite correlations. The F111E bomb impacts are all long and to the left of the predicted impact with little or no difference between the high and low altitude deliveries. The A6E bombs released from the inboard wing stations are mostly short of the predicted impact, especially those released from 5000 ft altitude. The outboard station releases from the A6E, on the other hand are all long with respect to the predicted impact point, and there is little or no difference between the high and low altitude drops.

In level deliveries of low drag bombs from different altitudes, the miss sensitivity to variation in horizontal release velocity varies directly as the time-of-fall, while the sensitivity to variations in vertical release velocity is nearly independent of altitude. This fact tells us that the appropriate component of jump velocity to use for downrange compensation of the outboard station releases from both types of aircraft is the vertical component, $V_{J\psi}$. On the other hand, $V_{J\phi}$ is a better component to use for compensating the A6E inboard station releases, because those impacts did exhibit downrange misses which were correlated with release altitude. For the left-biased F111E impacts, a $V_{J\theta}$ component is needed. Table IV shows the numerical values of the jump velocities as determined for each weapon station.

TABLE IV
JUMP VELOCITY FOR MK 84 LDGP BOMBS BY WEAPON STATION

Weapon Station	Jump Velocity (fps)		
	$V_{J\theta}$	$V_{J\psi}$	$V_{J\phi}$
F111E, Left Outboard	-1.0	2.0	0
A6E, Left Inboard	0	0	-1.3
Right Inboard	0	0	-1.3
Left Outboard	0	3.0	0
Right Outboard	0	3.0	0

Applying the above set of jump velocities to each of the impact points plotted in Fig. 5, we obtain the corrected impact plot of Fig. 6.

DISCUSSION

A comparison between Fig. 5 and Fig. 6 shows that apparent bomb dispersion can be reduced significantly by calibrating and assigning a "jump velocity" compensation for each weapon station on an aircraft. The example illustrated herein revealed a reduction in apparent dispersion of MK 84 LDGP bombs from 47 ft (CEP) to 20 ft (CEP). This residual ground plane dispersion of 20 ft (CEP) represents an angular dispersion of less than 1 mil for those bombs released from 5000 ft above ground level.

In order to account for the long impacts from the outboard wing station, it was necessary to postulate an upward jump velocity component $V_{J\psi}$ of 2 fps for the F111E and 3 fps for the A6E. These upward components cannot be attributed to angular oscillations of the bomb as theorized in the preceding analysis, because such oscillations should also produce induced drag and an associated rearward jump velocity component.

Because these upward jump velocities occur only on the outboard wing stations and amount to about 20 percent of the total ejection velocity (10 fps for the F111E and 15 fps for the A6E) in each case, the best explanation for their occurence is that they really represent a 20 percent reduction in the effective downward ejection velocity. Such a reduction could be caused by an upward reaction of the wing or a

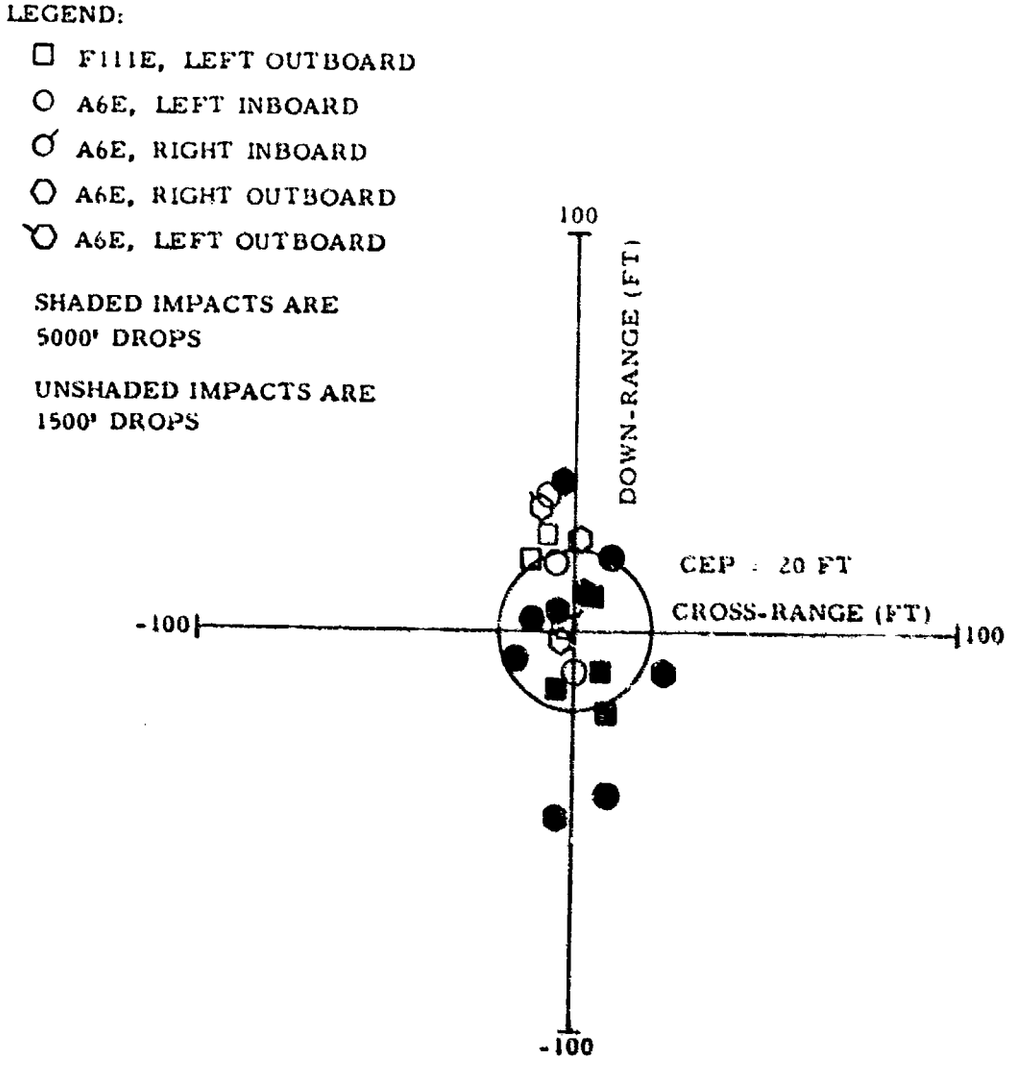


Figure 6. MK 84 LDGP Bomb Impacts Relative to Predicted Impacts Corrected for Jump Velocity

roll reaction of the whole aircraft when ejecting a 2000 lb bomb off an outboard wing pylon station.

The leftward jump velocity ($V_{J\theta}$ = -1 fps) observed for the MK 84 releases from the left outboard station of the F111E can be attributed to a systematic aerodynamic separation disturbance such as outflow along the wing. The amplitude of the initial yawing oscillation necessary to cause this outward jump velocity can be estimated from Fig. 2 to be about 3 deg. Figure 2 actually pertains to a MK 82 LDGP bomb instead of a MK 84, but a simple dimensional analysis of Eq. (27) will demonstrate that for similar bombs the slope of the straight line representing the jump velocity theory in Fig. 2 is independent of bomb size.

The same type of dimensional analysis shows that Fig. 3 applies equally well to any bomb in the MK 81-84 series as long as the aerodynamic coefficients remain the same. Hence, the 3 deg yawing oscillation should produce a slight, rearward jump velocity amounting to 0.2 fps (4 ft range decrement divided by an 18 sec time-of-fall) to account for the induced drag effect of the yawing oscillations. However, such a small magnitude is less than the measurement error previously ascribed to these particular test data. In the interests of simplicity, $V_{J\phi}$ was left at zero and is so listed in Table IV.

Although no bombs were released from the right wing of the F111E, we can anticipate a symmetrical outflow of air away from the fuselage to cause an outward jump velocity of $V_{J\theta}$ = +1.0 fps for MK 84 bombs released from the right outboard pylon station of the F111E.

The rearward jump velocity ($V_{J\phi}$ = -1.3 fps) attributed to the inboard station releases of MK 84's from the A6E has no corresponding $V_{J\theta}$ or $V_{J\psi}$ components. This can be explained as being an initial angle-of-attack effect rather than an angular rate effect, but the initial angle-of-attack would have to be 7 deg (see Fig. 3) in order to account for the 23 ft average range decrement observed in the 5000 ft drops. Perhaps a more accurate model would include a $V_{J\psi}$ component as well as a $V_{J\phi}$ component and follow a characteristic similar to that shown in Fig. 4, where a -2.5 deg initial oscillation amplitude accounts for the 23 ft range decrement.

This points up one shortcoming of the impact point method of measuring jump velocities. It is difficult to split the observed downrange discrepancies into $V_{J\psi}$ and $V_{J\phi}$. In effect, there are two unknowns and only one observable. Releases from different altitudes coupled with the theoretical equations which predict the jump velocity interelationships

and their variation under different release conditions can help to clarify the picture.

CONCLUSIONS

1. Initial pitching or yawing rate of a bomb has an order of magnitude larger effect on the angular dispersion of the bomb than does an initial pitch or yaw offset angle even though the angular oscillations have the same amplitude.

2. Rearward dispersion due to induced drag, on the other hand, depends only on the amplitude of the oscillation.

3. Systematic separation effects causing a bomb to diverge from its nominal, unperturbed trajectory, can be adequately described by jump velocity, a 3-dimensional ejection-like velocity imparted to the bomb at release.

4. Analysis of actual bomb drops shows that jump velocity compensation for systematic separation effects can reduce the apparent bomb dispersion by more than a factor of 2.

REFERENCES

1. J.D. Nicolaides, "Missile Flight and Astrodynamics", Bureau of Naval Weapons, Technical Note No. 100A, 1959 - 61.

2. "Close Air Support System (CLASS) F-4D Flight Test", Air Force Avionics Laboratory, Technical Report No. AFAL-TR-73-363, Sept. 1973.

3. "Summary of the NOL Investigations to Date of the Aerodynamic Characteristics of the Navy Low Drag Bomb", Naval Ordnance Report No. 5673, 8 Feb. 1960.

4. "Aircraft Store Information Catalog", David Taylor Model Basin publication, May 1966.

5. "Theoretical Sensitivity Analysis and System Delivery Computations for High and Low Drag Weapons at Several Subsonic and Supersonic Delivery Conditions", Air Force Armament Laboratory, Technical Report No. AFATL-TR-70-110, Oct. 1970.

6. "Operational Test and Evaluation of Tactical Radar Bombing Systems - Results of Demonstration Test of a Bomb Scoring System", Weapons Systems Evaluation Group (WSEG) Report 253 including IDA Study 5-444, Nov. 1974.

7. "Test and Evaluation of Tactical Radar Bombing Systems - Development Testing of Bomb Scoring System", Air Force Special Weapons Center (AFSWC) - TR-74-49, Dec. 1974.

8. "Verification Test Data Report for the Airborne Range Instrumentation System (ARIS)", Litton Systems, Guidance and Control Division Document No. 402395, Mar. 1975.

AUTHOR'S BIOGRAPHY

Dr. J. Stanley Ausman is Chief Scientist for the Guidance and Control Systems Division of Litton Systems Inc. located in Woodland Hills, California. He has been with Litton for 14 years directing advanced analytical studies of navigation and bombing systems as well as their subsystems and components. He is the inventor of Litton's CLASS, a precision weapon delivery system, and ARIS, a precision bomb scoring system, and has closely followed and supported both of those systems through their development and flight test phases.

He received his B. S. degree in Engineering Physics from the Berkeley campus of the University of California in 1950 and his M. S. and PhD degrees in Mechanical Engineering in 1952 and 1954, respectively, from the same University.

His professional affiliations include ASME, Tau Beta Pi, Sigma Xi, AIAA, ION and AOA. He is a former member of the ONR Gas Bearing Advisory Board and in 1963 received the ASME Melville Award for the best technical paper of the year. He has authored or co-authored 18 technical papers in the fields of shock and vibration, gas lubricated bearings, gyrodynamics, system control theory, and weapon delivery. He holds two patents on augmented inertial systems.

SYSTEM SAFETY

(ARTICLE UNCLASSIFIED)

BY

James C. Phillip
System Safety Engineer
McClellan AFB, California 95652

In some circles, safety is a dirty word. No one says safety is not good. That would be like you're against motherhood. But: "It costs money!" "It takes time."

Engineers particularly resent it since everyone knows their whole objective is to be safe. Manufacturers claim, "We build safe systems."

Yet, accidents do occur, and malfunctions continue to plague us, costing money, time, and lives.

This morning, Ladies and Gentlemen, I'd like to tell you about a new concept in safety. It's not the hard hat/steel toe shoe approach; "It's a new science called the System Safety Engineering Concept."[1]

System Safety is defined as the optimum degree of safety within the constraints of operational effectiveness, time, and cost, attained through specific application of system safety management and engineering principles throughout all life cycle phases of a system. Proper application of the system safety concept provides a fundamental approach to accident prevention.

[1]Most of the following text is taken from Dr. Harold E. Roland's Workbook System Safety Course.

DISTRIBUTION STATEMENT A
Approved for public release;
Distribution Unlimited

In the past, safety programs have been established entirely on an after-the-fact philosophy of accident prevention which is commonly referred to as the "Fly-Fix-Fly" approach. When an accident occurs, an investigation is conducted to determine the cause. Accident data are thus reviewed and discussed in an effort to determine what is needed to prevent similar accidents from occurring in the future. The resulting system modification, retrofit, or other after-the-fact correction of design is made to the existing operational equipment. The system safety approach to accident prevention involves a before-the-fact process which is characterized as being identify-analyze-control safety. The emphasis is placed upon an acceptable safety level being designed into the equipment prior to actual production. The system safety approach provides for the early identification andanalysis of potential system hazards and subsequent synthesis of controls for residual hazards to provide a system which can be produced, tested, operated, and maintained safely. Required corrective action is made before-the-fact. Proper application of the system safety concept requires an understanding of the technical aspects of system safety as a systems engineering element, together with the management controls necessary to assure its timely and economical completion. A little history of system safety might be beneficial at this point.

In September, 1947, a paper entitled "Engineering for Safety" was presented to the Institute of Aeronautical Sciences. In this paper, it was stated that "Safety must be designed and built into airplanes, just as are performance, stability, and structural integrity. A safety group must be just as important a part of a manufacturer's organization as a stress, aerodynamics, or a weights group." This technical paper provides one of the earliest recordings of the system safety concept. It was not until the early 1960's that the system safety concept was formally applied by contractual direction. This formal delegation of safety responsibility by contractual requirement replaced the familiar practice in which every designer, manager, and engineer presumably assumed his share of the responsibility for safety. The growth and development of the system safety approach to accident prevention can, in fact, be keyed to the publication of exhibits, specifications, and standards. The Atomic Energy Commission had established very strict safety controls on the use and exposure to nuclear material. In April, 1962, the Air Force published a document, "System Safety Engineering for the Development of Air Force Ballistic Missiles," applicable to ballistic systems division programs. This document established system safety requirements for the associate contractors on the Minuteman missile program where the first real system safety groundwork was done. In September, 1963, the document was revised

into an Air Force specification, "General Requirements for Safety Engineering of Systems and Associated Subsystems and Equipment." With very minor revision, in June, 1966, this specification was made a Department of Defense requirement. Finally, in July, 1969, the specification was further revised and became what we now use: MIL-STD-882, "System Safety Program for Systems and Associated Subsystems and Equipment: Requirements For." Department of Defense approval of MIL-STD-882 for use has produced a mandatory requirement for a system safety program on all procured material. In order to comply with all facets of this military standard, the Department of Defense agencies must provide trained personnel to efficiently manage the system. Safety portion of procurement and contractors must provide trained, experienced personnel to manage and perform the required system safety efforts.

This redirection of safety efforts from the later operational phases of the system life cycle to the earlier design phases has resulted from a growing awareness that utilization of the system safety concept is the most effective and economical approach for accident prevention/control. The major reasons for this evolution of system safety philosophy into effective, thorough, analytical safety decision/making risk management programs include, in part:

(a) Cost.

In the twenty-year period from 1953 to 1972, the USAF aircraft accident rate was improved from 24 to 3 accidents per 100,000 flying hours. The number of

aircraft destroyed annually decreased from 900 to 137. The pilot fatality rate improved from 4.8 to approximately 1.0. The total fatality rate improved from 11.1 to approximately 3.0. The cost of aircraft accidents, both major and minor, in 1972 was three hundred twenty-eight million dollars which represents airframe cost only. This dollar loss is more than double the annual loss of twenty years ago.

(b) Complexity.

System complexity is increasing rapidly in order to meet changing mission requirements. Technological progress has been phenomenal. Today's highly automated systems incorporate instant communications, high speed transportation, information storage and retrieval, high energy sources, microminaturization, advanced manufacturing techniques, etc. As we design, develop, produce, and use these increasingly complex systems, we must concurrently develop the capability to analyze and understand them.

(c) Specialization.

Fragmentation of assignment and responsibility in design groups is making utilization of the systems concept increasingly more difficult. System safety engineering should be a process which is fully capable of assuming a leading role in system design analysis.

(d) Liability.

The legal considerations or product liability cases is causing an awareness of system safety principles in industry. Lawyers are becoming more cognizant of the safety aspects of product design, manufacture, test, transportation, and use.

(e) Response to Failure.

The response of government, the company, and the general public to failure/accident is becoming more critical. This responsiveness is due in part to a public which is easily aroused by consumer groups/advocates and is producing an increased management awareness of the safety implications of failure.

(f) Nature of Events.

Technological change has produced the discovery of energy sources which create hazard event potentials with most catastrophic effects. The effects of an inadvertent missile launch, nuclear explosion, or inadvertent bomb drop are so serious that even one of these events cannot be tolerated. Further, testing or otherwise assuring operational capability with these systems is limited. Therefore, application of system safety principles during design and development of these systems is imperative.

Now, I'll talk about system acquisition. The systems acquisition life cycle consists of five major phases, with high-level decisions required before proceeding with the second, third, and fourth phases. The phases and devision points are as follows:

Conceptual Phase - Program Decision.

Validation Phase - Ratification Decision.

Full-scale Development Phase - Production Decision.

Production Phase.

Deployment Phase.

System safety should be applied throughout each phase before moving to the next phase: Undoubtedly, the most important phase is the conceptual when the preliminary hazard analysis (PHA) should be completed as this PHA will be the road map for all further investigation.

The degree of safety achieved in a system is directly dependent upon management emphasis, i.e., the ability of the procuring agency to clearly state system safety objectives and requirements and the contractor's ability to translate these requirements into safe, functional hardware. An effective system safety program should result in the following management and technical information for decision-making:

(a) System Safety Plans.

(1) System Safety Program Plan.

(2) System Safety Engineering Plans.

(b) System Safety Inputs to Specifications.

(1) Facilities.

(2) Equipment.

(3) Procedures.

(c) System Safety Support to Design Reviews.

(1) Preliminary Design Reviews.

(2) Critical Design Reviews.

(d) Documented System Safety Analyses.

(e) Documented Reviews of Test Plans and Operating Procedures.

(1) Development Test.

(2) Qualification Test.

(3) Acceptance Test.

(4) Special Safety Tests.

(5) Potentially Hazardous Operations.

(f) Special Safety Studies.

(1) Hazardous Materials.

(2) Special Procedures.

(3) Safety Devices.

(4) Energy Sources.

(g) Risk Assessment.

(1) Hazard

a. Probability.

b. Severity

c. Exposure

(2) Identification.

(3) Evaluation.

Now, we get into the management side of system safety which is primarily the same as any management program. I'll dispense with that and get into some of the primary analyses that are used to identify hazards before the fact, prioritize them so that emphasis can be taken where needed, or where it can be afforded, and show how these analyses can be employed.

System Safety Analyses.

This section is used to identify the methods and the types of analyses that will be used to evaluate potential design and operational hazards. First let us define:

Hazard Identification.

The identification of hazards encompasses both surveillance and monitoring, as well as safety analyses. Surveillance and monitoring normally consists of an on-site review of the manufacturing, testing, handling, storage, transportation, and operation facilities, as well as determination of conformance with safety standards and requirements. Safety analysis is a detailed study of the design and hardware performed on a total system basis. It is this analysis which serves as the fundamental system safety baseline against which hardware changes, procedure changes, and the personnel influences can be measured to demonstrate an improvement or loss in total safety. A review of the technical safety activity at all levels should determine that:

a. Safety surveillance and monitoring is provided for all activities.

b. Results of these efforts are reported to management.

c. Management responds to the hazard reports in an appropriate manner.

d. Methods have been developed and imposed for safety analysis to be performed.

e. Analytical method used is adequate.

f. Effort is consistent among the various programs.

g. Hazard identified by safety analysis are reported in a suitable medium.

h. Corrective action recommendations influence the design.

i. Closed-loop hazard identification and corrective action systems are used.

Preliminary Hazard Analysis (PHA).

A preliminary hazard analysis is an inductive process which should be conducted early in the design phase of the system life cycle to identify in broad or gross terms the potential hazards associated with the postulated operational concept. The analysis is a comprehensive, qualitative, evaluation of the system which considers the system from the viewpoint of its operational environment. As potentially hazardous operations, materials, and designs are identified, this information should be used in the development of safety criteria to be imposed in the performance/design specifications. Preliminary hazard analysis, therefore, becomes a necessary system safety program element to provide assurance that the system safety requirements become an integral part of the overall technical design requirements.

The preliminary hazard analysis should include, but not be limited to, the following activities:

(a) A review of pertinent historical safety experience data.

(b) A categorized listing of basic energy sources including an identification of possible causes in each category.

(c) An investigation of the various energy sources to determine the provisions which have been developed for their control.

(d) Identification of energy sources for which inadequate control has been provided in the proposed design/procedures.

(e) The provision of specific safety requirements/criteria which should be incorporated into the program documentation to ensure control of the energy sources which present unacceptable hazard levels.

A general listing of areas in the system design to be considered should include the following:

(a) Isolation of energy sources.

(b) Fuels and Propellants: Their characteristics, hazard levels, quality distance constraints, handling, storage and transportation safety features, compatibility factors, etc.

(c) Explosive devices and their hazard constraints.

(d) Material compatability.

Subsystem/System Hazard Analyses.

These are described in MIL-STD-882, and several techniques, including the fault tree analyses (FTA) may be employed. The purpose is to verify design criteria prior to the critical design review (CDR).

To be effective there must be a very close working relationship between the SSO and designer.

Operating Hazard Analysis (OHA).

The OHA covers the safety critical aspects in such areas as testing, maintenance, storage, shipping and handling, training, facility operations and deployments. The OHA should be initiated sufficiently early to provide inputs to test requirements, preliminary technical orders and shipping/storage criteria.

An example of a hypothetical, single hazard, preliminary hazard analysis entry would be Figure Number 1. Figures Number 2 and 3 depict a system and a fault tree analysis of the system. These are only a few of the tools used by the latest System Safety Engineers. Unfortunately, this paper barely opens the doors to the possibilities of system safety engineering. Be prepared, it's on its way. The growth of consumerism has recently brought about an almost universal concern with system safety aspects of most all equipment and activities that touch upon human affairs. If you, the designers and managers work closely with your System Safety Engineers you will find that everyone will benefit as there is much to be gained from a well-conducted system safety engineering program.

PRELIMINARY HAZARD ANALYSIS FOR HORSELESS CARRIAGE

BASIC ENERGY/ HAZARD SOURCES	CAUSE	PROVISION FOR CONTROL	ADEQUATE	IF NOT ADEQUATE, SPECIFIC PROVISION TO ASSURE SAFETY
MAN IN MOTION	INHERENT	A. BRAKING SYSTEM	NO	PROVIDE REDUNDANCY
		B. STEERING SYSTEM	YES	
		C. SPEED CONTROL		
		D. LIGHTING		

FIGURE 1

WATER HEATER SYSTEM

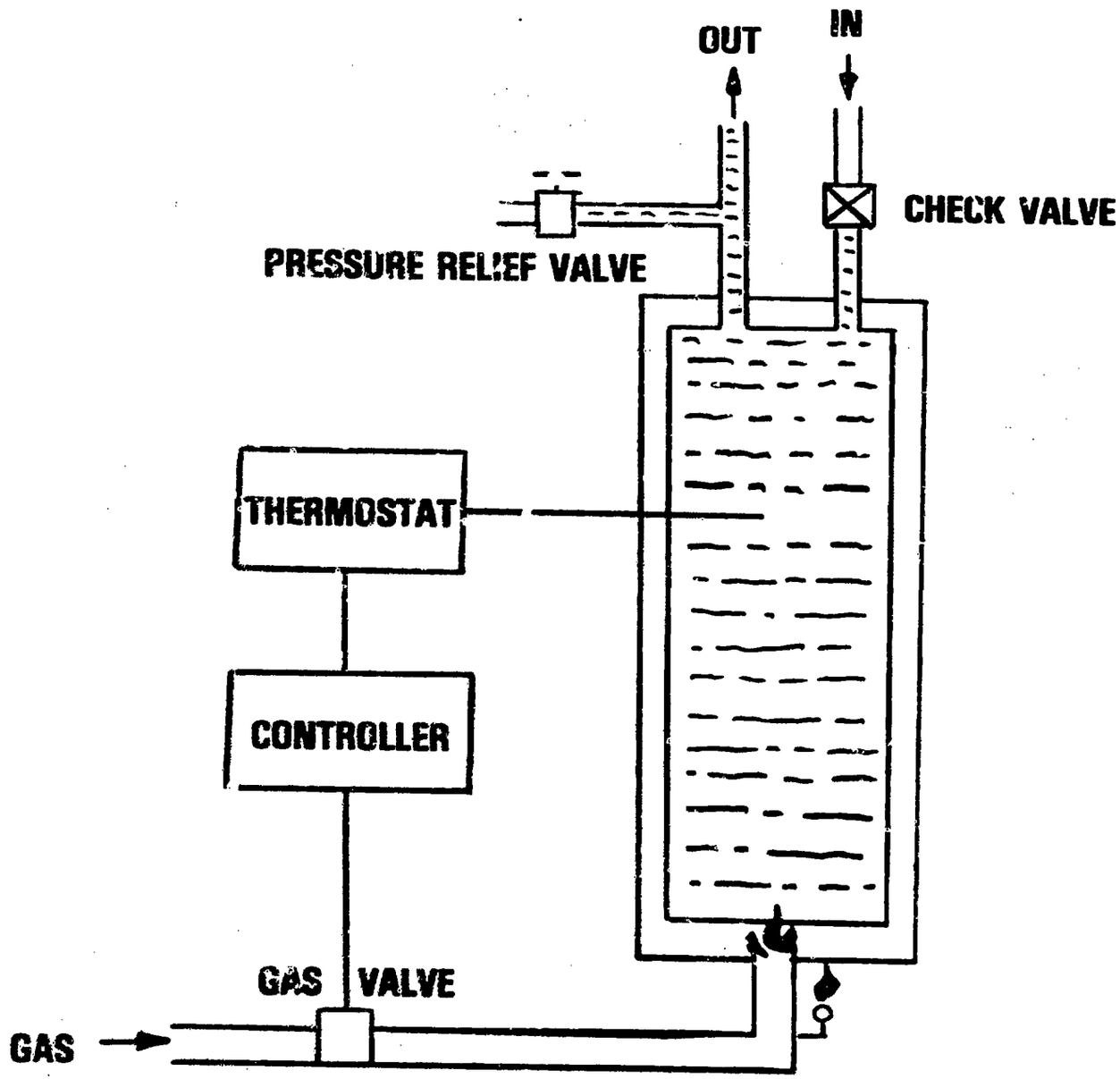
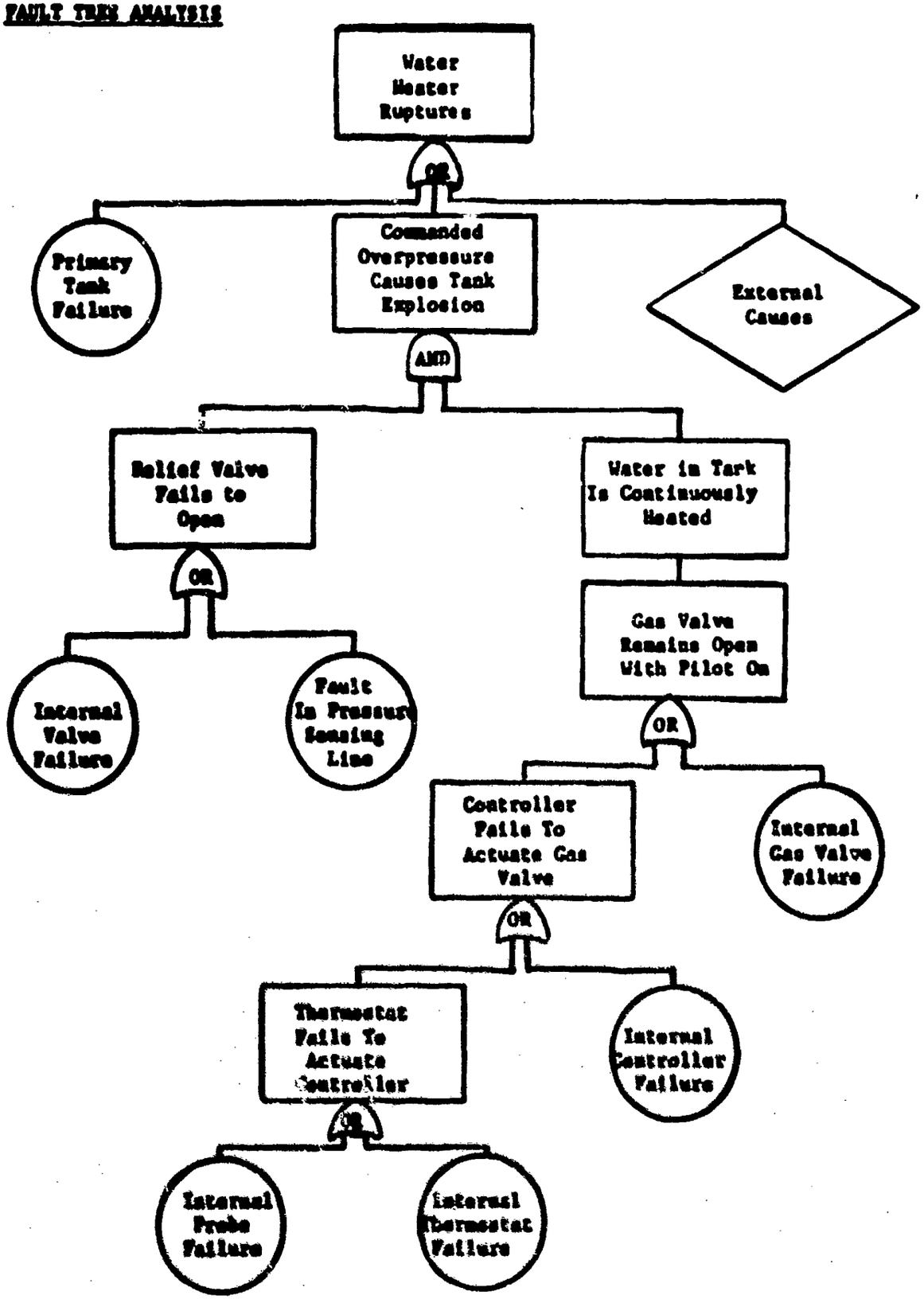


FIGURE 3

FAULT TREE ANALYSIS



AUTOBIOGRAPHY

James C. Phillip

Mr. Phillip received his BS in Civil Engineering from the University of Illinois in 1952. He was soon employed by Douglas Long Beach as a structural engineer where he worked on the C-124, C-133 and B-66 aircraft programs. In 1955 he accepted a position with the Air Force at Tachikawa, Japan as a structural engineer. After approximately one year he took over as Branch Chief, and later as Deputy, Engineering. Upon his return to the United States he took a job with the Air Force at McClellan AFB, California. He was lead project engineer in development of the Cal-30 Gun Pod System for the T-28/T-33 aircraft. He was also lead project engineer for installation of the DECA Navagational System in 4 AF aircraft as well as several lesser systems. He became deeply involved in Aircraft/Stores Compatibility in 1967 when he was appointed as the AFLC Representative to the JTGE/MD Working Party for Aircraft/Stores Compatibility. As of January 1975 he is the Sacramento ALC System Safety Engineer responsible for System Safety at McClellan AFB. He is a member of the "McClellan Society of Professional Engineers" (MSPE), the "American Society of Safety Engineers" (ASSE) and the "System Safety Society."

PREDICTION TECHNIQUE TO DETERMINE EFFECTS OF EXTERNAL STORES ON AIRCRAFT PERFORMANCE (U) (Article UNCLASSIFIED)

by

R. D. DYER
Air Force Flight Dynamics Laboratory
Wright-Patterson Air Force Base, Ohio 45433

and

R. D. GALLAGHER
Vought Systems Division
LTV Aerospace Corporation
Dallas, Texas 75222

ABSTRACT. (U) The Air Force Flight Dynamics Laboratory (AFFDL) is currently developing under contract with the LTV Aerospace Corporation, an analytical technique to provide design, development, and certifying engineers with a rapid, and accurate means of determining the interference effects of external stores on the parent aircraft in the subsonic, transonic, and supersonic speed regimes. This paper presents the formulation and application of generalized techniques for predicting the aerodynamic effects of external stores on the lift, drag and side force as well as the pitching and yawing moment of the carrier aircraft.

An earlier AFFDL contractual effort verified the feasibility of using an empirical approach for technique development for the lift, drag, and pitching moment terms. At the conclusion of this effort the predicted accuracies of the force terms were generally within ten percent of the incremental loads, with neutral point prediction accuracies less than one percent of the mean geometric chord. The current technique development refines the performance equations originally derived and extends their applicability as well as deriving new correlative techniques for side force and yawing moment.

Due to the complex flow patterns associated with the various aircraft/store configurations, empirical relations must be developed since there are no theoretical techniques available at present for

(Article Unclassified)

Approved for public release; distribution unlimited.

handling the local shock waves, viscous effects and flow separation. The method development is based upon a parametric correlation of extensive test data of many aircraft types obtained from a comprehensive data search of both contractor and military facilities as well as data from a parametric wind tunnel test of the A-7 and F-4 aircraft. These wind tunnel tests enabled the developers to readily define the correlation parameter trends. By perturbing only one variable independent of the other geometric and flight parameters, detailed flight correlations were developed. This method of development although costly with respect to test time enabled reliable correlations and well qualified prediction techniques.

All techniques are capable of calculating the parent aircraft performance for both single and multiple carriage on arbitrary aircraft configurations for any number of store stations. In addition the prediction equations can determine performance decrements for parent aircraft with leading edge sweeps up to 75^{0} and for high, mid, and low wing placement aircraft. The paper presents sample formulations and accuracy comparisons for various store configurations. Each equation delineates the interference variables of importance which will enable designers of future aircraft to better determine store/hard point placement. This new methodology will be available for application in September 1975.

Approved for public release; distribution unlimited.

LIST OF SYMBOLS

C_D	=	Drag coefficient, (Drag)/($q \cdot S_{REF}$)
C_L	=	Lift coefficient, (Lift)/($q \cdot S_{REF}$)
C_M	=	Pitching moment coefficient, (Pitching moment)/($q \cdot S_{REF} \cdot \bar{c}$)
C_Y	=	Side force coefficient, (Side force)/($q \cdot S_{REF}$)
C_n	=	Yawing moment coefficient, (Yawing moment)/($q \cdot S_{REF} \cdot b$)
C_l	=	Rolling moment coefficient, (Rolling moment)/($q \cdot S_{REF} \cdot b$)
q	=	Free stream dynamic pressure, lb/ft^2.
S_{REF}	=	Aircraft wing reference area, ft^2.
$\bar{c}$	=	Aircraft Wing mean geometric chord, ft.
b	=	Aircraft wing span, ft.
ΔC_{D_o}	=	Basic store installation incremental drag coefficient at zero lift coefficient.
$\Delta C_{D_{o_A}}$	=	Additional incremental drag coefficient at zero lift coefficient due to the mutual interference of adjacent store installations.
$\Delta C_{D_{o_{AF}}}$	=	Additional incremental drag coefficient at zero lift coefficient due to the mutual interference of store installation and fuselage.
ΔC_{D_i}	=	Additional incremental drag coefficient due to lift, as a result of adding external store installations to the clean aircraft.
PFA	=	Pylon frontal area, in^2.
XAFT	=	Longitudinal distance from the local wing trailing edge to the trailing edge of the given store, in. The reference point is the wing T.E. and distances upstream are negative.
XFWD	=	Longitudinal distance from the local wing leading edge to the nose of the given store, inch. The reference point is the wing L.E. and distances upstream are negative.
PTMAX	=	Maximum pylon thickness, in.
PC_{TOP}	=	Pylon chord length at the wing-pylon juncture, in.

PC_{LOW}	=	Pylon chord length at the bottom edge, in.
c	=	Local wing chord length, in.
$C_{D_{\P}}$	=	Drag coefficient based on maximum cross-sectional area.
$S_{\P}$	=	Store maximum cross-sectional area, ft.^{2}
CDB	=	Ballistic store drag coefficient based on maximum cross-sectional area, ft.^{2}
CE	=	Effective wing local chord, inch. Obtained by the vertical projection of the store installation on the aircraft wing.
D_W	=	Maximum width of a store installation, in.
D_S	=	Maximum store diameter, in.
G	=	Store-to-store minimum clearance, in. Applicable to multiple store installations only.
L	=	Total store installation length, in. Distance from the nose of the forward store to the trailing edge of the aft store. For single store installations, L is equal to the length of the store.
TN	=	Tail to nose longitudinal distance for adjacent store installations, in. That is, the longitudinal distance from the nose of the aft store installation to the tail of the lead adjacent store installation.
N_S	=	Total number of stores attached to a multiple or triple ejector rack.
Y	=	Wing spanwise distance between two given points, in.
Δy	=	Minimum clearance between adjacent store installations, in.
AR	=	Geometric aspect ratio of the aircraft wing.
Z	=	Maximum depth of a store installation (pylon included), in.
P_H	=	Reference pylon height = 1.883 ft.
P_h	=	Average pylon height, in.
DEPTH	=	$Z - P_h$
α	=	Aircraft model angle of attack, degree.
Ψ	=	Aircraft model angle of yaw, degree.

LIST OF SYMBOLS (Continued)

AWA	=	Affected wing area, the area defined by projecting that portion of the store installation beneath the wing vertically upon the wing chord plane, $in.^2$
a.c.	=	Aerodynamic center of a body, in.
NP	=	Aircraft neutral point location relative to the aircraft wing leading edge at the MGC, in.
MER	=	Multiple ejector rack.
TER	=	Triple ejector rack.
$C_{L_{\alpha_S}}$	=	Lift curve slope of an isolated store, per degree.
$C_{L_{\alpha_A}}$	=	Lift curve slope of an aircraft model, per degree.

LIST OF FIGURES AND TABLES

Figures

Figure No.	Title
1.	Model Installation - F-4 Aircraft
2.	Model Installation - A-7 Aircraft
3.	Drag Correlation - BXX Factor
4.	Drag Correlation - Effect of Longitudinal Location
5.	Neutral Point Correlation - Store C_{L_α} Adjustment
6.	Drag Prediction Accuracy
7.	Side Force Prediction Accuracy
8.	Lift Prediction Accuracy
9.	Yawing Moment Prediction Accuracy
10.	Neutral Point Prediction Accuracy
11.	Summary of Technique Capabilities

Table

I	Program Variables

INTRODUCTION

Performance analysts are continually faced with the problem of determining the interference flow field between the attack aircraft and its external stores for mission analyses. The inability to predict the interference performance losses is particularly evident when considering the non-linear aerodynamic effects in the transonic speed regime. There are no known theoretical techniques available which predict aircraft performance while carrying external stores in the complex flow field. Therefore, the Air Force Flight Dynamics Laboratory (AFFDL) initiated a program in 1970 to determine if it was possible to determine the symmetric forces and moments on attack aircraft in the subsonic, transonic, and supersonic speed regimes, by developing empirically based methods from existing data. The results of the effort described in AFFDL TR-72-24 entitled, "Technique Development for Predicting External Store Aerodynamic Effects on Aircraft Performance", displayed the fact that it is feasible to develop prediction techniques with reasonable accuracies (10-20 percent of the incremental load) for the lift, drag, and pitching moment terms. While these accuracies were considered generally good within the limitations imposed by the data available for method development, areas existed where improvements were needed. Consequently the AFFDL initiated a follow-on program with LTV Aerospace Corporation, Vought Systems Division to refine and extend the range of application of the original baseline prediction techniques and to develop new techniques for side force and yawing moment. The follow-on effort had as its objectives to develop prediction methods for all aerodynamic performance variables and to increase the accuracy and extend the applicability of the initial programs techniques. In addition, AFFDL desired a performance prediction method that could be applied to both single and multiple carriage for both wing and fuselage mounted stores and a method capable of predicting the influence of partially loaded multiple store rack installations on aircraft performance. This paper briefly describes the results of the current effort and presents the equations developed, emphasizing the important variables, and presents some of the significant findings.

DISCUSSION

At the initiation of this program, a literature search was performed whose objective was to gather specific types of data identified as needed from the previously mentioned 1970 effort. The original baseline techniques were developed from existing data and the definite shortage of data imposed limitations on accuracies and capabilities. In this program specific areas of data deficiency were concentrated on. These data concentrated on higher Mach number, wing sweep, and angle-of-attack data as well as conformal stores data. As the result of this literature search and data retrieval an aerodynamic data catalog on both aircraft and store installation airloads was compiled for many tactical aircraft. These data are indexed according to data type(s), aircraft type(s), store type(s), etc. accompanied by the corresponding title of the reference. The catalog contains some 600 references. This data catalog is a valuable tool for obtaining airloads data on arbitrary aircraft/store configurations. This data index is included in the final report of the subject program which is available through the Air Force.

The data from the literature search did not permit independent variable isolation due to more than one test variable changing at a time. Therefore, two wind tunnel tests were performed to systematically "isolate" the variable effects. One major problem associated with correlating existing data from the literature is that these data entail different aircraft/store configurations and flight conditions. Therefore, the parametric wind tunnel tests enabled the engineer to control the aircraft configurations and testing parameters for the explicit purpose of better defining correlation parameter influence. The tests were performed on five percent scale models of the A-7 and F-4 aircraft. The stores and racks were identical for both models, as well as the test conditions. The tests were performed in the Arnold Engineering and Development Center four foot trisonic test facility. From the testing, both parent model and store pylon installation loads were obtained by use of strain gage balances. Fig. 1 and 2 are photographs of typical installations of the F-4 and A-7 aircraft in the test section. Fig. 1 displays the various store stations tested on the F-4, with clean pylons visible on the left wing (inboard and outboard stations) as well as the fuselage centerline. A fully loaded MER with M-117 bombs is discernable on the right wing inboard station. Parent aircraft data were obtained in the wind tunnel test for many different variable changes, Table I summarizes the types of conditions tested for each aircraft. The main geometry test variables included spanwise store location shifts, pylon height variations, chordwise movement of the store-pylon installation relative wing, store chordwise shifts relative to pylon, store nose bluntness, and adjacent store variations. As can be seen from Table I a wide variety of flight conditions, aircraft/store configurations and store/rack types were considered. This

broad variable coverage was tested due to the desirability of isolating and ranging as many primary interference variables as possible in the limited test time provided. The A-7 and F-4 aircraft models were chosen as candidate airplanes due to their availability, performance capability differences, and configuration differences. These aircraft were also chosen for testing because of the extensive amount of existing data on these two systems for the parameters analyzed.

From the airloads data obtained in the wind tunnel test and from the data survey effort, detailed data correlations were performed with identification of pertinent correlation variable trends. Prediction techniques were then developed based on the previous correlations. The following sections give the final developed equations for each of the performance variables.



Figure 1 Model Installation - F-4 Aircraft



Figure 2 Model Installation - A-7 Aircraft

TABLE I

TEST PROGRAM VARIABLES

A-7 and F-4 Aircraft Models

- FLIGHT CONDITION - (WIND TUNNEL AND FLIGHT TEST DATA)
  - Angle of Attack - -4 to + 16 Degrees
  - Angle of Sideslip - -8 to + 8 Degrees
  - Mach Number - 0.6 to 1.2, 1.6, and 2.0
  - Reynolds Number - 3.9 to 4.9 X 10^6/ft
- AIRCRAFT-STORE INSTALLATION DESIGN -
  - Relative Wing-Fuselage Design
  - Wing or Fuselage Mounted
  - Tangent or Pylon Mounted
  - Relative Spanwise, Vertical or Longitudinal Placement
  - Adjacent Store Presence
  - Horizontal Tail Influence
- STORE AND RACK DESIGN -
  - Store Diameter
  - Store Type
  - Nose Bluntness
  - Rack Type (MER, TER, Single)
- Loading Arrangements -
  - Wing Stations - Six (A-7); Four (F-4)
  - Fuselage C_L Stations - Two (A-7); One (F-4)
  - Symmetrical and Unsymmetrical
  - With/Without Adjacent Stores

PREDICTION EQUATIONS:

In the following paragraphs the prediction equations will be summarized for all the performance variables. However, only the drag force and neutral point prediction equations will be presented in sufficient detail to enable the reader to understand the technique development.

Drag Equations:

The basic technique approach for the drag equation, consists of obtaining incremental drag "build-ups" to account for each of the various store installation hardware items carried externally on the aircraft model such as pylon, rack, store, etc. The summation of these drag increments yields the individual store installation drag contribution. These drag contributions for all individual store installations can be combined with the clean aircraft drag to determine the total aircraft-with-stores drag. The method presented here is an extension to that developed earlier. The additional data from the wind tunnel program permitted a more comprehensive correlation to improve accuracy and include additional types of store carriage. The present method has equations for the following aircraft-store installation cases: wing pylon-mounted single and multiple stores, fuselage tangent-mounted single and multiple stores, and fuselage pylon-mounted single and multiple stores. A more detailed explanation of this buildup is provided in the following delineation which explains the drag make-up for generalized aircraft-with-stores configurations. Consider aircraft with external store installations in a steady-state flight condition, that is, in equilibrium flight at a constant altitude and speed. The total aircraft-with-stores drag coefficient for this steady state flight condition is:

$$C_{D_{TOTAL}} = DRAG_{\substack{AIRCRAFT \\ WITH \\ STORES}} / (q \cdot S_{REF})$$

The equations developed for each loading case are presented below in generalized form as Equations (1) through (6). In each of the equations presented the value calculated is the incremental drag coefficient due to the addition of the store installation to the aircraft. Remember, our definition of store installation is any armament-associated hardware which are external to the clean aircraft. Thus an empty pylon or a pylon with an empty MER/TER rack is considered a store installation. The K-terms used in defining some of the equation terms identify that an equation or relationship has been developed to account for that specific variable.

Case 1: Wing Pylon-Mounted Single Store(s)

$$\Delta C_{D_{\substack{\text{Store}\\\text{Installation}}}} = \Delta C_{D_{o_{\text{Pylon}}}} + \Delta C_{D_{o_{\substack{\text{Pylon-}\\\text{Rack}}}}} + \Delta C_{D_{o_{\substack{\text{Isolated}\\\text{Store}}}}} + \Delta C_{D_{\substack{\text{Pylon-Store-}\\\text{Aircraft}\\\text{Interference}}}} + \Delta C_{D_{o_{\substack{\text{Adjacent Store}\\\text{Interference}}}}} + \Delta C_{D_{o_{\substack{\text{Adjacent}\\\text{Fuselage}\\\text{Interference}}}}} + \Delta C_{D_{i_{\substack{\text{Drag Due}\\\text{to Lift}}}}} \quad (1)$$

Case 2: Wing Pylon-Mounted Multiple Stores

$$\Delta C_{D_{\substack{\text{Store}\\\text{Installation}}}} = \Delta C_{D_{o_{\text{Pylon}}}} + \Delta C_{D_{o_{\substack{\text{Pylon-}\\\text{Rack}}}}} + \Delta C_{D_{o_{\substack{\text{Store-}\\\text{Rack}}}}} + \Delta C_{D_{o_{\substack{\text{Sway}\\\text{Braces}}}}} + N_{\substack{\text{No. of}\\\text{Stores}}} \cdot \Delta C_{D_{o_{\substack{\text{Isolated}\\\text{Store}}}}} + \Delta C_{D_{o_{\substack{\text{Store-Rack-}\\\text{Aircraft}\\\text{Interference}}}}} + \Delta C_{D_{o_{\substack{\text{Adjacent}\\\text{Store}\\\text{Interference}}}}} + \Delta C_{D_{o_{\substack{\text{Adjacent}\\\text{Fuselage}\\\text{Interference}}}}} + \Delta C_{D_{i_{\substack{\text{Drag Due}\\\text{to Lift}}}}} \quad (2)$$

Case 3: Fuselage Tangent-Mounted Single Store (s)

$$\Delta C_{D_{\substack{\text{Store}\\\text{Installation}}}} = \Delta C_{D_{o_{\substack{\text{Isolated}\\\text{Store}}}}} \cdot K_{\substack{\text{No. of}\\\text{Stores}}} \cdot K_{\substack{\text{Wing-Fuselage}\\\text{Position}}} \cdot K_{\substack{\text{Store}\\\text{Tandum}\\\text{Spacing}}} \cdot K_{\substack{\text{Store}\\\text{Lateral}\\\text{Spacing}}} \cdot K_{\substack{\text{No. of}\\\text{Store}\\\text{Rows}}} \cdot K_{\substack{\text{No. of}\\\text{Stores}\\\text{Per Row}}} \quad (3)$$

Case 3 (Cont'd)

$$\cdot K_{\substack{\text{Store}\\\text{Longitudinal}\\\text{Location}}} + N_{\substack{\text{No. of}\\\text{Stores}}} \cdot \Delta C_{D_{o_{\substack{\text{Fuselage}\\\text{Rack}}}}}$$

Case 4: Fuselage Tangent-Mounted Multiple Stores

$$\Delta C_{D_{\substack{\text{Store}\\\text{Installation}}}} = \Delta C_{D_{o_{\substack{\text{Store}\\\text{Rack}}}}} + \Delta C_{D_{o_{\substack{\text{Sway}\\\text{Braces}}}}} + N_{\substack{\text{No. of}\\\text{Stores}}} \cdot \Delta C_{D_{o_{\substack{\text{Isolated}\\\text{Store}}}}} \cdot (1 + K_{\substack{\text{Store-Rack-}\\\text{Aircraft}\\\text{Interference}}}) \quad (4)$$

Case 5: Fuselage Pylon-Mounted Single Store(s)

$$\Delta C_{D_{\substack{\text{Store}\\\text{Installation}}}} = \Delta C_{D_{o_{\substack{\text{Isolated}\\\text{Store}}}}} \cdot K_{\substack{\text{No. of}\\\text{Stores}}} \cdot K_{\substack{\text{Wing-}\\\text{Fuselage}\\\text{Position}}} \cdot K_{\substack{\text{Store}\\\text{Tandum}\\\text{Spacing}}} \cdot K_{\substack{\text{Store}\\\text{Lateral}\\\text{Spacing}}} \cdot K_{\substack{\text{No. of}\\\text{Store}\\\text{Rows}}} \cdot K_{\substack{\text{No. of}\\\text{Stores}\\\text{per Row}}} \cdot K_{\substack{\text{Store}\\\text{Longitudinal}\\\text{Location}}} \cdot K_{\substack{\text{Store}\\\text{Depth}}} \cdot K_{\substack{\text{Pylon}\\\text{Depth}}} + (\Delta C_{D_{o_{\substack{\text{Pylon}}}}} + \Delta C_{D_{o_{\substack{\text{Fuselage}\\\text{Rack}}}}}) \cdot N_{\substack{\text{No. of}\\\text{Stores}}} \quad (5)$$

Case 6: Fuselage Pylon-Mounted Multiple Stores

$$\Delta C_{D_{\substack{\text{Store}\\\text{Installation}}}} = \Delta C_{D_{o_{\substack{\text{Pylon}}}}} + \Delta C_{D_{o_{\substack{\text{Pylon-}\\\text{Rack}}}}} + \Delta C_{D_{o_{\substack{\text{Store}\\\text{Rack}}}}} + \Delta C_{D_{o_{\substack{\text{Sway}\\\text{Braces}}}}} \quad (6)$$

Case 6 (Cont'd)

$$+ N_{\substack{\text{No. of}\\ \text{Stores}}} \cdot \Delta C_{D_{\substack{\text{Isolated}\\ \text{Store}}}}$$

Some identical terms appear in both the wing mounted (Equations (1) and (2) and fuselage mounted(Equations (3) and (5) store cases. This is the result of numerous commonalities in pylon-store geometry and placement that are relatively independent of whether the store installation involves a single, multiple, pylon or tangent mounting arrangement. By proper summation of the drag increments (from Equations (1) through (6) into Equation (7) below, the total drag coefficient of the aircraft with stores can be determined.

$$C_{D_{\substack{\text{Aircraft with}\\ \text{Stores}}}} = C_{D_{\substack{\text{Clean}\\ \text{Aircraft}}}} + \sum_{i=1}^{N_I} \left(\Delta C_{D_{\substack{\text{Store}\\ \text{Installation}}}}\right) \qquad (7)$$

where N_I is the total number of store installations.

Empirical curves are provided to permit the engineer to manually determine the incremental performance values. The general nature of the correlation efforts and the variables involved in evaluating the various drag contributors are suggested by an examination of Figures 3 and 4. Figure 3 is the basic correlation for predicting the pylon drag increment for wing and fuselage pylon-mounted single and multiple store cases. As evident from the figure, the geometric and flight condition variables involved in deriving the correlation are the pylon frontal area (height and thickness) and Mach number. The data presented in this figure represent slopes of the parameter BXX as a function of pylon thickness-to-length ratio. Therefore, the parameter BXX can be computed for many values of pylon thickness to length ratio. The aerodynamic data used in developing Figure 3 involves ten different aircraft types selected to encompass as many variables as possible, i. e., spanwise and longitudinal armament station location, relative wing-fuselage position, etc. Wind tunnel test data points for the A-7 and F-4 aircraft are shown in this figure. The correlation shown in Figure 4 predicts the single store drag increment due to longitudinal location along the wing chord. Test data for MK-84, 300 tank and Mk-82 stores carried on A-7 and F-4 aircraft models are shown in this figure. These data are for pylon heights of 11.5, 17.0 22.6 and 28.2 inches. In summarizing the total correlation task involved in the development of the resultant drag equations, over 70 final correlation plots involving approximately 240 data curves were prepared.

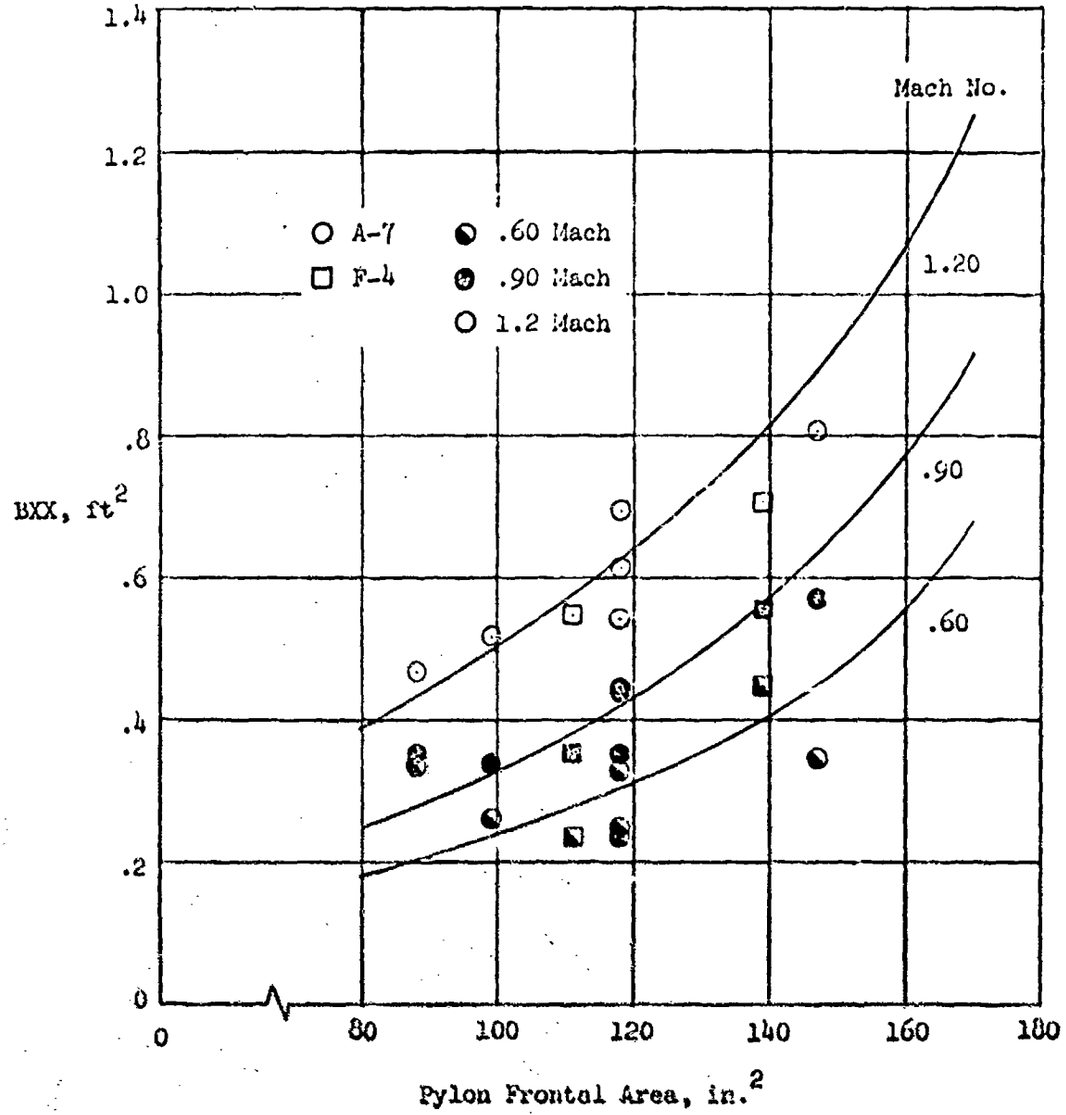


Figure 3. Drag Correlation - BXX Factor

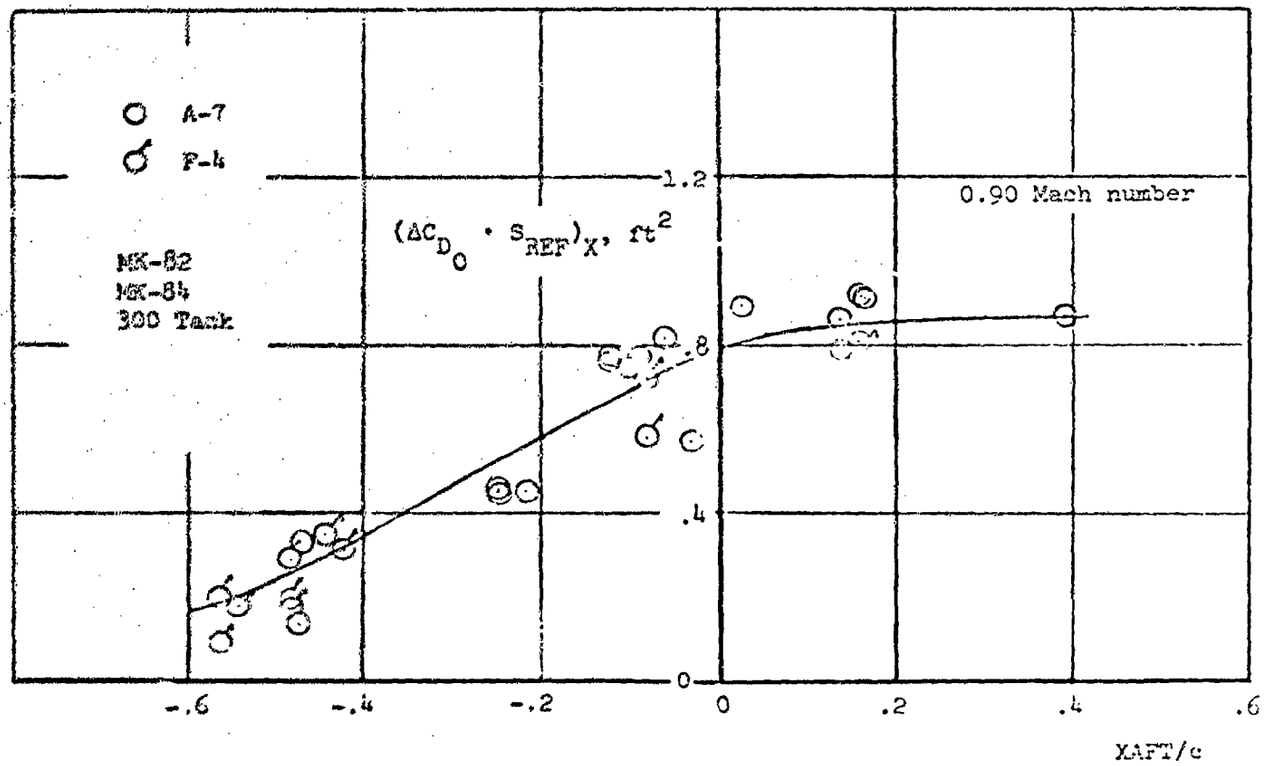


Figure 4. Drag Correlation - Effect of Longitudinal Location

Neutral Point Equations:

The neutral point of an aircraft defines the longitudinal position of the aircraft center of lift. The neutral point, NP, position relative to the aircraft center of gravity can be used with the lift coefficient to determine the aircraft pitching moment. The aircraft-store loading types to which the method applies include wing pylon-mounted single and multiple loadings as well as fuselage pylon and tangent mounted single and multiple loadings.

The equations were developed entirely from wind tunnel data for various symmetrically loaded aircraft. The correlation approach is basically the same as the previously developed effort. However, the expanded data base has provided the increased capabilities herein.

The basic definition of neutral point is as follows:

$$NP = X_{c.g.} - \bar{c} \left(\frac{dC_m}{dC_L}\right), \text{ inches} \tag{8}$$

where $X_{c.g.}$ = Aircraft c.g. location relative to the leading edge of the mean geometric chord, inches.

$\left(\frac{dC_m}{dC_L}\right)$ = Slope of the $C_m - C_L$ curve for the particular configuration.

The neutral point can be broken into parts given by

$$(NP)_{\substack{\text{Aircraft} \\ \text{with Stores}}} = (NP)_{\text{Clean A/C}} + \Delta(NP)_{\text{Stores}} \tag{9}$$

$\Delta(NP)_{\text{Stores}}$ is to be separated into three parts defined as follows:

$\Delta(NP)_1$ - An increment obtained by transferring the lifting characteristics of the various stores to the clean aircraft aerodynamic center.

$\Delta(NP)_2$ - An increment due to the interference effects of the store configuration on the wing flow field.

$\Delta(NP)_3$ - An increment developed from a gain/loss of horizontal tail effectiveness generated by the store loading.

The developed equations for the individual increments are as follows:

$$\Delta(NP)_1 = \frac{\sum_{i=1}^{N_I} \sum_{j=1}^{N_{S_i}} \left(C_{L_{\alpha_{S_{ij}}}}\right)_{INST} \cdot \left[X_{S_{ij}} - X_{A/C}\right]}{\left(C_{L_\alpha}\right)_{A/C} + \sum_{i=1}^{N_I} \sum_{j=1}^{N_{S_i}} \left(C_{L_{\alpha_{S_{ij}}}}\right)_{INST}} \qquad (10)$$

$$\Delta(NP)_2 = \delta\,(S_{REF}) \left\{ \sum_{i-1}^{N_I} \sum_{1}^{\dot{N}_{S_i}} \left(C_{L_{\alpha_{S_{ij}}}}\right)_{\infty} \right\} \cdot \left\{ \sum_{i=1}^{N_I} \right. \qquad (11)$$

$$\left. \left[\Delta(NP)_{2_{BASIC}} + K_1\,(\bar{y}_i) \cdot K_2\,(\bar{X}_{ML_i}) \cdot K_3\,(M)\right] \right\} / N_I$$

$$\Delta(NP)_3 = \sum_{i=1}^{N_I} \left[\Delta(NP)_{3_{BASIC}}\right]_i \cdot K_1\,(\bar{y}_{T_i}) \cdot K_2\,(\bar{Z}_{T_i}) \qquad (12)$$

Where N_I = Number of store installations on the aircraft.

N_{S_i} = Number of stores on installation i.

$X_{S_{ij}}$ = Distance from aerodynamic center of store j on store installation i to the leading edge of the aircraft mean geometric chord (the aerodynamic center of each store is assumed to be its mid-lug point).

$X_{A/C}$ = Aerodynamic center of clean aircraft.

$\left(C_{L_{\alpha_{S_{ij}}}}\right)_{INST}$ = Installed value of C_{L_α} of store j on store installation i (The subscript "∞" implies freestream value).

$C_{L_{\alpha_{A/C}}} = C_{L_\alpha}$ of clean aircraft.

$\bar{y}_i$ = Span location of installation i (non-dimensional with respect to wing semi-span).

$\bar{X}_{ML_i}$ = Distance from local wing leading edge to mid-lug point of store installation i (non-dimensional with respect to the local wing chord).

$\bar{y}_{T_i}$ = Span location of store installation i (non-dimensional with respect to horizontal tail semi-span).

$\bar{Z}_{T_i}$ = Distance from wing lower surface to horizontal tail mid-line of store installation i (non-dimensional with respect to local wing chord).

The functions $\Delta(NP)_{2_{BASIC}}$ and $\Delta(NP)_{3_{BASIC}}$ are correlation curves which depend upon loading type and Mach number while the functions K_1, K_2, and K_3 are correction factors which depend on the independent variable cited.

The major portion of the correlation effort was devoted to the $\Delta(NP)_1$ term. This increment is analytical in concept and represents the transfer of the lifting characteristics of each store to the clean aircraft aerodynamic center.

One of the most difficult and time consuming developmental efforts on $\Delta(NP)$, was for the calculation of installed store C_{L_α}. These quantities were calculated as follows:

$$\left(C_{L_{\alpha_{S_{ij}}}}\right)_{INST} = K_{S_{ij}} \left(C_{L_{\alpha_{S_{ij}}}}\right)_{\infty} \qquad (13)$$

Where $\left(C_{L_{\alpha_{S_{ij}}}}\right)_{\infty}$ is the freestream value of the store C_{L_α} curve and $K_{S_{ij}}$ is a correction factor to produce the installed value. K_S depends on the store position relative to the aircraft wing, store geometry, and Mach number. Figure 5 gives the variation of K_S at M = 0.6 with the distance from the local wing leading edge to the store nose. Note the large variation in K_S for stores placed on MER shoulder stations. In fact, negative values of K_S are common. However, in absolute magnitude, the aft store stations have K_S

values approximately half the forward stations. The data points which do not agree well with the faired curve were brought into line with a pylon height correction.

The $\Delta(NP)_2$ term assesses the effects of the store installation on the aircraft flow field. This term is difficult to develop directly due to the large number of significant independent variables. For this reason this increment was developed in a strictly empirical fashion. The equation indicates the influence of four basic variables: Mach number, store size, store longitudinal position, and store spanwise location. Both $\Delta(NP)_2$ and K_3 depend on Mach number

$$\left(C_{L_{\alpha_{S_{ij}}}}\right)_{\infty_{BASIC}}$$

while K_1 and K_2 are functions of span location and position relative to the wing leading edge respectively. The effects of store size are reflected in the $\left(C_{L_{\alpha_{S_{ij}}}}\right)_{\infty}$ terms.

The horizontal tail increment, $\Delta(NP)_3$, was developed from an extremely limited data base (A-7 and F-4 aircraft). Evaluating this increment for specific aircraft configurations is often difficult. Finding enough data to correlate a general method was not possible. Tail effects data were not included in the wind tunnel program because of compromises necessary to meet tunnel allocations. This term depends on Mach number ($\Delta(NP)_{3_{BASIC}}$) and position of the store installation relative to the horizontal tail. Although these parameters are certainly reasonable, insufficient data were available to precisely define their effect. Care must be exercised in applying this correction to aircraft having tail spans and longitudinal and vertical tail locations differing substantially from the two reference aircraft. However, even with the neutral point method limitations, quite acceptable results were obtained as will be seen later in the "Accuracy" section.

$$K_S \equiv \frac{(C_{L_{\alpha_S}})_{INSTALLED}}{(C_{L_{\alpha_S}})_{\infty}} \qquad \bar{X}_{SN} \equiv \frac{\text{Dist. from local wing L.E. to store nose}}{\text{Local wing chord}}$$

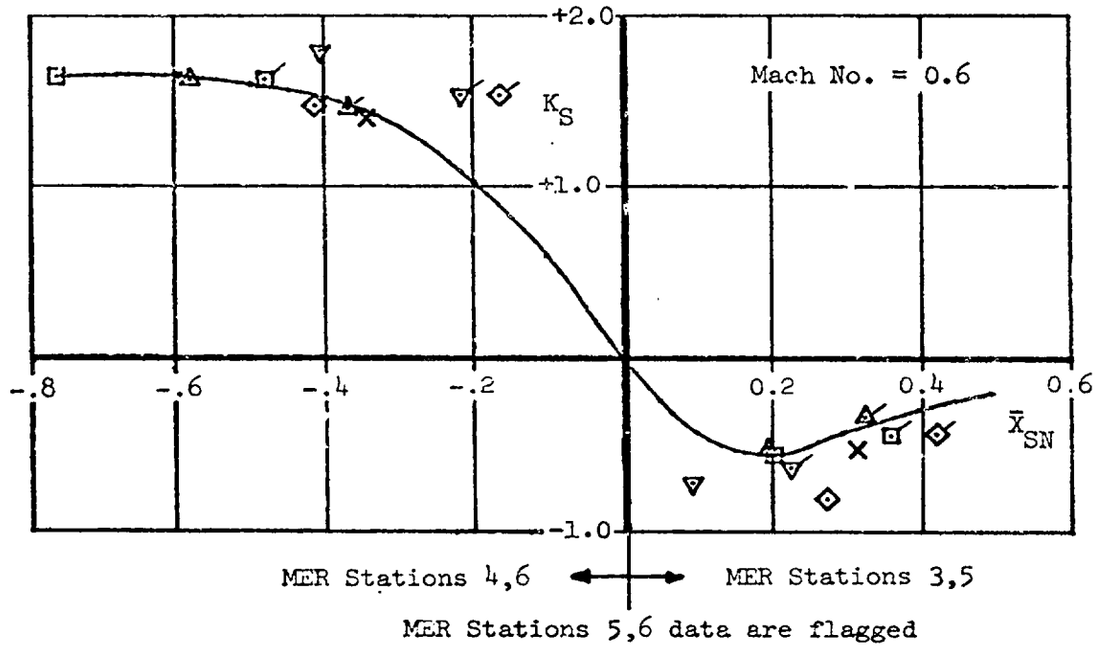


Figure 5. Neutral Point Correlation - Store C_{L_α} Adjustment, MER Shoulder Stations

Lift, Side Force and Yawing Moment Equations:

Time only permits presenting a summary of the developed performance equations for the lift force, side force and yawing moment, accompanied by a brief definition of what variables are in each equation.

Lift Force Equations:

The general form of the lift coefficient equations for an aircraft with stores configuration is the algebraic sum of the clean aircraft lift coefficient and the increments due to all store installations carried i.e.,

$$C_{L_{\substack{\text{Aircraft}\\\text{With}\\\text{Stores}}}} = C_{L_{\text{Clean}}} + \Delta C_{L_{\substack{\text{Store}\\\text{Installations}}}} \qquad (14)$$

The incremental lift due to all store installations consists of the sum of the individual lift effects from each pair of symmetrical store installations. The prediction equations for the various loading cases are presented below.

Wing-Mounted Single Stores:

$$\Delta C_{L_{\substack{\text{STORE}\\\text{INSTALLATION}}}} = \Delta C_{L_{\text{BASIC}}} (K_{\Lambda} \cdot K_{\text{PYLON}} + K_{\text{FUSE}}) + \Delta C_{L_{\alpha}} (\alpha - 4) \qquad (15)$$

Wing-Mounted Multiple Stores:

$$\Delta C_{L_{\substack{\text{STORE}\\\text{INSTALLATION}}}} = (\Delta C_{L_{\text{BASIC}}} + \Delta C_{L_{\substack{\text{LONGIT}\\\text{EFFECT}}}} \cdot K_{AWA}) \cdot (K_{\Lambda} \cdot K_{\text{PYLON}} + K_{\text{FUSE}}) + \Delta C_{L_{\alpha}} (\alpha - 4) \qquad (16)$$

Fuselage-Mounted Stores:

$$\Delta C_{L_{\substack{\text{STORE}\\\text{INSTALLATION}}}} = \Delta C_{L_{\text{BASIC}}} (K_{\text{WING}} \cdot K_{\text{SPAN}}) + \Delta C_{L_{\alpha}} (\alpha - 4) \qquad (17)$$

Where $\Delta C_{L_{\text{BASIC}}}$ = Basic lift effect of the store installation at 4° angle of attack. The term is a function of store installation type, store installation planform, location and Mach number.

K_{Λ} = Parameter to account for aircraft wing sweep effect, function of wing leading edge sweep and store installation.

K_{PYLON} = Parameter to account for pylon height effect; function of pylon height, store installation location and Mach number.

K_{FUSE} = Parameter to account for the effect of store installation proximity to the fuselage, function of minimum lateral clearance between the store installation and the side of the fuselage and Mach number.

$\Delta C_{L_{\alpha}}$ = Effect of aircraft angle of attack relative to the reference case of 4^{0} , function of store installation location and Mach number.

$\Delta C_{L_{LONGIT\ EFFECT}}$ = Effect of longitudinal location of multiple-mounted stores along the local wing chord; function of store installation planform and location, and Mach number.

K_{AWA} = Longitudinal location factor; function of store longitudinal placement on the aircraft wing, local wing chord and Mach number.

K_{WING} = Parameter to account for the effect of wing location on the fuselage, function of the percent of fuselage height from the top of the fuselage to the wing center line at the chord plane.

K_{SPAN} = Parameter to account for the effect of lateral placement of the store installation, function of percent distance from the fuselage center line to the side of the fuselage.

Side Force Equation:

As a result of the small quantities of correlatable data available on other aircraft-store configurations, the correlations are predominately based on F-4 and A-7 experimental data. Those data were almost exclusively obtained at an angle of attack of 5 degrees for the angle of yaw range of -6 to +8 degrees. Equations were developed for essentially all conventional store installation cases. The resultant equations will predict either the incremental aerodynamic effect of the store installation or the combined aircraft

with stores configuration. The store loading cases for which these equations are applicable are: wing pylon mounted single and multiple stores and fuselage pylon and tangent mounted single and multiple stores. The procedure was developed on the concept of combining individual effects to predict the resultant side force. The general form of the prediction equation for a reference angle of attack is presented below.

$$\Delta C_{Y_{\substack{\text{STORE} \\ \text{INSTALLATION}}}} = (\Delta C_Y)_{BASE} + (\Delta C_Y)_{Z\ BASIC} + (\Delta C_Y)_X + (\Delta C_Y)_Y \cdot K_M + (\Delta C_Y)_{\substack{\text{STORE-TO-STORE} \\ \text{INTERFERENCE}}} \quad (18)$$

$(\Delta C_Y)_{BASE}$ = Base side force coefficient computed for a reference spanwise and longitudinal store location and flight condition, f(ψ, store diameter, store fin span, store fin configuration, rack type, store cluster span, store-to-store spacing within a cluster)

$(\Delta C_Y)_Z$ = Effect of pylon height, f(pylon height, stores installation type, ψ)

$(\Delta C_Y)_X$ = Effect of store longitudinal placement along the local wing chord, f(store diameter, store installation type, longitudinal location of the store, $\Delta C_{Y_{BASE}}$, ψ)

$(\Delta C_Y)_Y$ = Effect of store spanwise location on the wing, f (store installation depth, spanwise location of the store, ψ)

K_M Effect of Mach number relative to a reference Mach number of 0.60, f(Mach number, spanwise location of the store)

$\Delta C_{Y_{\substack{\text{STORE-TO-} \\ \text{STORE} \\ \text{INTERFERENCE}}}}$ = Effect of mutual interference due to adjacent store installations, f(Mach number, relative longitudinal location of adjacent stores, relative spanwise location of adjacent stores, length of adjacent stores, ΔC_Y computed for each of the adjacent store installations)

By using the store installation component build-up feature of these equations, the incremental side force contribution of pylons alone, the pylons plus racks, or the complete store installation may be computed. Prediction of the total aircraft with stores side force coefficient is determined by summing the total increment predicted due to stores and the clean aircraft side force.

Yawing Moment Equations:

The yawing moment is considered the product of incremental store drag and side forces times a moment arm, ℓ_M. Though there is some unsymmetrical lift and drag induced by symmetric store loadings, this is normally very small and most of it can be related directly or indirectly to side force. Therefore, yawing moment has been correlated as a function of incremental side force times the moment arm, ℓ_M.

$$(\Delta C_{n_{\substack{\text{STORE} \\ \text{INSTALLATION}}}}) = (\Delta C_{Y_{\substack{\text{STORE} \\ \text{INSTALLATION}}}}) \left(\ell_M / b_{REF}\right) \tag{19}$$

The arm, ℓ_M is defined as the longitudinal distance from the airplane c.g. to the point of side force application. In this way, the incremental yawing moment contributed by an element of the store installation (store fin, nose, pylon, etc.) is the product of ℓ_M times the incremental side force due to that element.

Wind tunnel test data for metric pylons, racks, and stores were used to derive methods for predicting the distance ℓ_M. The procedure to predict the distance ℓ_M requires three basic predictions; the first involves prediction of the incremental forces acting on each individual hardware item comprising the store installation such as pylon, store nose, store fin, store rack, etc. Second, the point of force application for each of the contributing elements noted above must be predicted. Finally, the distance ℓ_M can be computed by dividing the summation of moments about the aircraft c.g. due to the predicted incremental forces described above by the sum of these same incremental forces. In equation form,

$$\ell_M = \frac{\sum_{i=1}^{I} (\Delta F_i \cdot \ell_{M_i})}{\sum_{i=1}^{I} (\Delta F_i)} \tag{20}$$

Where ΔF_i is the estimated incremental force due to an element of the store installation such as a store fin, store nose, etc., and ℓ_M is the distance from the point of force application of that incremental force predicted for the element, to the aircraft c.g. location. The variable I is the total number of elements for the given store installation.

The general form of the prediction equation for yawing moment coefficient is,

$$C_{n_{\substack{\text{AIRCRAFT}\\\text{WITH}\\\text{STORES}}}} = C_{n_{\substack{\text{CLEAN}\\\text{AIRCRAFT}}}} + \Delta C_{n_{\substack{\text{DUE TO EXTERNAL}\\\text{STORE INSTALLATIONS}}}} \qquad (21)$$

Where,

$$\Delta C_{n_{\substack{\text{DUE TO EXTERNAL}\\\text{STORE INSTALLATIONS}}}} = \sum_{i=1}^{N_I} \left(\Delta C_{n_{\substack{\text{INDIVIDUAL}\\\text{STORE INSTALLATION}}}}\right)_i + \Delta C_{n_{\text{INTERFERENCE}}} \qquad (22)$$

for N_I number of store installations carried on the aircraft. Correlation curves have been generated to obtain the incremental yawing moment due to the individual store installations and interference. That is, for a given Mach number,

$\Delta C_{n_{\substack{\text{INDIVIDUAL}\\\text{STORE}\\\text{INSTALLATION}}}}$ = Function of pylon geometry and pylon location, store geometry and store location, rack geometry and rack location, and aircraft center of gravity location.

And $\Delta C_{n_{\text{INTERFERENCE}}}$ = Function of ΔC_n for individual store installations as noted above, and their proximity to other store installations.

The equations are generally applicable to pylon-mounted stores on the wing, as well as pylon and tangent mounted stores on the fuselage. The procedure is intended primarily for symmetrical store installations.

ACCURACY:

Accuracy assessment is performed by comparing the actual test data with that predicted by the developed equations. Figs.6 to 10 provide the accuracy assessment for all the performance variables considered. Comparisons are presented for numerous wing and fuselage mounted store arrangements involving various aircraft at subsonic, transonic, and supersonic Mach numbers. Single, MER, and TER store loadings are included in the data shown.

The drag force and side force accuracies Fig.6 and 7 respectively, display overall accuracies of approximately 10 to 15 percent of the incremental value. The drag predictions are equally accurate for both single and multiple store loadings. When compared to the total aircraft airloads, these accuracies are usually much less than ± 5 percent. Prediction errors for lift (Fig. 8) are nominally 20 percent of the incremental load but only about ± 2 percent of the total aircraft lift. Similar incremental errors are noted for yawing moment (Fig. 9) as for the lift term. However, yawing moment is very dependent on the aircraft configuration of interest i.e. the distance from the aircraft center of gravity to the point of application. The neutral point shift accuracies are shown in Fig.10. Generally most of the comparison data lie within a ± 1.0 inch (full scale)error band with over 90 percent of the data within a ± 4.0 inch band. With respect to the mean geometric chord of most present day aircraft, these accuracies are generally less than ± 3 percent and usually on the order of ± 1 percent or less. As expected, the general accuracy of this method decreases with increasing Mach number, due to the flow complexity at transonic and supersonic speeds. The data indicate neutral point predictions are more accurate for the higher density loadings.

PREDICTION CAPABILITY:

Fig. 11 provides a good summary of the overall Mach number capability of the prediction methods. As noted for the performance variables, most carriage configurations display a supersonic prediction capability. In addition the methods will predict the lift for angles of attack of 0^0 to 8^0, drag and neutral point at cruise conditions (generally 2^0 to 6^0, but will provide acceptable accuracies for small variances on either side of this band) and side force and yaw at $+5^0$. The directional terms are able to be predicted for angles of sideslip between $\pm 8^0$. The method can handle high, mid and low wing aircraft, with wing leading edge sweep angles up to 75^0. The methods are applicable to any aircraft of conventional design provided no prominent flow disrupting devices exist either forward

or closely adjacent to the store stations. In general most stores can be used with and without fins. The technique can determine the interference terms for any number of store stations per aircraft side. In addition the program accounts for the interference effects between both single and multiple loadings or even mixed loadings.

Whereas the 1970 prediction method was computerized with a manual technique supplement. The performance prediction from this effort is presently in manual technique only. This will enable the compatibility engineer to observe prediction trends for his particular airplane/external store configuration.

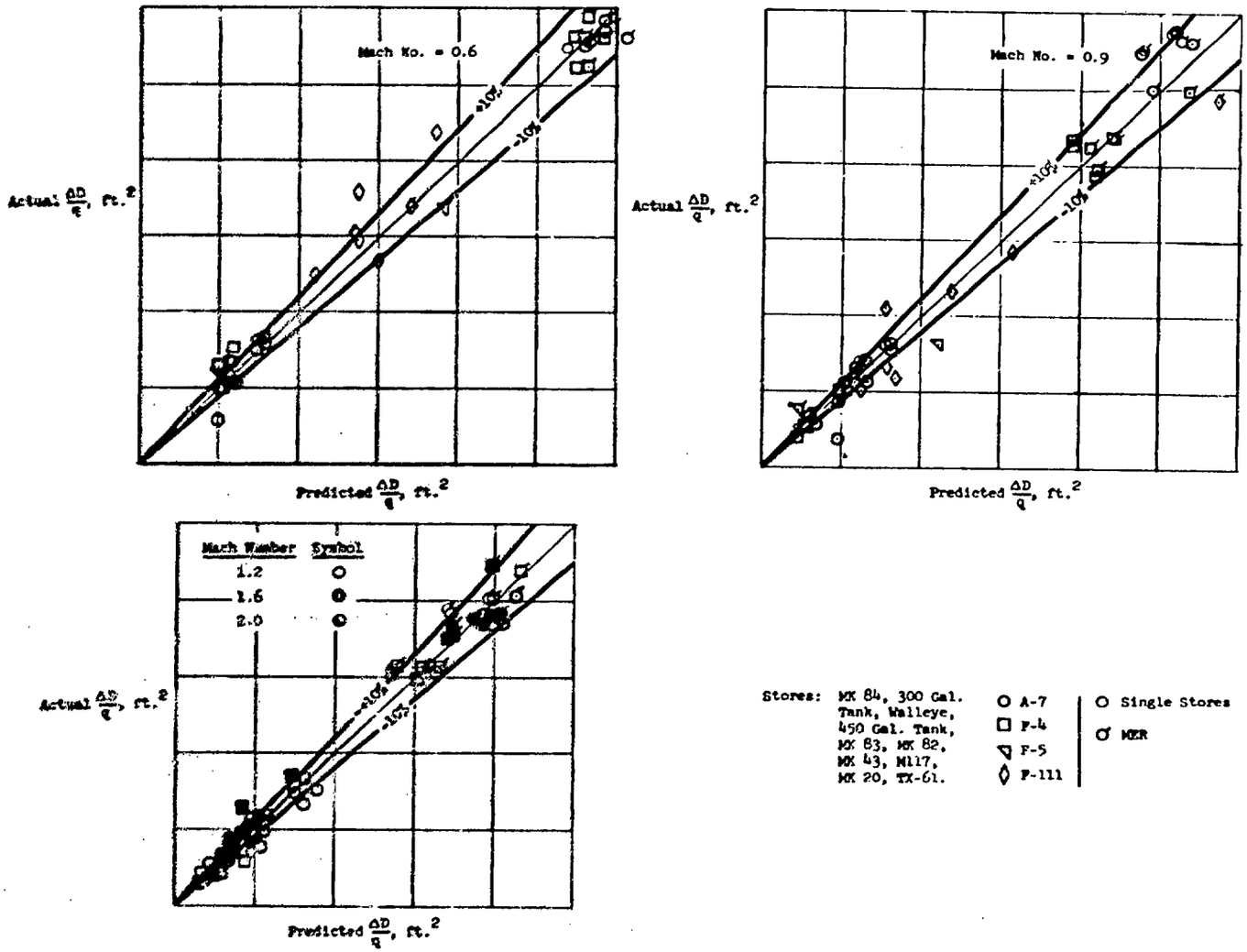


Figure 6. Drag Prediction Accuracy

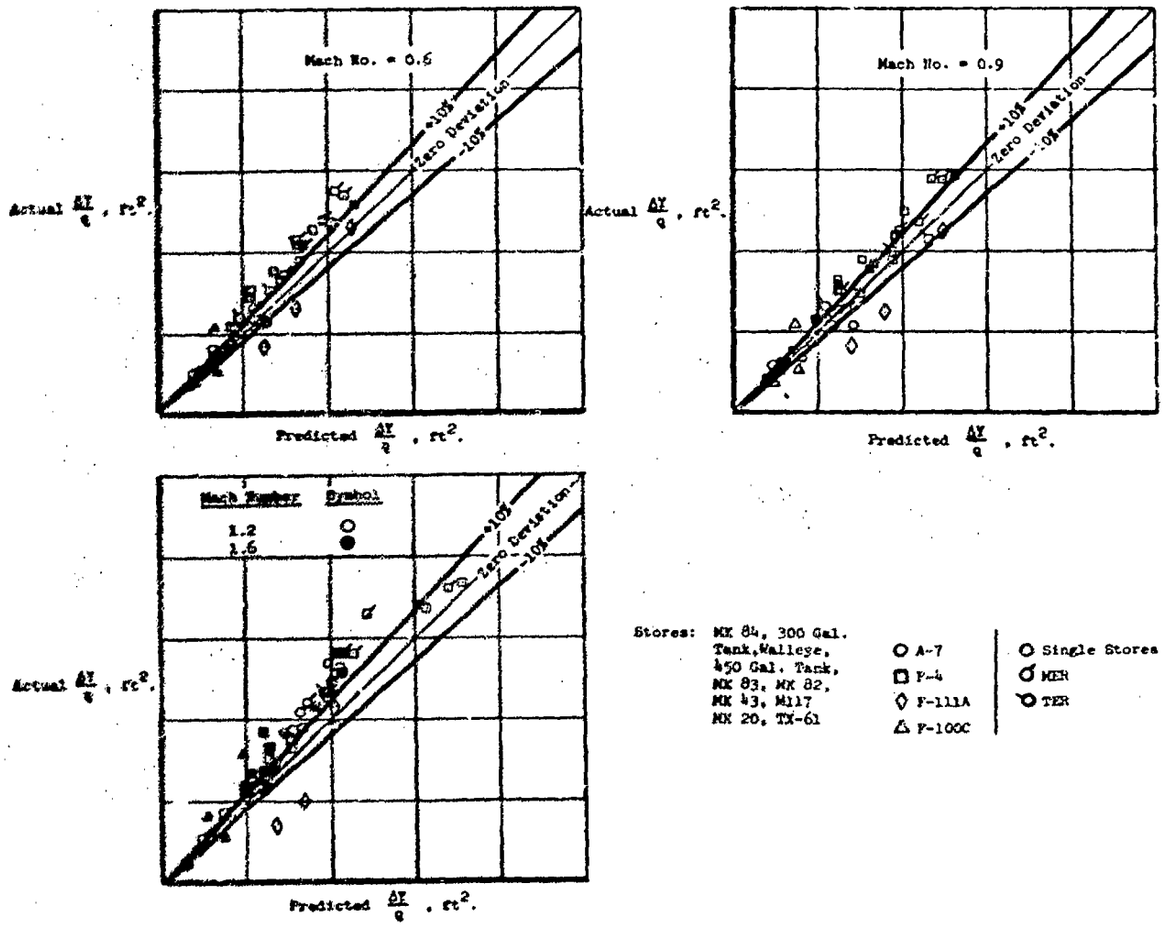


Figure 7. Side Force Prediction Accuracy

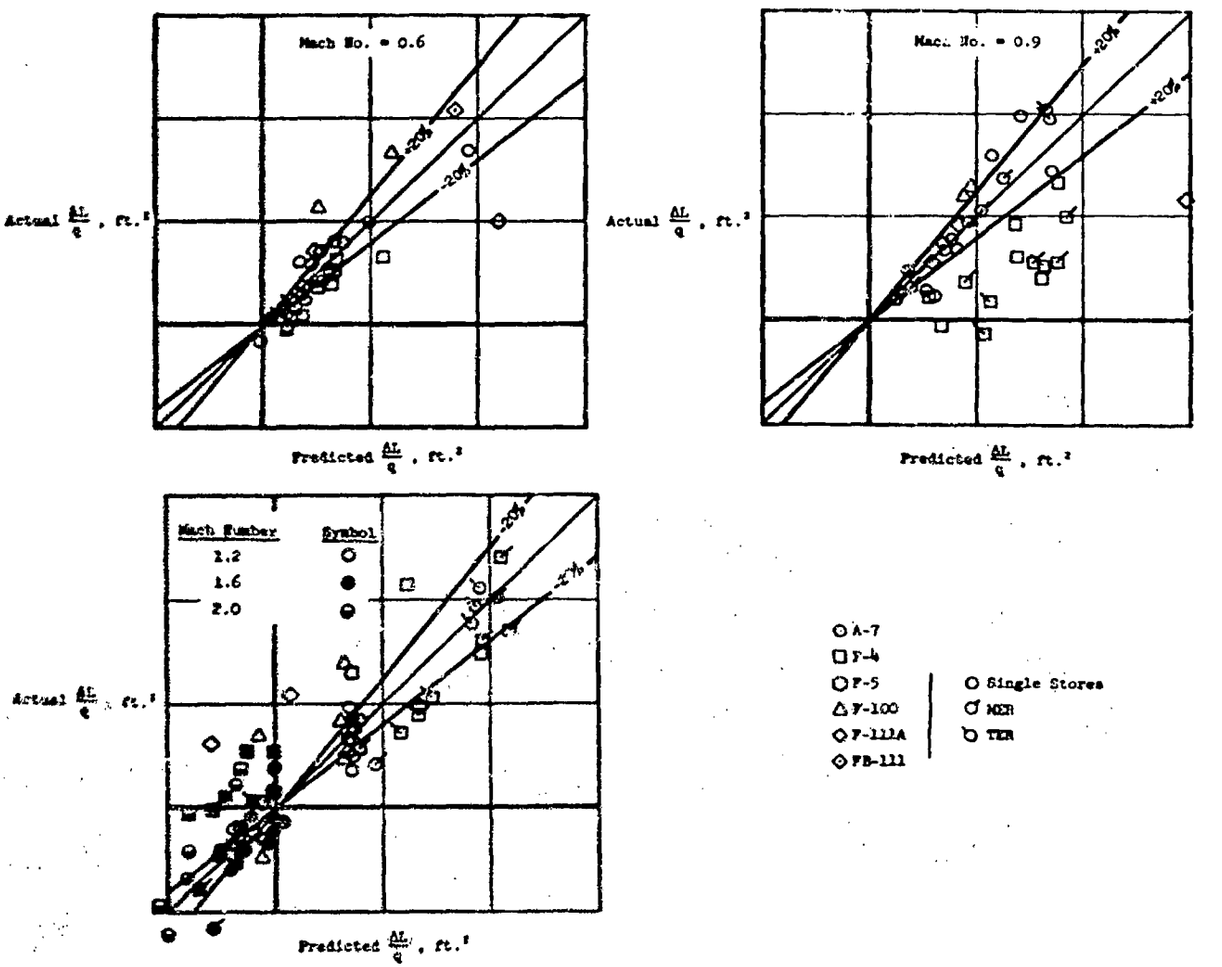


Figure 8 Lift Prediction Accuracy

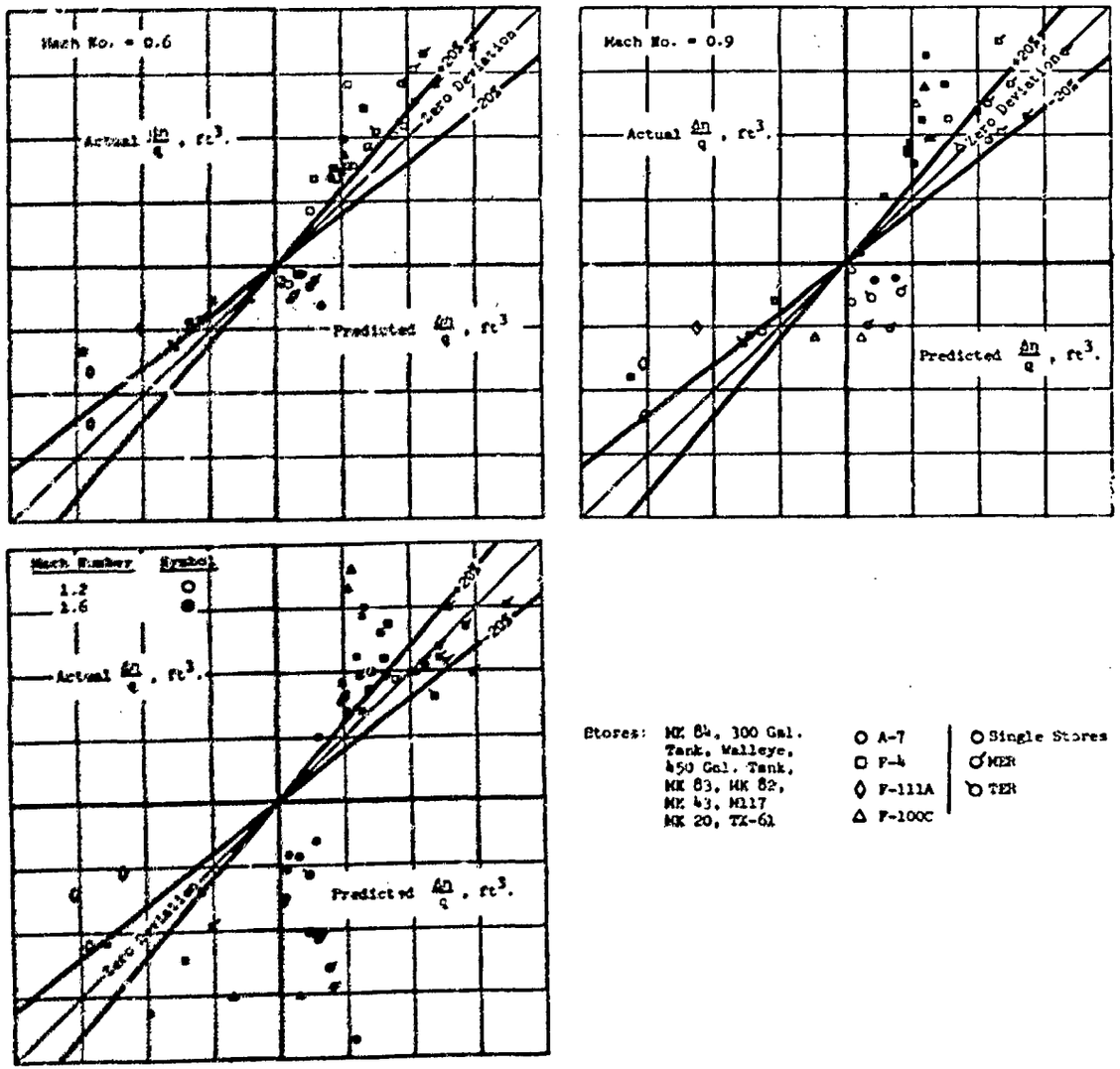


Figure 9 · Yawing Moment Prediction Accuracy

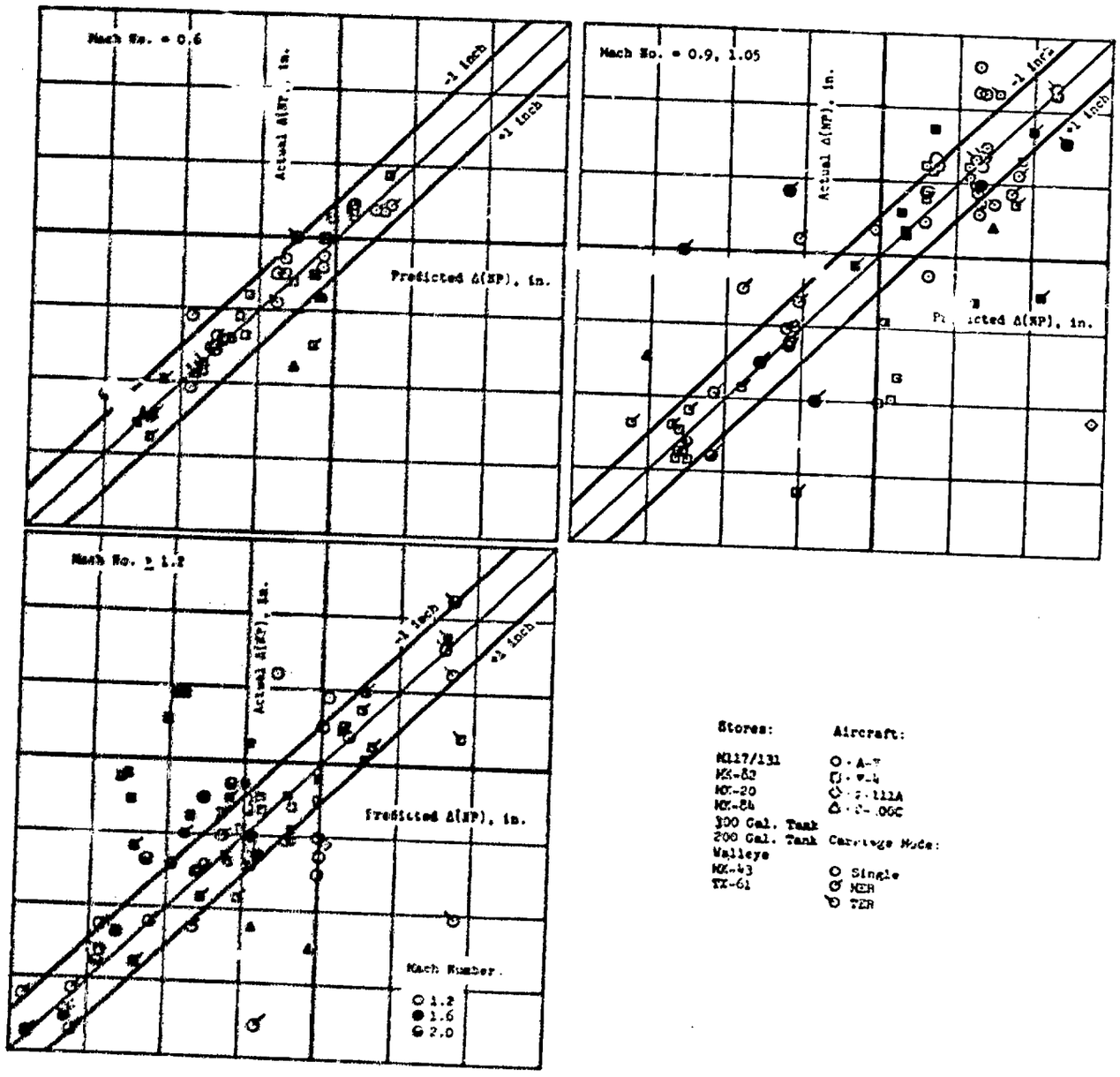
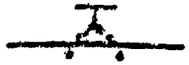
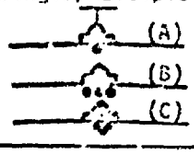
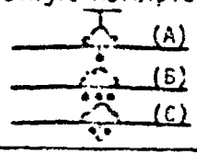


Figure 10. Neutral Point Prediction Accuracy

TYPE OF STORE LOADING ARRANGEMENT -	WING		FUSELAGE	
	Pylon-Mounted Single	Pylon-Mounted Multiple	Tangent-Mounted Single/Multiple	Pylon-Mounted Single Multiple
			 (A) (B) (C)	 (A) (B) (C)
MACH RANGE -		(HER/TER)		
• Drag	0.0 - 2.0 MN	0.0 - 1.6 MN	0.0 - 2.0 MN(A) 0.0 - 0.9 MN(B) 0.0 - 1.6 MN(C)	0.0 - 1.6 MN(A,C) 0.0 - 0.9 MN(B)
• Lift	0.0 - 2.0 MN	0.0 - 1.6 MN	0.0 - 2.0 MN(A) 0.0 - 1.6 MN(B,C)	0.0 - 2.0 MN(A) 0.0 - 1.6 MN(B,C)
• Neutral Point	0.0 - 2.0 MN	0.0 - 1.6 MN	0.0 - 1.6 MN(A,C)	0.0 - 1.6 MN(A,C)
• Side Force	0.0 - 2.0 MN	0.0 - 1.6 MN	0.0 - 1.6 MN(A,C)	0.0 - 1.6 MN(A,C)
• Yawing Moment	0.0 - 2.0 MN	0.0 - 1.6 MN	0.0 - 1.6 MN(A,C)	0.0 - 1.6 MN(A,C)

ANGLE-OF-ATTACK RANGE - Lift - 0° to 8°, Drag, Neutral Point, Side, and Yaw - Cruise.

ANGLE-OF-YAW RANGE - -8 to +8° (Directional terms only)

Figure 11. Summary of Technique Capabilities

CONCLUSIONS

A prediction technique has been developed which can determine the aerodynamic interference effects caused by the carriage of external stores on aircraft lift, drag, and side force, neutral point, and yawing moment. These empirical methods provide the aircraft/store compatibility engineer with a design tool to predict the incremental aerodynamic effects of adding external stores to arbitrary aircraft. The empirical approach taken proved to provide adequate accuracies for preliminary design and in most cases even for engineering development application. Accuracies for most of the performance variables are with 10-20% of the incremental value and generally within 1.0% MGC in neutral point shift. Whereas the prediction accuracies from this effort are comparable to the previous program accuracies, the current techniques are broader in scope with fewer limitations, as well as providing additional performance prediction capability. The technique(s) are applicable to high, mid, and low wing aircraft at subsonic, transonic, and supersonic speeds. The technique can handle both full and down loaded configurations and aircraft with wing sweeps from 15^{o} to 75^{o}.

The technique is in "handbook" form where as noted in the above discussion, figures and charts will provide the necessary dependent variables based on the aircraft configuration. The parametric test data and the bibliography of aircraft/store, pylon, rack, and store aerodynamic data compiled and indexed through this program provide the aircraft/store compatibility community with a unique data base for performing related efforts.

When applying the technique to advanced systems, the dependent variables may not be within the given bounds of the ordinate or abscissa. However, sufficient data is provided that will enable reasonable extrapolation to provide minimal prediction error for the desired dependent variable.

AUTOBIOGRAPHY

by

R. D. DYER
Air Force Flight Dynamics Laboratory
Wright-Patterson Air Force Base, Ohio 45433

Mr. Dyer graduated with a Bachelor's Degree in Aeronautical and Astronautical Engineering from Ohio State University in 1968 and is currently studying for his Master's Degree at O.S.U. In 1968, he assumed his present position as an Aerospace Engineer in the Aeromechanics Branch at the Air Force Flight Dynamics Laboratory where his primary field of responsibility is in internal and external weapons carriage. Mr. Dyer is also an associate member of the American Institute of Aeronautics and Astronautics and the American Defense Preparedness Association.

AUTOBIOGRAPHY

by

R. D. GALLAGHER
Vought Systems Division
LTV Aerospace Corporation
Dallas, Texas 75222

Mr. Gallagher graduated with a BSME (Aeronautical) Degree from Oklahoma State University in 1961. He has since been employed within the Vought Aeronautics Company of the LTV Aerospace Corporation where his present position is Engineer-Specialist. His technical experience has been concentrated in the area of weapons carriage and separation and has involved numerous advanced aircraft and weapon systems. His primary assignment is in an R&D environment where he is responsible for conceiving and performing programs involving aircraft-store aerodynamic problems. Mr. Gallagher presently serves as LTV principal investigator for this program, as well as principal investigator for the VSD/AFATL "Captive Store Airloads Prediction Technique" program.

THE REDUCTION OF THE INSTALLED DRAG OF MULTIPLE STORE CARRIERS
(U)
(Article UNCLASSIFIED)

by

A.B. Haines
Chief Aerodynamicist
Aircraft Research Association Ltd.
Bedford, U.K.

ABSTRACT. (U) During the past few years, ARA has conducted various research programmes with two main aims: to improve the methods for predicting, and to find means for reducing the installed drag of external stores. This paper concentrates on one particular area where the research has shown that striking improvements are possible. Evidence is presented to show that the installed drag of multiple carriers particularly in underwing locations can be reduced substantially by

(i) better aerodynamic cleanliness: typically, an excrescence that is estimated to give one 'drag count' (i.e. $\Delta C_D = 0.0001$) on an empty carrier can give '1½ counts' on the loaded assembly and 2½ 'counts' when the loaded assembly is installed underwing,

(ii) fore-and-aft stagger of the stores,

(iii) slightly increased lateral spacing of the stores.

Proportionately, (i) is most effective at the lower Mach numbers and (ii) and (iii) at high subsonic speeds but all give major reductions in drag that should be highly significant in terms of the operational capability of a strike aircraft.

The modifications are based on simple established aerodynamic principles; some pictures from oil flow tests are included to show why and how they are successful.

Approved for public release; distribution unlimited.

LIST OF FIGURES

1. ΔC_D for multiple and single underwing installations.

2. Isolated store drag rig with fully loaded ¼ scale standard C.B.T.E.

3. Standard triple carrier.

4. Drag increment due to adding a single bomb. Interference within assembly.

5a. Oil flow at M = 0.75; α = 0. Fully loaded standard C.B.T.E. Side view.

5b. Oil flow at M = 0.75; α = 0. Fully loaded standard C.B.T.E. View with bottom bomb removed.

6. Staggered cleaned-up C.B.T.E. assembly.

7. Reduction of drag of loaded triple carrier 'assembly' by removing excrescences and by staggering bombs.

8. Drag reductions for two stages of cleaning up the C.B.T.E. assembly.

9. Cross-sectional area distributions for fully loaded cleaned-up and staggered C.B.T.E.

10. Aircraft-store assembly interference. Fully loaded standard triple carrier.

11. Aircraft-store assembly interference. Fully loaded cleaned-up triple carrier.

12. Drag reduction for cleaning up C.B.T.E. installation.

13. Tests on idealised carriers. Effects of lateral spacing.

14. Effects of lateral spacing.

1. INTRODUCTION

The Aircraft Research Association Ltd. was set up in 1952 with the prime purpose of building and operating a large 9ft x 8ft transonic tunnel. The tunnel first ran in 1956 and since then, has been used extensively for research and development tests for member firms in the U.K. and for customers elsewhere. The facilities and activities at ARA have also been extended to include several additional subsonic, supersonic and hypersonic tunnels, groups working on theoretical aerodynamics and in particular, in the present context, a Drag Analysis Group which is engaged in comparing model and flight test drag data with the aim of improving drag prediction methods. The drag of external stores has figured as a high priority item in the work of this Group; also, in the last few years, various systematic research programmes have been undertaken in the transonic tunnel to find methods for drag reduction. The present paper is concerned with the achievements in one particular area viz. the reduction of the installed drag of loaded multiple carriers particularly when mounted in underwing locations.

Fig.1 is a convincing illustration of the importance of the problem as seen some years ago. The curves in Fig.1 are based on actual measured results for a complete aircraft model in the ARA transonic tunnel. The figure presents a comparison between the drag increments due to two No.2 Mk.1 C.B.T.E. triple carriers (i.e. one per wing panel) fully loaded with Mk.10 1000 lb bombs, the increments due to two single bombs and the drag of the clean model without stores. Both the carriers and the single stores were pylon-mounted under the wing of the aircraft at about mid-semi-span. It will be seen that the drag increment of the loaded carrier is far greater than three times the increment due to the single bomb/pylon and indeed, above $M = 0.75$, it is greater than the drag of the clean aircraft model without stores. Three factors contribute to these high drag values: the aerodynamic dirtiness of the carrier installation, the mutual interference within the store assembly and third, the interference between the assembly and the parent aircraft wing. The evidence presented in this paper shows how the drag can be reduced substantially by better aerodynamic cleanliness, by fore-and-aft stagger of the stores and by slight increases in the lateral spacing of the stores.

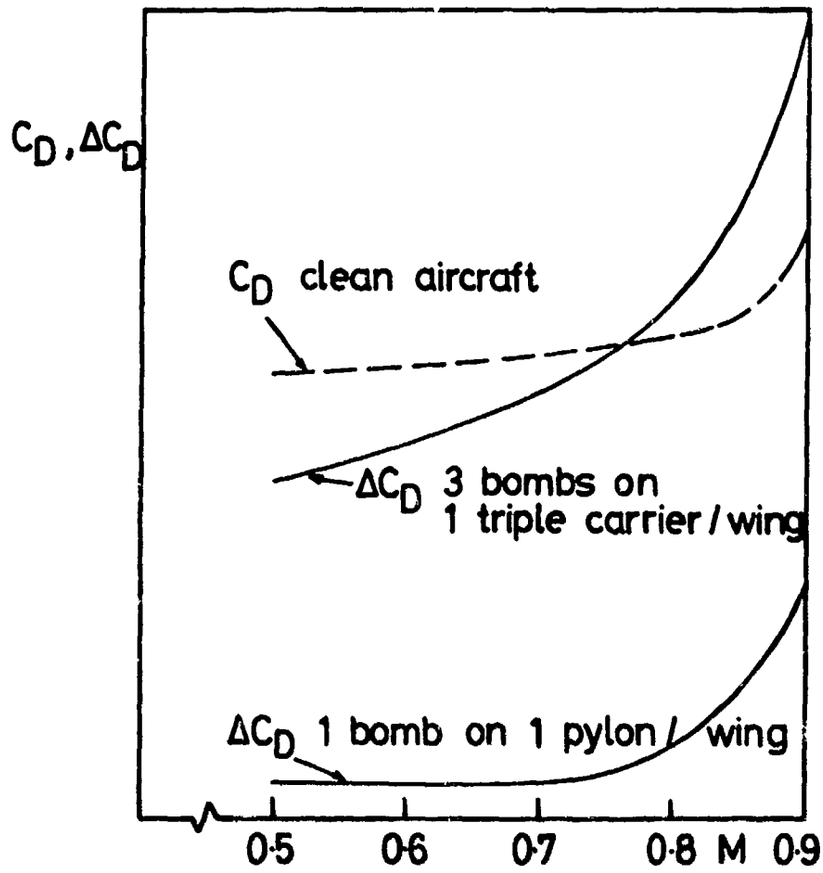


Figure 1. ΔC_D FOR MULTIPLE AND SINGLE UNDERWING INSTALLATIONS

2. THE DRAG OF A STANDARD TRIPLE CARRIER (NO.2 MK.1 C.B.T.E.)

Much of the research has been undertaken by testing relatively large, e.g. ¼ scale store assemblies mounted in the tunnel below a long slender body as shown in the photograph in Fig.2. At this scale, most of the detailed features of the full-scale store assembly can be adequately reproduced. For example, Fig.3 shows the ¼ scale standard triple carrier as tested on this rig. It will be seen that not only are major items e.g. the pylon adaptor and the ejection release units fully represented but also details such as the crutch arms, crutch pads and crutch pad rests. Tests have confirmed that the store assemblies are mounted well clear of the body boundary layer and sufficiently far aft of the body nose to be in essentially an undisturbed stream. Interference effects from the body can therefore be treated as trivial at least at subsonic speeds. A sensitive balance inside the body measures the drag of either the store assembly or the store/pylon combination and for the purpose of this paper, the data from this rig are described as "isolated drag data".

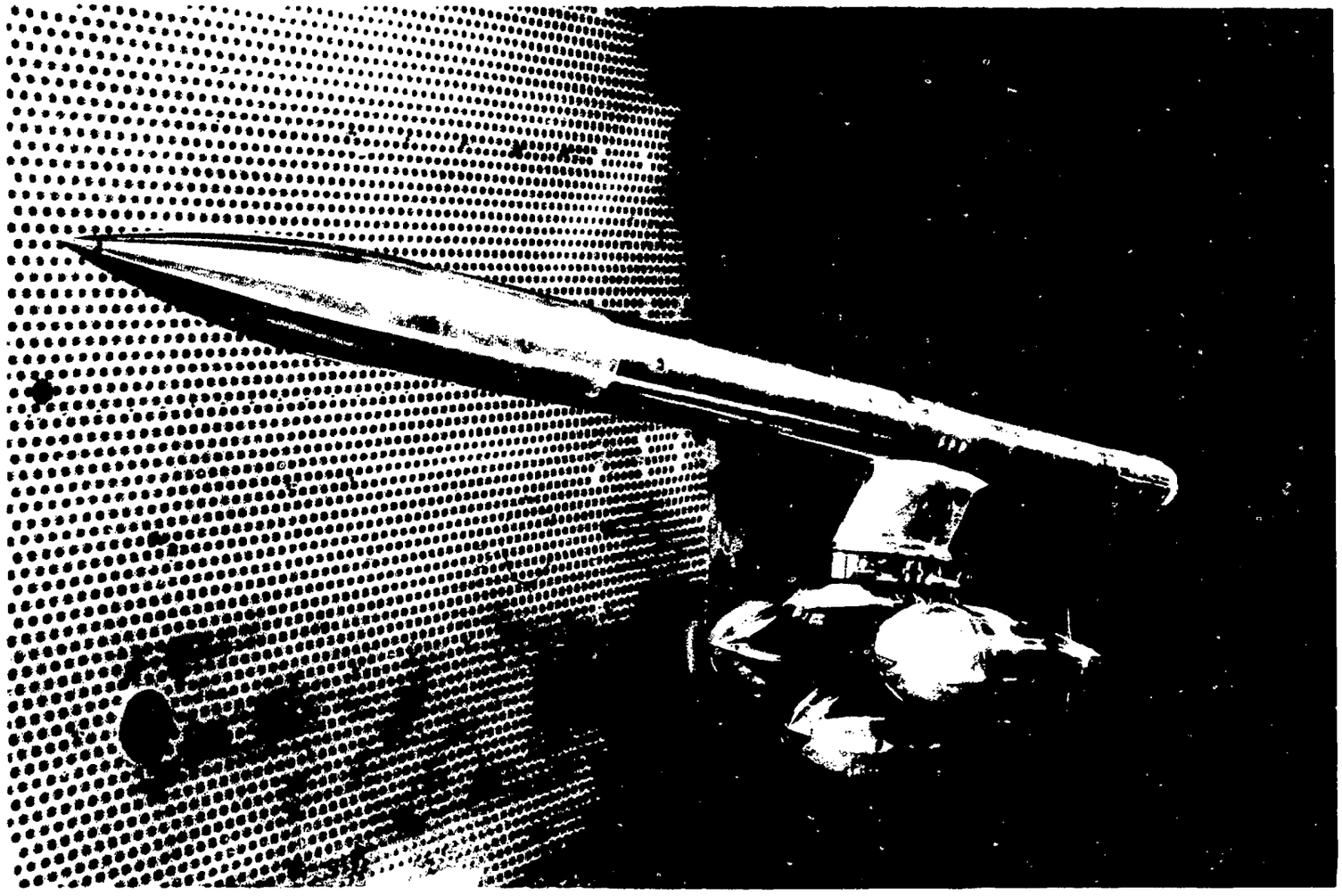


Figure 2. ISOLATED STORE DRAG RIG WITH FULLY LOADED
1/4 SCALE STANDARD C.B.T.E.

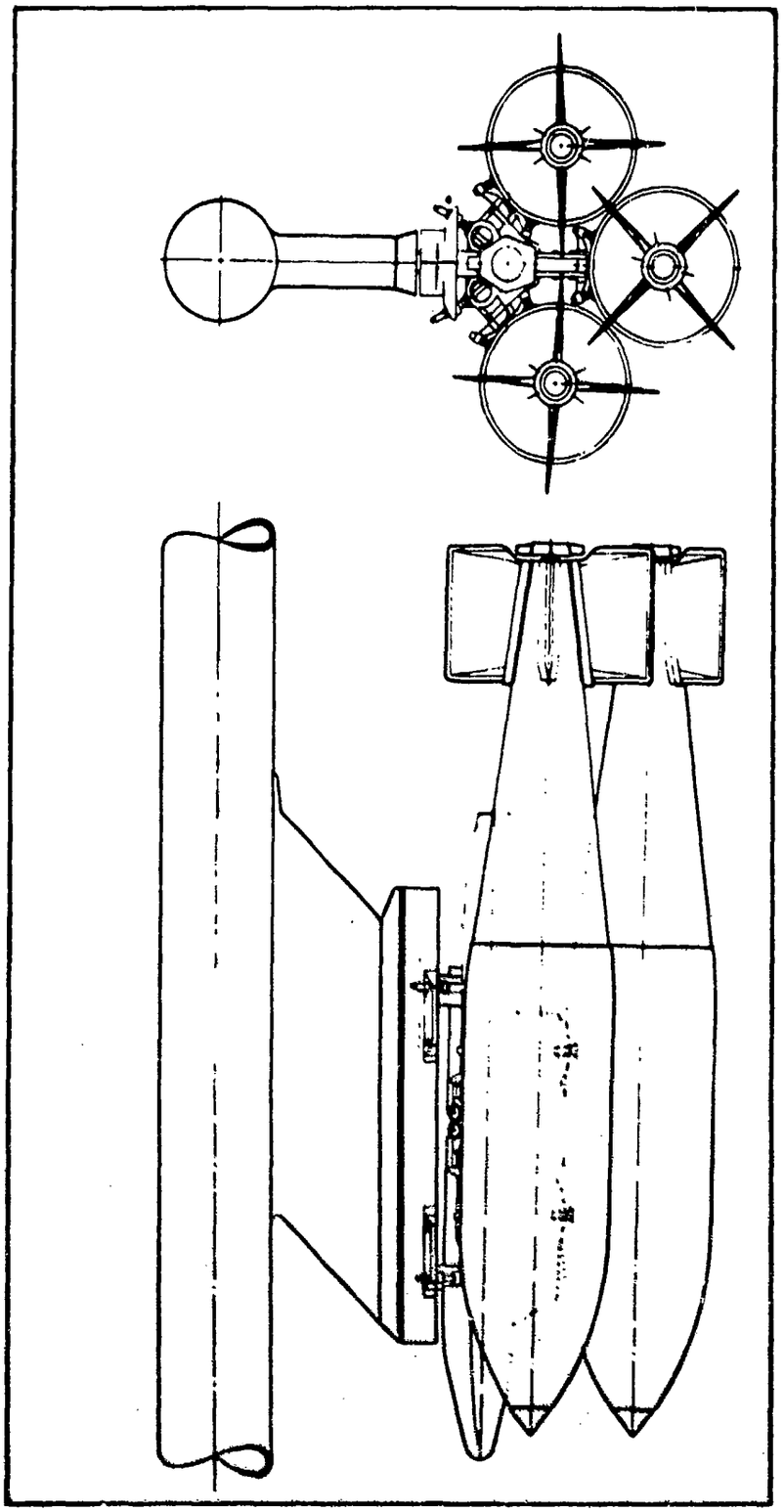


Figure 3. STANDARD TRIPLE CARRIER

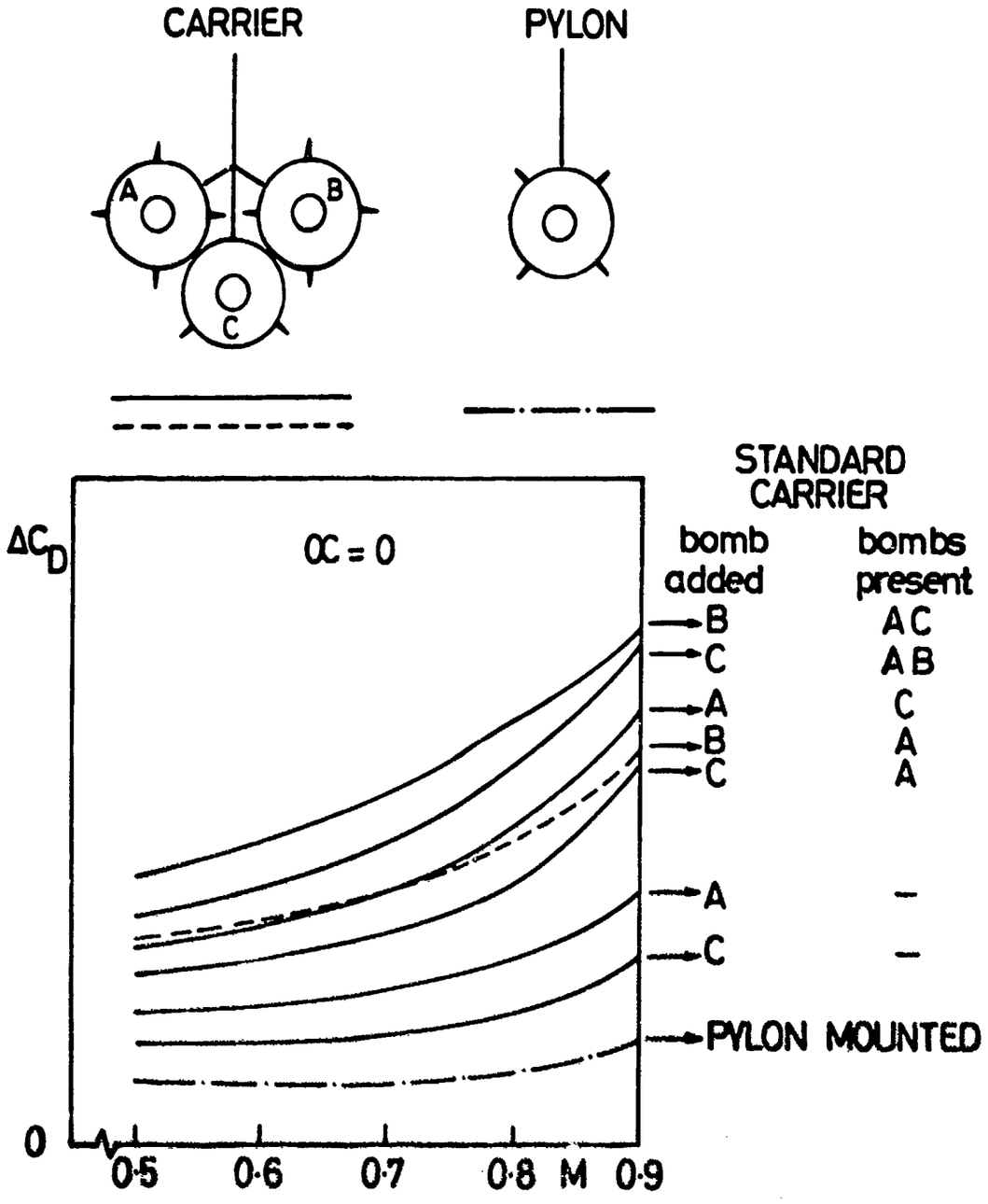


Figure 4. DRAG INCREMENT DUE TO ADDING A SINGLE BOMB INTERFERENCE WITHIN ASSEMBLY

Tests were made on the standard triple carrier of Fig.3 with various loads of Mk.10 1000 lb bombs. Fig.4 presents the data in a form that enables one to appreciate how the mutual interference effects within the assembly - at least at the test Reynolds numbers - become more serious as extra bombs are added to the carrier. ΔC_D in this picture is the drag increment due to adding a single bomb either to a pylon or to an empty triple carrier or to a triple carrier with one bomb already present or to a triple carrier with two bombs already present. The first and most obvious point is the steady increase in ΔC_D through this progression. Second, with a given number of bombs present, ΔC_D due to adding a shoulder bomb is always greater than ΔC_D due to adding a bottom bomb thus implying significant interference between the shoulder bombs and the body of the carrier. Third, it will be noted that the rate of increase with Mach number in the adverse interference is greater for a shoulder and a bottom bomb than for two shoulder bombs.

It has been common practice at ARA to express the data at low speed as either an "assembly factor" (A.F.) or an "installation factor" (I.F.) where

$$\text{A.F.} = \frac{\text{Measured drag of store assembly}}{\Sigma \text{ Estimated drag of individual components}}$$

$$\text{I.F.} = \frac{\text{Measured drag increment of store installation (on aircraft)}}{\Sigma \text{ Estimated drag of individual components}}$$

"Components" in this context implies not merely the stores, carrier and pylon but also the individual excrescences. If the estimates are accurate, A.F. and I.F. are a measure respectively of the interference within the assembly and the interference between the assembly and the parent aircraft. Any inaccuracy in the drag estimates obviously confuses the issue and in the present case, it is known for example that the ARA methods tend to overestimate the drag of the empty carrier. If one then replaces this term in the denominator of the expression for A.F. by the measured drag of the empty carrier, one finds that the low speed assembly factors for the results just discussed vary from 1.0 for the empty carrier (by definition) to values between 1.1 and 1.2 for the single bomb cases, to values between 1.4 and 1.5 for the two bomb cases, and 1.75 for the fully loaded carrier, these figures thus giving an idea of the increase in the low speed interference within the assembly. Further increases occur with Mach number as shown in Fig.4. For example, by M = 0.9, the drag due to adding a single bomb expressed as a percentage of the drag of a pylon-mounted bomb has increased to 190% for a bottom bomb or 250% for a shoulder bomb in cases with only one bomb fitted or to figures as high as 400% and 500% for the shoulder bomb in two-bomb and three-bomb configurations.

In an attempt to interpret these high drag values, oil flow tests were made on the fully loaded standard carrier. Figures 5(a) and (b) are photographs of the oil flow at M = 0.75. In Fig.5(b) the bottom bomb has been removed to show the oil flow pattern in the channel formed by the three bombs and the carrier. As might be expected, the flow is

very complicated and, before discussing in detail, it may be helpful, for the purpose of identifying the features associated with high drag, to note some relevant features of the flow about a single isolated bomb of this type. The bomb has a clearly defined forebody, parallel centrebody and boattailed afterbody. A calculated inviscid pressure distribution is characterised by marked suction peaks, followed by strongly adverse pressure gradients, at the start of both the centrebody and the afterbody. A reduction of surface shear stress would be predicted for these regions of adverse pressure gradient and this is indicated in Fig.5(a) by the thicker oil deposit in the region of the shoulder bomb centrebody, with virtually straight streamlines, not notably affected by the other bombs or by the carrier. It can be concluded that the boundary layer would be highly sensitive to any further increases in local velocity, cross-flow or local disturbances in these regions, and would be particularly liable to separate on the



Figure 5a. OIL FLOW AT M = 0.75; α = 0
FULLY LOADED STANDARD C.B.T.E.
SIDE VIEW



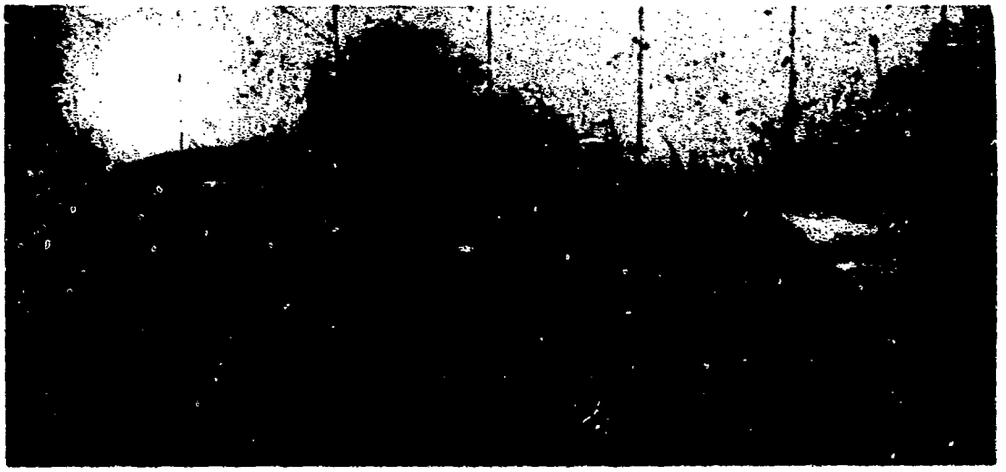


Figure 5b. OIL FLOW AT M = 0.75; α = 0
FULLY LOADED STANDARD C.B.T.E.
VIEW WITH BOTTOM BOMB REMOVED

boattail and afterbody. Returning to Fig.5(b) and starting at the nose of the bombs, the flow diverts away from the small passages between the bombs and C.B.T.E. body. Between the bombs at the nose-parallel portion junction, a combination of the high diversionary flow angles and the high local velocities due to both the bomb shape and proximity, cause a small region of shock-induced separation to be present even at this relatively low Mach number of M = 0.75. The effects of these separations convect downstream in the channel to produce very extensive separations and rolled-up vortex type flows over the rear of the bombs. The flow out of the channel creates a marked cross-flow over the top of the shoulder bombs. The shoulder E.R.U. forward crutching arms form a bluff excrescence situated directly in this cross-flow and in the region of strong adverse pressure gradient at the start of the bomb centrebody - as noted above, an ideal location to induce boundary layer separation. Fig.5(a) shows the separation spreading behind the forward crutching arms, and causing a large area of separated flow over the top and inside surfaces of the shoulder bomb afterbodies. The top and inner fins of the shoulder bomb and the top fins of the bottom bomb are apparently immersed in a highly confused wake. These oil flow pictures demonstrate how the separate direct drag-producing effects, i.e. the proximity of the bombs and bluff crutching arms, probably combine to magnify the total drag of the store plus carrier assembly. In particular, consistent with the drag data, one can note the greater extent and severity of the separations on the shoulder bombs compared with the flow over the bottom bomb.

3. IMPROVEMENTS DUE TO CLEANING-UP THE TRIPLE CARRIER

The cleaning-up exercise on the isolated ¼ scale triple carrier was undertaken in two stages. First, the crutch arms and resting pads were removed from the E.R.U. units and the pylon adapter and then second, a fully cleaned-up design with the E.R.U.s completely faired into the C.B.T.E. body was devised as shown in the picture for the staggered cleaned-up assembly in Fig.6. It is thought that both these cleaned-up versions (note: stagger is not yet being considered) are completely practical derivatives of the original standard carrier and that they could be achieved with little or no weight penalty.

Fig.7 shows that the isolated drag of the triple assembly is substantially reduced at both stages of this exercise. The drag of the fully cleaned-up version is only about 55% of the drag of the standard carrier at the lower Mach numbers. At higher Mach numbers, the improvement becomes less pronounced, this ratio rising to more than 80% at M = 0.9 and this implies that at the higher Mach numbers, removing the excrescences and thus refining the passages between the stores is not sufficient; the basic store-store interference has to be reduced. Nevertheless, throughout the Mach-number range, the removal of the excrescences clearly represents a major achievement.

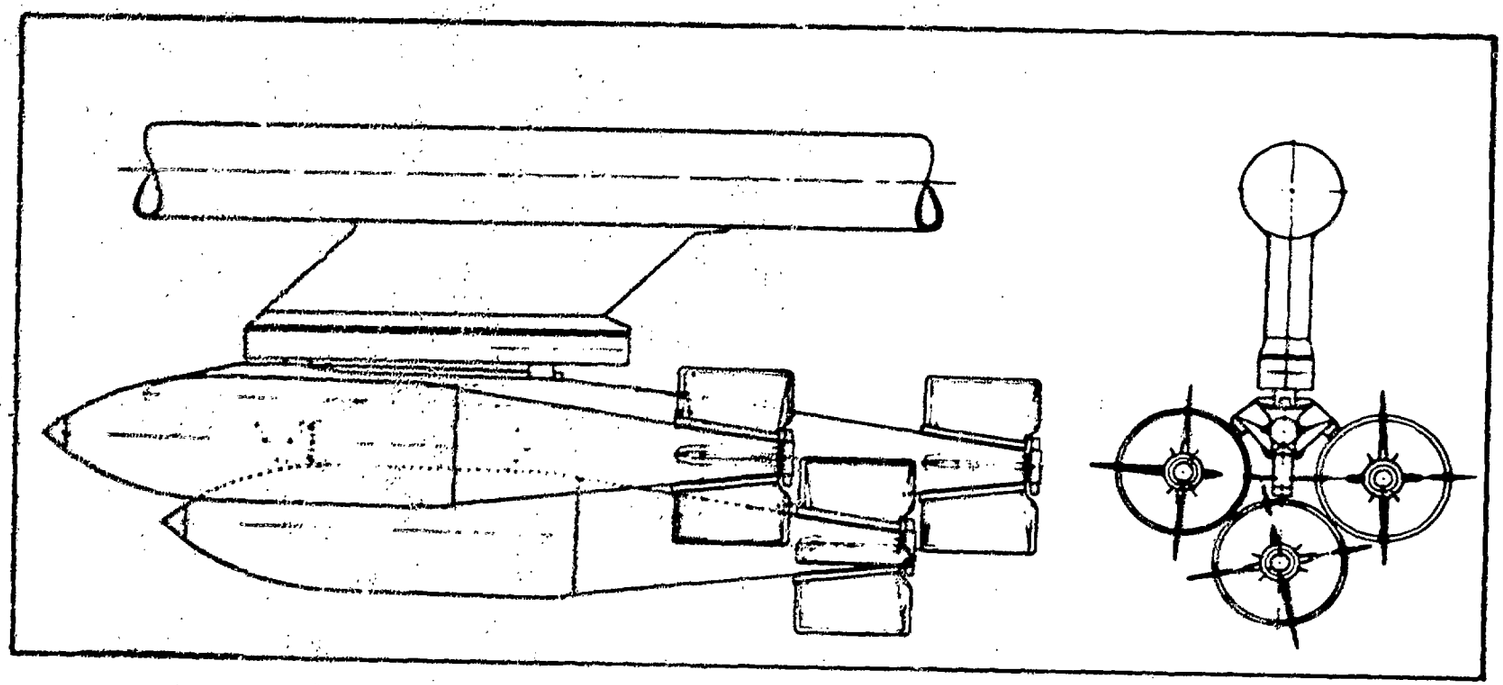


Figure 6. STAGGERED CLEANED-UP C.B.T.E. ASSEMBLY

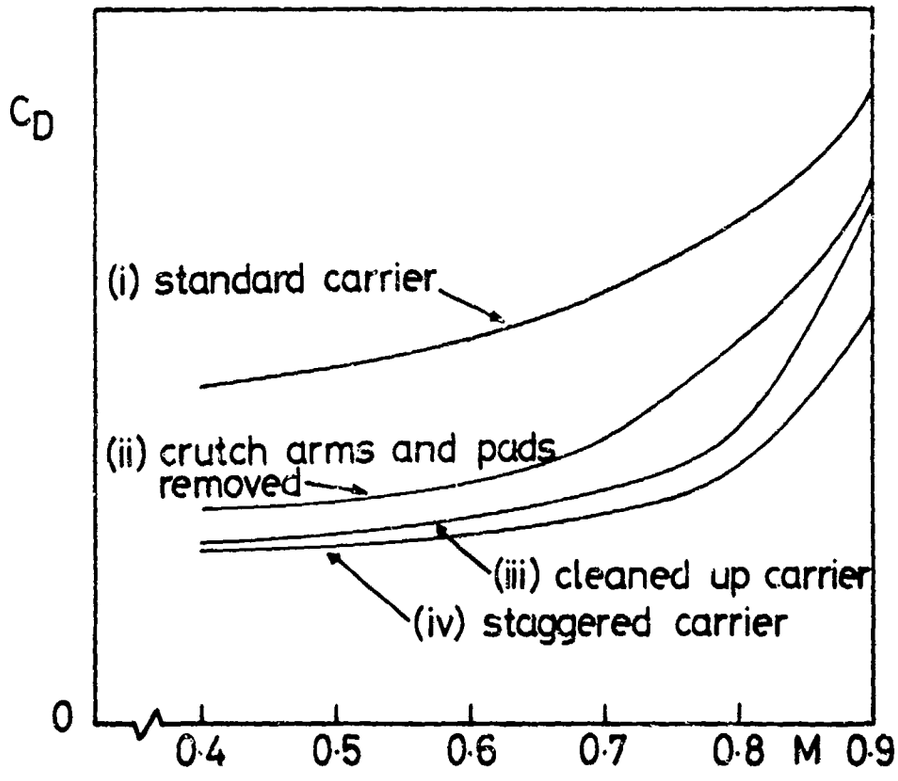


Figure 7. REDUCTION OF DRAG OF LOADED TRIPLE CARRIER 'ASSEMBLY' BY REMOVING EXCRESCENCES AND BY STAGGERING BOMBS

In Fig.8, the drag reductions are compared with the estimated low speed drag of the deleted excrescences. One has to distinguish here between the drag saving (B) from removing the crutch arms and pads and from the final fairing (A - B). In the first case, the drag saving is substantially greater than the estimated low speed drag of these items. This implies that when they are present, there is not only a direct drag force on the actual excrescences but also severe adverse interference effects on the flow over for example, the rear of the bombs as suggested by the oil flow pictures. On the other hand, the extra drag saving (A - B) due to removing excrescences other than the crutch arms and pads, is only about half the estimated extra saving from these items. The contrast between these two results illustrates the weakness of an estimation technique in which one merely adds the drag of the individual excrescences. In general, it is found that this simple technique provides an overestimate of the excrescence drag for cases where some of the excrescences lie downstream and in the wake of other excrescences or an underestimate in cases where the excrescences induce

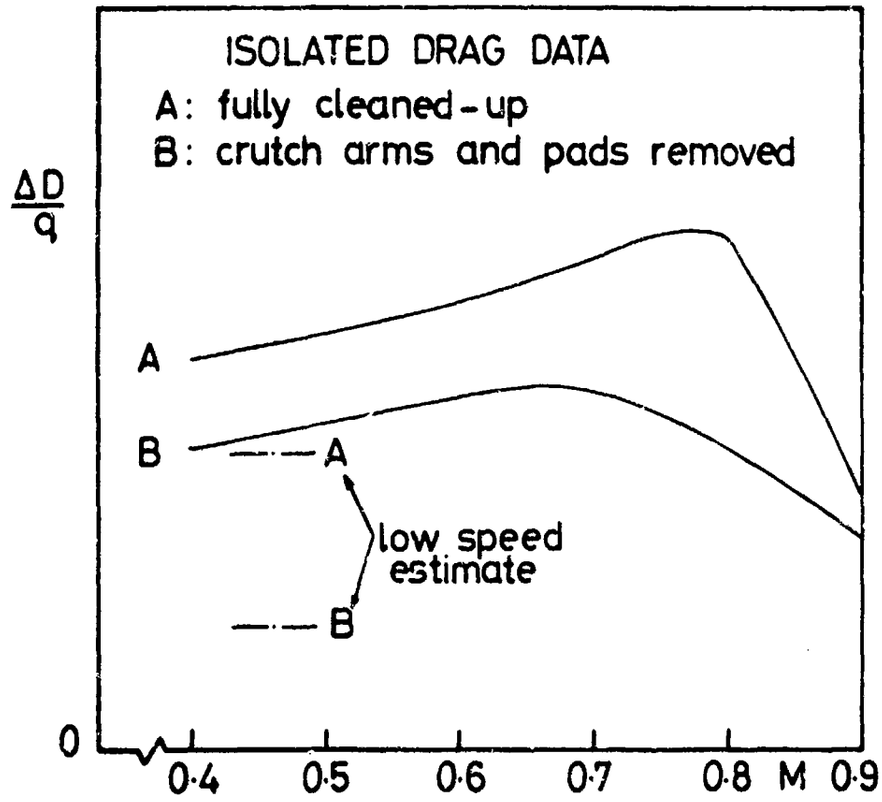


Figure 8. DRAG REDUCTIONS FOR TWO STAGES OF CLEANING UP THE C.B.T.E. ASSEMBLY

flow separations on major components of a store assembly.

It should be noted that if the interference within the assembly had not been improved by the deletion of the excrescences, the assembly factor as defined earlier would be higher for the cleaned-up assembly. In fact, the assembly factor for the fully loaded carrier has improved from 1.75 to about 1.50, thus implying as would be expected, reduced interference.

4. EFFECTS OF FORE-AND-AFT STAGGER OF THE STORES

The results of the clean-up exercise above were impressive but nevertheless somewhat disappointing at high Mach number. Other concepts are therefore needed. One of these is to stagger the stores longitudinally relative to each other. Tests were therefore made on a $\frac{1}{4}$ scale model of the staggered faired assembly shown in Fig.6. The bombs in the shoulder locations were staggered forward and aft of the bottom bomb by 0.92 calibre. This distance is near the practical maximum available without a complete redesign of the carrier. It is sufficient to give a notable improvement in the longitudinal cross-sectional area distribution of the store assembly as shown in Fig.9.

The drag data for the loaded staggered carrier are given in Fig.7. Reductions in drag are obtained at all Mach numbers; they become greater as the Mach number is increased until by M = 0.90, they are of a similar order to those obtained from cleaning-up the carrier. The ratio of the drag of the staggered cleaned-up carrier to the drag of the original standard carrier varies from about 50% at M = 0.4 to about 65% at M = 0.9.

No attempt was made to optimise this staggered carrier. Indeed, oil flow tests suggested that the version might be far from the optimum. The pictures suggested that the high velocity region near the junction of the nose and parallel portion of the most rearward bomb is too close to the maximum thickness of the particular pylon used for this investigation and that as a result, a shock wave is present between the pylon and this bomb even at M = 0.75. It is possible therefore that repositioning the starboard rearward bomb relative to the pylon or a change to a thinner pylon of different shape could further reduce the interference drag at high Mach number. Nevertheless, in other respects, the oil flow tests confirmed that the general flow over the stores was far better than with the original standard carrier. The flow over the noses of the bombs still tries to avoid entering the channel between the C.B.T.E. and the bombs but the deflection of the surface streamlines is considerably smaller. There is still a shock-induced separation near the high velocity peak at the rear end of the bomb nose and also the forward fixation of the bomb to the carrier still causes a disturbance over the top of the shoulder bombs. However, both of these are very much smaller than with the standard carrier and there is a much reduced effect on the flow over the tail cones of the bombs. To sum up, much has been achieved but further improvement should still be possible.

5. RESULTS FOR INSTALLED CARRIERS

The results discussed in sections2-4 above have been for carriers tested "in isolation" on the rig shown in Fig.2. Both the standard and the fully faired triple carriers (but not the staggered carrier) have also been tested as pylon-mounted installations below the wing of a typical aircraft complete model. Naturally, this model was to a smaller scale but it was still possible to make a tolerable reproduction of the details of the carrier assembly. The smaller scale model was in fact tested on the isolated rig and the values of drag coefficient were very similar. The results from the installed and isolated tests are compared in Figs.10 & 11. Clearly, with the standard triple carrier, Fig.10, there is considerable excess drag due to interference between the store assembly and the parent aircraft wing. This is observed both at low C_L, and at high Mach number at all values of C_L. The excess interference drag is only trivial near $C_L = 0.4$ or, expressed more generally, near C_L for $(\Delta C_D)_{min}$ and up to M = 0.7 i.e. up to a Mach number about 0.1 below the drag-rise Mach number at this C_L for the clean aircraft. For a typical cruise condition for the aircraft-store combination, the increase in ΔC_D with Mach number from the low speed value is about twice as great as given by the isolated data.

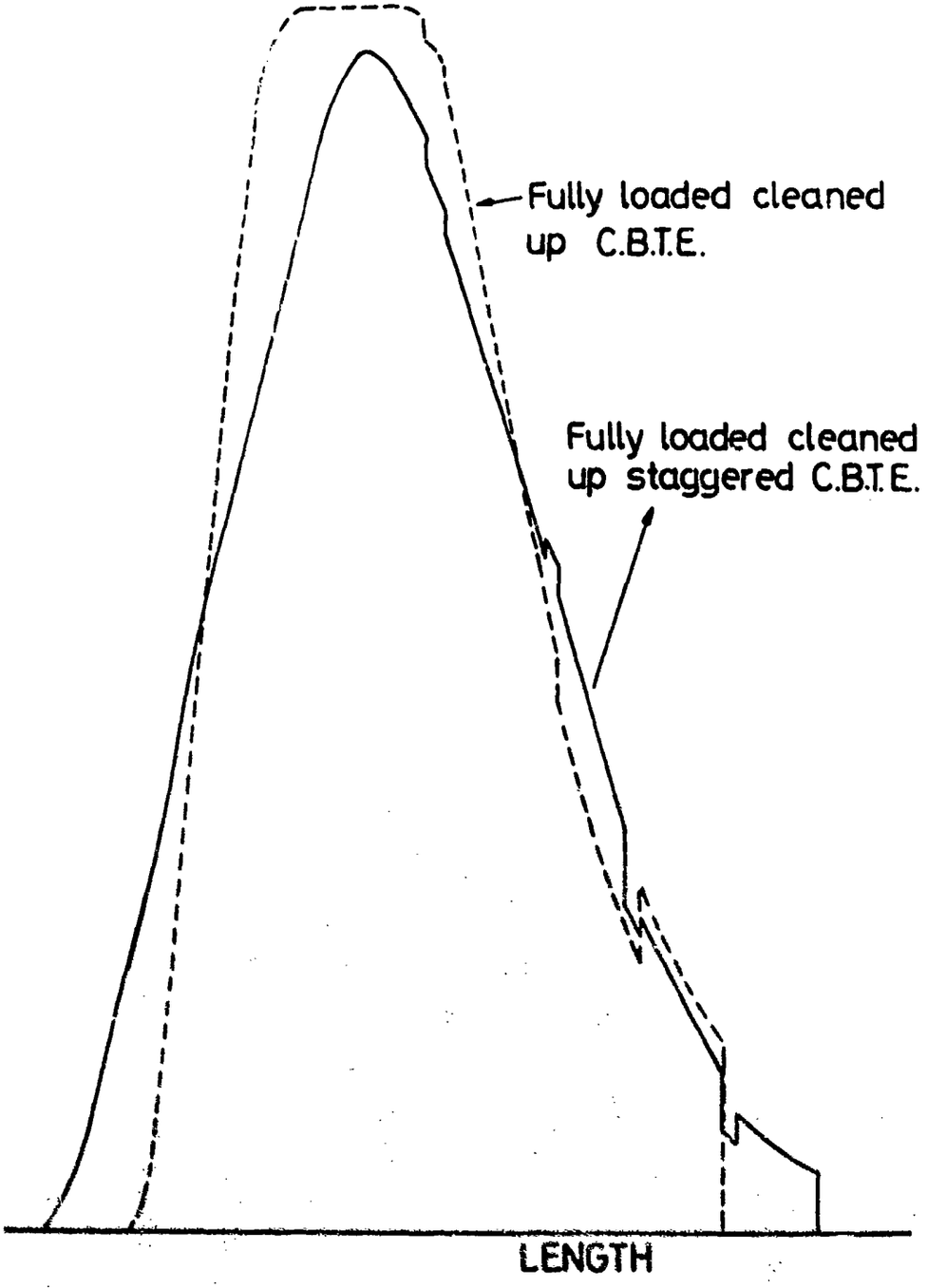


Figure 9. CROSS SECTIONAL AREA DISTRIBUTIONS FOR FULLY LOADED CLEANED-UP AND STAGGERED C.B.T.E.

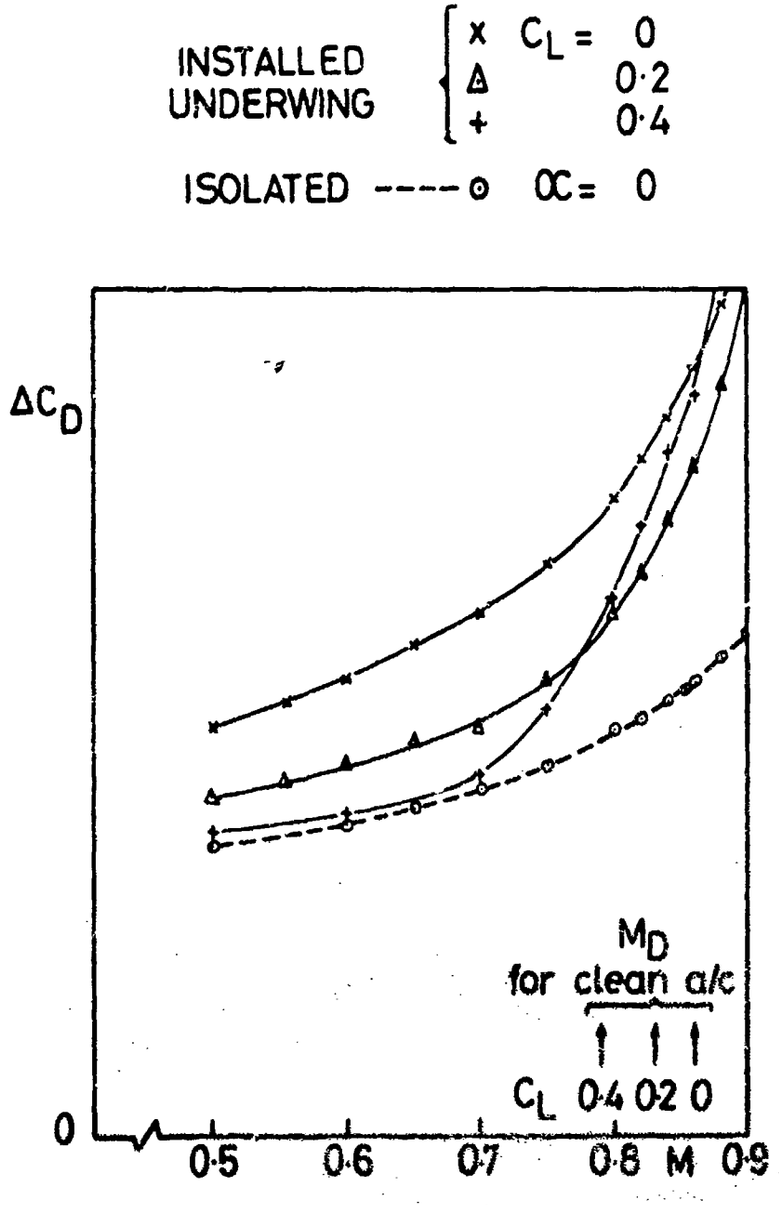


Figure 10. AIRCRAFT-STORE ASSEMBLY INTERFERENCE FULLY LOADED STANDARD TRIPLE CARRIER

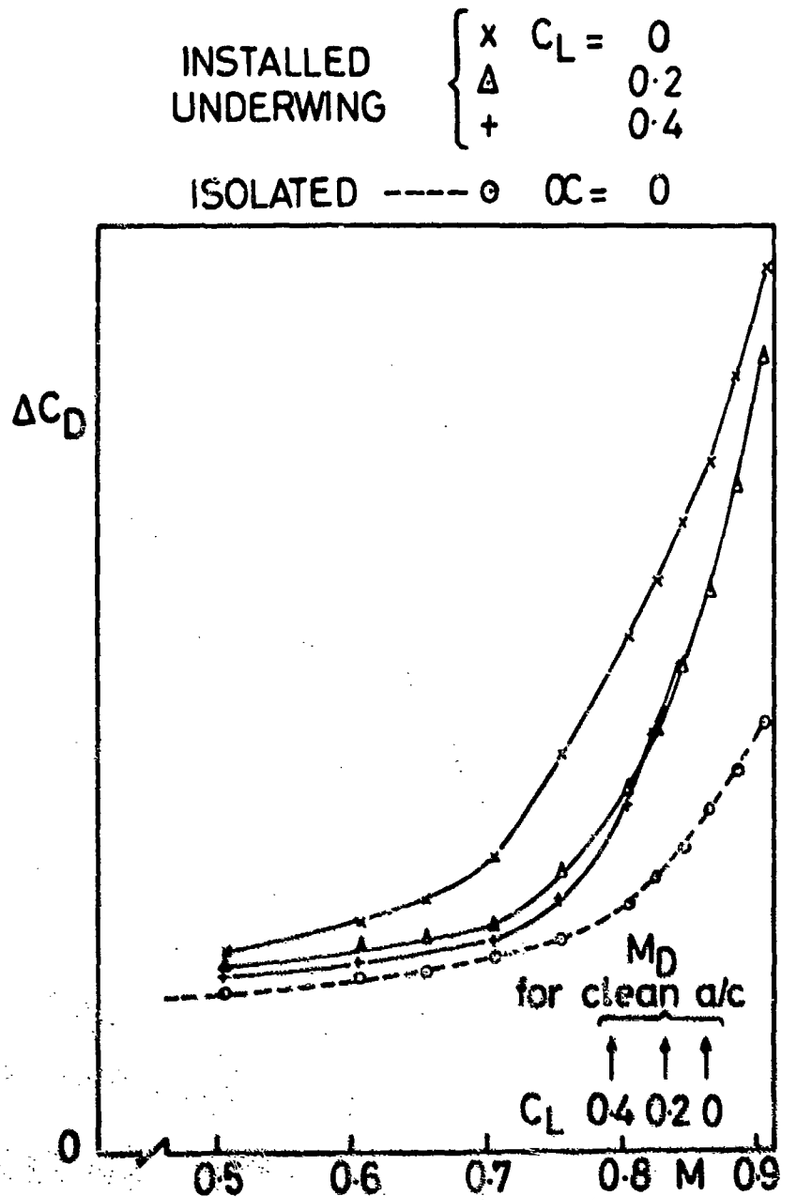


Figure 11. AIRCRAFT-STORE ASSEMBLY INTERFERENCE FULLY LOADED CLEANED-UP TRIPLE CARRIER

Comparison of Figs.10 & 11 show that the excess interference drag for the installed case can be reduced considerably by cleaning-up the carrier. This improvement is particularly noticeable at low Mach number and low C_L as can be seen perhaps more clearly from Fig.12 which compares the drag reduction from cleaning-up the carrier for the installed case at different values of C_L with the isolated data and with the simple low speed estimate for the drag of the deleted excrescences. The problem area at low C_L is almost solved at low Mach number by cleaning-up the carrier: at $C_L = 0$, one can sum up the results by saying that an excrescence which is estimated to give one drag "count" as a separate item contributes 1½ drag counts when part of the assembly and 2½ drag counts when the assembly is installed on the aircraft wing. At high Mach number, however, as with the isolated data, the improvements are still disappointing. It should be stressed that this does not mean that the excrescences in their effects are unimportant at high Mach number. Rather, it implies that the drag is then determined primarily by the proximity of the stores in the assembly and by the proximity of the assembly to the aircraft wing. If the basic interference between the major components could be reduced or if one was considering the drag of merely a partly loaded multiple carrier, it is probable that one would then find that the deletion of the excrescences was more rewarding.

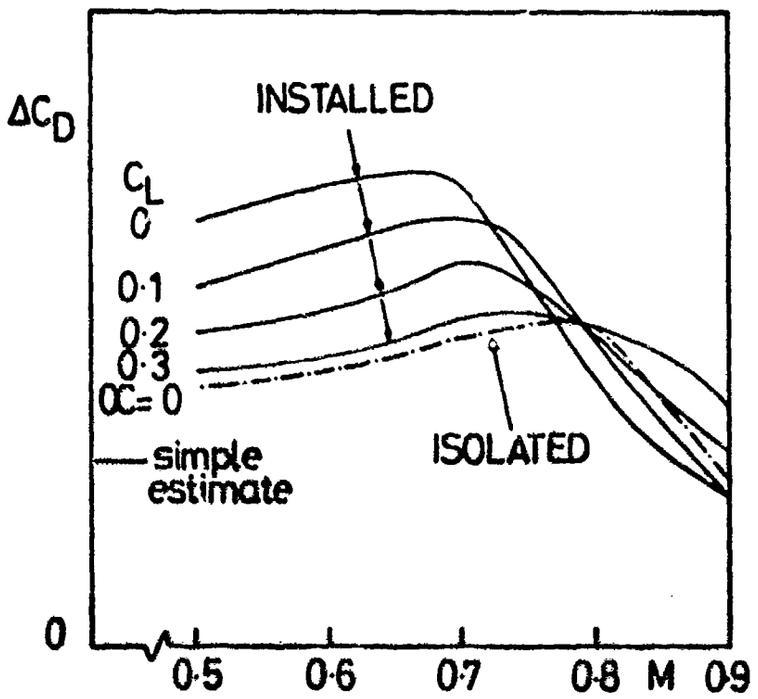


Figure 12. DRAG REDUCTION FOR CLEANING UP C.B.T.E. INSTALLATION

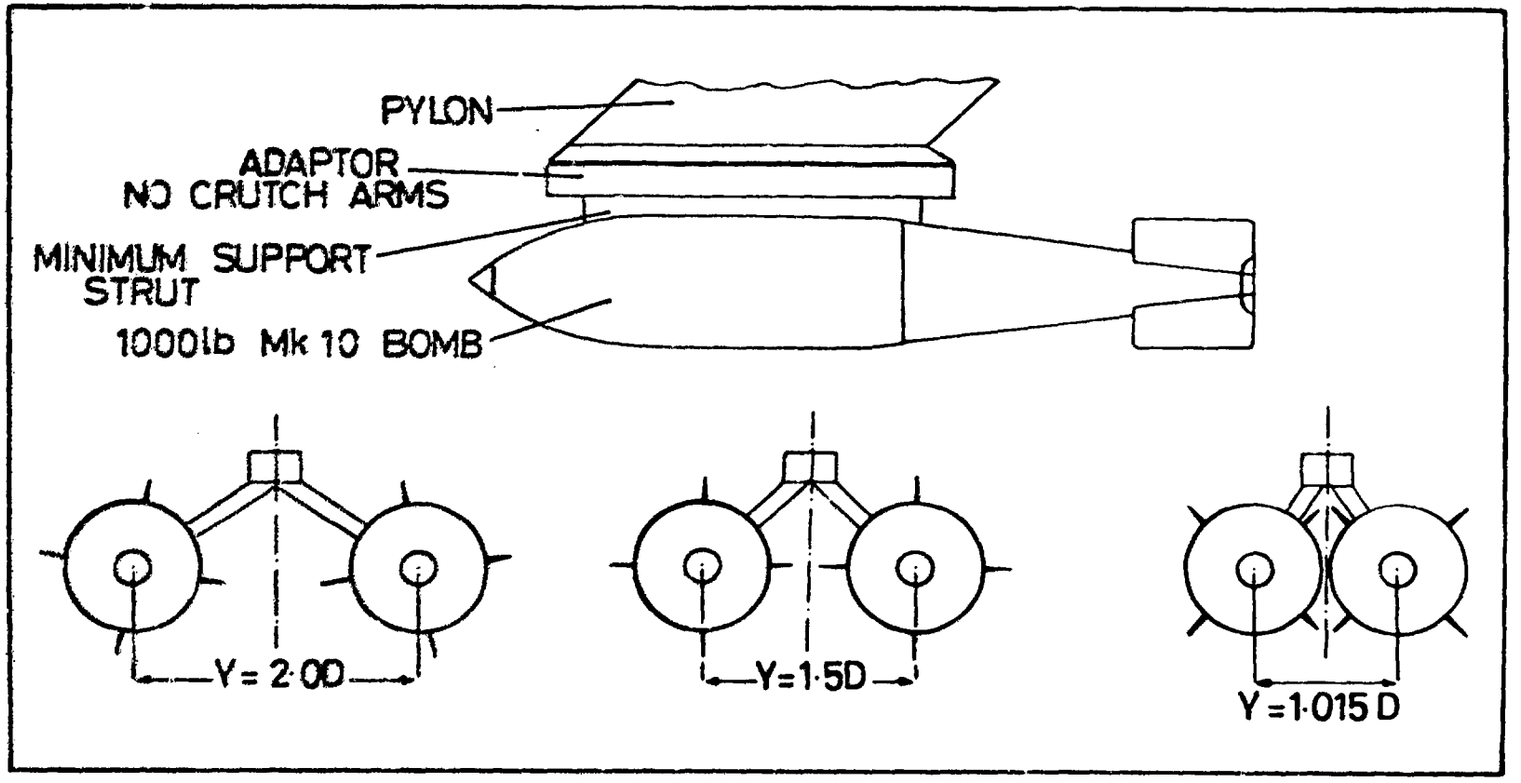


Figure 13. TESTS ON IDEALISED CARRIERS, EFFECTS OF LATERAL SPACING

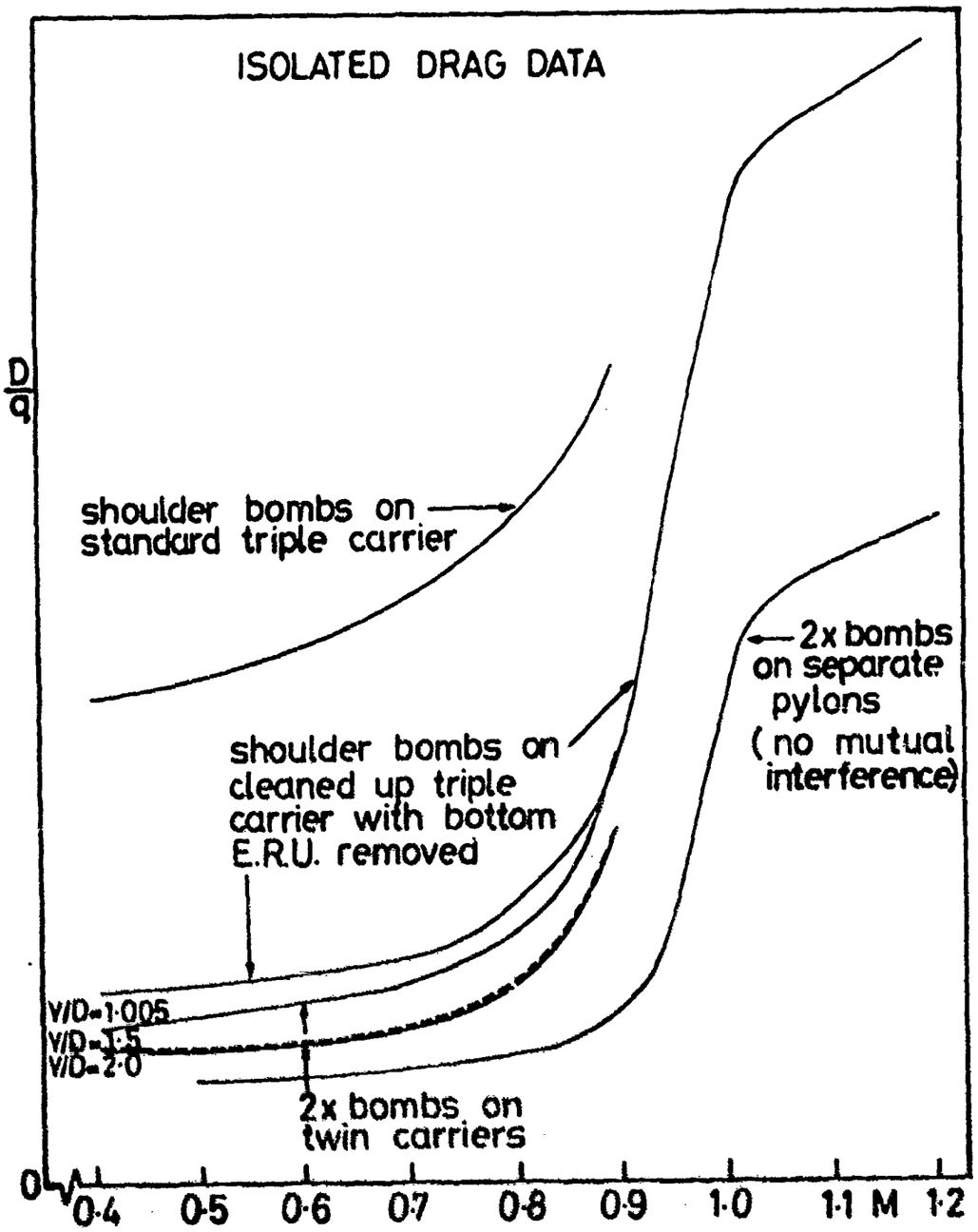


Figure 14. EFFECTS OF LATERAL SPACING

6. EFFECTS OF STORE LATERAL SPACING

The last remarks in the previous section suggest that it would be possible to reduce the effects of the lateral spacing of the stores within a triple assembly. This has not been specifically investigated but some related experiments on idealised twin carriers have been made. The arrangements tested are shown in Fig.13; the aim in these tests was to use carriers that would create minimum interference so that the data would give a clear idea of the interference between the actual stores. Measured results are presented in Fig.14. This figure also contains for comparison, data for the standard triple carrier with two shoulder bombs, for the cleaned-up triple carrier with the bottom E.R.U. removed also carrying two shoulder bombs and finally, for two bombs on separate pylons assuming there is no mutual interference between the bombs. It will be seen that throughout the test Mach-number range, increasing the lateral spacing in the idealised twin carrier from the minimum value (0.015D separation of bomb surfaces) to the mid-spacing (0.50D) reduces the drag significantly but the further increase to the maximum spacing (1.00D) has little effect. It should be remembered however that since the length of the twin carriers was altered as the spacing was changed, the results in Fig.14 contain an element due to the different drag of the carriers and when one allows for this, one finds that there is actually a small reduction in interference drag between the mid and maximum spacings. The results still suggest however that little further reduction would come from increasing the spacing further and it is intriguing to note that the apparently asymptotic values that have been attained are still, at high Mach number, much greater than the values for the two bombs on separate pylons. This suggests that probably, even with these idealised carriers, there is some major interference at high Mach number due to the pylon adaptor and carrier struts. Alternatively, it is possible that the variation of drag with lateral spacing is not a smooth monotonic curve and that the results for the widest spacing shown here are near a second local maximum in this curve.

It should be stressed that as plotted (and measured), the data in Fig.14 does not include the drag of the pylon(s). This means that Fig.14 is meaningful in showing the aerodynamic interference of the twin carrier installations but for the practical designer, the separate pylon case would have to bear the penalty of the drag of the extra pylon. This could be sufficient to offset the apparent drag advantage of this case at low Mach number but would have little effect on the more striking differences in the variation of drag with Mach number.

Many existing carriers provide lateral spacing between the store centres in the range $1.05 < Y/D < 1.25$ and so Fig.13 suggests that if these lateral spacings could be increased slightly, there would be significantly less store-store interference drag. It seems possible that the savings in drag would be more important than any associated increase in the weight of the carrier.

7. CONCLUDING REMARKS

Evidence has been presented showing that appreciable reductions in the excessive drag of a standard triple carrier should be feasible by a combination of improved aerodynamic cleanliness, fore-and-aft stagger of the stores and increased lateral spacing of the stores. It is not unrealistic to think in terms of installed drag increments for a good fully loaded triple carrier that are only about a third of those for the original standard carrier and which therefore are comparable with or perhaps even better than the original carrier loaded with merely a single bomb. Also, many of the modifications would not lead to any significant weight penalty.

The examples in the paper show that the application of simple established aerodynamic principles, involving relatively minor modifications and redesign of existing store carriers and assemblies, can achieve large reductions in the installed drag increments that are highly significant in terms of the total drag and operational capability of a strike aircraft.

AUTOBIOGRAPHY

Mr. Haines graduated at Birmingham University with a B.Sc.(Hon) degree in Mathematics in 1941. He then joined the staff of the Aerodynamics Department, R.A.E. Farnborough where he served in the 24ft tunnel on propellor research and then in the 10ft x 7ft high speed tunnel. In 1955 he joined the Aircraft Research Association Ltd., Bedford as Chief Aerodynamicist, a position he still holds. In the past 20 years, Mr. Haines has been concerned with the planning, execution and interpretation of tests in the Association's transonic tunnel and has specialised in problems of transonic flow, sweptback wing design, scale effect and the assessment of aircraft drag standards both for civil and military aircraft.

He has been a member of the Performance Sub-Committee of the Aeronautical Research Council from 1958 - 1973 and again since 1975 and was the Chairman of this Committee from 1963 to 1971. He is also a member of the Aerodynamics Committee of this Council; also, since 1971 he has been Chairman of the S.B.A.C. Aerodynamics Research Sub-Committee.

AN EXTENSION OF THE FACES TECHNIQUE FOR RAPID WING STORE FLUTTER CLEARANCE* (U) (Article UNCLASSIFIED)

by

M. A. FERMAN** and W. H. UNGER***

McDonnell Aircraft Company
St. Louis, Mo. 63166

ABSTRACT. (U) An extension of the FACES Technique (Ref 1) which provides a rapid wing store flutter clearance procedure is presented. This extension consists of an improved analytical technique expanding both engineering idealizations and the accompanying computer program. This broadens the coverage thus providing a more useful method. The extended FACES method now includes flexible fuselage and flexible control surface dynamics, with an improved pylon representation. The aerodynamics are also expanded to fully account for the new dynamics, and have been modularized to simplify user effort. Multicase aspects have been improved to enhance parametric study applications. A finite section method with programmed equations requiring only basic data input is the principal approach. This allows for single pass vibration and flutter for a wing with multiple sections, with up to two control surfaces per side, and with a multi section flexible fuselage. From 1 to 5 flexible pylons per side with any mix of single or multiple stores can be used. Two and three dimensional aerodynamics for all speed regimes are available.

The computer program is available in IBM and CDC forms in standard batch and in interactive graphics versions using Cathode Ray Tube (CRT) consoles.

Applications are shown for three modern military aircraft with both clean wing and external stores, and with flexible control surfaces and flexible fuselage.

---

* Work sponsored by Air Force Flight Dynamics Laboratory, Wright-Patterson Air Force Base under Contract F33615-74-C-3064.

** Senior Group Engineer, Structural Dynamics

*** Engineer, Structural Dynamics

Approved For Public Release, Distribution Unlimited

LIST OF FIGURES

Figure No.	Title
1	Idealization for Calculated Vibration Option
2	FACES Substructure Method
3	Improved Fast Flutter Routine
4	CRT Version FFR
5	Typical CRT Results for Aircraft 1

LIST OF TABLES

Table No.	Title
I	Application Cases
II	Aircraft 1 with Modified Control Surface - Piano Hinge Attachment - Symmetric Motion
III	Aircraft 2 with Four Pylons Per Side - Symmetric Motion

LIST OF ABBREVIATIONS AND SYMBOLS

Symbol	Description
AC	Aerodynamic Center
C	Chord
CEAC	Computer Engineering Associates Analog Computer
C_{L_α}	Lift Curve Slope $\frac{\partial C_L}{\partial \alpha}$
CID	Calculation - Interpolation Decision Process
DLM	Doublet Lattice Method
DIAPR	Diagnostic Process
D/F	Degree of Freedom
EA	Elastic Axis
EI	Bending Rigidity
FFR	Fast Flutter Routine
GJ	Torsional Rigidity
g	Structural Damping Coefficient
i	$\sqrt{-1}$
I	Imaginary Part of Aerodynamic Derivatives
MER	Multiple Ejector Rack
q_b, q_t	Wing Relative Bending and Twist Angles
$q_{\gamma 1}, q_{\gamma 2}$	Upper and Lower Pylon Roll
$q_{\theta 1}, q_{\theta 2}$	Upper and Lower Pylon Pitch
$q_\beta, q_{\beta 3}, q_{\beta 4}$	Pylon Yaw, Forward and Aft Rack Yaw
$q_{\gamma 3}, q_{\gamma 4}$	Forward and Aft Rack Roll
$q_{\theta 3}, q_{\theta 4}$	Forward and Aft Rack Pitch
q_r, q_p	Root Roll and Pitch
q_{VB}, q_{LB}	Fuselage Relative Vertical and Lateral Bending Angles
q_{TO}	Fuselage Relative Twist Angles

LIST OF ABBREVIATIONS AND SYMBOLS (Continued)

Symbol	Description
q_ζ, q_ϕ, q_H	Control Surface Relative Bending, Twist, and Rotation Angles
R	Real Part of Aerodynamic Derivatives
SURF	Surface Fit Program
TER	Triple Ejector Rack
V	Velocity
α	Pitch or Twist Angle
Λ	Sweep Back Angle
ω	Circular Frequency, Radians per Second
∂	Partial Derivative

INTRODUCTION

The flutter clearance of modern aircraft carrying external stores can be a costly and time consuming effort. An earlier effort, References 2 and 3, was aimed at providing a rapid analytical means for improving store flutter clearance. This approach has been extended in both the engineering idealizations and the associated computer programs, see Reference 1. A finite section approach was again used as the main computational method. The addition of control surface and flexible fuselage dynamics including an improved pylon representation has been made to the computer program. The computer program was also simplified to improve the handling of multicase analyses. The original job stepped doublet lattice aerodynamics was put in modular form to expedite use, and a routine for interpolating aerodynamic forces versus 1/K was added to reduce analysis costs. Single pass vibration and flutter, storage of results for future work, flutter estimates of new stores from existing data are still retained. The modifications made were only in the vibration and flutter routines. No changes were made in the routines related to data storage, retrieval, and diagnostics. Data is passed to the storage and retrieval system as it was in the original program, see References 1 - 3.

Batch and graphics version for CDC and IBM computers again are available.

DYNAMICS IDEALIZATIONS

VIBRATION METHODS

The original concepts embodied in the earlier program have been retained. Flutter computations can be accomplished in one of two processes. One process uses vibration data computed external to FACES employing any method including finite element dynamics. The other process is a single pass, highly optimized vibration and flutter operation with the vibration data computed inside FACES using an extremely rapid, finite section analysis. This latter method is the core of the FACES technique. It operates directly with basic data, and is called the Calculated Vibration Module.

Figure 1 shows the basic idealization of mass and structural modeling, degrees of freedom and geometry. The wing is allowed to have up to 14 sections per semi-span with a serially kinked elastic axis (EA), i.e., the EA may have a different sweep in each section. Each section may have mass, roll, pitch and yaw inertia about its c.g. The mass and inertia can be based on streamwise cuts through the wing, or cuts perpendicular to the EA. Wing EA stiffness data can be directly used, employing the bending and torsion rigidities, EI and GJ, or it can be based on deflection methods. Alternately, the corresponding influence coefficients referred to the EA can be used. If a reference axis rather than the EA is employed, the coupled wing influence coefficients can be used. Root springs or influence coefficients defining the fuselage/wing root restraint are permitted. The relative bending and twisting motions between sections are used as the wing degrees of freedom (D/F). These quantities are respectively denoted by q_{bn} and q_{tn} in the figure. The wing roll and pitch motions relative to the fuselage are denoted by q_r and q_p in the figure.

Up to two control surfaces per side can be included with a total of 14 sections allowed. Each section may have mass, and roll, pitch and yaw inertia about axes aligned either streamwise, or at the angle Λ_s from streamwise. A straight elastic axis with sweep Λ_e is considered, with stiffness defined by EI and GJ data or by deflection methods, or by influence coefficients. The hinge axis is treated as a straight line with sweepback angle Λ_H. Either continuous hinges (piano hinges) or discrete hinges at two more points are allowed. An actuator can be included at each control surface section, with the rotary stiffness defined perpendicular to the hingeline. Control surface relative bending $q_{\zeta j}$ and relative torsion $q_{\phi j}$ freedoms at each section are allowed along with one rotational freedom q_H relative to the wing. A constraint technique is used to couple the q_ζ and q_ϕ terms to account for hinge attachment to the wing. See Appendix A of Volume I, Reference 1, for more details on the method.

Up to 24 fuselage sections can be allowed with each section having mass, and roll, pitch and yaw inertia, which are all based on

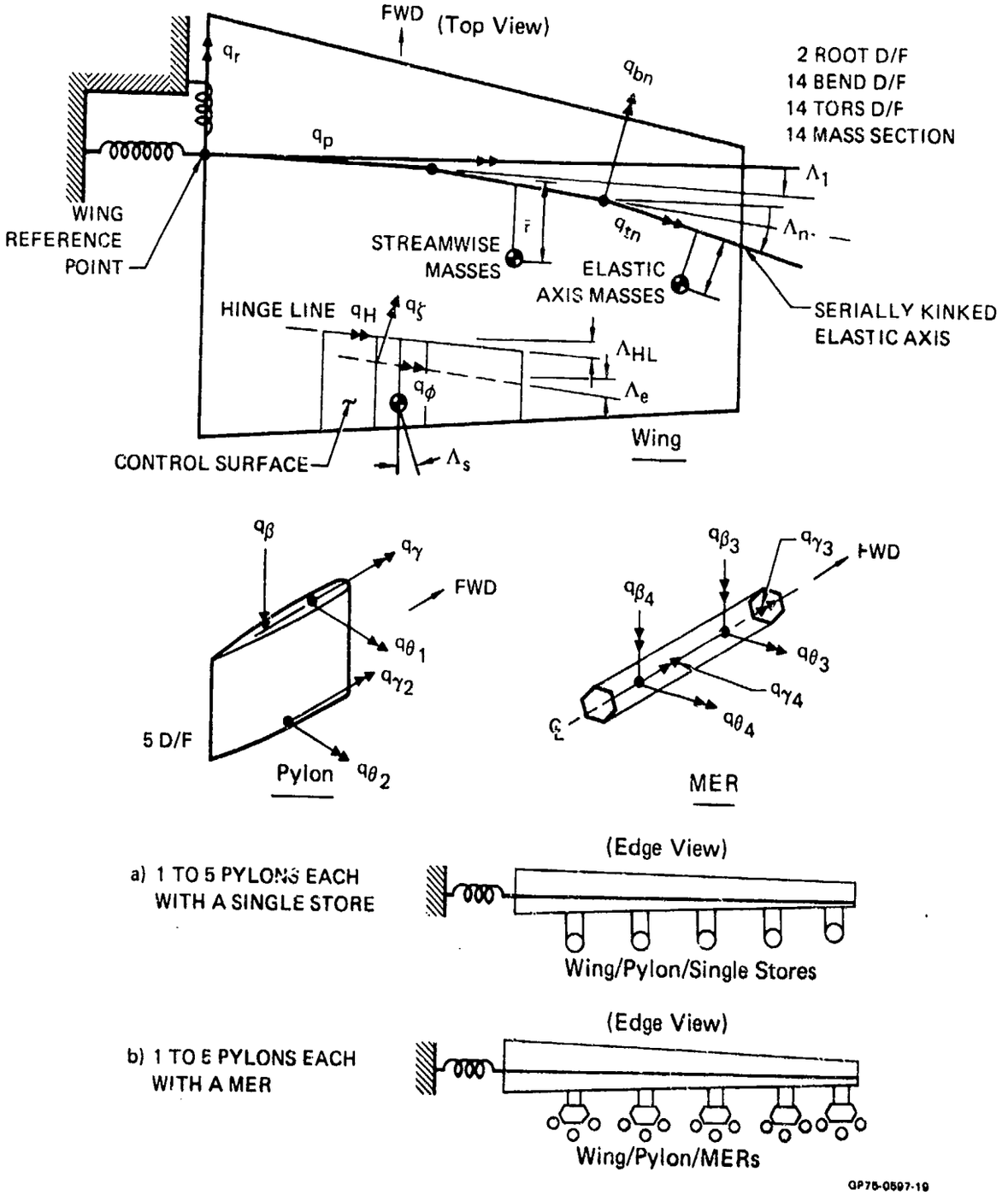
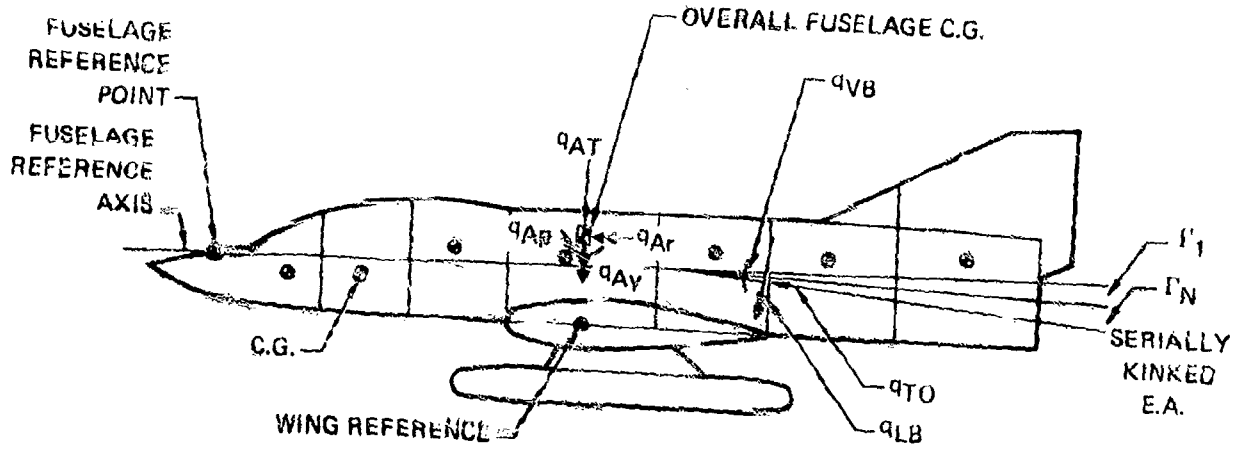
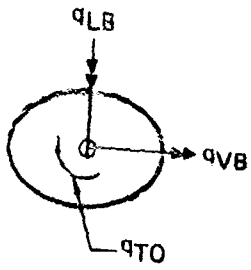
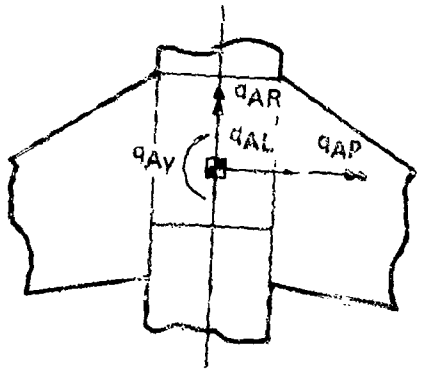


FIGURE 1 IDEALIZATIONS FOR CALCULATED VIBRATION OPTION
Part 1





Aft View



Top View

FIGURE 1 IDEALIZATION FOR CALCULATED VIBRATION OPTION GP78-0697-15
Part 2

streamwise section properties. A serially kinked elastic axis with up to 24 kinks in the vertical plane is allowed, with the EA defined as a straight line in the horizontal plane. Fuselage stiffness data can be based on simple EI and GJ data, uncoupled stiffness from deflection methods, or influence coefficients. If a reference axis rather than an e.a. is used, then coupled influence coefficients can be used. For symmetric analysis, the elastic fuselage freedoms are vertical bending freedoms q_{VB_j}. For antisymmetric analyses, the elastic freedoms are lateral bending q_{LB_j} and tortion q_{TO_j}.

The equations include provisions for one to five pylons per side, with single, TER or MER carriage of multiple weapons. Each pylon is idealized as having from one to five freedoms relative to the wing. These freedoms are roll, pitch and yaw relative to the wing at the upper end of the pylon, and roll and pitch of the rack/store relative to the lower end of the pylon. These D/F are respectively denoted by $q_{\gamma 1}$, $q_{\theta 1}$, q_{β}, $q_{\gamma 2}$, $q_{\theta 2}$. The upper and lower pylon roll axes can be arbitrarily located vertically along the pylon. The upper pitch axis can now be arbitrarily located along the upper roll axis, and the lower pitch axis can now be arbitrarily located along the lower roll axis. Pylon stiffness or influence coefficients can be directly used. Elastic coupling between the freedoms of each pylon is permitted, but none is allowed between different pylons nor between the pylon and the wing. Pylon mass, moments and products of inertia are used. Single store mass and inertia can be included.

Figure 1 also highlights the idealization for multiple store carriage (MER's, TER's). Each rack is idealized as having from one to six relative degrees of freedom; namely, roll, pitch, and yaw angles for the front and aft ends of the rack relative to the center. These D/F are respectively noted as $q_{\gamma 3}$, $q_{\theta 3}$, $q_{\beta 3}$, $q_{\gamma 4}$, $q_{\theta 4}$, $q_{\beta 4}$. Rack springs or influence coefficients may be used to define elastic properties. Elastic coupling is permitted between the freedoms at each end of a rack, but not between various racks, nor the pylons, nor the wings. Mass and inertia of the rack and MER (TER) stores can be included.

For symmetric vibration, the rigid aircraft freedoms of translation, q_{AT}, and pitch, q_{AP}, were used. For antisymmetric vibration, the rigid aircraft freedoms of lateral translation, q_{AL}, roll, q_{AR}, and yaw, q_{AY}, were used.

The coupled vibration for flexible wing/control surface/pylons/stores/fuselage were obtained in a substructure method from two uncoupled solutions; namely, (a) the uncoupled vibration case of flexible wing/control surfaces/pylon/stores with rigid fuselage, and (b) the uncoupled case of flexible fuselage with rigid wing/control surfaces/pylons/stores. This is depicted in Figure 2. This approach was used to keep the total vibration solution size equal to or less than the uncoupled solution sizes, which thus requires no larger computer core size than that used for the uncoupled cases.

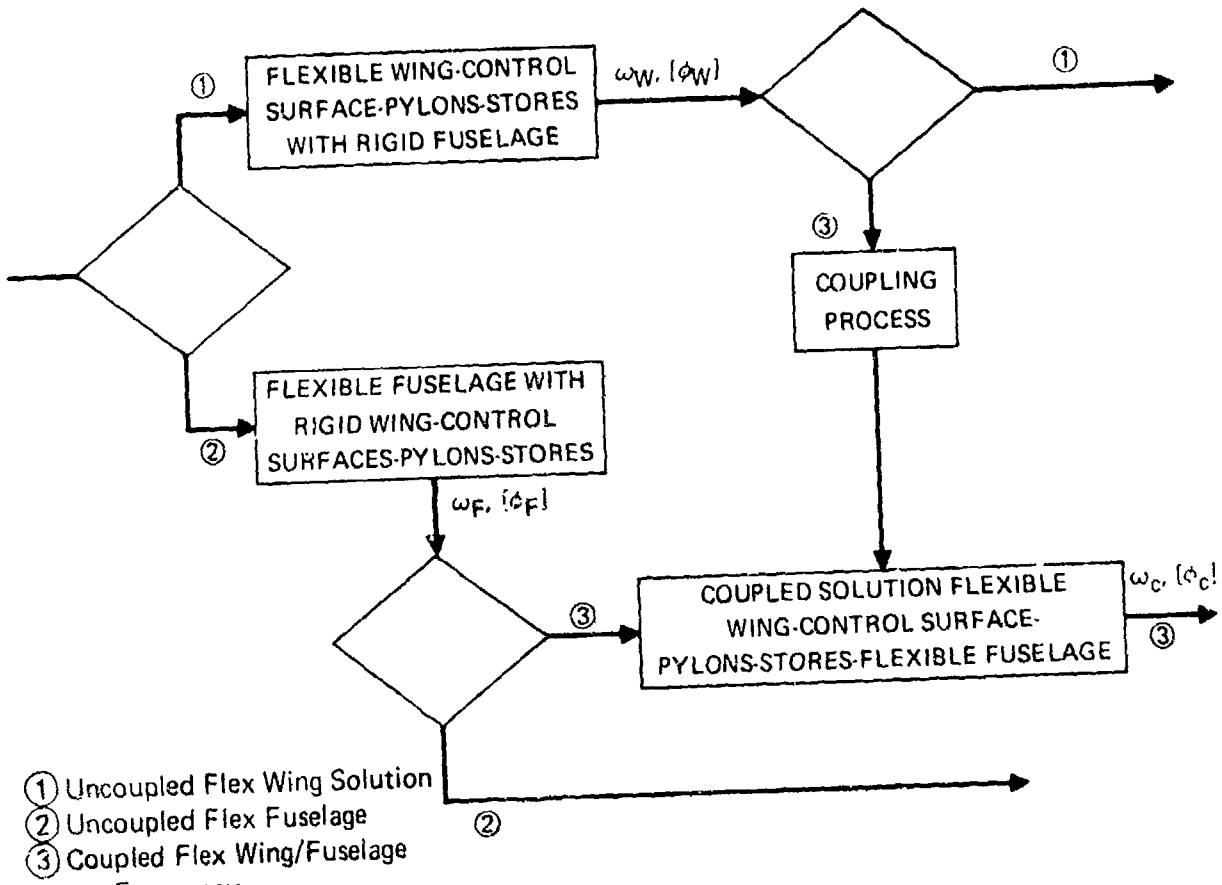


FIGURE 2 FACES SUBSTRUCTURE METHOD

The program is designed only for symmetrical carriage of stores from each side of the aircraft. Within this constraint, any combination of single store carriage and MER (TER) carriage can be accommodated for up to five pylons per wing semispan.

AERODYNAMICS

Three types of aerodynamics are used in FACES, and are described in detail in Appendix C of Volume I, Reference 1. A Modified Strip Theory method is available as a basic aerodynamics approach for the standard application. It is used to calculate wing and control surface aerodynamics based on streamwise aerodynamic strips when employing the calculated vibration approach. The sectional values of the lift curve slope and aerodynamic center location must be submitted in the analysis. The corresponding control surface parameters can be submitted or used as two dimensional quantities. These quantities can reflect values applicable to either two or three dimensional incompressible or compressible flow. Either the average values of the lift curve slope and aerodynamic center for the complete wing or the local values can be used. For cases where predetermined vibration data is input, streamwise aerodynamic strips can be used, as can those cut perpendicular to the elastic axis (or a reference axis). The pylons, racks, stores, and fuselage can be accounted for by use of equivalent flat-plate or primary surface elements.

The Doublet Lattice Method (DLM) from Program N5KA of Reference (4) is available for computation of lifting surface aerodynamics for all lifting surfaces and bodies. This program is now available as a module to simplify its use. It interfaces with FACES via the Surface Fit Program, SURF, which is now a module. The SURF program calculates the polynomial surface fit coefficients required in DLM. SURF is now expanded to include control surface and fuselage coefficients computations. Both calculated and predetermined vibration data can be used. Calculated vibration data is always taken through SURF to DLM to maintain single pass flutter. Predetermined vibration data whether finite element or finite section can be handled in SURF if the polynomial coefficients are needed. If the polynomial coefficients are also predetermined, SURF is bypassed. Appendix B of Volume I, Reference (1), presents the analytical methods in SURF. A method for interpolating the aerodynamic forces versus reduced frequency (1/k) was added to reduce the cost of using the DLM option.

The Piston Theory method is included for supersonic aerodynamics. This version is based on the third order type of approximation applied to airfoils with control surfaces, but is not applicable to thick bodies such as a fuselage or stores. This method is directly applicable to both finite section and finite element vibration modeling. For obtaining best results, it is not advised to use the Piston Theory below Mach 2.

FLUTTER EQUATION AND SOLUTION

A standard V-g solution is used to determine flutter speeds and frequencies. The standard formulation of aerodynamic derivatives (R + iI) is combined with generalized mass and stiffness to form the flutter equations of motion. Either predetermined data which is directly input, or calculated vibration data which is passed internally is used. A mode tracking method is used to locate flutter crossings to aid the user in reviewing results.

THE FACES COMPUTER PROGRAM

The FACES computer program is a system of modular computer programs divided into four procedures. The four procedures are: a) Fast Flutter Routine (FFR), b) Data Sotrage and Retrieval System (DSRS), c) Diagnostic Process (DIAPR), and d) Calculation-Interpolation-Decision Process (CID). The first procedure is the Fast Flutter Routine which is a collection of modules under the control of a main program. This allows for a selection of various flutter analysis methods without the necessity of changing the program or the job control cards. The second procedure is the Data Storage and Retrieval System which allows for the accumulation of large quantities of calculated and experimental flutter data for an aircraft system with a multiple of external stores on various pylon/rack combinations, and retrieval of user selected cases. The last two procedures, the Diagnostic Process and the Calculation-Interpolation-Decision Process, provide engineering information obtained from the DSRS data for use in flutter analysis, flutter clearance and other design purposes. CID allows estimation of flutter characteristics for new stores while DIAPR checks the acceptability of the interpolated data. References 1 and 3 give a detailed account of the DSRS, DIAPR and CID procedures.

The Fast Flutter Routine (FFR) is a procedure containing modules for calculating vibration results, surface fit coefficients, oscillatory aerodynamics, an aerodynamic interpolation procedure, and a V-g-flutter solution.

Figure 3 shows a program schematic of the Fast Flutter Routine. Each module has been assigned a number for internal usage.

The Calculated Vibration module (050) provides a rapid means of calculating vibration characteristics of a wing/fuselage/control surface/pylon/rack/store system based on the direct input of basic data. The module utilizes programmed equations for a finite section wing with control surfaces, pylons and stores; and for a flexible fuselage having symmetric and/or antisymmetric rigid body motion. The input consists of the wing, control surface and fuselage sectional mass, geometry and stiffness along with the mass, geometry and stiffness for the pylons, racks and stores. The substructure vibration solutions are computed. The uncoupled wing vibration solution is made for the wing system, and the results are passed to the flutter modules, or to the coupled vibration solution. The Calculated Vibration module will calculate the uncoupled vibration properties of the fuselage and will pass the necessary data to the coupled flexible fuselage/flexible wing vibration solution.

Once both sets of uncoupled vibration properties have been calculated, then the coupled vibration solution is made and the results are passed to the remaining user specified aerodynamics and flutter module

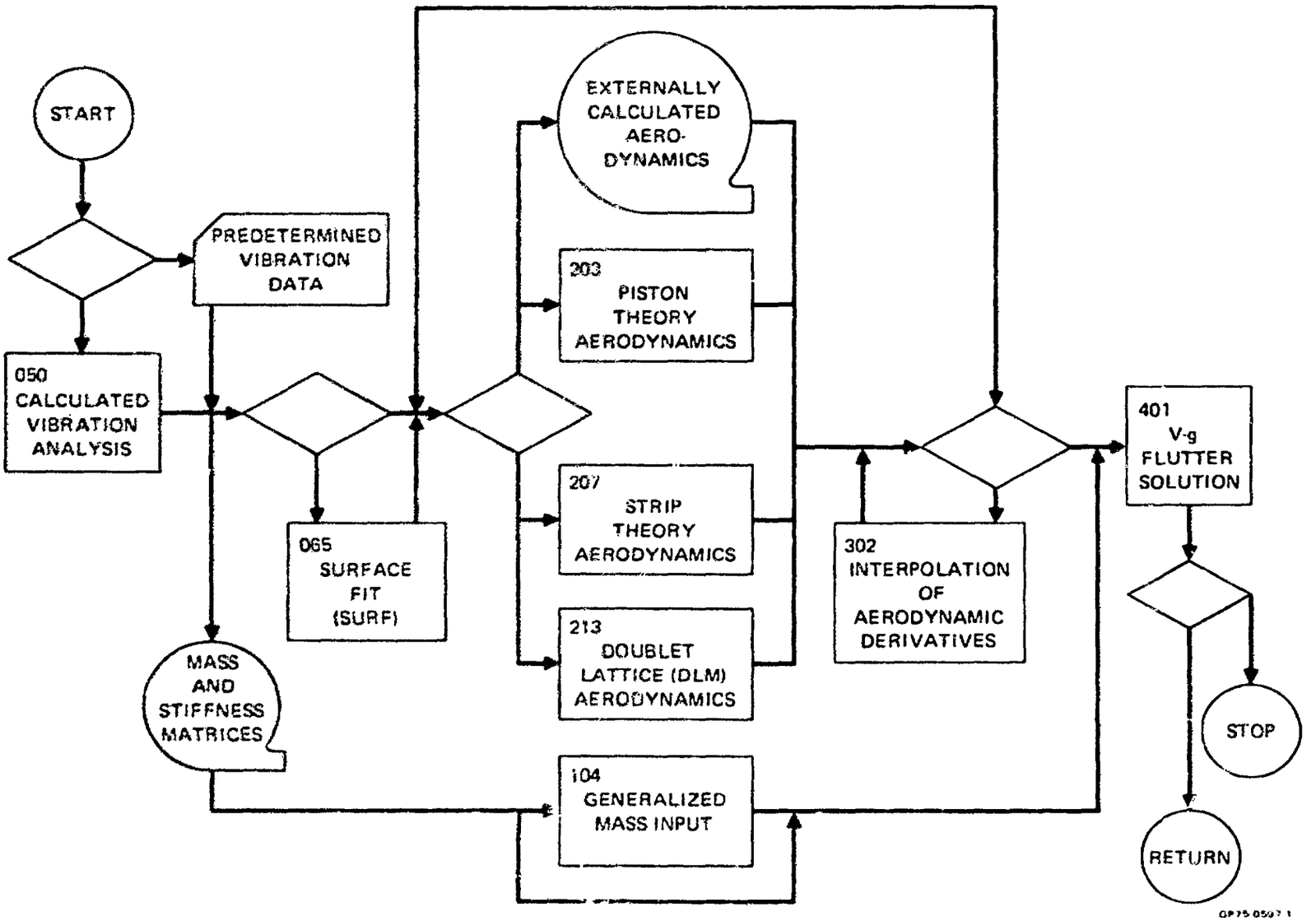


FIGURE 3 IMPROVED FAST FLUTTER ROUTINE

Three aerodynamics modules are shown in Figure 3. They are the Piston Theory Module (203), the Modified Strip Theory Module (207) and the Doublet Lattice Unsteady Aerodynamics Module (213). In addition to these three modules, an option is available whereby aerodynamics calculated externally to the program may be input.

Modules 065, 213, and 302 have been added as a block so that Doublet Lattice Unsteady Aerodynamics may be more easily obtained than was originally available in the earlier FACES program. Instead of a three job step procedure, Doublet Lattice Aerodynamics may now be obtained in a simple one step submittal. The Surface Fit module performs a least squares polynomial surface fit on data passed from the Calculated Vibration module to obtain the polynomial coefficients required by Module 213.

Module 213 can calculate data for only a limited number of reduced frequencies because of the size of the program and the cost of calculating the unsteady aerodynamic derivatives. The Interpolation of Aerodynamic Derivatives Module (302) has been added to allow the user to obtain more reduced frequency data at a fraction of the cost of obtaining the original Doublet Lattice data. Module 302 can also use aerodynamic derivatives obtained externally to FACES, interpolate them and add them to the derivatives computed by the aerodynamic modules within FACES.

The classical V-g flutter solution is carried out in Module 401. A root sorting routine in 401 enables the program to track modes with airspeed, allowing flutter speeds to be extracted automatically from the V, g, ω data. Printer plots are also generated which show the V-g and V-ω plots with the points given mode numbers so that g and ω can be followed on the plots.

THE FACES INTERACTIVE GRAPHICS PROGRAM

In addition to the standard batch process version (FACES 1B), the FACES system has been interfaced with a CRT interactive graphics console. The CRT program (FACES IIIB) provides the FACES capabilities under the direct control of the user at the console so that rapid changes in parameters can be made with their effects on flutter rapidly seen.

FACES IIIB has been made available on two computer systems: the CDC 6600 driving a 274 graphics console and an IBM 360 driving a 2250 graphics console. Printer output is available in both cases.

The main graphics feature is that the user/engineer is in the flutter calculation loop for efficient computer utilization and rapid turnaround. Figure 4 shows a schematic of the FACES FFR/CRT program. The four blocks within the FACES program which contains CRT console displays are shown on the figure. They are: a) the uncoupled wing vibration solution, b) the uncoupled flexible fuselage vibration solutions, c) the coupled vibration solution, and d) the V-g flutter solution.

The FFR/CRT program starts by calculating the uncoupled wing vibration properties in the Uncoupled Wing Vibration Solution. The vibration frequencies are displayed on the CRT. After they have been examined, the user has a number of options to choose from. They include:

- o Displaying the eigenvectors
- o Displaying the numerical values of the deflection data
- o Plotting the deflection data
- o Changing input matrix data to do a parametric vibration analysis
- o Continuing to the next part of the analysis.

The next analysis the user can choose is the uncoupled flexible fuselage solution. The program calculates the uncoupled fuselage vibration frequencies and displays them on the CRT screen. After they have been examined, the user again has a number of options to choose from. It includes options similar to the list shown immediately above except that they pertain to a flexible fuselage. After examining any data he wishes to see, the user may return to change data for a parametric study or he may continue to the coupled vibration solution.

The coupled vibration solution calculates the coupled frequencies and displays them. Again, the user has several options to choose from once he has examined the coupled frequencies. These include:

- o Displaying the coupled wing deflections
- o Plotting the coupled wing deflections
- o Displaying the coupled fuselage deflections

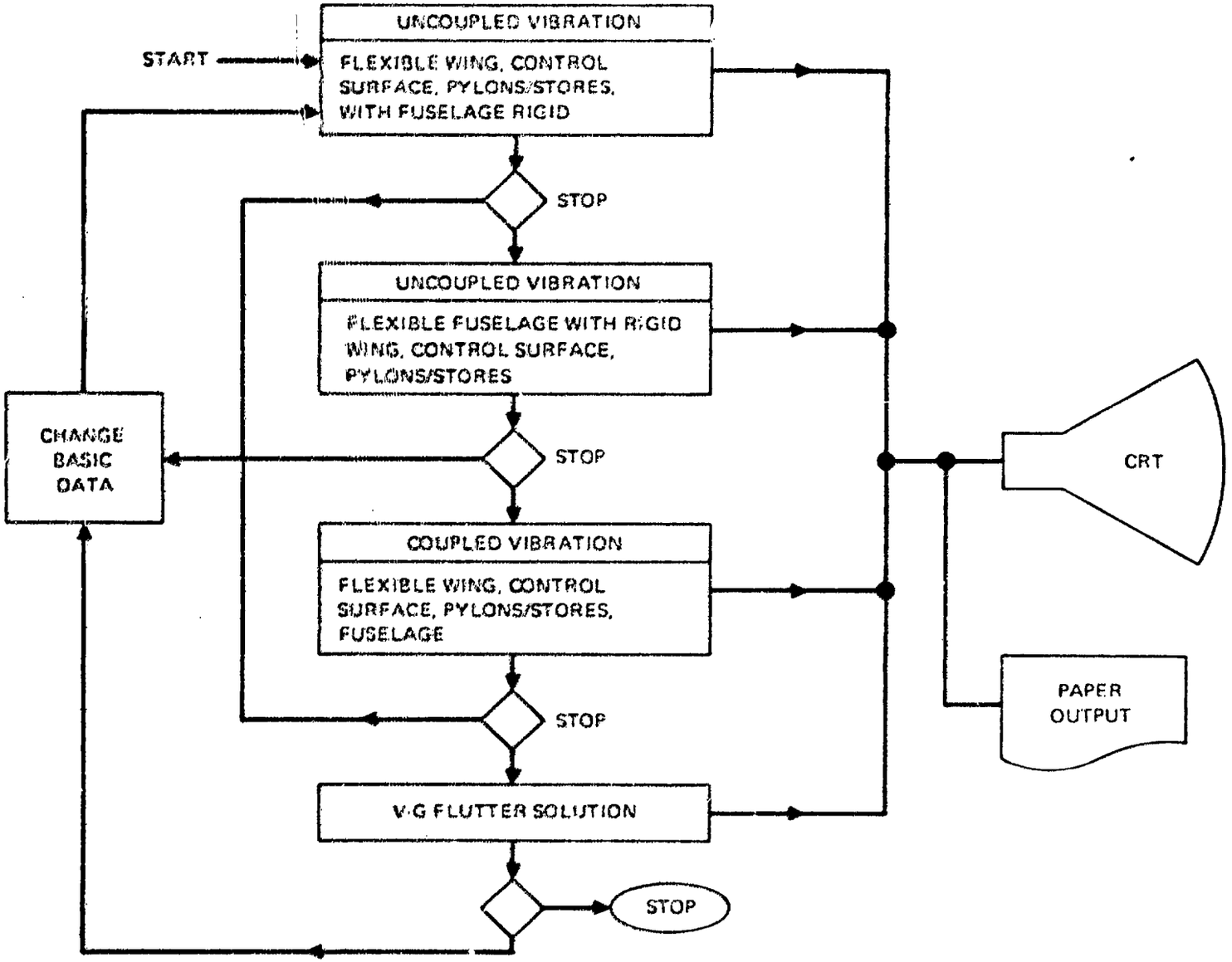


FIGURE 4 CRT VERSION - FFR

- o Plotting the coupled fuselage deflections
- o Changing the input matrix data and rerunning the vibration analysis
- o Continuing to the V-g flutter solution.

If he chooses to go to the V-g flutter solution, a summary of flutter crossings is displayed on the screen and plots of V-g and V-ω can be examined. After the results of the Flutter Solution has been examined, the program may be recycled back to the Calculated Vibration Analysis module to run another parametric case, or the program may be terminated.

APPLICATIONS

The FACES method has been applied to three modern military aircraft considering cases with a variety of stores, and with and without flexible control surface freedoms, and with and without flexible fuselage freedoms. This is summarized in Table I. These studies employed only the FFR procedure while earlier studies also investigated the DSRS and DIAPR/CID procedures, see References 1 - 3. Independent corroborating studies based on the McDonnell General Flutter Program and the earlier FACES programs (IA and IIA) were used to check the new FACES batch and graphics versions (IB and IIIB). Some GVT results were used to gauge the theoretical results. Only a few results are given here, while many more are covered in Reference 1.

Aircraft 1 is a fighter bomber of aspect ratio 2.76 and is normally equipped to carry stores from two pylons at 35.7% and 57.3% of semispan. This aircraft was used to check clean wing, single store carriage, flexible control surfaces, and flexible fuselage using the FFR option. Earlier use was made of this aircraft for DSRS and DIAPR/CID studies.

Aircraft 2 is a variation of aircraft 1 and has an aspect ratio of 2.8. This was used to check single and multiple pylon carriages with up to three hypothetical pylons added at 75.2%, 82.2% and 92% of semispan. Cases with flexible fuselage were investigated.

Aircraft 3 is a fighter and was used to investigate a wing with streamwise mass sections for three configurations, namely, a wing with flexible fuselage, a wing with flexible control surfaces, and a wing with single store with flexible fuselage.

Table II shows results of FACES IB and corroborating studies of symmetric vibration and flutter of aircraft 1 with a clean wing and a flexible control surface having a continuous or piano hinge attachment. The actuator was attached in the second control surface section. The FACES IB results are shown for all substructure cases, while the corroborating study results are given for only the uncoupled wing with control surface. Good agreement is shown between FACES IB and the corroborating study for the uncoupled wing with control surface cases. An uncoupled control surface rotation frequency of 40.6 Hz was used.

Flutter results are shown for both studies. These used two dimensional flow aerodynamics, i.e., an average lift curve slope $C_{L_\alpha} = 2\pi$, and an average aerodynamic center location at the quarter chord, AC = .25C. FACES IB results are shown for the uncoupled case of flexible wing and control surface and for the coupled case of flexible wing/control surface/fuselage. Corroborating study results are shown for the uncoupled flexible wing-control surface case. Good agreement between the two studies is shown for the uncoupled wing case. The effect of fuselage flexibility in the coupled FACES IB results is slight.

TABLE I APPLICATION CASES

AIRCRAFT	NO. OF CASES	PYLONS/STORES	FLEX CONTR.	FUSEL	
				FLEX	RIGID
1	2	CLEAN		X	X
	2	CLEAN	X	X	X
	1	ONE PYLON WITH A TANK		X	X
2	3	ONE PYLON WITH MERS		X	
	1	FOUR PYLONS WITH TWO SINGLE STORES, ONE TER, ONE MER		X	X
	1	FIVE PYLONS WITH, THREE SINGLE STORES, ONE TER, ONE MER		X	X
3	2	CLEAN WING		X	X
	1	CLEAN WING	X		X
	1	ONE PYLON WITH 600 GALLON TANK		X	X

GP76-0587 10

TABLE II AIRCRAFT 1 WITH MODIFIED CONTROL SURFACE PIANO HINGE ATTACHMENT - SYMMETRIC MOTION

CONFIGURATION	B.L.	PYLON	RACK	RACK CONFIG.	STORE	REMARKS

	FACES IB				CORROBORATING STUDY
	UNC. WING, C/S	UNC. FUS.	COUPLED		UNC. WING, C/S
VIBRATION FREQUENCIES HERTZ	8.21	12.18	8.01	49.37	8.21
	20.55	22.09	12.60	50.79	20.29
	27.05	32.29	20.52	59.84	27.86
	38.63	41.47	22.34	68.27	37.94
	48.80	47.99	27.10		48.95
	50.79	80.34	33.17		50.69
	67.82		37.82		67.85
	73.10		43.33		73.77

	UNC. WING/C/S		COUPLED		UNC. WING/C/S	
	SPEED KNOTS	FREQ HZ	SPEED KNOTS	FREQ HZ	SPEED KNOTS	FREQ HZ
FLUTTER $C_{L_\alpha} = 2\pi$ AC = 0.25c	976.	19.2	979.	20.3	950.	19.8
	1126.	33.8	1300.	33.4	1126.	33.7

GP75 0597 11

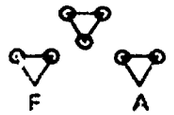
Table III shows results of symmetric vibration and flutter for aircraft 2 considering store carriage from four pylons per side. The actual pylons at 35.2% and 57.3% are supplemented by two hypothetical pylons at 75.2% and 92% of semispan. A TER is carried at the 35.2% pylon, a MER at the 57.3% pylon, an MK81 at the 82.2% pylon, and a LAU 32 A/A at the 92% pylon. The TER and MER loading configurations consist respectively of 3 M117's and 4 shoulder mounted M117's. Table III shows symmetric vibration and flutter results for FACES IB, FACES IA and corroborating studies. The FACES IB vibration results shown, cover all three substructure solutions. FACES IA vibration results are shown for the uncoupled flexible wing/stores case and show close agreement with those of FACES IB. Existing corroborating studies presented for the earlier configurations of Reference 3 are shown and correlate well.

FACES IB flutter results are shown for the uncoupled flexible wing/stores case and the coupled flexible wing/stores/fuselage case. Close agreement between the FACES IB results and the FACES IA results for the uncoupled wing cases are seen. The corroborating study results of Reference (3) for the uncoupled wing/stores case shows good agreement. Note that these flutters are very sensitive and that closer agreement would be difficult to establish. The coupled FACES IB flutter results show reasonable effects of the inclusion of flexible fuselage modes.

Thus, close agreement is seen between the vibration and flutter results of the studies, considering the overall complexity and sensitivity. The extreme sensitivity of flutter speed to damping for the flutter crossings is flagged by the symbols M and N. The latter, in particular, is so sensitive that its V-g plot would be difficult to separate from the V axis in any normal V-g presentation.

Figure 5 shows typical CRT graphics results for Aircraft 1. Part 1 shows coupled symmetric wing-store vibration and coupled symmetric fuselage vibration for a case with single pylon carriage of a large fuel tank. The upper picture shows the mode number, frequency, bending and torsion shapes and a tabulation of pylon/store deflection data. These latter quantities are arranged to show three linear deflections and three rotations at the pylon c.g. and store c.g. for each "store station". The first six numbers are pylon fore-aft, lateral and vertical translations, and roll, pitch and yaw angles. The next six are single store displacements and angles. If a MER is used, then there are two sets of six numbers following the pylon data, one for the front store cluster, and one for the aft store cluster. The lower picture shows the coupled symmetric fuselage vibration results. Note that only the bending deflection is given since there is no torsion for this case. In the antisymmetric case, both are shown. Part 2 shows vibration results for the uncoupled wing with control surface vibration case. The results are similar to those of Part 1 except that control surface motion is shown in the torsion plot. Part 3 shows flutter results for the first CRT example in Part 1. The upper part shows the flutter summary table which lists flutter crossing speeds and frequencies for

TABLE III AIRCRAFT 2 WITH FOUR PYLONS PER SIDE
SYMMETRIC MOTION

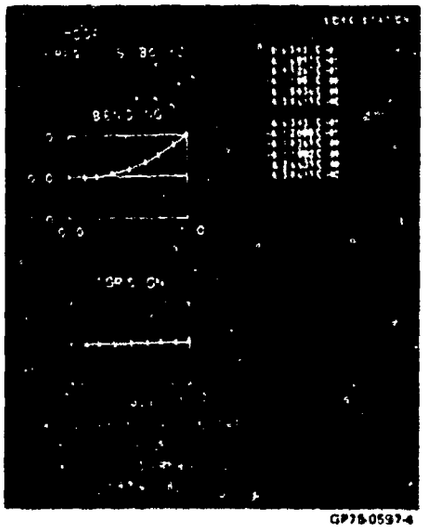
	B.L.	PYLON	RACK	RACK CONFIGURATION	STORE	REMARKS
CONFIGURATION	81.50 132.50 168.20 214.00	MAU 12 B/A MAU 12 B/A ECM PYLON ECM PYLON	TER-100 MER-100	 F A	3-M117 GP 4-M117 GP MK81 LAU 32A/A	

	FACES 1B UNC. WING	FACES 1B UNC. FUS.	FACES 1B COUPLED	CORROBORATING STUDY UNC. WING	FACES 1A UNC. WING
VIBRATION FREQUENCIES HERTZ	3.98 9.64	11.36	3.97 9.64	3.98 10.47	3.98 9.64
	4.20 10.[illegible]	17.93	4.19 10.47	4.19 11.01	4.19 10.47
	4.28 10.[illegible]	29.09	4.28 10.62	4.50 11.30	4.27 10.78
	4.55 1[illegible]	38.23	4.53 12.33	4.58 13.21	4.53 13.19
	6.33 16.[illegible]	44.05	6.26 13.40	6.36 16.35	6.33 16.22
	9.14 21.[illegible]	78.19	8.88 16.18	9.20 12.32	9.13 21.25

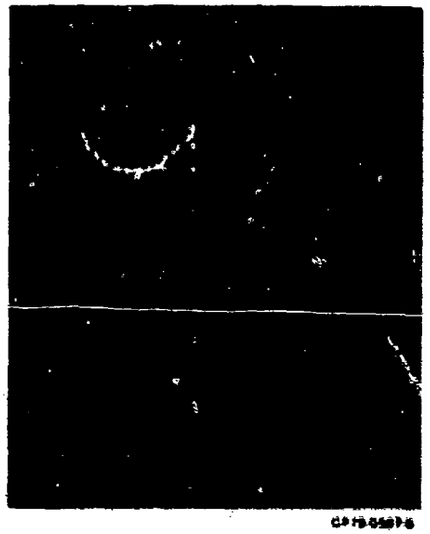
	UNC. WING		COUPLED		UNC. WING		UNC. WING	
FLUTTER $C_{L_\alpha} = 2\pi$ AC = 0.25c	SPEED KNOTS	FREQ HZ	SPEED KNOTS	FREQ HZ	SPEED KNOTS	FREQ HZ	SPEED KNOTS	FREQ HZ
	561.M	9.6	615.M	10.6	590.M	11.3	586.M	10.7
	656.N	9.6	627.	12.6	677.	12.4	666.N	10.7
	684.	12.3	659.N	10.5	720.N	10.5	685.	12.3
	980.M	4.4	697.	12.2	817.M	4.4	960.M	4.4
	1440.	19.0	980.M	4.4	1445.	19.0	1433.	19.0

GP75 0597 12

M - Mild Flutter Mode – $0.002 \leq g \leq 0.015$
N - Mild Flutter Mode – $0.0001 \leq g \leq 0.0001$

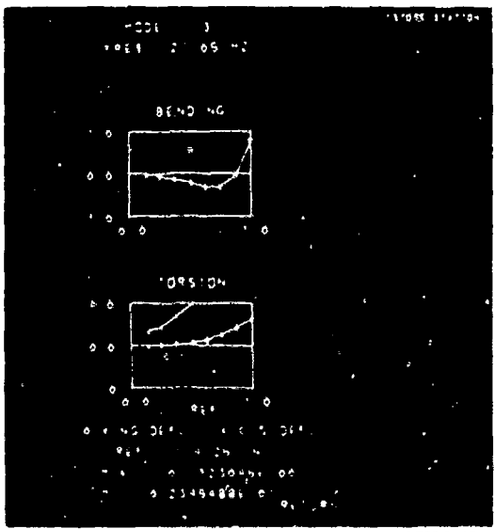


COUPLED WING/STORE MODE 1

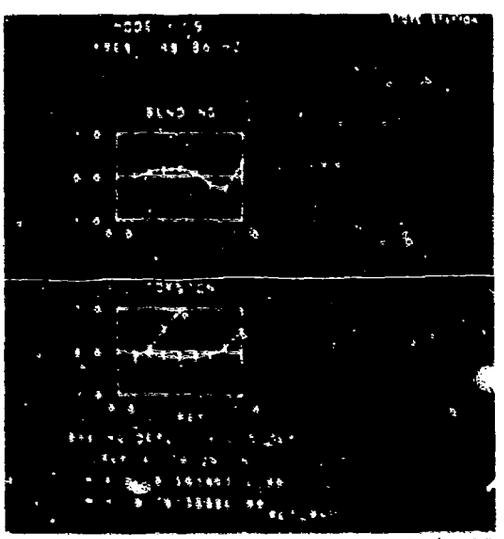


COUPLED FUSELAGE MODE 4

FIGURE 5 TYPICAL CRT GRAPHICS RESULTS FOR AIRCRAFT 1
Part 1 - Coupled Wing/Store/Fuselage Modes

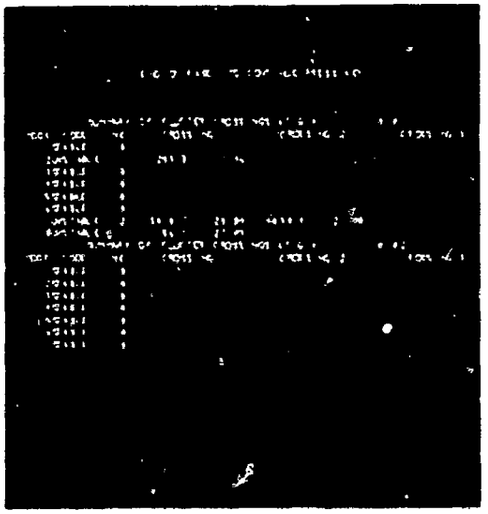


UNCOUPLED MODE 3

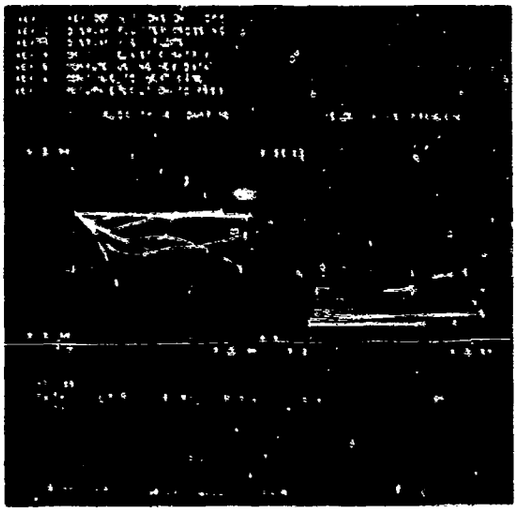


UNCOUPLED MODE 5

FIGURE 5 TYPICAL CRT GRAPHICS RESULTS FOR AIRCRAFT 1 (Continued)
Part 2 - Uncoupled Wing/Control Surface Modes



FLUTTER SUMMARY TABLE



V-g-ω PLOT

FIGURE 5 TYPICAL CRT GRAPHICS RESULTS FOR AIRCRAFT 1 (Concluded)
Part 3 - Flutter Results

various values of structural damping. The lower part shows the graphic display of the V-g-ω data. The damping versus speed (g vs V) and frequency versus speed (ω vs V) are shown. A user's menu showing various options for console operation (keys) is shown at the upper left.

CONCLUDING REMARKS

The current extension of the FACES method retains the same basic, rapid features of the earlier version, and gives much wider configuration coverage with a corresponding reduction of engineering effort. It is now possible to analyze the flutter properties of a general wing or lifting surface with or without control surfaces, and with or without pylons/stores. Flexible fuselage effects can be included in all analyses. The unique features of rapid single pass vibration and flutter, data storage and retrieval, data diagnostics, and estimation of new stores from accumulated data have been retained. The computer programs have been improved to enhance usage and are again available in both batch and CRT graphics versions for both IBM and CDC machines. Improved multicase capability with the option for back to back symmetric and antisymmetric results will provide a reduction of user labor. The employment of preprogrammed equations requiring only basic data input will free the user from much tedious effort. The CRT option provides a version with significant visibility to the user. It allows for direct and rapid data changes, and the ability to assess results between data changes.

REFERENCES

1. Ferman, M. A., Unger, W. H., Wells. J. R., "An Extension of the Rapid Method for Flutter Clearance of Aircraft with External Stores", Vols. I, II, III - to be released as an AFFDL Technical Report.

2. Ferman, M. A., Unger, W. H., "A New Approach for Rapid Flutter Clearance of Aircraft with External Stores", Aircraft/Stores Compatibility Symposium Proceedings, Sacramento, Calif., 18-20 September 1973.

3. Ferman, M. A., Unger, W. H., et al, "A Rapid Method for Flutter Clearnce of Aircraft with External Stores", AFFDL TR-73-74, July 1973.

4. Geising, J. P., Kalman, T. P., and Rodden, W. P., "Subsonic Unsteady Aerodynamics for General Configurations", AFFDL TR-71-5, Part II, Vol. I and II, April 1972.

AUTOBIOGRAPHY

M. A. Ferman
Senior Group Engineer
McDonnell Aircraft Company

Mr. Ferman received a B.S. in Aeronautical Engineering from Purdue University in 1957 and an M.S. in Applied Mechanics from Washington University (St. Louis, Mo.) in 1962. He joined McDonnell Aircraft Company in 1958 and has specialized in Structural Dynamics with particular emphasis on vibration and flutter of aircraft. This work has included theoretical and experimental areas related to advanced design, production aircraft, and methods and research. He was Principal Investigator on the "Conceptual Flutter Research" project sponsored by the Naval Bureau of Weapons from 1964 - 1968. His more recent assignments include supervision of Structural Dynamics aspects on the "F-15 Composite Wing", from 1971 to 1974, and Principal Investigator for the research project, "Flutter of Aircraft with External Stores", sponsored by the Air Force Flight Dynamics Laboratory from 1971 - 1973, and from 1974 until the present. He has authored and co-authored reports and papers in this field.

He was part-time Lecturer in Graduate Applied Mechanics at St. Louis University from 1965 - 1971, and is an Associate Fellow in the American Institute of Aeronautics and Astronautics.

AUTOBIOGRAPHY

W. H. Unger
Engineer
McDonnell Aircraft Company

Mr. Unger received a B.A. in Chemistry from Southern Illinois University at Edwardsville in 1969. Since joining the Structural Dynamics Department of McDonnell Aircraft Company in 1963, he has been concerned with vibration and flutter and has gained extensive experience with digital computer methods. He has worked on such projects as Gemini, F-15, Advanced Design and "Conceptual Flutter Research" (sponsored by the Naval Bureau of Weapons from 1964 - 1968). His most recent assignment was the "Flutter of Aircraft with External Stores" project sponsored by the Air Force Flight Dynamics Laboratory from 1971 - 1973, and 1974 until the present. He is also currently responsible for updating and maintaining the McDonnell General Flutter Program and other structural dynamics computer programs.

EXTERNAL STORE AIRLOADS PREDICTION TECHNIQUE
(U)
(Article UNCLASSIFIED)

by

A. R. RUDNICKI, JR.
E. G. WAGGONER, JR.
Vought Systems Division
LTV Aerospace Corporation
Dallas, Texas 75222

ABSTRACT. (U) A technique has been developed under Air Force sponsorship for predicting six-component airloads on captive stores for single and multiple carriage configurations. The prediction method includes techniques for predicting the basic airload as well as the incremental airloads due to aircraft yaw and adjacent store interference.

The basic approach to the prediction technique was an empirical correlation of a large experimental data base consisting of literature survey data and data obtained from a parametric wind tunnel test.

This paper summarizes the study program, presents the approach used and major variables considered in the technique development, and discusses the prediction results achieved.

"Approved for public release; distribution unlimited"

LIST OF FIGURES

Figure No.	
1	Instrumented Multiple Carriage Store Hardware
2	Instrumented Single Carriage Store Hardware
3	Typical Test Installation Configuration - Six Instrumented M117 Stores on F-4 Inboard Pylon
4	A-7 and F-4 Instrumented Store Test Capability
5	Typical Isolated Store Aerodynamic Characteristics
6	Captive Store Side Force Characteristics
7	Captive Store Yawing Moment Characteristics
8	Variation of σ with α for a 45° Swept Wing
9	Area Segments for a Typical Store
10	Typical Store Immersed in Aircraft Flow-Field
11	Derivation of Side Force Slope Spanwise Correction
12	Comparison of Pylon Height Correction Factors
13	Normal Force Prediction Results for Four Aircraft - Store Configurations
14	Pitching Moment Prediction Results for Four Aircraft - Store Configurations
15	Side Force Prediction Results for Four Aircraft - Store Configurations
16	Yawing Moment Prediction Results for Four Aircraft - Store Configurations
17	Axial Force Prediction Results for Four Aircraft - Store Configurations
18	Rolling Moment Prediction Results for Four Aircraft - Store Configurations

LIST OF SYMBOLS

b	Aircraft wing span
C_y	Side force coefficient, $\frac{SF}{qS_{REF}}$
d	Store maximum diameter, in.
K	Generalized factor
K_{NOSE}	Store nose lift efficiency factor
K_{WING}	Store wing/fin lift efficiency factor
K_{Λ_1}	Aircraft wing sweep correction factor, $\frac{\sin \Lambda}{\sin 45^\circ}$
K_σ	Partial derivative of sidewash with respect to α, $\frac{\partial \sigma}{\partial \alpha}$
L	Store length, in.
M	Mach number
q	Free-stream dynamic pressure, $\frac{lbs.}{ft^2}$.
SF	Side force, lbs.
SPA	Side projected area, $in.^2$
S_{REF}	Store reference area, $\frac{\pi d^2}{4}$, ft^2.
X_B, Y_B, Z_B	Store body axis coordinate system
$\frac{x}{c}$	Fraction of wing chord
Z	Distance from lower surface of wing to bottom of pylon at the mid-lug point
α	Angle of attack, deg.
α_ℓ	Local angle of attack, deg.
β, β_s	Store yaw angle positive nose outboard, deg.
Δ	Increment
η	Fraction of wing semi-span, $\frac{y_{BL}}{b/2}$, where y_{BL} is the distance from the aircraft centerline to the centerline of the pylon, measured in the wing plan view.
Λ	Aircraft wing quarter-chord sweep angle, deg.
σ	Sidewash angle, deg.
Ψ	Aircraft yaw angle, positive aircraft nose right, deg.

Subscripts

A/C	Aircraft
C	Aircraft local wing chord
INTF	Interference
ISO	Isolated
PRED	Predicted
α	Differentiation with respect to angle of attack
ψ	Differentiation with respect to yaw angle

1.0 INTRODUCTION

Determination of the aerodynamic forces and moments acting on individual components of an aircraft is a part of the design process to assure that adequate load carrying structure is provided for all design flight conditions. Accurate information on the aerodynamic loads is important to achieving aerodynamic compatibility between the aircraft and stores. The flow environment in which external stores are immersed is generally highly complex and affected by many variables; e.g., flight conditions and physical characteristics of the aircraft, store installation, and adjacent stores. Successful theoretical prediction of quantitative data has proven to be difficult, although some techniques have been used successfully to predict qualitative trends. The strong influence of viscous flow, particularly at transonic speeds with multiple carriage store arrangements, has made current methods inadequate for many applications. The most reliable method by which the engineer can provide store airloads continues to be through wind tunnel testing. This latter process is normally complex and expensive and too often provides airloads data late in the design effort, after many decisions influencing aircraft/store compatibility have already been made.

A study program was conducted by Vought Systems Division of LTV Aerospace Corporation under the sponsorship of the Air Force Armament Laboratory (DLJC), Eglin AFB, Florida to develop a generalized technique to predict aerodynamic loads acting on airborne external stores. As a consequence of the relatively low effectiveness and inherent limitations of present theoretical methods, an experimental data correlation approach was selected for developing the prediction technique. The major objective of this program was to provide a prediction technique that is rapid and easy to use, versatile in application to various aircraft and store configurations, applicable to maneuvering flight conditions at subsonic, transonic, and low supersonic speeds, and sufficiently accurate for store/store installation design purposes.

The objectives of this program were accomplished in two phases. The initial phase involved the collection, documentation, and correlation of existing airloads data upon which to initiate the technique development and preparations for wind tunnel testing. The second phase of the program consisted of conducting the wind tunnel test program to complete the required supporting data, performing detailed data correlations, and developing the final prediction technique.

This paper describes the work performed and the results obtained during all phases of the study program. The various sections delineate specific tasks which were performed. Descriptions of both the technical information survey and wind tunnel test planning and preparations are included. A discussion of the approach to the prediction technique including the dominant parameters is also presented. Finally, the capabilities and nominal accuracies of the method are assessed, including some comparisons with experimental data.

2.0 TECHNICAL INFORMATION SURVEY

An extensive data survey was performed by Vought Systems Division to locate and acquire data and related information on captive store and store installation airloads. Acquiring these data was necessary to develop correlations essential to the prediction technique development and to provide guidelines in planning the wind tunnel test program. Although data were known to exist on numerous store types and store installations, problems in acquiring useful airloads data were apparent. These problems included: the inter-industry and inter-service dispersion of data, the diverse origin of airloads data, and the assorted approaches used in measuring airloads. The following paragraphs explain the general survey approach, the type of data solicited and the broad survey results.

2.1 SURVEY PROCEDURE

Early survey planning indicated three primary avenues by which the required technical data could be identified. Selection of these avenues, which were chosen to encompass the majority of data sources, also provided a built-in cross-reference system which minimized the possibility of overlooking pertinent data. Listed below are the primary approach avenues followed:

- Airframe and weapon contractors and government agencies
- Aircraft/weapon system program offices
- Technical literature surveys.

A comprehensive stores data bank had been previously compiled by Vought Systems Division largely through in-house efforts and as a result of a previous Air Force study contract. Hence, data sought through the survey were largely data which had become available since the previous survey. Although all the data identified through the survey were not obtained, efforts to acquire those data deemed most relevant to the program were highly successful.

2.2 NATURE OF DATA SOLICITED

Aerodynamic data and information as summarized in this section were requested to support the study. The desired data involved stores, store installations, and parent aircraft. This information is classified in three broad categories: experimental data, existing prediction methods and data correlations, and related literature on the subject. A further breakdown of the experimental data includes aerodynamic force and moment data, both wind tunnel and inflight, and flow field information. The aerodynamic force and moment data include those obtained for individual stores, racks, pylons, or aircraft, such that airloads on individual installed stores can be defined. Free-stream store data were also sought to be used as a base in isolating store-aircraft interference effects. Data for all types of store loading arrangements were solicited. These included data for stores mounted singly or on MER or TER racks, single

and multiple rail launchers, conformal pallets, etc., on both wing and fuselage stations.

Techniques capable of predicting airload components for stores carried in the flow field of aircraft were also solicited. In general, these prediction methods were found to be limited in application. However, most techniques present an approach to the treatment of certain parameters which are considered primary independent variables influencing the store airloads. These include such parameters as aircraft attitude and flight condition, store geometry, location and installation, and adjacent interference. Hence, these correlation and prediction techniques were a useful aid in the formulation of the general prediction method.

2.3 SURVEY RESULTS

The data survey resulted in the acquisition of a considerable amount of data pertaining to stores and store installations which was not in the original VSD data bank. Much of the experimental data acquired provides total aircraft airloads due to the combined aircraft-store configuration. While useful in determining general store effects, it is difficult to isolate individual store or store installation airloads from these data. Extensive individual store and store installation airloads data were made available on the A-7, F-4, and F-111 aircraft. The majority of data on these aircraft consists of metric store and metric pylon airloads where a balance mounted internal to the store or pylon installation measures the applied aerodynamic forces and moments. Other aircraft for which store airloads have been acquired are the A-4, A-6, F-5, F-86, F-105, F-100 and various wing-fuselage combinations.

The following summary observations are made concerning the specific flight condition and geometry variables encompassed by the survey data and the general nature of the data. The significance of these observations is best realized when it is understood that the developed prediction capability for a given variable and the selected conditions/configurations for wind tunnel testing are a direct function of the available data quantity and quality.

Data coverage for the desired subsonic to supersonic Mach number range was generally acquired with lesser quantities being available for the supersonic region. The majority of acquired data defines airloads in the subsonic flight regime. In the supersonic flight regime data are generally limited to single store carriage installations; however, substantial multiple store installation data were obtained well into the transonic region. F-4 and F-111 store airloads data comprise the majority of the supersonic data. The available A-7 store airloads data are limited to subsonic and transonic flight although considerable A-7 supersonic data were acquired in wind tunnel tests conducted as part of this study.

Store and store installation airloads were acquired for a variety of store types. However, there has not been a great quantity of data acquired for any one store type mounted on various aircraft. These data are necessary to isolate the effects of certain variables, or at least to remove the variance in store geometry as an independent variable. Considerable free-stream store aerodynamic data were also obtained which were useful in isolating aircraft/store interference effects. In regard to store installation type, the bulk of the data acquired consisted of wing pylon singly and multiply carried stores. Limited data are available on fuselage mounted installations, including multiply and singly carried stores, both tangent and pylon mounted. Sparse data exist for TER, wing tip mounted, fuselage semi-submerged, wing tangent and semi-submerged, and conformal store installations.

3.0 WIND TUNNEL TEST PROGRAM

Early in the study planning it was recognized that sufficient airloads data did not exist for developing the prediction techniques from empirical correlations. Also, it was impractical to expect that data accumulated from the varied sources would be thorough enough to establish predictable trends for all priority variables whose contributions collectively define captive store airloads. The practical solution seemed to be to compile all available airloads data, review these data to identify voids where additional data were needed, and then perform a wind tunnel test program to acquire complementary airloads data through a systematic approach. VSD possesses unique wind tunnel model instrumentation and hardware capable of acquiring extensive store airloads data in a single run. Much of the model hardware needed to test a wide variation of instrumented store arrangements was already available for high speed testing. It was decided to adapt this hardware to existing F-4 and A-7 wind tunnel models for a test program which would technically and economically satisfy the current study needs. The following sections describe the test program and include a description of test hardware, variables encompassed, and related test preparation.

3.1 PROGRAM DESCRIPTION AND TEST CAPABILITIES

The wind tunnel test program consisted of instrumenting 0.05 scale models of both the A-7 and F-4 aircraft to measure individual store airloads for both single and multiple carriage stores. In addition, the A-7 parent aircraft model was instrumented to obtain six-component aircraft force and moment data simultaneously with the instrumented store data.

Five component balances (excludes drag) were used on both F-4 and A-7 test programs to obtain multiple carriage store airloads data. The instrumented MER is designed to carry six of these balances simultaneously, one on each of the six MER stations. Data were obtained at all six MER stations continuously during a run. The M117 (MAU-103A/B fin) and BLU-1C/B (finned and unfinned) firebomb stores were utilized in obtaining multiple carriage rack airloads. Instrumented multiple carriage racks

were capable of being tested on all right-hand wing store stations and on fuselage centerline store stations on both the A-7 and F-4 aircraft models. The instrumented MER/store/balance arrangement is illustrated in Figure 1. All multiple carriage store airloads data for the wind tunnel test program were obtained using an instrumented MER since no instrumented TER hardware currently exists. Six component balances were used on both aircraft models to obtain individual store airloads for the single carriage stores. The 300 gallon fuel tank and the Walleye (AGM-62A) store models were used to obtain the single carriage airloads. Instrumented single carriage stores had the capability of being mounted at any wing store station on both the A-7 and F-4 models. Figure 2 illustrates the single store-balance hardware arrangement while Figure 3 depicts a typical multiple carriage test configuration. The illustrations presented in Figure 4 provide a summary description of instrumented single and multiple store testing capabilities.

Another test capability, which is not obvious from Figure 4, permits ±12 inch (full scale) longitudinal shift relative to the pylon in the instrumented F-4 single carriage store position for both inboard and outboard wing pylon stations. It provided additional parametric type store airloads data for the 300 gallon tank and Walleye stores by providing captive airloads data at several chordwise positions. These data were of considerable value to the technique development.

3.2 TEST VARIABLES

Any prediction technique derived through an empirical correlation of data requires an adequate data base to be meaningful. The data base must span the range of variables that dominate captive store airloads. These dominant parameters include store configuration; store spanwise, chordwise, and vertical position; aircraft configuration (wing sweep angle, high/low wing, etc.); aircraft attitude; and flight conditions.

Many of the variables examined during the wind tunnel test program concerned with aircraft/store configuration effects were included in the discussion of test capabilities above (aircraft type, chordwise position, spanwise position, etc.). Remaining variables include the range of flight conditions tested. The Mach number range for single carriage configurations varied from 0.5 to 2.0 with data obtained specifically at M=0.5, 0.7, 0.9, 1.05, 1.2, 1.6, and 2.0. The Mach number range for multiple carriage configurations varied from 0.5 to 1.6 with data obtained at the same Mach numbers as single carriage excluding Mach 2.0. Difficulties were encountered with model dynamics when testing multiple carriage configurations at Mach 2.0; therefore, this higher Mach number was deleted from the test program. The angle of attack range for all test data varied from -4 to +12 degrees while the yaw angle range varied from -8 to +8 degrees in four degree increments.

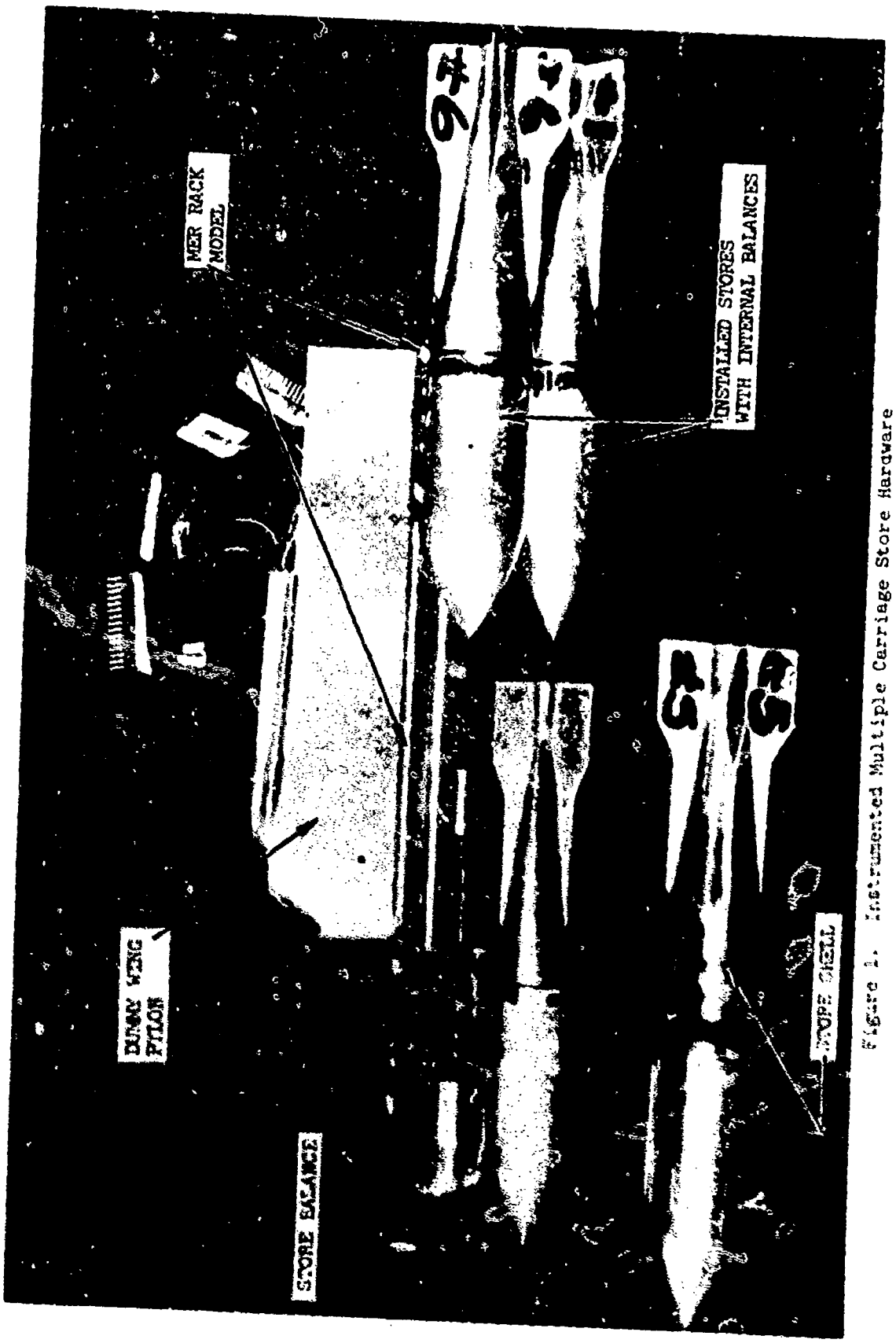


Figure 1. Instrumented Multiple Carriage Store Hardware

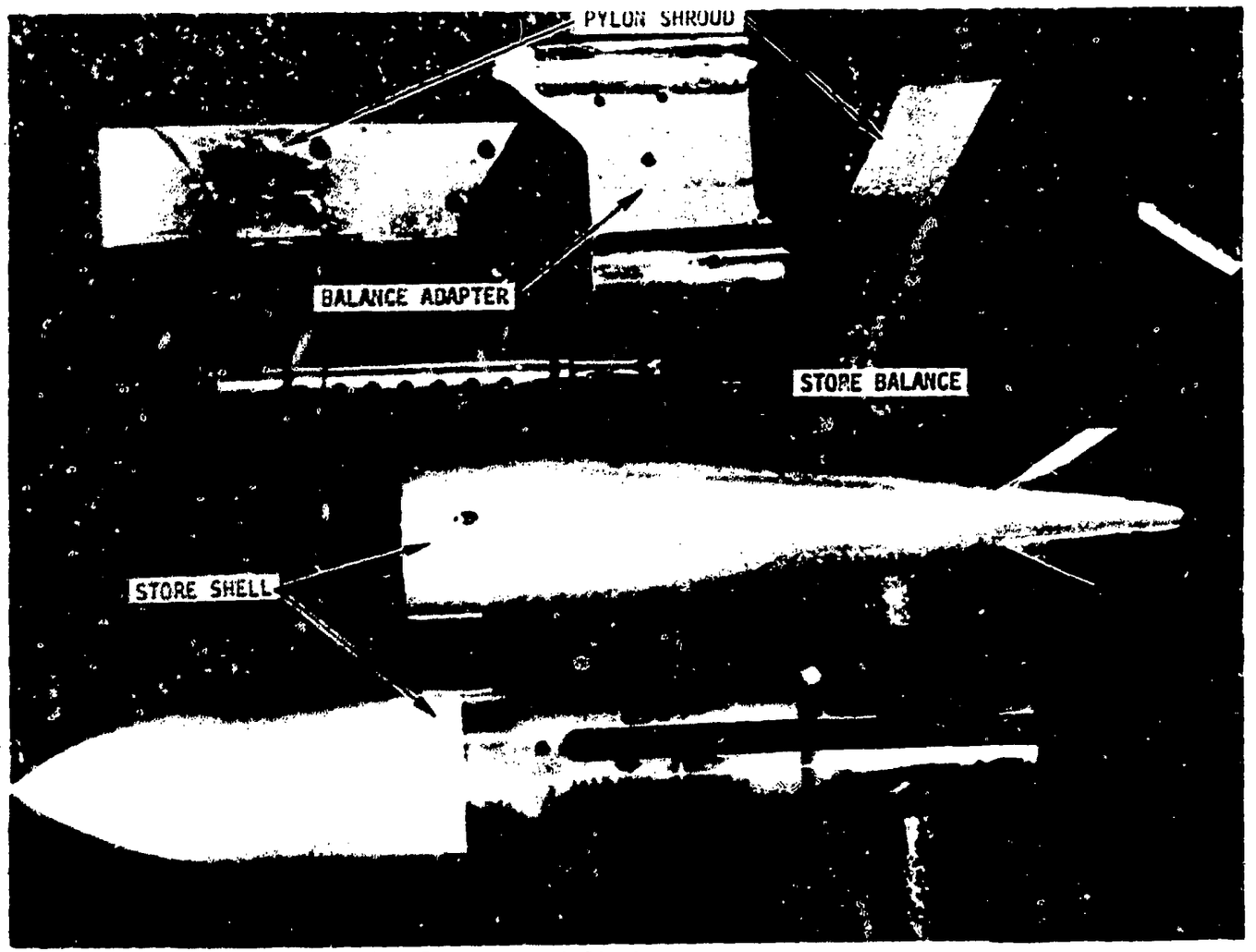
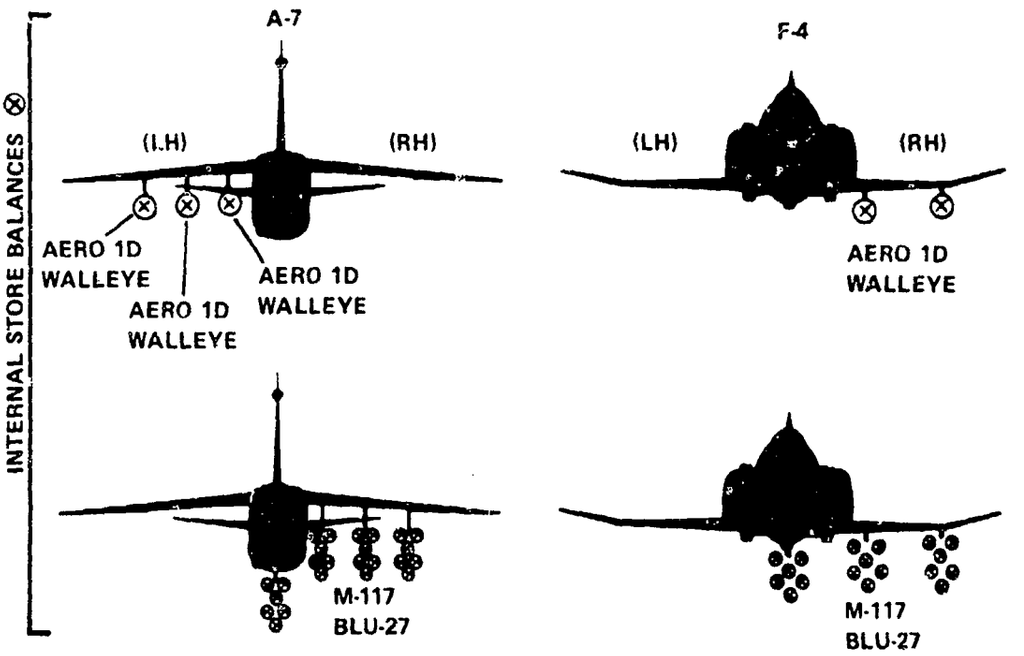


Figure 2. Instrumented Single Carriage Store Hardware

Figure 1. Typical Test Installation Configuration - Six Instrumented M117 Stores on F-4 Inboard Pylon.



NOTES

1. INSTRUMENTED MER RACKS CAN BE CARRIED AT EACH OF THE PYLON STATIONS ON THE A-7 AND F-4 AS SHOWN ABOVE, BUT NOT AT MORE THAN ONE STATION SIMULTANEOUSLY
2. THE INSTRUMENTED SINGLE-CARRIAGE STORE CAN BE CARRIED AT THREE A-7 OR TWO F-4 PYLON STATIONS SIMULTANEOUSLY

Figure 4 A-7 and F-4 Instrumented Store Test Capability

4.0 PREDICTION TECHNIQUE

Development of the prediction technique was approached as an empirical correlation of existing airloads data combined with the parametric type wind tunnel data obtained from tests conducted as part of this program to complement the existing data.

The question of how to correlate these data into a prediction method that is both simple and accurate was answered by preliminary comparisons of captive and isolated store data. Aerodynamic characteristics of the captive stores were observed to possess much the same linear nature as isolated stores. The isolated characteristics are presented in Figure 5 for the same store whose captive side force characteristics are shown in Figure 6. The linear approximation is indicated in each figure by a dashed line and is an adequate representation of the actual quasi-linear data.

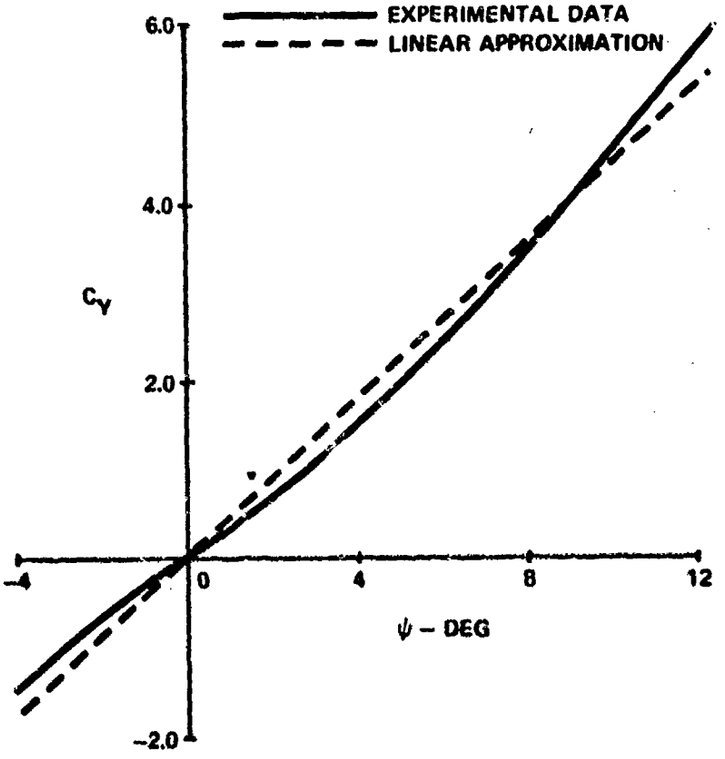


Figure 5 Typical Isolated Store Aerodynamic Characteristics

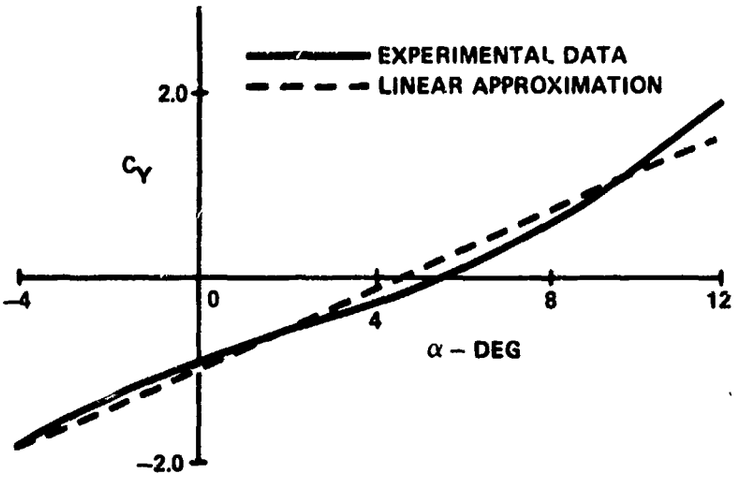


Figure 6 Captive Store Side Force Characteristics

This linear characteristic found in most of the data greatly simplifies the mathematical expressions needed. Unfortunately, the quasi-linear relationship displayed by the captive side force component does not extend to all components for the angle of attack range desired for the prediction technique (-4/12 degrees). The captive yawing moment component for the subject store is presented in Figure 7 along with the linear approximation covering the largest portion of the desired angle of attack range. As shown in the figure, significant errors will result using the linear approximation above approximately 8 degrees angle of attack. Even so, there is a linear region to represent a significant part of the airplane's flight envelope, and the advantages of using the linear approximation for each component far outweigh the disadvantage of some loss in accuracy in a portion of the desired angle of attack range. It should be noted that if the isolated aerodynamic characteristics of the store are non-linear in nature, then this non-linearity should be expected in the captive airloads. The advantages of linearizing the data base are (1) a simple representation of the component airload by a $y=mx + b$ type equation and (2) a major variable, aircraft angle of attack, is built into the mathematical component airload representation.

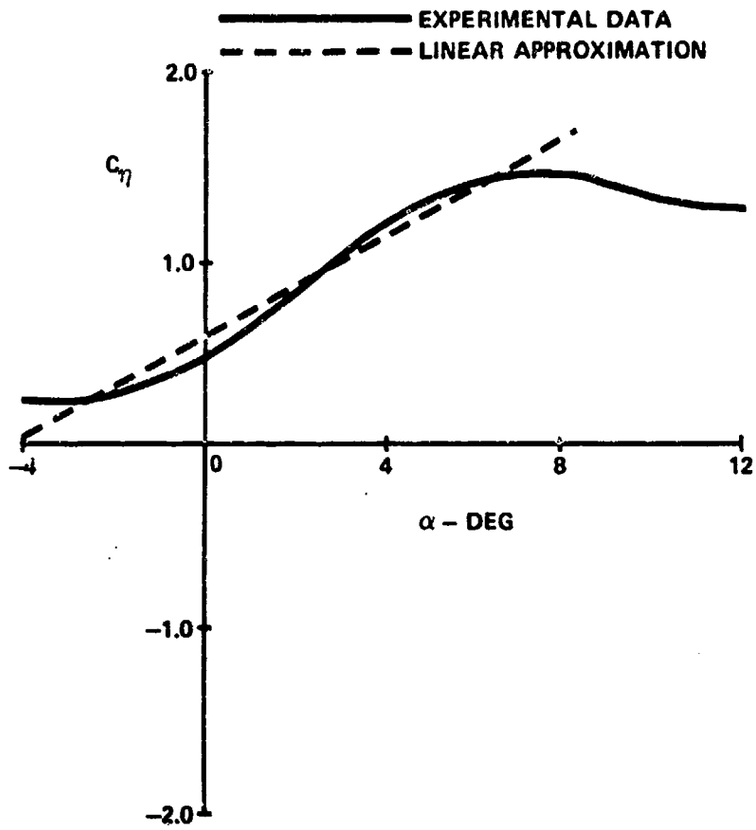


Figure 7 Captive Store Yawing Moment Characteristics

As a result, the data base was linearized so that each airload component could be expressed as a slope (force or moment as a function of angle of attack) and an intercept at zero angle of attack. As a result of the linearized data base, all predictions are accomplished in the form of a predicted slope and intercept for each of the airload components. Because of increasing non-linearity at the larger aircraft angles of attack and yaw angles, significant errors are likely outside the range of applicability stated for these variables. A summary of nominal method accuracy including some comparisons with experimental data is presented in Section 5.0.

4.1 BASIC APPROACH

A theoretical method must rely on mathematical descriptions of the aircraft components, pylons, racks and stores to implement potential flow solutions of the store airloads. Any corrections for viscous effects must be handled separately. An empirical method allows much simplification to that approach. The basic approach used in this method applies the concept that captive airloads are the result of a free-stream flow plus the interference effects. In this way, work that has been previously accomplished for free-stream aerodynamic predictions can be used as a base on which to relate captive airloads. This permits the prediction procedure to be a summation process as indicated below.

Captive Store Airloads = Isolated Store Airloads
+ Interference Effects

Applying the summation approach to interference increments depends first on airloads for some base configuration. Corrections can then be added to these initial airloads to account for differences between the base configuration and the desired configuration. Predicting these initial airloads is called the initial prediction. It involves assuming the store is in the flow field of a base wing with 45° sweep and installed at a specific spanwise. chordwise, and vertical location. The next step is to obtain a final prediction by applying empirically derived corrections to the initial prediction to compensate for aircraft configuration differences and to account for the effects of the store being in the desired spanwise, chordwise, and vertical location.

This approach was used in correlating the experimental data to develop the prediction method presented here. Correlations to identify airloads for the base configuration implement the initial prediction procedure and were basic to the entire development process. These correlations were performed with M=0.5 data to avoid the increased complexity of compressible flow corrections and shock induced effects. This is the lowest Mach number of the test data from the wind tunnel tests of this program. Because compressibility effects are normally small at speeds below M=0.5, the method is considered valid for low subsonic speeds without Mach number corrections.

Correlations of the data to identify corrections needed to account for Mach number and configuration differences were much more difficult than those for the base data. This greater difficulty results from the many factors which contribute to the aerodynamic differences between the various store installation configurations. Some of these factors are the reason rigorous mathematical solutions are not yet practical for prediction purposes on many installation , particularly for multiple carriage racks. Fortunately, experimental data indicate that some of these differences are either small or compensating so that empirical expressions are possible without including terms which evaluate each contributing parameter. A method has been developed by using the available data to establish predictable trends and these trends are expressed mathematically.

To apply the method, the initial prediction of captive airloads is always made first at M=0.5 by assuming the store is inserted into the flow-field of the base wing (45° sweep). The initial prediction is made for the basic airload case (i.e., the captive store airload generated by a zero-yaw pitch excursion of the parent aircraft). The incremental captive airloads due to aircraft yaw and the effects of adjacent store interference are predicted as increments to be added to the basic airload. The effects of Mach number are treated as an increment to be added to the prediction at M=0.5. At a particular Mach number the total captive airload experienced by a store can be obtained from the following generalized coefficient expression:

$$C_{x_{TOTAL}} = C_{x_{BASIC}} + \Delta C_{x_{\beta}} \cdot \beta + \Delta C_{x_{INTF}}$$

where:

- x - y, η, N, M, A, ℓ representing side force, yawing moment, normal force, pitching moment, axial force, and rolling moment, respectively.
- $C_{x_{BASIC}}$ - Basic captive airload generated by a zero yaw pitch excursion of the parent aircraft.
- $\Delta C_{x_{\beta}}$ - Incremental airload due to aircraft yaw per degree store yaw angle, β.
- β - Store yaw angle equal to $\Psi_{A/C}$ for a right wing store installation and $-\Psi_{A/C}$ for aleft wing store installation.
- $\Delta C_{x_{INTF}}$ - Incremental airload due to the effect of adjacent store interference

In summary, the total captive airload experienced by a store can be calculated by incrementing the isolated store aerodynamic characteristics through the initial prediction summation procedure for the base wing (45° sweep), applying empirical corrections to arrive at the final prediction for the subject wing, and using the generalized coefficient expression above to sur the major contributions to the installed airload.

4.2 PREDICTION EQUATIONS

The variables used in deriving the final prediction equations for both single and multiple carriage configurations were essentially the same. These variables accounted for store configuration characteristics (both physical and aerodynamic); store spanwise, chordwise, and vertical location in the aircraft flow-field; the interference effect of the aircraft fuselage and adjacent stores; parent aircraft attitude (pitch and yaw); and Mach number.

As a result of the similarities in the equation forms, only the single carriage M=0.5 side force slope prediction equation is presented and discussed here. The intent is to describe typical procedures used in developing the prediction method.

4.2.1 Initial Airload Prediction

Initial prediction calculations begin by assuming the store is inserted into the flow field of the base wing (45° sweep) at the mid-semispan (η=0.5) position. Longitudinally the store is placed at the true captive position and the local wing chord is assumed to be the same as the captive position for the subject aircraft wing. The sidewash characteristics of the base wing are known from an analysis of the flow field data presented in Reference 1. This analysis yielded the rate of change of sidewash angle, σ, with respect to angle of attack, α. This term, $\frac{\partial \sigma}{\partial \alpha}$, is known as a function of x/c for the base wing, Figure 8.

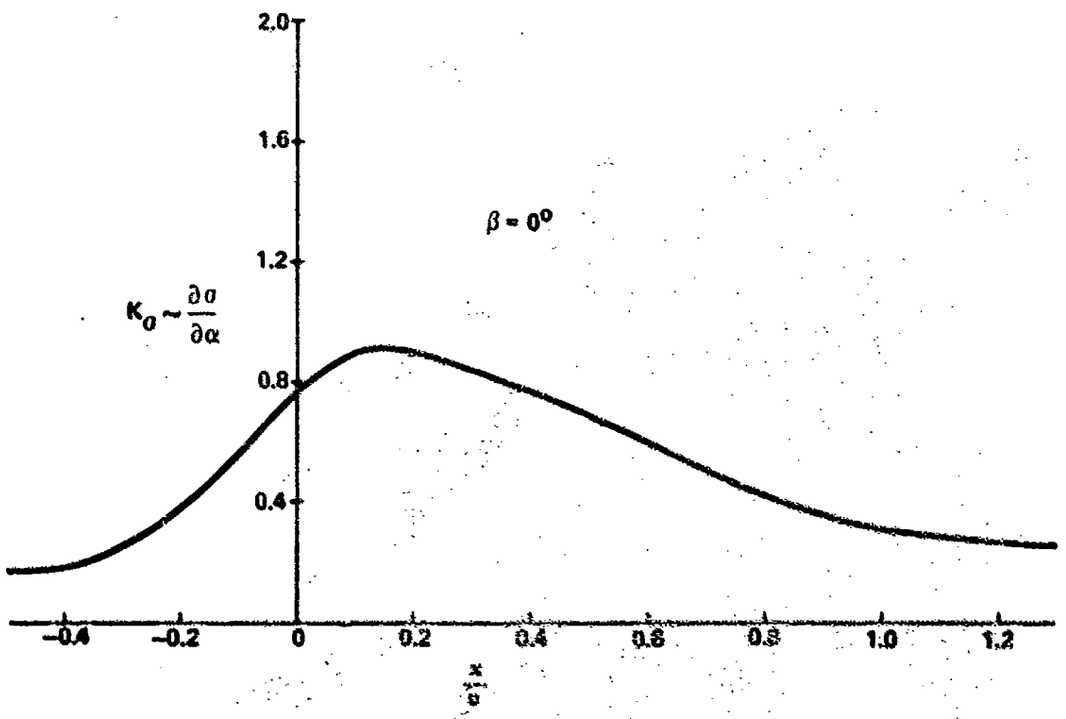


Figure 8 Variation of σ with α for a 45° Swept Wing

Several definitions concerning the store and aerodynamic characteristics must also be made. The total store planform area is divided into nose area, body area, and wing area as shown in Figure 9. The distinction

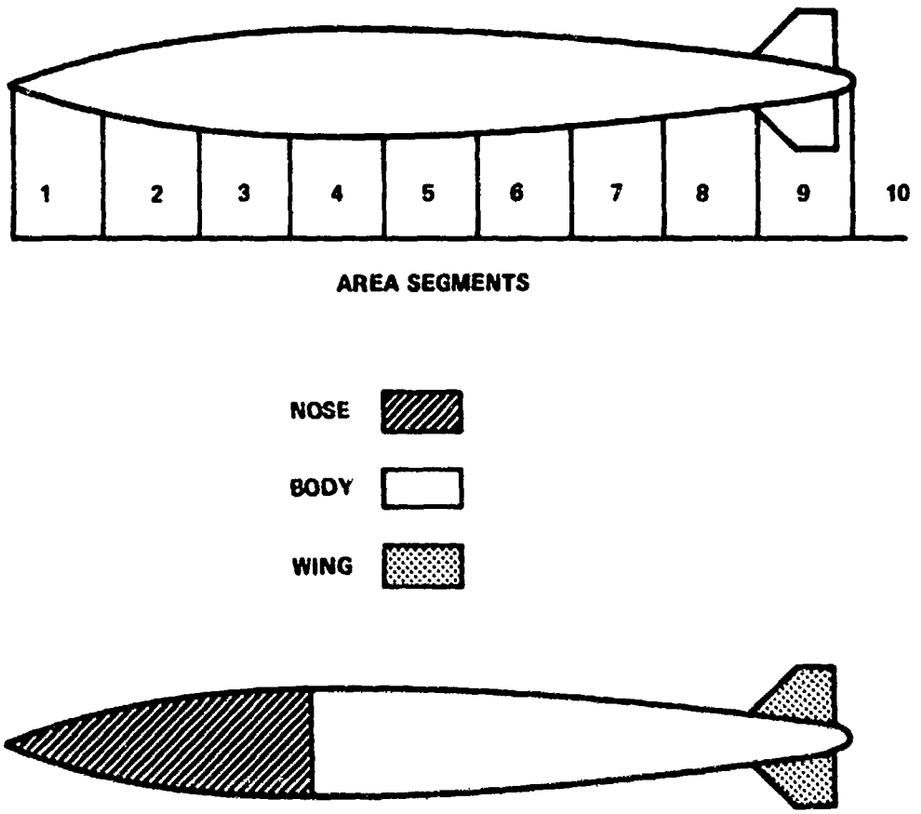


Figure 9 Area Segments for a Typical Store

in planform areas is required since aerodynamically the nose and wing are more efficient producing lift (or side force in this case) than the store body. Because of this efficiency distinction, factors have been defined using Reference 2 for the store nose, K_{NOSE}, and wing(s), K_{WING}, to weight their respective planform areas in relation to the store body planform area.

With a knowledge of the store geometric and isolated aerodynamic characteristics, a summation procedure is performed along the store in the aircraft flow-field to obtain an initial prediction of side force slope. The store is positioned in the aircraft flow field as shown in Figure 10. The planform area of the store is projected into the X_B, Z_B

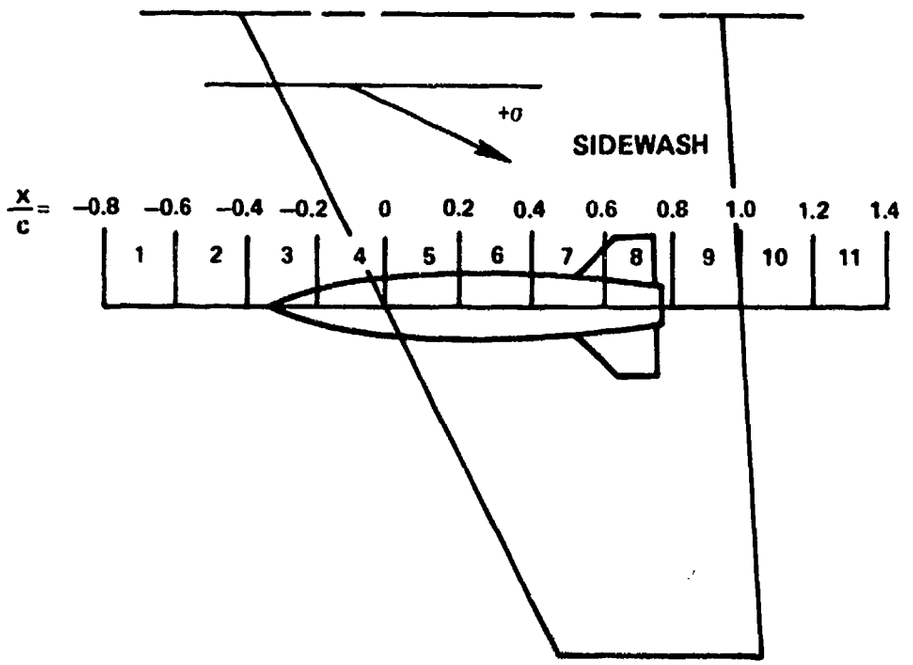


Figure 10 Typical Store Immersed in Aircraft Flow-Field

plane and is defined as side projected area, SPA. The store is divided into constant length segments from nose to tail, Figure 9, and the SPA is computed for each of the segments with distinction made as to nose, body, or wing areas.

With the segmented side projected areas defined and the store inserted into flow field of the base wing, the summation procedure is given by the following relationship.

$$\text{ADJUSTED SPA} = \sum_{n=1}^{m} K_{\sigma_n} K_{\text{NOSE}_n} K_{\substack{\text{WING} \\ \text{(TAIL)}}_n} \text{SPA}_n$$

where:

m - Number of constant length area segments as computed from store nose to tail

K_σ - Rate of sidewash variation with angle of attack, $\frac{\partial \sigma}{\partial \alpha}$, Figure 8.

K_{NOSE} - Store nose lift effectiveness.

$K_{\substack{\text{WING} \\ \text{(TAIL)}}}$ - Store wing or tail lift effectiveness.

SPA - Store side projected area, in^2., Figure 9.

then:

$$K_{C_{SF}} = \frac{\text{ADJUSTED SPA}}{\text{SPA}_{\text{TOTAL}}}$$

where:

ADJUSTED SPA - Adjusted side projected area of the store as given by the summation equation above.

$\text{SPA}_{\text{TOTAL}}$ - Total side projected area of the store. The sum of nose, body, and wing side projected areas.

The initial side force slope prediction is given by the following equation.

$$\frac{d\left(\frac{SF}{q}\right)}{d\alpha_{\substack{\text{INITIAL} \\ \text{PRED}}}} = K_{C_{SF}} \frac{d\left(\frac{SF}{q}\right)}{d\psi_{ISO}}$$

where:

$\frac{d\left(\frac{SF}{q}\right)}{d\psi_{ISO}}$ - Isolated aerodynamic characteristics of the subject store. Equal to $C_{L_{\alpha_{ISO}}} S_{REF}$, $\frac{ft^2}{deg.}$. Computed from the method of Reference 2.

It should be noted that if experimental isolated store characteristics are used in the above equation, the user must still perform most of the computations of Reference 2 since many of the terms of the computation are used in defining the store nose and wing weighting factors.

The discussion in this section has been limited to the single carriage side force slope initial predictions. Initial predictions of normal force, pitching moment, and yawing moment slopes for both single and multiple carriage, are similar. An additional term is added to the summation procedure for the moment terms to account for the displacement of the area segment with respect to the moment reference point. Initial predictions of axial force and rolling moment are somewhat different with a complete discussion included in Reference 3.

4.2.2 Aircraft/Store Interference Prediction

The single carriage side force slope prediction equation is presented below.

$$\left(\frac{SF}{q}\right)_{\substack{\alpha \\ PRED}} = K_{C_{SF}} \left(\frac{SF}{q}\right)_{\substack{\psi \\ ISO}} K_\eta K_{INTF} \frac{K_L}{C} K_Z K_{A_i}$$

The initial term, $K_{C_{SF}} \left(\frac{SF}{q}\right)_{\substack{\psi \\ ISO}}$, in the above equation is the initial prediction discussed in Section 4.2.1. The remaining factors are empirical corrections to the initial prediction to compensate for the effects of the parameters previously mentioned in this section.

The first empirical correction,term, K_η, is a factor to compensate for the spanwise position of the subject store. This factor was derived from three independent data sources, all of which were contained in the data base consisting of the survey data and the wind tunnel test data. In order to derive a spanwise correction factor, it is desirable to have captive airloads data for several store types on all wing pylons for as many parent aircraft as possible. Two of the previously mentioned data sources came from the survey. One source, Reference 4, contained the BULLPUP "A" missile on F-4 inboard and outboard wing pylons. A second source, Reference 5, came from the test program in which the 300 gallon tank and Walleye stores were tested on all wing pylons of both the A-7 and F-4 aircraft. The third and final data source was a flow-field investigation of a wing-body combination at low subsonic speeds reported in Reference 1. The flow-field investigation reported flow angularities both in the lateral and vertical planes for semi-span stations η= 0.25, .50, and .75 for a number of chordwise and vertical locations beneath the test wing. Ratioing the sidewash flow angularities from the flow-field data, assuming the mid-semispan position, η=0.5, as the base, the solid curve in Figure 11 was derived. Through a similar analysis the data

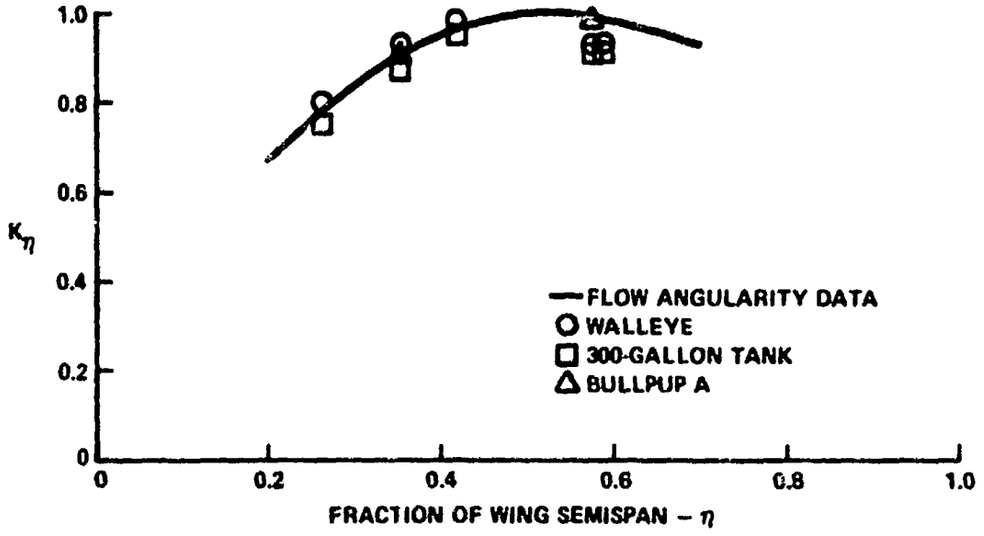


Figure 11 Derivation of Side Force Slope Spanwise Correction

points represented by symbols were derived as also shown in Figure 11. Hence, from three independent data sources, essentially the same spanwise trends were obtained for single carriage side force slope. The final correlation curve presented for this term is basically the average of the solid curve and the data points shown in Figure 11.

The next empirically derived correction to the initial prediction is the factor K_{INTF}. This term accounts for the interference effect of the fuselage on the captive store side force slope for high-wing aircraft. The presence of the fuselage near the installed store prevents the full development of a sidewash flow-field and, therefore, modifies the spanwise trends established earlier.

The term $K_{L/C}$ is an empirical factor based on the length of the store divided by the local aircraft wing chord. In addition to the chordwise location of the captive store, this factor gives an indication of the amount of the store contained in the non-uniform wing flow-field.

The next term, K_Z, in the side force slope equation is a factor to account for pylon height variation. Sidewash angularity beneath a swept wing is strongest near the wing surface and decays to zero at some distance, on the order of a local wing chord length, beneath the wing.

Experimental flow-field data indicate that the decay is exponentially shaped. Other investigators (Reference 6) have developed an empirical pylon height correction factor for side force slope which is presented in Figure 12 as a function of vertical distance beneath the wing surface to the store longitudinal axis. Figure 12 also presents the pylon height correction factor for side force slope developed from the present study for comparative purposes and is presented as a function of vertical displacement from the wing lower surface to the pylon rack mid-lug point. The exponential variation with pylon height is apparent in both cases.

The final empirical factor, K_{Λ_1}, is a first order correction for aircraft wing sweep angle. The factor is defined as $\sin \Lambda / \sin \Lambda_{BASE}$ where Λ is the quarter chord sweep of the subject aircraft wing. The base sweep angle, Λ_{BASE}, for this factor is 45° since the initial prediction discussed in Section 4.2.1 was made for a base wing with 45° sweep angle. This factor has been suggested by several investigators including those of Reference 6 and is adequate for wing sweep angles that do not vary significantly from the base wing sweep (45°). For this reason the range of sweep angles for which the technique is recommended is limited to quarter chord sweep angles between 30 and 60 degrees.

The discussion is in this section has been limited primarily to those empirical factors pertaining to the single carriage side force slope prediction for M=0.5. Presented in Reference 3 are the prediction equations for all applicable rack types, store carriage locations, and aircraft speed regimes. Inspection of these equations reveals a large number of empirical correction factors which have not been discussed here. However, the development of those terms was similar to those presented here, and detailed descriptions of these terms are included in Reference 3.

5.0 ASSESSMENT OF APPLICABILITY AND ACCURACY OF THE PREDICTION METHOD

In undertaking this research program, there was some question regarding the degree of success that could be expected from a data correlation approach to developing a store airloads prediction technique. Experience in developing other empirical methods gave reasonable assurance that a method was possible. However, the goal for this program was a method that was easy to use and would provide sufficient accuracies to make the predictions suitable for preliminary design purposes. The results reported in Reference 3 indicate that this goal was achieved. One of the important factors influencing these results was the quantity and quality of data used in the correlation. Because of the limited data obtained in the survey, the wind tunnel data produced as part of the program made possible the versatility which was accomplished.

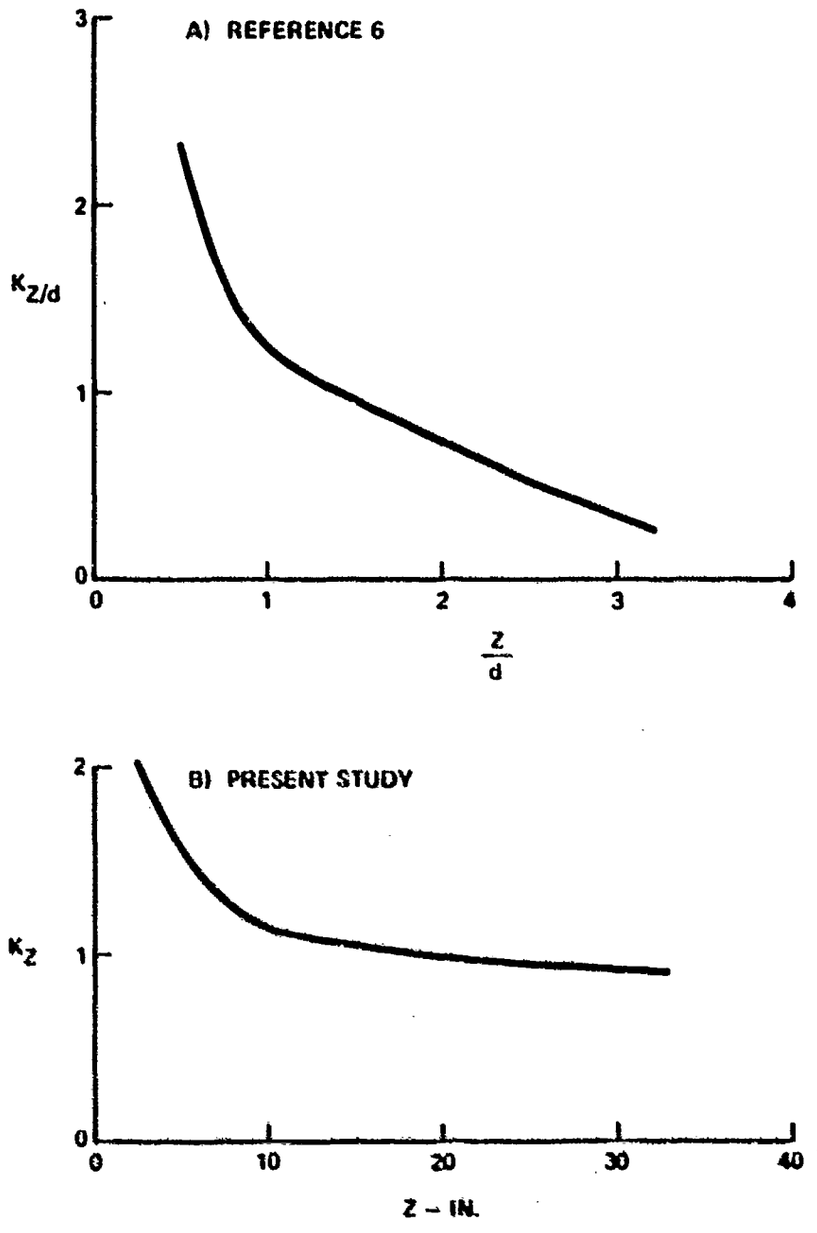


Figure 12 Comparison of Pylon Height Correction Factors

Simplicity was achieved in the sense that there are no complicated steps required to apply the method. There are many factors to be evaluated, but the process is outlined in a systematic sequence of simple steps. Because there are numerous calculations required for a complete prediction of six component airloads for multiple store installations, computerization of the method for practical applications appears appropriate.

The method has a wide range of applications and capabilities. The method is capable of predicting the captive airloads for single carriage and multiple carriage store configurations for a generalized aircraft including the basic airload (that airload generated by a zero-yaw pitch excursion of the parent aircraft) and the incremental airloads due to aircraft yaw and adjacent store interference. Establishing absolute limits of applicability is difficult since this is often a function of the accuracy that is acceptable. Recommended limits are submitted and sufficient data are presented to implement the method for those limits. Applications beyond the stated limits will normally mean a decay in accuracy.

The single carriage method is valid over the Mach number range 0.5 to 2.0 while the multiple carriage Mach range varies from 0.5 to 1.6. Both single and multiple carriage prediction techniques are valid over the angle of attack range of -4 to +12 degrees and the aircraft yaw angle range of -8 to +8 degrees although best accuracy for the increments due to aircraft yaw are for the range -4 to +4 degrees. The aircraft wing sweep angle (quarter chord) range of validity is from 30 to 60 degrees although the method can be applied to a wider sweep angle range (say 20 - 70 degrees) with decreased accuracy. The method is applicable to all wing/pylon and fuselage centerline carriage configurations. It is not intended for fuselage configurations off the centerline nor to semi-submerged or conformal carriage.

An assessment of the accuracy of the method has been conducted through comparisons with the data base used in the technique development. The first accuracy check, and possibly the most meaningful, was a comparison of predicted values of individual airload components with the linearized representation of the data obtained from the test of that configuration in the wind tunnel. This check is meaningful because accurate linearized representations, like those shown in Figures 5 and 6, are adequate for most engineering applications. Wind tunnel tests for airloads data can often be avoided if this type prediction has sufficient accuracy. The accuracy comparisons with the linearized data base indicate that all components for both single and multiple carriage configurations are nominally within ±10% of the base value.

Additional comparisons were made to check predicted values with specific data points. This check does include the effects of scatter in the wind tunnel data which is not necessarily a true test of the method. However, it does indicate something of the data non-linear effects on accuracy. Comparisons with the experimental data base for two single and two multiple carriage configurations are presented in Figures 13 through 18. These comparisons allow the reader to see the effects of data non-linearity on accuracy in portions of the angle of attack range.

6.0 CONCLUSIONS AND RECOMMENDATIONS

With the conclusion of the program we are left with a few summary comments and observations which are mentioned here.

- It is possible to take experimental captive store airloads data and correlate these data into mathematical expressions for predicting store airloads for the generalized aircraft/store configuration.

- Accuracy is sufficient for preliminary design.

- The number of steps required for a six-component airloads solution suggests that computerization of the method is desirable.

- Better accuracy is attained for the force components than the moment components due to the sensitivity of the moment components to the factors affecting the local flow-field such as viscous effects and adjacent store installations.

- Further work should include parametric data obtained on a generalized wing/body aircraft model utilizing generalized store shapes to generate larger ranges of data for the most influential variables. An improvement in accuracy should naturally result.

- Additional work should consider using higher order curve fits of the data base for possible accuracy improvements.

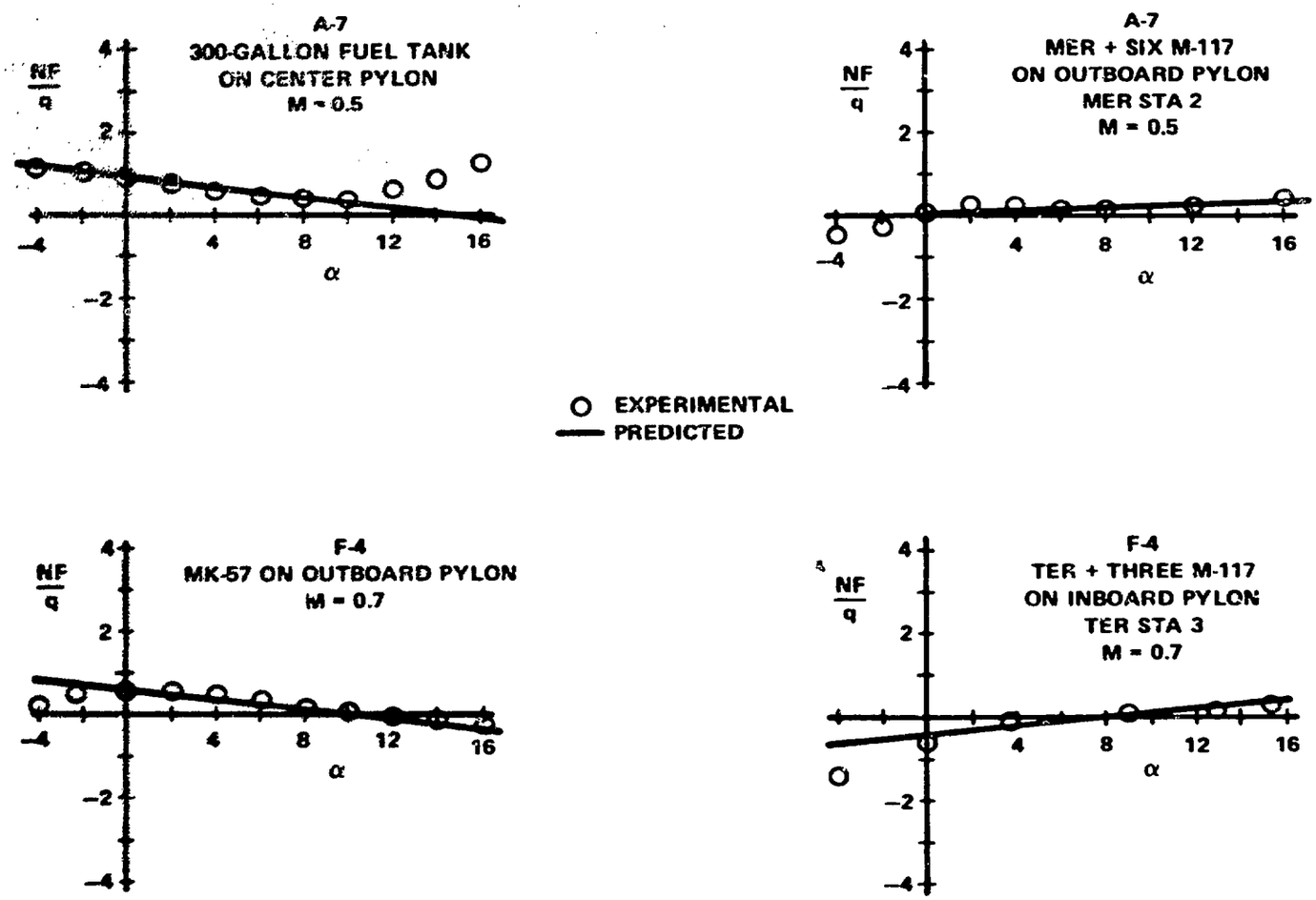
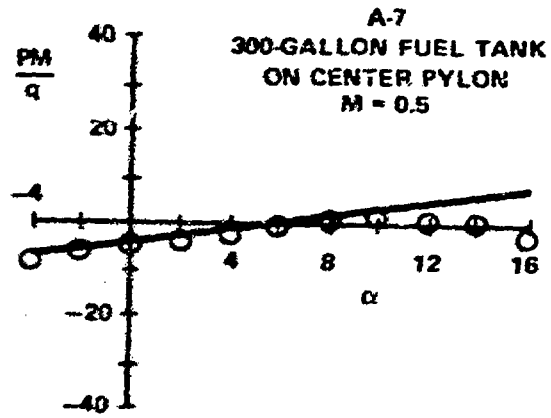
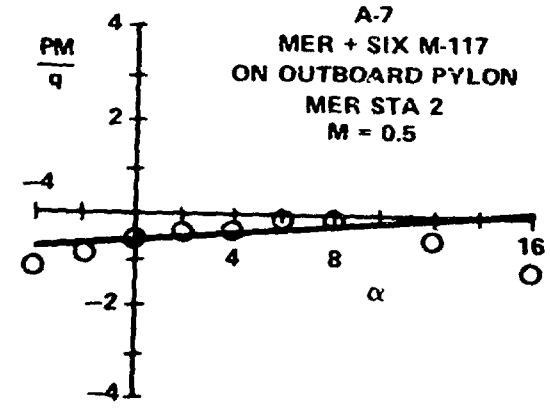
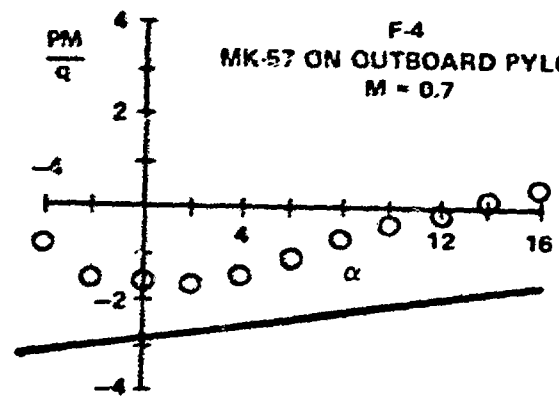


Figure 13 Normal Force Prediction Results for Four Aircraft - Store Configurations





O EXPERIMENTAL
PREDICTED



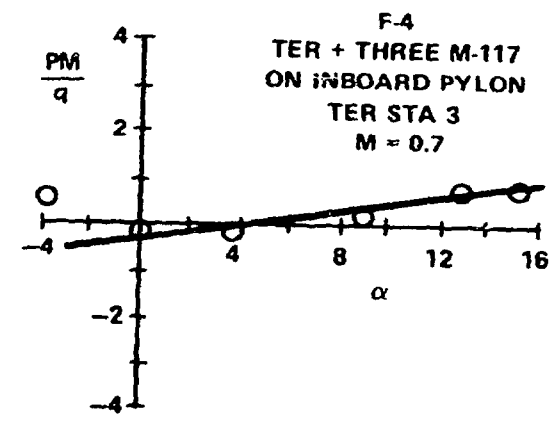


Figure 14 Pitching Moment Prediction Results for Four Aircraft - Store Configurations

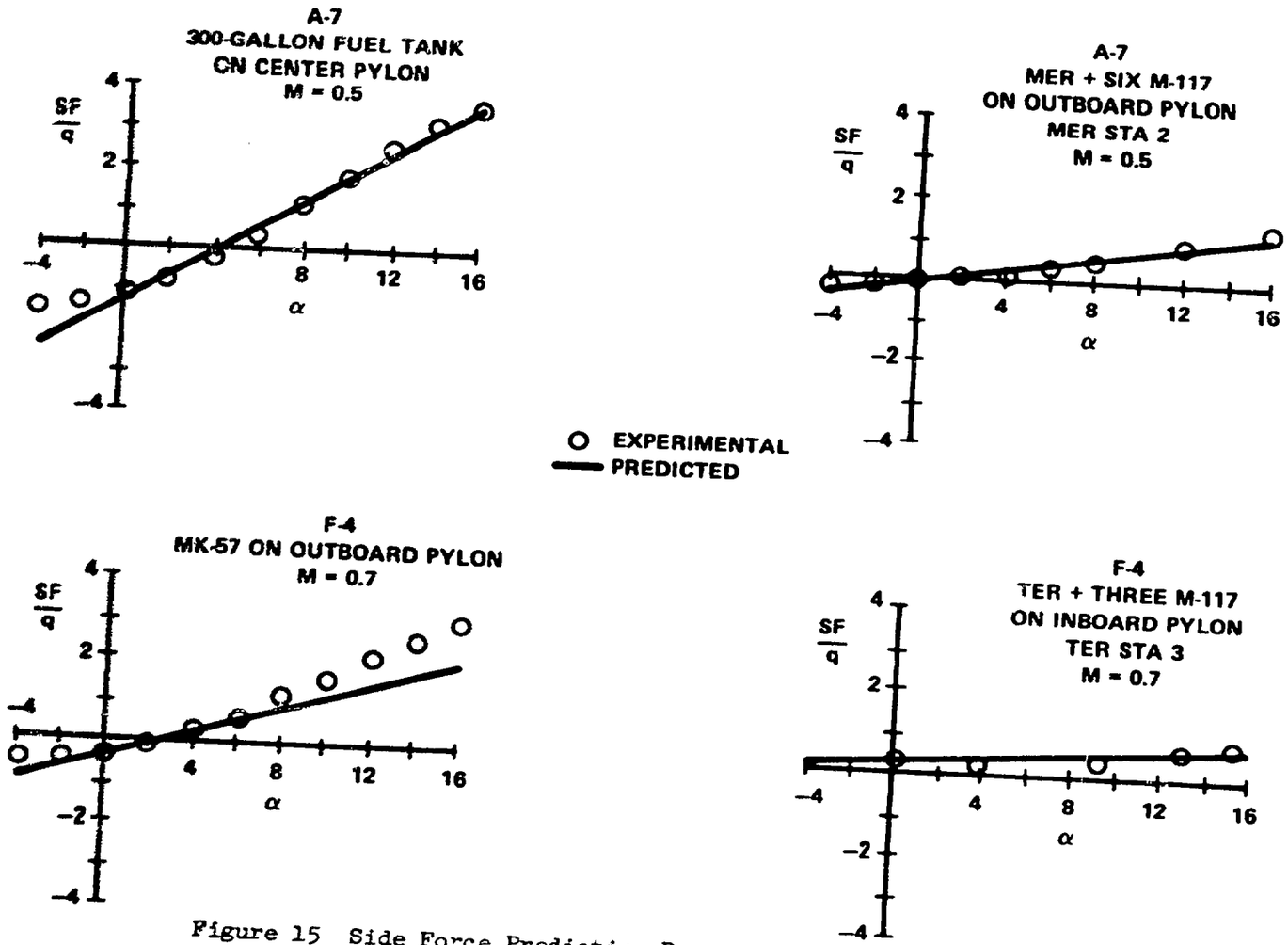


Figure 15 Side Force Prediction Results for Four Aircraft - Store Configurations

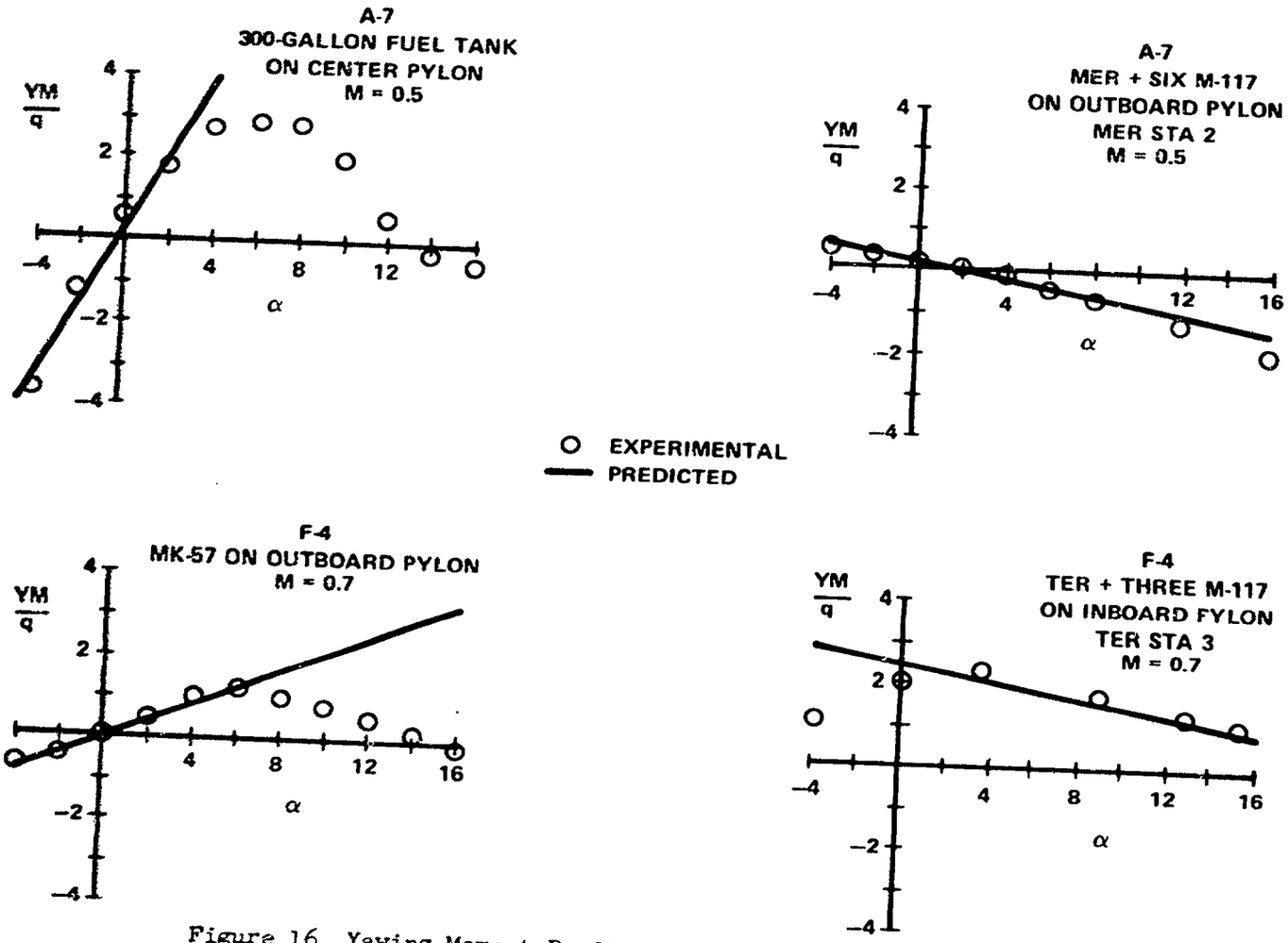


Figure 16 Yawing Moment Prediction Results for Four Aircraft - Store Configurations

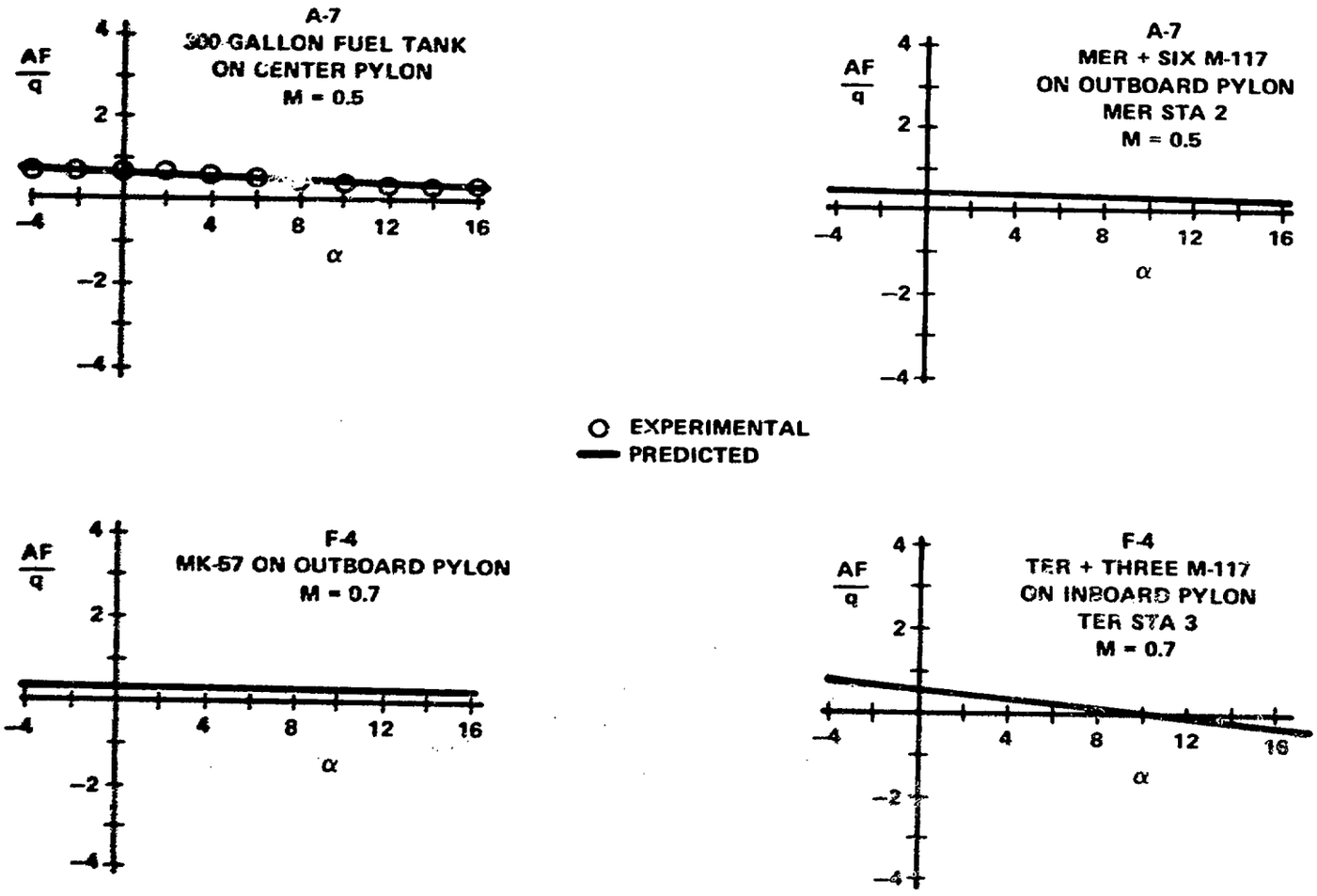


Figure 17 Axial Force Prediction Results for Four Aircraft - Store Configurations

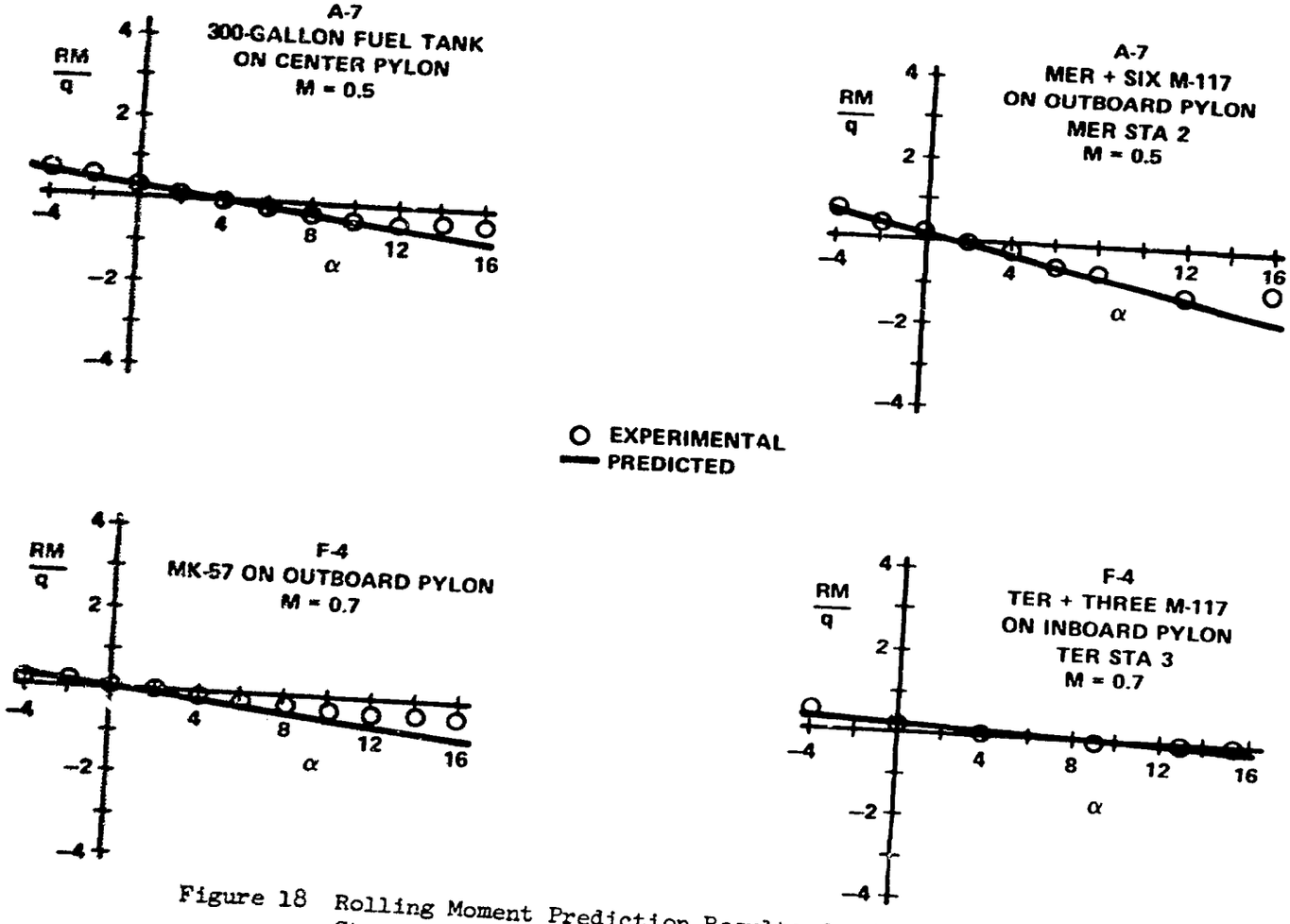


Figure 18 Rolling Moment Prediction Results for Four Aircraft - Store Configurations

REFERENCES

1. Alford, W. J. Jr., "Theoretical and Experimental Investigation of the Subsonic Flow-Fields Beneath Swept and Unswept Wings with Tables of Vortex - Induced Velocities," NACA Report 1327, 1957.

2. Nielsen, J. N., Pitts, W. C., and Kaattari, G. E., "Lift and Center of Pressure of Wing-Body-Tail Combinations at Subsonic, Transonic, and Supersonic Speeds," NACA Report 1307, 1957.

3. Rudnicki, A. R. Jr., Waggoner, E. G. Jr., Alexander, C. T., and Gallagher, R. D., "External Store Airloads Prediction Technique," Vought Systems Division Report 2-57110/5R-3225, June 1975.

4. Gregoire, J. E., "Wind Tunnel Tests on the 7.5% F-4C Store Loads Model in the McDonnell Polysonic Wind Tunnel, Series II," Report A879, McDonnell Aircraft Corporation, January 1965.

5. Hill, D. W. Jr., and Mattasits, G. R., "Aerodynamics Loads on Four External Stores in the Carriage Position on the A-7D and F-4C Aircraft at Mach Numbers from 0.5 to 2.0," AEDC-TR-74-29, AFATL-TR-74-64, Arnold Engineering Development Center, May 1974.

6. Marsden, P. and Haines, A. B., "Aerodynamic Loads on External Stores" A Review of Experimental Data and Method of Prediction," R. & M. No. 3503, November 1962.

AUTOBIOGRAPHY

A. R. Rudnicki, Jr.

Mr. Rudnicki received a Bachelor of Science degree in Mechanical Engineering from Louisiana State University in 1966. Upon graduation he entered graduate school at the Massachusetts Institute of Technology and obtained a Master of Science degree in Aeronautics and Astronautics in 1968.

Mr. Rudnicki joined the Aerodynamics Group of Vought Systems Division in 1968 and was assigned to the A-7 Aircraft Project. From 1968 to 1969 he participated in the A-7D/Maverick compatibility program including the planning and execution of various missile captive airloads and captive trajectory wind tunnel tests and the associated data analysis. During this period he developed a six-degree-of-freedom trajectory routine for predicting A-7D/Maverick launch envelopes. His primary responsibility from 1969 through 1972 was to conduct captive store airloads wind tunnel tests and complete the data analysis associated with the A-7D "Seek Eagle" stores compatibility program. Since 1973 he has been associated with an Air Force sponsored R&D program designed to develop a generalized technique for predicting six component captive store airloads.

AUTOBIOGRAPHY

E. G. Waggoner, Jr.

Mr. Waggoner received a Bachelor of Science degree in Aerospace Engineering from Auburn University in 1969 and a Master of Science degree in Mechanical Engineering from Southern Methodist University in 1972.

After joining the Aerodynamics Group of Vought Systems Division in 1969 he was engaged in an R&D effort concerned with predicting 3-dimensional pressure distributions on wings. Since 1971 he has been involved in various aspects of external stores technology. From 1971 to 1972 he participated in an effort to develop external store aerodynamic effects on aircraft performance. During 1972 his assignments centered around development of a six-degree-of-freedom store trajectory routine, wind tunnel test planning and support, and evaluation of store airloads data in conjunction with the A-7D "Seek Eagle" program. Since 1973 he has had responsibilities in all phases of an Air Force sponsored R&D program to develop a store captive airloads prediction technique. This includes data survey efforts, wind tunnel test planning and support, as well as the detailed correlation effort associated with developing the prediction technique.

ADVANCED LAUNCHING AND SUSPENSION TECHNOLOGY (ADLAST) PROGRAM PLAN (U) (Article UNCLASSIFIED)

by

THOMAS E. MILHOUS
Naval Air Development Center
Warminster, Pa. 18974

ABSTRACT. (U) Based on projected Navy aircraft development efforts, a compatible weapons suspension equipment research and development program has been formulated to complement the conventional and nuclear weapon attack missions. The Navy weapon carriage philosophy requires that four distinct classes of suspension systems be developed as follows:

a. 2000-lb Gravity Release System for low performance ASW, sea control and reconnaissance aircraft.

b. 2000-lb Ejector Bomb Rack for high performance attack and fighter aircraft.

c. 2000-lb Ejector Bomb Rack for use in multiple carriage installations on all aircraft.

d. 4500-lb Ejector Bomb Rack for high performance attack aircraft and ASW mining operations.

All of the above systems should exhibit features acceptable to or readily adaptable to nuclear and conformal carriage in addition to their conventional role. These systems would also exhibit a high degree of standardization as regarding aircraft fit to negate the requirement for different models within each class.

Additional new system features will include: adjustable dual ejection (where applicable), programmable store release attitude, quick adjust sway braces, built-in-test (BIT) capability and store status monitor. Generalized design objectives will exhibit: rapid turn around capability, low maintenance requirements, high interchangeability index, standardized interfaces, high mission reliability,

improved mission safety characteristics, multiple mode capability and minimal skill operations.

In order to attain the goals of the above systems at a minimum cost and maximum efficiency to the Navy, the following multi-faceted, flexible program will be pursued on a priority basis as dictated by Navy aircraft requirements:

a. Development of individual detail design guidelines for each class of equipment. These documents shall define the performance and operational criteria required for each system.

b. Preparation of request for proposals (RFPs) for solicitation of industry and Navy proposals for the design and development of each system.

c. Evaluation of all responses to the RFPs to decide the optimum course of action in pursuance of the programs, i.e.,:

   (1) Contractor developed with Navy monitor and control.

   (2) Navy developed.

   (3) Combination contractor/Navy development with Navy monitor and control.

APPROVED FOR PUBLIC RELEASE; DISTRIBUTION UNLIMITED

INTRODUCTION

The basic problem facing the Navy in the area of weapons suspension equipment is one of operational limitations and penalties imposed by lack of state-of-the-art equipment and the current philosophy regarding research and development in this critical area. Current suspension equipment available for use on new and proposed aircraft is of b ·ic design and 1955 state-of-the-art vintage. This is not meant to indicate that the Navy faces a catastrophic or unsolvable situation in its current daily operations. However, it does point out that, in light of current aircraft technology, the weapons suspension equipment is marginal and, as such, does impose rather heavy restrictions on the system. In its daily operations, due to this situation, the fleet faces:

a. Personnel and mission safety hazards.

b. Excessive turnaround or rearming time.

c. High volume maintenance cycles at all levels.

d. High volume preoperational checks and tests.

e. Frequent component replacement and redesign programs.

f. Restricted flight envelopes.

g. Restricted delivery envelopes.

h. Restricted weapons carriage requirements.

i. Excessive administrative controls.

j. Excessive on-site support equipment and spares requirements.

k. Excessive minor failure rates.

l. Continual need for improvement and modification via ECP to meet requirements.

m. Lower delivery accuracy and reliability level than would be desired.

The above indicates the extent of penalties the Navy pays in terms of cost, time and delivery accuracy due to use of existing equipment. This overall problem can be directly related to the current research and development approach to weapons suspension equipment design that only allows a hindsight, minor development effort to modify an existing rack to meet the requirements of a new aircraft.

This philosophy is purportedly based on the fact that independent R&D funding is not available in this area and must wait until an aircraft is designed and funded prior to receiving any support. This philosophy has its obvious drawbacks as can be seen with the Navy's two newest aircraft, the S-3A and the F-14. The prime aircraft bidders are forced to bid their proposals based on using an existing item of government furnished weapons suspension equipment and by the time funds are available for development, the airframe and avionics designs are too firm to accept the cost and time impact of incorporating newly designed equipment.

The S-3A aircraft which is the Navy's prime carrier based ASW threat was saddled with modification to two racks:

a. The Aero-65A1/B1 in the bomb bay.

b. The MAU-9A/A on the wings.

The modifications resulted in two racks, the BEU-14/A in the bomb bay and the BRU-11A/A on the wings that will perform the functions required of the aircraft. However, the S-3A has been penalized due to this philosophy with:

a. Excessive program costs and delays to cope with the out of specification electromagnetic compatibility outputs of the racks.

b. Highly restricted delivery envelopes in the bomb bay installations.

c. Excessive weight penalties on the wing stations.

d. Relatively high equipment maintenance cycles.

e. Tedious loading requirements.

f. Excessive administrative controls for nuclear safety.

A very similar situation has occurred with the F-14 aircraft in that it has been forced to utilize two racks, the BEU-19/A (MAU-9A/A modified) and a modified MAK-79 in installations for which they were not designed. The results have been:

a. An extremely cumbersome and trouble prone operating interface linkage on the BRU-19.

b. A questionable use of the secondary release system on the BRU-19.

c. The design and incorporation of an aircraft pylon to provide the structural integrity missing in the MAK-79.

d. Excessively low ejection forces on the MAK-79 stations.

e. Questionable safety and reliability of the MAK-79 stations.

f. A complicated and time-consuming loading procedure for all stations.

g. Restricted delivery envelopes.

The Navy has been slow to learn its lesson and is approaching a situation similar to those outlined above in its implementation of the F-18 or NACF program.

Two specifications, XAS-3759 and XAS-3760, have been developed to outline the guidelines for development of future weapons suspension equipment and update the state-of-the-art to match the aircraft and the balance of the avionics system. However, unless a design program is implemented on an independent basis, and sufficiently funded, new equipment will continually lag service aircraft by as much as two decades.

BACKGROUND

R&D effort and funding in recent years for design and development of new suspension and release mechanisms to fulfill the Navy's conventional and nuclear attack bombing role has been minimal. This has created a situation where the use of prior art in fleet operations has resulted in massive inefficiencies and failures in both tactical and logistic operations. No bomb rack to date has been developed specifically to fulfill the stringent nuclear carriage requirements. No new nonejector rack has been developed in over 20 years. The fleet has had to exist with utilization of modified in-service conventional racks to fulfill their nuclear role. The problems that have and are currently plaguing the fleet are of such a nature that each could probably be solved by modification and or adoption of current state-of-the-art techniques. However, to fully optimize the weapons suspension and release system and maximize fleet efficiency, a novel future state-of-the-art system integration of multiple current state-of-the-art techniques is required. Although the need for this type of improvement has been well recognized by many lab and fleet activities, it has not, in the past, been supported by the magnitude of funding required to even approach final problem solutions.

To attain the projected fleet objectives resulting from a reduction in manpower, future weapons suspension equipment will have to exhibit:

a. Rapid turnaround capability.

b. Low maintenance requirements.

c. High interchangeability index.

d. Standardized interfaces.

e. High mission reliability.

f. Improved mission safety characteristics.

g. Multiple mode capability.

h. Minimal skill operations.

To the maximum extent possible, the requirements of the Navy and Air Force should be addressed in an effort to attain joint service standardization.

DEVELOPMENT HISTORY

Although recent funding has not been sufficient to support a full R&D effort on weapons suspension equipment, expertise and maintenance of state-of-the-art has been attained through minor design efforts to provide the fleet with equipment that would, at least, meet their minimal operational requirements. The latest available systems (BRU-10, BRU-11, BRU-14, BRU-15 and BRU-19), although they have received flight and in some cases nuclear certifications, are basically updates of twenty plus year old bomb rack designs. The modifications performed on these systems and the extent of the effort required to make them flight worthy have allowed the Navy to maintain, practice and utilize latest state-of-the-art subsystems and concepts at a relatively low research and development cost, but the overall operations and performance to the fleet are marginally acceptable as previously noted. In addition, the overall logistics cost and burden, due to the proliferation of racks, are horrendous.

OBJECTIVES

The philosophy of the Navy requires that four distinct types of weapons suspension systems be developed for future aircraft:

a. 2000-lb Gravity Release System for low performance ASW, sea control and reconnaissance aircraft. This type of system would also be used inside sealed bomb bay aircraft.

b. 2000-lb Ejector Bomb Rack for high performance attack and fighter aircraft. This would essentially be a lightweight rack with low drag characteristics.

c. 2000-lb Ejector Bomb Rack for use in multiple carriage installations on all aircraft. This rack should essentially be a derivative of the 2000-lb system discussed above.

d. 4500-lb Ejector Bomb Rack for high performance attack aircraft and ASW mining operation. This rack would be a heavy parent rack capable of supporting individual stores or multiple carriage systems.

All of the above systems should exhibit features acceptable or readily adaptable to nuclear and conformal carriage in addition to their conventional role. These systems would also exhibit a high degree of standardization as regards aircraft fit and will thus do away with the requirement of different models within each class and the continuing proliferation of type and series of each rack, resulting in reduced costs.

APPROACH

In order to attain the goals of the above systems at a minimum cost and maximum efficiency to the Navy, the following multifacet flexible program shall be employed:

a. Establish liaison with the cognizant Air Force Suspension Equipment Design activity.

b. Development of individual detail design guidelines for each category of equipment. These documents shall define the performance and operational criteria required for each system and shall be coordinated with the Air Force to insure that all their requirements are included.

c. Preparation of request for proposals (RFPs) for solicitation of industry and in-house proposals for the design and development of each system.

d. Joint Air Force/Navy evaluation of all responses to the RFP to decide the optimum course of action in pursuance of the programs, i.e.,

(1) Contractor developed with Navy monitor and control.

(2) Joint Services developed.

(3) Combination contractor/Joint Services development.

e. Development of the system with a major emphasis on the research, development, test and evaluation RDT&E and Reliability/Maintainability development programs to substantially reduce risk.

All design and specification guidelines to be utilized in the above programs would be based on the findings and directions of

Specifications XAS-3759 and XAS-3760. These documents are general design guides developed by a team of Navy personnel considered as experts in the field of weapons suspension equipment, and address all past, current and foreseeable future problem areas of this equipment. These industry and tri-service coordinated documents may be invaluable in determining the detail requirements and specifications for each of the above classes of racks and should considerably lower the risk factor of the overall program.

The actual approach for the design of the 2000-lb Gravity Release System would be to design, develop, fabricate and test a new 14 - 30 inch nonejector bomb rack with conventional nuclear carriage capability for ASW, sea control, reconnaissance fixed and rotary wing aircraft. This rack would incorporate features such as: 2000-lb store capacity; integral, quick adjust, indicating sway braces; new high reliability low cost release unit; inflight operable locking system, secondary independent release and unlock systems; manual ground operational capability; and built-in-test (BIT) adapter jack as a minimum. The purpose of this program would be to replace current racks such as the BRU-12, BRU-14, BRU-15 and MK-8 shackle, and thus vastly improve the Navy ASW patrol aircraft capability.

The 2000-lb ejector bomb rack would incorporate all of the criteria of the nonejector rack, but in addition, would have a dual ejector pitch control system and low profile for use on high speed light attack aircraft in a wing mounted, multiple or conformal carriage installation. Semi or fully automatic features would be stressed to reduce manpower and turnaround time requirements.

The 4500-lb ejector bomb rack would have essentially the same basic design requirement as the 2000-lb ejector rack with a proportional increase in payload and performance characteristics. Its primary mission would be for heavy air-to-ground attack missions but consideration will be given to the incorporation of an air-to-air missile carriage role.

Although the two specifications, XAS-3759 and XAS-3760, have been developed to outline the guidelines for development of future weapons suspension equipment and update the state-of-the-art to match the aircraft and the balance of the avionics system, unless a design program is implemented on an independent basis and sufficiently funded, new equipment will continually lag service aircraft by as much as two decades. In addition, the fleet will of necessity continually be plagued with the horrendous logistic and operational nightmare caused by the unending march of rack models, makes, series, types, etc.

The time is now to grasp the situation and approach the solution by designing and implementing a new weapons suspension system for future use in its true perspective - that it is a major subsystems, one that is the primary system in many missions - by funding and

controlling its development on an independent and self-sustaining basis. It is only in this manner that the Navy can ever hope to attain the standardization and reliability within its own house that it is recommending to all outside contractors and foreign nations.

AUTOBIOGRAPHY

Mr. T. E. Milhous received his B.S. degree in Mechanical Engineering from Widener College in 1968. Upon graduation, he joined the Naval Ordnance Laboratory under the work-study program and received his M.S. degree in Mechanical Engineering from the University of Maryland in 1971. His work assignments at NOL included environmental testing of conventional weapon fuzing systems and Navy member ship on JTCG Working Party for Fuzes. For the past four years he has been employed by the Weapon Suspension Design Branch at the Naval Air Development Center as a project engineer. At NADC, areas of responsibility have included subsystem and system research and development of suspension equipment and committee memberships is follows:

a. JTCG/MD Working Party for Racks and Ejection Cartridges - principal Navy member

b. NATO Air Armament Working Party - Navy technical representative

c. ASCC Conventional Aircraft Armament Working Party - Navy representative

Mr. Milhous is a member of the Tau Beta Pi engineering society.

HYDRAULIC CONSTANT RECOIL PROGRAM (U)

(Article UNCLASSIFIED)

P.E. Townsend
Rock Island Arsenal
Gen Thomas J. Rodman Laboratories
Rock Island, Illinois

R.F. Gartner
Honeywell Inc.
Government and Aeronautical Products Division
St. Louis Park, Minnesota

R.E. Rasmussen
Tri-Tec Associates
Minneapolis, Minnesota

Approved for public release; distribution unlimited.

ABSTRACT. With the maturing role of the attack helicopter in the mid-intensity conflict environment, high impulse armament is desired to maximize mission effectiveness. This paper will report on the Army's efforts to develop a hydraulic recoil control system for use in integrating weapons with high recoil loads on helicopter structures. Past and present airborne armament systems employ automatic weapons using spring-type recoil adaptors to absorb the impact of the weapon impulse. This typically generates a high peak load at firing, a counter-recoil load as the weapon comes into battery, and resultant structural ringing. This type of loading not only results in localized structural flexure, causing weapon inaccuracy, but generates structural vibration throughout the aircraft that contributes to control and reliability problems. The hydraulic servo unit being developed integrates the impulse over the entire firing cycle resulting in a constant load at a minimum level as much as 80% lower than peak loads now experienced. In addition, the unit senses and compensates for other system variables, such as ammunition impulse variation, acceleration loads due to aircraft maneuvers, and weapon misfires. A state-of-the-art development is required in the central servo control valve that combines rotary and longitudinal motion to sense and meter the working fluid within the servo loop. The rotary motion determines the weapon position in the

firing cycle while the longitudinal displacement measures the recoil stroke during firing. Also designed into the same valve is the misfire compensation network that assumes control when a round falls to fire during a burst. This unique control device represents a breakthrough in servo valve development with wide application potential in fields other than armament systems integration. Design studies, computer simulations, and critical components testing have demonstrated concept feasibility. A flight-worthy prototype is currently being developed using the 20mm M197 automatic cannon as the test vehicle. Flight test evaluation is planned in FY76 on the Army's Multiweapon Fire Control AH-1G helicopter. Successful demonstration of this concept will have the following benefits for future attack helicopter development:

a. The ability to mount higher impulse gun-type weapon systems.

b. Reduced structural requirements in the helicopter airframe.

c. Increased system accuracy due to reduced structural flexure.

d. Reduced stabilization requirements in sighting and turret systems.

e. Reduced flight crew stress during weapon firing operation.

f. Increased aircraft component life and reliability due to reduced vibrational disturbances now generated during weapon firing.

LIST OF ILLUSTRATIONS

Figure 1. Force Pulses from Present Recoil Adaptors

Figure 2. Force Pulses from Laboratory Model and Recoil Adaptors

Figure 3. Recoil Velocity vs Time for Constant Recoil Force

Figure 4. Recoil Displacement vs Time for Constant Recoil Force

Figure 5. Laboratory Concept

Figure 6. Force Pulse from Laboratory Model

Figure 7. Rotary Valve Concept

Figure 8. Rotary Valve Assembly

Figure 9. Rotary Valve/M197 Assembly

Table I Computer Predicted Forces

INTRODUCTION

The attack helicopter is proving to be an effective weapon system in the mid-intensity conflict; further increases in mission effectiveness can be gained by increasing the fire power of the automatic weapons. This increase can best be gained through automatic weapons firing larger projectiles at greater muzzle velocities. However, the more powerful weapons cannot be mounted on the lighter weight helicopters because of their large cylic recoil forces. This paper is a report on the Army's effort to develop a hydraulic recoil control system to overcome the recoil problem.

THE PROBLEM

Past and present airborne armament systems employ automatic weapons using spring-type recoil adaptors to absorb the weapon recoil impulse. These adaptors typically transmit a high peak force during firing and a counter recoil force as the weapon comes into battery. Figure 1 is a typical force-time history measured during the firing of the 3-barrel 20MM M197 gatling gun at a rate of 750 shots per minute. This type of force loading not only results in localized structural flexure, causing weapon inaccuracy, but also generates vibration throughout the aircraft that contributes to helicopter control and reliability problems.

ARMY PROGRAM

The Army is investigating mechanisms that will reduce the transmitted recoil forces to a much lower level than presently obtained from the spring-type recoil adaptors. One of the mechanisms being studied is the hydraulic recoil control system described in this paper. It is a hydraulic servomechanism that reduces the transmitted recoil forces from firing the M197 weapon to a near constant level over the entire firing cycle. Figure 2 shows, the measured transmitted force from the laboratory model this recoil control mechanism and the forces from the conventional recoil adaptors, repeated from Figure 1 for comparison. As can be seen from the comparison, a four to one reduction in peak recoil forces was obtained with a total amplitude reduction of five to one.

A test prototype model is presently being developed by the Government and Aeronautical Products Division of Honeywell. This prototype will undergo extensive ground firings and then flight tested in the AH-1G helicopter.

A complete system that can be mounted in the XM97 turret, it requires only electric power lead in parallel with the gun motor and hydraulic power from the helicopter secondary hydraulic system. It uses approximately one pint of oil for a 20-round burst. (Other than requiring a power lead and two additional hydraulic lines the weapon system function will not be altered.

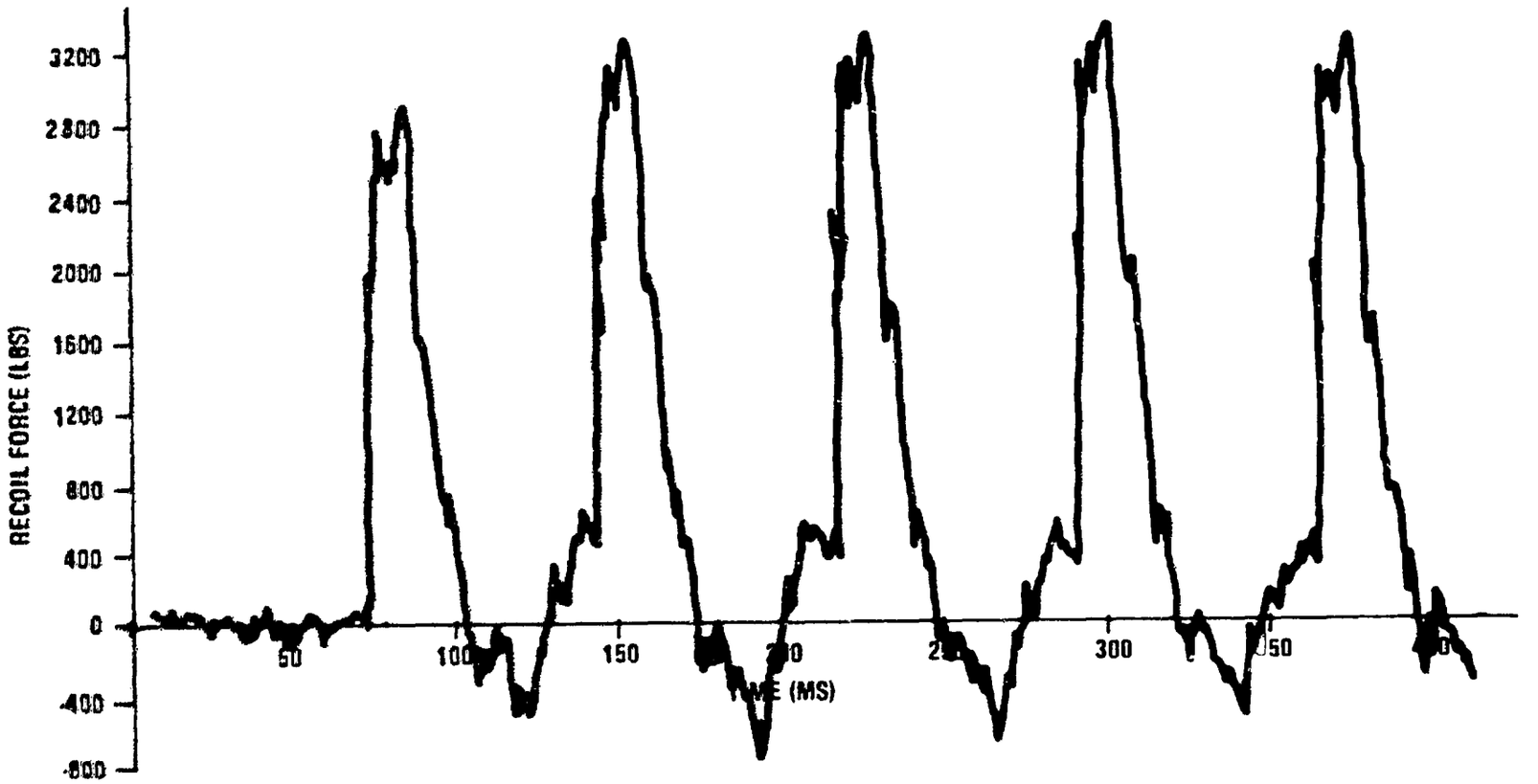


Figure 1. Force Pulses From Current Recoil Adaptors

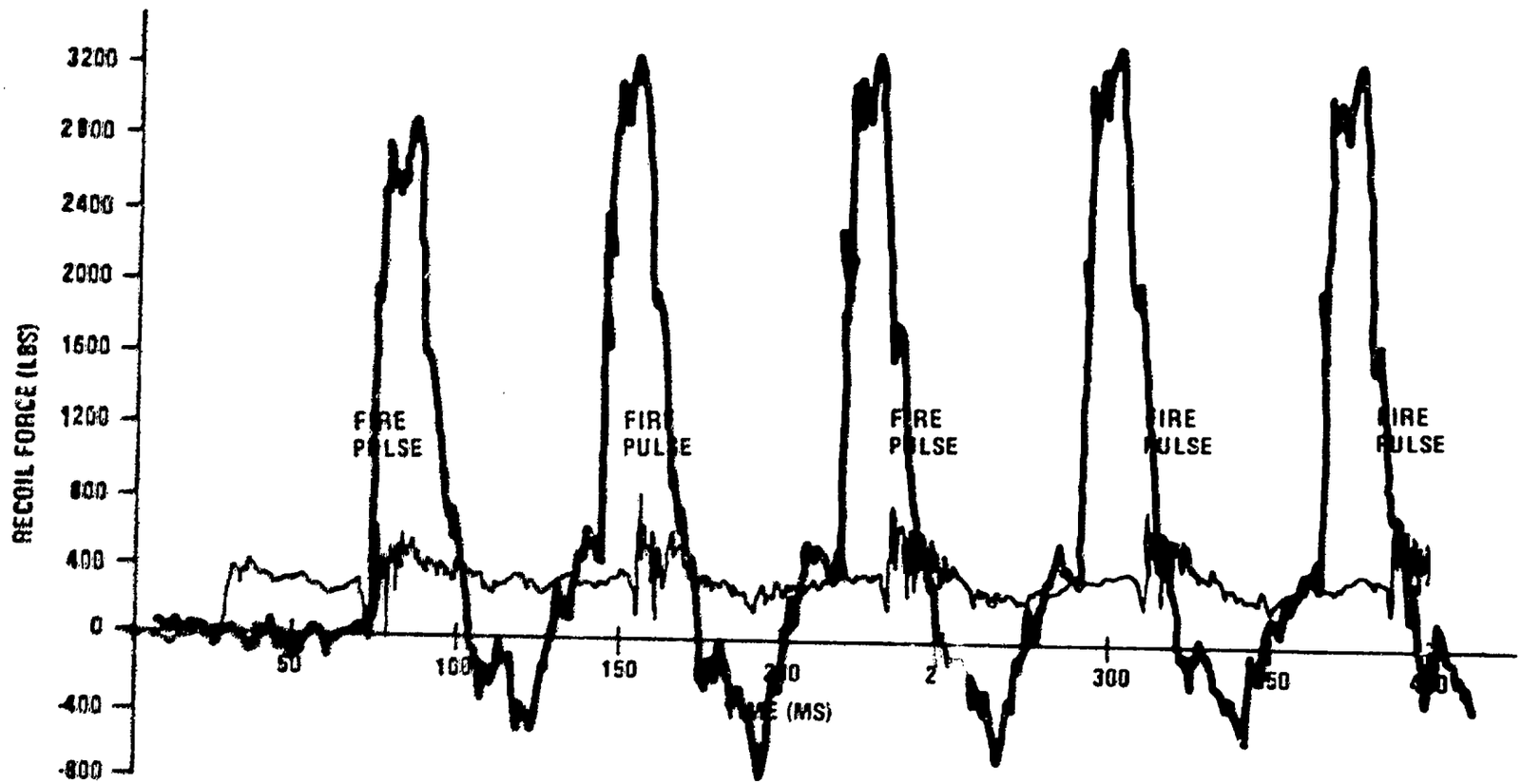


Figure 2. Force Pulses From Laboratory Model and Recoil Adaptors

This paper will describe the function of the system, a hydraulic servomechanism that controls the recoil forces and the weapon movement.

FUNCTIONAL CONCEPT

REQUIREMENTS

The test prototype recoil control system meets the following program requirements:

- Reduce transmitted recoil force to near constant level
- Control weapon recoil travel
- Compensate for
  - Weapon elevations +50 to -90 degrees
  - Firing rate variations of ±10 percent
  - Ammunition impulse variations of ±10 percent
  - Random misfires, including two consecutive misfires
- Consume less than 3 GPM hydraulic flow, average

TECHNICAL APPROACH

Many combinations of passive and active recoil systems were examined through computer simulations. In addition to indicating that the forces, rates, and cylic frequencies encountered were well within the capabilities of hydraulic servomechanisms, the simulations showed that the following were necessary if recoil forces were to be constant:

- Weapon must be fired "out of battery"
- Net cycle displacement must be zero
- Net cycle velocity must be zero

These rules are illustrated graphically in Figures 3 and 4. The analysis is based on the assumption that the transmitted recoil forces are constant. If the dynamics of a given weapon are examined, definite relationships can be established between weapon recoil position, velocity, acceleration and firing rate, and ammunition impulse. These relationships are:

$$\text{Recoil force (lb)} = \text{Impulse (lb - sec)} \times \text{shots per second} \qquad (1)$$

$$\text{Recoil displacement (in)} = \frac{1.5 \times \text{impulse}}{\text{recoiling mass (slugs)}} \times \text{shots per second} \qquad (2)$$

By using these relationships, the basic characteristics of a hydraulic system that will enable the weapon to recoil in a predictable manner can be determined. If hydraulic components with the proper specifications are used, the system requirements can be met by a hydraulic servomechanism which:

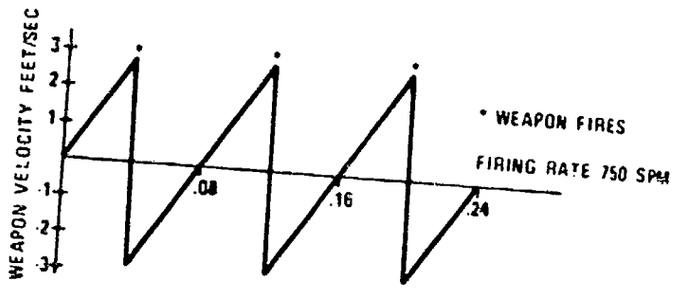


Figure 3. Recoil Velocity vs Time for Constant Recoil Force

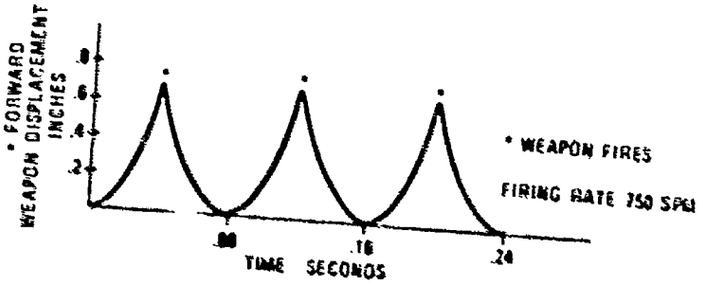


Figure 4. Recoil Displacement vs Time for Constant Recoil Force

- Commands weapon recoil motion to follow a prescribed position and velocity pattern
- Senses errors between actual and prescribed position and velocity
- Adjusts recoil forces to reduce these errors to zero

INITIAL CONCEPT

Figure 5 shows the first concept of which a laboratory model was mounted on the M197 gun and fired on the Honeywell range. The mechanization consists of a simple unequal area hydraulic piston connected to the weapon; forces on the cylinders are transmitted to the supporting structure representing the helicopter. The greater part of the force is supplied by the hydraulically coupled accumultor --- essentially a hydraulic spring with a very low rate. The force from the accumulator is close to the prescribed force. A hydraulic servomechanism, consisting of the small servo piston, a three-way servovalve and positioning cam, causes the pressure on the servo piston to be the precise amount necessary for the net force to be identical to the prescribed force of equation 1. This net force is the sum of the accumulator-produced pressure force, sliding friction force, and servo piston force. The force required by the cam to move the three-way servovalve is negligible. The force control positioning of the servovalve is accomplished by a cam mounted so that it both rotates and recoils with the weapon. Rotation provides synchronization with weapon firing, and the recoil motion positions the valve to provide the proper flow-pressure relationships for each instant of time over the entire cycle shown in Figures 3 and 4.

COMPENSATION FOR ERRORS

If the weapon, with a recoil system as shown, is fired at a specified rate with specified ammunition, the flow-pressure relationships of a suitable servovalve can be defined. Furthermore, with extensive computational analysis, the contour of the cam can be determined exactly. Assume, however, that the variables (primarily firing rate and impulse) are not as specified. Obviously, the weapon would respond to these differences by moving at a non-prescribed velocity to a non-prescribed position. These velocity and positional differences (servosystem error) will result in a different servovalve position and different flow-pressure response. However, computation analysis has predicted the effect of these errors, permitting selection of valve parameters (port width, length, overlap and underlap) such that the errors normally encountered will cause only slight changes in the prescribed forces, thereby resulting in a gradual trend of weapon movement back toward the prescribed recoil path.

The transmitted forces measured in the firing of the laboratory model without the force from the recoil adaptors for comparison, are shown in Figure 6. Careful study of the fluid flow between the cylinder and accumulator revealed the generation of high pressures resulting from the rapid weapon deceleration during firing.

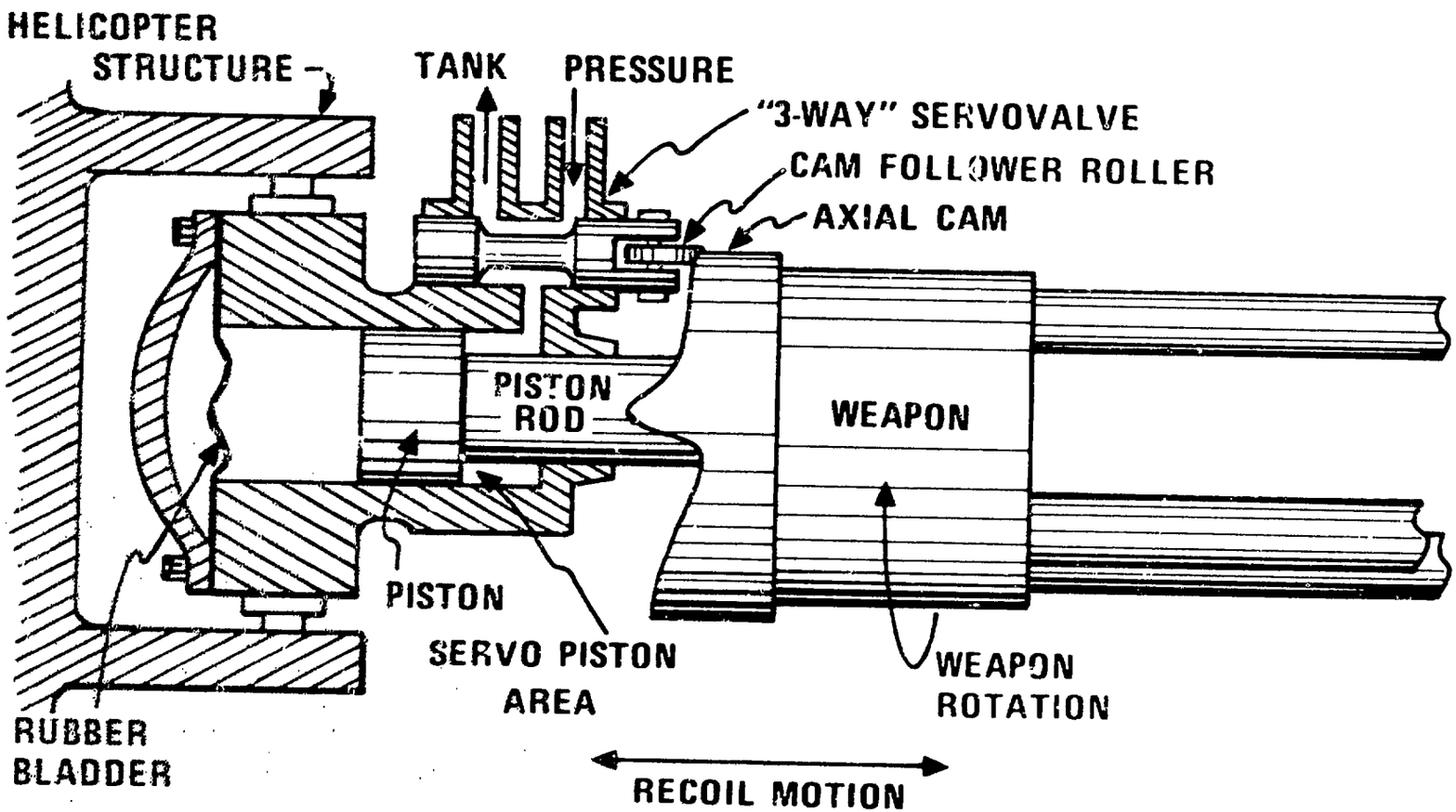


Figure 5. Laboratory Concept

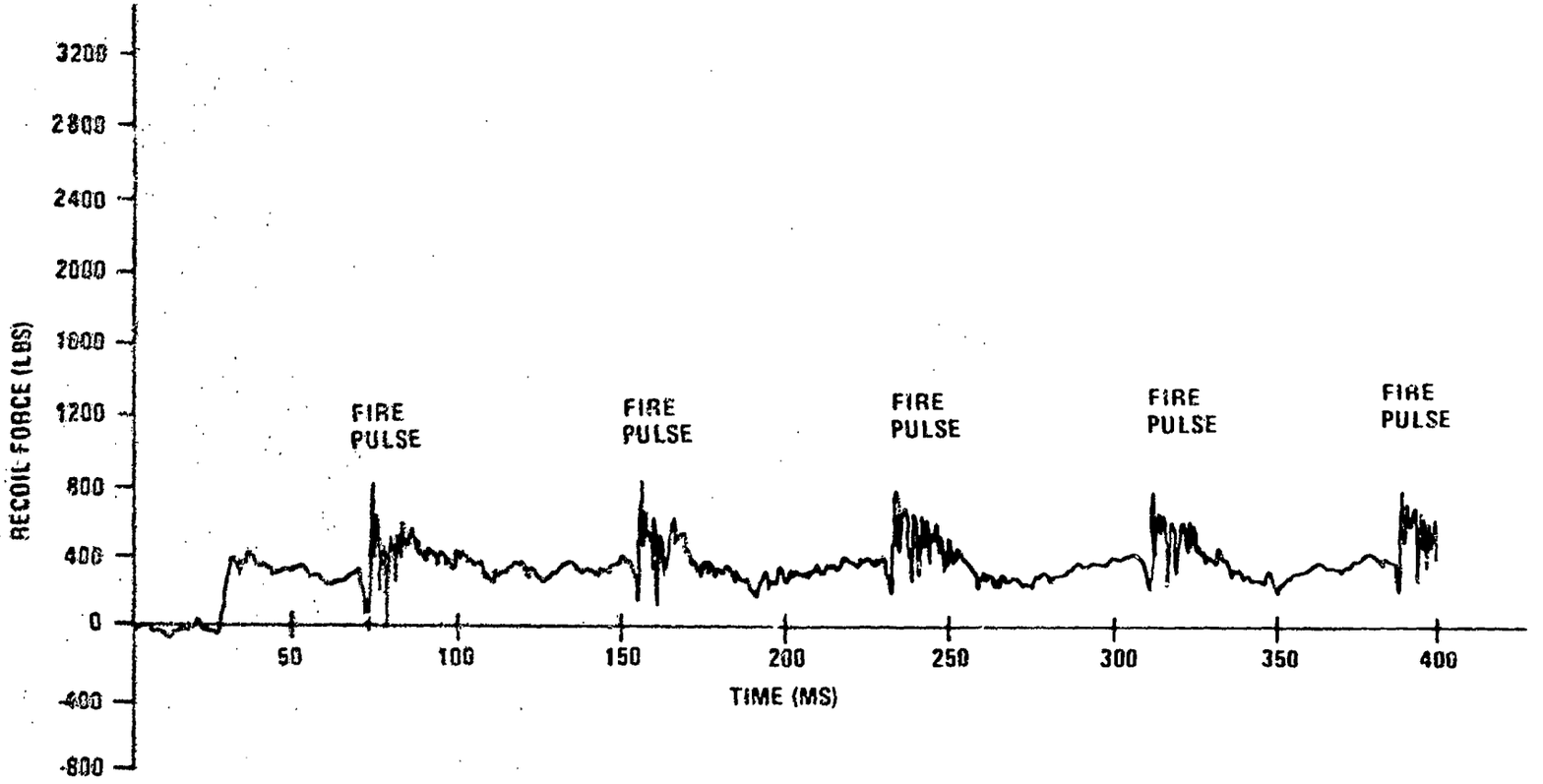


Figure 6. Force Pulse From Laboratory Model

PRESENT CONCEPT

The first objective in the design of the present concept was to redesign the piston/cylinder/accumulator configuration to minimize the generation of the high pressure pulse. In addition, a redesign of the cam/follower arrangement to improve servovalve/cam tracking capabilities eliminated the large, awkward cam arrangement. The present design concept is shown in Figure 7. In this arrangement, the recoil cylinder and accumulator were made integral and shaped to provide dispersion of the pressure pulse over the surface of the accumulator bladder. The servovalve, servopiston, and cam of the laboratory design were replaced by a rotary valve of unusal design (Figure 7) that combines the function of all three. The difference in the valve land diameters became the servopiston area and the valve lands were shaped to perform, in conjunction with hydraulic pressure and return ports, the function of the cam and roller follower of the laboratory model.

Figure 8 is a photograph of the rotary valve assembly. It consists of a spool and a sleeve. In this photograph the spool of the valve is positioned to the left of its operating position to display the rounded end of the piston and the curved lands that control the flow of oil in and out of the servocylinder. The sleeve is attached to a vertical member of the saddle in the turret. The receiver of the weapon slides over the sleeve with the spool attached to the weapon rotor as shown in Figure 9.

In addition to the rotary servovalve the hydraulic recoil system consists of subsystems hich

- Hold the weapon in a fixed position during the non-firing portions of helicopter flight.
- Sequence the operation of the recoil system with the firing of the ammunition, not with rotation of the empty weapon.
- Adjust accumulator pressure to compensate for weapon elevation or aircraft maneuvers.
- Detect misfires and control subsequent recoil motion without stopping firing.
- Ensure safety-of-flight with a monitoring subsystem that prevents damage to the aircraft in event of hydraulic malfunction.

Preliminary reliability estimates indicate more than adequate reliability based upon comparable data from hydraulic servomechanisms used in aircraft control systems.

Table I contains the computer predicted force values for the test prototype system over the complete range of operating conditions.

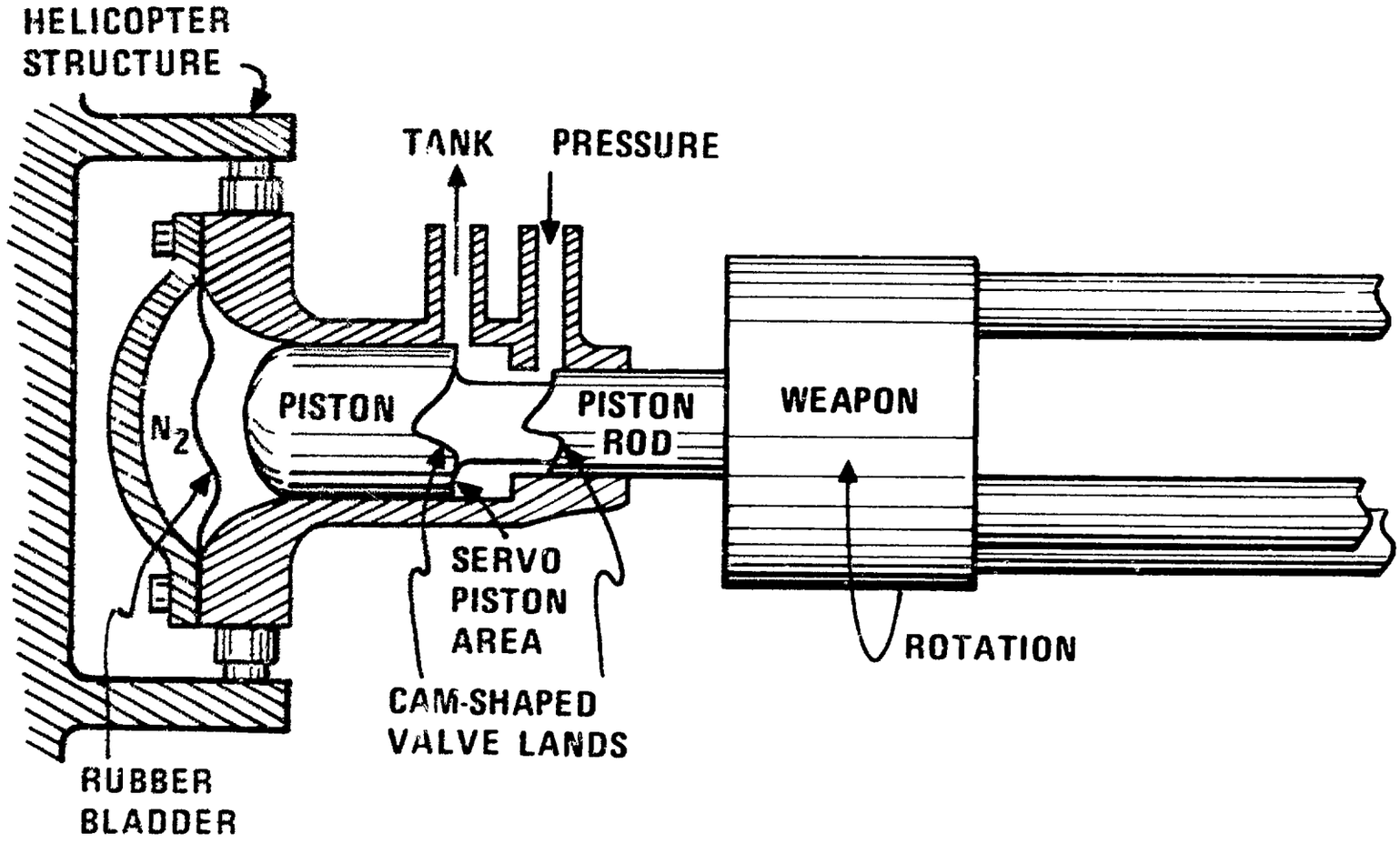


Figure 7. Rotary Valve Concept

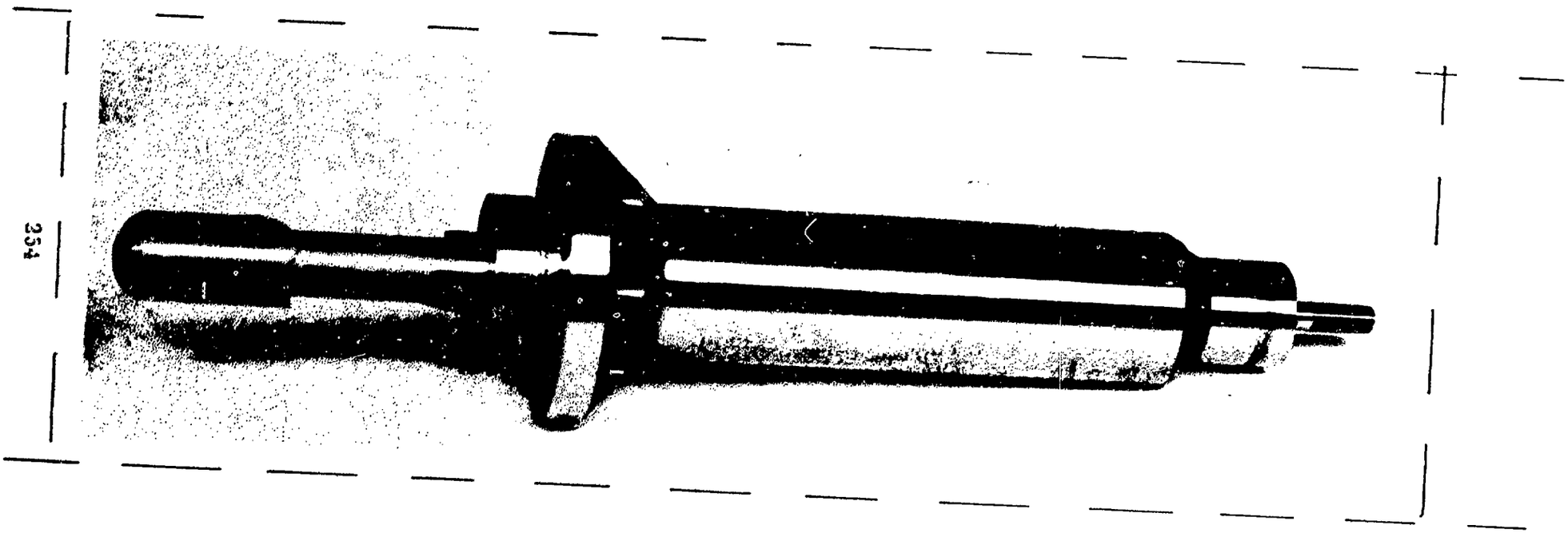


Figure 8. Rotary Valve Assembly

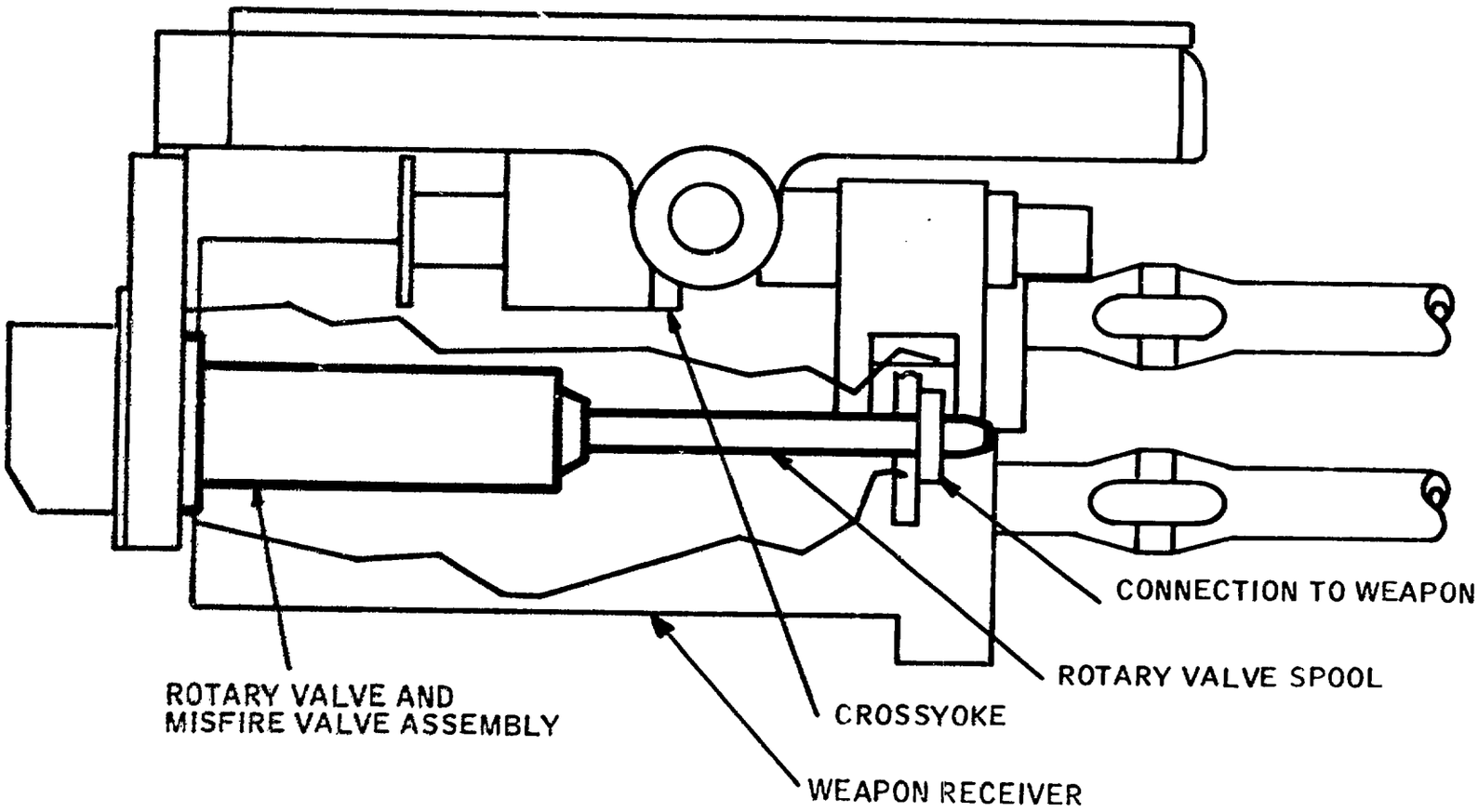


Figure 9. Rotary Valve/M197 Assembly

TABLE I COMPUTER PREDICTED FORCES

	STANDARD	TEST PROTOTYPE SYSTEM EXTREMES	MISFIRE
RECOIL FORCES			
MAXIMUM (lbs)	450	626	591
MINIMUM (lbs)	431	473	1016
DIFFERENCE (lbs)	19	153	1607

PRESENT STATUS

The total system has been tested statically on a hydraulic flow bench with results close to design values. Firing tests will be initiated in the near future. These tests will include firings to evaluate performance over the required variations in weapon elevation, firing rate and ammunition impulse as well as tolerance to random misfires.

CONCLUSIONS

The results of the program to date demonstrate that hydraulic servomechanisms can be applied to the recoil systems of automatic weapons to reduce significantly the recoil forces transmitted to the helicopter structure. The lower level, near constant forces offer significant potential benefits to the attack helicopter:

- Ability to mount higher impulse gun-type weapon systems.
- Reduced structural requirements in the helicopter airframe.
- Increased system accuracy due to reduced structural flexure.
- Reduced stabilization requirements in sighting and turret systems.
- Reduced flight crew stress during weapon firing operation.
- Increased aircraft component life and reliability due to reduced transmitted vibration.

Philip E. Townsend is currently a project engineer in the Advanced Concepts Group of the Aircraft/Air Defense Weapon Systems Directorate in the GEN Thomas J. Rodman Laboratoty at the Army's Rock Island Arsenal. He is engaged in Systems Integration of Helicopter Weapons Systems. Prior assignments include Aircraft Weaponization Exploratory Development Program control in the Army Weapons Command and dynamic analysis of artillery weapons systems at Rock Island Arsenal. Mr. Townsend received a Bachelor of Science degree in Mechanical Engineering from the State University of Iowa and is currently engaged in study to earn a Master of Science degree in Systems Management from the Flordia Institute of Technology.

Robert F. Gartner is currently a Senior Principal Development Engineer in the Fire Control Systems Section of the Honeywell Government and Aeronautical Products Division. He is engaged in the development of helicopter fire control systems with primary emphasis on hydraulic recoil control servomechanism. Prior assignments involved the development small arms and airborne munition. Mr. Gartner received a Bachelor of Science degree in Mechanical Engineering from the Illinois Institute of Technology.

Robert F. Rasmussen is a Consulting Engineering and president of Tri-Tec Associates of Minneapolis. Mr. Rasmussen speciality are hydraulic servo-mechanism, holding over 30 patents in this field. Mr. Rasmussen is a registered Professional Engineer and has received a Bachelor of Science degree in Mechanical Engineering from the University of Minnesota.

BOMB RACK SUSPENSION HOOK

IMPROVEMENT PROGRAM
FOR
NAVAL AIR SYSTEMS COMMAND
(U)
(ARTICLE UNCLASSIFIED)

by

Edward Turissini
Naval Avionics Facility, Indianapolis
and
Lynn Seal
Dayton T. Brown, Inc.

ABSTRACT. (U) Bomb rack hooks have always presented a safety and maintenance problem, to Fleet personnel, due to the evident hazards caused by their failure. Extremely rigid quality control procedures are applied during the manufacturing of these hooks which include preproduction, first article and sample testing for fatigue life, ultimate strength, plating thickness, salt spray and chemical analysis of the steels used for the hooks. During the course of these tests, numerous design discrepancies and material and manufacturing faults were detected and reported. Fatigue failure coupled with stress corrosion cracking accounts for most hook failures. The ramifications of the situation are obvious. Failure of a hook under the stress of launch or arrested landing can cause inadvertent release of stores or fuel tanks, thereby endangering the pilot, launch crew, aircraft, and carrier. Inadvertent release of a store over populated areas endangers both people and property on the ground. Failure of a hook in flight can cause non-release of a store of fuel tank endangering both crew and aircraft.

As a result of persisting Fleet failures, complex maintenance procedures and manufacturers' difficulty in producing hooks that consistently meet specification requirements, it was imperative that a thorough investigation be conducted of hook design, manufacturing, and testing methods.

APPROVED FOR PUBLIC RELEASE:

DISTRIBUTION UNLIMITED

PRECEDING PAGE BLANK-NOT FILMED

The purpose of this paper is to describe the investigation being performed by Dayton T. Brown, Inc. and Naval Avionics Facility, Indianapolis (NAFI) funded by Naval Air Systems Command (AIR 5321). It encompasses investigation of hook materials, hook shapes, plating methods, forming techniques, heat treatment and non-destructive inspection techniques.

LIST OF APPENDICES

Appendix I - Marine Stress Corrosion of PH 13-8Mo Corrosion Resistant Steel

Appendix II - List of Sources for Detailed Test Information

HISTORICAL BACKGROUND

Over the past 25 years, several methods have been utilized in the manufacture of bomb rack hooks. The following is a listing of the various methods (material, plating, etc.) used:

(a) Chrome plated 4140 steel - This material is used for MAU-9, BRU-10, Aero 1A Adapter, Aero 15 and Aero 65 bomb rack hooks.

(b) Chrome plated 4140 steel, with cadmium plate on non load bearing areas - This material is used for Aero 7 and Aero 20 bomb rack hooks.

(c) AISI 431 corrosion resistant steel (CRES) - This material was used on early versions of Aero 7 and Aero 20 bomb rack hooks.

(d) 17-4PH CRES - This material is used for Aero 27 bomb rack hooks.

(e) Chrome over nickel plated 4140 steel - This system was used on some MAU-9 and BRU-10 bomb rack hooks.

Various problems have been encountered during fabrication and Fleet use of these different bomb rack hooks. These problems have resulted in excessive maintenance (hook cleaning and replacement) by the Fleet user and reluctance of prospective vendors to fabricate hooks.

Specifically, in the case of both the 431 CRES and the 17-4 PH CRES, the problems have centered around stress corrosion cracking during Fleet use. The 431 CRES, has adequate resistance to stress corrosion cracking; however, the heat treatment procedures for this material are extremely complex and very critical, and the properties of the material cannot always be controlled adequately for this application. The 17-4 PH CRES is an inadequate material because it must be heat treated to a condition of H875 to meet the ultimate strength requirements necessary for bomb rack hooks. When heat treated to this condition, this material loses much of its resistance to corrosion and stress corrosion cracking and has considerably reduced impact strength.

The 4140 steel has proven to be the most suitable material currently being used for bomb rack hooks. However, the various plating systems for this material present serious problems which render 4140 steel hooks unsatisfactory from both the production and Fleet use standpoint.

The chrome over nickel plating has been abandoned by vendors due to production problems which were to costly to overcome. The chrome and chrome/cadmium plating systems are presently being used on 4140 steel. However, these plating systems also present problems because the chrome plate reduces fatigue life up to 50%, chips, breaks down in service use, and is costly to apply.

The current bomb rack hook designs also present problems with respect to their geometries, which cause production problems and reduce fatigue life as a result of stress concentrations. For example, the MAU-9 and BRU-10 bomb rack hooks have a cut-out which is formed during the forging process. This, many times, causes cracks to form on the edges of the cut-out area. Also, sharp corners, inside radii, cut-outs, reduced cross-sections, etc. on all hooks coupled with the chrome plating greatly reduce the fatigue life, and require all hooks to be prestressed prior to use. Prestressing is the operation of tensile loading the hook slightly above its yield strength so that residual compressive stresses remain on the critical surfaces of the hook, thus increasing the fatigue life many times longer than the unprestressed hooks.

APPROACH

As a result of the problems, an investigation was undertaken to improve hooks by:

(a) Changing of design (geometry) to eliminate stress concentrations.

(b) Use of a material that required no plating.

(c) Use of a material that required no prestressing.

(d) Use of a material that was not susceptible to stress corrosion cracking.

(e) Maintaining a low cost of the end items to include low initial cost (manufacture and testing) and maintenance cost.

Initially an investigation was undertaken to determine the most suitable materials for bomb rack hooks. PH 13-8Mo CRES and MP35N multi-phase alloy were found to be the materials which most closely met the requirements.

PH 13-8Mo CRES possesses very satisfactory fatigue properties, excellent resistance to stress corrosion (see Appendix I), can be heat treated to a hardness of Rockwell C45 while maintaining adequate impact strength, and does not require plating for corrosion resistance. This material can also be forged and exhibits adequate machinability.

MP35N multi-phase alloy also possesses all of the properties necessary for its use in bomb rack hooks with the exception of producibility. Since this material is only hardened by cold working, it must be machined at hardnesses of Rockwell C40 to C43.

Drawings were prepared reflecting changes in hook geometry, which were empirically derived through observations of bomb rack hooks that failed laboratory fatigue tests. Hook design changes were also made to simplify the production of bomb rack hooks during forging and machining operations. An additional benefit of the program was that one hook design could replace the two different hooks presently used in the 14 inch and 30 inch stations of the Aero 7 Bomb Ejector Rack.

Concurrent with drawing update, BRU-10 and Aero 7 bomb rack hooks were produced from PH 13-Mo CRES, while one Aero 7 and one Aero 65 bomb rack hook were produced from MP35N for the purpose of determining the feasibility of the use of these materials in this application. All hooks were made to present production drawings. All PH 13-Mo CRES bomb rack hooks were subjected to the following tests:

(a) Ultimate load

(b) Fatigue (prestress evaluation also conducted)

(c) Salt [illegible]

(d) Stress corrosion (60% of yield load)

(e) Life (installed in bomb rack)

(f) Vibration (installed in bomb rack)

(g) Limited flight tests

FINDINGS

The two MP35N bomb rack hooks were only fatigue tested. Although the results were favorable, it was decided to eliminate further evaluation of the MP35N because of its cost and the difficulty of machining this material.

The bomb rack hooks made from PH 13-8Mo CRES passed all tests and equaled or exceeded the performance of presently used hooks. During evaluation of these hooks it was noted that the BRU-10 hooks made from this material did not require prestressing to pass fatigue tests and the Aero 7 hooks, while still requiring prestressing, would not require critical prestress load determination as had been necessary with present bomb rack hooks. Since results were encouraging, it was decided to fabricate final verification samples of the new designs. At the time of this report, these hooks are presently being fabricated with evaluation planned to the completed by December 1975.

NEW INSPECTION TECHNIQUES

The life of bomb rack hooks made from the PH 13-8Mo CRES will be greatly increased, due to deterioration of the plating no longer being a factor, and changes in Fleet maintenance concepts will be required. Since corrosion is presently the determining factor of hook life in a Fleet environment, the improved corrosion resistance, fatigue life, and resistance to stress corrosion cracking of the PH 13-8Mo CRES will be the limiting factors for length of service life.

Failures due to fatigue and stress corrosion cracking always begin as minute cracks in the surface of the bomb rack hook. Consequently, inspection techniques which will increase the probability of detecting these minute cracks are required. An investigation into non-destructive testing techniques is being undertaken to determine the most suitable method of inspecting hooks at the depot maintenance level. This investigation will cover techniques currently in use such as magnetic particle and dye penetrant inspection, as well as new techniques such as acoustic emission and wink flourescent dye penetrant inspection.

Aero 15 bomb rack hooks will be used for the evaluation of the non-destructive testing techniques. These hooks will be stripped of plating and cyclically loaded to induce fatigue cracks. The cracks in the hooks will be measured and their location noted by use of the Replication Technique. The Replication Technique is a method of making a cellulose acetate replica of a surface and then examining this replica under a microscope at 100X to 500X for cracks. Initial tests using the Replication Technique have shown cracks as small as .001 inch in length.

Hooks having cracks of known location and size will be standards for comparison of the techniques to be investigated. The techniques to be investigated are as follows:

(a) The wink flourescent penetrant technique is a process which requires the application of flourescent penetrant to the area being inspected while the part is being cyclically loaded. After several cycles, the part is held in tension while the excess penetrant is removed. When the part is loaded in compression, the penetrant retained in a crack will be forced out so that it can be detected. As the part is slowly cycled, the fluid will be drawn back into the crack when a tensile load is applied and forced out as a compressive load is again applied. The crack will appear to "wink" at the observer. The developer of this technique claims that defects as small as .005 inches in length can be detected.

(b) The acoustic emission technique of inspection is a method of crack detection based on the Kaiser Effect to monitor growing cracks. The Kaiser Effect is the name given to the phenomenon that no acoustic emission can be detected from a loaded specimen until the load exceeds the highest previous load to which the specimen has been subjected. The presence of a crack;

however, will cause acoustic emission due to the propagation of the crack. In the case of bomb rack hooks, no emission should be detectable at loads lower than the prestress load the hook was subjected to during manufacturing, unless a crack is present.

These methods of inspection will be compared with presently used methods such as magnetic particle and dye penetrant inspection techniques to determine if any advantage can be obtained by their use.

CONCLUSIONS

The investigation is presently continuing with a proposed completion date of December 1975. Based on the successful completion of preliminary evaluations of PH 13-8Mo CRES bomb rack hooks, no problems are foreseen with the redesigned hooks made from this material.

Use of the new bomb rack hooks will increase safety, reliability, and maintainability of Fleet equipment.

Additional, detailed, information concerning this program can be obtained by contacting the individuals listed in Appendix II.

APPENDIX I

Marine Stress Corrosion[1]

Tests were conducted on PH 13-8 Mo samples, .062" (1.6 mm) strip, exposed in triplicate on a location 80 feet (24 m) from the ocean at Kure Beach, North Carolina.

Condition	Applied Stress[1] ksi (MPa)	Results[2]
H 950[3]	204.0 (1417)	1 Sample failed after 353 days; 1-1077 days, 1NF[2]
	183.5 (1264)	1 Sample failed after 51 days; 2NF
	153.0 (1055)	1 Sample failed after 1077 days: 2 NF
H1000[3]	199.0 (1372)	3NF
	179.0 (1234)	3NF
	149.0 (1027)	3NF
H1050[3]	172.0 (1186)	3NF
	155.0 (1069)	3NF
	129.0 (889)	3NF
Solution treated, welded, aged at 1000 F (538C) for 4 hrs	195.0 (1345)	3 Samples failed after 43 days
	175.5 (1108)	3 Samples failed after 43 days
	146.3 (1008)	1 Sample failed after 43 days; 1 - 100 days
Solution treated, welded, solution treated and aged at 1000 F (538C) for 4 hrs	195.0 (1345)	3NF
	175.5 (1108)	3NF
	146.3 (1008)	3NF

(1) Applied stresses were 100%, 90%, and 75% of the 0.2% yield strength, using smooth bent beam specimens tested in the longitudinal direction.

(2) NF indicates NO FAILURE in 1405 days exposure.

(3) Heat treatment includes solution treatment at 1700 F (927C), 15 minutes.

* Condition being used for bomb rack hooks.

[1] Chart obtained from Armco Steel Corporation Product Data Publication S-33C.

APPENDIX II

Mr. Harold Ornoff
Naval Air Systems Command
AIR-53213

Phone: Autovon: 222-3845
Commercial: 202-692-3845

Mr. Edward Turissini
Naval Avionics Facility, Indianapolis
Code 921

Phone: Autovon: 634-1911, Ext. 3873
Commercial: 317-353-3873

Mr. Lynn Seal
Dayton T. Brown, Inc.

Phone: Commercial: 516-589-6300

EDWARD F. TURISSINI

Mr. Turissini is a graduate of Indiana Institute of Technology and holds a Bachlor of Science Degree in Mechanical Engineering. He has been employed by the Naval Avionics Facility since 1969. Mr. Turissini's responsibilities at NAFI have included design engineer for the BRU-8 Bomb Rack, design engineer SKQ-3 Telemetry Antenna, Project Engineer BRU-14/A, BRU-15/A Bomb Racks, and Project Engineer Bomb Rack Hook Improvement Program.

LYNN D. SEAL

Mr. Seal is a graduate of Case Institute of Technology and holds a Bachelor of Science Degree in Metallurgy. He served four years with the U.S. Air Force as an Aircraft Maintenance Officer and joined Dayton T. Brown, Inc. in 1969. Upon joining the laboratory, Mr. Seal was assigned as a project engineer to the Mechanical Laboratory responsible for the qualification and acceptance test programs of mechanical, electromechanical, and explosively activated aircraft equipment and material. Mr. Seal is presently the technical supervisor in the Mechanical Test Department, responsible for all aircraft equipment and material testing.

EJECTION RELEASE OF AERODYNAMICALLY UNSTABLE STORES
(Article Unclassified)

by

STEVE J. JENDRAS
Staff Engineer
McDonnell Aircraft Company
St. Louis, Missouri 63166

ABSTRACT. The ejection of externally mounted aerodynamically unstable stores from high speed fighter aircraft has resulted in numerous collisions of the store with the aircraft, and/or limited speed envelopes for safe store release.

An analytical study was undertaken to determine the ejector/release-mechanism characteristics required to provide safe separation of unstable stores throughout the flight envelopes of modern fighter-bomber aircraft and to provide insight into the effect of the physical characteristics of the stores. The purpose was to provide a means of improving aircraft/store compatibility by: (1) further acquainting store designers with the effect of variations in store physical characteristics on separation. (2) providing bomb rack designers with indications of desired performance, for both constrained and unconstrained store release systems, and (3) providing information to aircraft designers to aid them in selecting bomb racks with capabilities compatible with the weapon-carrying and performance capabilities of their designs.

Study results indicate that the performance capabilities of selected existing bomb racks (having high end-of-stroke velocity), may be sufficient to achieve safe release of most of the stores in existence. New ejectors which constrain the angular motion of the store during ejection show a considerable improvement over unconstraining types in terms of the end of stroke velocities required.

The results of the analytic technique used in this study have correlated reasonably well with F-4 flight test results, and the general trends indicated are considered applicable - as a first approximation - to other aircraft utilizing similar stores installations. Recommendations for follow-on effort include analyses of the effect of:

- Variations in store static stability
- Flow field variances
- Airplane maneuvering

"Approved for public release; distribution unlimited."

LIST OF FIGURES

Figure	Title	Page
1	Study Matrix	
2	BLU-1/B Napalm Bomb	
3	Release Conditions	
4	Typical Store Installation	
5	Typical Store Collision Boundary	
6	Store Aerodynamic Characteristics	
7	Length vs Store Weight	
8	Moment of Inertia vs Store Weight	
9	Flow Angularity - γ	
10	Typical Ejection Mechanisms	
11	Release Envelope Comparison - 100 Lb Store (LAU-10)	
12	Release Envelope Comparison - 400 Lb Store (CBU-30A)	
13	Release Envelope Comparison - 400 Lb Store (LAU-3A)	
14	Release Envelope Comparison - 800 Lb Store (BLU-27B)	
15	Required End of Stroke Velocity, Unconstrained, Maximum L-Minimum I_y, 150-750 Kts	
16	Required End of Stroke Velocity, Unconstrained, Maximum L-Minimum I_y, 150-650 Kts	
17	Required End of Stroke Velocity, Unconstrained, Maximum L-Minimum I_y, 150-550 Kts	
18	Required End of Stroke Velocity, Unconstrained, Maximum L-Maximum I_y, 150-750 Kts	
19	Required End of Stroke Velocity, Unconstrained, Maximum L-Maximum I_y, 150-650 Kts	
20	Required End of Stroke Velocity, Unconstrained, Minimum L-Minimum I_y, 150-750 Kts	
21	Required End of Stroke Velocity, Unconstrained, Minimum L-Maximum I_y, 150-750 Kts	
22	Effect of Ejector Moment Arm, 400 Lb Store, Zero Moment Arm	
23	Effect of Airspeed, 400 Lb Store, V_{eos} = 10 Ft/Sec	
24	Effect of Airspeed, 400 Lb Store, V_{eos} = 13 Ft/Sec	
25	Effect of Ejector Moment Arm, 400 Lb Store, Moment Arm = -0.1 Ft	
26	Effect of Ejector Moment Arm, 400 Lb Store, Moment Arm = +0.1 Ft	
27	Effect of Ejector Moment Arm, 400 Lb Store, Moment Arm = -0.4 Ft	
28	Effect of Ejector Moment Arm, 400 Lb Store, Moment Arm = -0.917 Ft	
29	Effect of Ejector Moment Arm, 400 Lb Store, Moment Arm = +0.917 Ft	
30	Required End of Stroke Velocity, Maximum L-Minimum I_y, $\Delta\theta_{eos} = 0$, $\dot{\theta}_{eos} = 0$	

LIST OF FIGURES (Continued)

Figure	Title	Page
31	Required End of Stroke Velocity, Maximum L-Maximum I_y, $\Delta\theta_{eos} = 0$, $\dot{\theta}_{eos} = 0$	
32	Required End of Stroke Velocity, Maximum L-Minimum I_y, $\Delta\theta_{eos} = +2^o$, $\dot{\theta}_{eos} = 0$	
33	Required End of Stroke Velocity, Maximum L-Minimum I_y, $\Delta\theta_{eos} = +4^o$, $\dot{\theta}_{eos} = 0$	
34	Required End of Stroke Velocity, Maximum L-Minimum I_y, $\Delta\theta_{eos} = +2^o$, $\dot{\theta}_{eos} = 2^o/t_{eos}$	
35	Required End of Stroke Velocity, Maximum L-Minimum I_y, $\Delta\theta_{eos} = +4^o$, $\dot{\theta} = 4^o/t_{eos}$	
36	Unconstrained Store Release, 1200 Lb Store	
37	Constrained Store Release, 1200 Lb Store, $\Delta\theta_{eos} = +4^o$, $\dot{\theta}_{eos} = 0$	
38	Constrained Store Release, 1200 Lb Store, $\Delta\theta_{eos} = +4^o$, $\dot{\theta}_{eos} = 4^o/t_{eos}$	
39	Required End of Stroke Velocity, Maximum L-Minimum I_y, $\Delta\theta_{eos} = 50\ t_{eos}$, $\dot{\theta}_{eos} = 50$ Deg/Sec	
40	Required End of Stroke Velocity, Unconstrained Release	
41	Required End of Stroke Velocity, Constrained Release	
42	Required End of Stroke Velocity, Unconstrained Release, Airspeed Effects	
43	Summary of Unstable Stores Ejection	
44	Required End of Stroke Velocity, Unconstrained Ejection Stroke = 4 Inches, Speed Envelope 150-750 Kts	
45	Required End of Stroke Velocity, Unconstrained Ejection Stroke = 4 Inches, Speed Envelope 150-550 Kts	
46	Typical Performance, Unconstrained Bomb Racks, Stroke = 4 Inches	

LIST OF TABLES

Table	Title
I	Store Pitch Acceleration Parameters
AI	Physical Characteristics - Existing Stores
AII	Physical Characteristics Summary - Parametric Stores

ABBREVIATIONS AND SYMBOLS

C_M	Pitching Moment Coefficient
C_N	Normal Force Coefficient
C.G.	Center of Gravity
I_y	Pitch Moment of Inertia, slug-ft^2
KCAS	Knots Calibrated Airspeed
L	Store Length, Feet
MER	Multiple Ejector Rack
S	Store Reference (Maximum Cross-Sectional) Area - Ft^2
t_{eos}	Ejector Stroke Time - Seconds
TER	Triple Ejector Rack
V_{eos}	Store Velocity End-of-Stroke - Ft/Sec
W	weight - Pounds
Z	Vertical Displacement - Ft
Z_{eos}	Ejector Stroke Length - Inches
α	Store Angle of Attack
γ	Gross Airplane Flow Field Angularity
θ	Store Pitch Angle - Degrees
$\dot{\theta}$	Store Pitch Rate at End-of-Stroke Position - Deg/Sec
$\ddot{\theta}$	Store Pitch Acceleration
$\Delta\theta_{eos}$	Change in Store Pitch Angle Between Stowed and End-of-Stroke Position

INTRODUCTION

Improvements in bomb rack design have been made over the years to better utilize the store carrying capability of modern fighter-bombers. In particular, store separation characteristics have been improved by means of force ejection techniques. However, the safe separation envelopes for many stores remain very restricted when compared to the aircraft flight envelope, largely due to adverse aircraft flow field effects, insufficient ejection forces, ejector-induced moments, and the unstable characteristics of some weapons.

This study examined the interaction of release mechanisms and store physical properties on the separation characteristics of an aerodynamically similar family of unstable stores. The basic intent was to define those features which would enhance the utility of future release mechanism designs, and to provide insight, from its initial design stages, of the separation envelope to be achieved with the store, using existing release hardware.

An existing digital computer program was used to simulate store separation characteristics, permitting a rapid method of parametrically evaluating the interaction of body physical characteristics and various release mechanism concepts. Given the flight condition and the physical characteristics of the store, the program output provided the trajectory of the store in the pitch plane as a function of time. The author is indebted to Mr. W.B. Hollingsworth of the McDonnell Aircraft Company Aerodynamics department for the trajectory computations, and much of the analysis used in this paper.

The types of store ejection mechanisms investigated were broadly subdivided into two general categories - those capable of controlling store motion during the stroke (constrained), and those for which the store was a free body during the stroke (unconstrained). No attempt was made to study specific ejection devices, although the performance of a given device can be superimposed on the summary data plots derived from the analysis.

This study was parametric in nature, and therefore the numerical results should not be considered directly applicable to any particular weapon/store location/aircraft combination. However, the general approach used in the study has indicated a reasonable correlation with F-4 flight test results, and it is expected that the trends obtained should be similar to those observed for store separation from any external weapon station of most modern fighter-bomber aircraft.

The manner in which the analysis was performed is described in the following paragraphs.

PROCEDURE

In order to examine the interaction of store physical properties and release mechanism effects on store separation characteristics, the following factors were parametrically evaluated:

- Store length (L), weight (W) and inertia (Iy)
- Ejection velocity and stroke (4-12 inches)
- Constraint of angular motion during ejection
- Applied ejector moments
- Airspeed (dynamic pressure) effects

A summary matrix of conditions evaluated in the study is presented in Figure 1.

STORE		UNCONSTRAINED EJECTION			CONSTRAINED EJECTION		
LENGTH	INERTIA	EJECTION STROKE	APPLIED MOMENT	AIRSPEED EFFECT	CONSTANT ANGLE RATE		VARIABLE ANGLE CONSTANT RATE
					VARIABLE	ZERO	
MAX	MAX	X		X	X		
MAX	MIN	X		X	X	X	X
MIN	MAX	X					
MIN	MIN	X	X				

FIGURE 1 - STUDY MATRIX

The physical characteristics of a broad range of existing stores were utilized to formulate the bounds of length and pitch inertia used for a given weight parametric store. The aerodynamic shape used for the parametric stores was the ogive-cylinder-ogive configuration of the BLU-1B napalm bomb shown in Figure 2. The theoretical aerodynamic characteristics of these stores were superimposed on generalized F-4 aircraft fuselage centerline flow fields to evaluate the release characteristics of tangentially mounted stores in a level flight speed range from 150 to 750 knots at an altitude of 10,000 feet, see Figure 3.

For this study, the store was assumed to be installed as shown in Figure 4. The unstable store was selected as representative of a worst case for separation characteristics, with the tangent mounting providing a limiting case for store clearance with the aircraft. The store was assumed to be installed on an aircraft fuselage centerline, permitting the simplification of a three degree of freedom (pitch plane) computation. Because of its straightforward nature, the details of the computer program are not discussed herein.

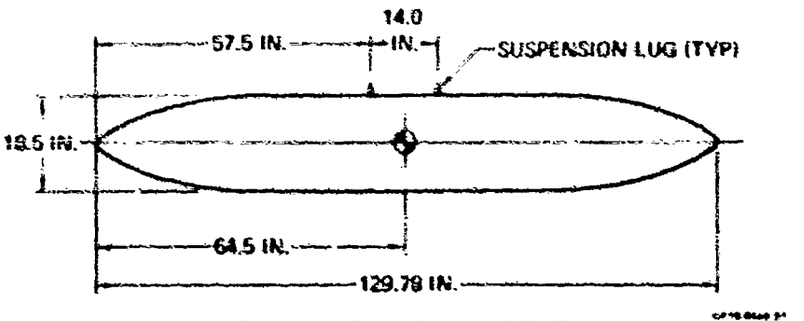


FIGURE 2 - BLU-1/B NAPALM BOMB

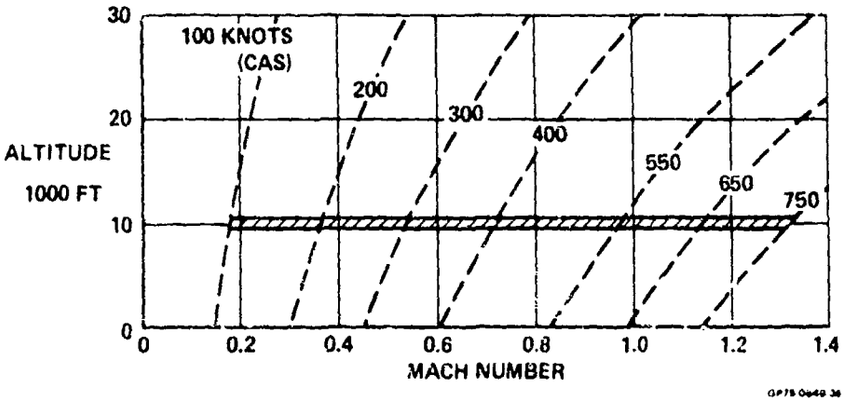


FIGURE 3 - RELEASE CONDITIONS

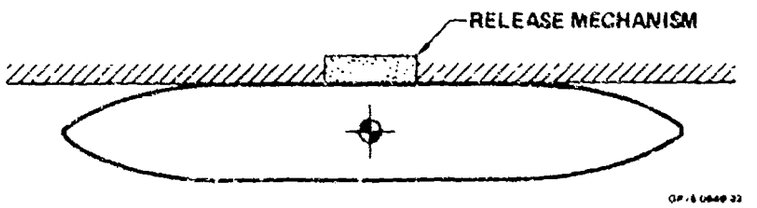


FIGURE 4 - TYPICAL STORE INSTALLATION

DATA PRESENTATION

The computed trajectories provided the pitch angle and vertical displacement of the store as a function of time. Using this data, time-independent pitch angle vs vertical displacement plots were then constructed upon which appropriate collision boundaries were superimposed (Figure 5). From an analysis of this data, the minimum end-of-stroke velocity required for safe separation was determined for each of the various combinations of store characteristics, release mechanisms and airspeed envelopes considered. For this study, safe separation was based on positive clearance with the stowed surface. These basic results are presented in a series of plots showing the required end-of-stroke velocity as a function of store weight, and in bar-graph form showing allowable release envelopes for various ejection techniques. The final results of the study are presented in a series of plots showing the minimum end-of-stroke velocity required for safe release throughout the speed envelope, as a function of store weight, length and inertia.

STORE CHARACTERISTICS

The store characteristics which have the most significant influence on separation characteristics are the aerodynamic shape, the length/moment-of-inertia combination, weight and the store C.G. location.

For clarity and consistency, one generalized store shape with a constant length-to-diameter ratio was used for the various store length/moment-of-inertia combinations considered. As noted previously, the basic store shape selected was that of the unfinned BLU-1/B napalm bomb. The aerodynamic coefficients for this store were analytically determined by the method presented in USAF Stability and Control DATCOM, WADD TR-60-261, dated October 1960. A sample of the estimated normal force and pitching moment coefficients is presented in Figure 6.

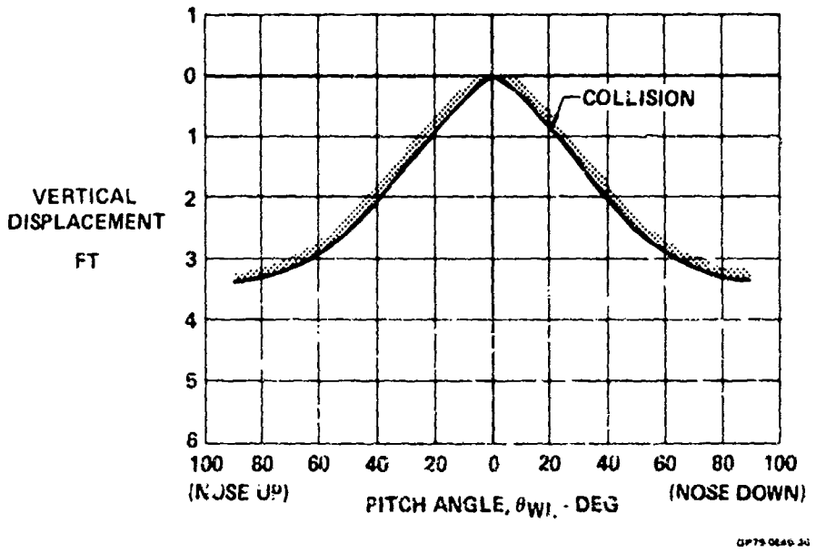


FIGURE 5 - TYPICAL STORE COLLISION BOUNDARY

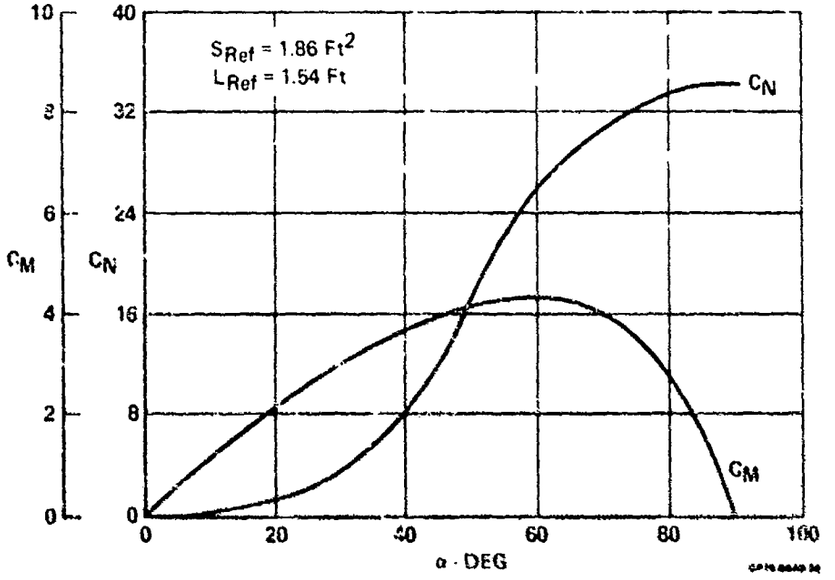


FIGURE 6 - STORE AERODYNAMIC CHARACTERISTICS
M = 0.85

The weights of the parametric stores used in this study were 100, 400, 800 and 1200 pounds. Each weight class was further subdivided into four general categories based on length and inertia, as follows:

- maximum L/minimum Iy
- maximum L/maximum Iy
- minimum L/maximum Iy
- minimum L/minimum Iy

The maximum and minimum length/inertia combinations were determined by summarizing the characteristics of a broad spectrum of existing stores as a function of weight, see Figures 7 and 8. As shown, maximum and minimum lines were constructed to encompass almost all of the stores considered. It is noted that fuel tanks were not considered in this study. A summary of the characteristics of the stores considered is presented in Appendix A.

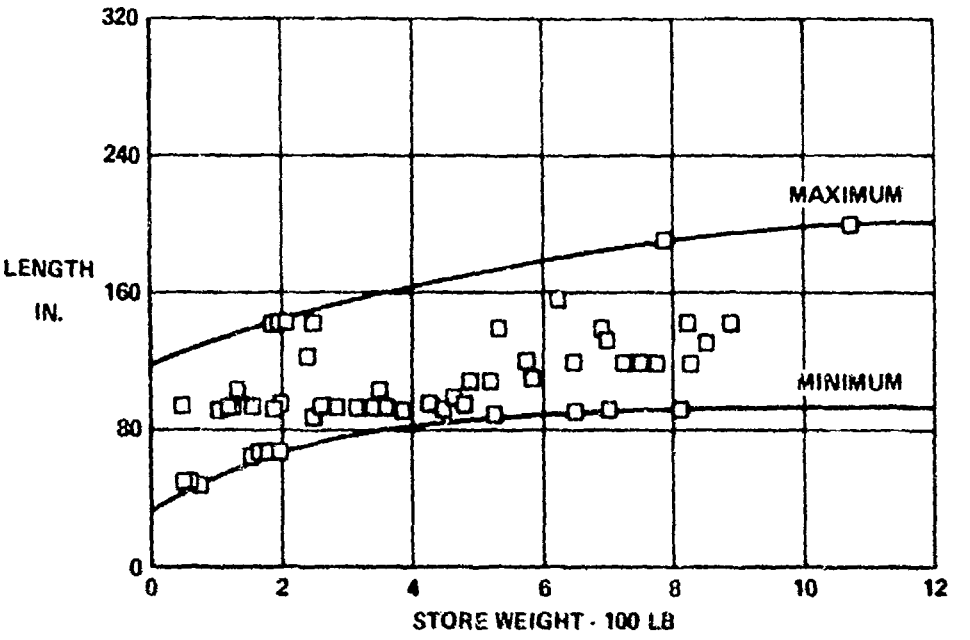


FIGURE 7 - LENGTH vs STORE WEIGHT

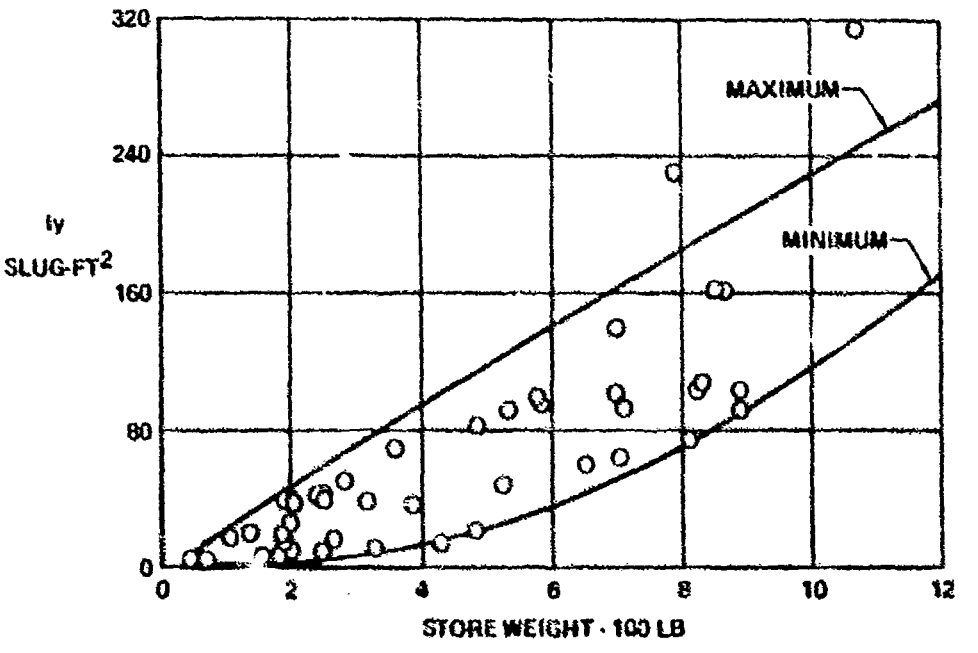


FIGURE 8 - MOMENT OF INERTIA vs STORE WEIGHT

Throughout the analysis the weapon C.G. was assumed to be located at the midpoint of the store centerline. Variations in C.G. were not considered because, as long as the C.G. shifts are not large and the ejector moment arm is not changed, the trends observed will be similar as store physical characteristics, ejector force, and release mechnaisms are varied. The effect of varying the ejector moment arm was briefly analyzed.

FLOW FIELD DETERMINATION

Due to the flow field about the aircraft, the angle of attack of the store is not the same as the angle of attack of the aircraft. In order to account for this difference, while maintaining a simplicity of computation, an incremental angle, gamma (γ), was used. Gamma, the gross flow angularity, is a nonlinear function of Mach number ranging from about $+3^{0}$ to about -9^{0} for a flight velocity regime of Mach 0.3 to Mach 1.3, see Figure 9. Although this angle does vary with store shape and store position on the aircraft, the gamma used in this study was considered to be independent of these variables. The values for gamma were determined empirically by comparing analytical results with flight test data for specific stores.

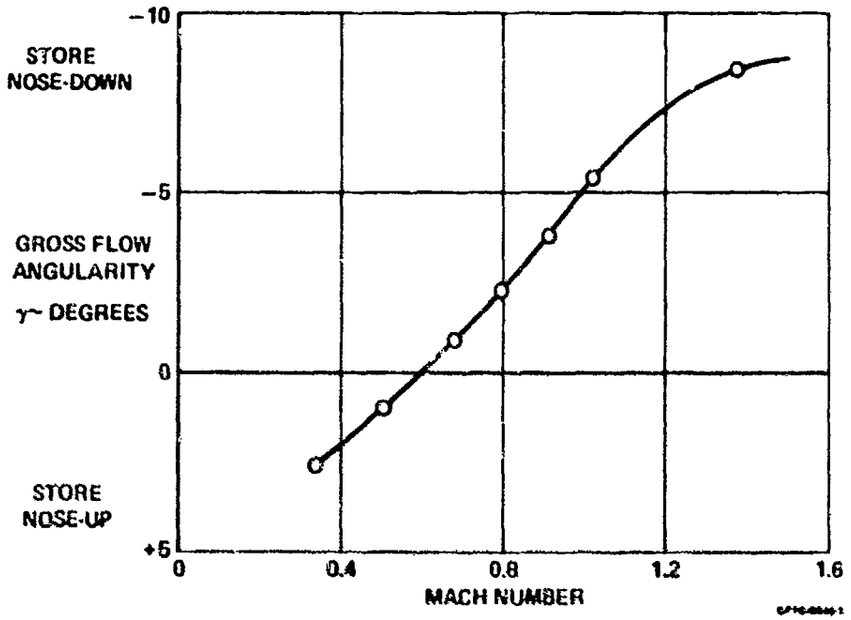


FIGURE 9 - FLOW ANGULARITY - γ

RELEASE MECHANISMS

The release mechanism (bomb rack) concepts considered in this study were assumed to be the force ejection type. No attempt was made to evaluate or simulate any specific device, although the parametric results of the study permit an evaluation of a given design on store release envelope. As shown in Figure 10, two types of mechanisms were considered:

- Unconstrained Ejection - The store is a free-body at hook release, which occurs at the start of the ejection stroke. Most of the ejectors in use today are of this type. This design can impart a translational velocity to the store, with or without an applied moment.
- Constrained Ejection - Store motion is controlled to the end of the ejection stroke, where hook release occurs. The basic design concept of this type of ejector is to impart a translational velocity to the store, while limiting its angular excursions (angle and/or rate) to specified values during the stroke.

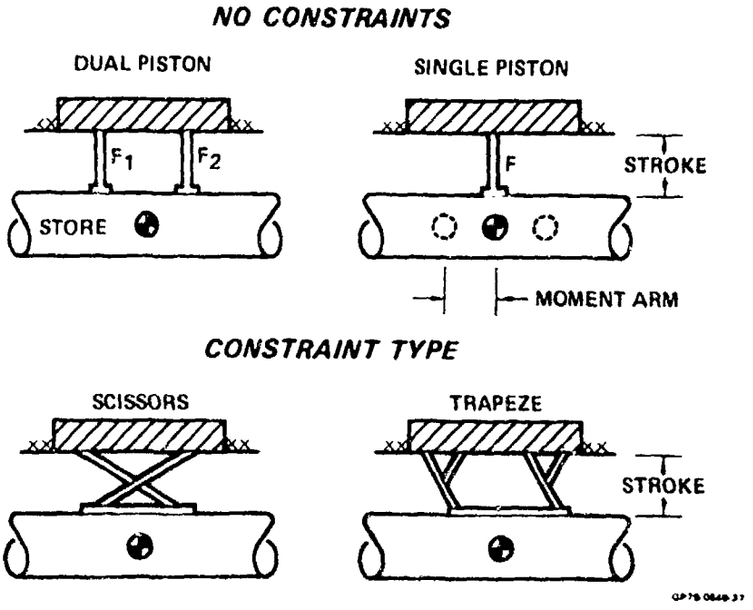


FIGURE 10 - TYPICAL EJECTION MECHANISMS

Another type of constrained ejection - a bomb rack in combination with an aft pivot - was not considered in this study, since this type of system is utilized primarily for jettison of pylons, fuel tanks and multiple external racks.

Unconstrained ejectors were evaluated in terms of stroke length (4-12 inches) and applied moments. Constraint type ejectors, because of their geometric characteristics, tend towards longer strokes and, for most cases, were evaluated for a 12-inch stroke. The combinations of these design variables were felt to encompass those release devices in existence or in development study.

Because of the parametric nature of this study, it was assumed that a given release mechanism was capable of imparting any velocity to the store required for safe separation;

TECHNIQUE VERIFICATION

Various existing stores were selected for the comparison of analytical results with flight test data. The choice of stores was based on: 1) the proximity of the weight of these stores to one of the four weights considered for the parametric store, 2) an aerodynamically unstable shape, and 3) the availability of flight test data. The stores used in the comparison were: (1) an empty rocket launcher, the LAU-10/A; (2) a loaded dispenser, the CBU-30/A; (3) a loaded rocket launcher, the LAU-3/A; and (4) a napalm bomb, the BLU-27/B. For each store selected, analytical trajectories were computed at various values of airspeed and gamma utilizing the generalized store shape and the moment of inertia and length for the given store. The analytical separation envelopes obtained were then compared to the envelopes obtained from flight testing. As shown in Figures 11 through 14, the results of the analysis show good general agreement with flight test results. It is particularly interesting to note that the flight test results represent stores carried on wing pylons or multiple external bomb racks.

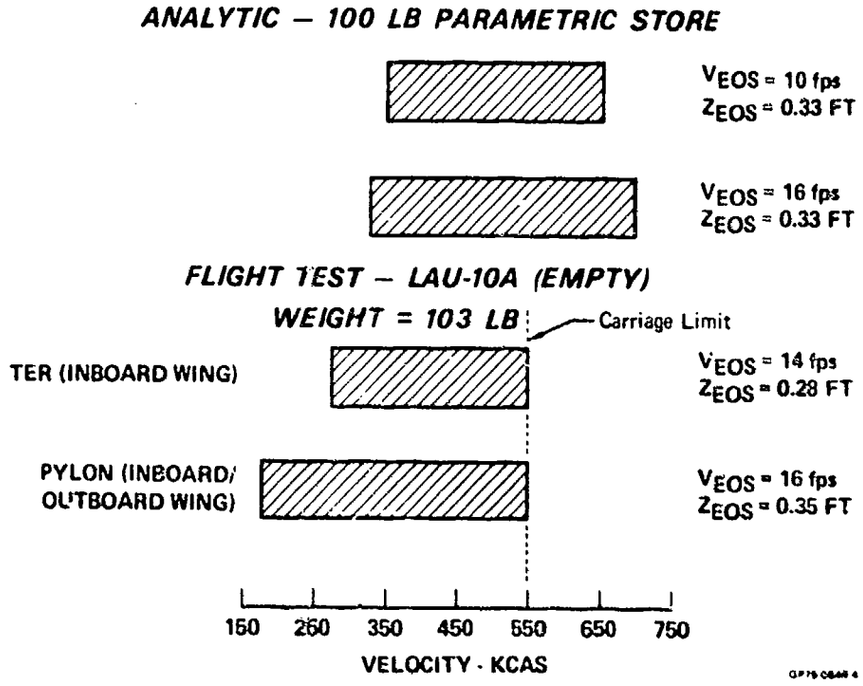


FIGURE 11 - RELEASE ENVELOPE COMPARISON - 100 LB STORE

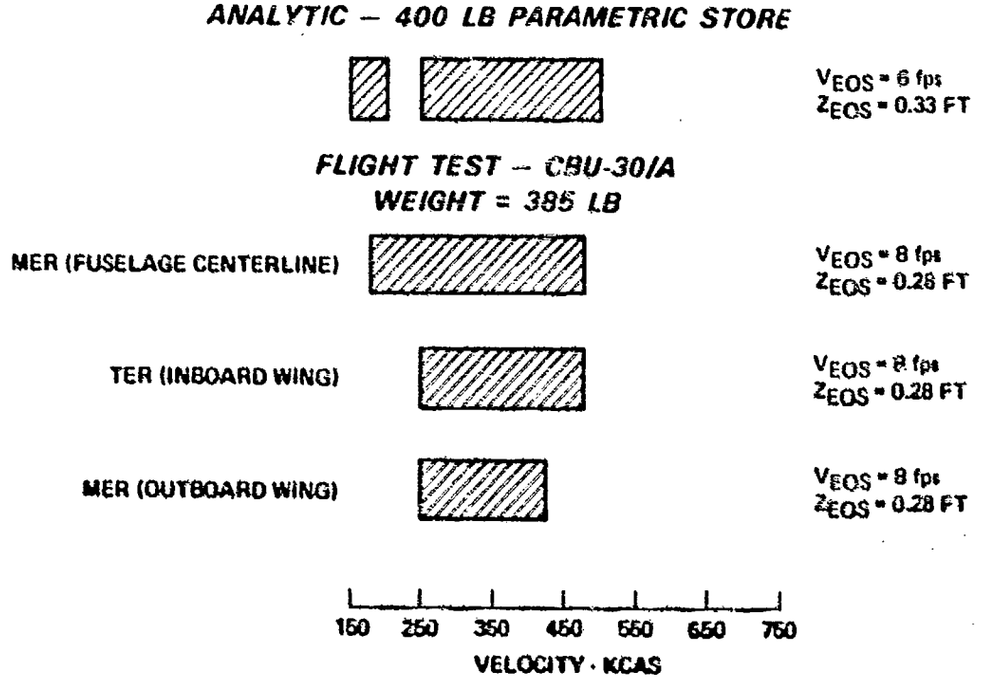


FIGURE 12 - RELEASE ENVELOPE COMPARISON - 400 LB STORE

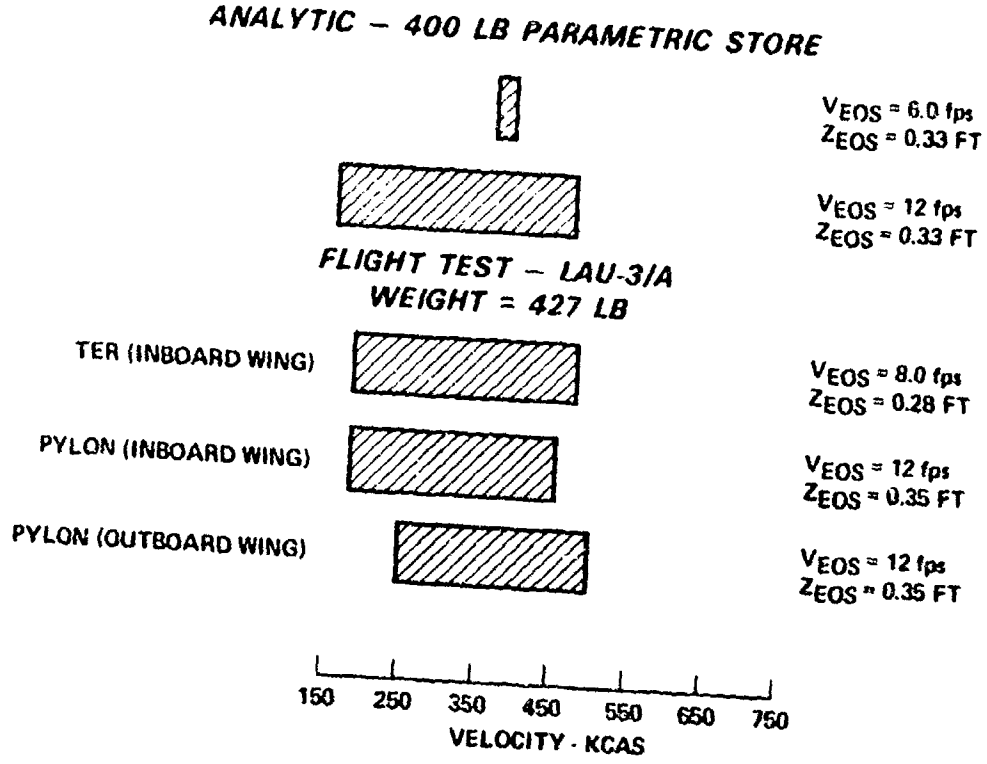


FIGURE 13 - RELEASE ENVELOPE COMPARISON - 400 LB STORE

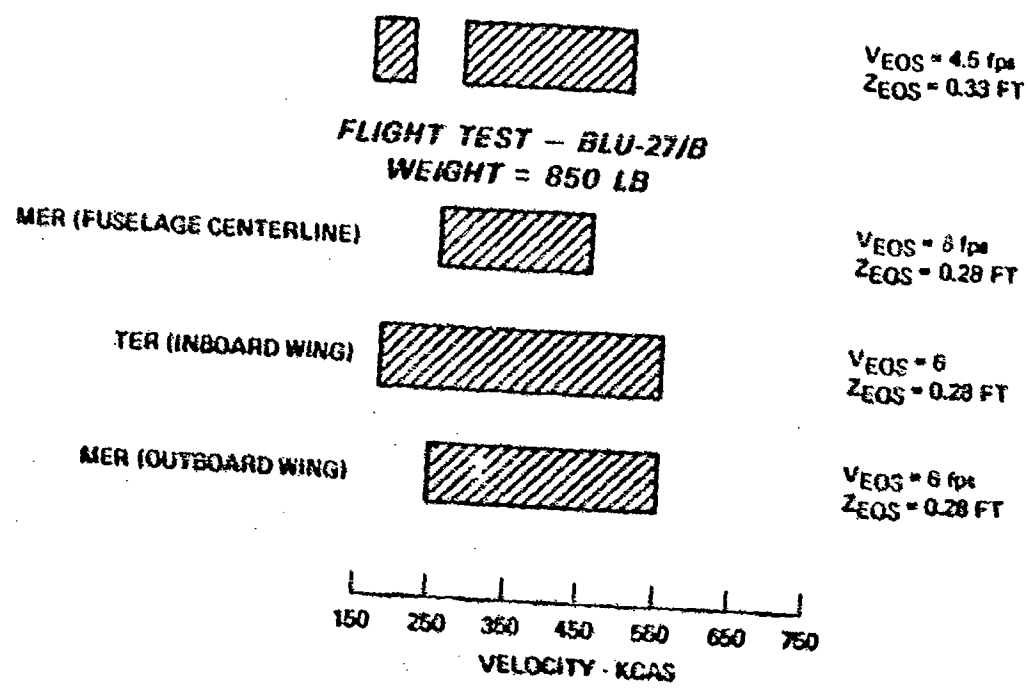


FIGURE 14 - RELEASE ENVELOPE COMPARISON - 800 LB STORE

RESULTS

The results of the study are presented for constrained and unconstrained release mechanisms in terms of velocity required at end of ejection stroke for a given set of store physical characteristics and a given release speed envelope. These data are presented in summary form due to the large quantities of trajectory data required to evaluate a given set of parameters.

The effect of applied moments is presented for the unconstrained ejector, as are the effects of stroke length. In order to reduce the quantity of computation, moment effects were evaluated only for a 400-pound minimum length, minimum inertia store.

The required end of stroke velocities are correlated in terms of the parameters

$$W^{\frac{1}{3}}\frac{L^3}{I_y} \text{ and } \frac{L^3}{I_y} \qquad (1)$$

for each of the release mechanism categories and speed envelopes considered. Constrained ejection effects are summarized to show a direct correlation with the unconstrained case for a 12-inch stroke, and also show the effects of variations in store angular motion constraints during the ejection cycle.

The following paragraphs discuss the detailed results of the study.

UNCONSTRAINED RELEASE

As previously discussed, in the unconstrained-release method of store separation, the store is free to react to aerodynamic forces as soon as it is released. Values of the minimum end-of-stroke velocity (V_{eos}) required for safe separation throughout the release envelopes considered were obtained for each of the four store length/moment-of-inertia combinations. The effect of applied ejector moments is presented for the minimum length/minimum inertia case only.

Length/Moment-of-Inertia Effects - The minimum end-of-stroke velocities required for safe separation were determined for all four generalized length/moment-of-inertia combinations using ejector stroke lengths of four, eight, and twelve inches. The effect of reduced separation envelopes on minimum required end-of-stroke velocity was also investigated. For all cases discussed in this section the ejector force was applied at the weapon C.G.

Maximum Length-Minimum I_y - Figure 15 shows the minimum required end-of-stroke velocity vs store weight for stores with the maximum values of length and the minimum values of moment-of-inertia. Although the ejection forces required to attain these high values of V_{eos} are unrealistic in terms of current bomb rack capabilities, the trends indicated by the data are of importance since similar trends are observed throughout the unconstrained release analysis. First, the data indicate that for any given store weight, the required end-of-stroke velocity decreases with decreasing piston length. This is because as stroke length is increased, required ejection forces decrease and the stroke time increases. As a result, the total time required for the store to reach a given vertical displacement early in the trajectory (1st few feet) is shorter for the shorter stroke. With constant flow field effects, the angular motion of the store as a function of time is essentially independent of stroke length, so that for a given vertical displacement, store angular displacement is reduced for the shorter stroke. It can also be observed that the required end-of-stroke velocity decreases with increasing store weight. This is due to the fact that, as the store weight and size are increased, the larger moments-of-inertia and increased aerodynamic forces acting normal to the store tend to compensate for the more restrictive collision boundaries and the increased values of store pitching moment.

Because of the high end-of-stroke velocities required for safe separation for the 150-750 knot envelope, the effect of reducing the upper speed to 650 knots was investigated. This resulted in a significant decrease in required V_{eos} as shown in Figure 16. The upper speed limit was further reduced

to 550 knots, and the results are shown in Figure 17. Although further reductions in required V_{eos} were achieved, the effect is not nearly as large, due to dynamic pressure effects.

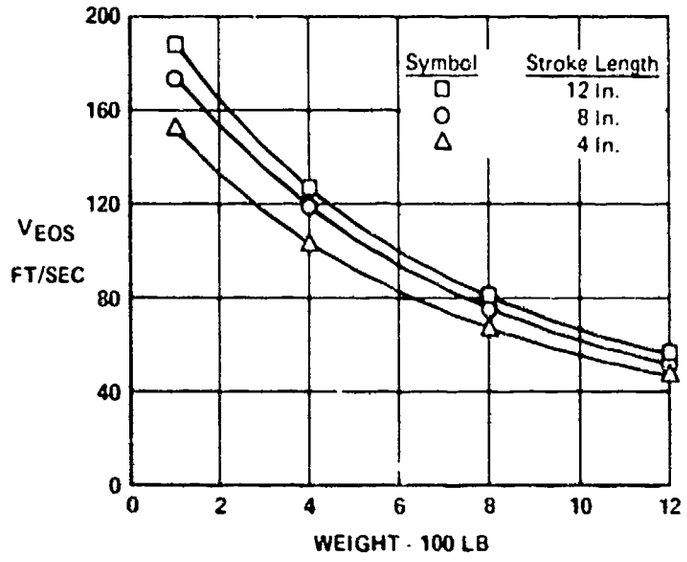


FIGURE 15 - REQUIRED END OF STROKE VELOCITY
Unconstrained
Maximum L - Minimum Iv
Flight Envelope: 150 - 750 kts

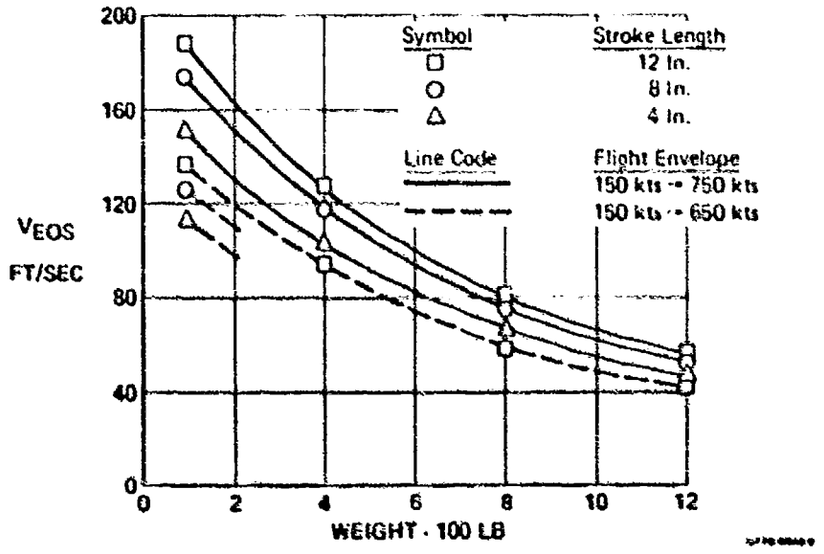


FIGURE 16 - REQUIRED END OF STROKE VELOCITY
Unconstrained
Maximum L - Minimum Iy

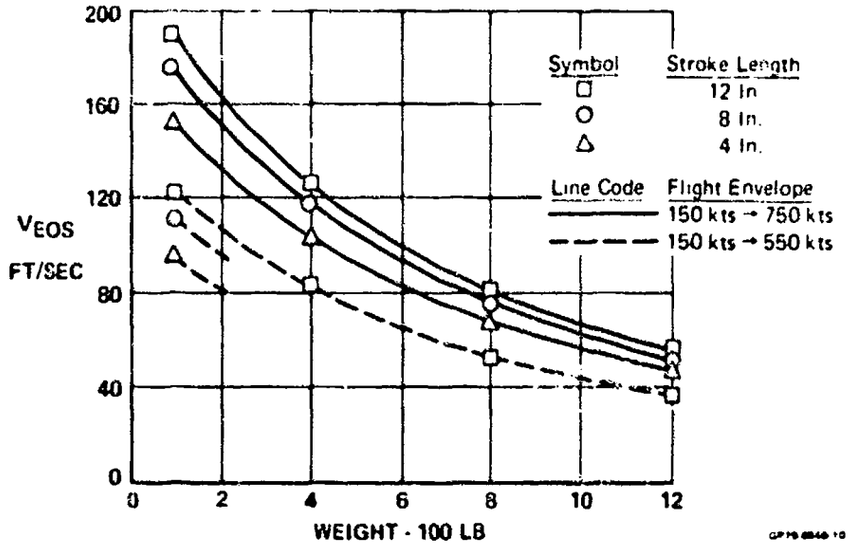


FIGURE 17 - REQUIRED END OF STROKE VELOCITY
Unconstrained
Maximum L - Minimum Iy

Maximum Lenght/Maximum I_y - The result of the increased moment of inertia is a significant decrease in the end-of-stroke velocities required for safe release as shown in Figure 18. This occurs because the large increase in moment-of-inertia decreases the pitch acceleration and, consequently, the pitch angle at a given vertical displacement.

The effect of reducing the required separation envelope to 150-650 knots was also investigated for this case and the results are shown in Figure 19. For stores heavier than 400 pounds, approximately the same percentage reduction in V_{eos} was achieved as was obtained for the maximum length/minimum moment-of-inertia case. There is no reduction, however, in the end-of-stroke velocity required for the 100-pound store, because the critical speeds for separation of this 100-pound store occur in the 280-380 knot range.

Minimum Length/Minimum I_y - As shown in Figure 20, the end-of-stroke velocity required for safe release of stores in this category is less than for the previous two cases at all weights and stroke lengths. Although the low values of moment-of-inertia tend to increase the pitch acceleration, the shorter lengths result in enlarged collision boundaries and reduced aerodynamic moments. The relationship of store weight to end-of-stroke velocity for constant stroke lengths is generally the same as indicated in previous cases for weights between 200 and 1200 pounds. However, the 100-pound store fails to fit into the general trend of the previous cases in which the end-of-stroke velocity increased as weight decreased.

The apparent inconsistency of the 100-pound store can be explained by the differences in the moment-of-inertia and reference area between the 100, 200, and 300 pound stores. The pitch acceleration, $\ddot{\theta}$, is a function of the aerodynamic moment acting on the store and the moment of inertia of the store, i. e.,

$$\ddot{\theta} = \frac{M}{I_y} = \frac{C_{M_q} qSL}{I_y} \qquad (2)$$

Since the aerodynamic characteristics of the generalized store were constant for this study, $\ddot{\theta}$ is a function of S/I_y. Table I lists the reference areas, moments-of-interia, and S/I_y for the corresponding store weights.

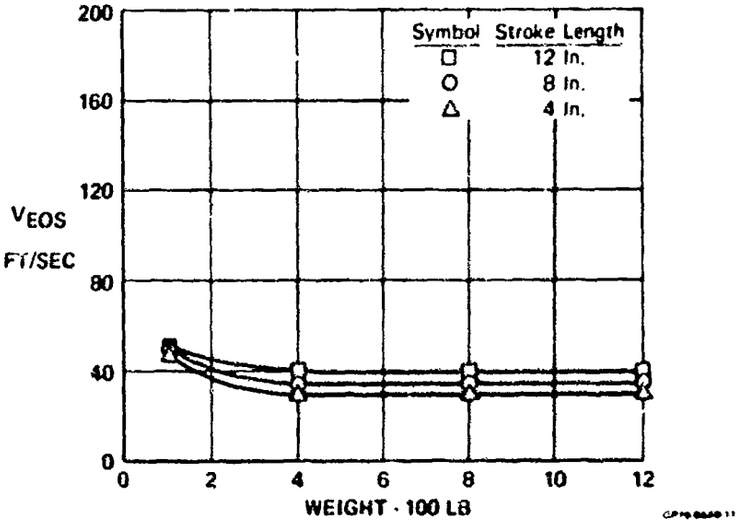


FIGURE 18 - REQUIRED END OF STROKE VELOCITY
Unconstrained
Maximum L - Maximum Iy
Flight Envelope : 150 - 750 kts

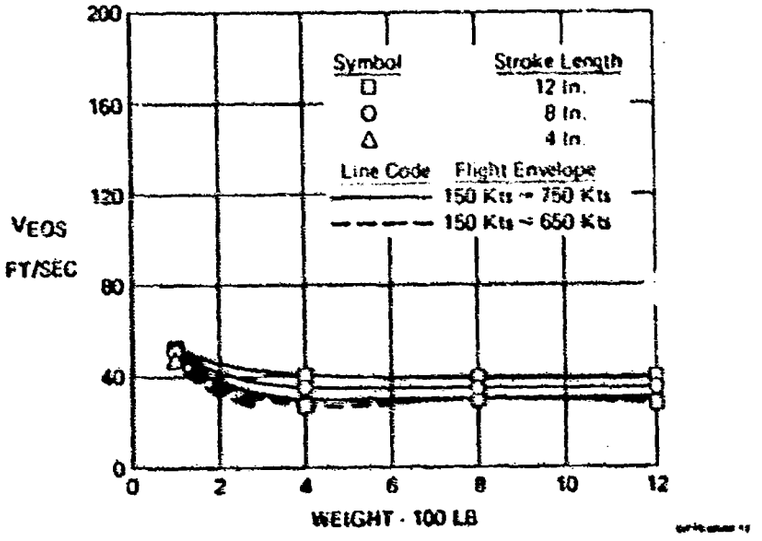


FIGURE 19 - REQUIRED END OF STROKE VELOCITY
Unconstrained
Maximum L - Maximum Iy
Flight Envelope: 150 - 750 kts

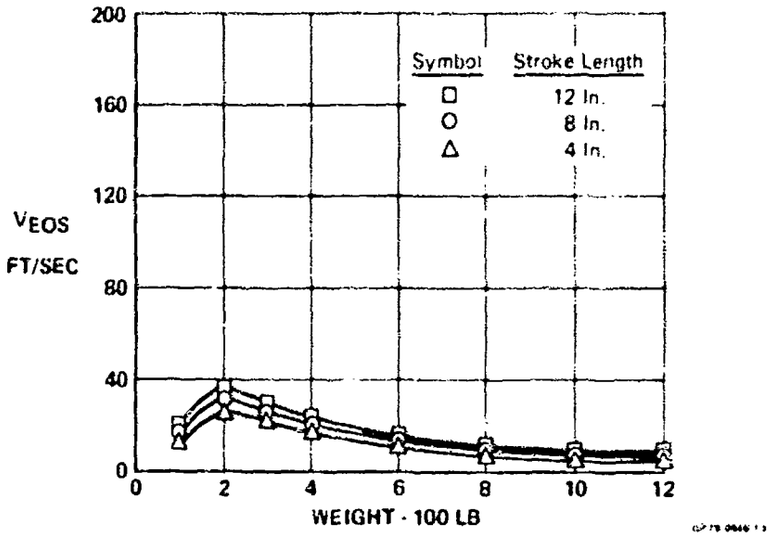


FIGURE 20 - REQUIRED END OF STROKE VELOCITY
Unconstrained
Minimum L - Minimum Iy
Flight Envelope: 150 - 750 kts

TABLE I - STORE PITCH ACCELERATION PARAMETERS

	STORE WEIGHT (LB)					
	100	200	300	400	800	1200
I_y (SLUG-FT^2)	2.50	3	7	14	71	170
S (FT^2)	0.30	0.500	0.640	0.740	0.9200	0.9500
S/I_y (SLUGS)	0.12	0.167	0.092	0.053	0.0129	0.0056

The table indicates a 28% decrease in S/I_y as the weight is decreased from 200 to 100 pounds, due largely to the large decrease in area. The resultant decrease in pitch acceleration, along with the less restrictive collision boundary for the shorter store, results in a lower V_{eos} being required. The table also indicates a 45% decrease in S/I_y as the weight is increased from 200 to 300 pounds. This results in a lower pitch acceleration, permitting a reduced V_{eos} for safe release for the 300 pound store. The latter trend is maintained for the remainder of the store weights.

Minimum Length/Maximum I_y - This combination is the least critical of the four cases investigated, since its length results in the least restrictive collision boundary, and the high moments of inertia result in the lowest pitch acceleration. For this case, safe separation can be attained without an ejector force (free-fall release) for all weights and stroke lengths. The end-of-stroke velocities shown in Figure 21 are the result of the acceleration of gravity.

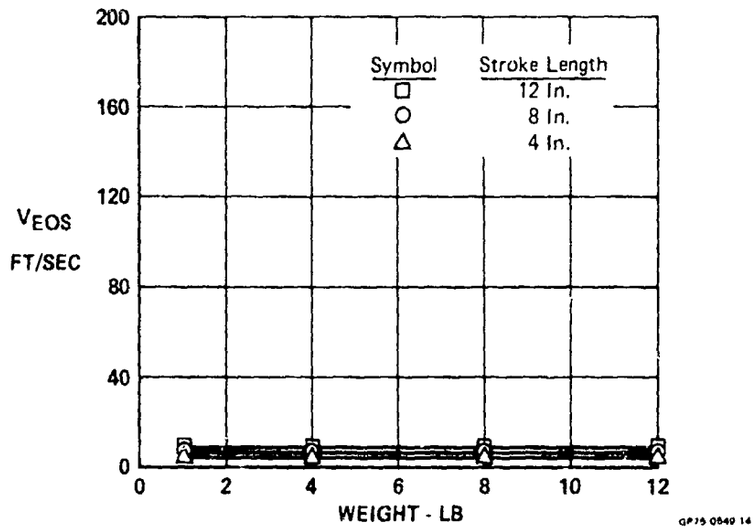


FIGURE 21 - REQUIRED END OF STROKE VELOCITY
Unconstrained
Minimum L - Maximum Iy
Flight Envelope: 150 - 750 kts

Effect of Applied Ejector Moment - Moments may be applied through the use of a force differential on a duel piston ejector, but for this study, a single piston ejector was assumed to determine the effect of the ejector foot being located various distances forward and aft of the store C.G.

The results are summarized in a series of bar graphs, showing the safe release envelopes of a 400-pound generalized store for various end-of-stroke velocities. The store characteristics were the minimum length-minimum inertia case, and ejector stroke was 8.0 inches. Safe separation envelopes with the ejector force applied at the weapon C.G. are shown in Figure 22. For this case increased values of V_{eos} cause expansions in the separation envelope - a trend observed in other phases of this study. For the smallest value of V_{eos} the separated weapon pitches strongly nose-up at low speeds and severely nose-down at high speeds and, as a result, only a small safe release envelope is achieved.

When the end-of-stroke velocity is increased to 10 ft/sec, a significant expansion of the separation envelope occurs because the increased velocity increases the store vertical displacement at a given pitch angle. Figure 22 indicates, however, that a discontinuity exists in the safe separation envelope for this end-of-stroke velocity. To examine the reasons for this phenomenon, a pitch angle vs vertical displacement plot, illustrating the trajectories obtained at various release Mach numbers, is presented (Figure 23). Due to the instability of the generalized store, the large nose-up stowed angle of the weapon at Mach 0.3 (the result of the high aircraft angle-of-attack) causes the store to pitch nose-up during separation; however, safe separation is achieved because the dynamic pressure at Mach 0.3 is too low to produce large values of store lift or pitch acceleration. As the release Mach number is increased from 0.3 to 0.45 the store trajectories penetrate the nose-up collision boundary. At 0.6 Mach, nose-up tendencies are less severe and safe separation is again possible. Reductions in aircraft angle of attack and changes in the aircraft flow field account for the tendency of the store to pitch nose-down at higher Mach numbers. Between Mach 0.7 and Mach 0.8 the store trajectories penetrate the nose-down collision boundary, establishing the upper speed limit for safe separation.

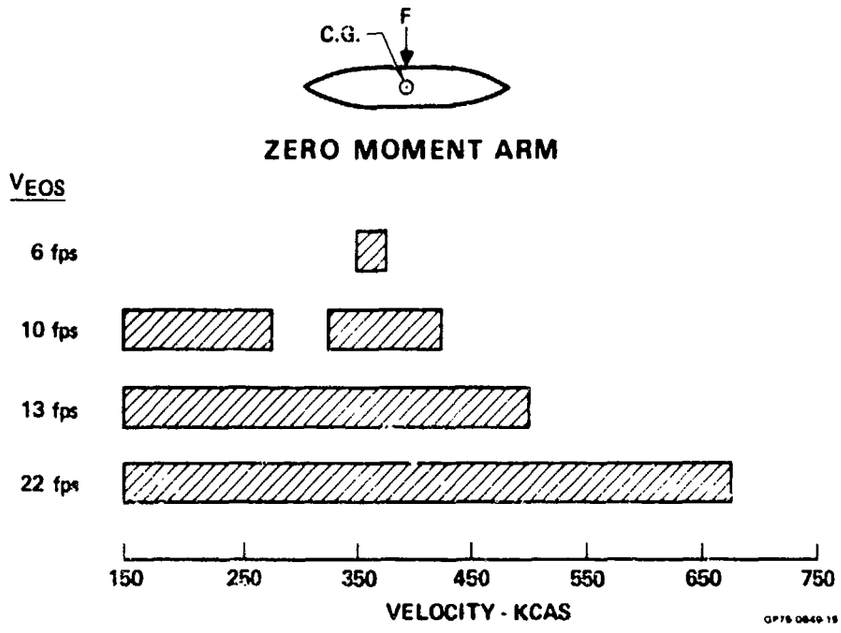


FIGURE 22 - EFFECT OF EJECTOR MOMENT ARM - 400 LB STORE

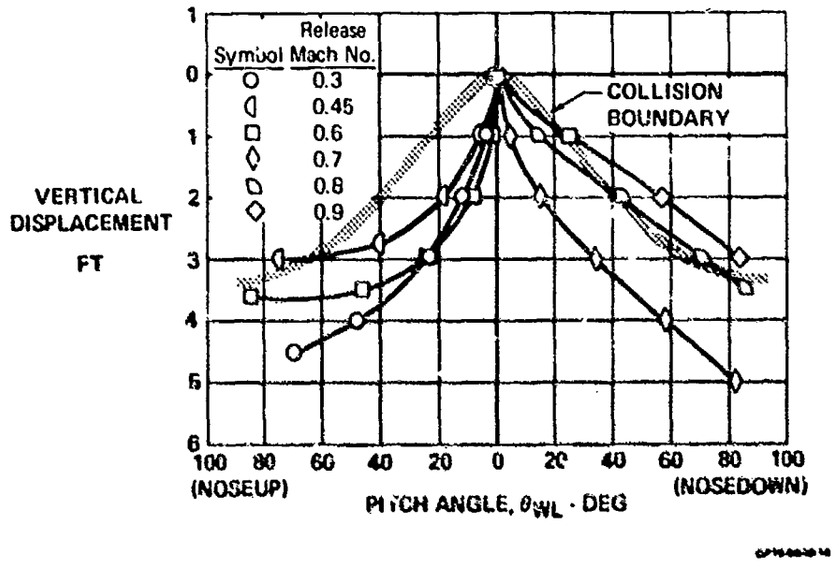


FIGURE 23 - EFFECT OF AIRSPEED - 400 LB STORE
V_{EOS} = 10 ft/sec

As V_{eos} is decreased, discontinuities in the envelope are eliminated and the upper speed limit for safe separation is increased, due to the increased vertical displacement at a given pitch angle, as indicated by a comparison of Figures 23 and 24.

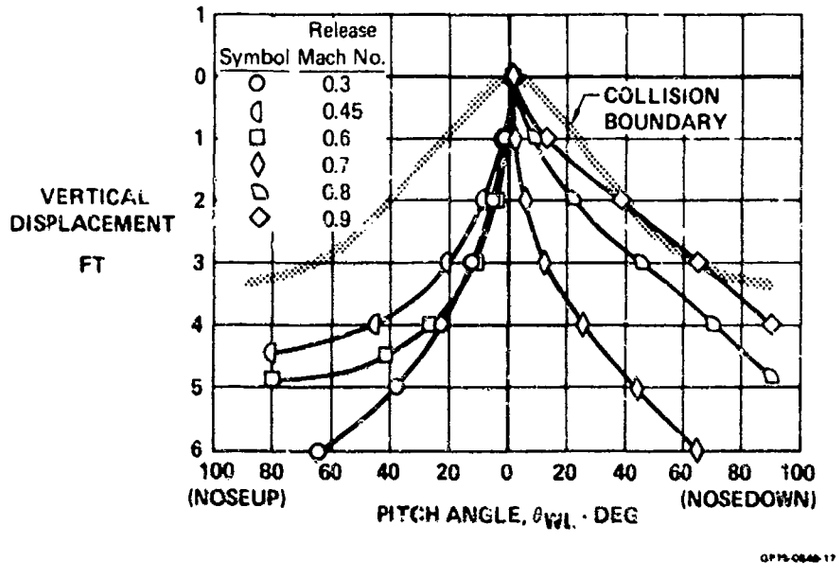


FIGURE 24 - EFFECT OF AIRSPEED - 400 LB STORE
V_{eos} = 13 ft/sec

Ejector Moment Arms of ±0.1 Feet - Figures 25 and 26 present the separation envelopes obtained with the ejector foot located 0.1 foot forward and aft of the weapon C.G. A comparison of Figure 25 with Figure 22 shows that although no discontinuities are obtained with the nose-down moment, a general reduction in maximum release speed occurs, since induced moments are additive to nose-down flow field effects at the higher Mach numbers.

Figure 26 shows that with nose-up moment, large discontinuities are obtained in release envelopes, with the envelope almost eliminated at an ejection velocity of 6 ft/sec. At 22 ft/sec, however, the separation envelope is slightly increased in comparison to the zero-moment-arm case. This is because the nose-up pitch acceleration caused by the ejector reduces the tendency of the store to pitch nose-down at high speeds, while at lower speeds the pitching moment, in combination with the higher ejection velocity, is not large enough to cause collision.

Ejector Moment Arm of -0.4 Feet presents the separation envelopes obtained with the ejector foot displaced 0.4 ft forward of the store C.G. In contrast to previous cases, a general reduction in separation envelopes is observed as V_{eos} is increased, due to the larger ejector moment arm. As ejector force becomes larger, the corresponding increase in ejector-induced, nose-down pitching moment is more significant than the increase in store vertical velocity. Consequently, the store pitch angle becomes greater for a given vertical displacement as V_{eos} is increased.

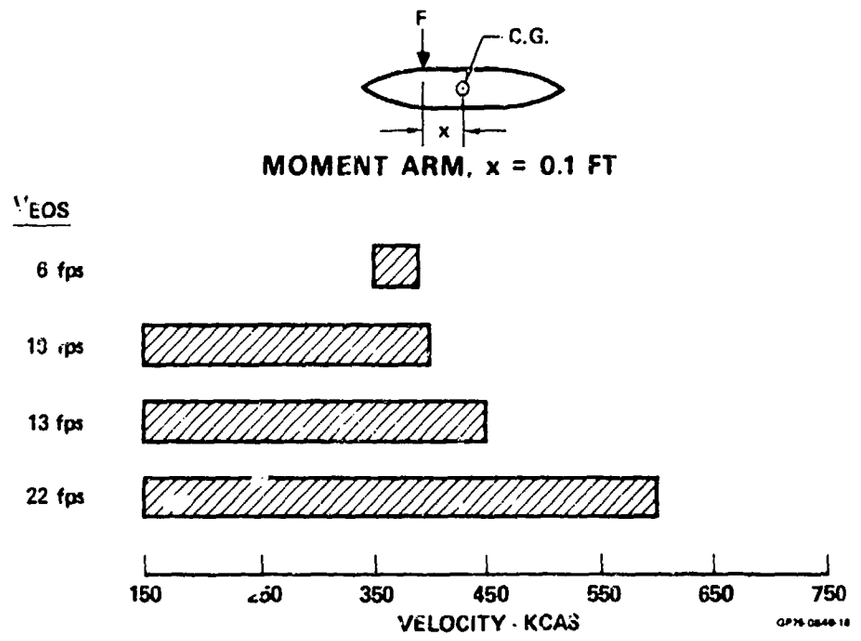


FIGURE 25 - EFFECT OF EJECTOR MOMENT ARM - 400 LB STORE

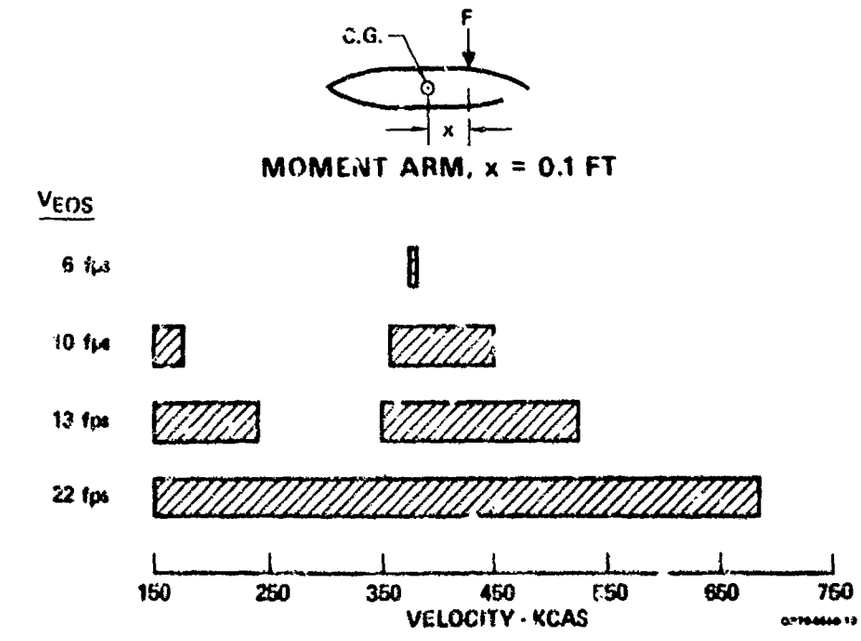


FIGURE 26 - EFFECT OF EJECTOR MOMENT ARM - 400 LB STORE

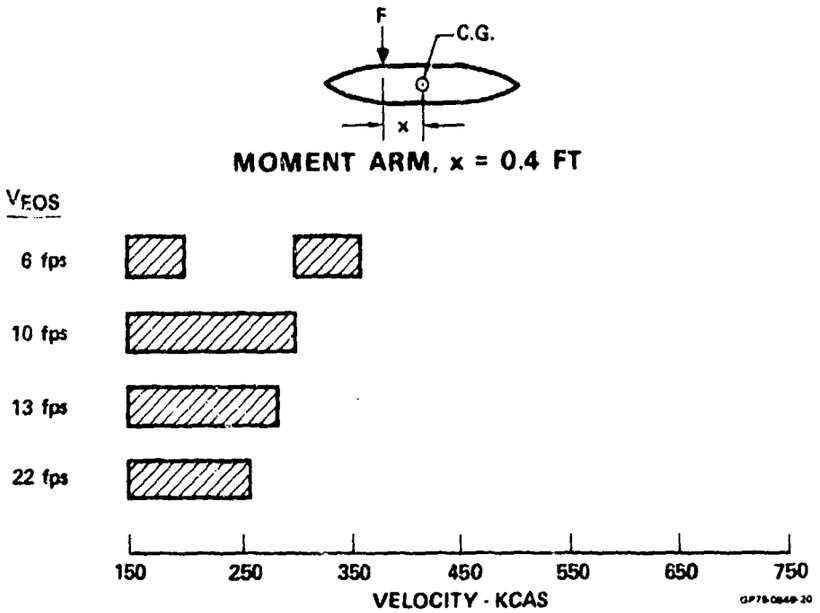


FIGURE 27 - EFFECT OF EJECTOR MOMENT ARM - 400 LB STORE

Ejector Moment Arms of ±0.917 Feet - Figures 28 and 29 present the safe release envelopes obtained with the ejector foot located 0.917 ft forward and aft of the store C.G. Figure 28 indicates that, while some improvement over the sero-moment-arm case occurs for the smallest V_{EOS} considered, for values greater than 10 ft/sec the associated ejector induced nose-down pitching moments become large enough

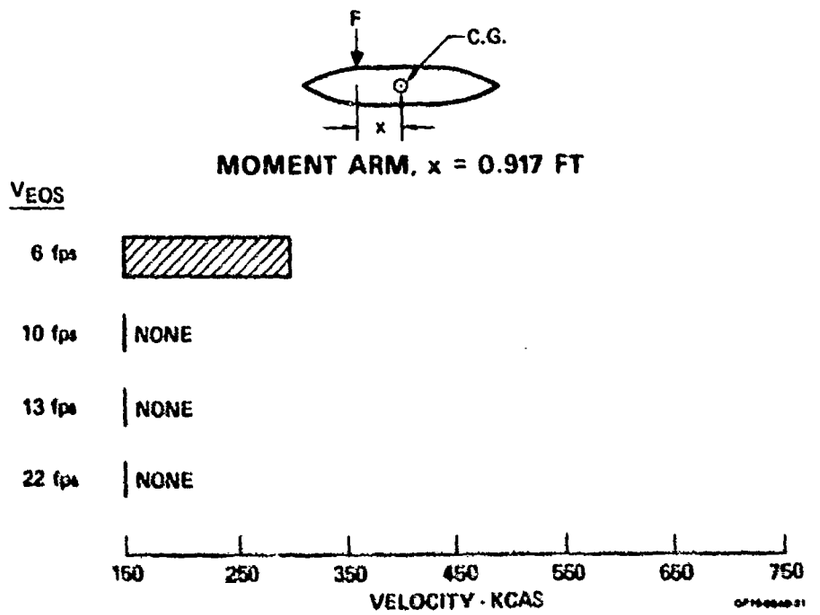


FIGURE 28 - EFFECT OF EJECTOR MOMENT ARM - 400 LB STORE

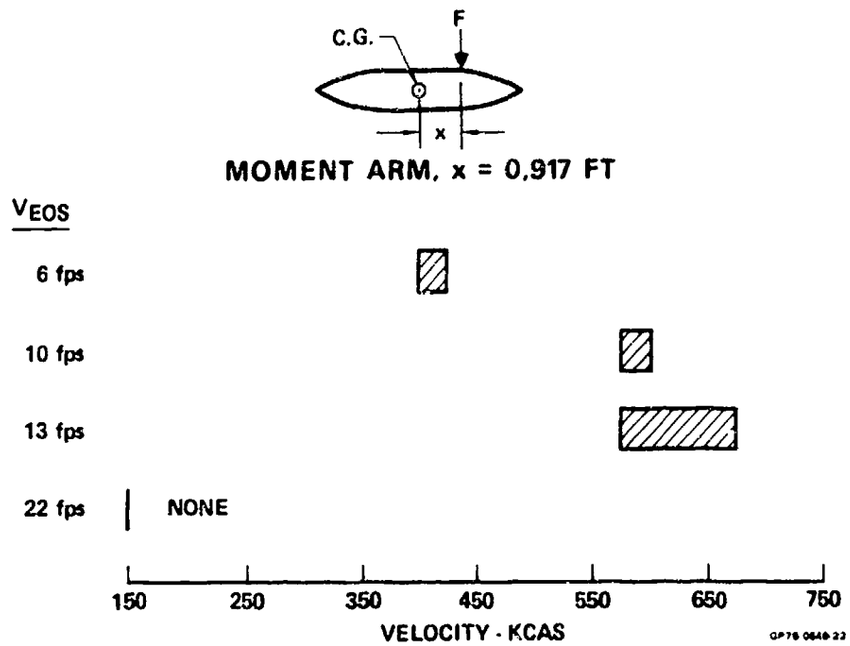


FIGURE 29 - EFFECT OF EJECTOR MOMENT ARM - 400 LB STORE

to make separation unsafe at any speed. Figure 29 indicates that the effect of displacing the ejector foot well aft of the C.G. is also to greatly reduce the safe separation envelope. It is estimated that for the 0.4 and 0.917 ft moment arms, the desired 150-750 knot separation envelope would be essentially impossible, regardless of the ejection force.

CONSTRAINED RELEASE

Constrained store release mechanisms, typified by the scissors and four-bar linkage concepts shown in Figure 10, control store angular motion during the ejection cycle. Hook opening does not occur until the end of the ejection stroke, thereby eliminating airload effects for that portion of the trajectories.

Only a 12-inch stroke was evaluated over the full weight range because it tends to be more representative of current design concepts. In addition, the V_{eos} vs weight curves for the 4 and 8-inch strokes are similar in shape to those obtained for the 12-inch stroke, based on analogy to the unconstrained ejection results, and limited computations for a 100-pound store.

Three general types of release mechanisms were considered, associated with the following conditions at the end of the ejection stroke :

- Constant pitch angle (θ), zero pitch rate ($\dot{\theta}$)
- Constant pitch angle and variable rate
- Constant pitch rate and variable pitch angle

Constant Pitch Angle, Zero Pitch Rate - In this type of constrained store release, the release mechanism rotates the weapon to a constant, predetermined pitch angle during ejection. For this case it was assumed that the store would reach this angle prior to the end of the ejector stroke, and that the store would not have a pitch rate at hook release.

$\Delta\theta_{EOS}$ = 0 Degrees - In this case, the stowed pitch angle of the store is held constant throughout the ejector stroke. The only benefit is that the effect of the aerodynamic forces on the store angular motion is delayed until the end-of-stroke position is reached. Figures 30 and 31 present the end-of-stroke velocities required for safe separation of parametric store shape with the maximum length/minimum moment-of-inertia, and maximum length/maximum moment-of-inertia combinations. For the 100-pound store negligible improvement over the unconstrained case is noted with the four-inch stroke; however, for the longer strokes, significant reductions in required end-of-stroke velocities are achieved, especially for the heavier stores.

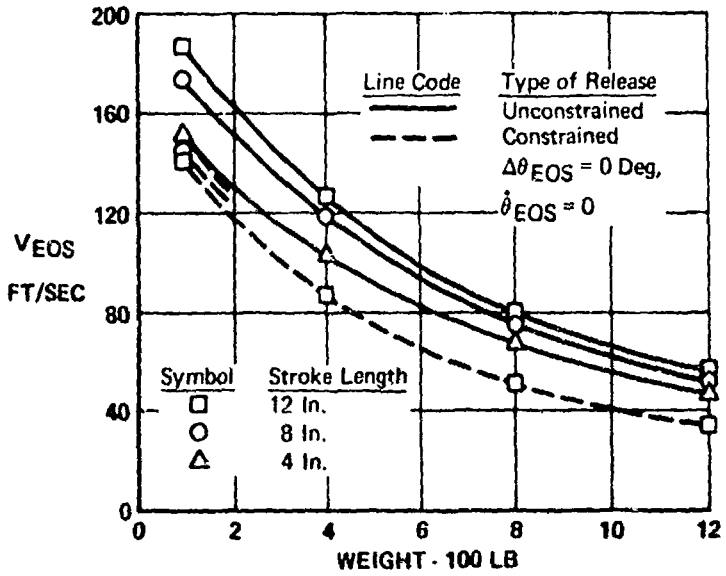


FIGURE 30 - REQUIRED END OF STROKE VELOCITY
Maximum L - Minimum Iy

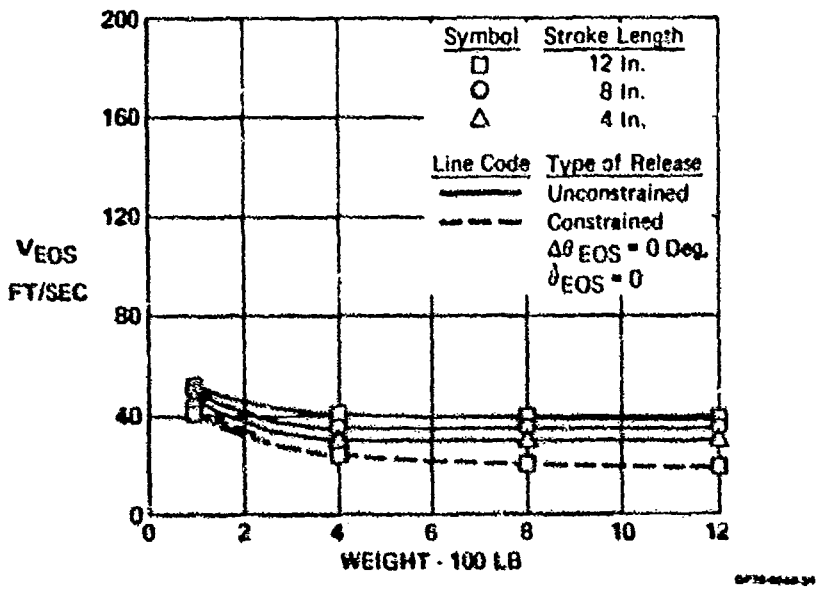


FIGURE 31 - REQUIRED END OF STROKE VELOCITY
Maximum L - Maximum Iy

$\Delta\theta_{eos}$ = +2 Degrees - This case is similar, except that the store is rotated two degrees nose-up by the release mechanism before the ejector stroke ends. A positive value of θ_{eos} was selected since most of the trajectories for the unconstrained release cases are strongly nose-down at high speeds. Figure 32 shows that this system results in significant improvements over the unconstrained case for all stroke lengths. However, a comparison of Figures 30 and 32 reveals that the reductions in end-of-stroke velocity achieved by the $+2^{o}$ constraint, as compared to $\Delta\theta_{eos} = 0^{o}$, are significant only for the lighter store weights.

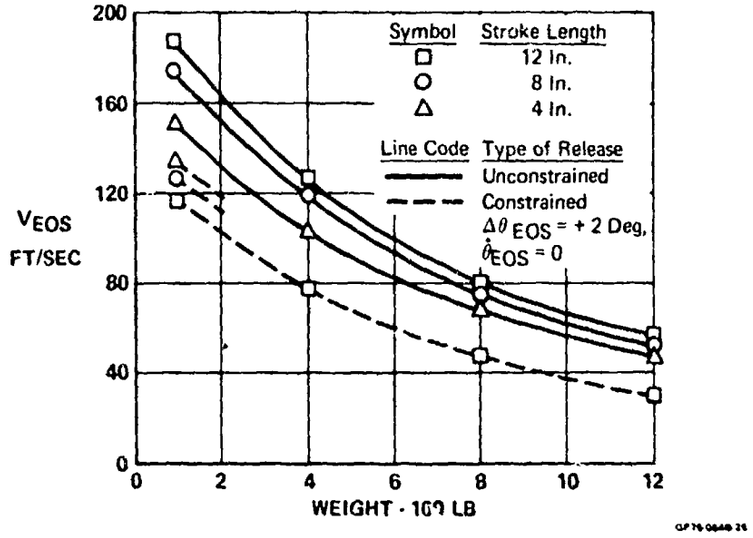


FIGURE 32 - REQUIRED END OF STROKE VELOCITY
Maximum L - Minimum Iy

$\Delta\theta_{eos}$ = +4 Degrees - The results, shown in Figure 33, for constrained store release with $\Delta\theta_{eos} = +4^{o}$ are similar to those obtained for the previously discussed conditions. While there is, again, a large improvement over the unconstrained case, significant reductions in end-of-stroke velocity over the $\Delta\theta_{eos} = 0^{o}$ and $+2^{o}$ conditions are obtained only for the lighter weight stores.

Constant θ_{eos} and a Variable θ_{eos} - In this technique the release mechanism also rotates the store to a predetermined pitch angle during ejection. However, the desired $\Delta\theta_{eos}$ is not attained until the ejector stroke ends and the store has a pitch rate when released from its constraints. It was assumed that the store pitch angle during ejection would vary linearly with stroke time; therefore, θ_{eos} was determined by dividing the value of $\Delta\theta_{eos}$ by the stroke time.

$\Delta\theta_{eos}$ = +2 Degrees, $\dot{\theta}_{eos} = +2/t_{eos}$ Degrees/Second - Figure 34 indicates that the utilization of this type of constrained release system results in a considerable improvement over unconstrained separation in terms of required end-of-stroke velocity. However, a comparison of Figures 32 and 34 reveals that the effect of inducing a nose-up pitch rate is small.

$\Delta\theta_{eos}$ = +4 Degrees, $\dot{\theta}_{eos} = +4/t_{eos}$ Degrees/Second - The required end-of-stroke velocities for this case are shown in Figure 35 and indicate that the reductions in required end-of-stroke velocity, when compared to unconstrained release, are significant - as has been true for all constrained release techniques studied. However, a comparison of Figures 33 and 35 reveals that, for stores heavier than 600 pounds, the induced pitch rate increases the required end-of-stroke velocity - a trend not observed in the previous comparisons.

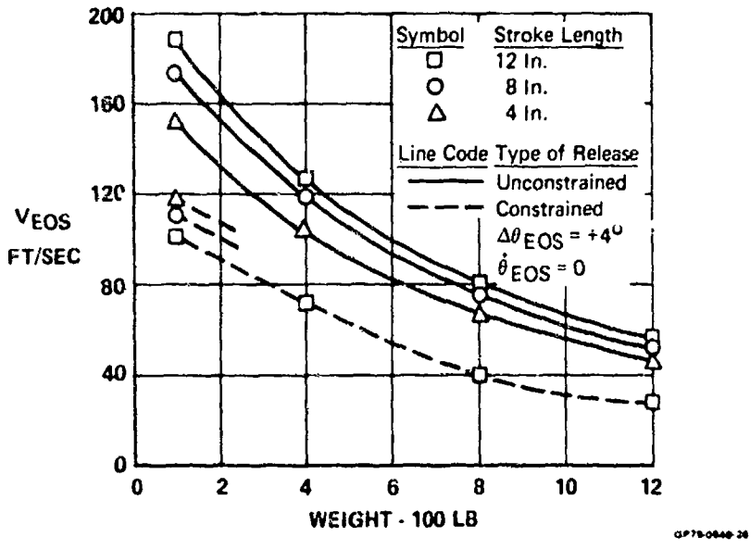


FIGURE 33 - REQUIRED END OF STROKE VELOCITY
Maximum L - Minimum Iy

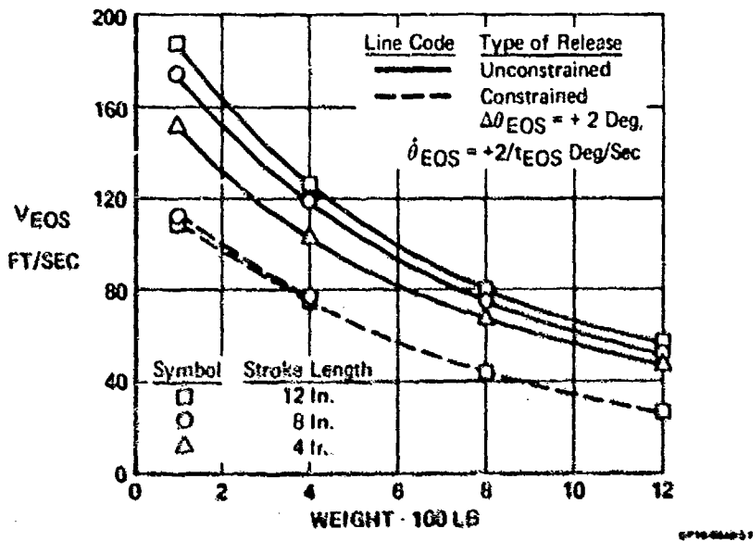


FIGURE 34 - REQUIRED END OF STROKE VELOCITY
Maximum L - Minimum Iy

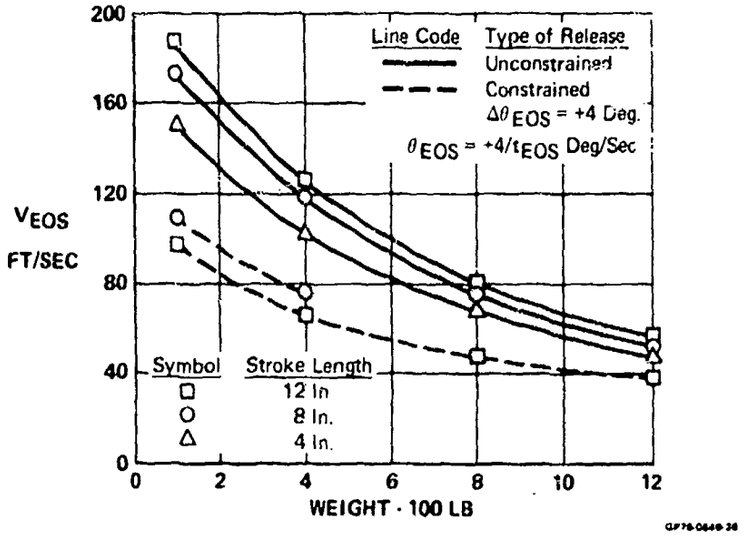


FIGURE 35 - REQUIRED END OF STROKE VELOCITY
Maximum L - Minimum Iy

For most of the unrestrained-release conditions investigated, separations at high speeds, during which the stores pitched strongly nose down, were the most critical. Although stores separated in the low subsonic speed range often exhibited nose-up tendencies, rarely were their trajectories as close to the collision boundary. This trend is exemplified in Figure 36, a pitch angle vs vertical displacement plot for the unconstrained release of a 1200 lb generalized store with the maximum length/minimum moment-of-inertia combination. Constrained release methods generally require less end-of-stroke

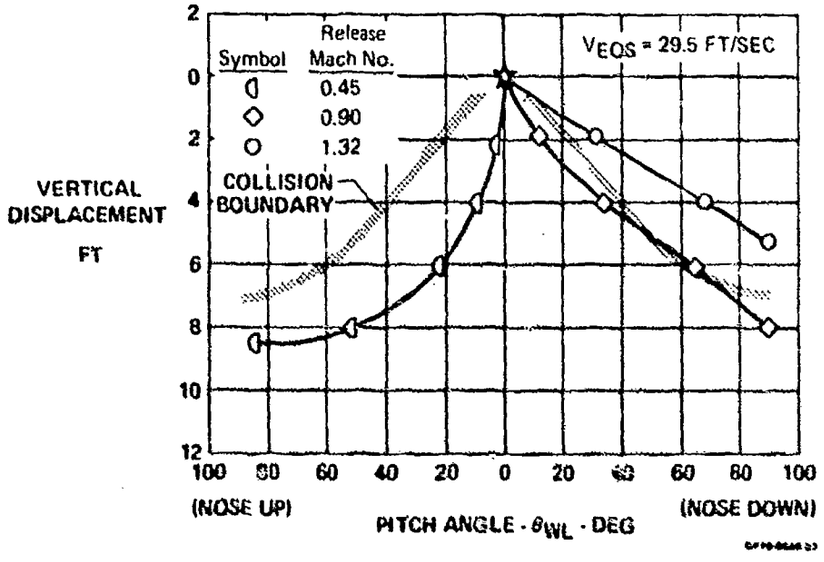


FIGURE 36 - UNCONSTRAINED-STORE-RELEASE
1200 Lb Generalized Store

velocity than the unconstrained-release case because, by inducing a nose-up pitch angle or pitch rate, stores do not pitch as severely nose-down at high speed. The general improvement obtained by utilizing restrained-store-release techniques can be seen by comparing Figure 36 with Figure 37, which shows the effect of a $\Delta\theta_{eos} = +4^{o}$, $\dot{\theta}_{eos} = 0$ release constraint.

However, when a pitch rate is added to the 4° constrained case, it can be seen in Figure 38, that the low-speed trajectory characteristics become critical, resulting in a requirement for more end-of-stroke velocity.

Constant Pitch Rate, Variable Pitch Angle - For the last restrained-store-release technique analyzed, a constant nose-up pitch rate of 50 degrees/second was applied to the store during ejector stroke by the release mechanism. The store pitch angle at release is then the product of the induced pitch rate and the ejector stroke time. Figure 39 indicates that the results obtained for this case are generally similar to those noted for the other restrained-release techniques.

DATA CORRELATION AND SUMMARY

A method has been derived for correlating the variances in store physical characteristics and ejection concepts evaluated in this study, to provide a more workable tool for the designer of aircraft, bomb racks, and stores. Since in conceptual design stages, whether they be aircraft, bomb rack or store related, the aerodynamic portions of the store release problem are frequently not known, a method of relating study results to store physical characteristics was sought. Considering that the required end-of-stroke velocity is a function of store pitching acceleration, then

$$V_{eos} = f(\ddot{\theta}) = f\,\frac{C_{mqsl}}{I_y} \tag{3}$$

But since the store aerodynamic characteristics were essentialy constant, equation (3) reduced to

$$V_{eos} = f\,L^3/I_y \tag{4}$$

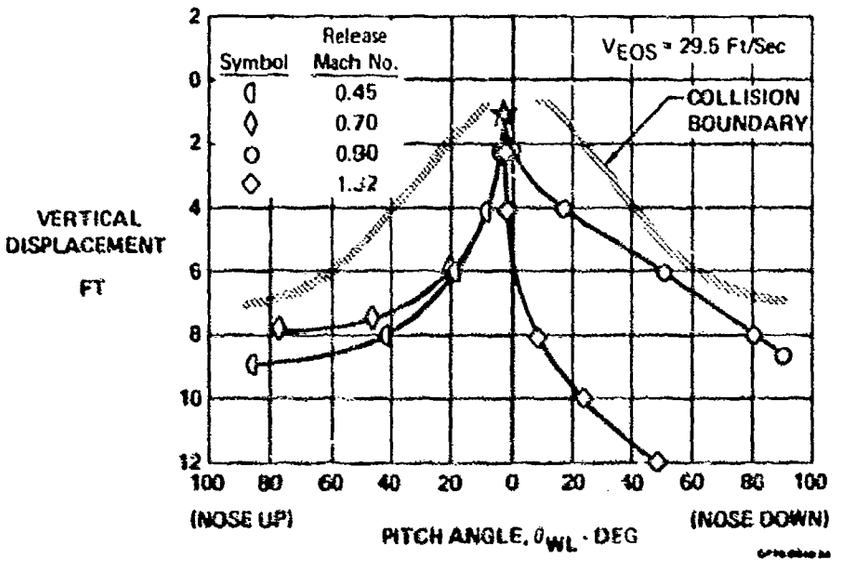


FIGURE 37 - CONSTRAINED-STORE-RELEASE
$\Delta\theta_{eos} = +4$ Deg, $\dot{\theta}_{eos} = 0$ Deg/Sec
1200 Lb Generalized Store

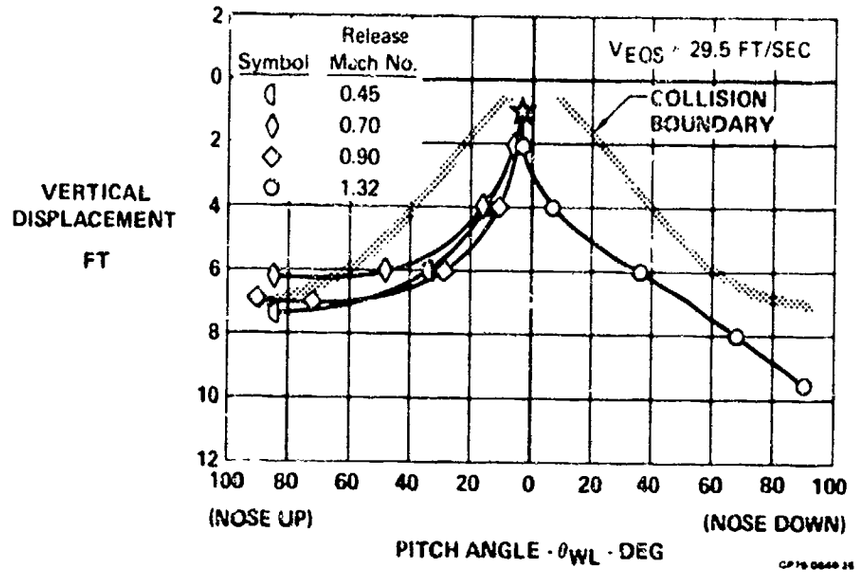


FIGURE 38 - CONSTRAINED-STORE-RELEASE
$\Delta\theta_{eos}$ = +4 Deg, $\dot{\theta}_{eos} = 4/t_{eos}$ Deg/Sec
1200 lb Generalized Store

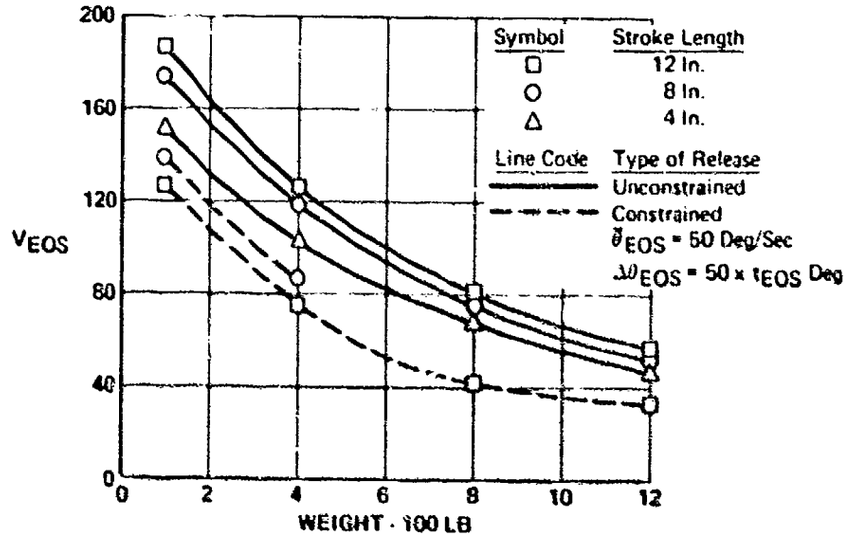


FIGURE 39 - REQUIRED END OF STROKE VELOCITY
Maximum L - Minimum Iy

In order to provide an additional correlation of required end of stroke velocity as a function of store weight, it was found by experimentation that the multiplier $W^{1/3}$ provided a satisfactory solution. The correlating function in equation (4) then becomes

$$V_{eos} = f\frac{L^3}{I_y} W^{1/3} \qquad (5)$$

A summary of th esults discussed in previous sections for unconstrained and constrained store release in the speed envelope of 150 and 750 knots are presented in Figures 40 and 41. The effects of maximum speed are presented in Figure 42 for the unconstrained, 12-inch stroke case.

Figure 43 compares unconstrained and constrained ejections (Figures 40 and 41), showing the actual bounds of existing stores and the postulated characteristics of bodies encompassing the bounds of the study.

In order to compare required ejection velocities with the performance capabilities of existing devices, the faired curves presented in Figures 40 and 42 were plotted for constant store weight as a function of L^3/I_Y for a 4-inch stroke, as shown in Figures 44 and 45. Superimposed on these figures is the performance of existing unconstrained ejectors, as shown in Figure 46. The range of L^3/I_Y shown is a reasonable representation of existing stores. Since these curves are derived from a fairing of computed data, certain cases (e.g., 100-pound store, max. L/max. I_y), are not in exact agreement with the calculated data.

The use of the summary data shown in Figures 44 and 45 provides a technique of evaluating airspeed effects, weapon physical characteristics and bomb rack performance.

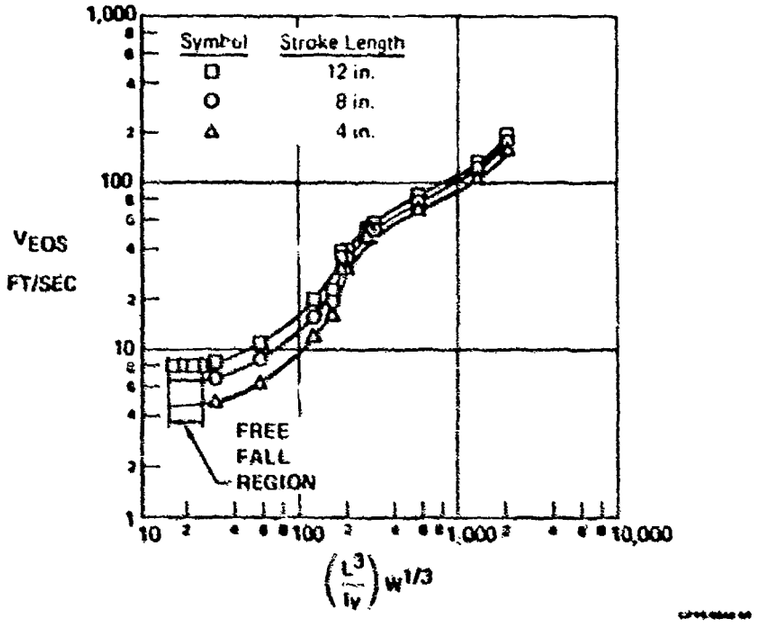


FIGURE 40 - REQUIRED END OF STROKE VELOCITY
Unconstrained Release
Release Envelope: 150-750 kts

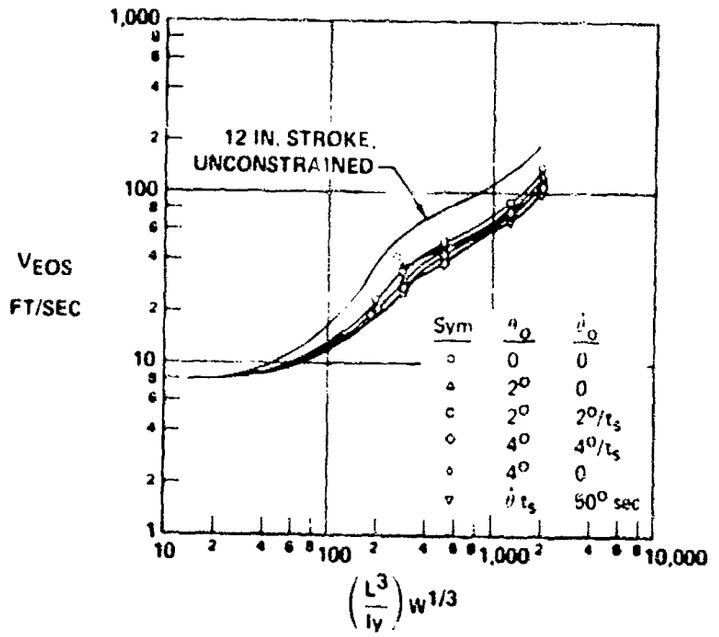


FIGURE 41 - REQUIRED END OF STROKE VELOCITY
Constrained Release
Release Envelope: 150-750 kts

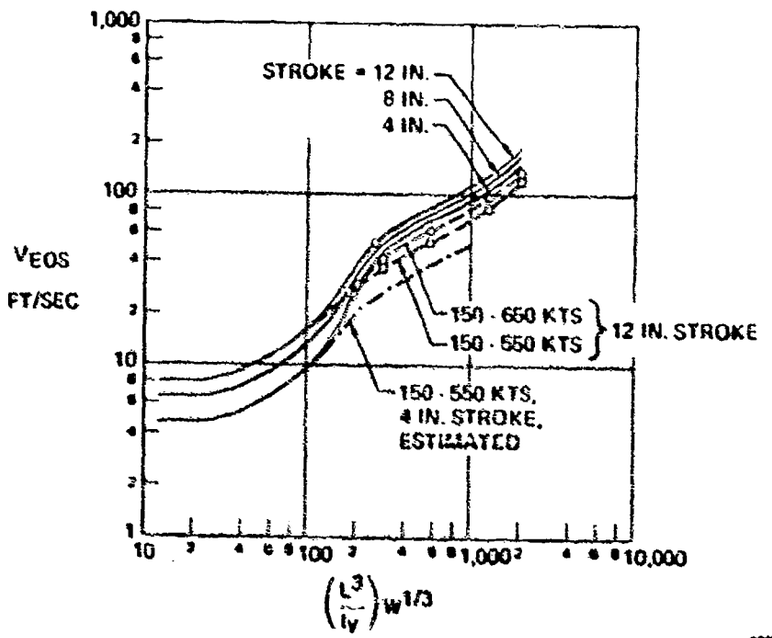


FIGURE 42 - REQUIRED END OF STROKE VELOCITY
Unconstrained Release
Release Envelope Effects

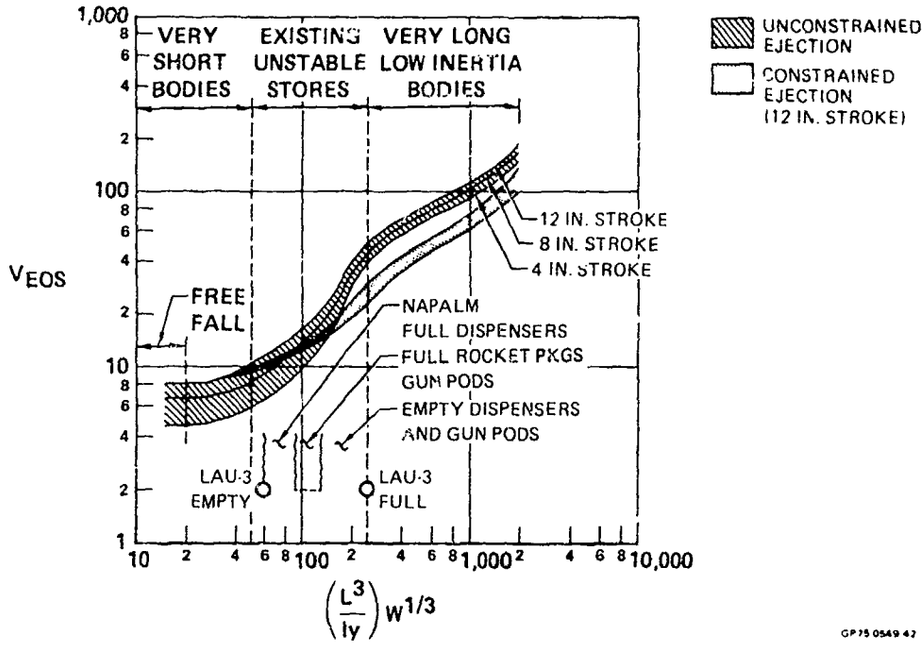


FIGURE 43 - SUMMARY OF UNSTABLE STORES EJECTION
Release Envelope: 150-750 kts

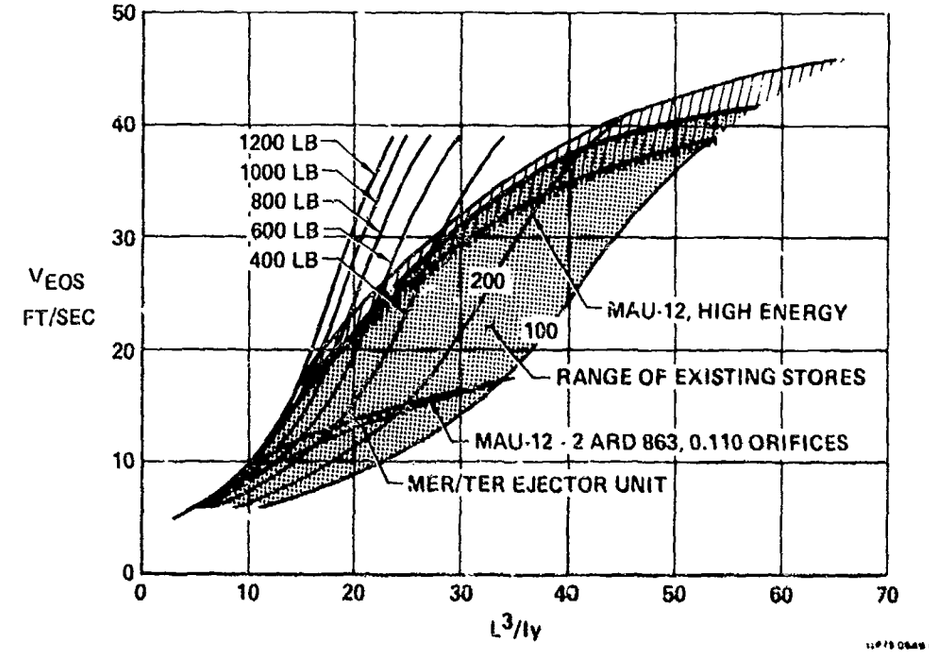


FIGURE 44 - REQUIRED END OF STROKE VELOCITY
Unconstrained Ejection
Speed Envelope: 150 - 750 kts
Stroke = 4 Inches

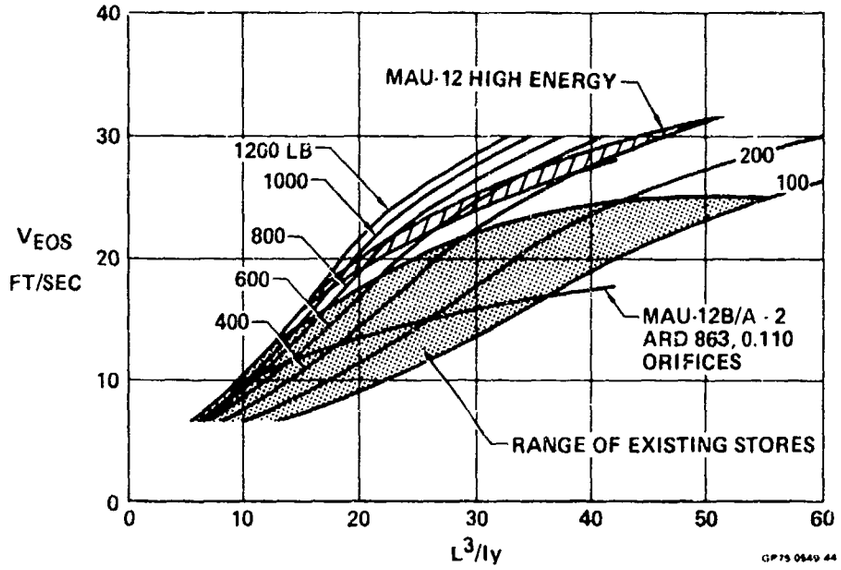


FIGURE 45 - REQUIRED END OF STROKE VELOCITY
Unconstrained Ejection
Speed Envelope: 150-550 kts
Stroke = 4 Inches

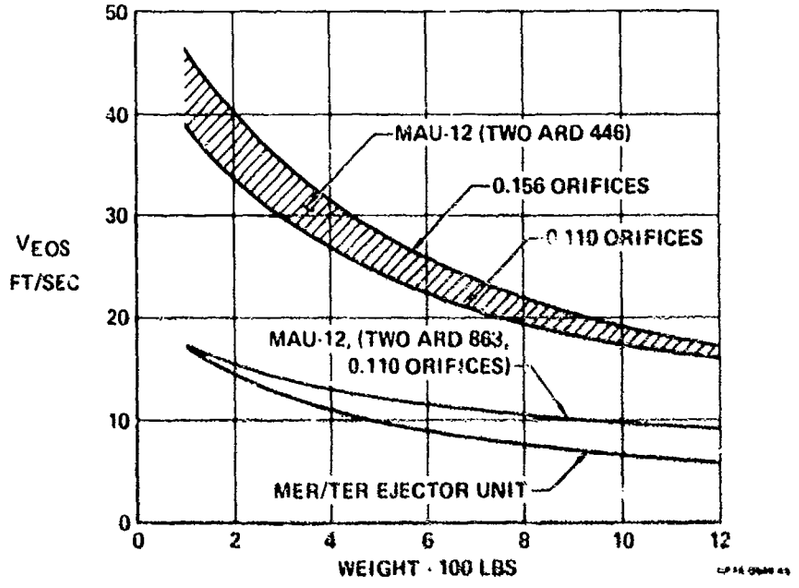


FIGURE 46 - TYPICAL PERFORMANCE
Unconstrained Bomb Racks
Stroke = 4 Inches (Nominal)

CONCLUSIONS AND RECOMMENDATIONS

CONCLUSIONS

The study discussed in this report is based on many simplifications, and therefore it would be imprudent to expect a one-for-one numerical correlation of the results obtained with an actual store/aircraft combination. The trends established, however, are considered valid. Based on these trends, the following conclusions are drawn:

- Constrained ejection offers an improvement over the unconstrained case in terms of required release velocities (and resultant reaction loads into the aircraft structure)
- For a constrained release ejector, control of pitch angle is the driving parameter. Pitch rate inputs produce small additional improvement.
- Within the weight-length-inertia range of existing stores, high energy unconstrained ejection may be sufficient to provide safe release up to 750 knots.
- Based on the limited analyses conducted in this study, applied moments generally do not have a positive effect on store release. (For a given individual store, this may not be a valid statement). Applied moments may, in fact, result in a net decrease in allowable release speeds, or discontinuities in the allowable release speed envelope.

RECOMMENDATIONS

As has been noted previously, many simplifications were made during this study, including the following.

- Constant store aerodynamic characteristics
- Constant flow field effects
- C.G. at the mid-point of the store
- Three-degree of freedom computation
- Non-maneuvering flight.

It is encouraging, however, to obtain the type of correlation established in this study, and these results should form a basis for additional work to establish a more general correlation.

It is recommended that further studies consider the effect of store stability and flow field variances to apply further bounds on the correlations discussed herein. The effect of store C.G. location (or applied moments) should be explored in greater depth for unconstrained ejection. In addition, the effect of maneuvering flight including yaw and rolling conditions should also be investigated.

AUTOBIOGRAPHY

The author, Steve J. Jendras, was born 13 July 1936, in Chicago, Illinois. He received the degree of Bachelor of Science in Aeronautical Engineering from the University of Notre Dame in June 1957. He received the degree of Master of Business Administration from St. Louis University in January 1961. He received the degree of Master of Science, Engineering Mechanics from St. Louis University in 1968.

The author has been employed by the McDonnell Douglas Corporation since June 1957, with nine years experience in aerodynamics on the F-4 aircraft and F-111 escape capsule projects, and nine years experience in armament systems design on the F-4, F-15 and F-18 aircraft. His current assignment is as a staff engineer for armament for various advanced design aircraft.

APPENDIX A

TABLE A-I - PHYSICAL CHARACTERISTICS

STORE	WEIGHT* (LB)	INERTIA - I_y (SLUG - FT^2)	LENGTH (FT)	L^3/I_y	$W^{1/3}$ (L^3/I_y)
UK 36 TUBE ROCKET PKG	574/214	36.5/18.5	8.33	15.9/31	132/188
UK 18 TUBE ROCKET PKG	394/195	24.6/16.5	7.74	18.9/28	139/163
PADEYE	520	96.3	9.06	7.68	60.5
SUU-43	282/194	50/42	7.75	9.2/10.9	60.3/63
CBU-38A	702/185	64.4/21	7.53	6.65/20	59.1/115
CBU-16A	650/186	59.3/16.9	7.53	7.26/25	62.8/145
CBU-15A	526/186	48/16.9	7.53	8.96/25	72.2/145
CBU-7/A	810/186	73.8/16.9	7.53	5.83/25	54.2/145
CBU-1A THROUGH 13A	830/122	107/19.5	9.88	8.88/48.8	83.4/242
SUU-40A	346.5/135	70.1/20.2	8.55	9.2/31.9	64.4/163
SUU-25 FLARE	315/	38.1	7.75	12	82.2
BRITEYE FLARE	154	7.45	5.25	19.50	104.0
SUU-20	455/240	71.0/42.0	10.15	14.8/25.0	113.5/155
MK-4 GUN POD	1390/787	358.5/2.90	15.95	11/17	123/160
SUU-1623 GUN POD	1720/1070	560/318	16.6	9/14	108/146
SUU-11 GUN POD	325/245	10.5/9.1	7.01	33.4/38	230/240.5
LAU-10A ROCKET PKG	533/105	94.9/16.4	11.62/7.63	16.5/27.4	134/129
LAU-3A ROCKET PKG	427/71	14.9/3.6	7.88/3.88	32.9/14.15	245/58.6
LAU-32 ROCKET PKG	179/47	6.75/2.3	5.59/3.88	26/25.6	146/90.7
M-116 A2 NAPALM	700	139.0	11.45	10.80	95.6
BLU-1/B NAPALM	697	138.5	10.80	9.24	81.2
BLU-27B NAPALM	850	162.0	10.80	7.90	75.0
BLU-23B NAPALM	480	82.8	9.92	11.90	93.0
BLU-32B NAPALM	515	98.5	9.92	10.00	80.0

*(/) Indicates Full/Empty, Typical to All Columns.

GP75 0849 46

TABLE A-II - STORE PHYSICAL CHARACTERISTICS SUMMARY

Parametric Stores

WEIGHT	I_{YMIN} SLUG - FT^2	I_{YMAX} SLUG - FT^2	L_{MIN} - (FT)	L_{MAX} - (FT)	MIN/MIN	L^3/I_y MAX/MAX	L^3/I_y MIN/MAX	L^3/I_y MAX/MIN	L^3/I_y MIN/MIN	$(L^3/I_y)(W^{1/3})$ MAX/MAX	$(L^3/I_y)(W^{1/3})$ MIN/MAX	$(L^3/I_y)(W^{1/3})$ MAX/MIN
100	3	23	4.33	11.00	27.00	57.80	3.52	444.0	125.5	268.0	16.35	2060
400	14	95	6.83	13.55	22.85	26.35	3.37	178.5	168.0	193.5	24.80	1310
800	71	185	7.55	15.90	6.06	21.65	2.32	56.4	56.3	201.0	21.50	523
1200	170	271	7.83	16.75	2.82	17.15	1.77	27.4	29.9	182.0	18.75	290

GP75 0849 47

ON THE FEASIBILITY OF INCLUDING THE EFFECTS OF STORE SEPARATION IN FREE-FALL WEAPON BALLISTICS

(U)

(Article UNCLASSIFIED)

by

LEROY DEVAN
Naval Surface Weapons Center
Dahlgren Laboratory
Dahlgren, Virginia 22448

ABSTRACT. (U) The effects of store separation are generally not intentionally included in the ballistics of air-launched, free-fall stores. However, some residual yaw drag effect probably remains when store trajectory data is fitted to establish the drag coefficient as a function of Mach number. Use of particle ballistics can cause large miss distances on the ground if the store undergoes significant angular motion in the vicinity of the aircraft.

This paper presents an investigation of the feasibility of including the effects of store separation in ballistics. Prediction techniques are naturally divided into two stages. The first stage predicts the flight state variables from separation to free field (no aircraft flow field influence). The second stage predicts the remainder of the trajectory to impact given the initial conditions from the first stage computation. This paper presents two prediction methods for the second stage for stores with roll orientation-independent aerodynamics.

The first method yields a closed form perturbation solution of the 5-DOF nonrolling equations of motion. The first-order solution is the particle solution; the perturbation solution estimates the difference in impact coordinates between a 5-DOF computation and a particle computation. The method of least squares is applied to an envelope of MK-82 bomb trajectories; the down-range and cross-range deviations from particle impact are fitted. The deviations are fitted as functions of the initial disturbance (angles of attack, angle of attack rates, and cross-range initial velocity). Cross-range impact points are predicted with good accuracy, but down-range accuracy is only fair. Computation times are short.

The second method utilizes the averaging technique of Krylov-Bogoliubov for almost period functions applied to the epicyclic functional form for the complex angle-of-attack vector. A modified second-order Runga-Kutta integration scheme which retains the harmonic functions in the lift terms permits large variable integration step lengths. Computations for MK-82 rolling trajectories yield accuracy approaching the 6-DOF computation, but in about 1/40 of the computational time (nonrolling case) or less. This technique thus seems to be an important

"Approved for public release; distribution unlimited."

contribution to rapid, accuracte computation techniques. However, for adaption of this technique to current airborne computers, the computing time should be reduced from about 0.5 second to less than 0.100 second (CDC 6400 time).

This work is sponsored by the Naval Air Systems Command under AIRTASK A320320C/0098/SF3202000.

"Approved for public release; distribution unlimited."

LIST OF FIGURES

Figure		Page
1	Store Trajectory Coordinates	
2	Perturbation Solution Impact Geometry	

LIST OF TABLES

Table		Page
I	MK-82 Fit Envelope	
II	MK-82 Epicyclic Computation Comparison With 5-DOF	
III	MK-82 Epicyclic Computation Comparison With 6-DOF	

LIST OF SYMBOLS

C_D $= C_{D0} + C_{D2} \sin^2 \alpha_T + C_{D4} \sin^4 \alpha_T = -\gamma C_x + C_{N\alpha} \sin^2 \alpha_T$, Drag Coefficient

$C_{\ell p}$ Roll damping coefficient

$C^*_{\ell p}$ $= \tilde{C}_D + \tilde{C}_{\ell p} \frac{mD^2}{2I_x} = \frac{\rho_0 S}{2m} \hat{C}_{\ell p} = C^*_{\ell p 0} + \sin^2 \alpha_T C^*_{\ell p 2}$

$C_{L\alpha}$ $= \gamma C_{N\alpha} + C_x = C_{L\alpha 0} + \sin^2 \alpha_T C_{L\alpha 2}$ (rad^{-1})

$C_{\ell\delta}$ Roll moment coefficient due to fin cant

$C^*_{\ell\delta}$ $= \tilde{C}_{\ell\delta} \frac{mD}{I_y} \delta = \frac{\rho_0 S}{2m} \hat{C}_{\ell\delta} = C^*_{\ell\delta 0} + \sin^2 \alpha_T C^*_{\ell\delta 2}$

C_{mq} Pitch damping coefficient

C^*_{mq} $= (\tilde{C}_{mq} + \gamma \tilde{C}_{m\dot{\alpha}}) \frac{mD^2}{2I_y}$

$C_{m\dot{\alpha}}$ Pitch damping coefficient due to angle-of-attack rate

C_{np} Magnus moment coefficient

C_N Normal force coefficient

$C_{np\alpha}$ $C_{np}/\sin \alpha_T$ (rad^{-1})

$C_{N\alpha}$ $= C_N/\sin \alpha_T$ (rad^{-1})

C_x $= C_{x0} + \sin^2 \alpha_T C_{x2}$, Axial force coefficient

D Store reference diameter (ft)

g $= 32.174$, Acceleration of gravity (ft/sec^2)

G $Pg(1 - z'^2)^{1/2}/V^2 (ft^{-2})$

h Arc length integration step length (ft)

H $= \tilde{\rho}(\gamma\tilde{C}_{L\alpha} - \tilde{C}_D - C^*_{mq}) - gz'/V^2 = \tilde{\rho}\frac{\rho_0 S}{2m}\hat{H} - gz'/V^2$

$= H_0 + \sin^2\alpha_T H_2\ (ft^{-1})$

i $= \sqrt{-1}$

I_x Roll moment of inertia (slug-ft^2)

I_y Pitch moment of inertia (slug-ft^2)

K_1 Amplitude of the first arm of the epicyclic (rad)

K_2 Amplitude of second arm of the epicyclic (rad)

m Store mass (slugs)

M $= \gamma\tilde{\rho}\tilde{C}_{m\alpha}\frac{mD}{I_y} = \tilde{\rho}\frac{\rho_0 S}{2m}\hat{M} = M_0 + \sin^2\alpha_T M_2\ (ft^{-2})$, also Mach number.

p Spin rate (rad/sec)

P $= \frac{I_x p}{I_y V}\ (ft^{-1})$

Q $= \frac{1}{2}\rho V^2$ Dynamic pressure (ft^2)

s Arc length (ft)

S $= \frac{\pi D^2}{4}\ (ft^2)$

t Time (sec)

T $= \tilde{\rho}\gamma(\tilde{C}_{L\alpha} + \frac{mD^2}{2I_x}\tilde{C}_{np\alpha}) = \frac{\rho_0 S}{2m}\hat{T} = T_0 + \sin^2\alpha_T T_2\ (ft^{-1})$

V Velocity (ft/sec)

x Down-range store c.g. position (ft)

y Cross-range store c.g. position (ft)

z	Height of store c.g. above mean sea level (ft)
α	Aeroballistic pitch angle of attack (rad)
$\sin \alpha_T$	$= (\sin^2 \beta + \sin^2 \alpha \cos^2 \beta)^{1/2}$
β	Aeroballistic yaw angle of attack (rad)
γ	$= \cos \alpha_T$
δ_g	$= -G/[M_0 + M_2(K_1^2 + K_2^2)]$ (rad)
θ	Elevation angle of velocity vector (rad)
λ_1	$= K_1'/K_1$ (ft^{-1})
λ_2	$= K_2'/K_2$ (ft^{-1})
ρ	Air density ($slug\text{-}ft^2$)
$\tilde{\rho}$	$= \rho/\rho_0$
ρ_0	Mean sea level air density ($slug/ft^3$)
$\sigma(\ )$	= Standard deviation ( )
ϕ_1	Phase angle of first epicyclic arm (rad)
ϕ_2	Phase angle of second epicyclic arm (rad)
ω_1	$= \phi_1'$ (ft^{-1})
ω_2	$= \phi_2'$ (ft^{-1})

Superscripts

$\dot{(\ )}$ = d/dt ( )

$(\ )'$ = d/ds ( )

$\tilde{(\ )}$ = $\frac{\rho_0 S}{2m}$ ( )

$\bar{(\ )}$ = Estimated value at and of integration step or mean value

Subscripts

p	Particle value
o	Initial value or zero yaw value
f	Final value
i	Value at beginning of integration step
i + 1	Value at end of integration step

INTRODUCTION

The effects of store separation are generally not intentionally included in the ballistics of air-launched free-fall stores. Current trajectory models used to generate a fire-control algorithm are based upon particle ballistics (Reference 1). However, some residual yaw drag effects probably remain when store trajectory data is fitted to establish the drag coefficient as a function of Mach number; in Reference 2 the fit begins only .8 seconds after release.

Use of particle ballistics can cause large miss distances on the ground if the store undergoes significant angular motion in the vicinity of the aircraft, as indicated schematically in Figure 1.

It is assumed that a given store has been designed with enough static stability in order to insure an adequate damping of initial disturbances. In addition, it is assumed that a fin cant has been chosen to give steady-state roll rates which avoid asymmetry trim, roll-yaw resonance, roll lock-in and catastrophic yaw, as well as Magnus instabilities (see Reference 3 for instance).

Recently, ejection racks with adaptable ejection force characteristics have been proposed which would have the capability of producing minimum disturbances at the end of the aircraft interference flow field (References 4 and 5).

Computational algorithms have been developed which compute the ejection, aircraft flow field, and free-flight phases of a store trajectory (Reference 6). However, they require at least as much computing time on third generation computers (CDC 6700) as the time of fall. A long-range goal would be the prediction of store trajectories, including separation effects, on an airborne computer with limited storage capacity and basic computational cycle time which is not as fast as that of the general-purpose computer.

The problem addressed here is that of the feasibility of including store separation into rapid computation schemes for the prediction of impact coordinates for a store. Current fire-control algorithms compute the particle trajectory using curve fit approximations to the numerical solution. Typically, the time of fall and impact ranges are given as functions of release conditions (height above target, and elevation angle and magnitude of the release velocity). Store separation, of course, would introduce parameters characteristic of the store and aircraft. Some additional parameters would be aircraft pull-up rate (Reference 7), ejector characteristics, and location in the aircraft flow field. If the store were always dropped in the same flow environment and the same ejector were utilized, the only additional parameter would be the pull-up rate, however, the former case is usually true in practice.

Prediction techniques are naturally divided into two stages. The first stage predicts the flight state variables from separation to free field (no aircraft flow field influence). A simple store separation model for this stage would have as input data in-carriage loads (could be measured just before release by an in-carriage balance), ejector characteristics, and an estimate of the decay law for interference loads to free-field values. The second stage would predict the remainder of the trajectory to impact, given the initial conditions from first-stage computations. This paper is primarily concerned with prediction and application techniques for the second stage. Two different prediction techniques are presented below.

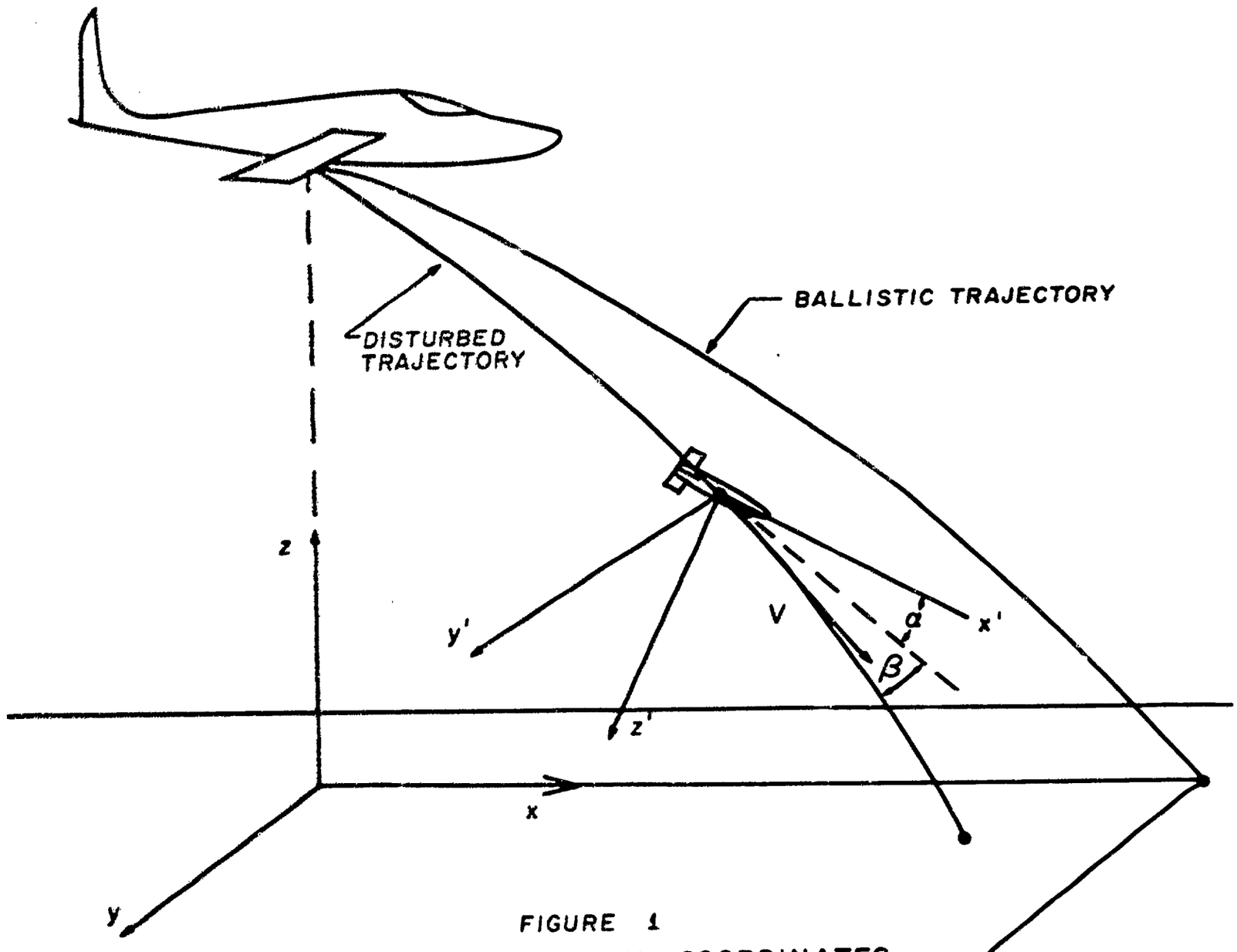


FIGURE 1

STORE TRAJECTORY COORDINATES

COMPUTATIONAL TECHNIQUES

Initial values in addition to ballistic initial conditions of velocity, V_0, height above mean sea level, z_0, and elevation angle of the velocity vector, θ_0, are aeroballistic angles of attack (Figure 1) α_0, β_0, and angle-of-attack rates $\dot{\alpha}_0$. $\dot{\beta}_0$, out-of-plane velocity component, $\dot{y}_0$, and roll rate, p_0. No roll-orientation-dependent aerodynamics are considered.

A. SIMPLE PERTURBATION APPROXIMATION

1. Basic Equations

For small angles (to order $\alpha^2 + \beta^2$) the c.g. equations of motion of a store are given by (wind is not considered):

$$\ddot{x} = -\frac{QS}{m}(C_D\dot{x} + \alpha C_{L\alpha}\dot{z})/V$$

$$\ddot{y} = -\frac{QS}{m}(C_D\dot{y}/V + \beta C_{L\alpha})$$

$$\ddot{z} = -\frac{QS}{m}(C_D\dot{z} - \alpha C_{L\alpha}\dot{x})/V - g \qquad (1)$$

α, β, and C_D are given by solution of the epicyclic equation. The computation ends at the target altitude, z_f.

Further assumptions are:

(1) Linear, constant aerodynamics.

(2) Angular disturbance is a small perturbation of particle equations.

(3) No rolling motion.

(4) No out-of-plane motion particle computation.

(5) Neglect perturbation in Q.

This approach seems to be almost identical to that of J. Ausman (References 8 and 9).

The usual equations of motion for the particle are

$$\ddot{x}_p = -\frac{\rho_p S}{2m} C_{D0} V_p \dot{x}_p$$
$$\ddot{z}_p = -\frac{\rho_p S}{2m} C_{D0} \dot{z}_p - g \qquad (2)$$

Perturbation equations are given by

$$\Delta\ddot{x} = -\frac{\rho_p S}{2m} V_p \dot{x}_p (\alpha^2 + \beta^2) C_{D2} - \frac{\rho_p S V_p}{2m} \dot{z}_p \alpha C_{L\alpha 0}$$
$$\Delta\ddot{z} = -\frac{\rho_p S V_p}{2m} \dot{z}_p (\alpha^2 + \beta^2) C_{D2} + \frac{\rho_p S V_p}{2m} \dot{x}_p \alpha C_{L\alpha 0} \qquad (3)$$

where

$$C_{D2} = C_{N\alpha 0} + C_{x0}/2 - C_{x2}$$
$$C_{L\alpha 0} = C_{N\alpha 0} + C_{x0}$$

In this case, the angle of attack is given by uncoupled damped harmonic motion

$$\alpha = e^{\lambda_0 t}\left(\alpha_0 \cos \omega_0 t + \frac{\dot{\alpha}_0 - \lambda \alpha_0}{\omega_o} \sin \omega_0 t\right)$$
$$\beta = e^{\lambda_0 t}\left(\beta_0 \cos \omega_0 t + \frac{\dot{\beta}_0 - \lambda_0 \beta_0}{\omega_o} \sin \omega_0 t\right) \qquad (4)$$

where

$$\lambda_0 = \frac{Q_p S D^2}{2 V_p i_y}\left(C_{mq0} + C_{m\dot{\alpha}0} - \frac{2 C_{N\alpha 0}}{\frac{mD^2}{i_y}}\right)$$
$$\omega_0^2 = -\frac{Q_p S D}{i_y} C_{m\alpha 0} \qquad (5)$$

The particle equations are integrated from initial conditions to $z = z_f$ at time, $t = t_f$. Subsequently, the perturbation corrections are made. Further approximations which avoid the nonconstant coefficient problem are

$$\dot{x}_p = \bar{\dot{x}} = \frac{(\dot{x}_{p0} + \dot{x}_{pf})}{2}$$

$$V_p = \bar{V} = \frac{(V_{p0} + V_{pf})}{2}$$

$$\dot{z}_p = \dot{z}_{p0} + \frac{(\dot{z}_{pf} - \dot{z}_{p0})t}{t_f} = \dot{z}_{p0} + \kappa t$$

$$\rho_p = \bar{\rho} = \frac{\rho_{p0} + \rho_{pf}}{2} \tag{6}$$

Double integrations of (3) then will yield perturbation corrections $(\Delta x)_f$ and $(\Delta z)_f$ at $t = t_f$. However, the combined solution leaves the store $(\Delta z)_f$ above the target. To obtain the down-range correction, ΔR_x, a simple extrapolation is assumed (see Figure 2).

$$\Delta R_x = (\Delta x)_f - \left(\frac{dx}{dz}\right)_f (\Delta z)_f$$

$\left(\frac{dx}{dz}\right)_f$ is obtained from the particle solution.

Further approximations are that oscillatory terms are neglected as well as terms of order $(\lambda_0/\omega_0)^2$.

The down-range correction is given by

$$\Delta R_x = -\frac{\bar{\rho}\bar{V}S}{4m} C_{D2} \left\{ \left[\bar{\dot{x}} - \dot{z}_{p0}\left(\frac{dx}{dz}\right)_f \right] \left[\frac{1}{2\lambda_0} ABP \left[t_f + \frac{1}{2\lambda_0}(1 - e^{2\lambda_0 t_f}) \right] + \frac{AB\, t_f}{\omega_0^2} \right] \right.$$
$$\left. - \frac{\kappa}{4}\left(\frac{dx}{dz}\right)_f \left[ABP \left[t_f (1 + e^{2\lambda_0 t_f}) + (1 - e^{2\lambda_0 t_f})/\lambda_0 \right] / \lambda_0^2 \right] \right\} - \frac{\bar{\rho}\bar{V}S}{2m} C_{L\alpha 0}$$
$$\left\{ \left[\frac{\alpha_0 (\lambda_0 t_f - 1)}{\omega_0^2} + \frac{(\dot{\alpha}_0 - \lambda_0 \alpha_0) t_f}{\omega_0^2} \right] \left[\dot{z}_{p0} + \left(\frac{dx}{dz}\right)_f \bar{\dot{x}} \right] - \frac{\alpha_0 \kappa t_f}{\omega_0^2} \right\} \tag{7}$$

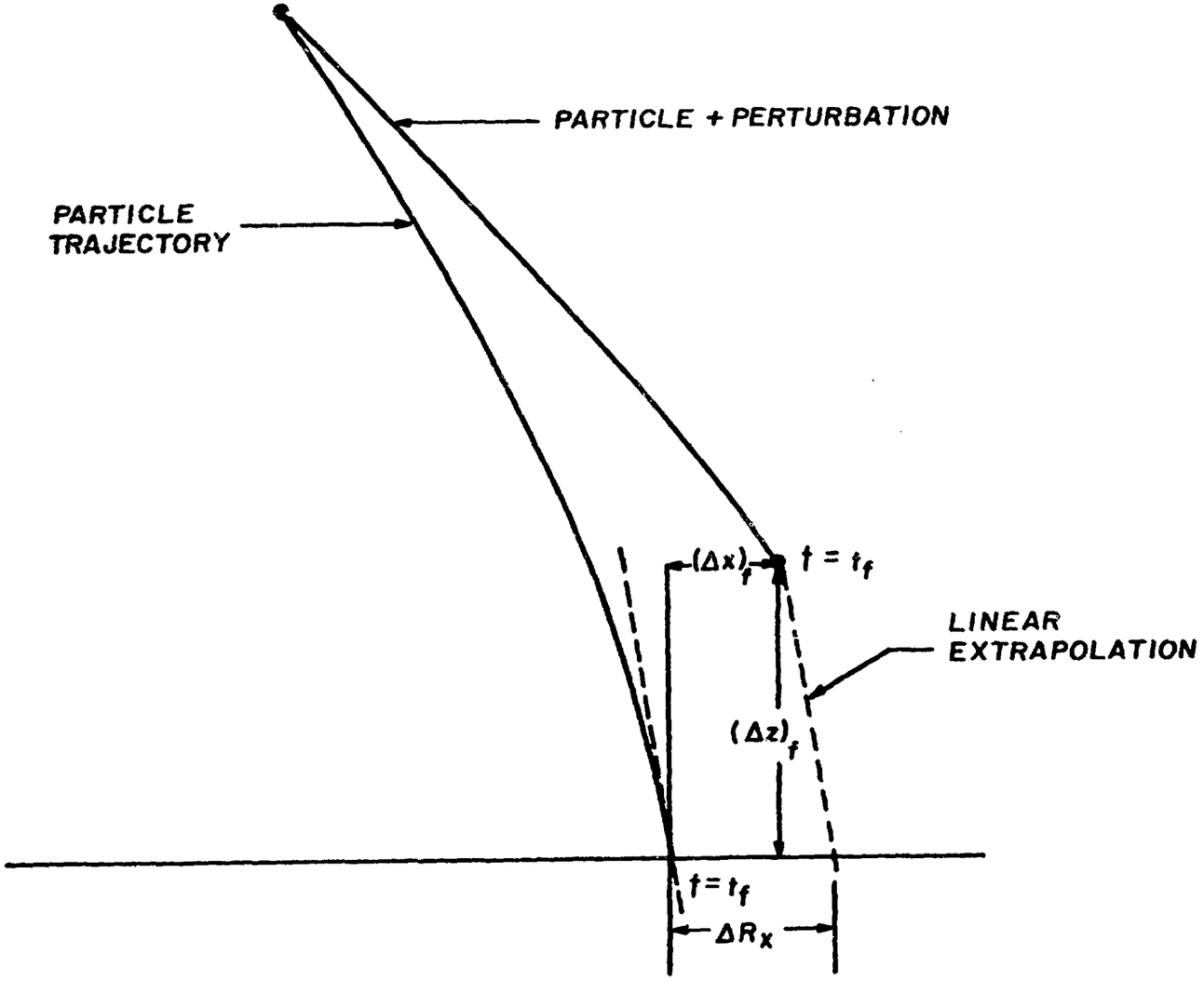


FIGURE 2

PERTURBATION SOLUTION IMPACT GEOMETRY

where

$$ABP = \alpha_0^2 + \beta_0^2 + \frac{(\dot{\alpha}_0 - \lambda\alpha_0)^2 + (\dot{\beta}_0 - \beta_0\lambda_0)^2}{\omega_0^2}$$

$$AB = \alpha_0(\dot{\beta}_0 - \lambda_0\beta_0) + \beta_0(\dot{\alpha}_0 - \lambda_0\alpha_0)$$

2. Applied Computations

Complete free-field aerodynamic data sets for a store are in short supply. One almost complete wind tunnel data set for the MK-82 bomb is given by References 10 and 11; an estimate of Magnus moment coefficient is obtained by scaling data from Reference 12.

First, a set of 72 5-DOF trajectories (no spin) was generated for an envelope of initial conditions using a Naval Surface Weapons Center, Dahlgren Laboratory (NSWC/DL), program known by the acronym SIMSTAB. Then, points on the trajectories were utilized to obtain a greater variation of initial conditions and target altitudes (and to save costly computer time). For the same ballistic initial conditions and target altitudes, particle computations were generated.

The variables which were fitted by the method of least squares are

$$\Delta x = x_f(5 - D) - x_{pf}$$

$$\Delta y = y_f(5 - D) \tag{8}$$

Statistics for the envelope of initial and target positions, Δx, and Δy are given in Table Ia.

A down-range estimate of Δx was based on the approximate solution given by ΔR_x. A number of fits were tried. One of the fits is given by

$$\begin{aligned}\frac{\Delta x - \Delta R_x}{t_f} &= a_1 + a_2\alpha_0 + a_3\dot{\alpha}_0 + a_4(\alpha_0^2 + \beta_0^2) \\ &+ a_5\frac{[(\dot{\alpha}_0 - \lambda_0\alpha_0)^2 + (\dot{\beta}_0 - \lambda_0\dot{\beta}_0)^2]}{\omega_0^2} + a_6[\alpha_0(\dot{\beta}_0 - \lambda\beta_0) \\ &+ \beta_0(\dot{\alpha}_0 - \lambda_0\alpha_0)]/\omega_0 + a_7(\alpha_0^2 + \beta_0^2)\dot{\alpha}_0 \\ &+ a_8\frac{[(\dot{\alpha}_0 - \lambda\alpha_0)^2 + (\dot{\beta}_0 - \lambda_0\beta_0)^2]\alpha_0}{\omega_0^2} + t_f\Big\{a_9\alpha_0 \\ &+ a_{10}\dot{\alpha}_0 + \cdots + a_{15}[(\dot{\alpha}_0 - \lambda_0\alpha_0)^2 + (\dot{\beta}_0 - \lambda_0\beta_0)^2]\alpha_0/\omega_0^2\Big\}\end{aligned}$$

TABLE I MK-82 FIT ENVELOPE

a. Envelope Properties
621 Trajectories, Standard Atmosphere

$0 \leq |\beta_0| \leq 10°$

$0 \leq |\dot{\beta}_0| \leq 1$ rad/sec

$3000' \leq z_0 \leq 10000'$

$300 \leq V_0 \leq 630$ Knots

$0 \leq |\dot{y}_0| \leq 10'$/sec

$0 \leq |\Delta y| \leq 311'$

$\sigma(\Delta y) = 79.6'$

$0 \leq |\alpha_0| \leq 20°$

$0 \leq |\dot{\alpha}_0| \leq 3$ rad/sec

$\theta_0 \leq 10°$

$20' \leq |\Delta x| \leq 424'$

$0 \leq z_f \leq 4000'$

$\sigma(\Delta x) = 103.7'$

b. Fit Properties

$\sigma(\Delta x - \Delta R_x) = 35.8'$ (Unfitted)

$\sigma(\Delta x - \Delta R_x) = 25.2'$

$|\Delta x - \Delta R_x|_{max} = 130'$ (Unfitted)

$|\Delta x - \Delta R_x|_{max} = 107'$

$\sigma(\Delta y) = 2.5'$

$|\Delta y|_{max} = 9.2'$

$$(\Delta y - \dot{y}_0 t_f)/t_f = b_1\beta_0 + b_2\dot{\beta}_0 + b_3\beta_0\dot{\beta}_0 + t_f(b_4\beta_0 + a_5\dot{\beta}_0 + a_6\beta_0\dot{\beta}_0) \quad (9)$$

Statistical properties of the fit are given in Table Ib. The properties labeled unfitted use ΔR_x as an estimate for Δx. The constant aerodynamics chosen for ΔR_x are typical of M = 0.9 and $\alpha_T = 10°$.

3. Discussion of Computational Results

The curve fit computations give good results in the cross-range. Down-range fit results are only fair. For a more limited envelope the down-range fit is better. Shortcomings of the simple approach are delineated below.

(a) For a limited envelope and no rolling motion, accuracy is only fair.
(b) For a good part of a trajectory, the drag due to angular motion is larger than the zero yaw drag, i.e., perturbation terms are larger than first-order terms.
(c) The extension of the method to rolling motion involves an estimate of the roll history and two sets of λ and ω. Significant differences in down-range and cross-range can occur for the loft case. Accuracy of an approximate method is expected to be worse than for the nonrolling case.
(d) Worst cases seem to be for large amplitude initial motion. Nonlinear aerodynamics are not modeled properly.

B. KRYLOV-BOGOLIUBOV AVERAGING APPROXIMATE INTEGRATION

1. Basic Equations and Numerical Approach

The formulation is based upon that used in the extensive work of C. H. Murphy (Reference 13). All aerodynamic coefficients are assumed to be quadratic in total angle of attack (see Nomenclature List and Equation 28 for details).

The basic equations with arc length as independent variable follow below.

$$V' = -\tilde{\rho}\tilde{C}_D V - \frac{gz'}{V} \quad (10)$$

$$z'' = \tilde{\rho}\tilde{C}_{L\alpha} \sin\alpha\cos\beta(1 - z'^2)^{1/2} - g/V^2(1 - z'^2) \quad (11)$$

$$y'' = -\tilde{\rho}\tilde{C}_{L\alpha} \sin\beta + g/V^2 y'z' \quad (12)$$

The complex equation of motion for the angle-of-attack vector is given by

$$\xi'' + (H - \gamma'/\gamma - iP)\xi' - (M + iPT)\xi = G \tag{13}$$

An approximate solution is given by the use of the epicyclic approximation plus slowly varying spin-gravity trim.

$$\xi = \xi_g + K_1 e^{i\phi_1} + K_2 e^{i\phi_2} = \sin\beta + i \sin\alpha \cos\beta \tag{14}$$

Note that the quasi-steady assumption, $\xi_g = -\delta_g$, is used since its contribution to $\sin\beta$ is very small for the low spin rate expected for stores ($p < 150$ rad/sec). ξ_g is also uncoupled from all other nonlinear aerodynamic relations. The case of strong coupling between gravity trim and the epicyclic is analyzed in an approximate manner in Reference 4.

Substitution of (14) into (13) and using the averaging method of Krylov-Bogoliubov (Reference 13) leads to expressions for the ω's and λ's (neglecting terms of order λ^2/ω^2) as follows below.

$$\begin{aligned} \omega_{10} &= P/2 + [P^2/4 - M_0 - M_2(K_1^2 + 2K_2^2)]^{1/2} \\ \omega_{20} &= P/2 - [P^2/4 - M_0 - M_2(2K_1^2 + K_2^2)]^{1/2} \end{aligned} \tag{15}$$

A correction for γ'/γ (about 5%) may be made by utilizing a perturbation approximation.

$$\begin{aligned} \omega_1 &= \omega_{10} - \frac{\omega_{20}}{\omega_{10}} \frac{(\omega_{10} - \omega_{20})K_2^2}{2(2 - P/\omega_{10})} \\ \omega_2 &= \omega_{20} + \frac{\omega_{10}}{\omega_{20}} \frac{(\omega_{10} - \omega_{20})K_1^2}{2(2 - P/\omega_{20})} \end{aligned} \tag{16}$$

For the λ's one obtains

$$\begin{aligned} &-\frac{2(K_1^2\lambda_1 + 2K_2^2\lambda_2)}{\omega_1^2(2 - P/\omega_1)} + \lambda_1(2 - P/\omega_1) = -H_0 \\ &-H_2(K_1^2 + K_2^2 + K_2^2\omega_2/\omega_1) + \frac{P}{\omega_1}[T_0 + T_2(K_1^2 + 2K_2^2)] \end{aligned}$$

$$-\frac{2(2K_1^2\lambda_1 + K_2^2\lambda_2)}{\omega_2^2(2 - P/\omega_2)} + \lambda_2(2 - P/\omega_2) = -H_0$$

$$-H_2(K_1^2 + K_2^2 + K_1^2\omega_1/\omega_2) + \frac{P}{\omega_2}[T_0 + T_2(2K_1^2 + K_2^2)] \qquad (17)$$

Finally, the roll equation must be integrated

$$P' = \tilde{\rho}[PC^*_{\ell p} + C^*_{\ell\delta}] + \frac{P_g z'}{V^2} \qquad (18)$$

The set of equations (10-18) together with initial conditions and target altitude constitute the initial value problem. It is proposed that these equations be integrated by a second-order numerical integration technique. The numerical technique is related to a second-order Runga-Kutta, but retains terms like $\sin\phi$, etc., in trigonometric form.

First, the initial value starting conditions must be matched to the epicyclic.

$$\xi_0 = \sin\beta_0 + i\sin\alpha_0\cos\beta_0 = K_{10}e^{i\phi_{10}} + K_{20}e^{i\phi_{20}}$$

$$\xi_0' = \cos\beta_0\beta_0' + i(\gamma_0\alpha_0' - \sin\alpha_0\sin\beta_0\beta_0')$$

$$= K_{10}(\lambda_{10} + i\omega_{10})e^{i\phi_{10}} + K_{20}(\lambda_{20} + i\omega_{20})e^{i\phi_{20}} \qquad (19)$$

If terms of order $(\lambda/\omega)^2$ are neglected, from (19) one can obtain

$$K_{10}^2 = \frac{(a_1\omega_{20}^2 + a_2 + a_3\omega_{20} - a_4\lambda_{10})}{(\omega_{10} - \omega_{20})^2}$$

$$K_{20}^2 = \frac{(a_1\omega_{10}^2 + a_2 + a_3\omega_{10} - a_4\lambda_{20})}{(\omega_{10} - \omega_{20})^2}$$

$$a_1 = 1 - \gamma_0^2$$

$$a_2 = (1 - \sin^2\beta_0\cos^2\alpha_0)\beta_0'^2 + \alpha_0'(\gamma_0^2\alpha_0' - 2\gamma_0\sin\alpha_0\sin\beta_0\beta_0')$$

$$a_3 = 2(\sin\alpha_0\beta_0' - \gamma_0\sin\beta_0\alpha_0')$$

$$a_4 = 2\gamma_0(\sin\beta_0\cos\alpha_0\beta_0' + \sin\alpha_0\cos\beta_0\alpha_0') \qquad (20)$$

For linear aerodynamics, λ_1, λ_2, ω_1, ω_2 are independent of amplitude. For the nonlinear case, an iterative solution with a linear first estimate converges to a desired accuracy fairly rapidly. Subsequently, one can compute the initial phases, ϕ_1 and ϕ_2.

The aerodynamic coefficients are also expanded in powers in Mach number as well as total angle of attack, α_T. The oscillating parts of $\sin^2 \alpha_T$ in $\tilde{C}_D$, $\tilde{C}_{L\alpha}$, $C^*_{\ell p}$, and $C^*_{\ell \delta}$ are neglected. Least-squares curve fits are used to obtain all coefficients.

The numerical scheme is outlined below. First, an estimate of the various functions is made for $s_i < s < s_i + h$.

$$V = -\left[\tilde{\rho}_i \tilde{C}_{Di} V_i + \frac{g\, z'_i}{V_i}\right](s - s_i) + V_i$$

$$= V_i + V'_i(s - s_i)$$

$$z' = \tilde{\rho}_i \tilde{C}_{L\alpha i}(1 - z'^2_i)^{1/2}\left[\frac{K_{1i}}{\omega_{1i}}(\cos\phi_{1i} - \cos\phi_1) + \frac{K_{2i}}{\omega_{2i}}(\cos\phi_{2i} - \cos\phi_2)\right] - g/V_i^2(1 - z'^2_i)(s - s_i) + z'_i$$

$$\phi_1 = \phi_{1i} + \omega_{1i}(s - s_i)$$

$$\phi_2 = \phi_{2i} + \omega_{2i}(s - s_i)$$

$$K_1 = K_{1i} e^{\lambda_{1i}(s - s_i)}$$

$$K_2 = K_{2i} e^{\lambda_{2i}(s - s_i)}$$

$$y' = -\tilde{\rho}_i \tilde{C}_{L\alpha i}\left[-\delta_{gi}(s - s_i) + \frac{K_{1i}}{\omega_{1i}}(\sin\phi_1 - \sin\phi_{1i}) + \frac{K_{2i}}{\omega^2_i}(\sin\phi_2 - \sin\phi_{2i})\right] + \frac{g}{V_i^2} y'_i z'_i (s - s_i) + y'_i \qquad (21)$$

First estimates for all these functions at the end of the interval are obtained by setting $s - s_i = h$. The quantities are indicated by an overbar.

Final estimates of z, y, P, t, and x at the end of the integration interval may be made by integrating first order estimates of z', y', P', $(dt/ds) = 1/V$, and $(dx/ds) = (1 - z'^2)^{1/2}$.

$$
\begin{aligned}
z_{i+1} &= z_i + \tilde{\rho}_i \tilde{C}_{L\alpha i}(1 - z_i'^2)^{1/2}\left\{\frac{K_{1i}}{\omega_{1i}}\left[h\cos\phi_{1i} - \frac{1}{\omega_{1i}}(\sin\bar{\phi}_1 - \sin\phi_{1i})\right] + \frac{K_{2i}}{\omega_{2i}}\left[h\cos\phi_{2i} - \frac{1}{\omega_{2i}}(\sin\bar{\phi}_2 - \sin\phi_{2i})\right]\right\} - \frac{g}{V_i^2}(1 - z_i'^2)\frac{h^2}{2} + z_i'h \\
y_{i+1} &= y_i - \tilde{\rho}_i \tilde{C}_{L\alpha i}\left\{-\frac{\delta_{gi}h^2}{2} + \frac{K_{1i}}{\omega_{1i}}\left[\frac{1}{\omega_{1i}}(\cos\phi_{1i} - \cos\bar{\phi}_1) - h\sin\phi_{1i}\right] + \frac{K_{2i}}{\omega_{2i}}\left[\frac{1}{\omega_{2i}}(\cos\phi_{2i} - \cos\bar{\phi}_2) - h\sin\phi_{2i}\right]\right\} + \frac{g}{V_i^2}y_i'z_i'\frac{h^2}{2} + y_i'h \\
P_{i+1} &= P_i + h\left[P_i' + \frac{g\,z_i'h}{2V_i^2}\left(P_i' - \frac{2V_i'P_i}{V_i}\right)\right] + \frac{P_i g}{V_i^2}(z_{i+1} - z_i - z_i'h) \\
t_{i+1} &= t_i + \frac{h}{V_i}\left(1 - \frac{hV_i'}{V_i}\right) \\
x_{i+1} &= x_i + x_i'\left[1 - \frac{z_i'}{1 - z_i'^2}(z_{i+1} - z_i - z_i'h)\right]
\end{aligned}
\tag{22}
$$

Values of $\tilde{\rho}$ and the speed of sound, c, at the end of the interval for the estimate and the final value are based on z_{i+1} above. The Mach number dependencies of all aerodynamic data, except C_D, are not estimated at the end of the interval (bar quantities). The amplitude dependencies are updated. Not updated are λ_1, λ_2, ω_1 and ω_2 (bar quantities).

It is convenient to introduce the notation $Z = \tilde{\rho}\tilde{C}_{L\alpha}(1 - z'^2)^{1/2}$, $Z_1 = ZK_1$, $Z_2 = ZK_2$, $Y = -\tilde{\rho}\tilde{C}_{L\alpha}$, $Y_1 = YK_1$, $Y_2 = YK_2$, and $\Delta = \tilde{\rho}\tilde{C}_{L\alpha}\delta g$. Final values of the derivatives are given as

$$
\begin{aligned}
z_{i+1}' &= \bar{z}' + \frac{\bar{Z}_1 - Z_{1i}}{h\omega_{1i}}\left[-h\cos\bar{\phi}_1 + \frac{(\sin\bar{\phi}_1 - \sin\phi_{1i})}{\omega_{1i}}\right] \\
&\quad + \frac{\bar{Z}_2 - Z_{2i}}{h\omega_{2i}}\left[-h\cos\bar{\phi}_2 + \frac{(\sin\bar{\phi}_2 - \sin\phi_{2i})}{\omega_{2i}}\right] \\
&\quad + \frac{g}{V_i^2}(1 - z_i'^2)\frac{V_i'}{V_i}h^2 + \frac{2g}{V_i^2}z_i'(z_{i+1} - z_i - z_i'h)
\end{aligned}
$$

$$y'_{i+1} = \bar{y}' + (\bar{\Delta} - \Delta_i)\frac{h}{2} + \frac{\bar{Y}_1 - Y_{1i}}{h\omega_{1i}}\left[h \sin \bar{\phi}_1 + \frac{(\cos \bar{\phi}_1 - \cos \phi_{1i})}{\omega_{1i}}\right] + \frac{\bar{Y}_2 - Y_{2i}}{h\omega_{2i}}\left[h \sin \bar{\phi}_2 + \frac{(\cos \phi_2 - \cos \phi_{2i})}{\omega_{2i}}\right] + \frac{g}{V_i^2}\left[\frac{-y'_i z'_i V'_i h^2}{V_i} + y'_i(z_{i+1} - z_i - z'_i h) + z'_i(y_{i+1} - y_i - y'_i h)\right] \tag{23}$$

If the lift terms could be neglected, these integration relations would essentially be identical with a second-order Runga-Kutta scheme. Equations 15-17 are utilized to update ω_1, λ_1, ω_2, λ_2. Finally, the amplitudes and phases are updated as

$$\begin{aligned} K_{1i+1} &= K_{1i} e^{h(\lambda_{1i} + \lambda_{1i+1})/2} \\ K_{2i+1} &= K_{2i} e^{h(\lambda_{2i} + \lambda_{2i+1})/2} \\ \phi_{1i+1} &= \phi_{1i} + \frac{h}{2}(\omega_{1i+1} + \omega_{1i}) \\ \phi_{2i+1} &= \phi_{2i} + \frac{h}{2}(\omega_{2i+1} + \omega_{2i}) \end{aligned} \tag{24}$$

The choice of step length is based upon an estimate of truncation error of $O(h^3)$. Third derivatives for z and x are estimated as

$$\begin{aligned} z'''_i &\approx \frac{2g}{V_i^3}(1 - z_i'^2)\left(V_i - \frac{g z'_i}{V_i}\right) - \frac{z'_i}{1 - z_i^2}\frac{(Z_{1i}^2 + Z_{2i}^2)}{2} \\ z''^2_i &\approx \left[\frac{g}{V_i^2}(1 - z_i'^2)\right]^2 + \frac{Z_{1i}^2 + Z_{2i}^2}{2} \\ x'''_i &\approx -\frac{1}{x'_i}[(z''_i/x'_i)^2 + z'_i z'''_i] \end{aligned} \tag{25}$$

If ϵ_i = a desired accuracy in length (i.e., truncation error), then the step length is computed as

If $|z'/x'| < 1$,

$$h = \left(\frac{6\epsilon_1}{|x_i'''|} \right)^{1/3} \tag{26}$$

If $|z'/x'| > 1$,

$$h = \left(\frac{6\epsilon_1}{|z_i'''|} \right)^{1/3} \tag{27}$$

These are not computed for every integration step.

In the early part of the trajectory, nonlinear aerodynamics are required. As the angular motion decays, reversion to linear aerodynamics is taken advantage of (by numerical test). Finally, when the yaw drag is small compared to zero yaw drag, reversion to particle motion or particle motion with steady-state gravity trim is made (again by numerical test). In the final stage, the accuracy requirement is changed to ϵ_2, a larger value.

2. Applied Computations

The above formulation was programmed for the CDC 6700 system with general input variables. Selected computations were made for the MK-82 bomb and compared with 5-DOF computations. The aerodynamic functions $\frac{C_D - C_{D0}}{\sin^2 \alpha_T}$, $\hat{M}$, $\hat{H}$, $\hat{C}_{\ell p}$, and $\hat{C}_{\ell \delta}$ were fitted to the following form

$$X = a_0 + a_1(M - M_0) + a_2(M - M_0)^2 + \sin^2\alpha_T [b_0 + b_1(M - M_0) + b_2(M - M_0)^2] \tag{28}$$

where M_0 = reference Mach number. C_{D0} was fitted as a polynomial in Mach number.

A number of computations are listed in Tables II and III with large disturbance inputs to test the numerical technique. Computations were for a standard atmosphere. All target levels were at sea level. All computations were made with an initial assumed truncation accuracy of 0.1 foot. For the nonoscillatory (particle) part of the trajectory the accuracy requirement was set at 1 foot.

3. Discussion of Results

In general, the computational results are in excellent agreement with 5 and 6-DOF computations. It must be kept in mind that there are also some computational error sources in the usual fourth-order Runge-Kutta computations.

TABLE II MK-82 EPICYCLIC COMPUTATION COMPARISON WITH 5-DOF

z_0 (ft) $\dot{\beta}_0$ (rad/sec)	V_0 (ft/sec) x_f (ft)	z'_0 $x_f^{(a)}$ (ft)	$\dot{y}_0$ (ft/sec) t_f (sec)	p_0 (rad/sec) $t_f^{(a)}$ (sec)	α_0 (deg) y_f (ft)	$\dot{\alpha}_0$ (rad/sec) $y_f^{(a)}$ (ft)	β_0 (deg) $\Delta z^{(b)}$
[c]5000	506.3	-0.5001	10		-.30	1.986	10
-0.880	4911	4924	11.68	11.66			-81
[c]9855	513.3	-0.5171	-0.63		-1.617	-1.827	-0.831
-0.907	7696	7696	17.99	18.00			-117
[d]4986	744.8	-0.3720	-13.22		-15.37	-2.059	-3.362
-1.282	12117	12118	16.79	16.80	-185	-184	-307
[c]10000	759.5	0.0	0.0		0.0	2.042	-2.0
-0.996	18609	18617	25.26	25.28			-130
[c]5000	759.5	0.5000	0.0		0.0	2.037	-10
1.020	20900	20938	32.86	32.92	-	-	-393
[d]10361	731.3	0.4730	11.54	-4.134	0.495	-2.997	-4.422
0.495	23551	23572	38.02	38.04	402	404	-739
[c]5000	1012.7	0.0	6.0		0.0	2.032	4.0
1.014	17226	17255	18.06	18.08			55

[a]5-DOF value.

[b]Δx = x(5-DOF) - x (particle).

[c]No out-of-plane approximate computation was made.

[d]Out-of-plane computation made.

TABLE III MK-82 EPICYCLIC COMPUTATION COMPARISON WITH 6 DOF

z_0 (ft) $\dot{\beta}_0$ (rad/sec)	V_0 (ft/sec) x_f (ft)	z'_0 $x_f^{(a)}$	$\dot{y}_0$ (ft/sec) t_f (sec)	p_0 (rad/sec) $t_f^{(a)}$	α_0 (deg) y_f (ft)	$\dot{\alpha}_0$ (rad/sec) $y_f^{(a)}$	β_0 (deg) $\Delta x^{(b)}$
10000	506.3	-.5000	2.0	0.0	0.0	2.055	0.0
1.0	7933	7941	18.54	18.56	11.2	5.6	-48
4986	744.8	-.057	-13.00	5.50	-15.39	2.155	-2.770
-1.079	12117	12122	16.78	16.80	-197	-194	-275
10000	759.5	0.0	0.0	0.0	0.0	2.042	-2
-.996	18601	18617	25.25	25.28	5.2	15.2	-121
5000	759.2	.5000	0.0	0.0	0.0	2.037	-10
1.020	20908	20955	32.86	32.93	-75.8	-96.9	-361
10361	737.2	.4729	11.8	4.63	-4.490	-2.974	-4.607
.668	23470	23501	38.01	38.03	337	341	-789
5000	1012.7	0.0	6.0	0.0	0.0	2.032	-4
1.014	17220	17255	18.05	18.08	62.5	64.7	55

(a) 6-DOF computations.

(b) Δx = x(6-DOF) - x (particle).

The most important feature of the approximate method are the short computation times. For a typical nonrolling computation, the approximate computation time is approximately 1/40 that of a 5-DOF computation and less compared to a 6-DOF computation. A time step size for the approximate computation is typically 30 times as long as a 5 or 6-DOF time step size for the large amplitude motion phase. The rapid computation time is due entirely to the retention of rapidly varying trigonometric functions in the numerical computation.

CONCLUDING REMARKS

Two different computational techniques for the prediction of the decay of store angular disturbances have been presented.

The perturbation technique allows short computational times, but seems to sacrifice too much accuracy. The MK-82 fit envelope results presented in Table I show adequate accuracy for cross-range estimates but much poorer results for down-range estimates. A measure of the adequacy of down-range prediction is the comparison of $\sigma(\Delta x)$ with $\sigma(\Delta x - \Delta R_x)$. If, by the combination of store aerodynamic design, good aircraft flow-field environment, and adaptable ejection, the store separation disturbance is reduced to an acceptable low level, then the perturbation technique holds some promise for adaption to present fire-control algorithms; perhaps the former will render the latter moot.

The second technique, based on a piecewise application of the epicyclic averaging method, seems to represent an important contribution to rapid, accurate computation techniques. Tables II and III give a comparison with 5-DOF and 6-DOF computations. The computations shown are, in general, for more severe initial disturbances and longer trajectories; Table III computations are for the case with roll. Computation times are of the order of 1/40 or less compared to 5-DOF or 6-DOF computation times. However, CDC 6400 (CDC 6700 times are quoted in equivalent CDC 6400 time) computation times are still of the order of 0.500 second. This computational time is much longer than for the perturbation method, which is probably about twice as long as a particle computation. Trajectory computation time for the epicyclic method should be reduced to 0.100 second or less to be adaptable for the purpose declared here.

One of the difficulties in store design for ballistic accuracy is the unavailability of aerodynamic characteristics. Reference 15 presents a possible instrumentation package which should be available for all major store drop programs. Free-flight aerodynamic data may be extracted by using the fitting techniques of Reference 16. An alternative approach would use a package containing a yawsonde (Reference 17).

REFERENCES

1. Barker, R. G., C. H. Frick, and L. J. McAnelly, A Method for Determining Drag Coefficients From Observed Position Data, Naval Weapons Laboratory, TR-2291, April 1970.

2. Reagan, J. F., Exterior Ballistic Analysis of General Purpose Bomb MARK-84 Assembled With 14-Inch Suspension Adapter, Naval Weapons Laboratory, TR-2472, October 1970.

3. Goodale, P. L., A Theoretical Study of the Flight Dynamics and Ballistic Consistency of a Research Bomb Having Cruciform Fins and Low Static Stability, Weapons Research Establishment (Australia) Technical Note ASA 117, June 1966.

4. Maestri, R. R., and L. H. Schindel, Self-Compensating Store Ejection, Naval Ordnance Laboratory NOL TR 74-32, February 1974.

5. Sun, J., "A Study of Variable Orifice Controlled Weapons Launching," 10th Navy Symposium on Aeroballistics, July 1975.

6. Maddox, A. R., "Parametric/Sensitivity Study of Store Separation," Aircraft/Stores Compatibility Symposium Proceedings, JTCG/ALNNO, WP-12-2, Vol. 3, pp 105-133, Sacramento Air Material Area/Air Force Logistics Command, September 1973.

7. Devan, L., An Estimate of the Effect of Multiple Ejection Rack Flexibility on Six-Degree-of-Freedom Store Ejection Conditions, Naval Weapons Laboratory TR-3252, March 1975.

8. Ausman, J., Modeling Aerodynamic Release Disturbances in Weapon Delivery Systems, Litton ARIS File Memo 8.3.7, August 1973.

9. Ausman, J., Computation and Calibration of Bomb Separation Jump Velocity, Litton ARIS File Memo 8.3.19, April 1974.

10. Piper, W. D., and F. J. DeMeritte, Summary of the NOL Investigations to Date of the Aerodynamic Characteristics of the Navy Low Drag Bomb, NAVORD Report 5679, February 1970.

11. Schermerhorn, V. L., and F. J. DeMeritte, Wind Tunnel Tests of the Navy Low-Drag Bomb at Angles of Attack up to 70 Degrees, NAVWEPS Report 7291, March 1961.

12. Regan, F. J., J. E. Holmes, and M. E. Falusi, Magnus Measurements on the M823 Research Store With Fixed and Freely Spinning Cruciform Stabilizer, Freely Spinning Monoplane Stabilizers and Split Skirt Stabilizers, NOL TR-69-214, November 1969.

13. Murphy, C. H., Free-Flight Motion of Symmetric Missiles, Ballistic Research Laboratory Report 1216, July 1963.

14. Murphy, C. H., "Gravity-Induced Angular Motion of a Spinning Missile," Journal of Spacecraft and Rockets, Vol. 8, No. 8, August 1971.

15. Gilbert, N. E., The Use of Rate Gyroscopes in the Free-Flight Measurement of Aerodynamic Lateral Force and Moment Coefficients, Weapons Research Establishment (Australia) Technical Note HSA 164, March 1970.

16. Chapman, G. T. and D. B. Kirk, "A Method for Extracting Aerodynamic Coefficients From Free-Flight Data," AIAA Journal, Vol. 8, No. 4, April 1970.

17. Whyte, R. H. and W. H. Mermagen, A Method for Obtaining Aerodynamic Coefficients from Yawsonde and Radar Data, Ballistic Research Laboratories Report No. 2280, March 1973.

AUTOBIOGRAPHY

Dr. Devan received his B.S., M.S., and Ph.D. in Engineering (Mechanics) from the University of California at Los Angeles. He held employment positions at McDonnell Aircraft Corporation (St. Louis) in the area of structures; at North American Aviation Inc., (Los Angeles) in the area of aeroelasticity; and at the University of Kansas as Assistant Professor of Aerospace Engineering. He has been at the Naval Surface Weapons Center, Dahlgren Laboratory, since 1969 and has worked in the areas of shock propagation, fire control aeroballistics, and store separation.

F-14/AIM-54 PHOENIX MISSILE SEPARATION PROGRAM

(U)

(Article UNCLASSIFIED)

by

Charles Dragowitz and Ralph Johnson
Grumman Aerospace Corporation
Bethpage, New York 11714

ABSTRACT. (U)

This paper presents an overview of the theoretical analysis performed by Grumman to establish separation compatibility between the F-14 Tomcat fighter and the AIM-54 Phoenix missile, with examples of analytical correlation with flight test results. The success of the correlation was good, leading to use of the analysis to reduce flight testing in the establishment of the final F-14/Phoenix launch and jettison envelopes. It also highlights significant F-14/AWG-9/ Phoenix weapon system capabilities which have been demonstrated to date.

"Approved for public release; distribution unlimited."

LIST OF FIGURES

Figure	Title
1	F-14 Six Phoenix Configuration
2	Separation Envelope
3	F-14 AIM-54 Phoenix Proposed Flight Test Drop 5* Station 4
4	F-14 Station 3 AIM-54 Phoenix Jettison Flight 230 Correlation Results
5	F-14 AIM-54 Phoenix Proposed Flight Test Drop 3* Station 1
6	F-14 Station 5 AIM-54 Phoenix Launch Flight 66 Correlation Results
7	Foxbat Target
8	Multiple Targets
9	ECM Jammer Target
10	Low Altitude Target
11	Distant Target

LIST OF TABLES

Table	Title
I	Demonstrated Phoenix Missile Capabilities

INTRODUCTION

Today, F-14 squadrons are deployed with both the Atlantic and Pacific fleets, providing the Navy with a unique air superiority fighter capability. Development of this capability began with the F-111B program in 1961 when the AWG-9/Phoenix system entered engineering development. By 1967, performance analyses had revealed that the F-111B could not serve effectively as a Navy air superiority fighter in other than its fleet air defense role. Consequently, in 1968, it was decided that a new highly maneuverable airframe would be developed which could utilize the AWG-9/Phoenix weapon system and effectively perform the other air superiority fighter roles. In February 1969, the Navy contracted with the Grumman Aerospace Corporation for the development of the F-14 fighter. Starting at this date, the F-14/AWG-9/Phoenix weapon system compatibility and capabilities had to be demonstrated.

The purpose of this paper is to provide an overview of the F-14/AIM-54 Phoenix missile separation program and to highlight the demonstrated capabilities of the F-14/AWG-9/Phoenix weapon system. To this end, the separation analysis and subsequent correlation with flight test results will be discussed along with the specifically demonstrated detection and intercept capability of the AWG-9/AIM-54 system.

F-14/PHOENIX MISSILE SEPARATION PROGRAM

The F-14 aircraft carries six Phoenix missiles, figure 1, one on each of two glove pylons and one on each of four fuselage weapon rails. These fuselage mounted Phoenix are carried two abreast between the engine nacelles. The weapon rails provide a mechanical and electrical interface between the F-14 and the Phoenix.

At the beginning of the F-14 program, it was estimated, based upon F-111 experience, that thirty demonstration points would be required to successfully complete a separation flight test program. Actually, due to successful correlation between the analysis and flight testing, only thirteen separation test points were required. This substantially reduced F-14/Phoenix flight test program costs. Figure 2 presents the F-14 flight envelope for the Phoenix missile configuration. It also depicts the launch and jettison limits cleared by the F-14/Phoenix separation test program. Flight test test separation conditions, six launches and seven jettisons, are denoted to illustrate that the entire flight envelope was spanned by these points.

The F-14/Phoenix separation analysis was performed by utilizing Grumman's six-degree-of-freedom store separation analysis code. Store body axis equations of motion are integrated, rotated into inertial coordinates and then integrated again to provide the store inertial displacements. A simulation of the aircraft dynamics is also coded to provide the inertial displacement of the aircraft. The difference between the two provides the trajectory of the store relative to the aircraft.

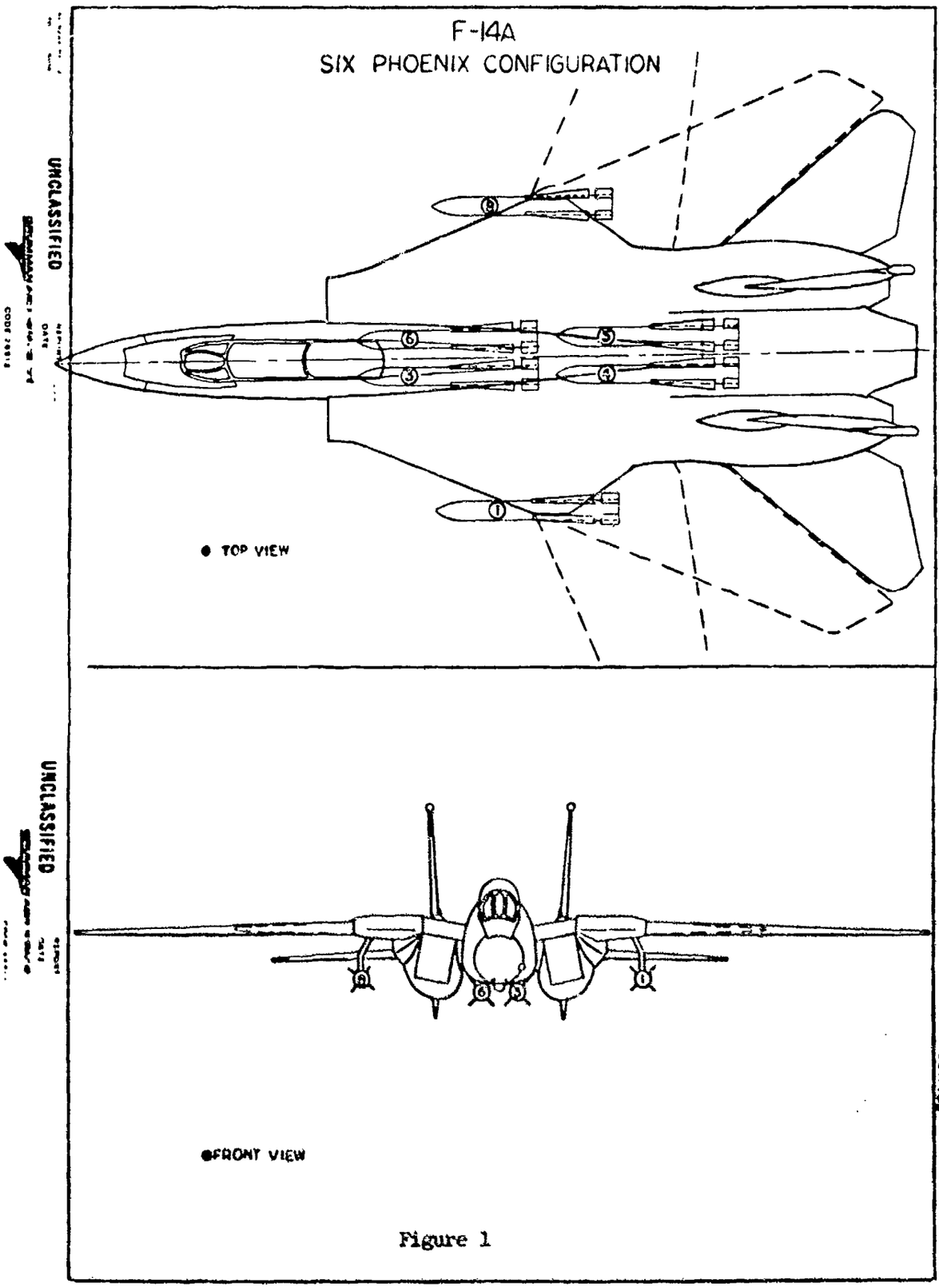

F-14A
SIX PHOENIX CONFIGURATION
UNCLASSIFIED
UNCLASSIFIED
● TOP VIEW
UNCLASSIFIED
UNCLASSIFIED
●FRONT VIEW

Figure 1

SYMBOLS

L-LAUNCH

J-JETTISON

NUMBERS DENOTE STATION

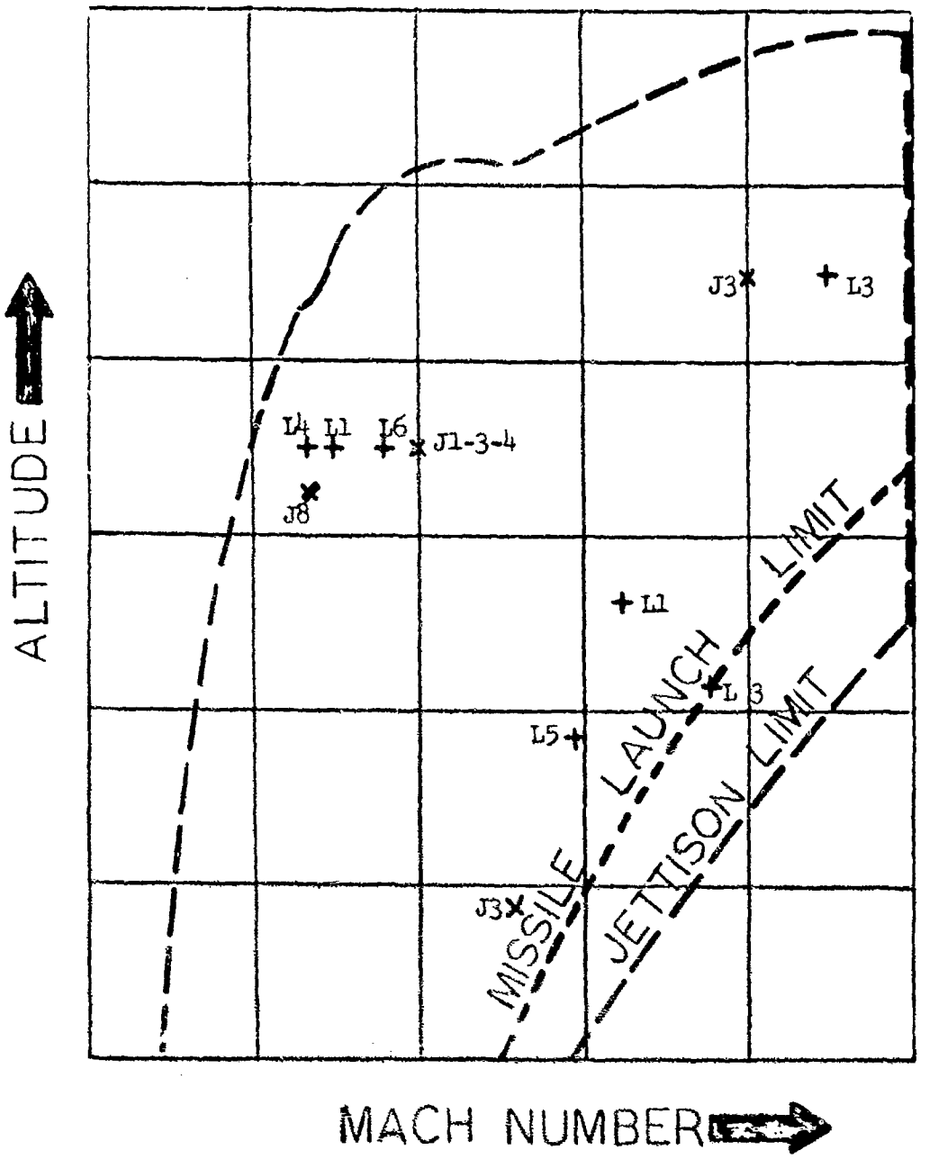


Figure 2 SEPARATION ENVELOPE

For the Phoenix, the control system characteristics were coded into the separation code. In addition, the separation code requires three general data sets for successful operation:

- Pertinent inertial and aerodynamic store characteristics including propulsive and control system effects and complete aircraft data for trajectory purposes.
- A description of the aircraft flowfield interference effects upon the store.
- Definition of the ejection/release mechanism.

The Phoenix characteristics were available from prior wind tunnel and flight testing performed by the Hughes Company. These data were modelled in detail as were the control system and thrust effects. The flowfield interference was modelled with two separate flowfields simulations, each of which was based upon F-14 wind tunnel test data. The first was a subsonic-transonic flowfield, obtained from yaw-head probe data, which mapped the flow angularities beneath the F-14 for the transonic Mach range. The second was a supersonic flowfield in which a metric sting mounted Phoenix was traversed beneath the F-14 to measure the forces and moments on the missile. For both simulations, the flowfield effect was coded as a function of fuselage station, butt line and waterline. At any point along the Phoenix trajectory, the effect of the flowfield is available for computational needs. In either case, these effects are superimposed upon the free air aerodynamic characteristics of the Phoenix. Finally, a detailed ejector simulation was modelled which imparted the proper energy level to the Phoenix and represented the aerodynamic-gas dynamic interaction which occurs during the ejection sequence.

The linearization of the flowfield with the free air effects, as described in the foregoing, are particularly noteworthy in the simplification of coding for analysis, low cost of analysis and high quality of results which it produces. The simplification occurs because each effect can be coded as a function of parameters pertinent to each, rather than to both (i.e. position for the flowfield versus angle of attack for freestream data). Costs are reduced because the freestream and flowfield are each measured or calculated once, not every time a trajectory is calculated. Finally, the quality of predicted results can be improved by spending more effort in obtaining both of the components. For the F-14 further simplifications were realized during the coding of the flowfield as a result of this methodology. Separate handling of the flowfield enabled common trends over a range of Mach numbers to be discerned. One basic flow model was therefore able to be used for supersonic Mach numbers with adjustments in magnitudes and location. With minor, empirically derived, modifications, this flow model provided excellent correlation when used in separation analyses.

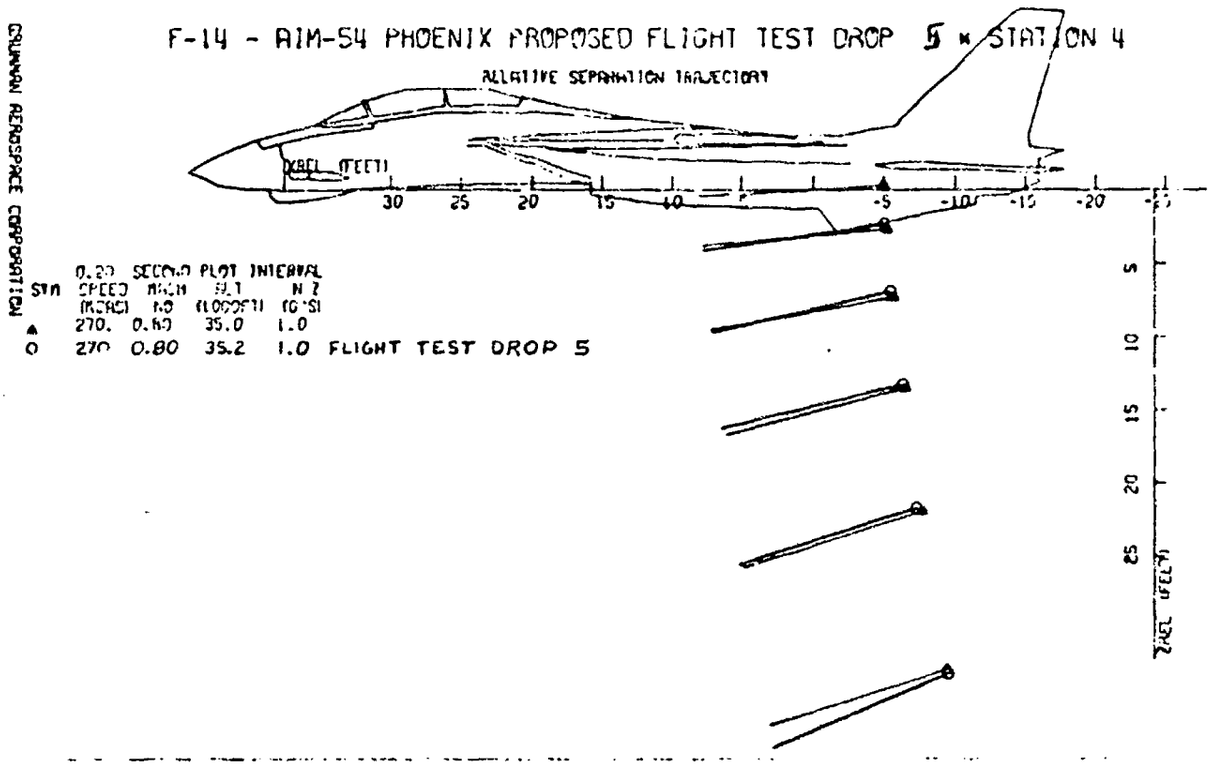
Examples of the quality of correlation obtained between the predictive separation analysis and flight test results are presented in figures 3 through 6. Side and front views of the aircraft are shown with the missile centerline representing the trajectory at 0.2

second time intervals after first motion. One launch and one jettison are presented for a subsonic and a supersonic flight condition. These illustrate typical problems in correlating analyses with flight test results. For jettisons, missile attitude is the predominant correlation problem. Figure 3 presents the predicted and flight test trajectories for a Phoenix jettison from station 4, the port aft channel F-14 store station. The analysis slightly underpredicted the nose down missile pitch. At high dynamic pressure supersonic conditions, greater discrepancy was observed in pitch and yaw while correlation in vertical and lateral displacement was very good. This is illustrated by the trajectories presented in figure 4 for a supersonic jettison of a Phoenix from station 3, the port forward channel F-14 store station.

Launches, in comparison, showed excellent attitude agreement, principally as a result of control system stabilization of the Phoenix. Thrust anomalies, however, produced substantial discrepancies between predicted and actual results. Figure 5 illustrates this by comparing the original prediction, the flight result and analytical trajectory generated at the specific flight conditions of a Phoenix launch from the port pylon F-14 station. The analysis contained a nominal thrust time history and rocket motor ignition time. As illustrated, there was a 50 ms (milliseconds) delay in motor ignition in the test. Matching this in the analysis produced excellent correlation for the first 800 ms. At approximately 750 ms, however, the test missile developed significantly greater than nominal thrust levels which resulted more rapid forward motion than the analysis would indicate. It should be noted that the analytical and test trajectories are almost identical with this exception.

An additional factor is the anomaly which occurred in ejector performance for this case. As shown, the original trajectory was predicted using an ejector produced velocity of 18 fps (feet per second) which represents nominal specified ejector performance. Correlation required a 14 fps velocity which matched the initial motion that was obtained in flight. For virtually all of the other test points, an 18 fps velocity level was required to correlate with flight. In the Phoenix program, early in the Sparrow program and during ground testing of the launchers for each missile, "soft shots" such as this were observed. The cause of this has been attributed to slow burning of the cartridges used to generate the gas to power the launchers.

Contrasting the foregoing, other launches resulted in nominal rocket motor and launcher performance. Figure 6 presents a supersonic Phoenix launch from store station 5 in the aft starboard channel. Correlation such as this and the three foregoing examples demonstrated that Grumman's six-degree-of-freedom store separation analysis code accurately predicted the trajectory of a Phoenix which was launched or jettisoned from the F-14. Once the analysis was substantiated by correlation, it was accepted for the purpose of establishing the limits of the F-14/AIM-54 Phoenix launch and jettison envelopes presented in figure 2. This reduced the scope of flight testing and costs substantially for this particular program and resulted in savings to the Navy as well as to the contractor.


F-14 - AIM-54 PHOENIX PROPOSED FLIGHT TEST DROP 5 w STATION 4
RELATIVE SEPARATION TRAJECTORY
GRUMMAN AEROSPACE CORPORATION
XREL (FEET)
30 25 20 15 10 5 -5 -10 -15 -20 -25
0.20 SECOND PLOT INTERVAL
STN SPEED MACH ALT N Z
(KCAS) NO (1000FT) (G'S)
▲ 270. 0.60 35.0 1.0
○ 270 0.80 35.2 1.0 FLIGHT TEST DROP 5
5 10 15 20 25
ZREL (FEET)

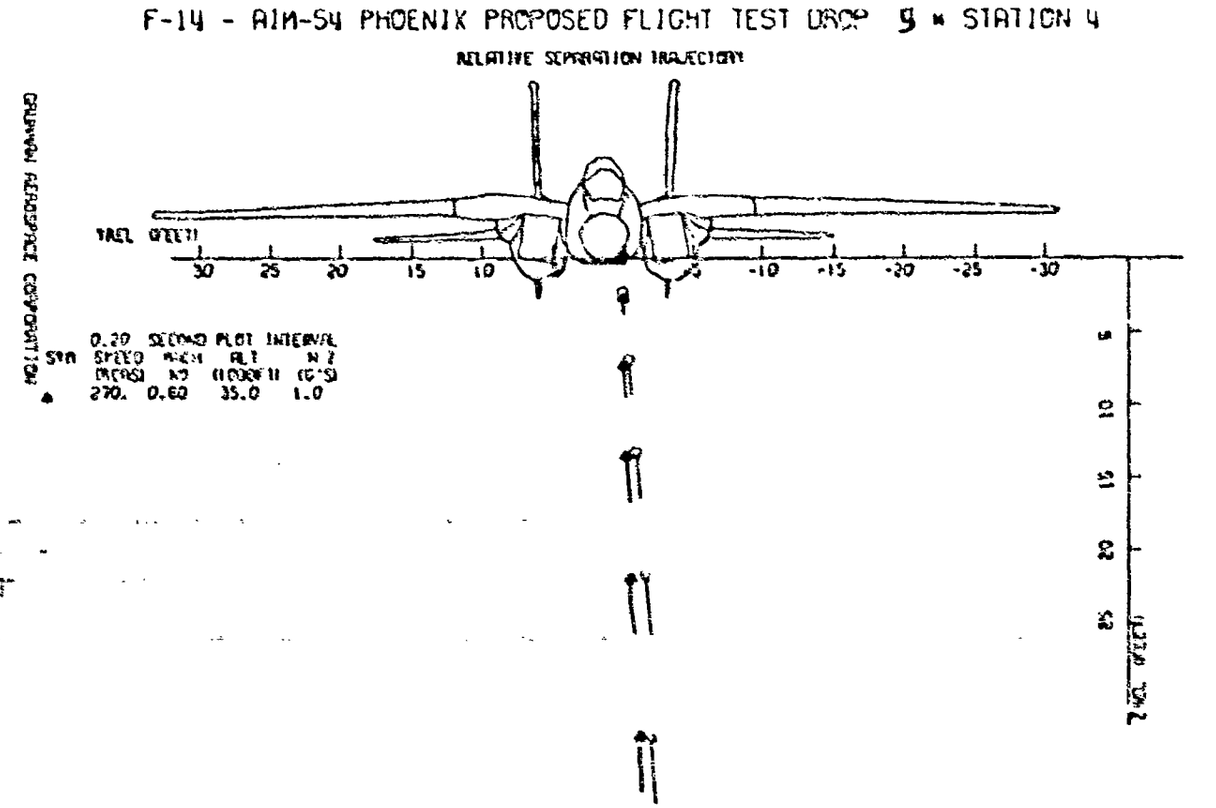
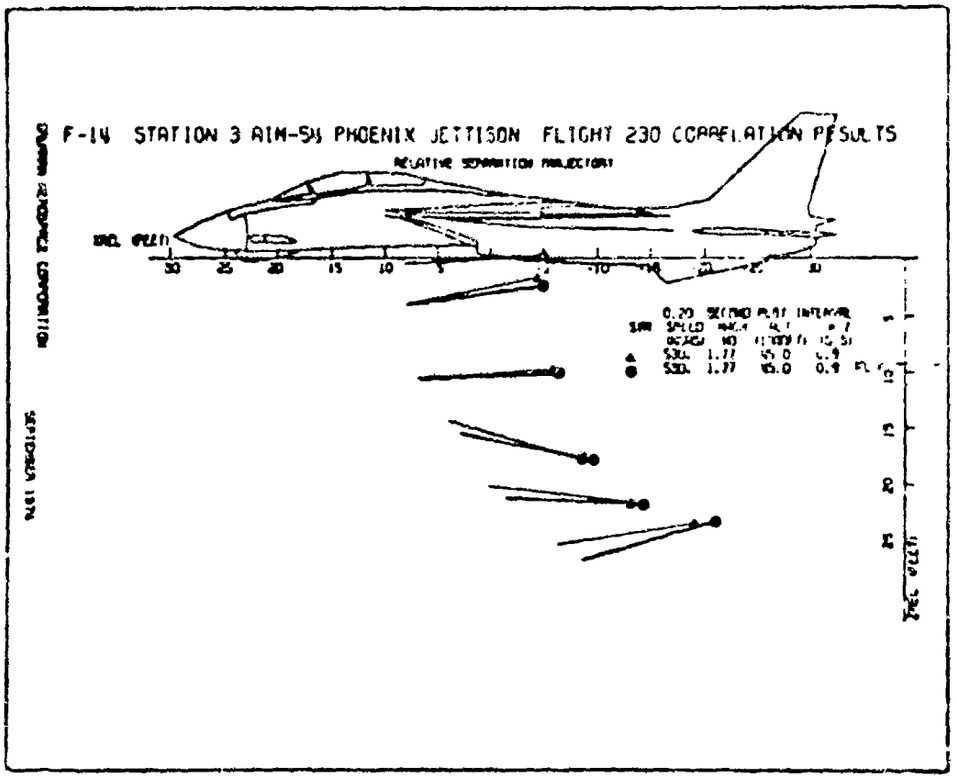

F-14 - AIM-54 PHOENIX PROPOSED FLIGHT TEST DROP 5 w STATION 4
RELATIVE SEPARATION TRAJECTORY
GRUMMAN AEROSPACE CORPORATION
YREL (FEET)
30 25 20 15 10 5 -5 -10 -15 -20 -25 -30
0.20 SECOND PLOT INTERVAL
STN SPEED MACH ALT N Z
(KCAS) NO (1000FT) (G'S)
▲ 270. 0.60 35.0 1.0
5 10 15 20 25
ZREL (FEET)

Figure 3


F-14 STATION 3 AIM-54 PHOENIX JETTISON FLIGHT 230 CORRELATION RESULTS

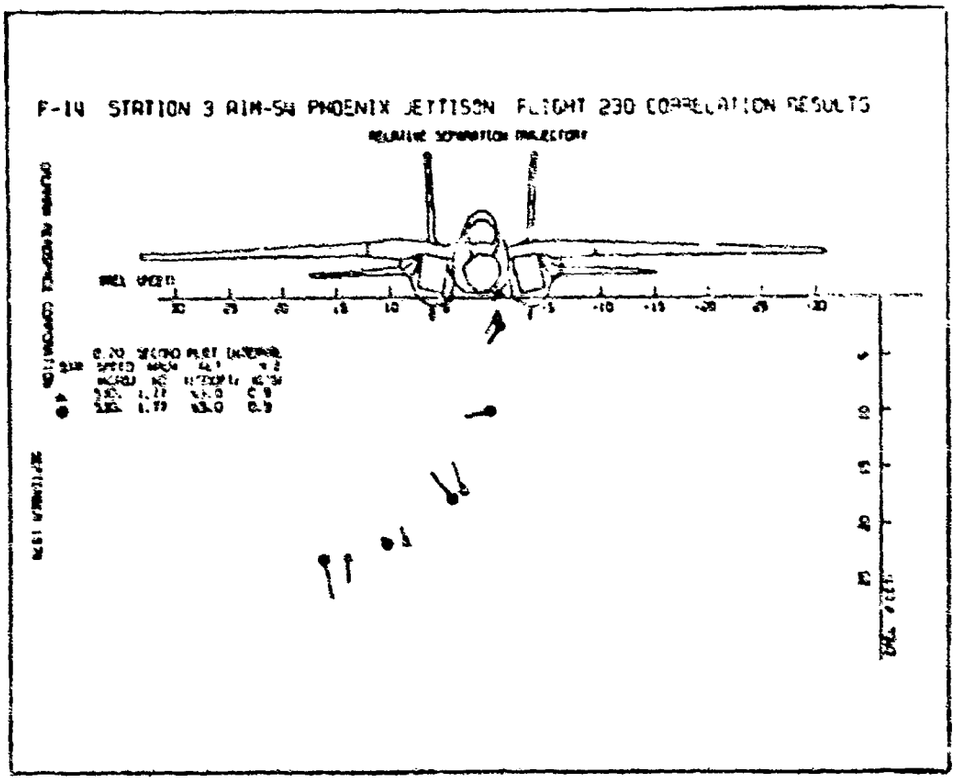
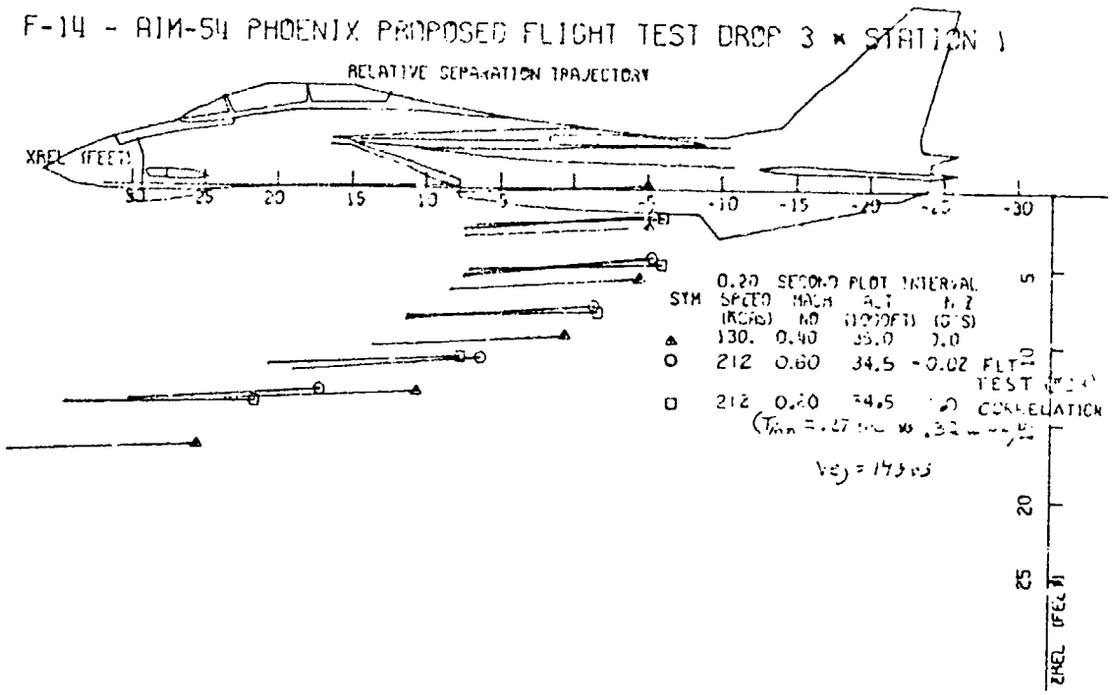

F-14 STATION 3 AIM-54 PHOENIX JETTISON FLIGHT 230 CORRELATION RESULTS

Figure 4



GRUMMAN AEROSPACE CORPORATION

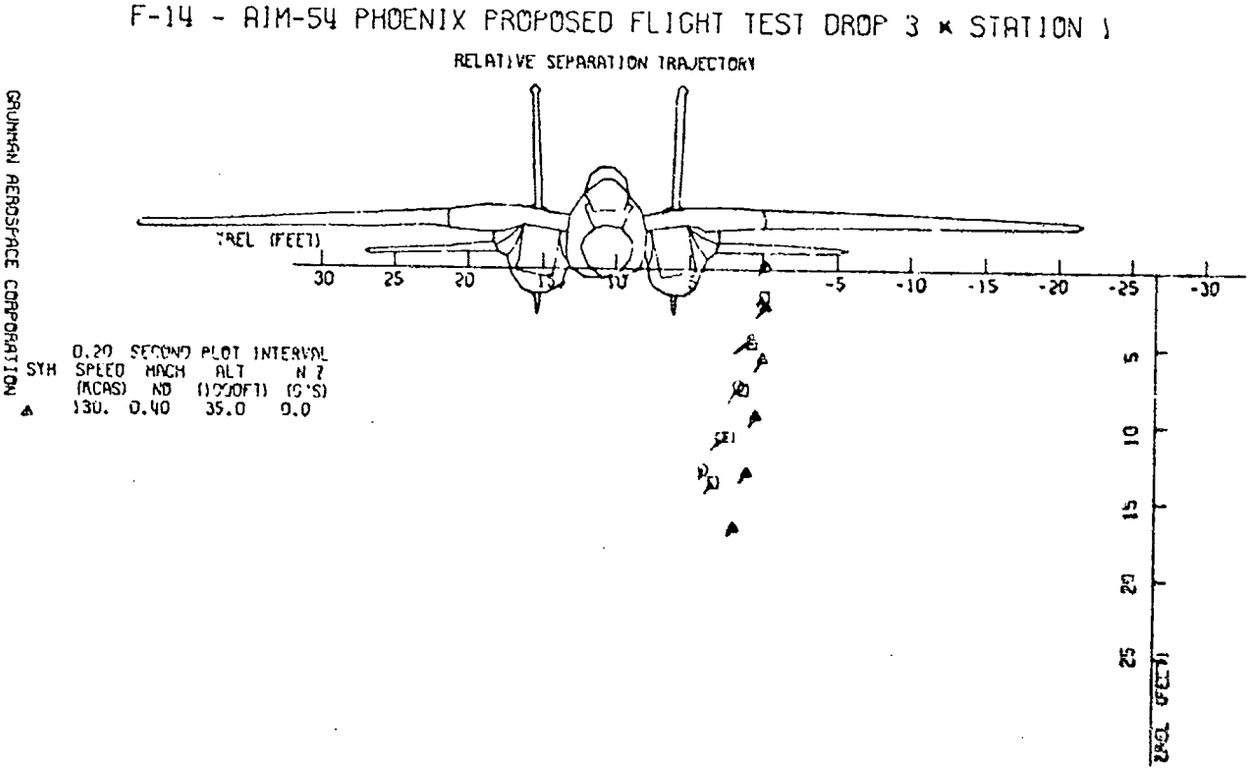
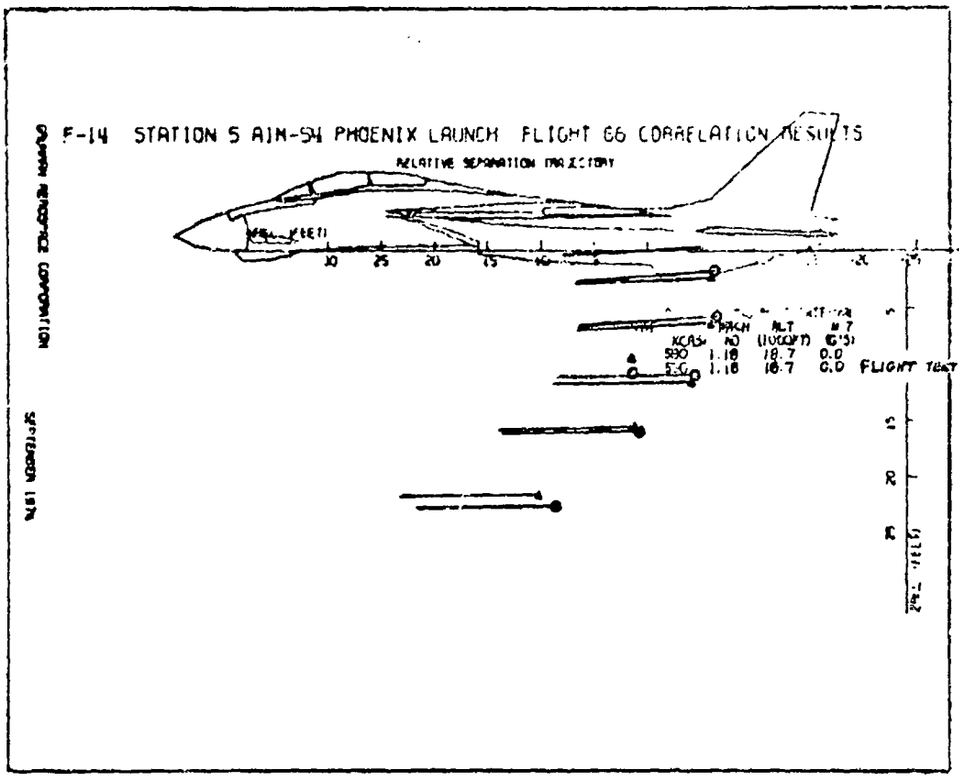


Figure 5


F-14 STATION 5 AIM-54 PHOENIX LAUNCH FLIGHT 66 CORRELATION RESULTS
RELATIVE SEPARATION TRAJECTORY
FLIGHT TEST

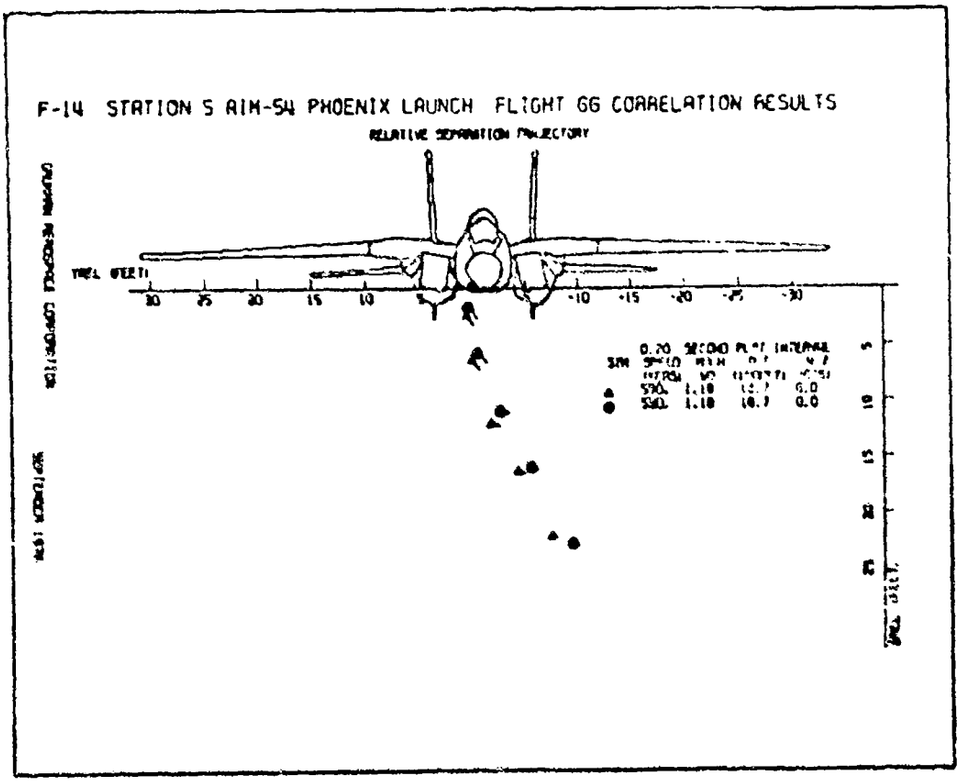

F-14 STATION 5 AIM-54 PHOENIX LAUNCH FLIGHT 66 CORRELATION RESULTS
RELATIVE SEPARATION TRAJECTORY

Figure 6

F-14/AWG-9/PHOENIX OPERATIONAL CAPABILITIES

The AWG-9/Phoenix weapon system forms the nucleus of the air superiority capabilities of the F-14. The AWG-9 radar provides large surveillance volume, long range detection and lookdown capabilities far in excess of that available with current fighter aircraft. Detection of fighter aircraft at any altitude can be made at ranges exceeding 100 nautical miles, more than double the current fighter capability. The AWG-9 is capable of tracking multiple targets and has simultaneously tracked 17 targets in flight and 24 targets in simulation. It can track and guide the F-14's six Phoenix missiles to six individual targets. The Phoenix missile is, by itself, an extremely effective weapon, being lethal against targets at launch ranges in excess of 50 nautical miles. The ability to detect, track and intercept targets at long range provides the F-14 with a unique capability. The F-14 can reduce the odds in a multiple threat environment with low risk and thereby employ its Sidewinder missiles and gun in close combat against a greatly reduced threat.

By the end of 1974, the Phoenix missile kill-success ratio was 0.78 (62 hits out of 80 launches) against a large variety of targets and environments. Table I summarizes the extremes under which the Phoenix has been employed in establishing this ratio.

TABLE I - DEMONSTRATED PHOENIX MISSILE CAPABILITIES

Simultaneous multiple launch and guidance
- 2 on 2, 4 on 4, 6 on 6

Unique threats
- 100 n. mile Backfire launch
- Low-altitude cruise missile
- Mach 2+, 82,000 ft Foxbats

Tactics
- Very low altitude targets
- ECM: Standoff and self-screening jammer
- Low-altitude shoot-up

Dogfights
- Evasively maneuvering target/launch during F-14 maneuvers
- Launch and leave during tail attack

Examples of some of the Phoenix missile launches that have been demonstrated are presented below:

FOXBAT THREAT

One of the primary missions for the F-14 is the interception of targets which fly at high speeds and high altitudes outside of the capabilities of other weapons systems. Figure 7 depicts one such mission demonstrated in flight. An augmented AQM-37A drone, simulating the radar cross section of a MIG-25 Foxbat, flying at Mach 2.2 at 82000 feet was successfully destroyed by a single Phoenix missile.

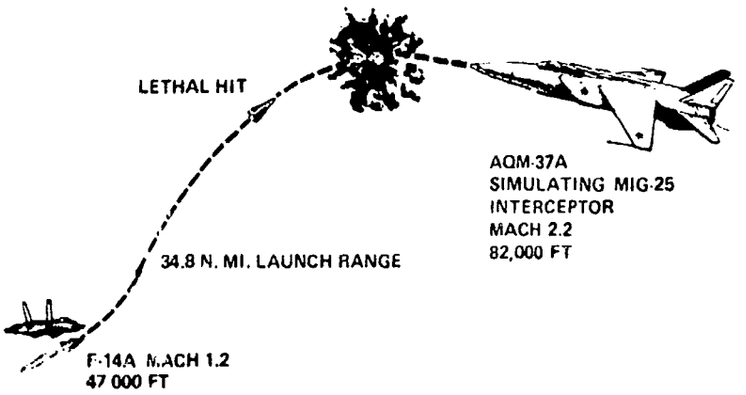


Figure 7 - FOXBAT TARGET

In another test, an augmented BOMARC drone flying at Mach 2.8 at 72000 feet was intercepted by a Phoenix. At launch the F-14 was flying at Mach 1.2 at 41000 feet and was over 50 nautical miles from the target.

MULTIPLE THREATS

In a multiple threat environment, the unique AWG-9 TWS (track-while-scan) mode enables the F-14 to launch several Phoenix missiles in rapid sequence against several targets. TWS also enables the F-14 to attack one or more targets while continuing a search for other targets. Figure 8 presents the details of one such multiple target mission. Within a 44 second timespan, four Phoenix were launched against five targets which were flying in a 20 nautical mile wavefront front formation at ranges up to 30 nautical miles. Within two minutes of first launch, one missile had scored a direct hit and the other three, lethal warhead hits.

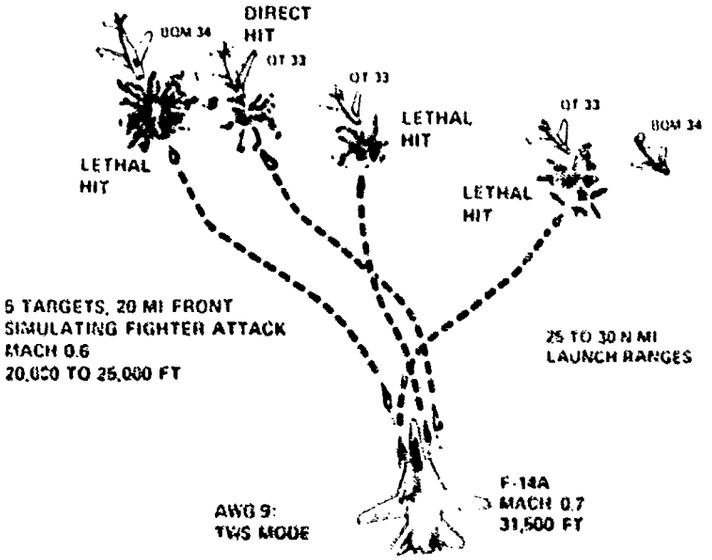


Figure 8 - MULTIPLE TARGETS

In another test, an F-14 flying at Mach 0.78 at 28000 feet intercepted two unaugmented QT-33 drones and two augmented BQM-34 drones. Another QT-33 was missed due to a missile antenna control loop failure and the loss of augmentation caused the miss of a third BQM-34. The drones were flying between Mach 0.6 and 1.1, nominally at 23000 feet at launch ranges between 30 and 50 nautical miles. The six missiles were launched within 38 seconds.

ECM ENVIRONMENT

The AWG-9/Phoenix had demonstrated unparalleled effectivity in adverse ECM environments. In a demonstration of this, figure 9, a QF-9 drone simulated a fighter threat and BQM-34 drone simulated a standoff jamming aircraft. Both were detected and, at 25 nautical mile range, a direct hit was scored on the fighter. Nine seconds after first launch, at a 47 nautical mile range, a second Phoenix was launched at the simulated jammer aircraft, scoring a lethal hit.

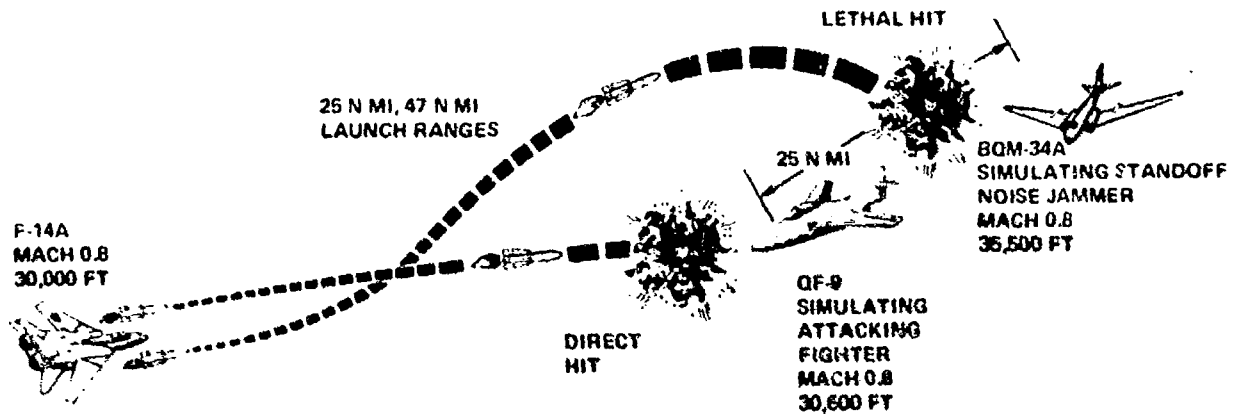


Figure 9 - ECM JAMMER TARGET

CRUISE MISSILE THREAT

The F-14A has demonstrated intercept capability against extremely low altitude (50-200 feet) targets. Cruise missile and attacking aircraft endeavor to avoid detection by flying at low levels. One example of the F-14's ability to counter this threat is shown in figure 10. A BQM-34 drone flying at Mach 0.75 at 50 feet was intercepted at a 22 nautical mile range by a Phoenix launched at a 10000 foot altitude.

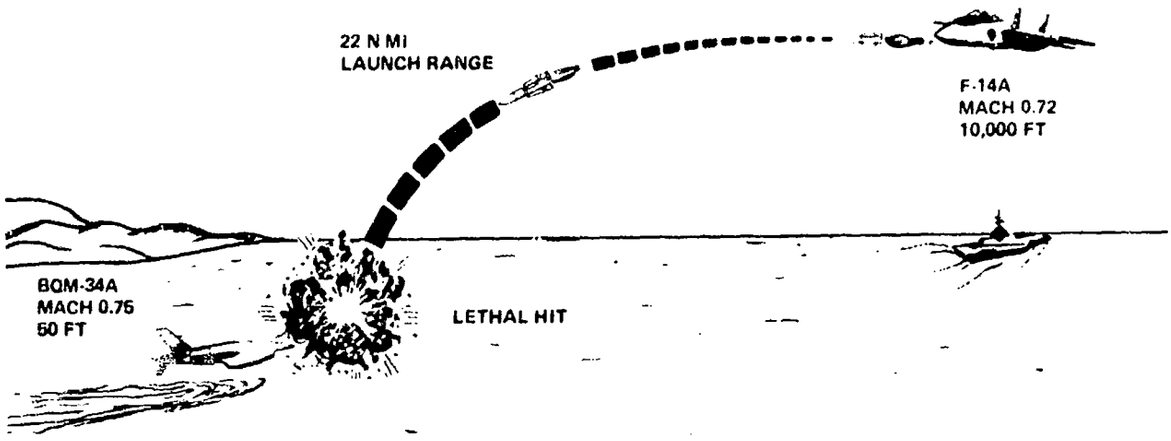


Figure 10 - LOW ALTITUDE TARGET

In another demonstration of this capability, a Phoenix launched at Mach 1.2 at 30000 feet intercepted a QT-33 flying at 200 feet at a 28 nautical mile range on a course 33 degrees to that of the F-14.

BACKFIRE THREAT

Figure 11 presents the target geometry for a simulated Backfire interception. An augmented BQM-34, simulating the radar cross section of a Backfire bomber, was flying at Mach 1.5 at 50000 feet. The drone was using a blinking jammer to confuse the F-14/Phoenix as would be expected of an attacking bomber. The Backfire was first tracked at 132 nautical miles with the AWG-9 in a track while scan mode. Launch occurred at a 110 nautical mile range and the Phoenix exceeded an altitude of 103000 feet during its flight to successful intercept.

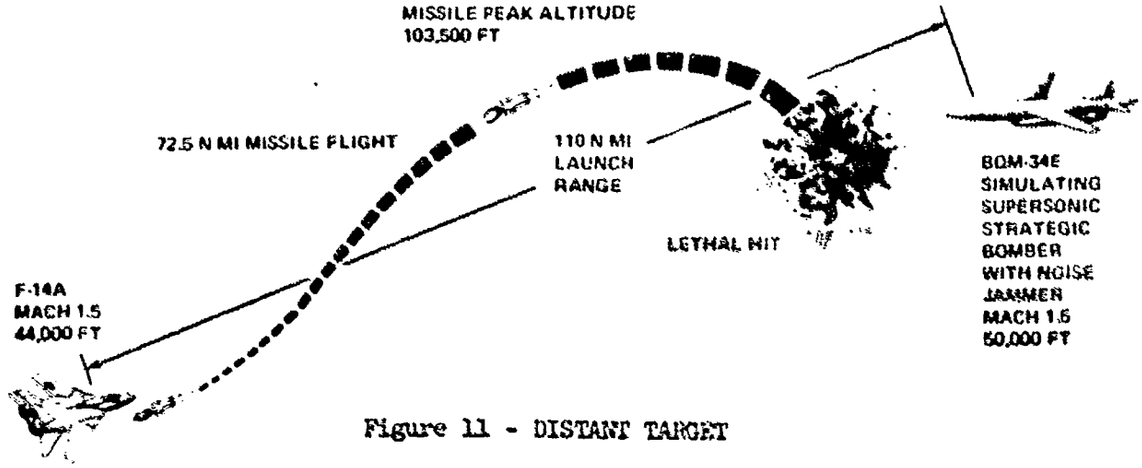


Figure 11 - DISTANT TARGET

MANEUVERING THREATS

In the air combat maneuvering environment, the F-14 is capable of launching a Phoenix at extreme load factors. The Phoenix, itself, is able to maneuver to counter evasive action by targets. This has been demonstrated by the interception of a QF-86 drone which dove vertically for 6200 feet, maneuvering at up to 6 g's after the Phoenix was launched in an attempt to evade the missile.

AUTOBIOGRAPHY

Mr. Dragowitz received his degree from Manhattan College, New York.

After military service, he joined the Aerodynamics Section of Republic Aviation Corporation. While there he worked on the F-84, XF-103 and the F-105 projects, in addition to advanced aircraft and weapon system programs. His primary duties were in the Aerodynamic Loads and Store Separation areas through various levels of responsibility, including Senior Group Leader.

Mr. Dragowitz later joined Grumman Aerospace Corporation and was responsible for all separation studies. He is currently Head of the Aerodynamic Design and Analysis Group which is responsible for Aerodynamic Aircraft/Store Compatibility, estimating aerodynamic and vehicle characteristics for configuration development and design as well as the development and use of theoretical and analytical estimating methods. Also, he is a member of the Aircraft/Stores Compatibility Study Group of the Joint Technical Co-ordinating Group and a member of the Launch Dynamics Panel of the Navy Aeroballistics Advisory Committee.

He has authored numerous papers and reports relating to aircraft/store compatibility.

Mr. Johnson received a B.S. degree in Aerospace Engineering from the Polytechnic Institute of Brooklyn. He received a M.S. degree in Mathematics at the C.W. Post College of Long Island University.

An employee of Grumman Aerospace Corporation for 10 years, his present position is Senior Aerodynamics Engineer responsible for separation and aircraft/store compatibility. He has completed analyses on various aircraft/stores programs and is presently involved in the F-14, A-6E and EF-111 programs. He co-developed the application of interactive computer graphics to store separation analyses and correlation with flight results.

He has authored several reports and papers on launch dynamics.

A TECHNIQUE FOR INVESTIGATING THE LAUNCH AND SEPARATION OF GUIDED WEAPONS (U) (Article UNCLASSIFIED)

by

MR CHARLES B. MATHEWS
CAPTAIN ROBERT D. CASON
LT PAGE G. MCGIRR
LT EDUARDO M. CARRERAS
Armament Development and Test Center
Eglin Air Force Base FL 32542

ABSTRACT. (U) In the past several years the trend in nonnuclear weapon development has shifted from the more conventional types of unguided weapons to extremely accurate weapons with complex guidance and control systems. The majority of the new guided weapons have flight control systems that are active during the launch phase to rate stabilize the weapon and reduce adverse perturbations. Because of present on-line computer limitations in the four-foot transonic wind tunnel at the Arnold Engineering Development Center, the usual technique (Captive Trajectory System or CTS) is inadequate for investigation of the launch phase of this type of guided weapon.

An approach was devised where the CTS hardware was used to obtain aerodynamic interference coefficients for the weapon with fixed control surfaces in a grid work pattern in proximity to the aircraft model. Aerodynamic models were developed for the aircraft/weapon combination and a generalized six-degree-of-freedom digital computer program was modified to incorporate subroutines containing mathematical models of the weapon seekers, autopilot, and flight control system.

This paper describes the techniques used for various aircraft and guided weapon configurations. It discusses the potential of the technique to solve weapon design problems and establish accurate and realistic specifications for seekers and flight control systems. The paper also describes how the technique has been used to investigate launch associated problems, such as seeker break-lock due to excessive weapon body rates and accelerations during the initial launch phase. Comparisons between the technique, CTS results and actual flight tests are discussed in detail.

Approved for public release; distribution unlimited

PRECEDING PAGE BLANK-NOT FILMED

LIST OF FIGURES

Figure 1. Typical Variation in Interference Pitching Moment Coefficient with Weapon Vertical Displacement

Figure 2. Variation in Interference Pitching Moment Coefficient with Weapon Vertical Displacement - F-4 Aircraft, .8 Mach

Figure 3. Variation in Interference Pitching Moment Coefficient with Weapon Vertical Displacement - F-4 Aircraft, 1.2 Mach

Figure 4. Block Diagram Showing Modules and Subroutines of the Computer Simulation

Figure 5. Aerodynamic Data for a Guided Weapon Installed on the A-7D Aircraft

Figure 6. Aerodynamic Data for a Guided Weapon Installed on the A-7D Aircraft

Figure 7. Aerodynamic Data for a Guided Weapon Installed on the A-7D Aircraft

Figure 8. Decay of Aerodynamic Data with Vertical Displacement for a Weapon Installed on the Inboard Pylon of the A-7D Aircraft

Figure 9.a. Comparison of CTS and Computer - Weapon Vertical Displacement and Pitch Angle versus Time

Figure 9.b. Comparison of CTS and Computer - Weapon Roll versus Time

Figure 9.c. Comparison of CTS and Computer - Weapon Lateral Displacement and Yaw Angle versus Time

Figure 10.a. Comparison of Flight Test Telemetry Data and Computer - Weapon Roll versus Time

Figure 10.b. Comparison of Telemetry Data and Computer - Gimbal Pitch Rate versus Time

Figure 10.c. Comparison of Telemetry Data and Computer - Gimbal Pitch Angle versus Time

Figure 11.a. Weapon Pitch, Yaw, and Roll vs Time - 15000 Ft, .9 Mach

Figure 11.b. Weapon Pitch, Yaw, and Roll Rates vs Time - 15000 Ft, .9 Mach

Figure 11.c. Weapon Pitch, Yaw, and Roll Accelerations vs Time - 15000 Ft, .9 Mach

Figure 11.d. Gimbal Pitch, Pitch Rate, and Pitch Acceleration vs Time - 15000 Ft, .9 Mach

Figure 11.e. Gimbal Yaw, Yaw Rate, and Yaw Acceleration vs Time - 15000 Ft, .9 Mach

Figure 12.a. Maximum Body Pitch Rate vs Mach Number

Figure 12.b. Maximum Body Yaw Rate vs Mach Number

Figure 12.c. Maximum Body Roll Rate vs Mach Number

Figure 12.d. Maximum Body Pitch Acceleration vs Mach Number

Figure 12.e. Maximum Body Yaw Acceleration vs Mach Number

Figure 12.f. Maximum Body Roll Acceleration vs Mach Number

Figure 13. Original Design

Figure 14. Nominal Weight Aircraft Jettison Envelope

Figure 15. Heavyweight Aircraft Jettison Envelope

Figure 16. Revised Design

Figure 17.a. Pitch versus Vertical Displacement - 13000 Ft, .8 Mach

Figure 17.b. Longitudinal Displacement versus Time - 13000 Ft, .8 Mach

Figure 17.c. Lateral Displacement versus Time - 13000 Ft, .8 Mach

Figure 18.a. Pitch versus Vertical Displacement - 40000 Ft, .9 Mach

Figure 18.b. Longitudinal Displacement versus Time - 40000 Ft, .9 Mach

Figure 18.c. Lateral Displacement versus Time - 40000 Ft, .9 Mach

Figure 19. Glide Bomb Configuration

Figure 20. CTS vs Simulation Comparison (Translational)

Figure 21. CTS vs Simulation Comparison (Angular)

Figure 22. CTS vs Simulation Comparison (Angular)

Figure 23. CTS vs Simulation Comparison (Angular)

Figure 24. CTS vs Simulation Comparison (Angular)

Figure 25. CTS vs Simulation Comparison (Angular)

Figure 26. Flight Test vs Simulation Comparison

Figure 27. Flight Test vs Simulation Comparison

Figure 28. Flight Test vs Simulation Comparison

INTRODUCTION

For many years the Air Force has relied heavily on the Arnold Engineering Development Center's (AEDC) four-foot transonic (4T) wind tunnel with its captive trajectory system (CTS) for determining external store and weapon separation trajectories. The efficiency and effectiveness of this system for the investigation of weapon delivery and jettison performance prior to flight testing have been well documented. The capability to accurately predict weapon separation trajectories has resulted in a tremendous savings of Air Force flight test time and dollars as well as considerably enhancing the safety aspects of the flight test programs.

In the past several years the trend in nonnuclear weapon development has shifted from the more conventional types of unguided weapons such as general purpose bombs, fire bombs, dispensers and rocket launchers to extremely accurate weapons with complex guidance and control systems. The 4T CTS retains the capability to study the fixed control surface jettison mode of these new weapons; however, the majority of the new guided munitions have flight control systems that are active during the launch phase for rate stabilization and reduction of adverse perturbations. The four-foot test section of 4T dictates that most aircraft (and weapon) models be no larger than 0.05-scale. It is not feasible to remotely control and accurately model the control surfaces of weapon models this small in size. Also, because of limited on-line computing capability it is not possible at this time to incorporate either the flight control system or the control effectiveness into the CTS. Therefore, it is not practical to use the 4T CTS for investigation of the launch phase of this type of guided weapon. Because of the above, an approach was devised where the CTS hardware was used to obtain basic captive balance coefficient data in a grid work pattern in proximity to the aircraft model. This data is then used in a six-degree-of-freedom digital simulation of the weapon that contains subroutines for the flight control system and complete three-dimensional free-stream aerodynamics.

METHOD DESCRIPTION

WIND TUNNEL GRID TESTS

The CTS was used to obtain the aerodynamic coefficients acting on an external store in the vicinity of the aircraft. As in CTS testing, the parent aircraft (usually 0.05-scale) is placed on a sting that is adjustable for angle of attack and angle of sideslip. Dummy store models (bombs, fuel tanks, etc.) are attached to the parent model to obtain the aircraft configuration desired. The weapon whose trajectory is desired is attached to a second sting having an internal six-component, strain gage balance system. Up to this point the procedure is identical to CTS testing. Instead of using the measured aerodynamic forces

to compute an on-line trajectory, however, the store model is translated and rotated by the CTS rig, and the aerodynamic coefficients are recorded.

It was determined by reference 1 that the interference coefficients varied considerably more with vertical displacement (Z direction) rather than with lateral or axial displacement and that rotations in pitch, yaw, and roll at various points in the grid have little effect on the interference properties. As a result, the variation in coefficients is normally obtained only as a function of vertical displacement for various Mach numbers and aircraft angles of attack. This procedure, which has proven satisfactory in most cases, serves to considerably reduce the wind tunnel testing and data handling requirements.

Figure 1 shows the typical variation in the pitching moment interference coefficient as the weapon moves in the Z direction away from the aircraft model. The internal balance measures the total coefficients which are composed of interference effects and free-stream effects due to the weapon angle of attack relative to the free-stream. The free-stream coefficients are obtained using the 0.05-scale weapon model which is displaced forward in the wind tunnel test section away from the aircraft model. Therefore, the interference coefficients may be obtained by subtracting the free-stream coefficients from the measured or total coefficients. For example, where Cm is the pitching moment,

$$C_{m_{INT}} = C_{m_{TOTAL}} - C_{m_{FS}} \qquad (1)$$

Figures 2 and 3 show typical variations in the pitching moment interferemce cofficients for a particular guided weapon which were calculated as described above. Inspection of these figures indicates the difficulty of curve fitting the interference data for a large range of Mach numbers and angles of attack, especially at the higher Mach numbers where shock effects cause large variations in the coefficients. As a result, a computer routine was developed where the interference coefficients are calculated as described above from magnetic tapes containing the wind tunnel data. The interference routine interfaces with a six-degree-of-freedom trajectory program. The arguments (which are outputs of the trajectory program) for obtaining the interference coefficients are Mach number, aircraft angle of attack, and Z. Routines are used for linear interpolation between the wind tunnel data points. Therefore, the interference coefficients are obtained point-by-point as the weapon traverses in the Z direction.

Sufficient grid work is usally obtained to cover the complete Mach and aircraft angle of attack range encompassed by the desired weapon launch and jettison envelope. In addition to the grid data, CTS trajectories with fixed controls are obtained at selected points within the envelope. Although the controls-fixed CTS trajectories

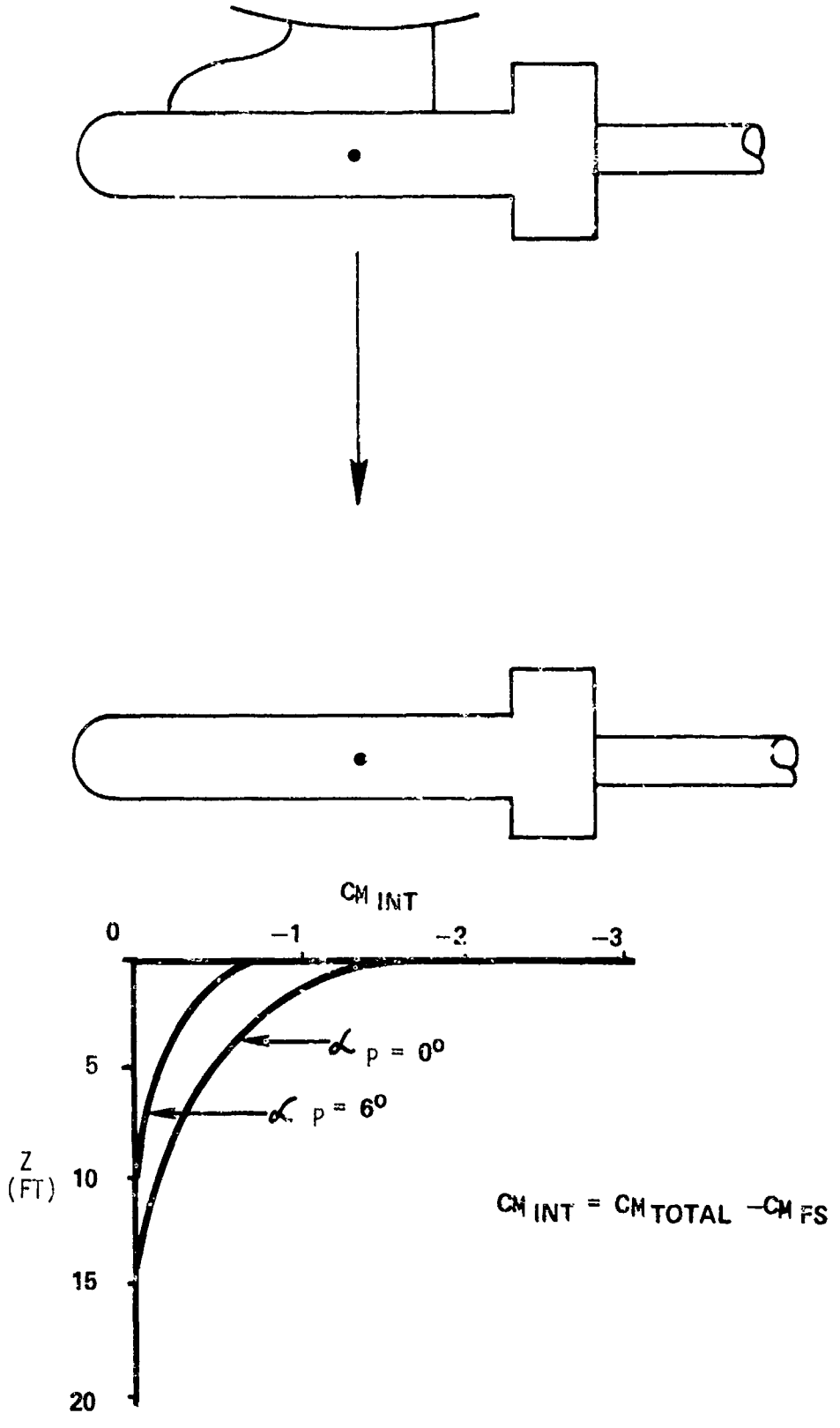


Figure 1. Typical Variation in Interference Pitching Moment Coefficient with Weapon Vertical Displacement

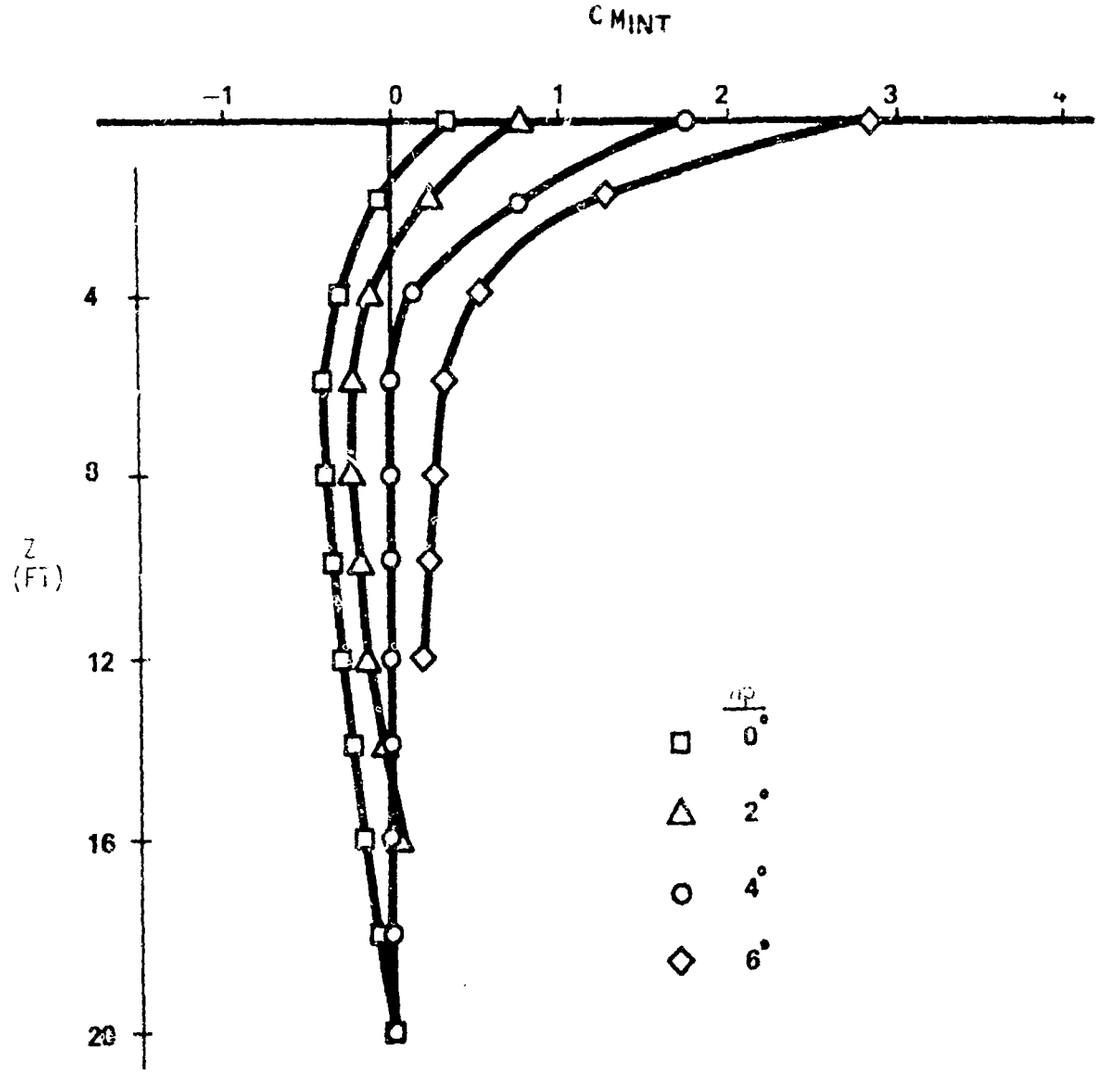


Figure 2. Variation in Interference Pitching Moment Coefficient with Weapon Vertical Displacement - F-4 Aircraft, .8 Mach

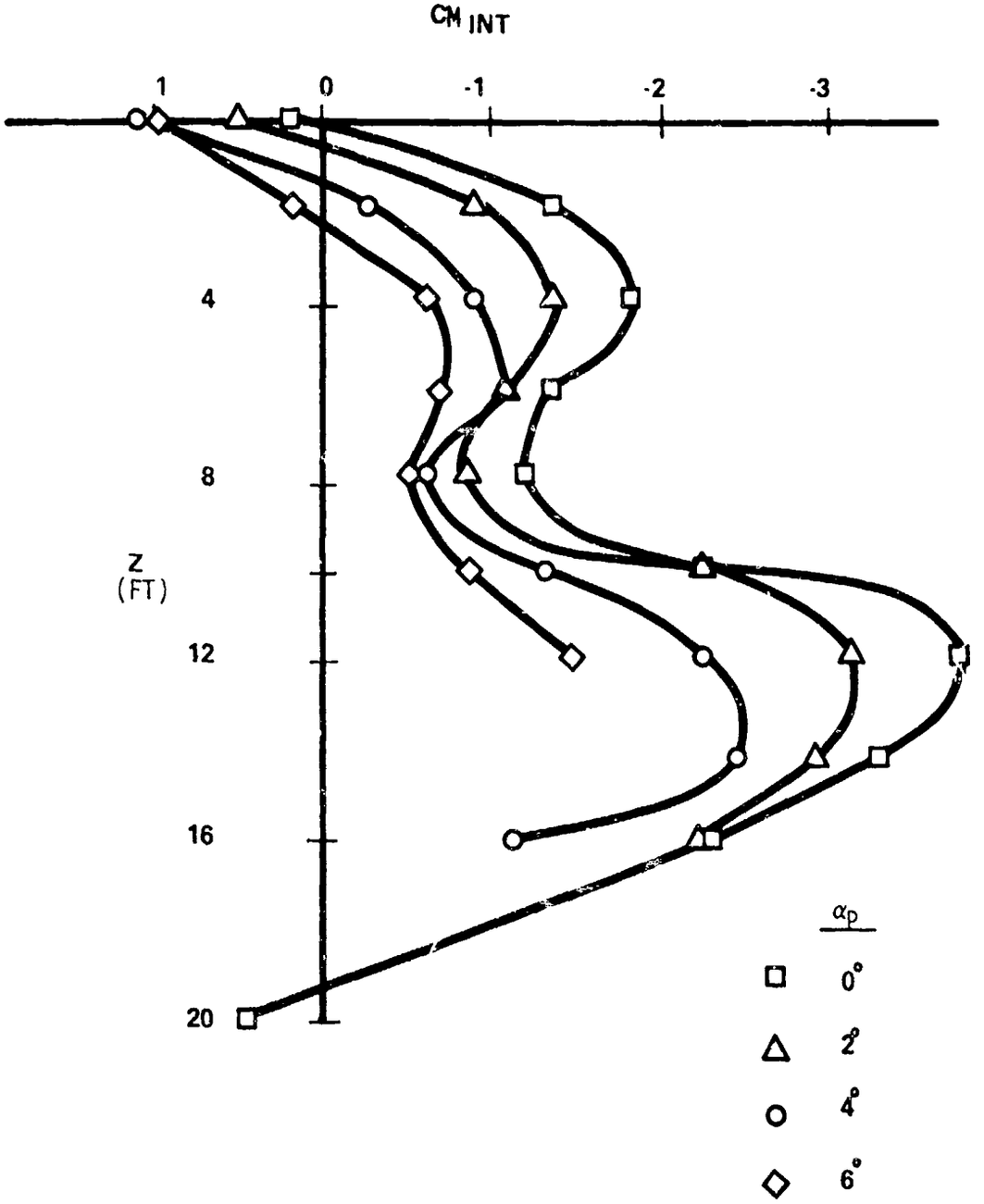


Figure 3. Variation in Interference Pitching Moment Coefficient with Weapon Vertical Displacement - F-4 Aircraft, 1.2 Mach

provide an actual simulation of the jettison mode, they are primarily obtained to provide a check for the computer/grid generated trajectories.

COMPUTER SIMULATION

Once aerodynamic models for the interference effects related to the aircraft/weapon combination are developed, a generalized six-degree-of-freedom (SIXDOF) digital computer program is modified to provide a complete simulation. Figure 4 is a block diagram of the computer simulation which includes mathematical models of the weapon seeker and flight control system. The simulation is modular in form and can readily be adapted to various weapons and aircraft simply by changing the applicable subroutines. For example, once the simulation is developed for a particular weapon, trajectories from various aircraft may be simulated by using the correct interference coefficients. The program also has the option of using flow field tabular data (as described in references 2 and 3) to calculate the interference coefficients in lieu of using grid data.

The free-stream aerodynamics for the weapon to be simulated are normally obtained from comprehensive wind tunnel tests of 0.20 (or larger) scale models of the weapon. The data, which is usually inputed in block data form, is normally a total three-dimensional aerodynamic model in the aeroballistic axis system containing control effectiveness and damping terms.

The total aerodynamic coefficients acting on the weapon at any given time during the trajectory are obtained by summing the free-stream, interference, and control contributions. For example, (where δ is control surface deflection)

$$Cm_{TOTAL} = Cm_{INT} + Cm_{FS} + Cm_{\delta}\delta \qquad (2)$$

PROCEDURE

The development of a complete trajectory simulation usually consists of building the applicable modules/subroutines of the SIXDOF program to include the aerodynamic interference coefficients, a complete aerodynamic model of the weapon with control effectiveness, and appropriate mathematical models of the weapon flight control system and seeker. Once this is accomplished, simulations may be made of the separation trajectories at various flight conditions throughout the desired envelopes. Uncontrolled, or jettison mode releases with fixed control surfaces, may be conducted by simply by-passing the seeker and flight control subroutines.

The first step in the procedure usually consist of conducting trajectory simulations for each flight condition where CTS trajectories were obtained. Good correlation between CTS and the SIXDOF simulations indicates a good aerodynamic model of the interference coefficients. Once this is obtained, which leads to confidence in the aerodynamic modeling, the flight control system can be activated to investigate the

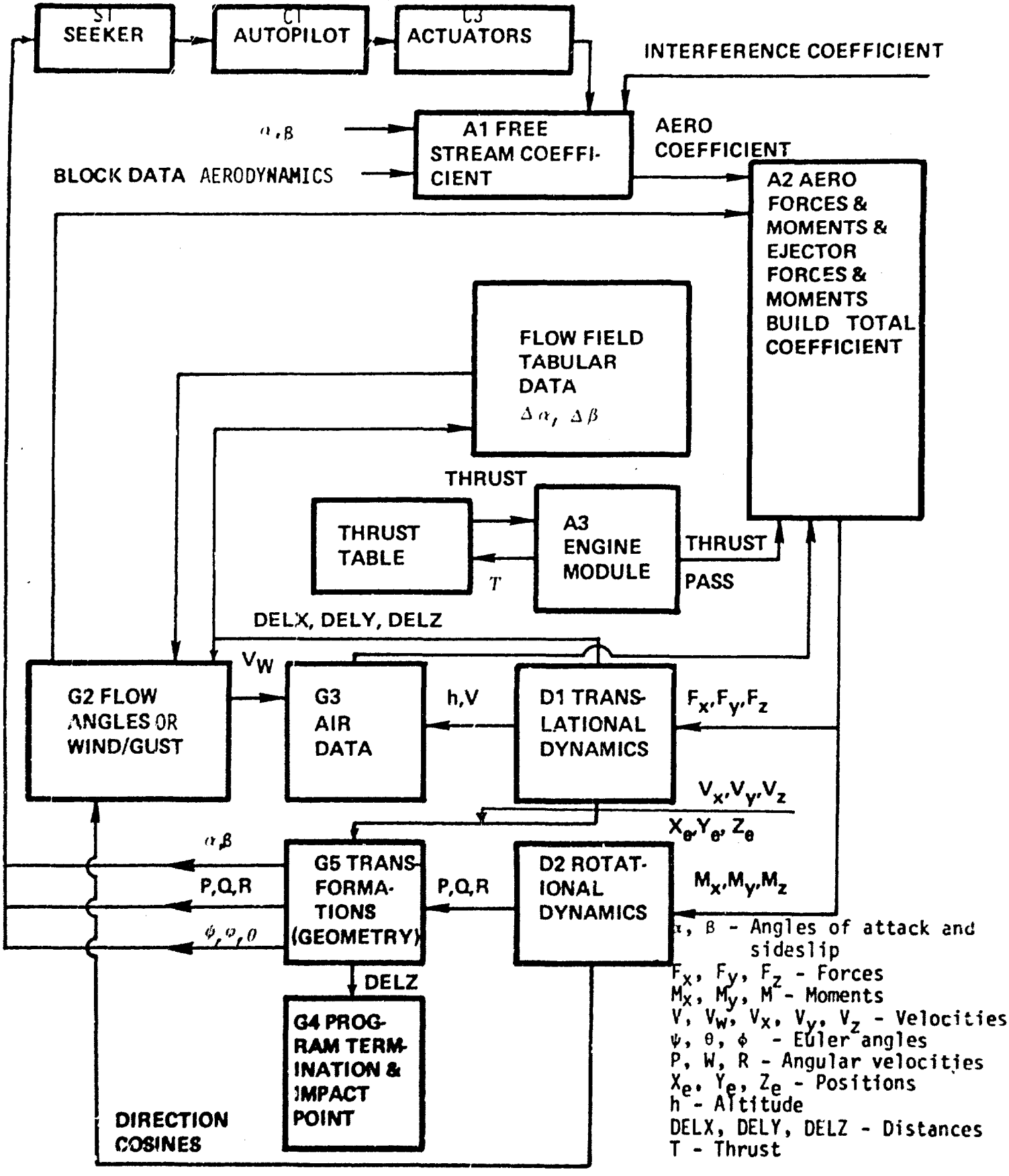


Figure 4. Block Diagram Showing Modules and Subroutines of the Computer Simulation

controlled launch mode. In addition to normal launches, the simulation can also be used to study the results of failure of such components as the weapon's flight control system or the aircraft ejector rack.

Normally the primary concern in a trajectory study is to insure that the weapon separates safely throughout the flight envelope and that chances of weapon-to-aircraft collisions are extremely remote. This applies to the controls-fixed jettison mode as well as the controls-active launch mode. Another, but much less studied aspect, is whether the weapon's aerodynamics and flight control system are capable of handling the launch transients. In other words, will the seeker and gimbal platform of a guided weapon maintain lock on the target during the launch transient? Both types of trajectory studies will be presented in the examples to follow.

EXAMPLES AND RESULTS

SEEKER BREAK-LOCK

An investigation was undertaken to determine the cause of excessive break-lock for a guided weapon launched from the inboard wing station of the A-7 aircraft. During flight tests, 6 out of 11 weapons released from the inboard wing station failed to guide properly. The problem was not apparent for the outboard wing station where seven launches were made with only one failure. The investigation consisted of:

a. A series of rate table tests to determine the maximum angular body rates for the guidance units.

b. Six-degree-of-freedom digital simulations to estimate weapon body/gimbal rates and accelerations expected during launches from the A-7 inboard wing station.

It was felt that the above two pieces of information would provide the basis for establishing a launch limit or envelope for the inboard wing station that would reduce the high occurrance of weapon break-lock.

The test results of a. above concluded that the guidance unit could withstand certain angular rates without breaking lock. However, no conclusions were made as to the effects of pitch/yaw/roll coupling or angular accelerations.

Wind tunnel data for the SIXDOF simulations was provided in the form of CTS and grid data by Mr R. J. Arnold of the Air Force Armament Laboratory. Figures 5 through 7 are installed rolling, pitching, and yawing moment coefficients. Configuration A is outboard data with a weapon on the intermediate pylon. Configuration B is inboard data with a 300-gallon fuel tank on the outboard pylon. Also included are recent inboard wind tunnel data from an AEDC test which represents the flight test configuration where the intermediate and outboard pylons were empty.

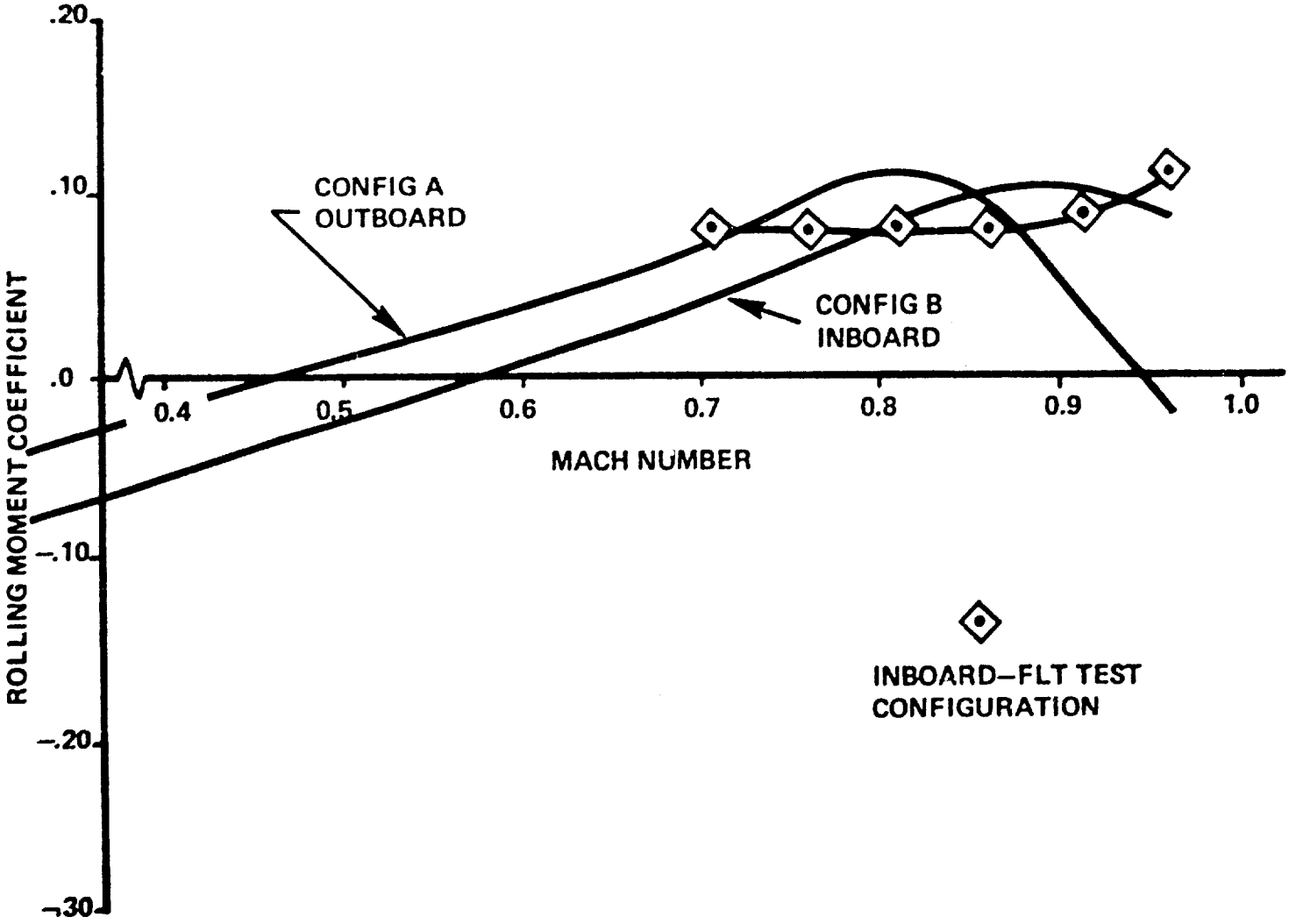


Figure 9. Aerodynamic Data for a Guided Weapon Installed on the A-7D Aircraft

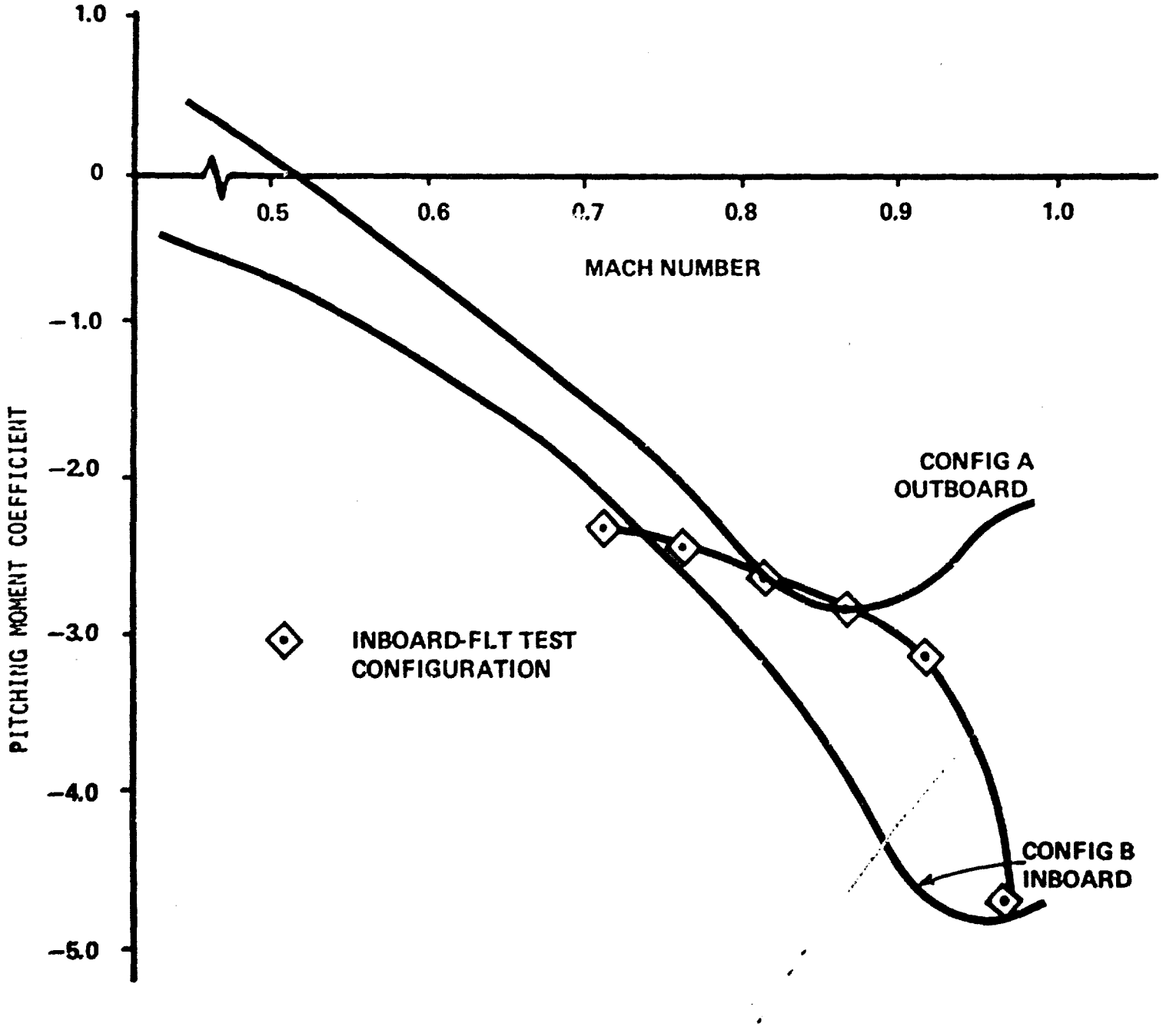


Figure 6. Aerodynamic Data for a Guided Weapon Installed on the A-7D Aircraft

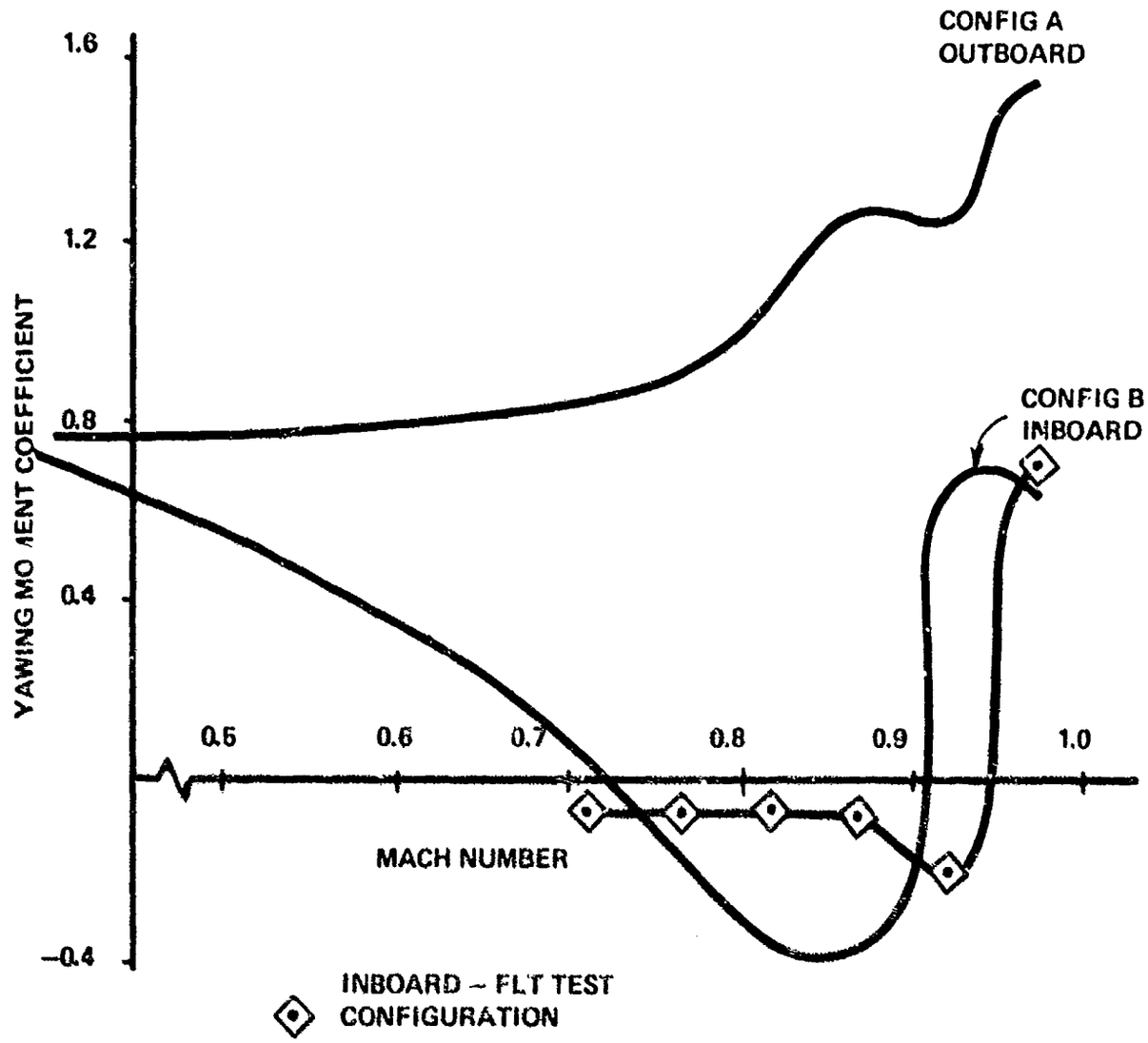


Figure 7. Aerodyne Data for a Guided Weapon Installed on the A-7D Aircraft

Note in Figure 5 that the rolling moment coefficients for all configurations, except the inboard, decrease to zero at 0.95 Mach whereas the rolling moment coefficient for the inboard remains in the vicinity of 0.1 or increases. Figure 6 shows the negative pitching moment coefficient to increase sharply for the inboard but decrease for the outboard at Mach 0.9 and above. However, Figure 7 shows the yawing moment coefficient to be consistently less for the inboard.

Again, as stated above it is not known if the primary causes of break-lock are angular rates, accelerations or some combination of both. Also, the effects of pitch/yaw/roll coupling are unknown. If, however, it is assumed that the inboard wing station break-lock problem can be attributed to pitch, yaw, and roll excursions caused by the interference aerodynamics, the trends in the installed coefficients discussed above lead to the following for the same flight conditions: (1) Pitch and roll excursions will be greater for the inboard, (2) Yaw excursions will be less for the inboard. Therefore, since the inboard wing station is the problem, a logical conclusion is that pitch or roll excursions (or a combination of both) rather than yaw excursions are the primary cause of the A-7 inboard break-lock problem.

During the wind tunnel tests, interference aerodynamic coefficients were obtained as a function of weapon vertical displacement below the aircraft (Figure 8 depicts the pitching moment coefficient). The interference coefficients decay to approximately zero at some distance below the aircraft depending on Mach number and angle of attack. A linear approximation to the decay curve based on the authors' judgment was used to model aerodynamic interference effects for the digital simulations. It will be noted later that even this simple linear approximation of the interference coefficients gives excellent results.

The procedure consisted of conducting six-degree-of-freedom launch simulations with the weapon autopilot off and comparing the trajectories to CTS results obtained for the same flight conditions. As noted earlier, it is presently impossible to obtain CTS trajectories for weapons with active controls because of scaling problems and on-line computer limitations. Therefore, CTS is capable only of providing inactive autopilot/control (or jettison) release trajectories. Good correlation between computer and CTS indicates that the aerodynamic models for the interference coefficients are fairly accurate (at least approaching that of CTS accuracy).

When good correlation is obtained, leading to confidence in the aerodynamics, the autopilot and actuator math models in the SIXDOF simulation are then activated to simulate a normal controlled launch. The program then merely adds the affect of the control deflections commanded by the autopilot which provides pitch and yaw rate and roll

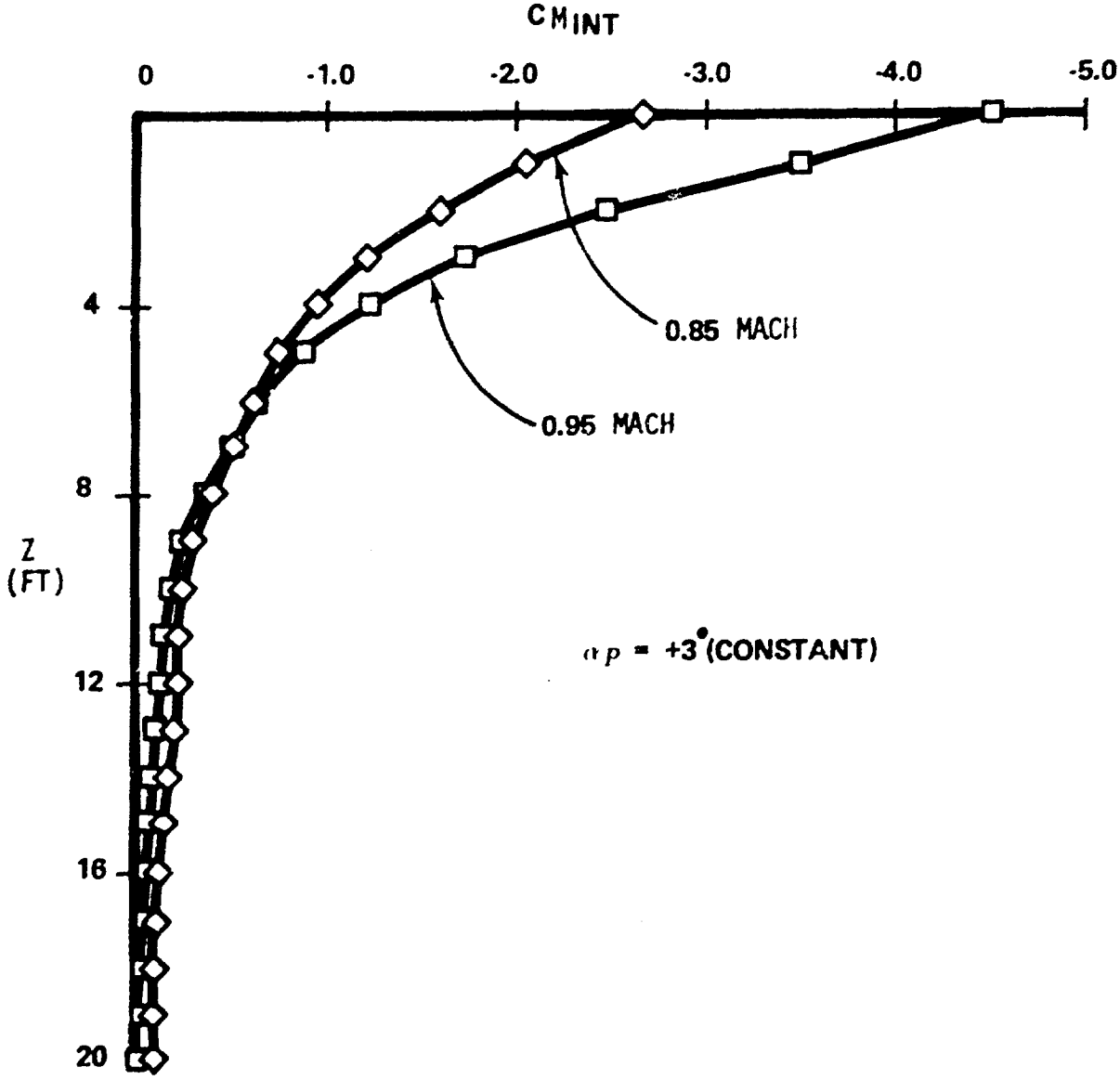


Figure 8. Decay of Aerodynamic Data with Vertical Displacement for a Weapon Installed on the Inboard Pylon of the A-7D Aircraft

position stabilization to the weapon during the first two seconds of the launch phase.

Figure 9 shows the excellent correlation obtained between the computer and CTS prior to activation of the autopilot and controls. Figure 10 shows the correlation between flight test telemetry data and the active autopilot computer simulations. Flight test data for inboard launches were obtained for only two missions.

From the above, it was concluded that the model for A-7 inboard launch dynamics was fairly accurate, and a parametric investigation was conducted in an attempt to find some logical basis for the break-lock and to establish a launch envelope. A-7 inboard wing station launches were simulated for Mach numbers of 0.7, 0.75, 0.8, 0.85, 0.9, and 0.95 at altitudes of 5, 10, 15, and 20 thousand feet. A 45° dive angle and a zero degree gimbal offset angle were used in all cases.

Figure 11 depicts typical time histories of the weapon angular positions, rates and accelerations and the seeker gimbal platform pitch and yaw positions, rates, and accelerations. Unfortunately the rate table tests did not define the coupled rates and accelerations that the seeker could tolerate without breaking lock on the target. Nevertheless, the investigation did prove the feasibility of this approach for defining the launch environment and the rates/accelerations the weapon seekers could expect to see during launch. Also, this type of study could assist in establishing seeker and guidance specifications.

The study provided guidelines for recommending a launch envelope for the inboard wing station. Figure 12 shows the maximum absolute value of the body/gimbal rates and accelerations as functions of Mach number and altitude. It should be noted that body/gimbal rates/accelerations differ only by gimbal friction which is small; therefore, only body excursions are shown. In almost every case a sharp break appears in the curve at about 0.9 Mach number indicating a large increase in the angular excursions at this point. At the lower altitudes this break moves toward 0.85 Mach suggesting that something lower than 0.9 Mach would be a realistic launch limit below 10,000 feet. Based on the above, it was recommended that the upper end of the A-7 inboard wing station launch envelope be restricted to 500 KIAS or 0.9 Mach, whichever is less.

SEPARATION CHARACTERISTICS DIRECTING DESIGN

A design for an improved guided bomb was proposed incorporating large strakes forward and large wings aft with pop-out tips to achieve significant increases in range and maneuverability. As shown in Figure 13, the design was approximately one and one-half calibers unstable when the pop-out tips were in the stored position. With the tips deployed the design was marginally stable.

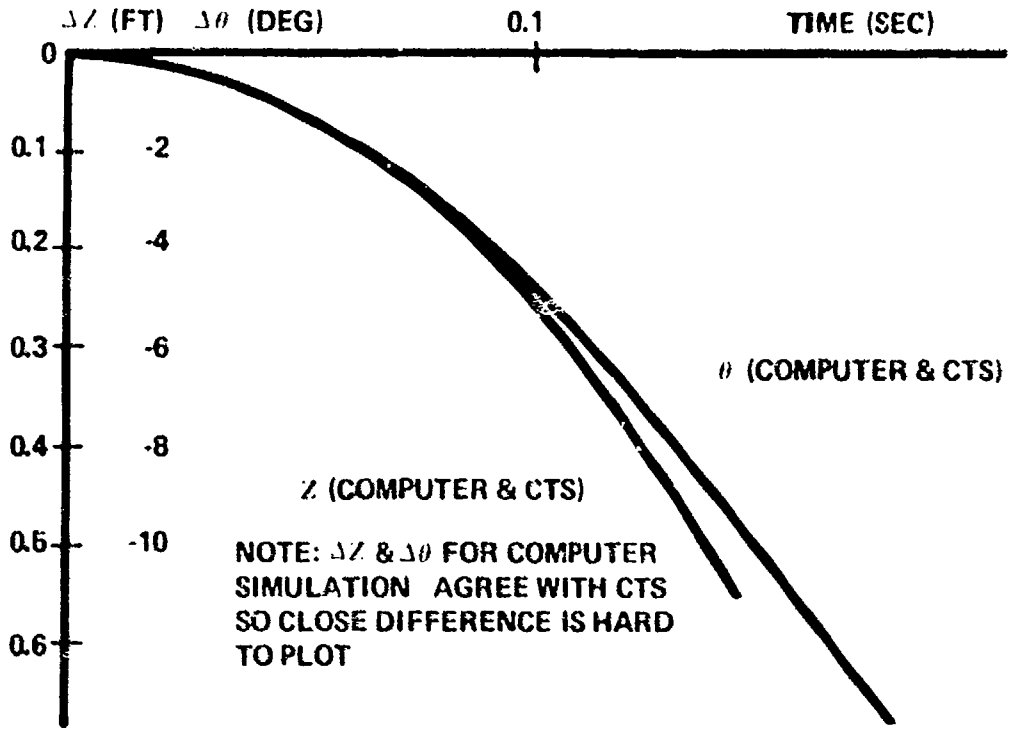


Figure 9.a. Comparison of CTS and Computer-Weapon Vertical Displacement and Pitch Angle Versus Time

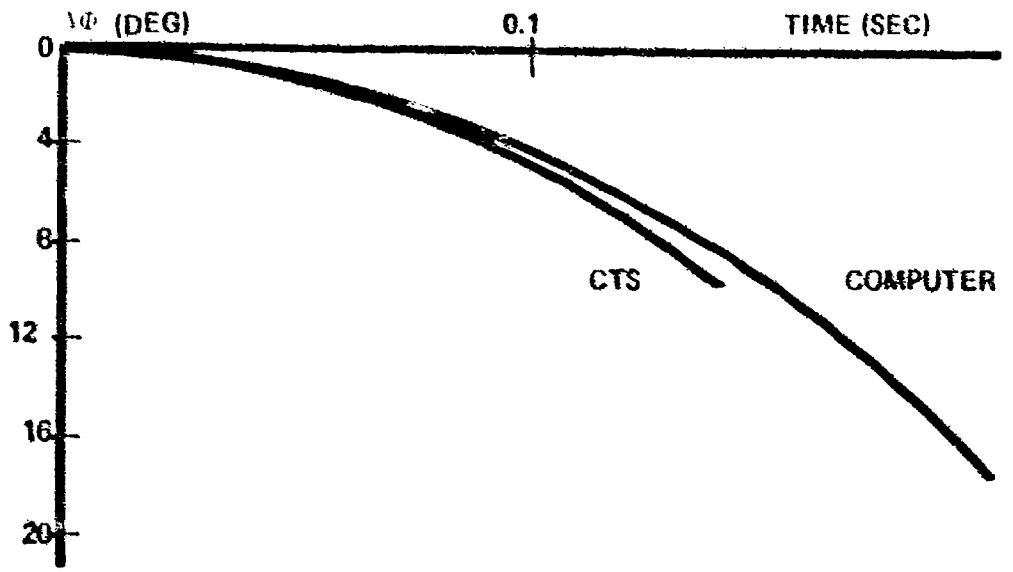


Figure 9.b. Comparison of CTS and Computer-Weapon Roll Versus Time

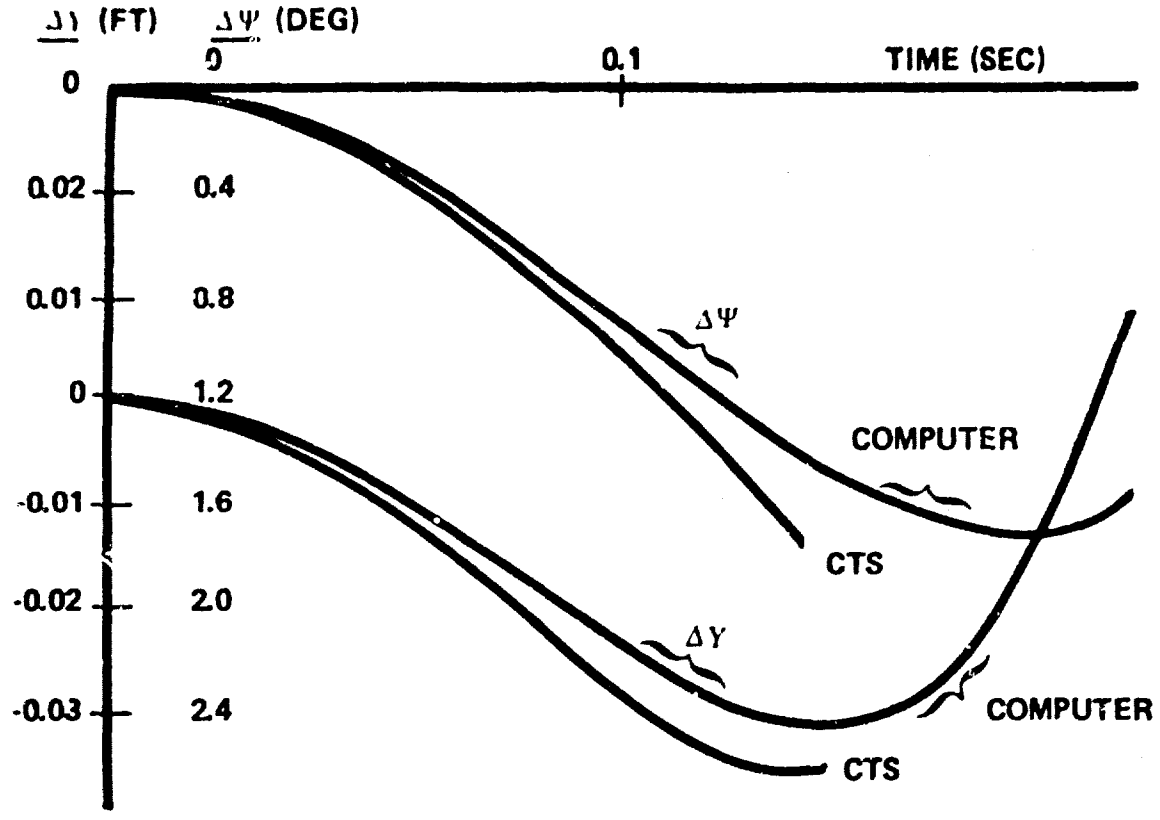


Figure 9.c. Comparison of CTS and Computer - Weapon Lateral Displacement and Yaw Angle Versus Time

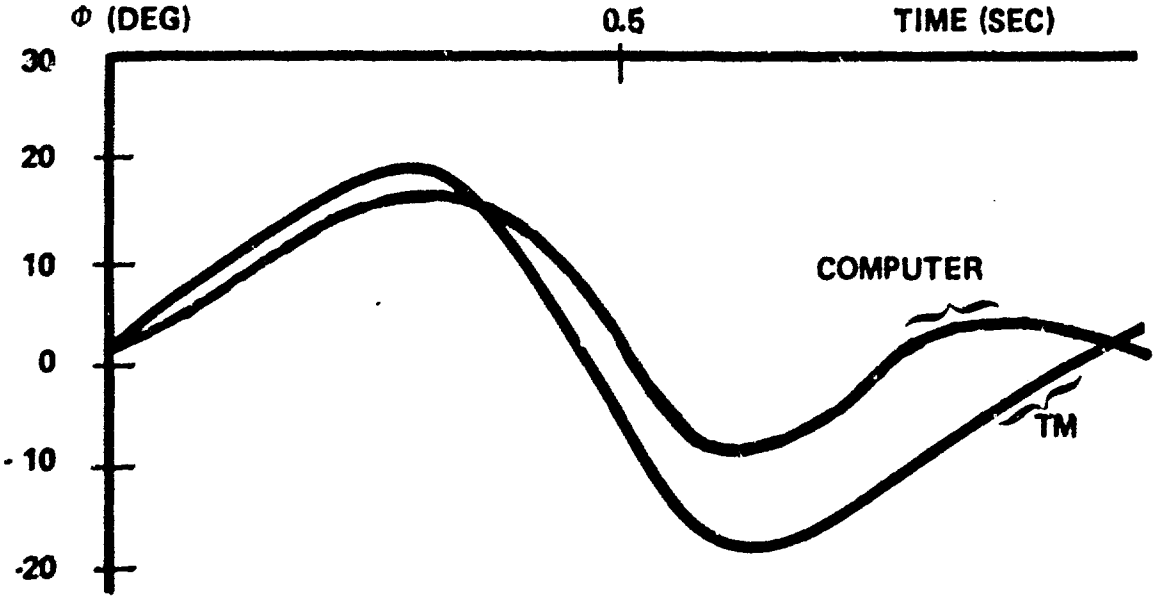


Figure 10.a. Comparison of Flight Test Telemetry Data and Computer - Weapon Roll Versus Time

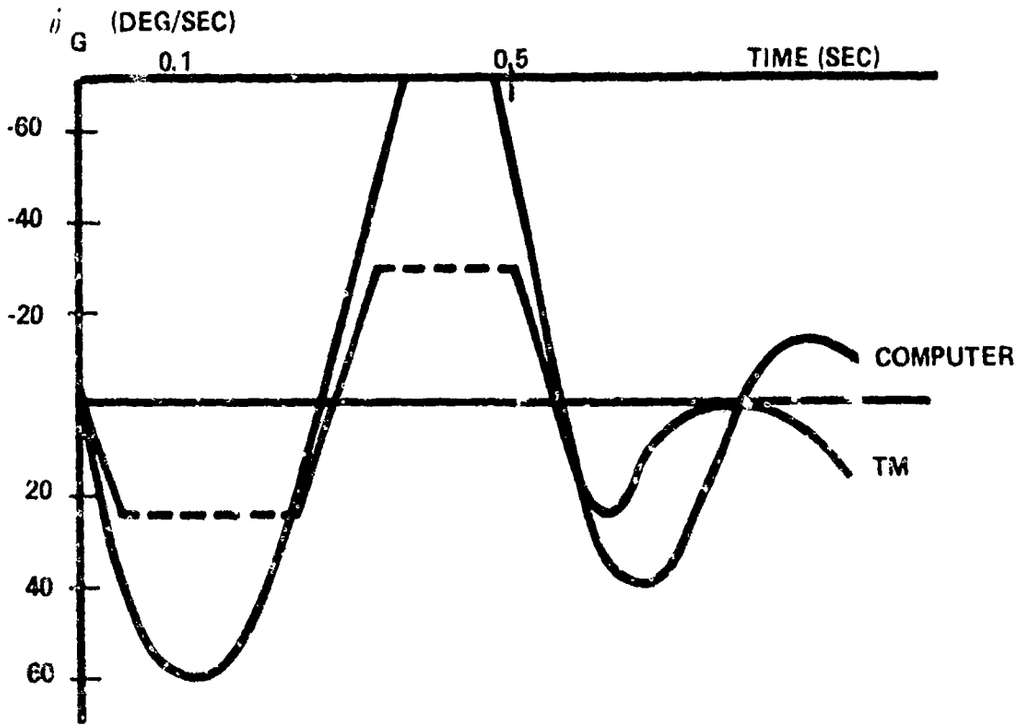


Figure 10.b. Comparison of Telemetry Data and Computer - Gimbal Pitch Rate Versus Time

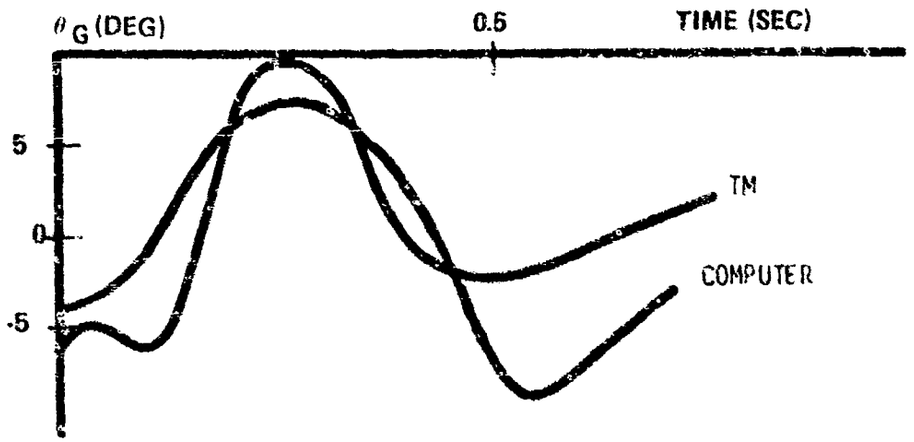


Figure 10.c. Comparison of Telemetry Data and Computer - Gimbal Pitch Angle Versus Time

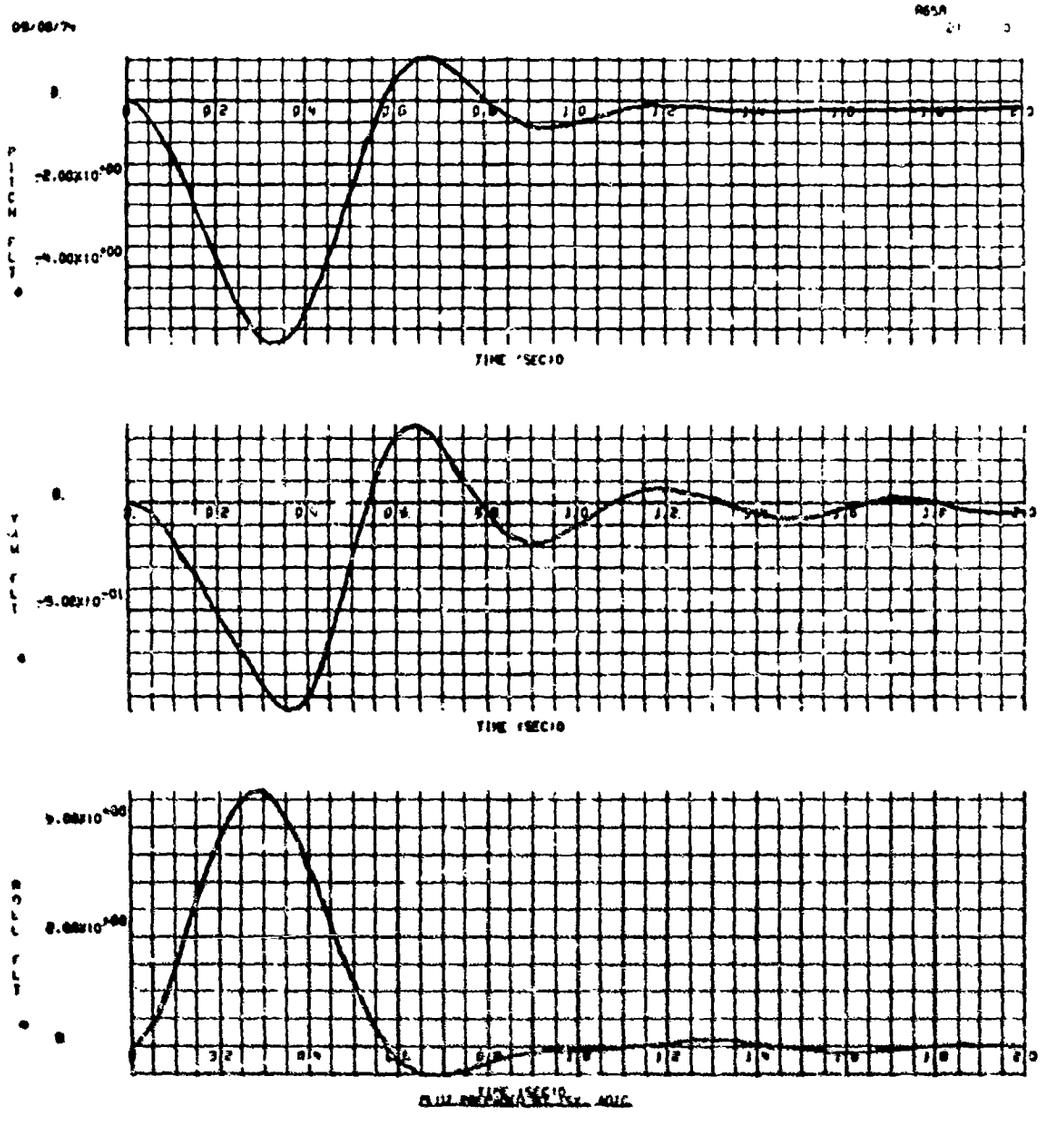


Figure 11.a. Weapon Pitch, Yaw, and Roll vs Time – 15000 Ft, .9 Mach

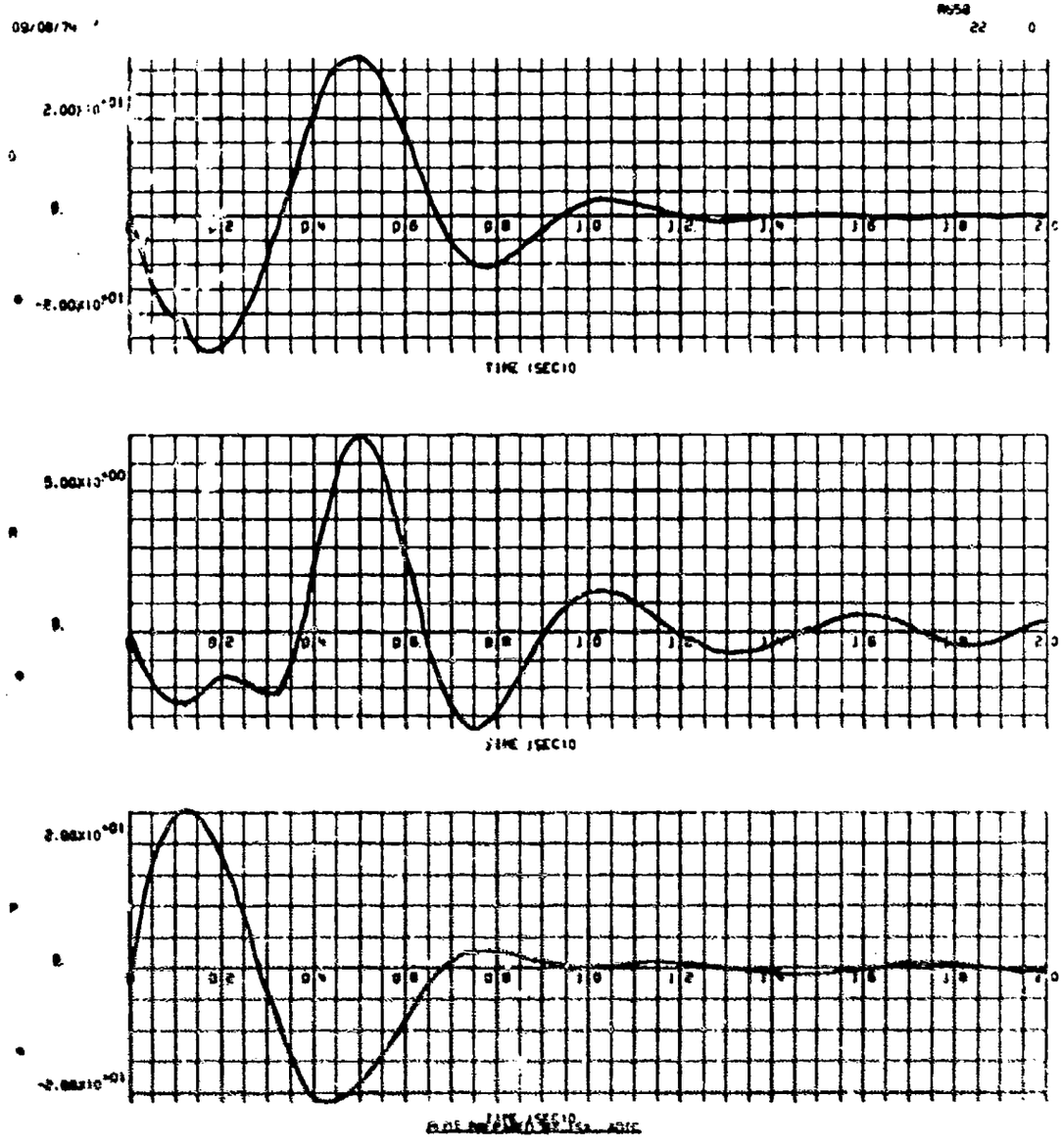


Figure 11.b. Weapon Pitch, Yaw, and Roll Rates vs Time - 15000 Ft, .9 Mach

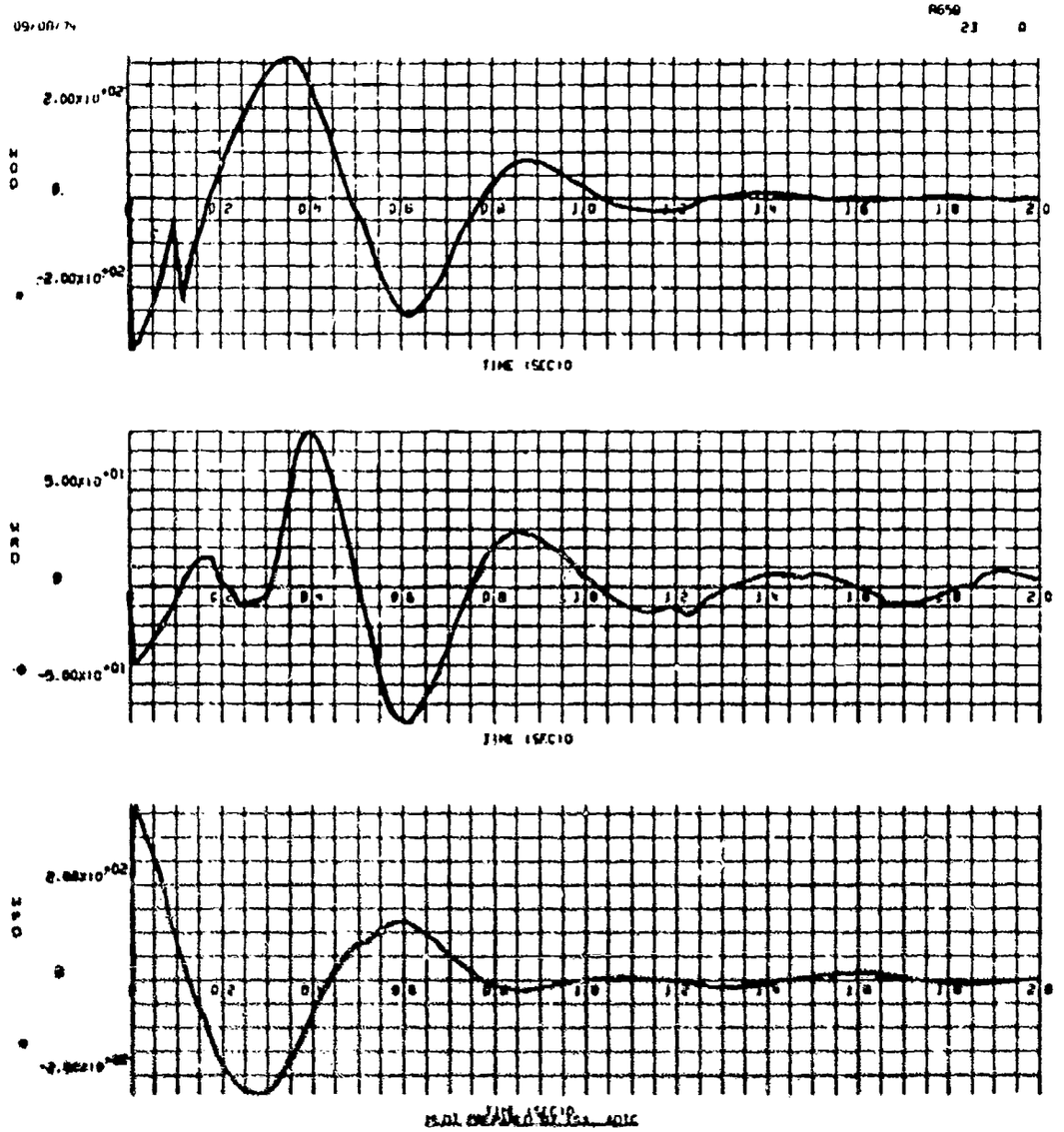


Figure 11.c. Weapon Pitch, Yaw, and Roll Acceleration vs Time - 19000 Ft, .9 Mach

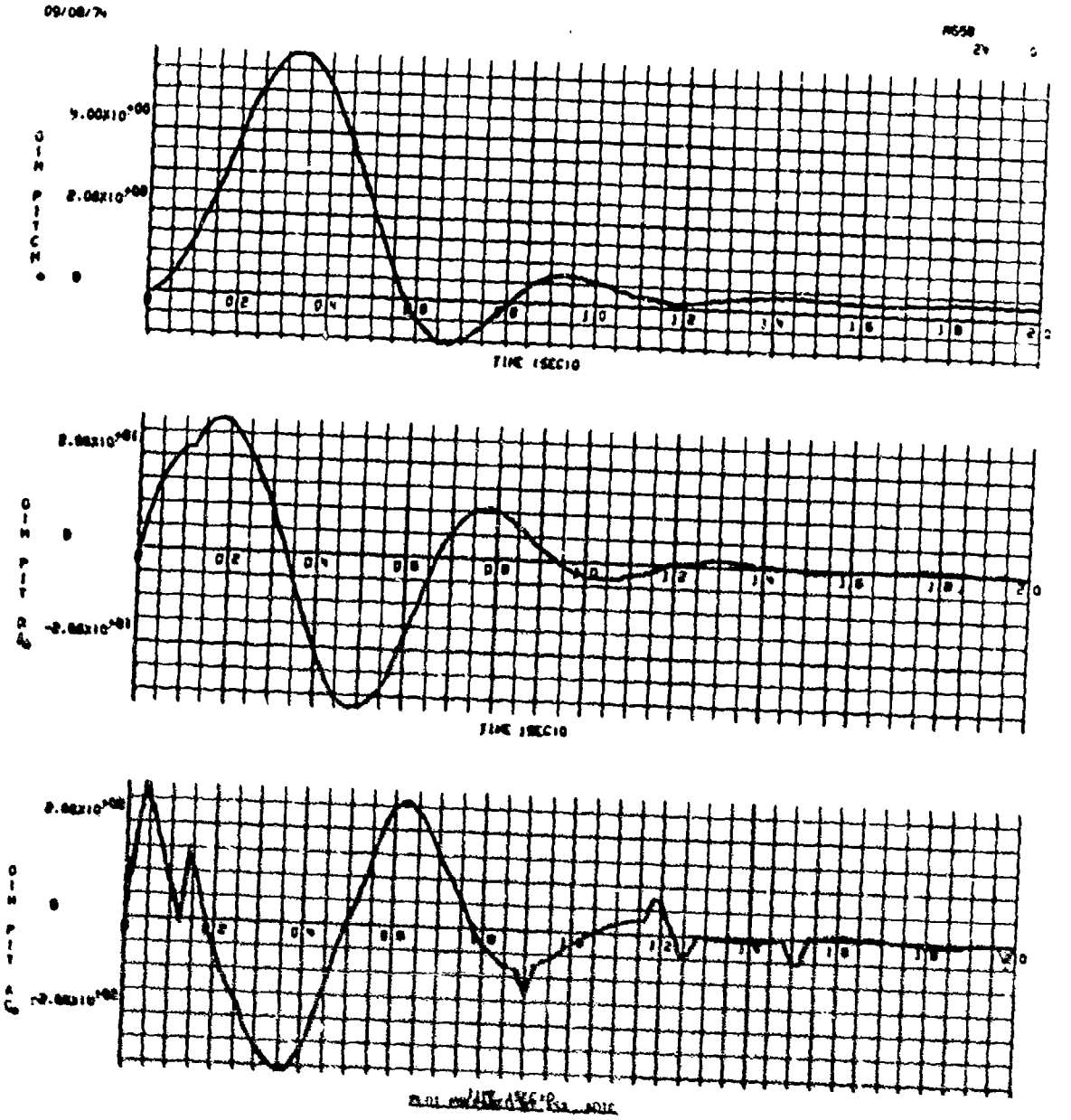


Figure 11.d. Gimbal Pitch, Pitch Rate, and Pitch Acceleration vs Time – 15000 Ft, .9 Mach

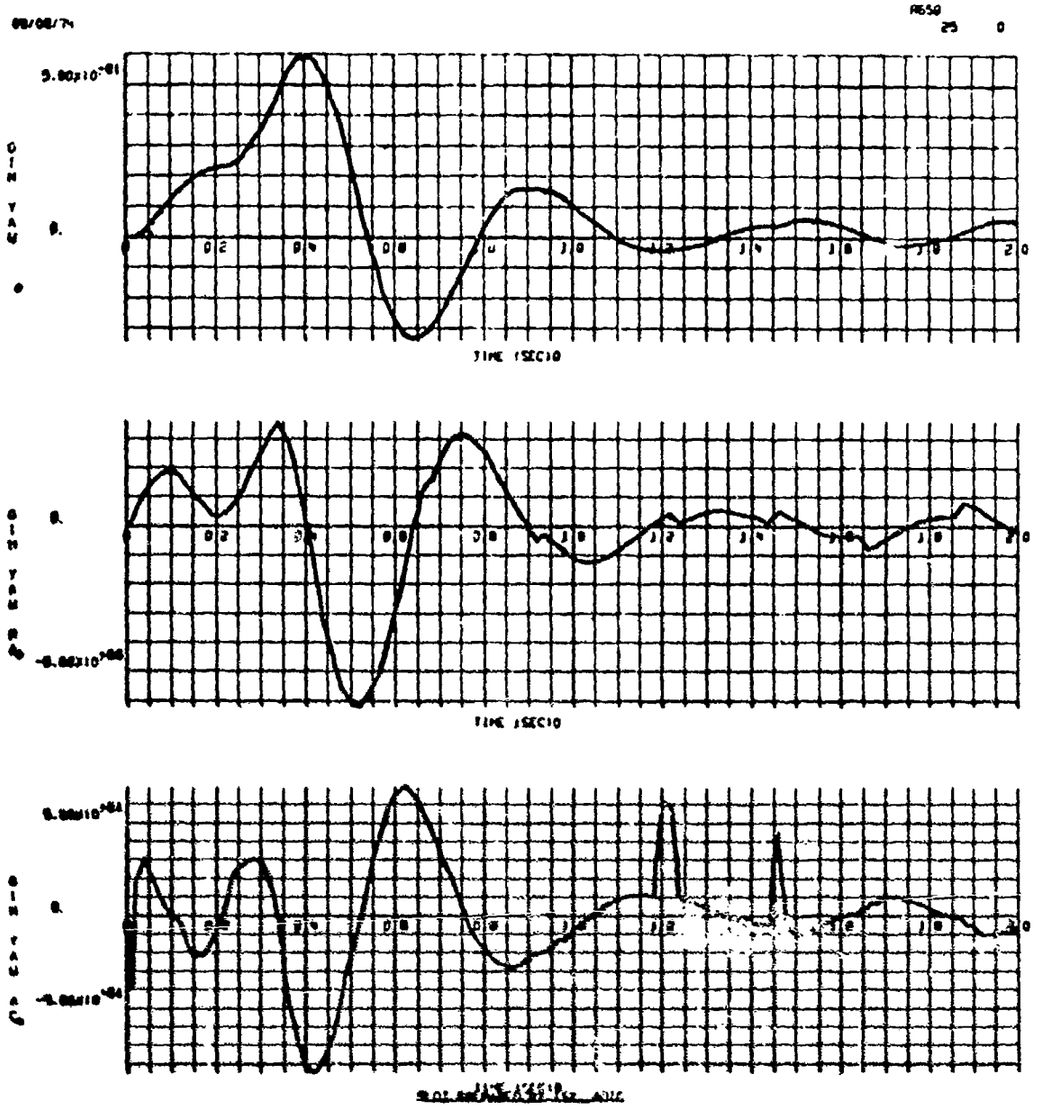


Figure 11.e. Gimbal Yaw, Yaw Rate, and Yaw Acceleration vs Time – 15000 Ft, .9 Mach

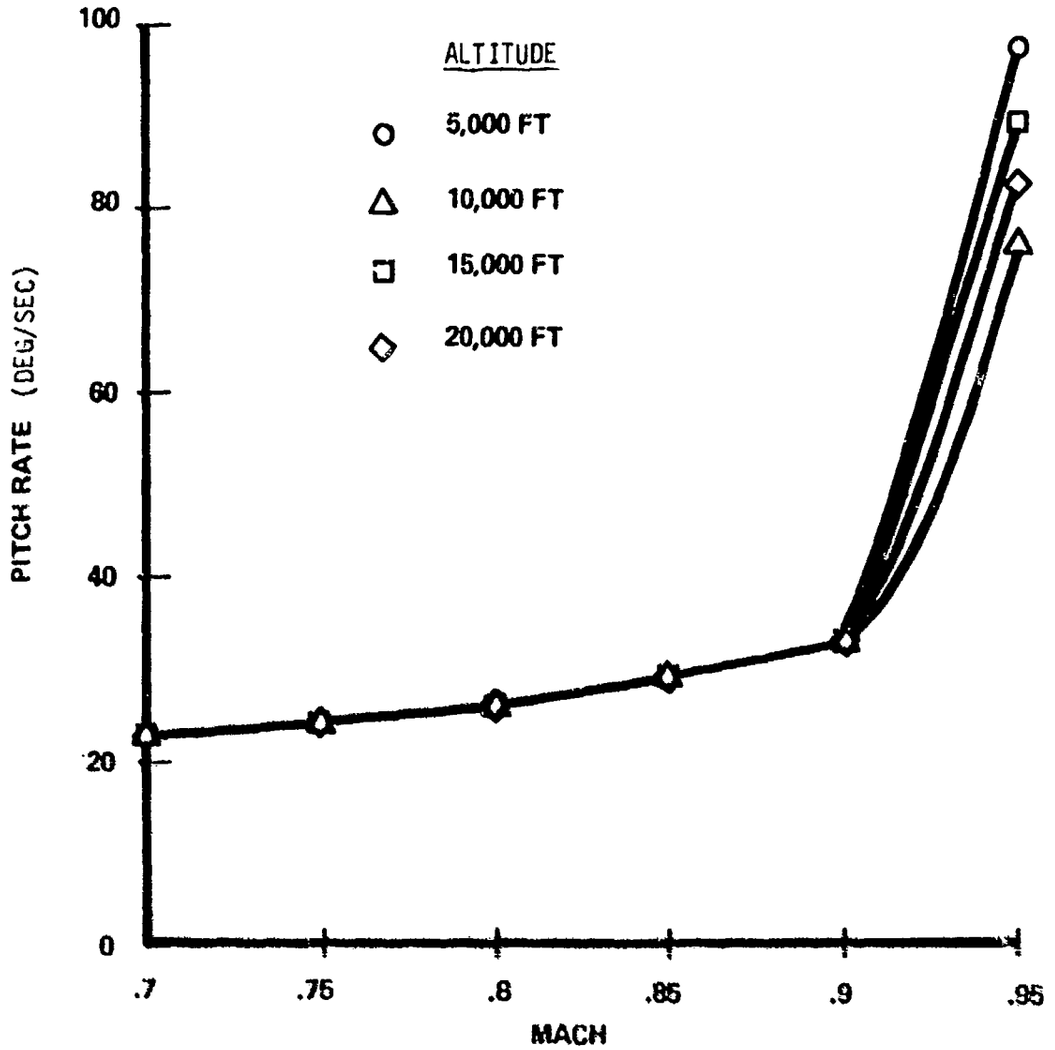


Figure 12.a. Maximum Body Pitch Rate Versus Mach Number

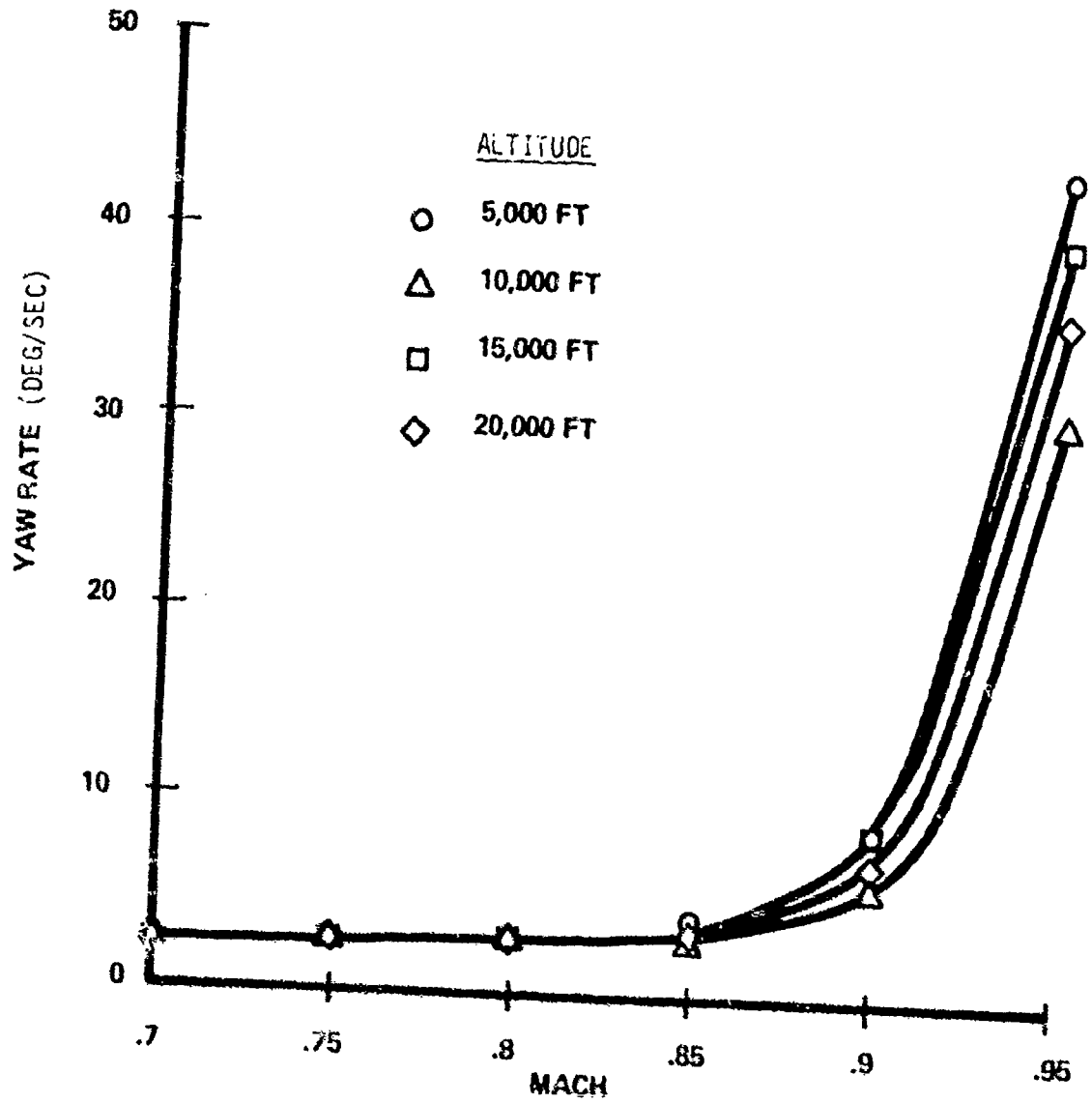


Figure 12.b. Maximum Body Yaw Rate Versus Mach Number

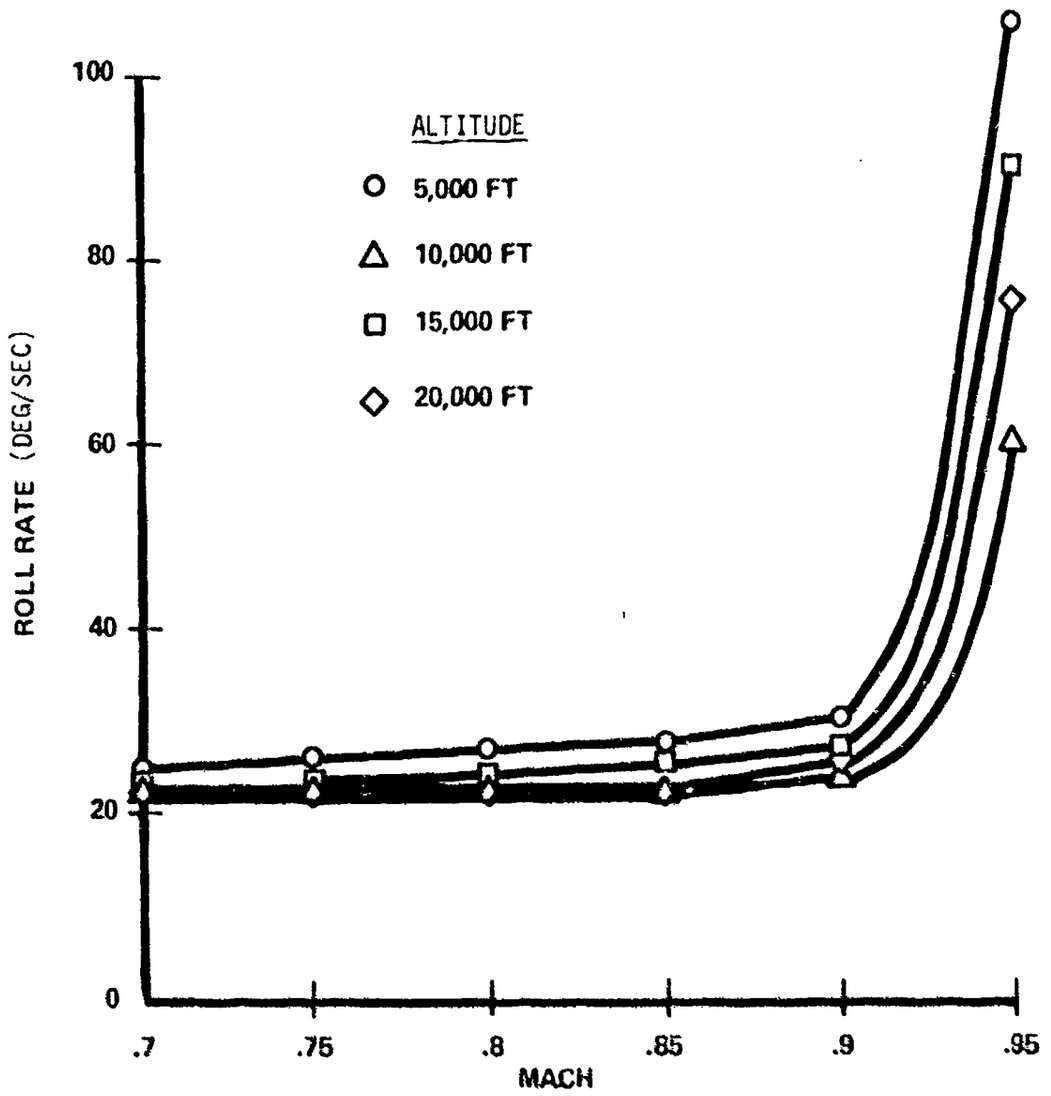


Figure 12.c. Maximum Body Roll Rate Versus Mach Number

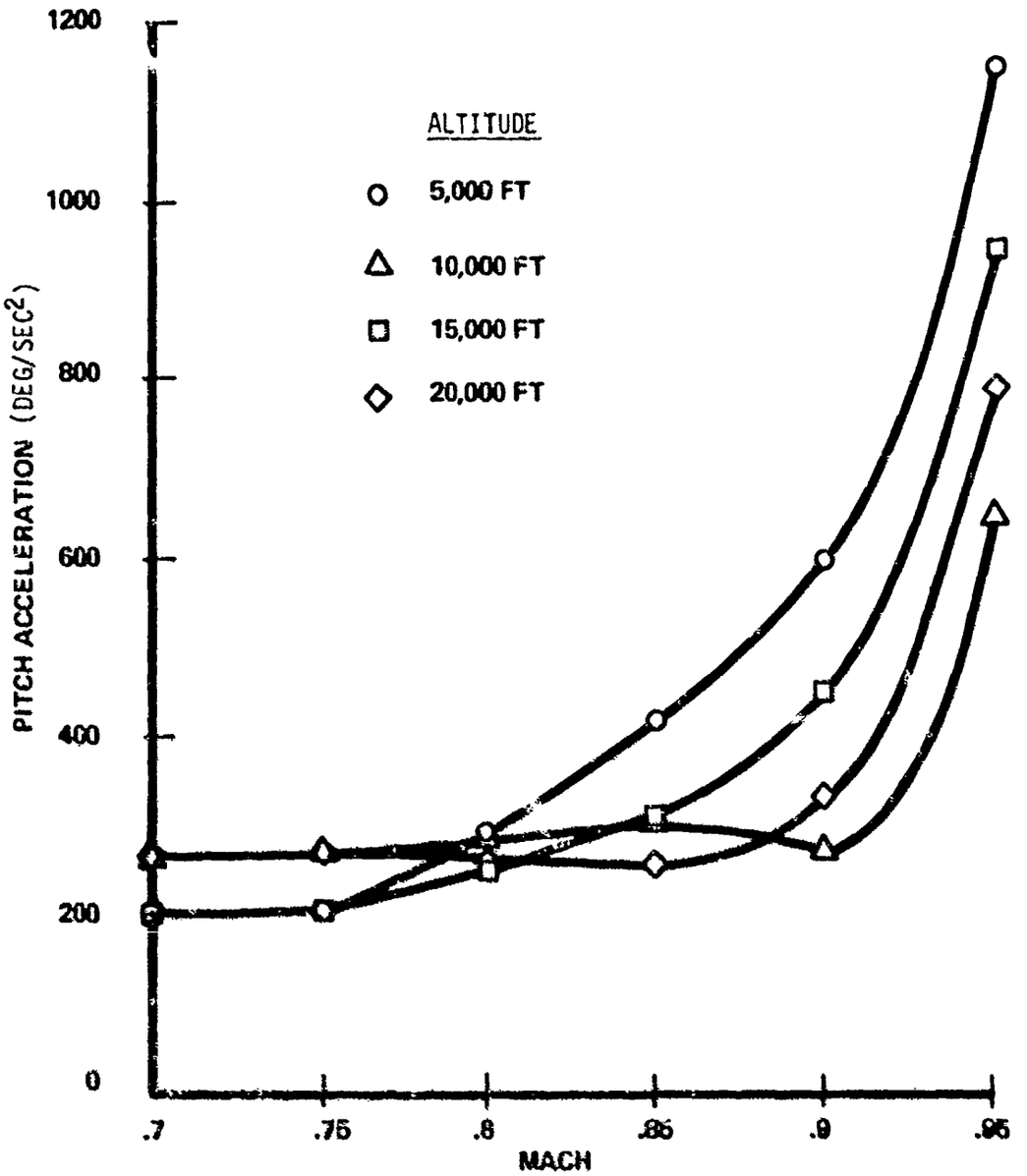


Figure 12.4. Maximum Body Pitch Acceleration vs Mach Number

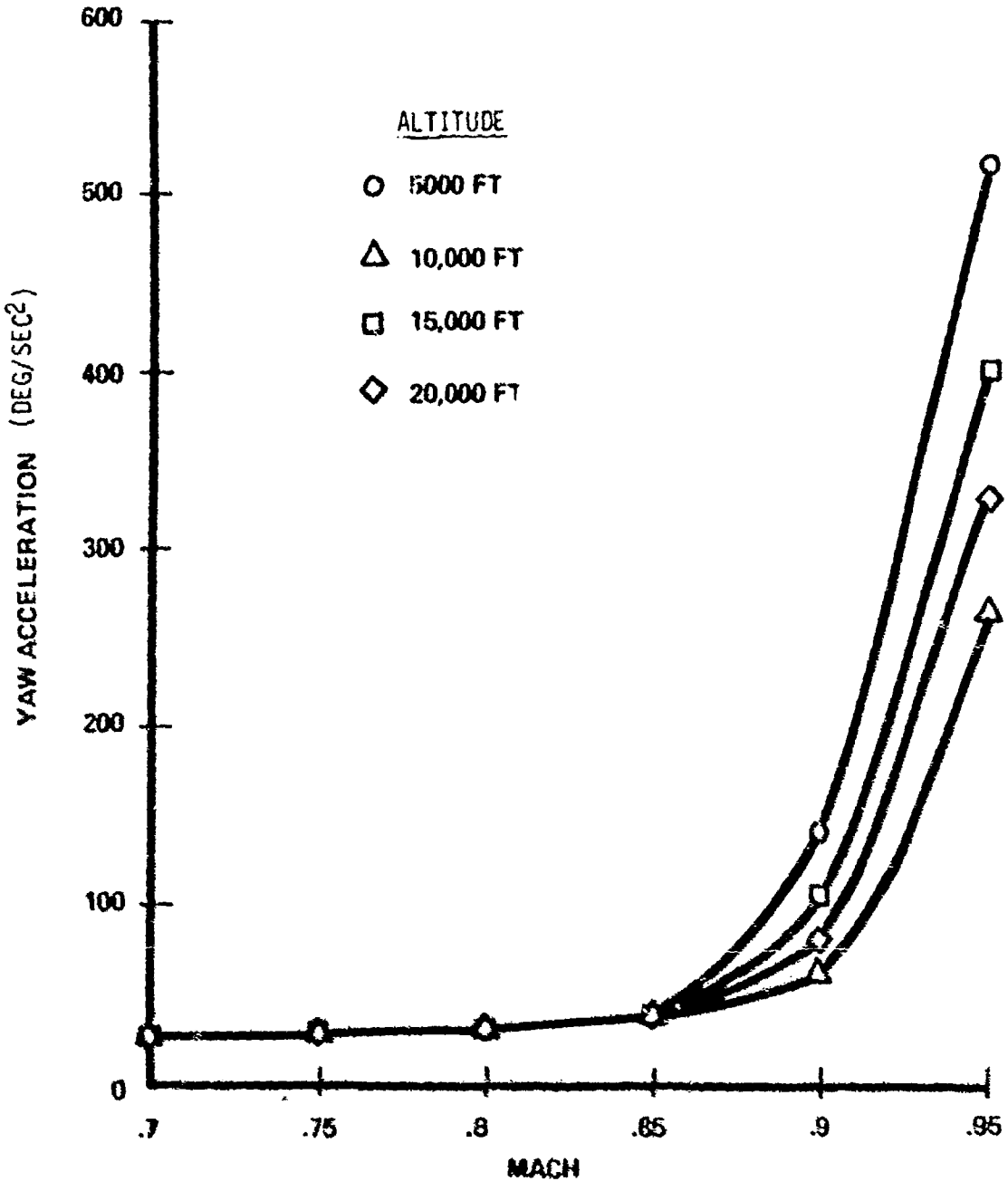


Figure 12.e. Maximum Body Yaw Acceleration Versus Mach Number

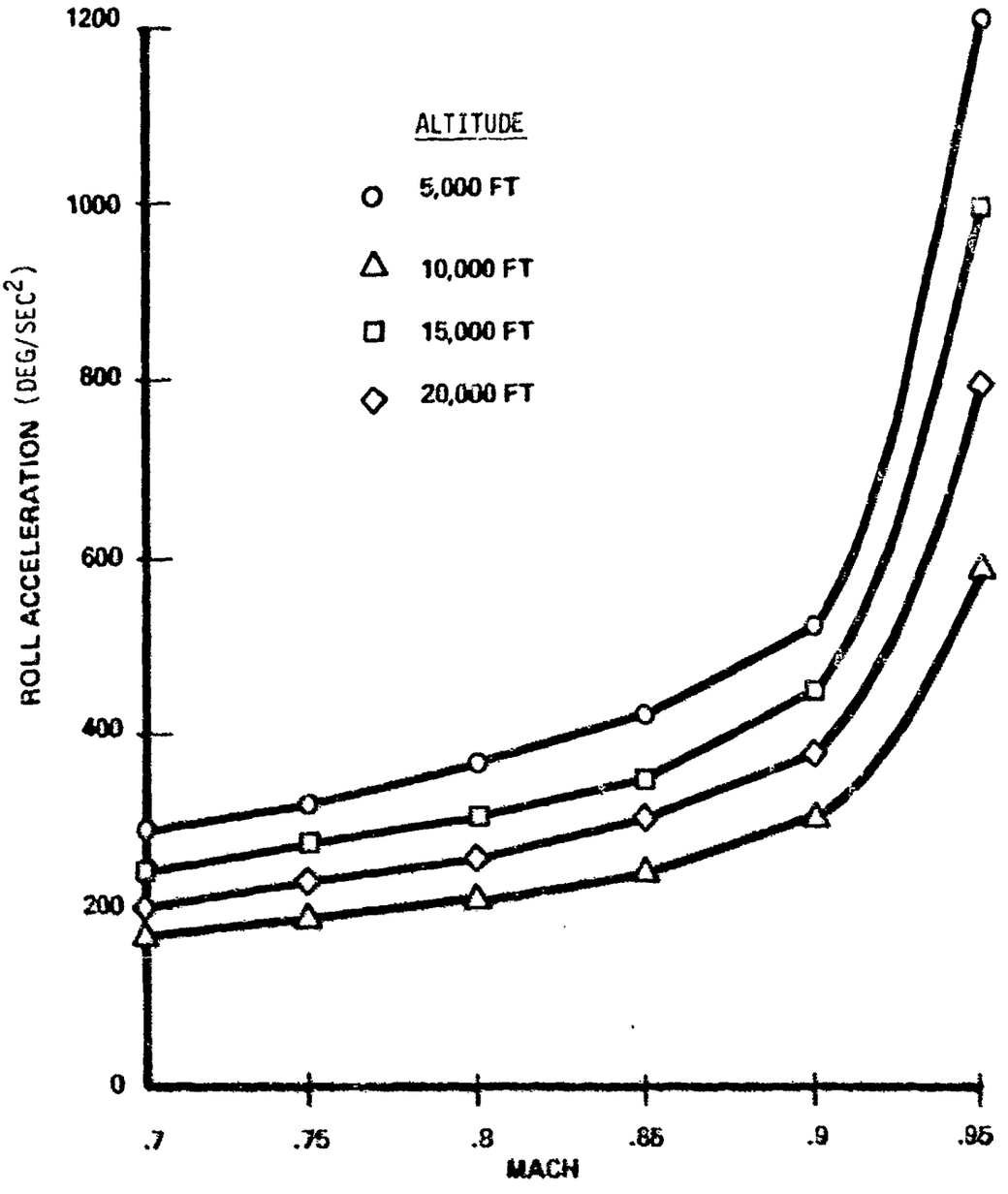


Figure 12.f. Maximum Body Roll Acceleration Versus Mach Number

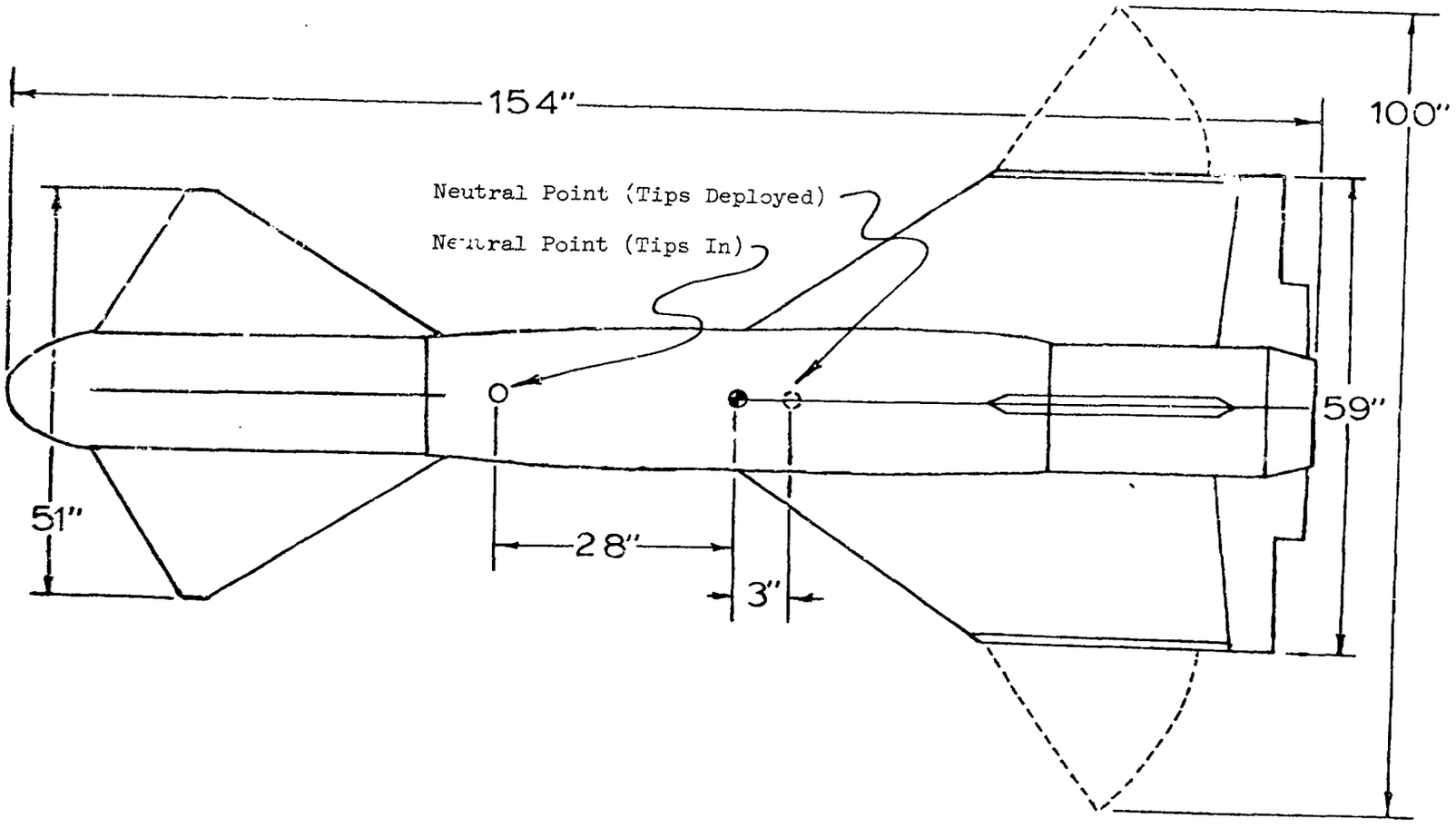


Figure 13. Original Design

A study was initiated to investigate the separation characteristics of the proposed design using the method described in the method description. After correlation runs were made with the CTS trajectories, a preliminary jettison envelope was constructed using a nominal weight F-4 aircraft and the standard ejection rack conditions. The results are shown in Figure 14. This preliminary envelope indicated that weapon separation was highly dependent on the initial aircraft angle-of-attack, and the worst case angle-of-attack condition occurs for a heavyweight aircraft. The obvious desirability of conservative results led to the selection of the heavyweight aircraft as a baseline.

Figure 15 shows the results of the jettison analyses for a heavyweight aircraft. These studies indicated that the weapon would not safely separate over a large portion of the jettison envelope. Without resorting to a total redesign, three solutions to the separation problem appeared feasible:

a. Early deployment of the wing tips to increase the stability of the weapon.

b. A preset pitch flap bias for the jettison mode.

c. Tuning the bomb rack to cause the weapon to pitch down.

The Air Force and the contractor conducted a comprehensive study to evaluate these options. The results of this analysis showed that none of the options, when considered singly or in combination would provide an acceptable solution. Early deployment of the wing tips was unacceptable for several reasons. The increase in stability occurred too late to appreciably change the early portion of the separation. Deployment of the tips would in some cases more than double the lift generated by the wings and strakes. Finally, deployment of the tips increased the wing span of the store by nearly 70 percent, which compounded the aircraft/weapon clearance problems.

The capabilities of the actuator limited the preset pitch flap bias to 7 degrees, which was not sufficient to provide safe separation throughout the envelope.

The best jettison results were obtained using a tuned bomb rack with the maximum allowable opening forward and the rear orifice blocked. Although this option allowed jettison over most of the captive flight envelope, it was felt that this solution would generate excessive angular rates and accelerations which might result in a weapon breaklock during launch.

At this point the Air Force and the contractor investigated the separation characteristics of a store that was statically stable in the carriage position. The force/moment grid program was modified to

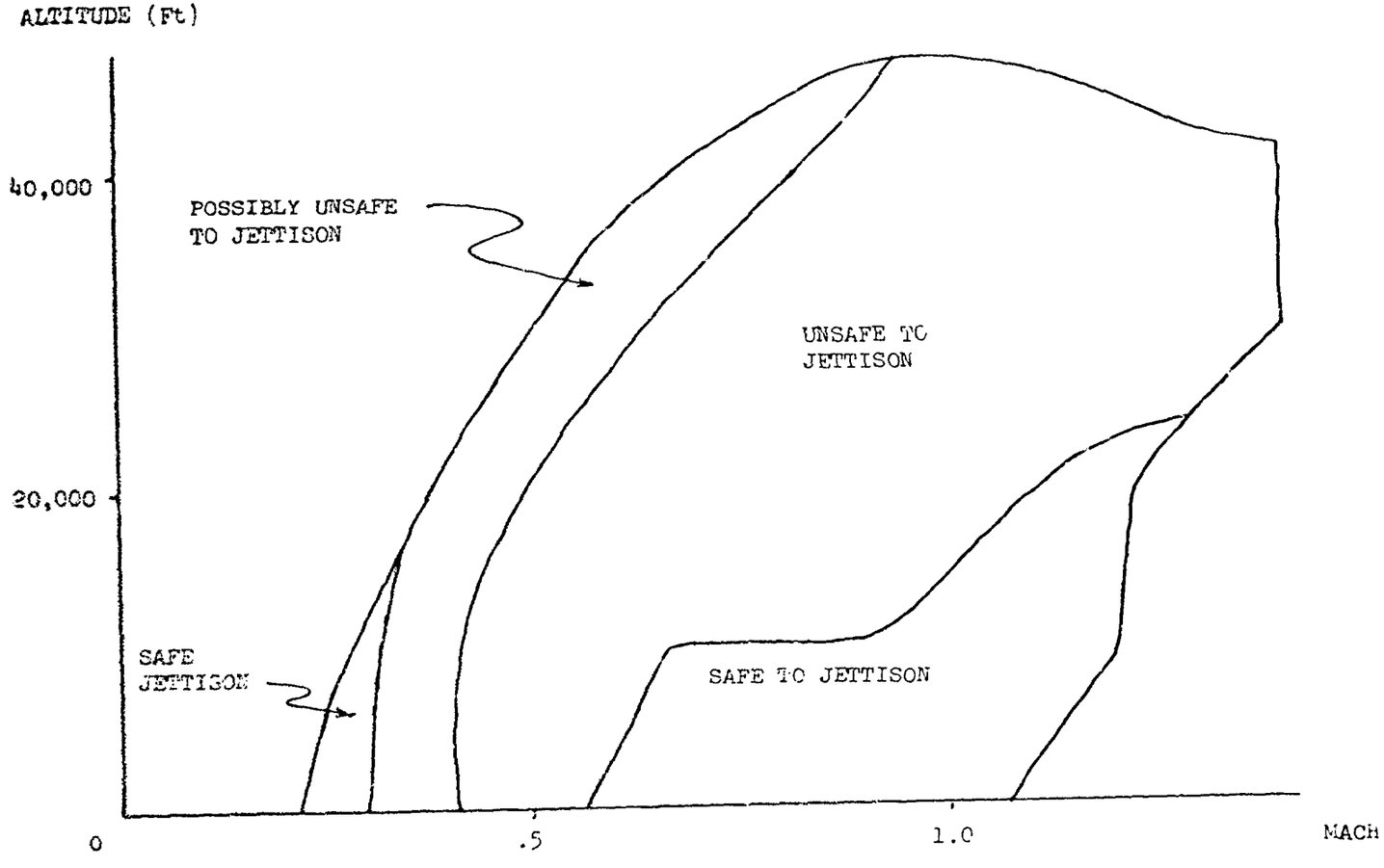


Figure 14. Nominal Weight Aircraft Jettison Envelope

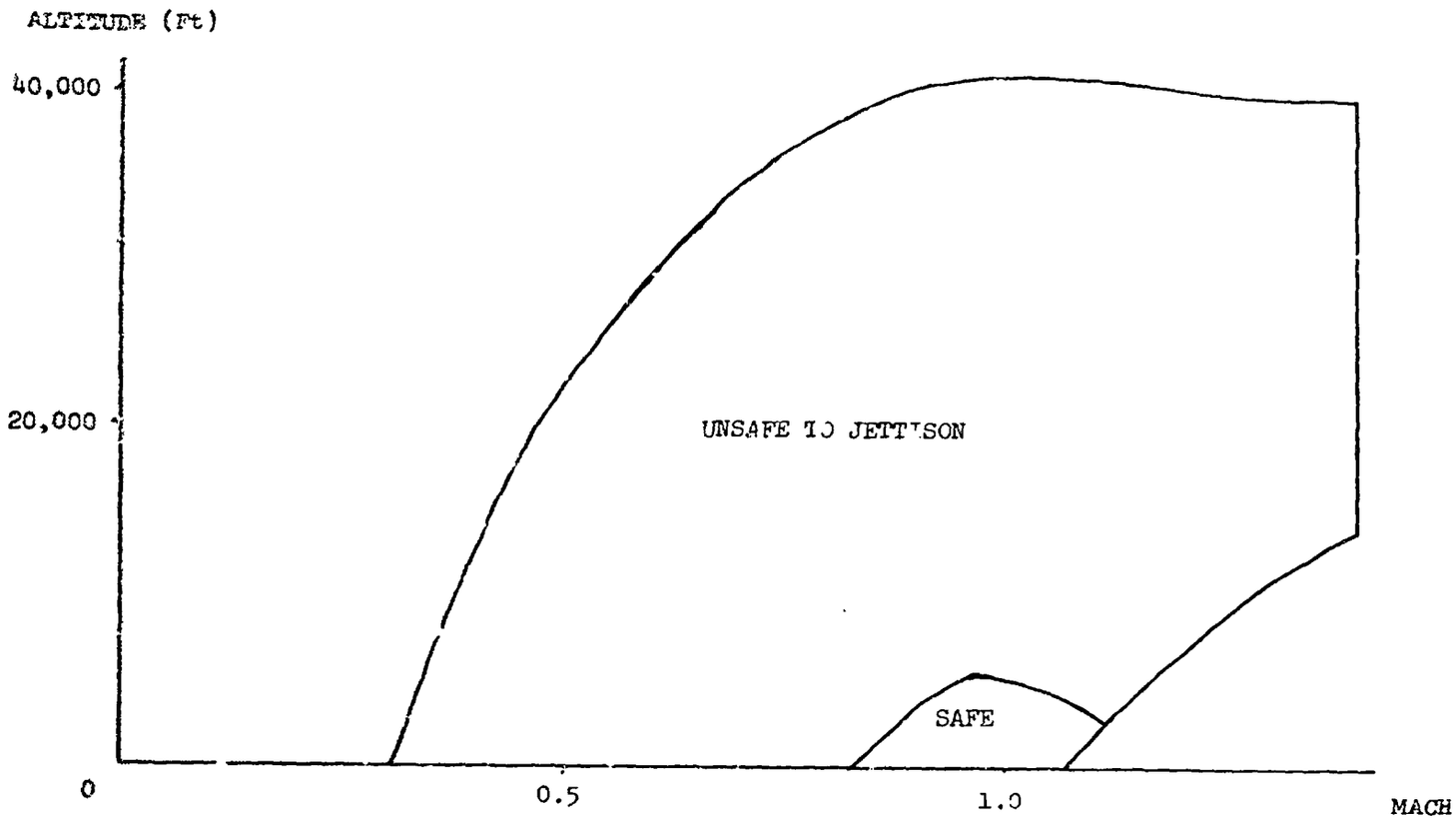


Figure 15. Heavyweight Aircraft Jettison Envelope

approximate the differences between the unstable and stable versions. The study showed that a marginally stable store with a pitch-flap-bias would adequately separate throughout the envelope. The impact on range and manueverability of a stable store was judged to be acceptable.

The desired increase in stability was accomplished by reducing the size of the forward strakes as shown in Figure 16. New grid coefficient runs were made with the store on the inboard station of an F-4 with a 370-gallon fuel tank outboard. In two hours and six minutes of testing, the following runs were completed:

Mach Number	Aircraft Angles of Attack
0.3	2, 4, 6, 8, 12, 16
0.65	0, 2, 4, 6, 8, 12
0.80	0, 2, 4, 6, 8
0.95	0, 2, 4, 6
1.05	0, 2, 4, 6
1.2	0, 2, 4

In two hours of tunnel testing, enough information was generated to allow almost complete coverage of the F-4 envelope. Computer analyses showed that the redesigned weapon would separate safely from the aircraft in the jettison mode. Five mass simulation vehicles were dropped at various points in the captive flight envelope to provide actual flight test data for comparison with the computer analysis. The results for two of these drops are presented in Figures 17 and 18.

COMPLETE SEPARATION ANALYSIS OF A NEW WEAPON

The glide bomb in Figure 19 is currently under development by the Air Force. This guided, 2000-pound bomb utilizes a set of folding wings to extend the range. At the request of the system program office (SPO) a study was undertaken to determine whether or not this weapon would safely separate from the F-4 aircraft.

The 4T wind tunnel at AEDC was used to collect three basic types of data with a 0.05-scale model: grid data, CTS trajectories, and free-stream data. The grid data consisted of total aerodynamic coefficients acting on the model in the vicinity of the F-4, as outlined in the method description. This data was collected with and without fuel tanks on the F-4 model and at various aircraft angles of attack and Mach numbers. The CTS trajectories were made at a wide range of flight conditions and with various tail deflection angles on the weapon to simulate jettison and to provide data to compare with future computer simulation. Finally the static aerodynamic coefficients of the weapon model with the wings folded were gathered and compared with those of the 0.20-scale model. The force coefficients

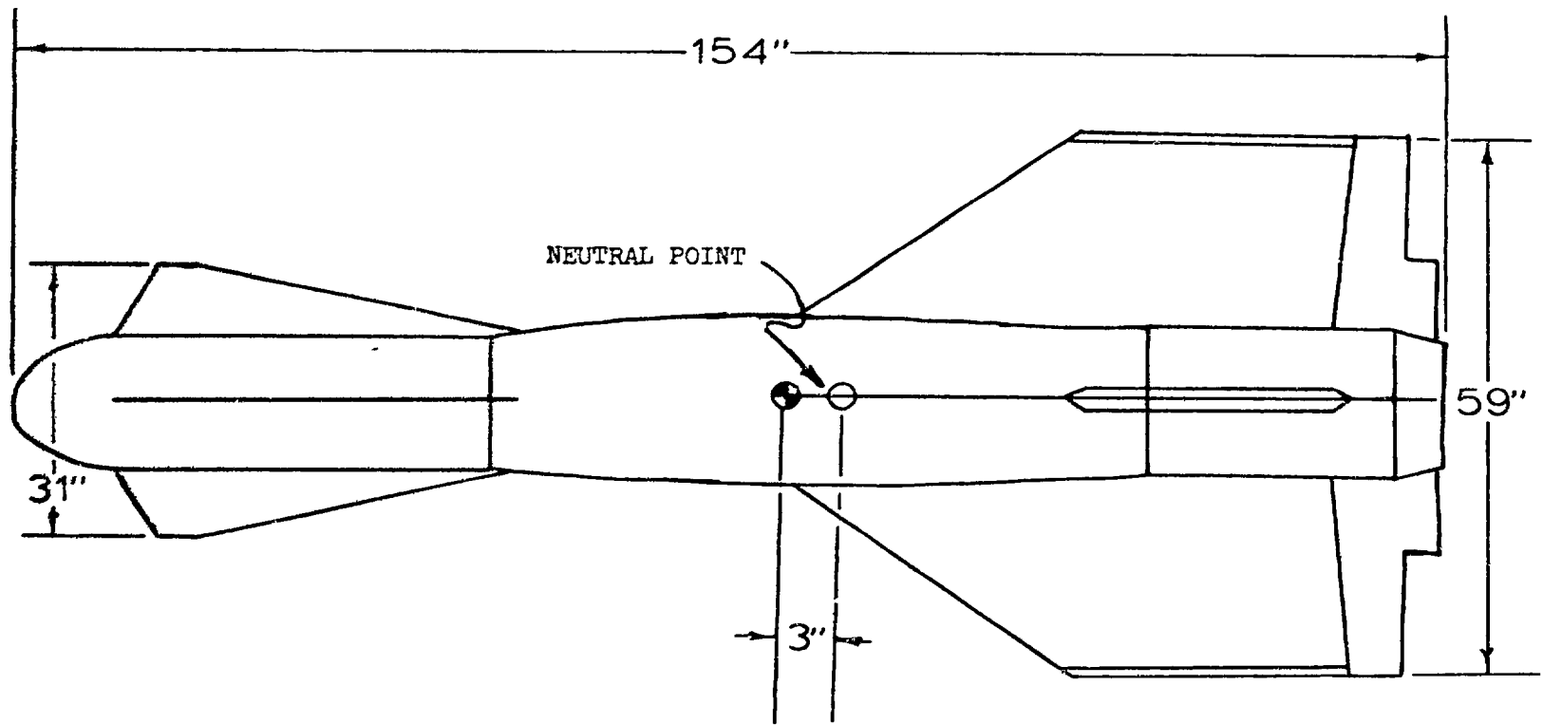


Figure 16. Revised Design

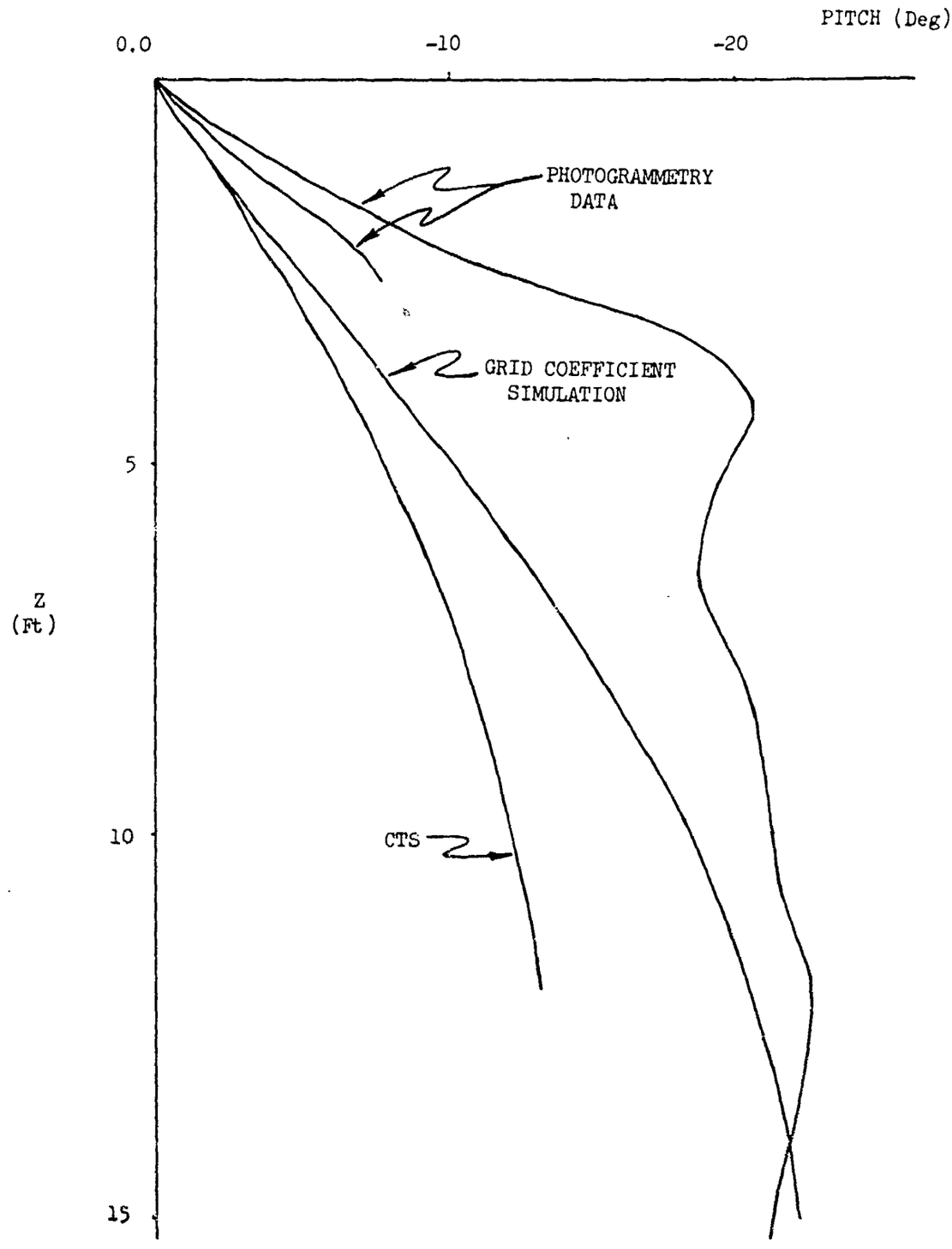


Figure 17.a. Pitch Versus Vertical Displacement – 13000 Ft, .8 Mach

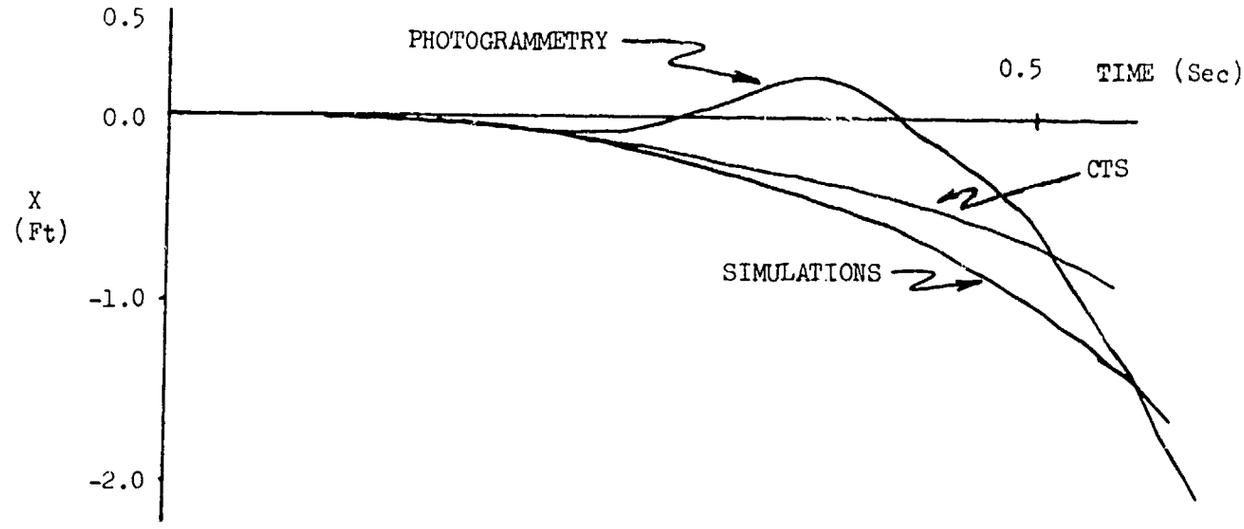


Figure 17.b. Longitudinal Displacement Versus Time. 13000 Ft, .8 Mach

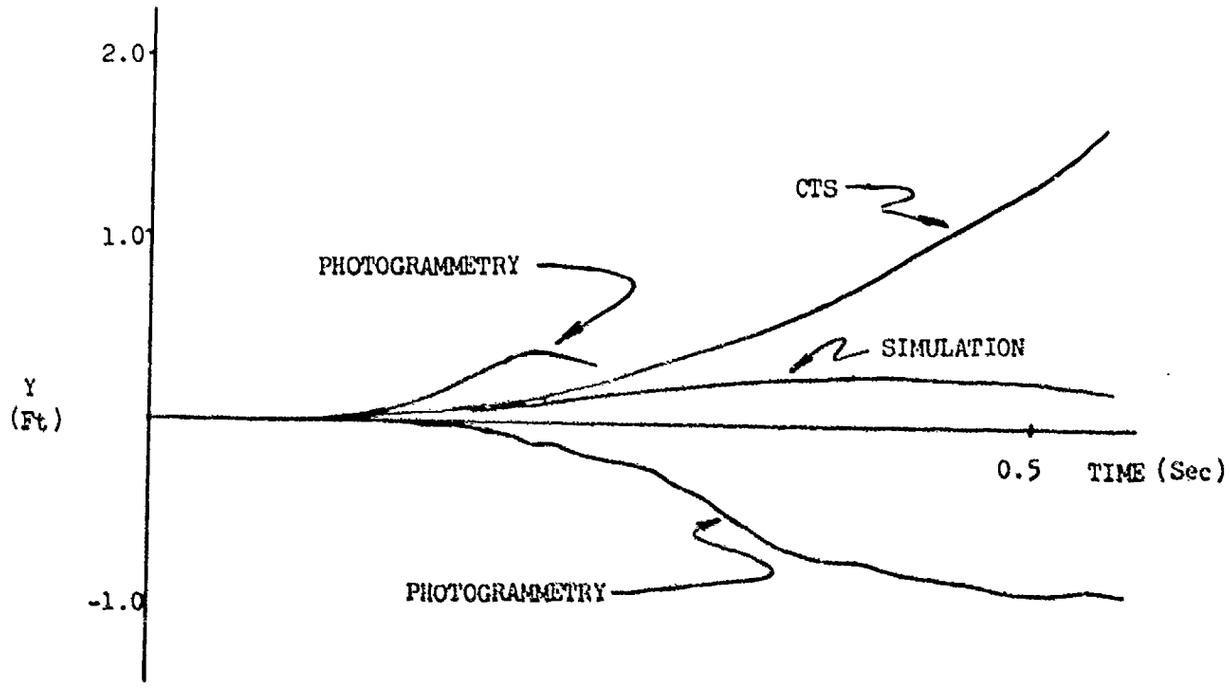


Figure 17.c. Lateral Displacement vs Time — 13000 Ft, .8 Mach

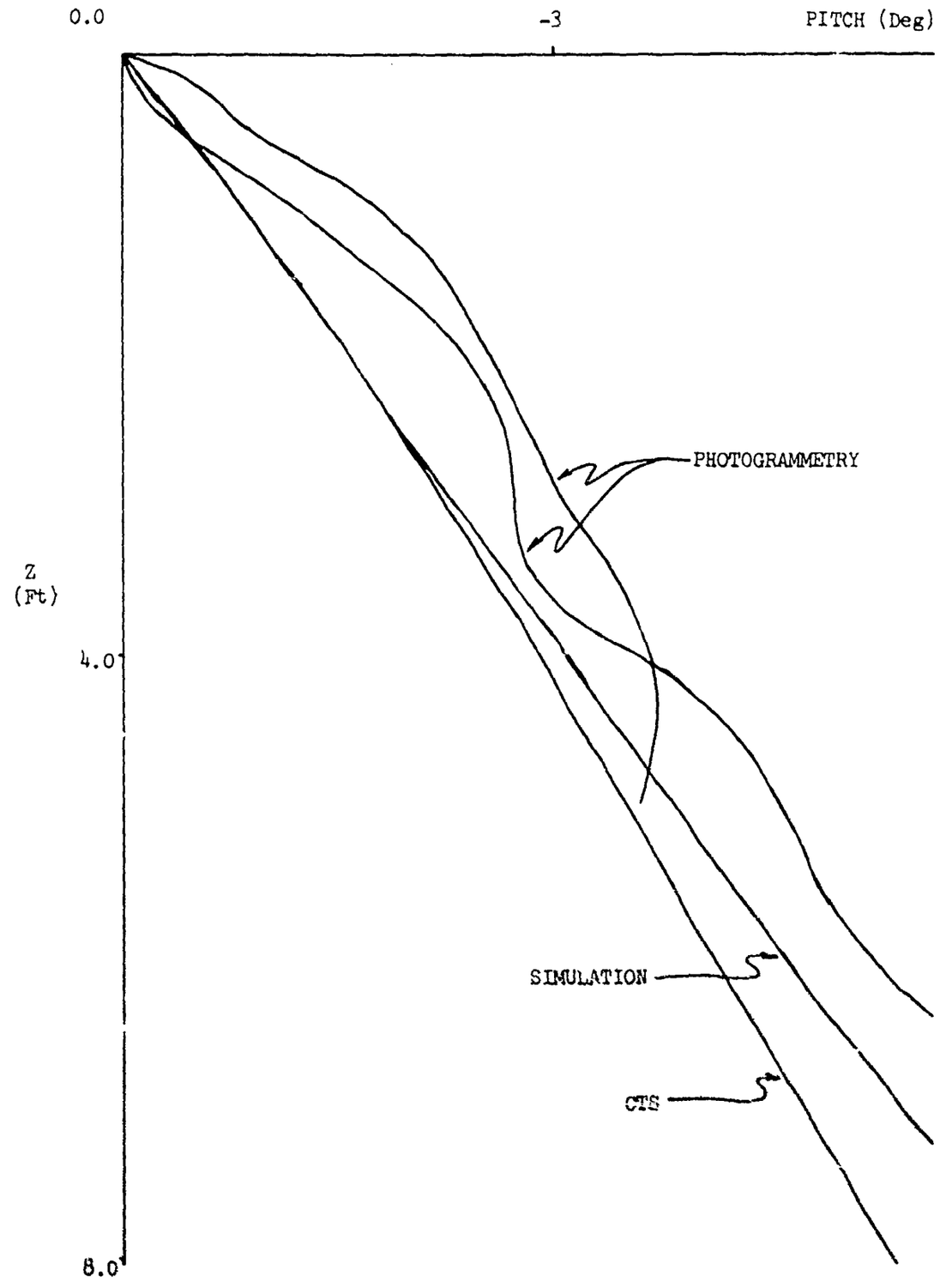


Figure 18.a. Pitch Versus Vertical Displacement – 40,000 Ft, .9 Mach

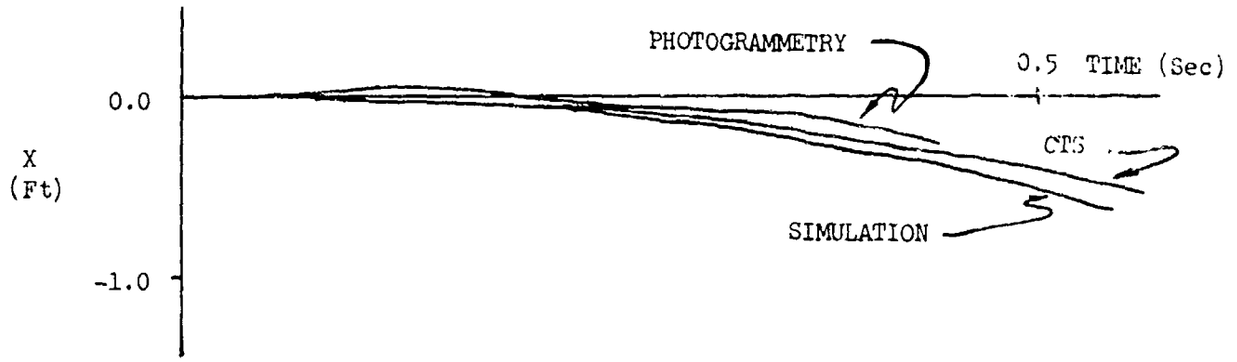


Figure 18.b. Longitudinal Displacement vs Time. 40,000 Ft, .9 Mach

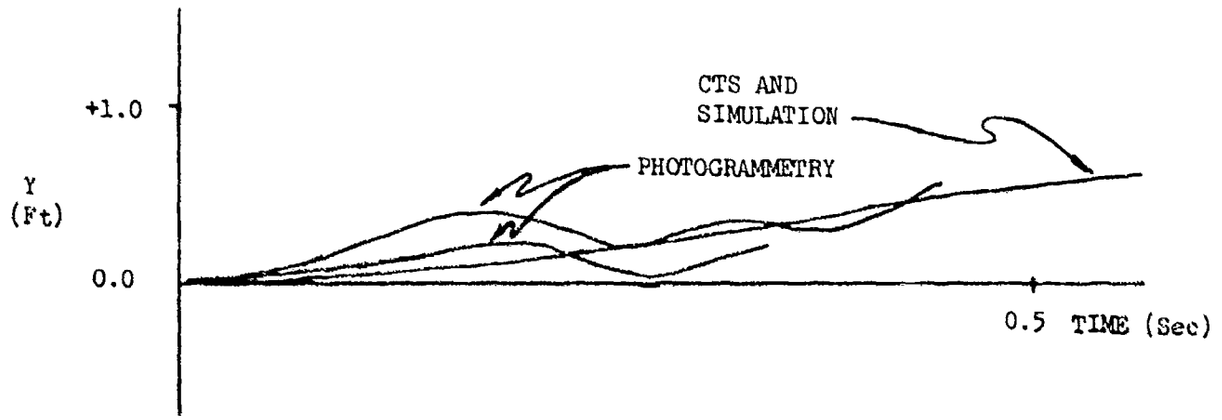


Figure 18.c. Lateral Displacement vs Time – 40,000 Ft, .9 Mach

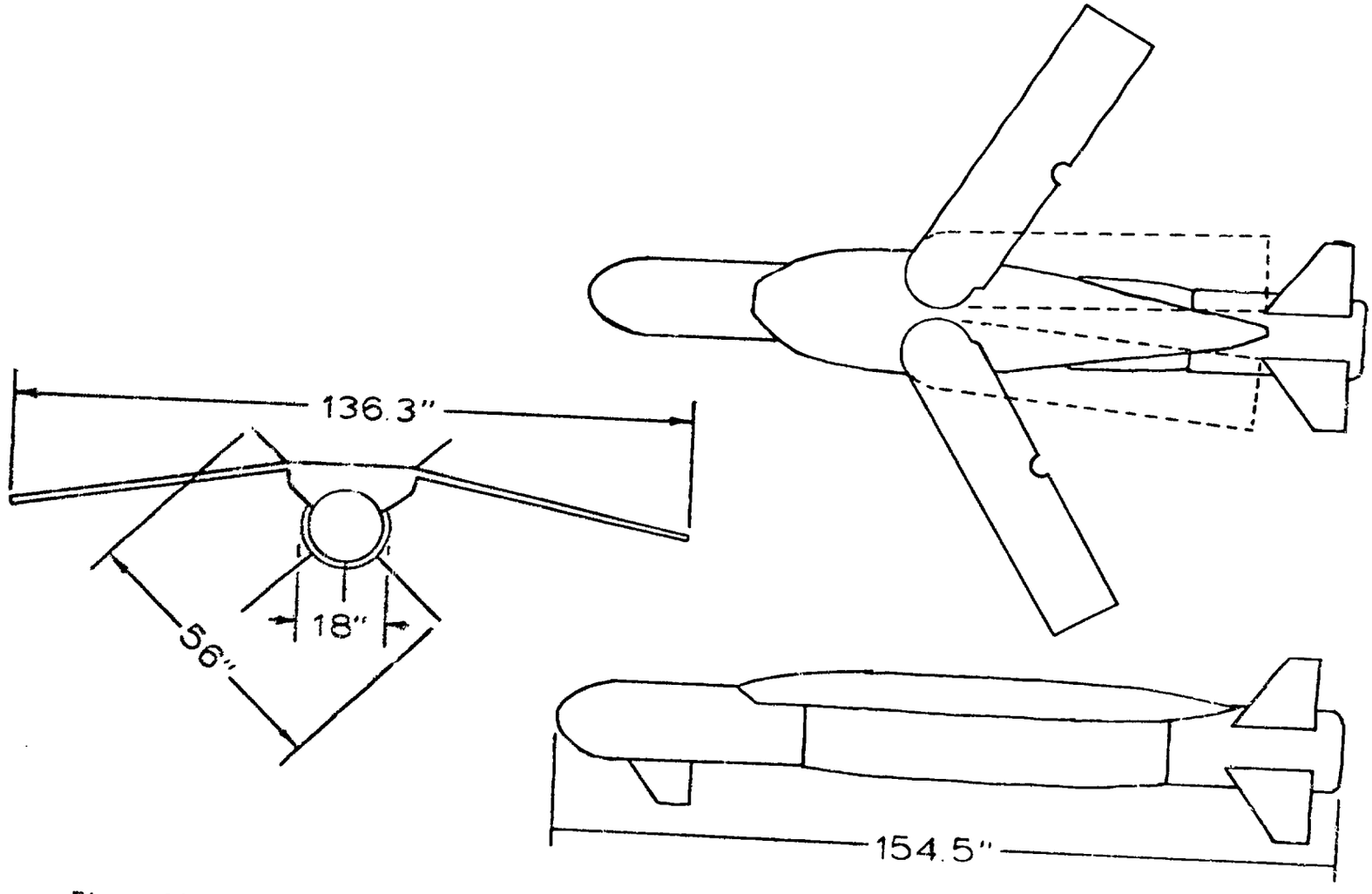


Figure 19. Glide Bomb Configuration

were in good agreement as were the moment coefficients at low ($\pm 4.0°$) angles of attack. At higher angles of attack, however, the moment coefficient of the smaller model was as much as 50 percent greater than the larger model.

The next task was to use this data along with information from the SPO to develop a digital computer simulation of the complete weapon. The 0.20-scale model data was used to calculate the free-stream aerodynamic characteristics of the weapon. The data for the inboard wing station of the F-4 with a MK-84 2000-pound bomb installed (Reference 4) was selected for the flow field data option in the program. For the grid data, the technique in the method description was used to obtain interference coefficients for the weapon. A digital model of the autopilot and a scheme for computing the wing opening aerodynamics were obtained from the SPO and incorporated into the basic program.

A study was initiated to evaluate the two simulation techniques--flow field data and grid data. To do this, computer simulations of jettison trajectories were made and compared to the CTF trajectories. Agreement with translational motion was excellent, as shown in a typical example by Figure 20. Agreement with pitching and yawing motion was generally good, as shown in Figures 21 to 25.

The disparities shown can be attributed to three factors. First, the free-stream aerodynamics of the 0.20-scale model used in the simulations are somewhat different from those of the 0.05-scale model of the CTS trajectories. For example, at 0.7 Mach and $-4.0°$ angle of attack, the pitching moment of the large model is only 50 percent that of the small model. Secondly, the flow field data on the F-4 was gathered at a single Mach number (0.85) and a single aircraft angle of attack ($0.3°$). Although this permits the prediction of general trends in the stores' motion, there are usually differences between the simulations and CTS or flight test trajectories. Finally, at supersonic Mach numbers, shock location plays a major role in determining separation trajectories.

A comparison of the two computer techniques indicated that the grid technique was the better method to use in analyzing the separation of the weapon with an active autopilot. The initial simulations showed that a normal launch with an autopilot posed no threat to the aircraft. The analysis then focused on single failures of three major components: the autopilot, the surface actuators, and the wing opening mechanism.

An autopilot failure could command full up on the tail surfaces causing the weapon to pitch up and possibly contact the aircraft. A flap position limiter was included in the original design preventing positions of more than five degrees from neutral for the first two seconds. The simulations showed that this limiter would be sufficient to protect the aircraft.

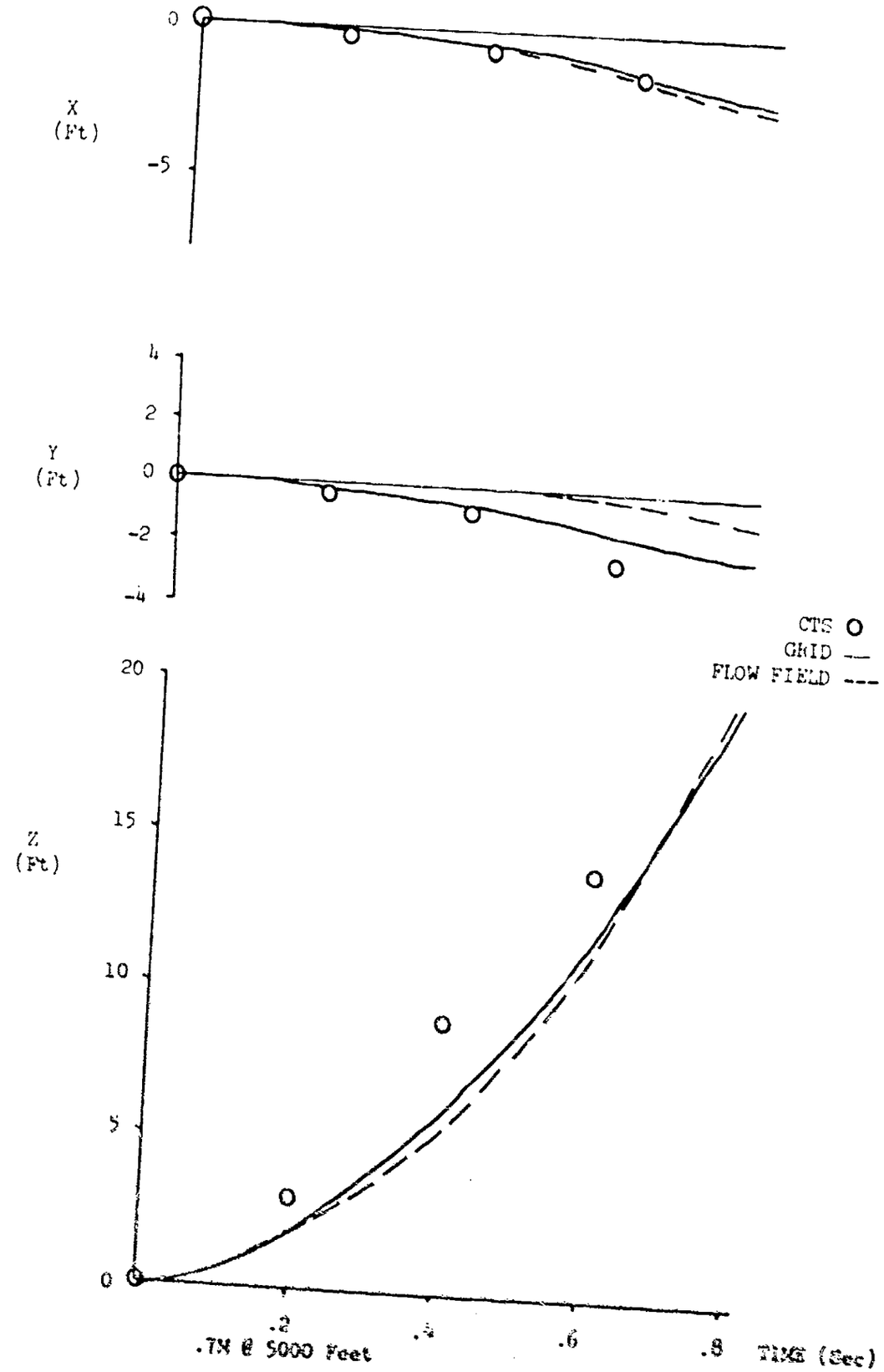


Figure 20. CTS vs Simulation Comparison (Translational)

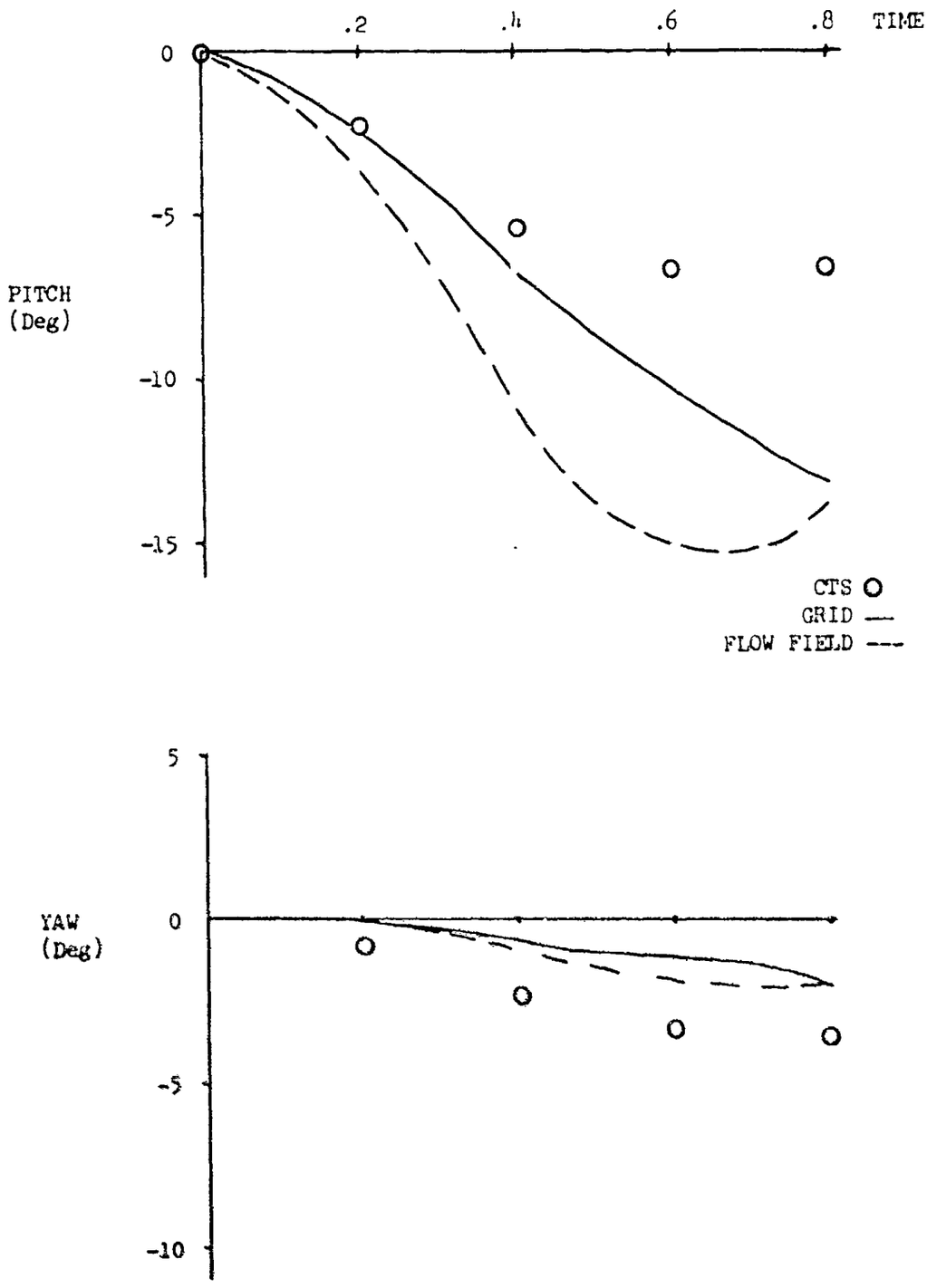
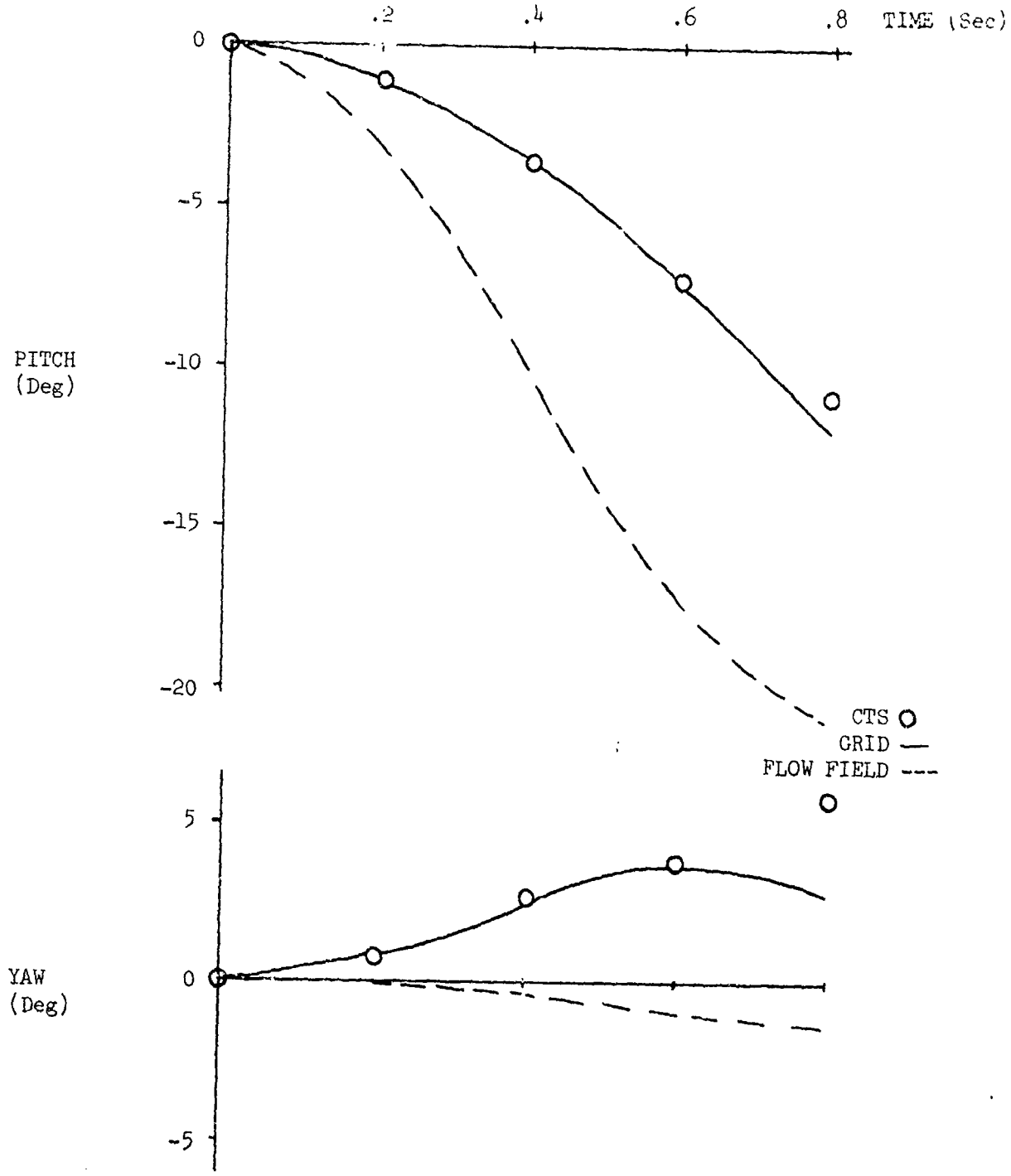
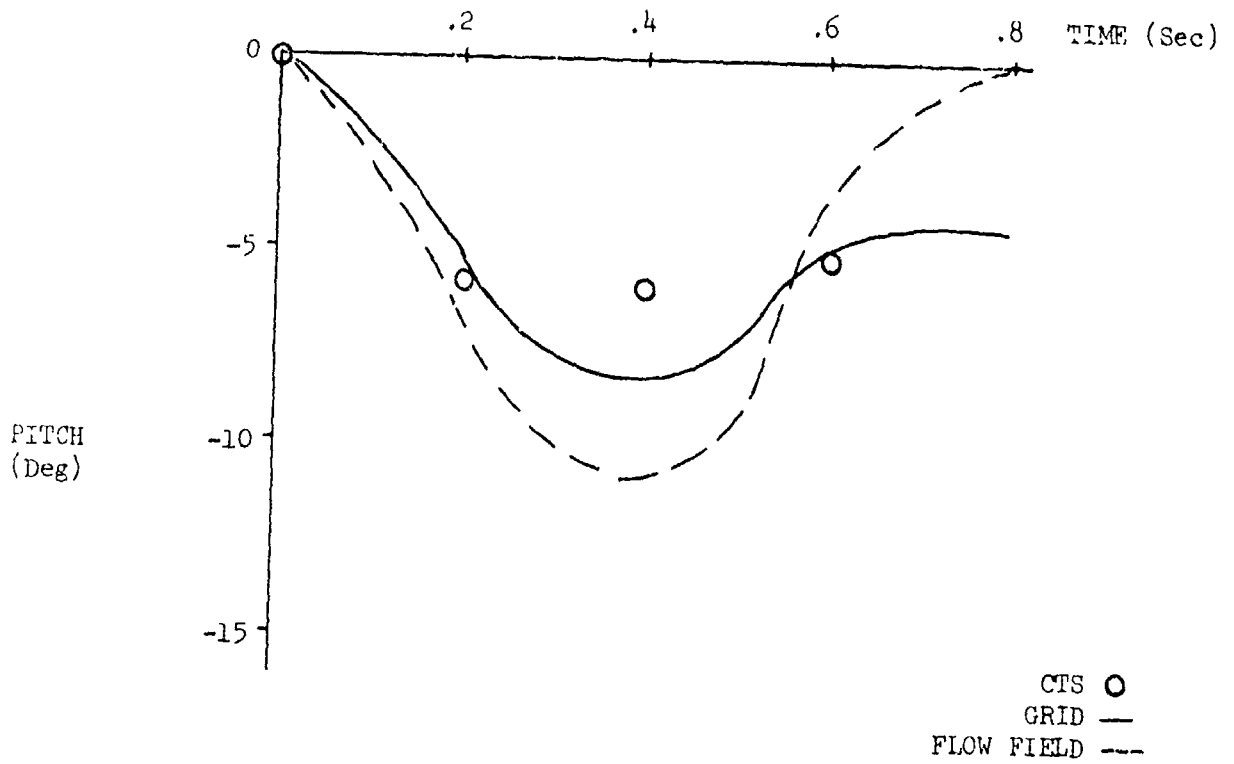


Figure 21. CTS vs Simulation Comparison (Angular)



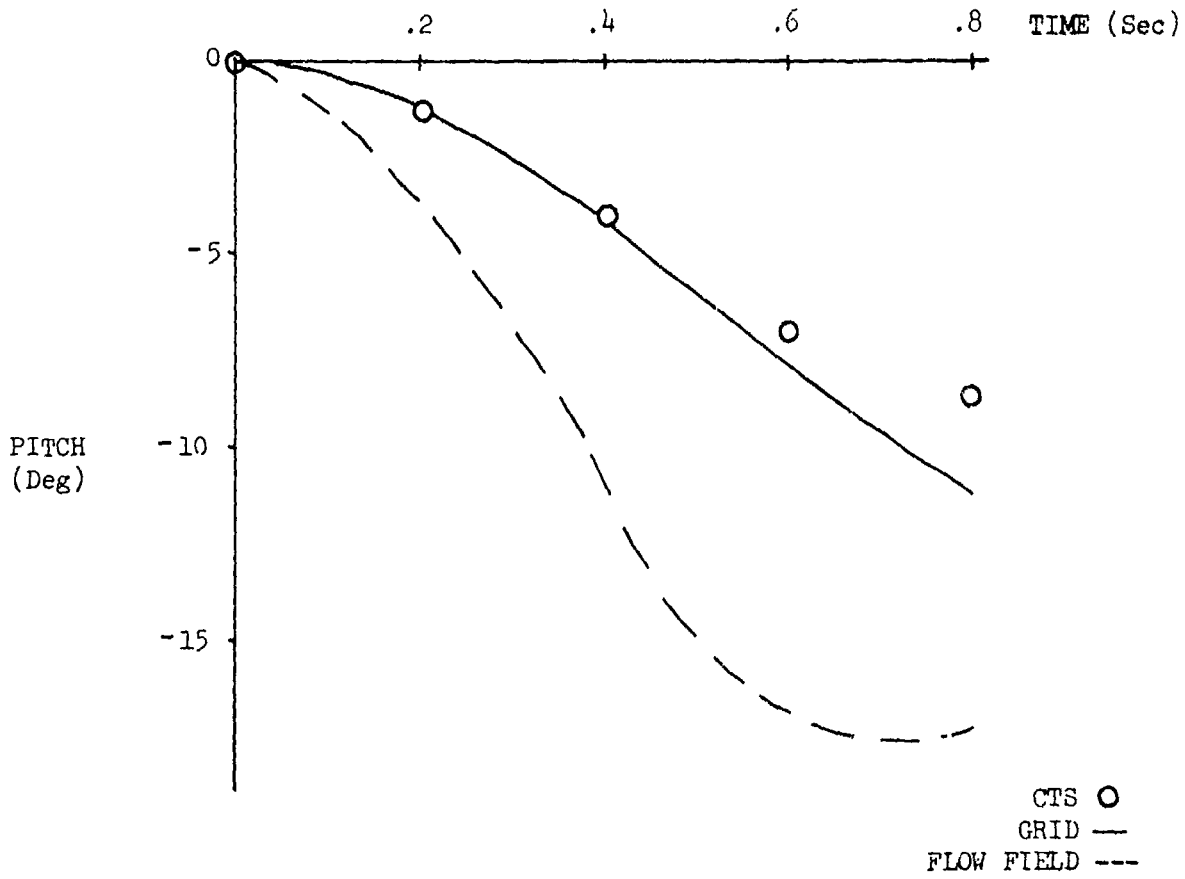
0.9M @ 40,000 Feet

Figure 22. CTS vs Simulation Comparison (Angular)



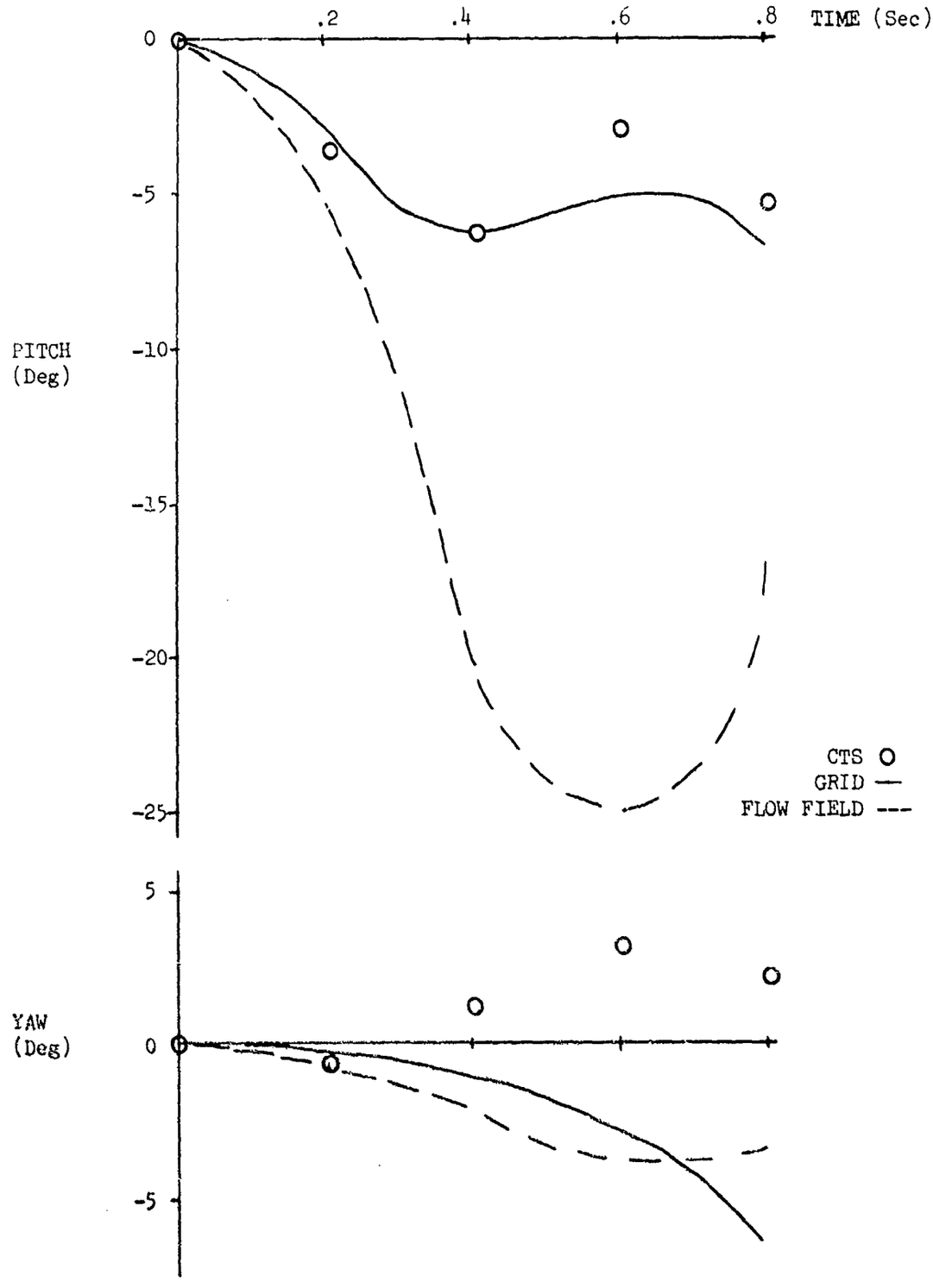
0.95M @ 5,000 Feet

Figure 23. CTS vs Simulation Comparison (Angular)



0.95M @ 40,000 Feet

Figure 24. CTS vs Simulation Comparison (Angular)



1.3M @ 40,000 Feet

Figure 25. CTS vs Simulation Comparison (Angular)

A single actuator failure in the full up or down position was also studied. It was determined that the autopilot could still control the vehicle during launch within acceptable limits.

Finally, the timing and a failure of the wing opening mechanism were investigated. The original design called for the wings to start deployment one second after weapon release. The analysis showed, however, that even with a pitch flap limiter, an autopilot failure would place the weapon precariously close to the aircraft as the wings deployed. The recommendation was made to the SPO that the design be changed to start wing deployment two seconds after weapon release. In addition, it was suggested that the wings be mechanically locked for 1.5 seconds to preclude any danger caused by early wing opening. Both of these features were later incorporated in the design by the contractor.

During the initial portion of the flight test program, three mass simulation vehicles were dropped to verify separation characteristics. These vehicles were configured with a seven-degree-down pitch-flap-bias on the tail surfaces to aid separation. A comparison of the flight test data with the flow field and grid techniques are shown in Figures 26 to 28.

These comparisons show good agreement between the experimental data and the two techniques, particularly the grid technique. The disagreement at the higher pitch angles (greater than 15.0°), is attributed to the lack of emperical data on the 0.20-scale model at these large angles.

In general, these simulation techniques provide the capability to accurately predict the motion of a guided weapon as it separates from the aircraft. They allow the identification of potential problem areas such as the wing opening time, before flight test, thereby permitting the necessary design changes. This permits a reduction in the number of both wind tunnel and flight test hours, resulting in a savings of expensive energy resources.

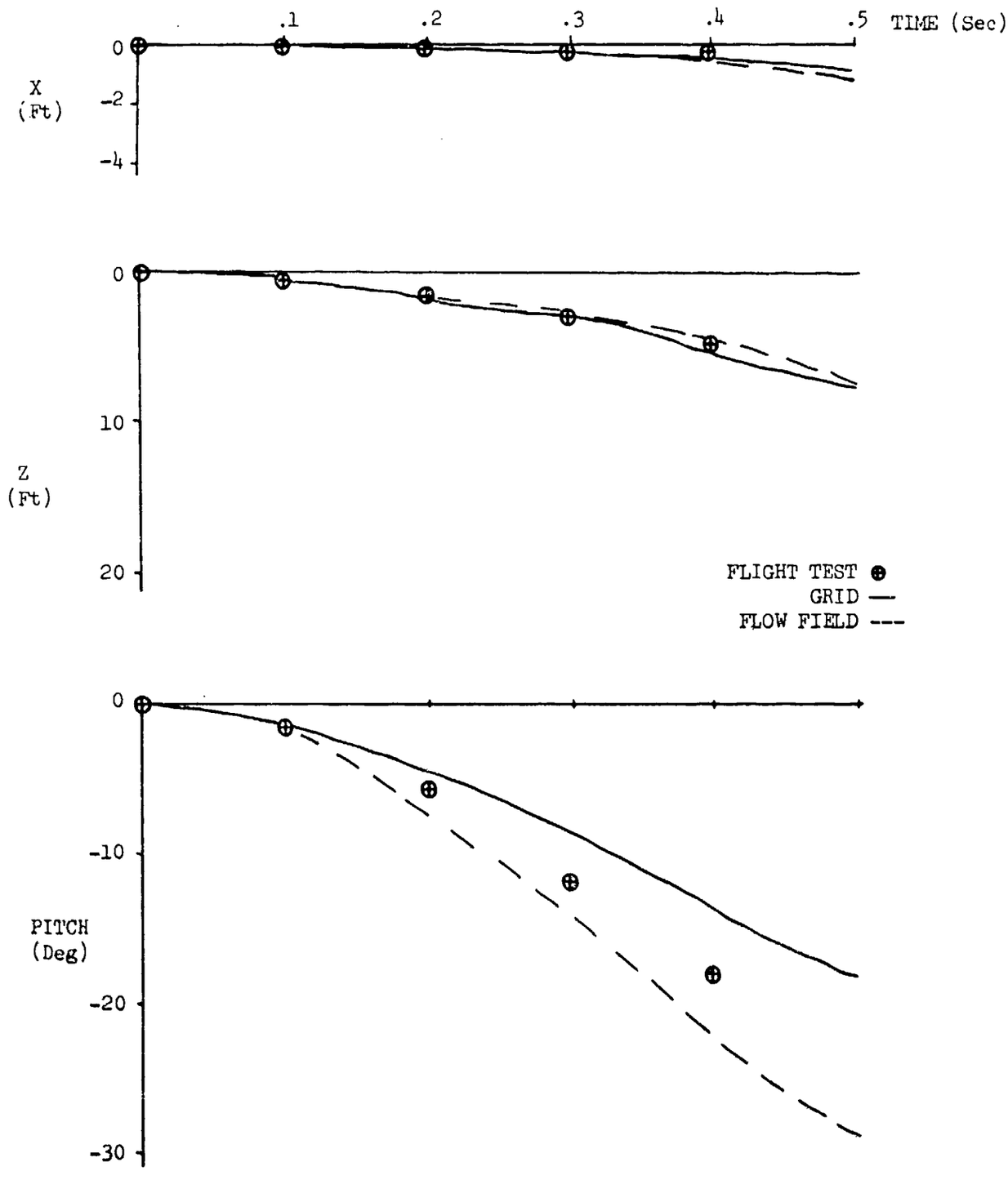


Figure 26. Flight Test vs Simulation Comparison

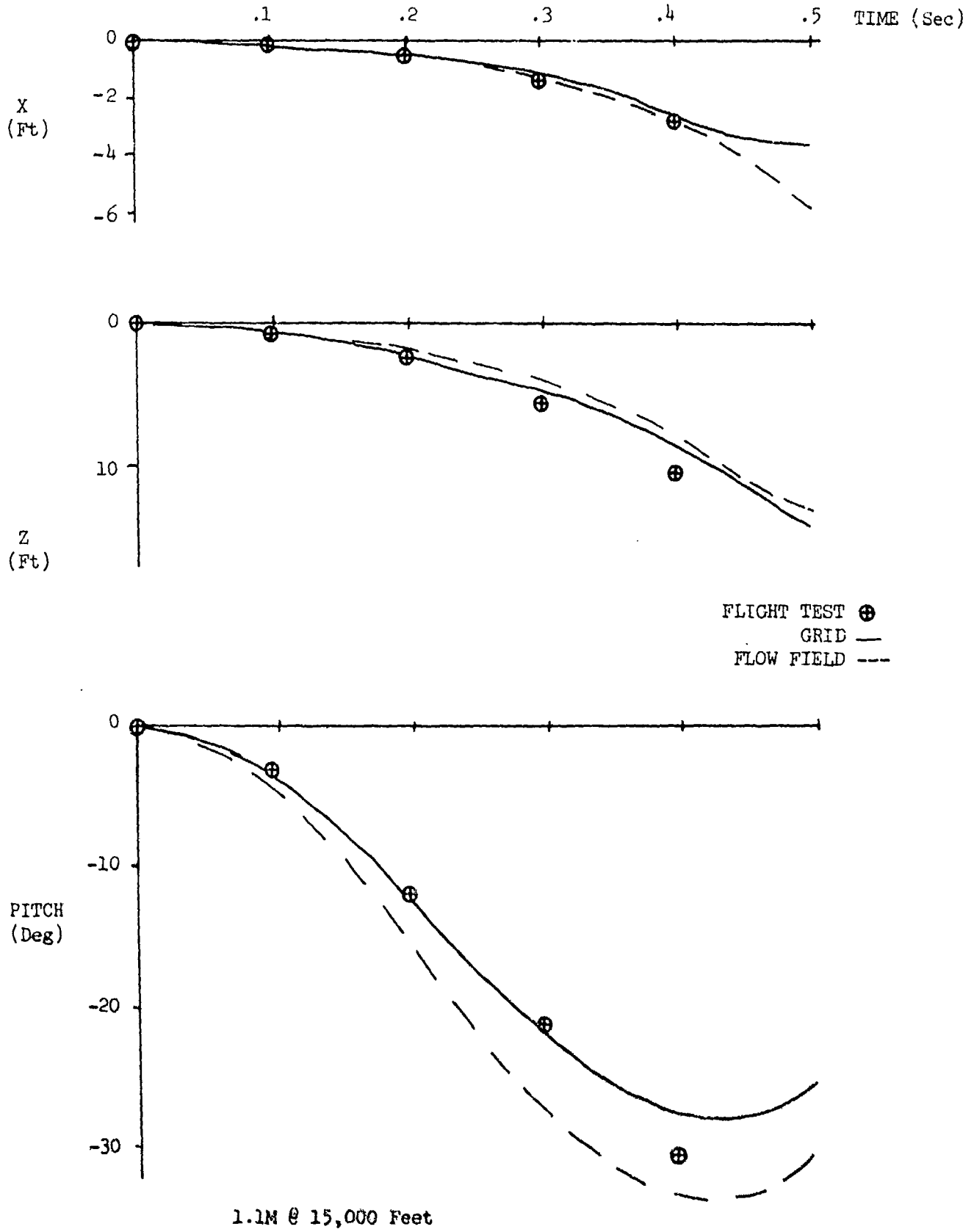


Figure 27. Flight Test vs Simulation Comparison

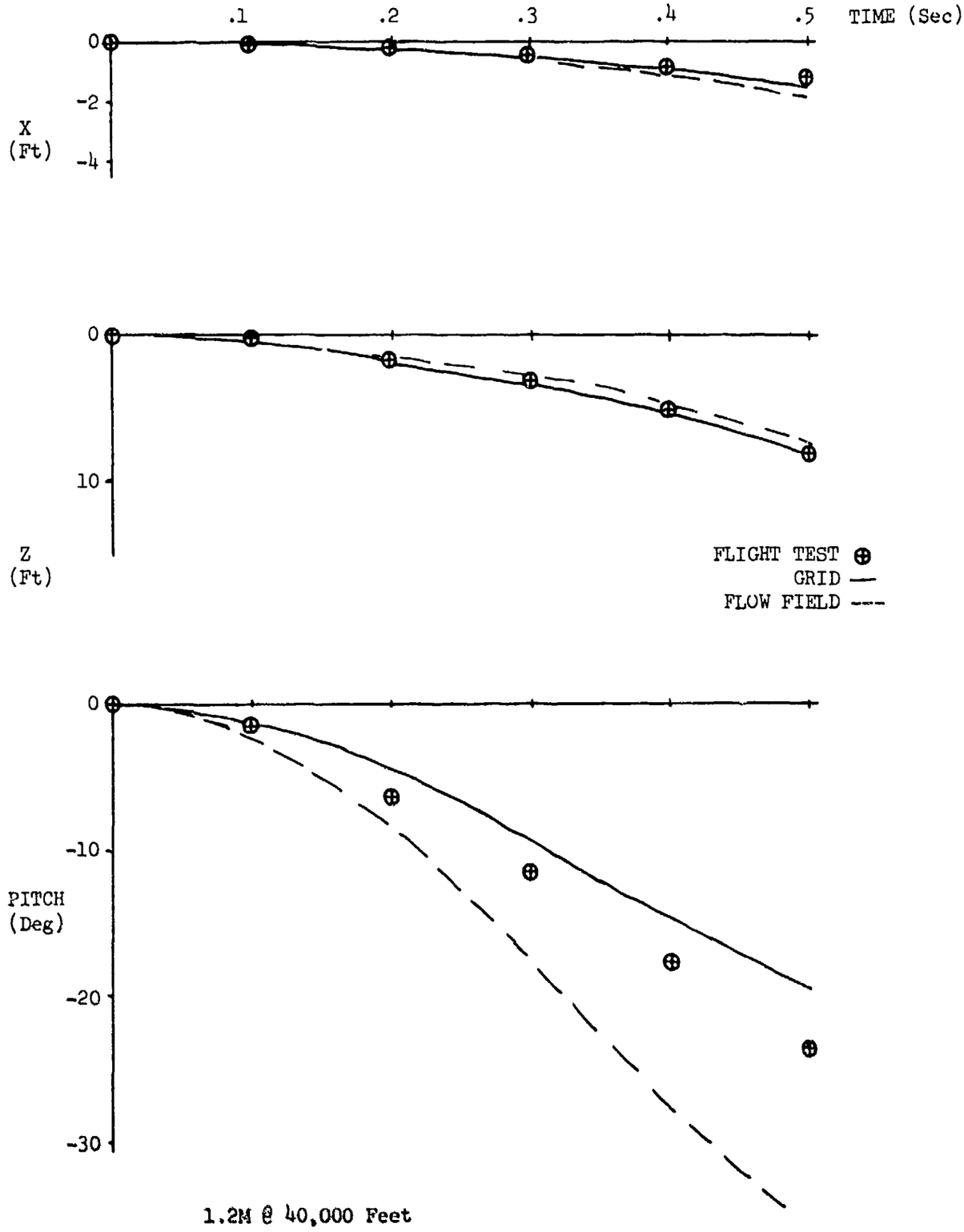


Figure 28. Flight Test vs Simulation Comparison

REFERENCES

1. Studwell, V. E., "Experimental Aerodynamics of Multiple Weapon Carriage," AFATL-TR-71-5, Air Force Armament Laboratory, January 1971.

2. Korn, S. C., "Use of the Flow Angularity Technique for Predicting Store Separation Trajectories," AFATL-TR-71-140, Air Force Armament Laboratory, October 1971.

3. Korn, S. C., "Validation and Expansion of the Flow Angularity Technique for Predicting Store Separation Trajectories," AFATL-TR-72-184, Air Force Armament Laboratory, September 1972.

4. Hill, D. W., "Investigation of the Flow Field Beneath the Wing of the F-4 Aircraft with Various External Stores at Mach Number 0.85," AEDC-TR-72-92, June 1972.

AUTOBIOGRAPHIES

Charles B. Mathews received his B.S. degree in Industrial Management and Aerospace Engineering from Auburn University in 1952 and 1956 respectively. From 1952 to 1956 he served as a pilot with the US Air Force in Korea and Hurlburt Field, Florida. His flying experience includes the B-26, B-57, and RF-84F. In 1968 he received his M.S. degree from Auburn University. He has been employed at the Air Force Armament Laboratory, Eglin AFB, Florida, from 1961 to the present, where he has had over thirteen years experience in aircraft/weapon compatibility work and aerodynamics related to aircraft and weapon design.

Robert D. Cason received his B.S. degree from the USAF Academy in 1967. After graduation from pilot training in 1968 he served as a wing operations officer at Hurlburt Field, Florida. He entered the Air Force Institute of Technology in June 1972 and received his Masters Degree in Aerospace Engineering in December 1973. Since then he has served as an aeronautical engineer, Aircraft Compatibility Branch, Air Force Armament Laboratory, Eglin AFB, Florida. He is a member of the AIAA.

Page G. McGirr received his B.S. degree in Aerospace Engineering from the University of Notre Dame in 1970 and his M.S.E. degree in Aerospace Engineering from The University of Michigan in 1971. Since graduation he has been assigned as an aeronautical engineer to the Air Force Armament Laboratory, Eglin AFB, Florida. He is currently with the Aircraft Compatibility Branch where he has been involved in decelerator design for nonnuclear munitions and wind tunnel tests and analysis of new weapon configurations. He is a member of Tau Beta Pi and the AIAA.

Eduardo M. Carreras received his B.S. degree in Mechanical Engineering from the University of Miami of Florida in 1972. Upon being commissioned by the Air Force, he attended the Air Force Institute of Technology and graduated with an M.S. degree in Aerospace Engineering. He has since been with the Aircraft Compatibility Branch of the Air Force Armament Laboratory at Eglin AFB, Florida, working on the compatibility of new weapons on aircraft.

LAUNCH TRANSIENT ANALYSIS: ESSENTIAL ELEMENT OF AIR LAUNCHED WEAPON CONFIGURATION DEVELOPMENT (U) (Article UNCLASSIFIED)

by

TERRY G. BLOSE AND RALPH M. BARNES
Rockwell International Corporation
Missile Systems Division
Columbus, Ohio

ABSTRACT. (U) Current development programs for improved air-launched weapon systems require consideration of weapon/aircraft compatibility during early weapon configuration definition and design.

An analytical technique for predicting launch and jettison separation characteristics of externally carried air-launched weapons is presented. The technique uses aircraft flow angularity data to determine the incremental forces acting on a weapon due to the aircraft flow field. A six degree-of-freedom program has been defined to calculate these incremental forces which, combined with weapon free stream aerodynamic characteristics and basic equations of motion, is used to predict weapon separation characteristics. Since the technique is based on the use of flow angularity data, numerous weapon configurations may be evaluated. Thus, the technique is particularly useful during initial weapon development.

Correlations of predicted jettison trajectories with wind tunnel and flight test data are presented to demonstrate the accuracy of the technique. For additional comparison, jettison trajectories determined using the Air Force Armament Laboratory (AFATL/DLJC) grid force/moment interference coefficient computer program are presented. The correlations were conducted for an improved modular guided weapon developed for the Air Force.

"APPROVED FOR PUBLIC RELEASE: DISTRIBUTION UNLIMITED"

NOMENCLATURE

a_{ij}	Direction cosines (see equation 1-3)
AVX	Aircraft free-stream velocity component along aircraft X-Axis ~ ft/sec
C.G.	Weapon center of gravity
C_{ℓ}', C_m', C_n'	Rolling moment, pitching moment, and yawing moment coefficients, respectively, in the weapon primed axis system
C_{ℓ}, C_m, C_n	Rolling moment, pitching moment, and yawing moment coefficients, respectively, in the weapon body axis system
$\Delta C_{\ell}'$, $\Delta C_m'$, $\Delta C_n'$	Incremental rolling moment, pitching moment, and yawing moment coefficients, respectively, in the weapon primed axis system
ΔC_{ℓ_i}, ΔC_{m_i}, ΔC_{n_i}	Interference rolling moment, pitching moment, and yawing moment coefficients, respectively, in the weapon body axis system
C_N', C_Y'	Normal force and side force coefficients, respectively, in the weapon primed axis system
C_N, C_Y	Normal force and side force coefficients, respectively, in the weapon body axis system
$\Delta C_N'$, $\Delta C_Y'$	Incremental normal force and side force coefficients, respectively, in the weapon primed axis system
ΔC_{N_i}, ΔC_{Y_i}	Interference normal force and side force coefficients, respectively, in the weapon body axis system
DV	Incremental local velocity component along the pylon Y-axis due to flow field angle of sideslip ~ ft/sec
DVX, DVY, DVZ	Incremental velocity components along the weapon body axes due to aircraft flow field ~ ft/sec

DW	Incremental local velocity component along the pylon Z-axis due to flow field angle of attack ~ ft/sec
k	Number of primary lifting components; for example, k is equal to 3 if the weapon is divided into body, strake, and wing components
M	Free-stream Mach number
S.M.	Weapon static stability margin ~ inches
VX, VY, VZ	Weapon free-stream velocity components along the weapon body axes ~ ft/sec
$\bar{V}X$, $\bar{V}Y$, $\bar{V}Z$	Effective velocity components along the weapon body axes ~ ft/sec
ΔX_p, ΔY_p, ΔZ_p	Weapon center-of-gravity position in the pylon axis system ~ feet
ΔXP_{CP}, ΔZP_{CP}	Aerodynamic center-of-pressure position in the pylon axis system ~ feet
α_{FRL}	Launch aircraft (fuselage reference line) angle of attack ~ degrees
α'	Weapon aerodynamic angle of attack in the primed axis system, measured between the free-stream velocity vector and the weapon centerline ~ degrees
$\bar{\alpha}'$	Effective aerodynamic angle of attack in the primed axis system, measured between the effective velocity vector and the weapon centerline ~ degrees
$\Delta\alpha$	Flow field angle of attack in the pylon axis system ~ degrees
$\Delta\beta$	Flow field angle of sideslip in the pylon axis system ~ degrees
ϕ'	Weapon aerodynamic roll angle in the primed axis system, measured between the plane of α' and the weapon reference orientation (zero ϕ' is "X" orientation) ~ degrees

$\bar{\phi}'$	Effective aerodynamic roll angle in the primed axis system, measured between the plane of $\bar{\alpha}'$ and the weapon reference orientation (zero $\bar{\phi}'$ is "X" orientation) ~ degrees
$\Delta\phi_p$, $\Delta\theta_p$, $\Delta\psi_p$	Weapon roll, pitch, and yaw angles, respectively, in the pylon axis system ~ degrees

SUBSCRIPTS

(α')	Due to aerodynamic angle of attack
($\bar{\alpha}'$)	Due to effective aerodynamic angle of attack
(ϕ')	Due to aerodynamic roll angle
($\bar{\phi}'$)	Due to effective aerodynamic roll angle
( )	For a given primary lifting component; for example, (W) indicates the wing component
FS	For the total weapon at free-stream conditions

INTRODUCTION

Recently, operational combat mission requirements for tactical aircraft have demanded development of new modular air-launched weapon systems. Improved high-lift aerodynamic concepts associated with many of the new weapon systems have placed increased emphasis on weapon/aircraft compatibility considerations throughout weapon design and development. Foremost among compatibility considerations are launch transient analyses which evaluate aircraft safety during weapon launch/jettison. The analyses are especially necessary during early configuration development to define design changes, if required, prior to design implementation.

The objectives of this paper are (1) to present a summary of an analytical technique which can be used during weapon definition and development to predict launch and jettison separation characteristics of air-launched weapons, and (2) to evaluate the accuracy of the prediction technique through correlation with both wind tunnel and flight test results. The correlations are performed for an improved modular guided glide weapon system developed by Rockwell International Corporation, Missile Systems Division, for the Air Force.

FLOW-ANGULARITY PREDICTION TECHNIQUE

The prediction technique, formulated during support of past Air Force/Navy programs for externally carried air-launched weapon systems, is based on determination of the aircraft non-uniform interference flow angularities combined with a digital six degree-of-freedom computer program.

The digital program utilizes the complete six degree-of-freedom equations of motion to predict either the launch or jettison trajectory of a weapon from a maneuvering aircraft. The program includes the effects of:

(1) Ejector rack characteristics (ejection force, ejector piston location, ejector stroke length, and total ejection time),

(2) Weapon mass properties (weight, moment of inertia, and center-of-gravity position),

(3) Launch aircraft flight conditions (Mach number, altitude, angles of attack and sideslip, body angular rates and Euler angles, and center-of-gravity position),

(4) Weapon/aircraft installation geometry (weapon center-of-gravity position on the aircraft, and weapon attitude relative to the aircraft reference axis),

(5) Atmospheric winds (optional),

(6) Launch aircraft flow field.

The weapon free-stream static force and moment coefficients obtained from either empirical/theoretical estimation methods or wind tunnel tests are defined in the weapon primed or aeroballistic axis system (α', ϕ'). Coefficients for both the total weapon and each individual primary component (e.g., body, wings) are incorporated into the program using multiple independent variable arrays with a linear-interpolation table look-up subroutine.

The prediction technique uses aircraft flow field angularity data ($\Delta\alpha$, $\Delta\beta$) to calculate the interference force and moment coefficients acting on a weapon in the presence of the launch aircraft. Flow-angularity data in the aircraft flow field may be obtained from theoretical/empirical methods or from wind tunnel tests. The data are obtained without the presence of the weapon (clean pylon only).

To calculate the interference coefficients on a weapon, the average flow field angularities acting on each primary lifting component are determined from the flow-angularity data. The angularities are

based on the vertical and axial position of the component's aerodynamic center of pressure in the pylon axis system. The center of pressure for the cruciform lifting surfaces is considered to be at the weapon centerline.

$$\Delta\alpha_{(\ )} = \mathcal{F}[\,M\ \ \alpha_{FRL}\ \ \Delta XP_{CP(\ )}\ \ \Delta ZP_{CP(\ )}\,] \qquad (1\text{-}1a)$$

$$\Delta\beta_{(\ )} = \mathcal{F}[\,M\ \ \alpha_{FRL}\ \ \Delta XP_{CP(\ )}\ \ \Delta ZP_{CP(\ )}\,] \qquad (1\text{-}1b)$$

The angularities are converted to incremental local flow velocity components (DW, DV) in the pylon axis based on the aircraft free-stream velocity X-component (AVX).

$$DW_{(\ )} = AVX \tan\left[\frac{\Delta\alpha_{(\ )}}{57.3}\right] \qquad (1\text{-}2a)$$

$$DV_{(\ )} = AVX \tan\left[\frac{\Delta\beta_{(\ )}}{57.3}\right] \qquad (1\text{-}2b)$$

The incremental velocity components are then transformed to the weapon body axis based on the weapon pitch, yaw, and roll ($\Delta\theta_p$, $\Delta\psi_p$, $\Delta\phi_p$) orientation in the pylon axis.

$$\begin{bmatrix} DVX_{(\ )} \\ DVY_{(\ )} \\ DVZ_{(\ )} \end{bmatrix} = \begin{bmatrix} a_{11} & a_{12} & a_{13} \\ a_{21} & a_{22} & a_{23} \\ a_{31} & a_{32} & a_{33} \end{bmatrix} \begin{bmatrix} 0 \\ DV_{(\ )} \\ DW_{(\ )} \end{bmatrix} \qquad (1\text{-}3)$$

where:

$$a_{11} = \cos\Delta\psi_p \cos\Delta\theta_p$$

$$a_{12} = \sin\Delta\psi_p \cos\Delta\theta_p$$

$$a_{13} = -\sin\Delta\theta_p$$

$$a_{21} = \cos\Delta\psi_p \sin\Delta\theta_p \sin\Delta\phi_p - \sin\Delta\psi_p \cos\Delta\phi_p$$

$$a_{22} = \cos\Delta\psi_p \cos\Delta\phi_p + \sin\Delta\psi_p \sin\Delta\theta_p \sin\Delta\phi_p$$

$$a_{23} = \cos\Delta\theta_p \sin\Delta\phi_p$$

$$a_{31} = \sin\Delta\psi_p \sin\Delta\phi_p + \cos\Delta\psi_p \sin\Delta\theta_p \cos\Delta\phi_p$$

$$a_{32} = \sin \Delta\psi_p \sin \Delta\theta_p \cos \Delta\phi_p - \cos \Delta\psi_p \sin \Delta\phi_p$$

$$a_{33} = \cos \Delta\theta_p \cos \Delta\phi_p$$

The transformed velocity components are combined with the weapon free-stream body axis velocity components (VX, VY, VZ) to obtain the effective velocity components ($\bar{V}X$, $\bar{V}Y$, $\bar{V}Z$) for each weapon component. The effective total aerodynamic angle of attack ($\bar{\alpha}'$) and roll angle ($\bar{\phi}'$) for each weapon component are then approximated based on the effective velocity components.

$$\bar{V}X_{(\ )} = VX + DVX_{(\ )} \tag{1-4a}$$

$$\bar{V}Y_{(\ )} = VY + DVY_{(\ )} \tag{1-4b}$$

$$\bar{V}Z_{(\ )} = VZ + DVZ_{(\ )} \tag{1-4c}$$

$$\bar{\alpha}'_{(\ )} = \tan^{-1}\left[\frac{\sqrt{\bar{V}Y_{(\ )}^2 + \bar{V}Z_{(\ )}^2}}{\bar{V}X_{(\ )}}\right] \tag{1-5}$$

$$\bar{\phi}'_{(\ )} = \tan^{-1}\left[\frac{\bar{V}Y_{(\ )}}{\bar{V}Z_{(\ )}}\right] \tag{1-6}$$

Using the weapon primed axis aerodynamic coefficient equations with the control effectiveness contributions eliminated, the aerodynamic coefficients for each weapon component and for the total weapon are obtained as functions of the effective velocity ($\bar{\alpha}'$, $\bar{\phi}'$) and the free-stream velocity (α', ϕ'), respectively.

WEAPON COMPONENT EFFECTIVE VELOCITY COEFFICIENTS - PRIMED AXIS

$$C_N'_{(\ )} = C_N'_{(\bar{\alpha}')} + \Delta C_N'_{(\bar{\phi}')} \sin^2\left[2\bar{\phi}'_{(\ )}\right] \tag{1-7a}$$

$$C_Y'_{(\ )} = \Delta C_Y'_{(\bar{\phi}')} \sin\left[4\bar{\phi}'_{(\ )}\right] \tag{1-7b}$$

$$C_m'_{(\ )} = C_m'_{(\bar{\alpha}')} + \Delta C_m'_{(\bar{\phi}')} \sin^2\left[2\bar{\phi}'_{(\ )}\right] \tag{1-7c}$$

$$C_n'_{(\ )} = \Delta C_n'_{(\bar{\phi}')} \sin\left[4\bar{\phi}'_{(\ )}\right] \tag{1-7d}$$

$$C_\ell'_{(\ )} = \Delta C_\ell'_{(\bar{\phi}')} \sin\left[4\bar{\phi}'_{(\ )}\right] \tag{1-7e}$$

TOTAL WEAPON FREE-STREAM COEFFICIENTS - PRIMED AXIS

$$C_{N'_{FS}} = C_{N'_{(\alpha')}} + \Delta C_{N'_{(\phi')}} \sin^2 [2\phi'] \quad (1\text{-}8a)$$

$$C_{Y'_{FS}} = \Delta C_{Y'_{(\phi')}} \sin [4\phi'] \quad (1\text{-}8b)$$

$$C_{m'_{FS}} = C_{m'_{(\alpha')}} + \Delta C_{m'_{(\phi')}} \sin^2 [2\phi'] \quad (1\text{-}8c)$$

$$C_{n'_{FS}} = \Delta C_{n'_{(\phi')}} \sin [4\phi'] \quad (1\text{-}8d)$$

$$C_{\ell'_{FS}} = \Delta C_{\ell'_{(\phi')}} \sin [4\phi'] \quad (1\text{-}8e)$$

The effective velocity and free-stream coefficients are transformed to the body axis system based on $\bar{\phi}'$ and ϕ', respectively.

INDIVIDUAL COMPONENT COEFFICIENTS - BODY AXIS

$$C_{N(\ )} = C_{N'(\ )} \cos \bar{\phi}'_{(\ )} + C_{Y'(\ )} \sin \bar{\phi}'_{(\ )} \quad (1\text{-}9a)$$

$$C_{Y(\ )} = C_{Y'(\ )} \cos \bar{\phi}'_{(\ )} - C_{N'(\ )} \sin \bar{\phi}'_{(\ )} \quad (1\text{-}9b)$$

$$C_{m(\ )} = C_{m'(\ )} \cos \bar{\phi}'_{(\ )} + C_{n'(\ )} \sin \bar{\phi}'_{(\ )} \quad (1\text{-}9c)$$

$$C_{n(\ )} = C_{n'(\ )} \cos \bar{\phi}'_{(\ )} - C_{m'(\ )} \sin \bar{\phi}'_{(\ )} \quad (1\text{-}9d)$$

$$C_{\ell(\ )} = C_{\ell'(\ )} \quad (1\text{-}9e)$$

TOTAL WEAPON FREE-STREAM COEFFICIENTS - BODY AXIS

$$C_{N_{FS}} = C_{N'_{FS}} \cos \phi' + C_{Y'_{FS}} \sin \phi' \quad (1\text{-}10a)$$

$$C_{Y_{FS}} = C_{Y'_{FS}} \cos \phi' - C_{N'_{FS}} \sin \phi' \quad (1\text{-}10b)$$

$$C_{m_{FS}} = C_{m'_{FS}} \cos \phi' + C_{n'_{FS}} \sin \phi' \quad (1\text{-}10c)$$

$$C_{n_{FS}} = C_{n'_{FS}} \cos \phi' - C_{m'_{FS}} \sin \phi' \quad (1\text{-}10d)$$

$$C_{\ell_{FS}} = C_{\ell'_{FS}} \quad (1\text{-}10e)$$

The interference coefficients (ΔC_{N_i}, ΔC_{Y_i}, ΔC_{m_i}, ΔC_{n_i}, ΔC_{ℓ_i}) for the total weapon are the summations of the effective velocity body axis coefficients for the weapon primary lifting components minus the free-stream body axis coefficients for the total weapon.

$$\Delta C_{N_i} = \left[\sum_{1}^{k} C_{N(\ )} \right] - C_{N_{FS}} \tag{1-11a}$$

$$\Delta C_{Y_i} = \left[\sum_{1}^{k} C_{Y(\ )} \right] - C_{Y_{FS}} \tag{1-11b}$$

$$\Delta C_{m_i} = \left[\sum_{1}^{k} C_{m(\ )} \right] - C_{m_{FS}} \tag{1-11c}$$

$$\Delta C_{n_i} = \left[\sum_{1}^{k} C_{n(\ )} \right] - C_{n_{FS}} \tag{1-11d}$$

$$\Delta C_{\ell_i} = \left[\sum_{1}^{k} C_{\ell(\ )} \right] - C_{\ell_{FS}} \tag{1-11e}$$

k = number of weapon primary lifting components considered

The interference coefficients in the body axis are incorporated with the complete free-stream aerodynamic coefficients (including control effectiveness and damping) in the six degree-of-freedom equations of motion.

APPLICATION OF THE TECHNIQUE

The flow-angularity technique, previously presented, was applied during configuration definition of an air-launched guided glide weapon required to be compatible with several Air Force/Navy tactical aircraft.

During definition of the weapon configuration, Rockwell International Corporation, Missile Systems Division, in coordination with the Aircraft Compatibility Group (DLJC) of the Air Force Armament Laboratory (AFATL/AFSC) at Eglin Air Force Base, Florida, conducted aircraft flow angularity wind tunnel tests, and performed separation analyses for weapon jettison from an F-4D/E aircraft.

The flow-angularity wind tunnel tests, Reference (1), were conducted in the Aerodynamic Wind Tunnel (4T) of the Propulsion Wind Tunnel Facility (PWT) at Arnold Engineering Development Center (AEDC/AFSC). The tests were performed using the AEDC captive trajectory store separation system (CTS). Flow-angularity data were recorded using a calibrated 40-degree conical tip pressure probe. The probe static and total pressure in the proximity of the aircraft were measured and reduced to flow field angularities using predetermined probe calibration data. The flow-angularity data were obtained at preselected coordinate locations in the pylon axis system as functions of aircraft angles of attack and sideslip, Mach number, and aircraft loading configuration. Data were obtained for the inboard wing stations of an F-4 aircraft for a Mach number range of 0.55 to 1.2.

Jettison (autopilot inoperative) trajectories of several configuration design concepts were predicted throughout the F-4 aircraft flight envelope using the previously discussed technique. The weapon weight for the concepts was assumed to be 2500 pounds. The control surfaces for all the concepts were locked in a trailing-edge down position to provide a nose-down pitch bias. The free-stream/build-up aerodynamic coefficient data for the various concepts were estimated based on development tests of similar configurations conducted in the NASA Ames 11-foot transonic, AEDC-4T and Rockwell low-speed NACAL wind tunnels. Parametric configuration variations for the following design concepts, shown in Figure 1, were evaluated:

Concept (1) Fixed span cruciform (X) wings and cruciform strakes; resulting in a statically stable configuration for jettison and launch.

Concept (2) Cruciform wings, with tips that extend after launch, and either (a) cruciform strakes, (b) cruciform strakes with retractable spoilers, (c) interdigitated cruciform strakes, or (d) interdigitated asymmetric span cruciform strakes; resulting in a statically unstable configuration during jettison.

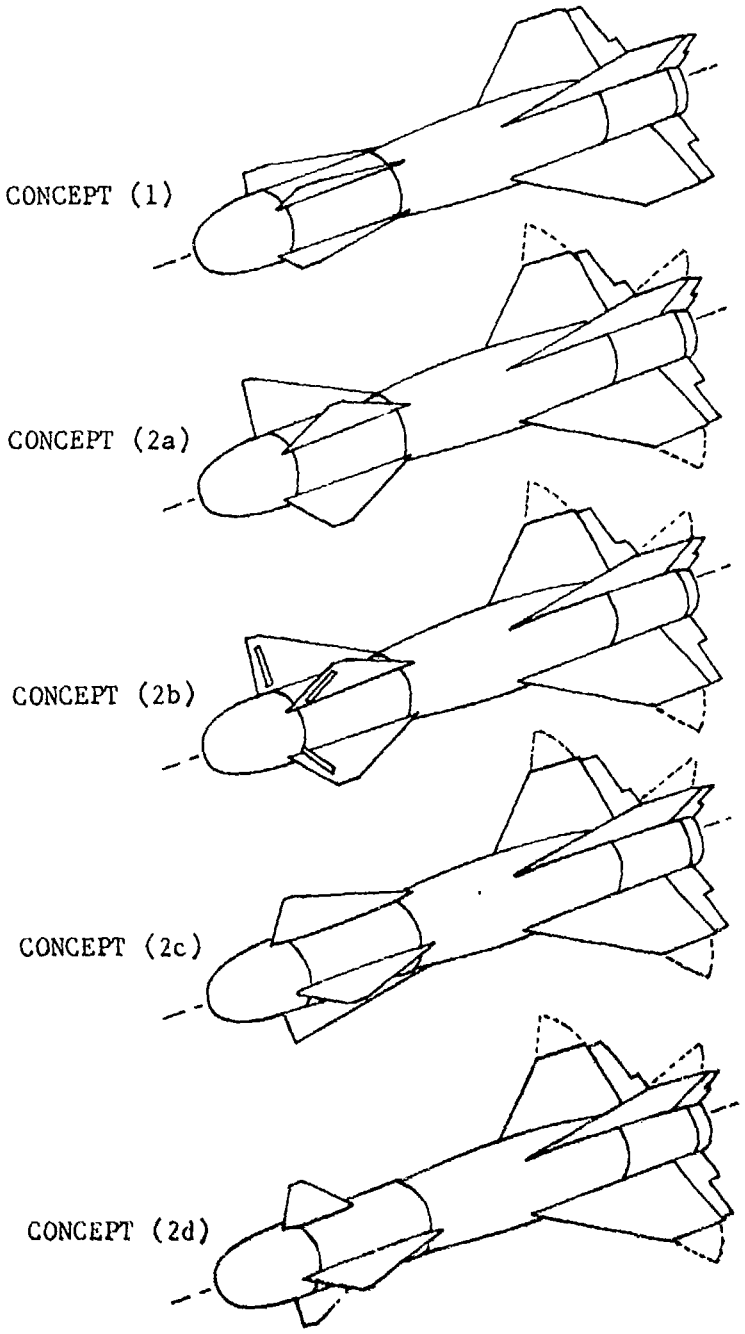


FIGURE 1 CONFIGURATION DESIGN CONCEPTS

Separation trajectories for the parametric configurations evaluated are shown in Figures 2 through 4 at a critical (high angle of attack) release condition - 0.65 Mach number at 30,000 feet altitude. The trajectories are from the left-wing inboard pylon of an F-4 aircraft with outboard 370-gallon external fuel tanks. The trajectories are for normal jettison (1.0 g level flight) with the aircraft landing gear, flaps, speed brakes, and wing-leading-edge slats retracted.

At the specific release condition, Figure 2 indicates that for jettison of Concept 1, longitudinal/directional static margins up to 13 inches stable have satisfactory jettison characteristics, and always produce nose-down and inboard incremental pitch and yaw angles, respectively.

Figure 2 also indicates that for Concept 2a,

(a) a longitudinal static margin at low angles of attack of 17 inches (0.944 diameters) unstable or less provides satisfactory vertical translation (ΔZ_p) of the weapon; that is, no weapon/aircraft contact, acceptable (safe) aircraft/adjacent store clearances, and vertical translation of the weapon center-of-gravity with respect to the aircraft is always increasing,

(b) a directional static margin of 4.5 inches unstable or less provides approximately zero lateral translation (ΔY_p) of the weapon center of gravity,

(c) during initial jettison, a longitudinal static margin of approximately 10 inches unstable produces zero incremental pitch angle ($\Delta \theta_p$),

(d) during initial jettison, a directional static margin of approximately 4.5 inches unstable produces zero incremental yaw angle ($\Delta \psi_p$).

For jettison of Concept 2b, Figure 3 shows that a longitudinal/directional static margin of approximately 8 inches unstable (which corresponds to 18-inch exposed semi-span strakes with retractable spoilers of approximately 1.2 square feet total frontal area) has satisfactory jettison characteristics and minimum (near zero) pitch/yaw dynamics.

Based on estimated aerodynamic coefficients, the jettison characteristics for Concept 2c, presented in Figure 4, are assumed to be the same as those for Concept 2a for equivalent strake exposed semi-span.

Figure 4 shows satisfactory jettison characteristics for Concept 2d with 17 inches unstable longitudinal and 4.5 inches unstable directional static margins. The static margins correspond to interdigitated

strakes with exposed semi-spans of 15 inches in the horizontal and 11 inches in the vertical.

In summary, the results of the analyses indicate that (1) from an F-4 aircraft with outboard fuel tanks, satisfactory jettison characteristics can be attained with some specific stability margins (e.g., strake span/spoiler combinations) for all the weapon concepts that were evaluated, (2) weapon translations and pitch/yaw dynamics during jettison are, as expected, directly associated with the aircraft flow field effects and the static longitudinal/directional stability of the aerodynamic configuration, and (3) for the configurations evaluated, the pitch/yaw dynamics are minimized with a moderately unstable static margin.

RELEASE CONDITIONS

MACH NUMBER 0.65
ALTITUDE 30,000 FT.
LOAD FACTOR 1.0 g

NOTES: (1) STATIC MARGIN AT LOW ANGLES OF ATTACK; POSITIVE MARGIN IS STABLE.

(2) SYMBOLS INDICATE 0.5 SECOND TIME INTERVAL.

STRAKE EXPOSED SEMI-SPAN ~ IN.	STATIC[1] MARGIN ~ IN.	CONCEPT
18	-28	2a
17	-24	
16	-20.5	
15	-17	
14	-14	
13	-10	
12	- 7	
11	- 4.5	
10	- 2	
9	+ 1	1
8	+ 3	
7	+ 5	
6	+ 6.5	
No Strakes	+13	

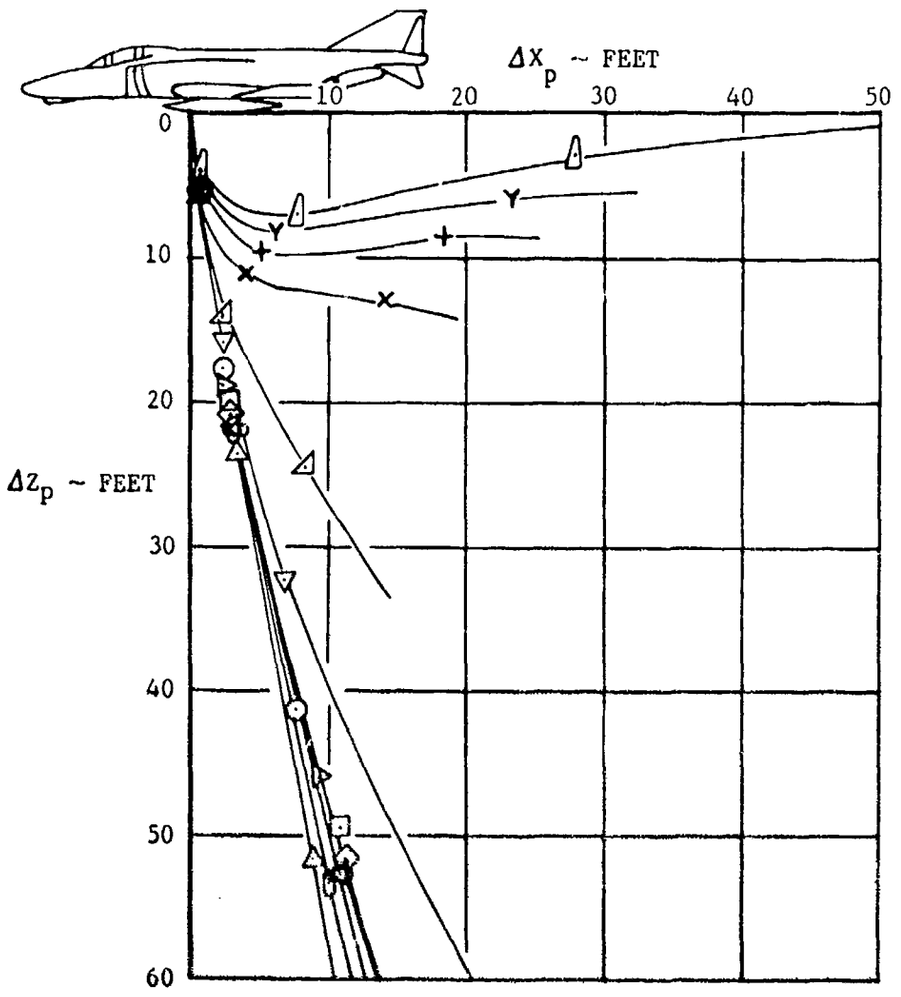


FIGURE 2 EFFECT OF CRUCIFORM STRAKES - CONCEPTS (1) AND (2a)

RELEASE CONDITIONS

MACH NUMBER 0.65
ALTITUDE 30,000 FT.
LOAD FACTOR 1.0 g

NOTES: (1) STATIC MARGIN AT LOW ANGLES OF ATTACK; POSITIVE MARGIN IS STABLE.

(2) SYMBOLS INDICATE 0.5 SECOND TIME INTERVAL.

	STRAKE EXPOSED SEMI-SPAN ~ IN.	STATIC[1] MARGIN ~ IN.	CONCEPT
	18	-28	2a
Y	17	-24	
+	16	-20.5	
X	15	-17	
	14	-14	
	13	-10	
	12	- 7	
	11	- 4.5	
	10	- 2	
	9	+ 1	1
	8	+ 3	
	7	+ 5	
	6	+ 6.5	
	No Strakes	+13	

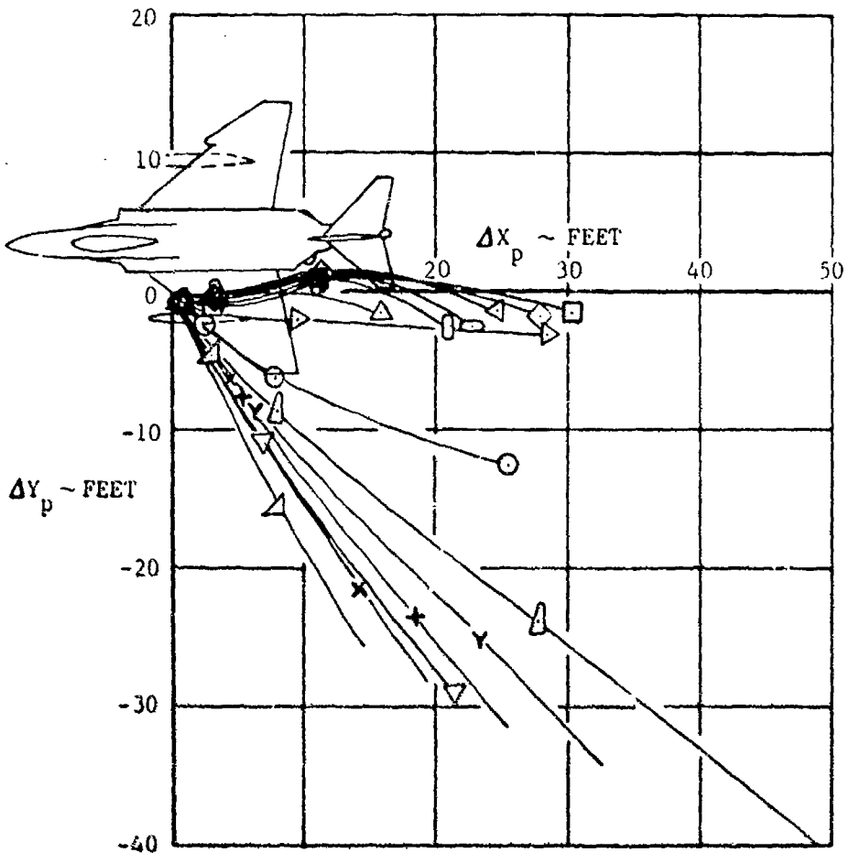


FIGURE 2 CONTINUED

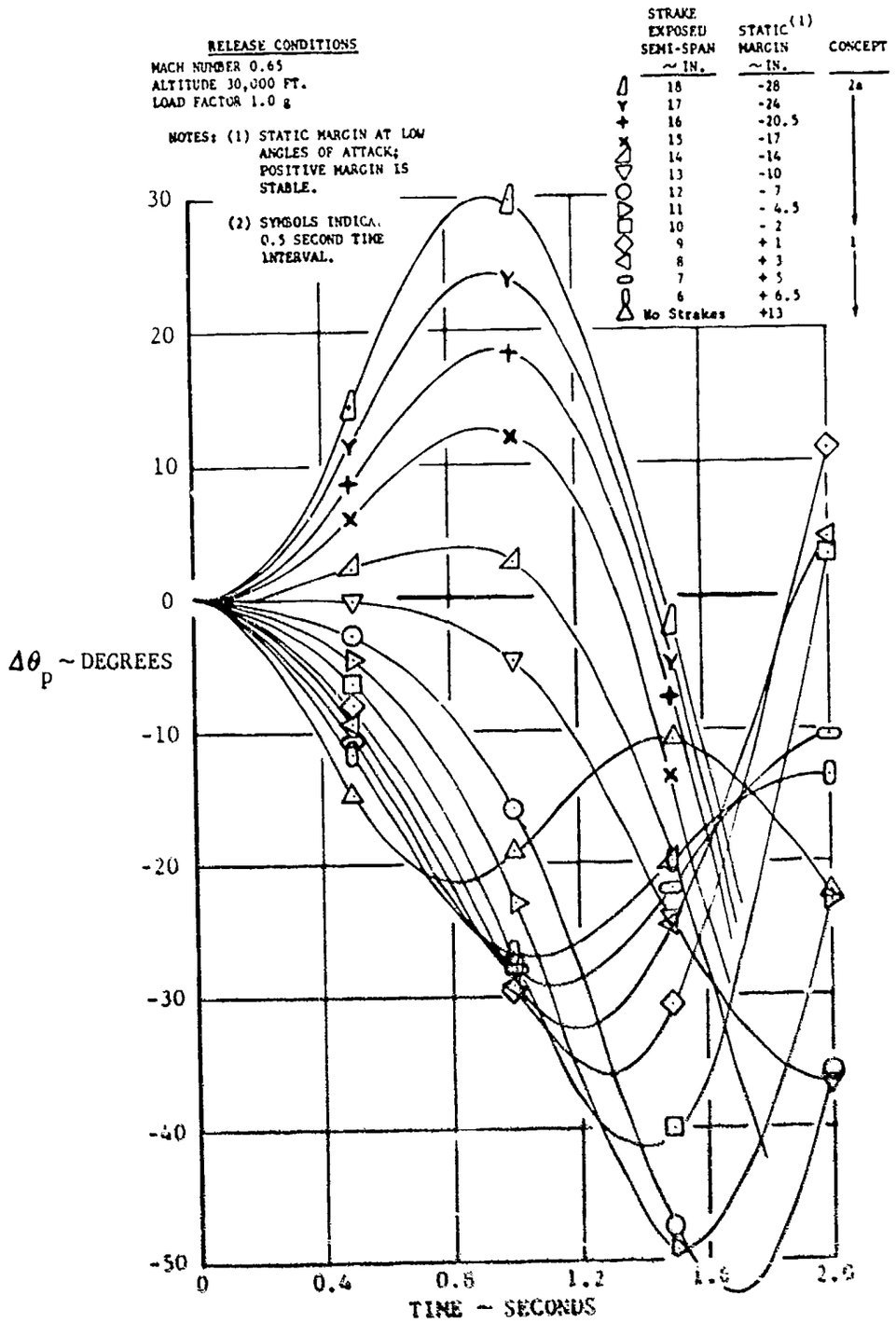


FIGURE 2 CONTINUED

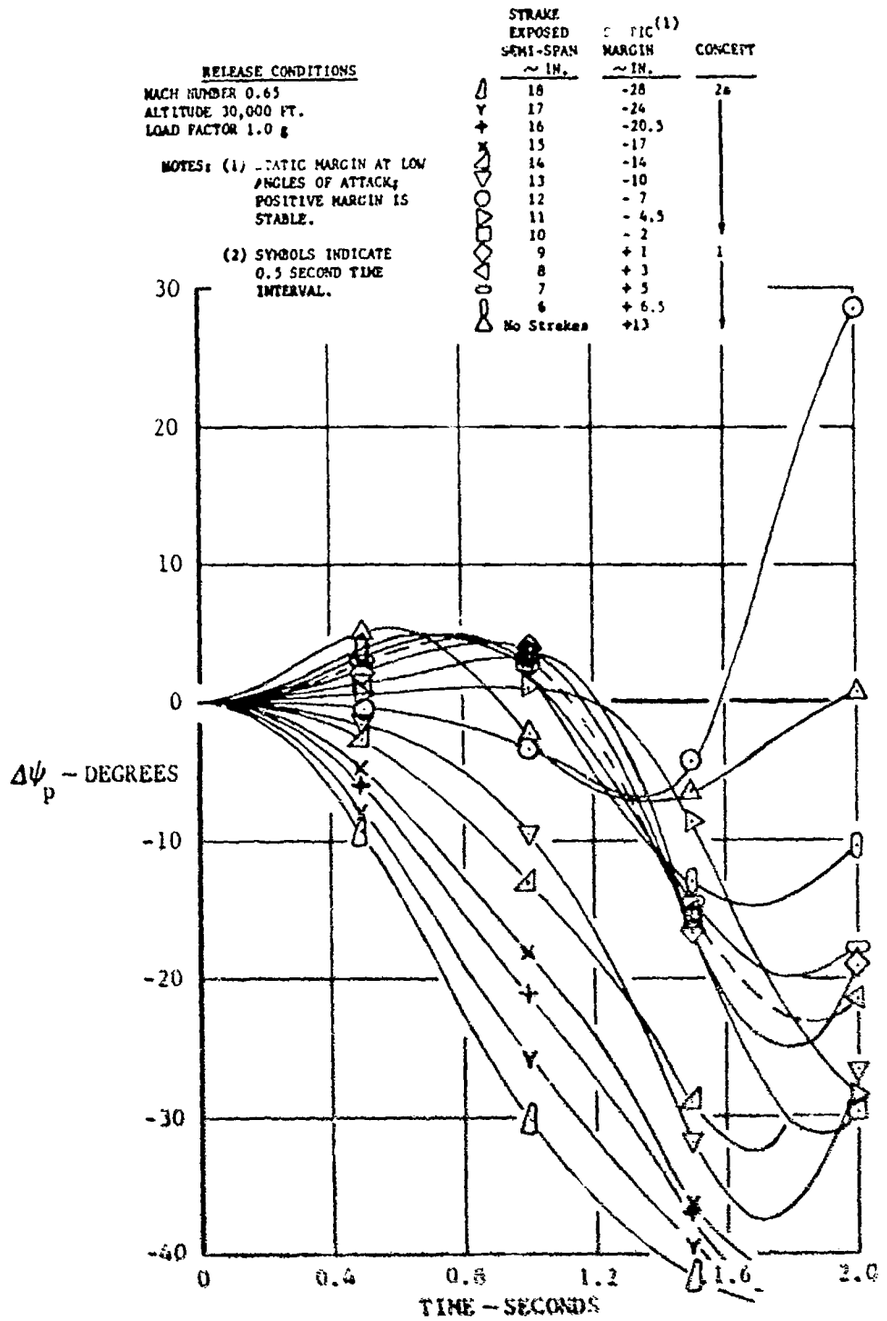


FIGURE 2 CONCLUDED

RELEASE CONDITIONS

MACH NUMBER 0.65
ALTITUDE 30,000 FT.
LOAD FACTOR 1.0 g

NOTES: (1) CRUCIFORM STRAKE EXPOSED SEMI-SPAN 18 INCHES.
(2) STATIC MARGIN AT LOW ANGLES OF ATTACK; POSITIVE MARGIN IS STABLE.
(3) SYMBOLS INDICATE 0.5 SECOND TIME INTERVALS.

	SPOILER FRONTAL AREA ~ SQ. FT.	STATIC[2] MARGIN ~ IN.	CONCEPT
○	3.3	+30	2b
□	2.5	+16	↓
Y	2.0	+ 7	
△	1.6	+ 1	
X	1.3	- 5	
▽	0.8	-13	
J	No Spoilers	-28	

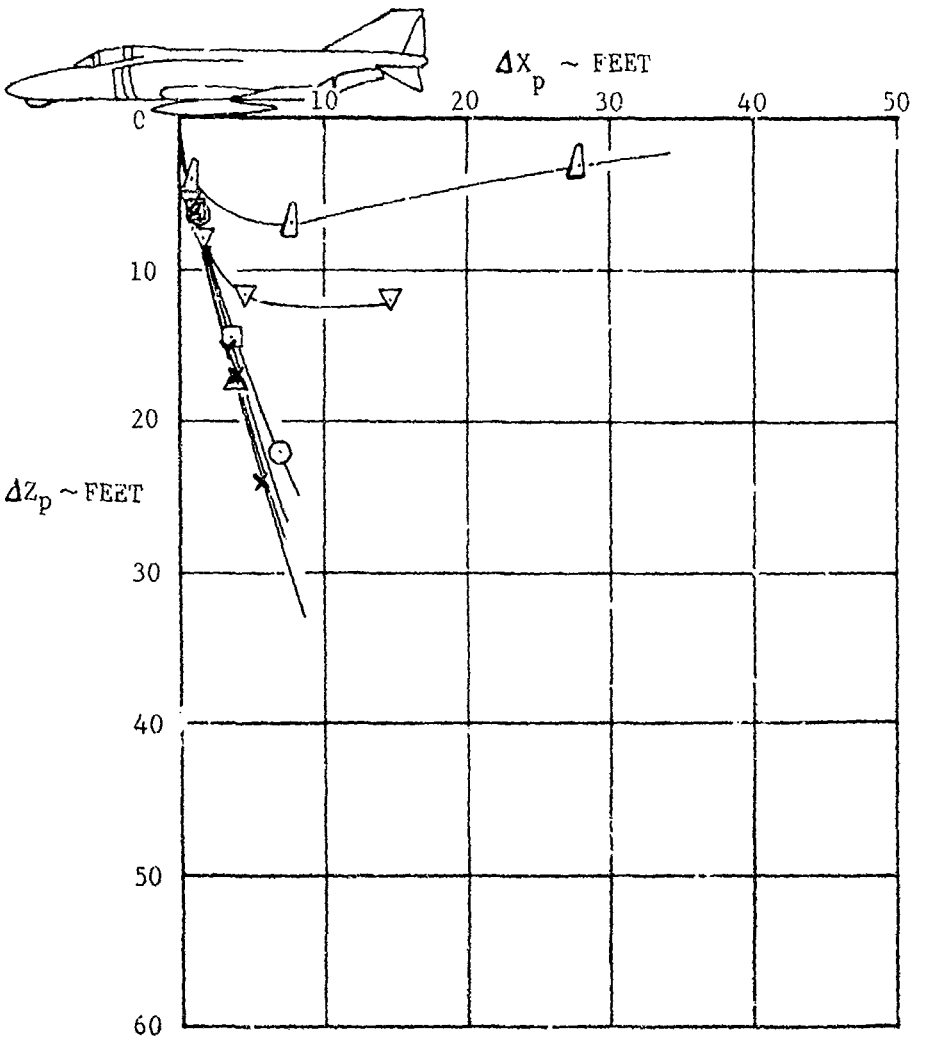


FIGURE 3 EFFECT OF CRUCIFORM STRAKES WITH SPOILERS ~ CONCEPT (2b)

RELEASE CONDITIONS		SPOILER FRONTAL AREA ~ SQ. FT.	STATIC(2) MARGIN ~ IN.	CONCEPT
MACH NUMBER 0.65	○	3.3	+20	2b
ALTITUDE 30,000 FT.	□	2.5	+16	
LOAD FACTOR 1.0 g	Y	2.0	+ 7	
	△	1.6	+ 1	
NOTES: (1) CRUCIFORM STRAKE EXPOSED SEMI-SPAN 18 INCHES.	X	1.3	- 5	
(2) STATIC MARGIN AT LOW ANGLES OF ATTACK; POSITIVE MARGIN IS STABLE.	▽	0.8	-13	
(3) SYMBOLS INDICATE 0.5 SECOND TIME INTERVALS.	△	No Spoilers	-28	

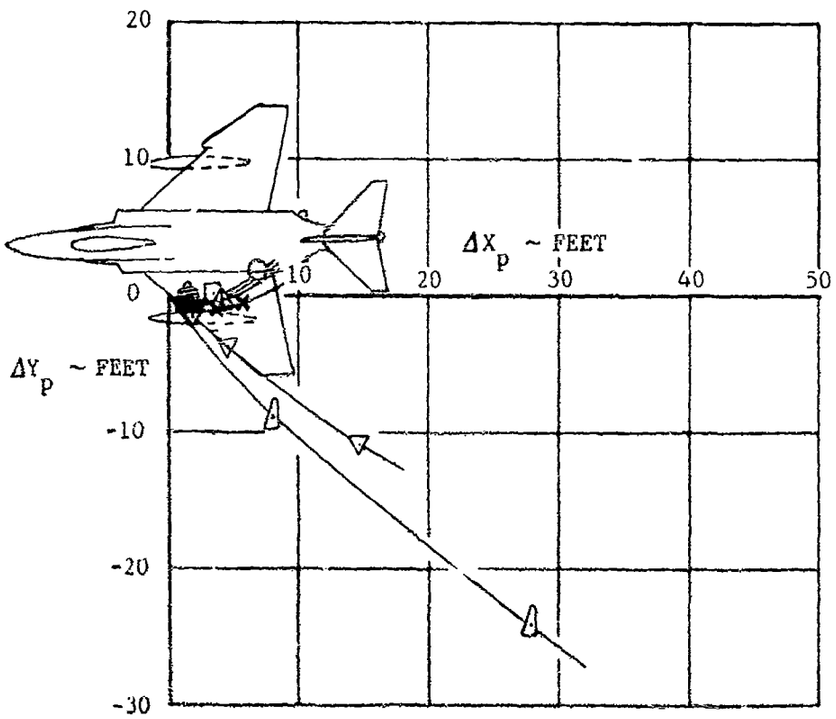


FIGURE 3 CONTINUED

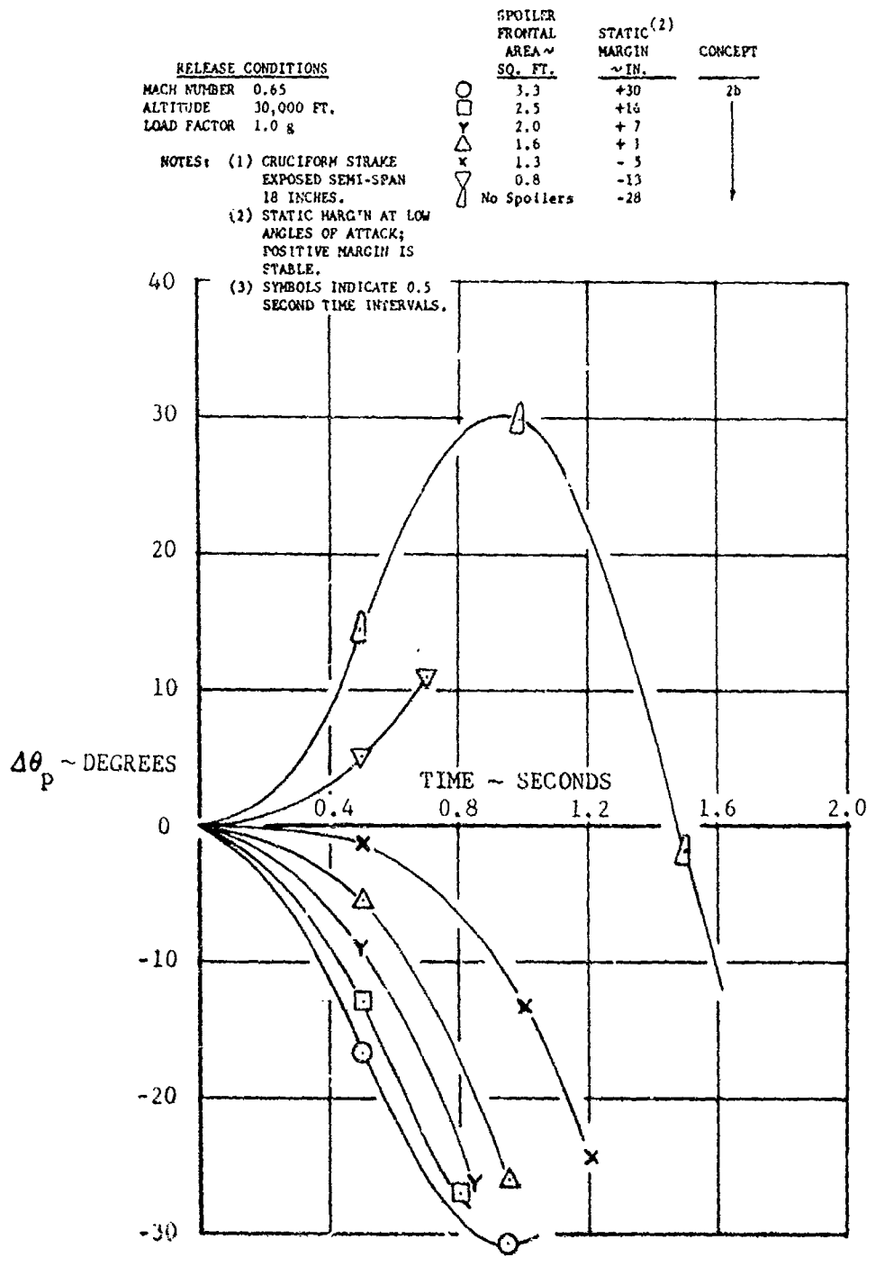


FIGURE 3 CONTINUED

RELEASE CONDITIONS		SPOILER FRONTAL AREA ~ SQ. FT.	STATIC(2) MARGIN ~ IN.	CONCEPT
MACH NUMBER 0.65	○	3.3	+30	2b
ALTITUDE 30,000 FT.	□	2.5	+16	↓
LOAD FACTOR 1.0 g	Y	2.0	+ 7	
	△	1.6	+ 1	
NOTES: (1) CRUCIFORM STRAKE EXPOSED SEMI-SPAN 18 INCHES.	×	1.3	- 5	
(2) STATIC MARGIN AT LOW ANGLES OF ATTACK; POSITIVE MARGIN IS STABLE.	▽	0.8	-13	
(3) SYMBOLS INDICATE 0.5 SECOND TIME INTERVALS.		No Spoilers	-28	

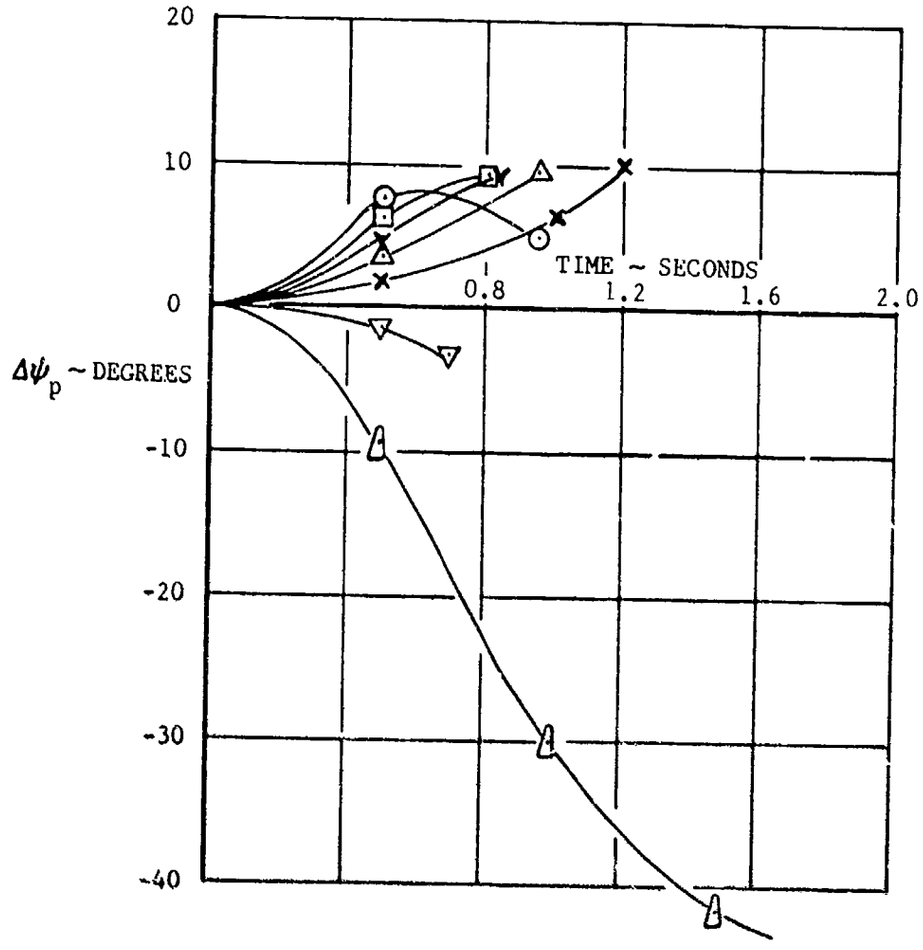


FIGURE 3 CONCLUDED

RELEASE CONDITIONS

MACH NUMBER 0.65
ALTITUDE 30,000 FT.
LOAD FACTOR 1.0 g

NOTES:
(1) STATIC MARGIN AT LOW ANGLES OF ATTACK; POSITIVE MARGIN IS STABLE.
(2) SYMBOLS INDICATE 0.5 SECOND TIME INTERVALS.

STRAKE EXPOSED SEMI-SPAN ~ IN. (HOR./VERT.)	STATIC[1] MARGIN ~ IN. (LONG./DIR.)	CONCEPT
18/18	-28/-28	2c
18/13	-28/-10	2d
18/10	-28/- 2	
18/ 5	-28/+ 8	
15/10	-17/- 2	
15/11	-17/- 4.5	

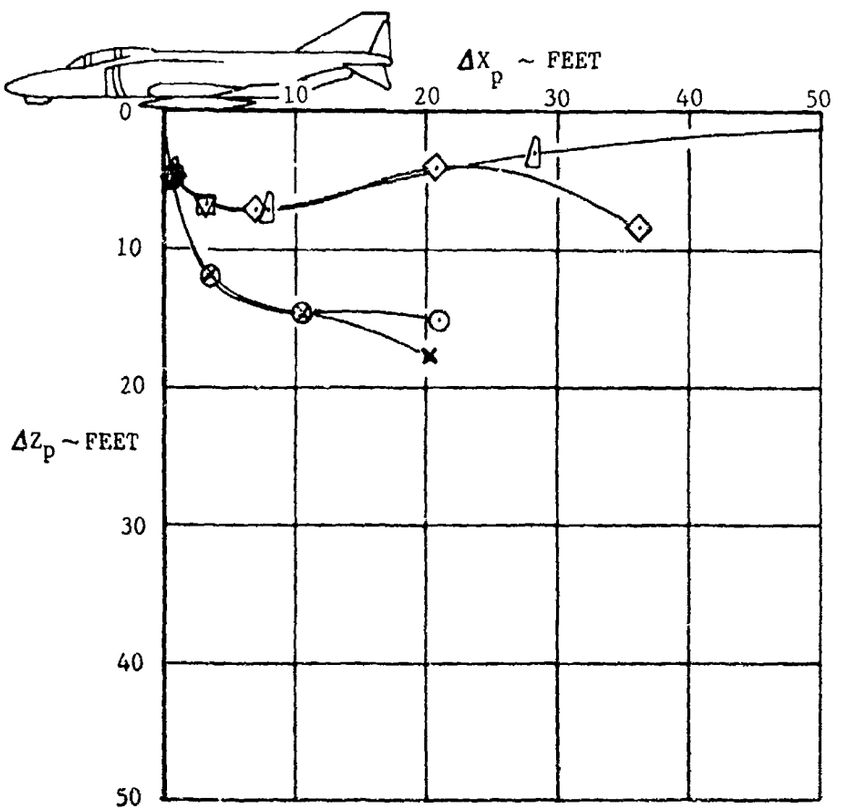


FIGURE 4 EFFECT OF INTERDIGITATED CRUCIFORM STRAKES ~ CONCEPTS (2c) AND (2d)

RELEASE CONDITIONS

MACH NUMBER 0.65
ALTITUDE 30,000 FT.
LOAD FACTOR 1.0 g

NOTES:
(1) STATIC MARGIN AT LOW ANGLES OF ATTACK; POSITIVE MARGIN IS STABLE.
(2) SYMBOLS INDICATE 0.5 SECOND TIME INTERVALS.

STRAKE EXPOSED SEMI-SPAN ~ IN. (HOR./VERT.)	STATIC[1] MARGIN ~ IN. (LONG./DIR.)	CONCEPT
18/18	-28/-28	2c
18/13	-28/-10	2d
18/10	-28/- 2	
18/ 5	-28/+ 8	
15/10	-17/- 2	
15/11	-17/- 4.5	

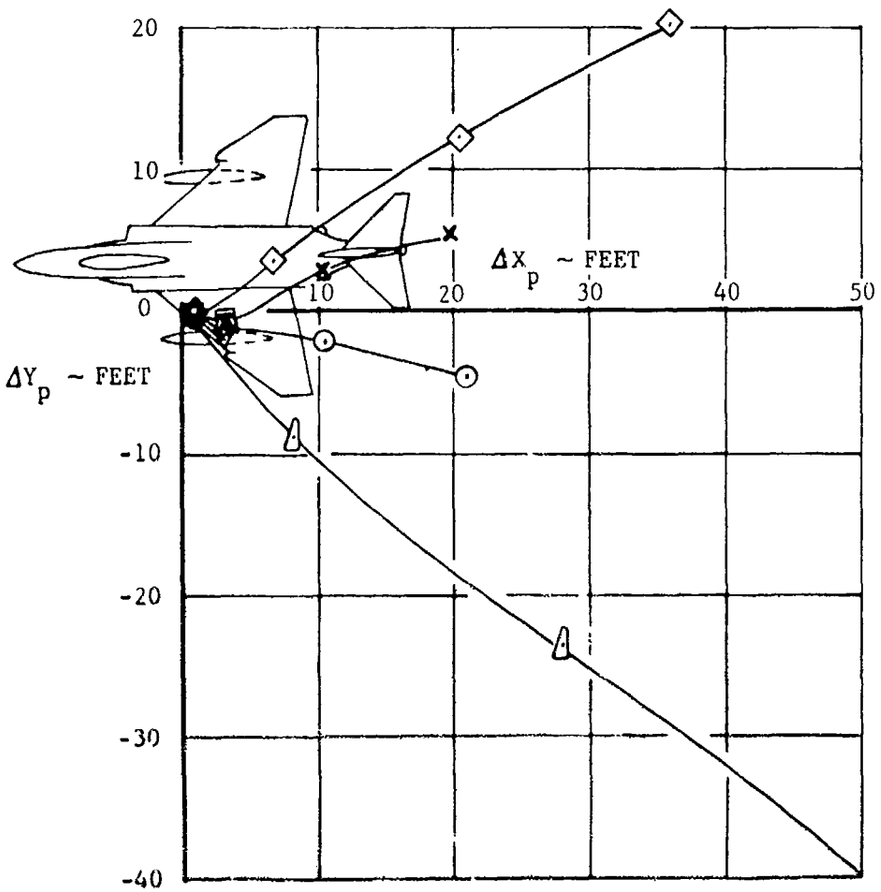


FIGURE 4 CONTINUED

RELEASE CONDITIONS	STRAKE EXPOSED SEMI-SPAN ~ IN. (HOR./VERT.)	STATIC[(1)] MARGIN ~ IN. (LONG./DIR.)	CONCEPT
MACH NUMBER 0.65	18/18	-28/-28	2c
ALTITUDE 30,000 FT.	18/13	-28/-10	2d
LOAD FACTOR 1.0 g	18/10	-28/- 2	↓
	18/ 5	-28/+ 8	
	15/10	-17/- 2	
	15/11	-17/- 4.5	

NOTES:
(1) STATIC MARGIN AT LOW ANGLES OF ATTACK; POSITIVE MARGIN IS STABLE.
(2) SYMBOLS INDICATE 0.5 SECOND TIME INTERVALS.

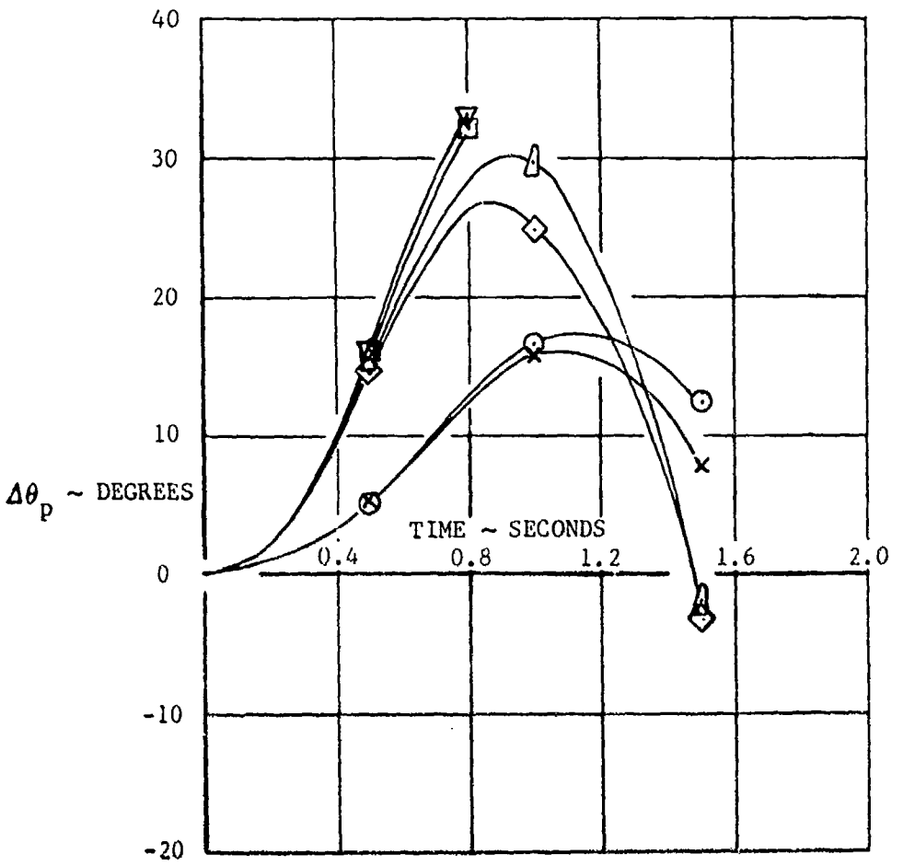


FIGURE 4 CONTINUED

RELEASE CONDITIONS

MACH NUMBER 0.65
ALTITUDE 30,000 FT.
LOAD FACTOR 1.0 g

NOTES:
(1) STATIC MARGIN AT LOW ANGLES OF ATTACK; POSITIVE MARGIN IS STABLE.
(2) SYMBOLS INDICATE 0.5 SECOND TIME INTERVALS.

	STRAKE EXPOSED SEMI-SPAN ~ IN. (HOR./VERT.)	STATIC(1) MARGIN ~ IN. (LONG./DIR.)	CONCEPT
◿	18/18	-28/-28	2c
▽	18/13	-28/-10	2d
□	18/10	-28/- 2	|
◇	18/ 5	-28/+ 8	|
×	15/10	-17/- 2	|
○	15/11	-17/- 4.5	↓

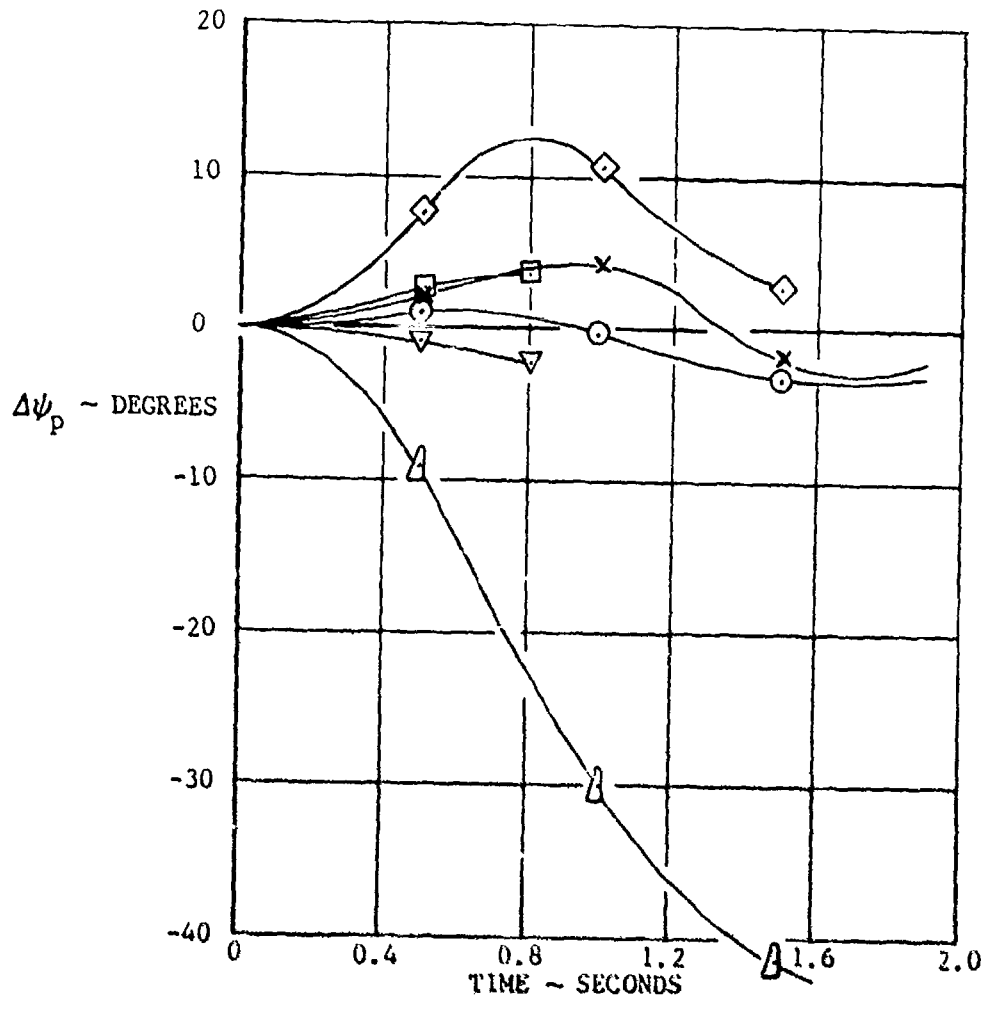


FIGURE 4 CONCLUDED

EVALUATION OF THE TECHNIQUE

To evaluate the accuracy of the flow-angularity technique, predicted separation trajectories are correlated with wind tunnel trajectories and flight test data. The predicted trajectories are also compared with trajectories determined using the grid force/moment interference coefficient computer program used by the Aircraft Compatibility Branch (DLJC) at Eglin AFB, Florida. The correlations and comparison are performed for a modular guided weapon which has cruciform (X) wings and strakes, and is statically stable during jettison. The weapon control surfaces are locked during jettison to produce a weapon nose-down pitch bias. The total weapon weight is approximately 2500 pounds.

The predicted separation trajectories were determined prior to the flight test program using the flow-angularity technique. The initial flight conditions for the trajectories are based on F-4 aircraft trimmed lift characteristics corresponding to 1.0 g level flight and nominal gross weight. Normal MAU-12 ejector rack conditions based on static ground tests for various store weight classifications were used.

The wind tunnel trajectory data were obtained during aircraft compatibility and separation tests, Reference (2). The tests were sponsored by the Air Force Armament Laboratory (AFATL) and conducted in the AEDC-4T wind tunnel in December, 1974. The tests were conducted with 0.05-scale aircraft and weapon models using the PWT Captive Trajectory Store Separation System (CTS) linked with a digital computer.

The flight test program was conducted at the Armament Development and Test Center (ADTC), Eglin Air Force Base, Florida, in February, 1975. The flight test data are obtained from photogrammetry results derived from on board high-speed camera coverage of Mass Simulation Vehicle (MSV) drops. It should be noted that although the photogrammetry results are digitized for each on board camera location, the accuracy is questionable, particularly in the yaw and roll motions of the weapon for this particular application.

Trajectories were determined by the Aircraft Compatibility Branch using the grid force/moment coefficient program described in Reference (3). The program makes two basic assumptions. The first is that the total coefficient on a weapon separating from an aircraft can be represented by a free-stream component and an interference component. The second assumption is that the interference coefficients vary only in vertical distance from the aircraft.

The weapon free-stream aerodynamics used in the DLJC program were obtained from wind tunnel tests using a 0.25-scale model. The data are input into the program in the aeroballistic axis system with a total three-dimensional aerodynamic model containing control, cross-coupling and damping terms.

The grid interference coefficients acting on the weapon were obtained with the AEDC-4T CTS system using 0.05-scale models of the weapon and F-4 aircraft. The aircraft model was mounted on the main strut and is adjustable in roll, pitch and yaw. The weapon with an internal six degree-of-freedom balance was mounted on a sting that can be positioned with the six degree-of-freedom CTS rig. The weapon model was translated in the aircraft pylon axis vertical direction (ΔZ_p) and the total coefficients acting on the weapon were measured every two feet (full-scale) up to 20 feet.

Taking measurements with the store translating only in the vertical direction greatly reduces the amount of time required to cover the Mach number/angle of attack range associated with the typical flight envelope of an aircraft. In this particular test, twenty-eight runs at Mach numbers ranging from 0.3 to 1.2 and angles of attack from zero degree to 16 degrees were made, in slightly over two hours.

After completion of the wind tunnel testing the interference coefficients were determined by subtracting the free-stream coefficients from the total coefficients that were measured in the tunnel. These interference coefficients were then entered on a data tape that is used by the computer program. Subroutines in the program read the tape, store the coefficients and do any interpolation required between points on the tape. The program uses the force/moment interference coefficients and free-stream coefficients with the six degree-of-freedom equations of motion to simulate the separation trajectory of a weapon.

DISCUSSION OF CORRELATIONS/COMPARISON

Correlations of the predicted and CTS separation trajectories with photogrammetry flight test results are shown in Figures 5 through 7 for both subsonic and supersonic release conditions. The weapon center-of-gravity translations, and angular rotations in the pylon axis system are presented as a function of flight time. In some cases, photogrammetry results for two different on board camera positions are shown.

The correlation between the predicted trajectories and the flight test data is, except for roll angle ($\Delta\phi_p$), reasonably good both subsonically and supersonically. The weapon roll angle is consistently underpredicted compared to the CTS wind tunnel and flight test data. The underprediction could be caused by an interaction effect of the aircraft pylon on the upper wing surfaces of the weapon which is not accounted for in the flow-angularity technique. The aircraft pylon probably reduces the aircraft spanwise flow field on the upper wing surfaces at the initial condition ($\Delta Z_p = 0$). An improvement in the technique would be to include the initial pylon effects on the weapon.

RELEASE CONDITIONS

MACH NUMBER 0.8
ALTITUDE 13,000 FEET
WEAPON RELEASED FROM RIGHT WING INBOARD PYLON
CLEAN OUTBOARD WING STATIONS

——— FLOW-ANGULARITY TECHNIQUE
○ CTS WIND TUNNEL TEST DATA
⊖ PHOTOGRAMMETRY FLIGHT TEST RESULTS

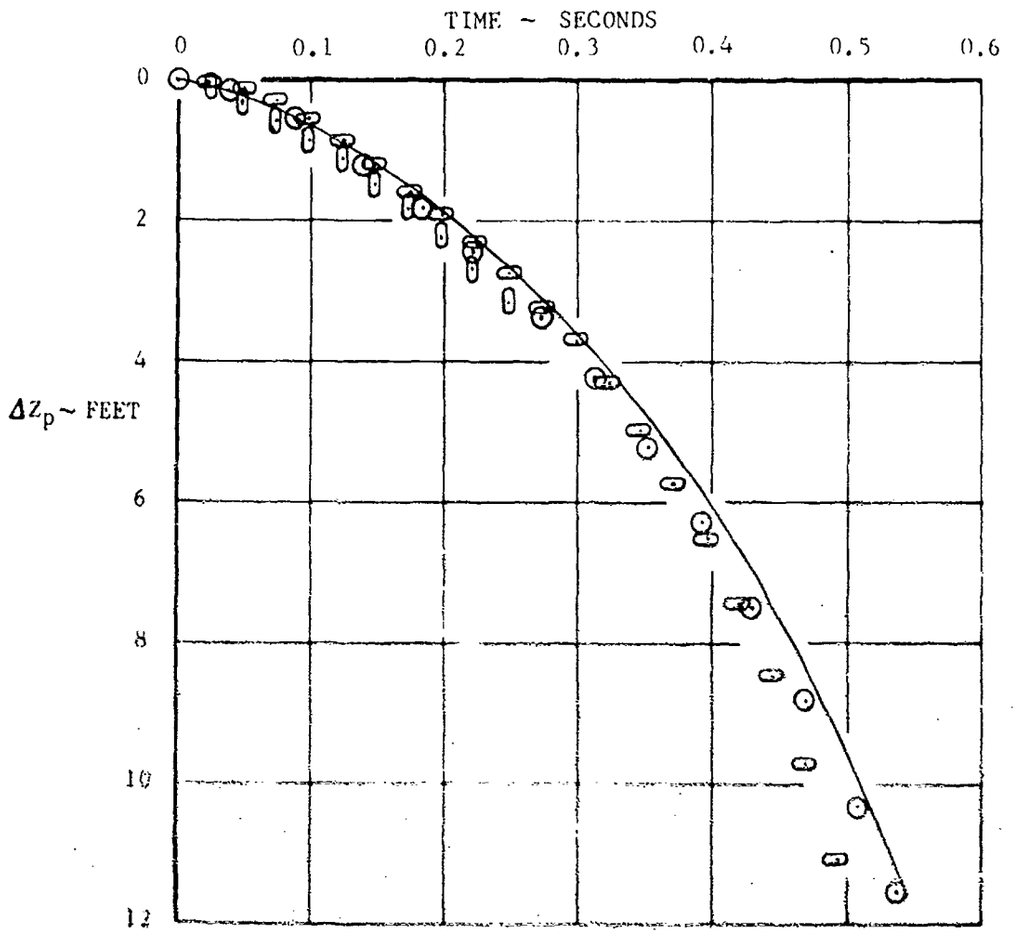


FIGURE 5 CORRELATION OF JETTISON CHARACTERISTICS ~ SUBSONIC, LOW ALTITUDE, CLEAN OUTBOARD WING STATIONS

RELEASE CONDITIONS
MACH NUMBER 0.6
ALTITUDE 13,000 FEET
WEAPON RELEASED FROM RIGHT WING INBOARD PYLON
CLEAN OUTBOARD WING STATIONS

——— FLOW-ANGULARITY TECHNIQUE
O CTS WIND TUNNEL TEST DATA
⊖ PHOTOGRAMMETRY FLIGHT TEST RESULTS

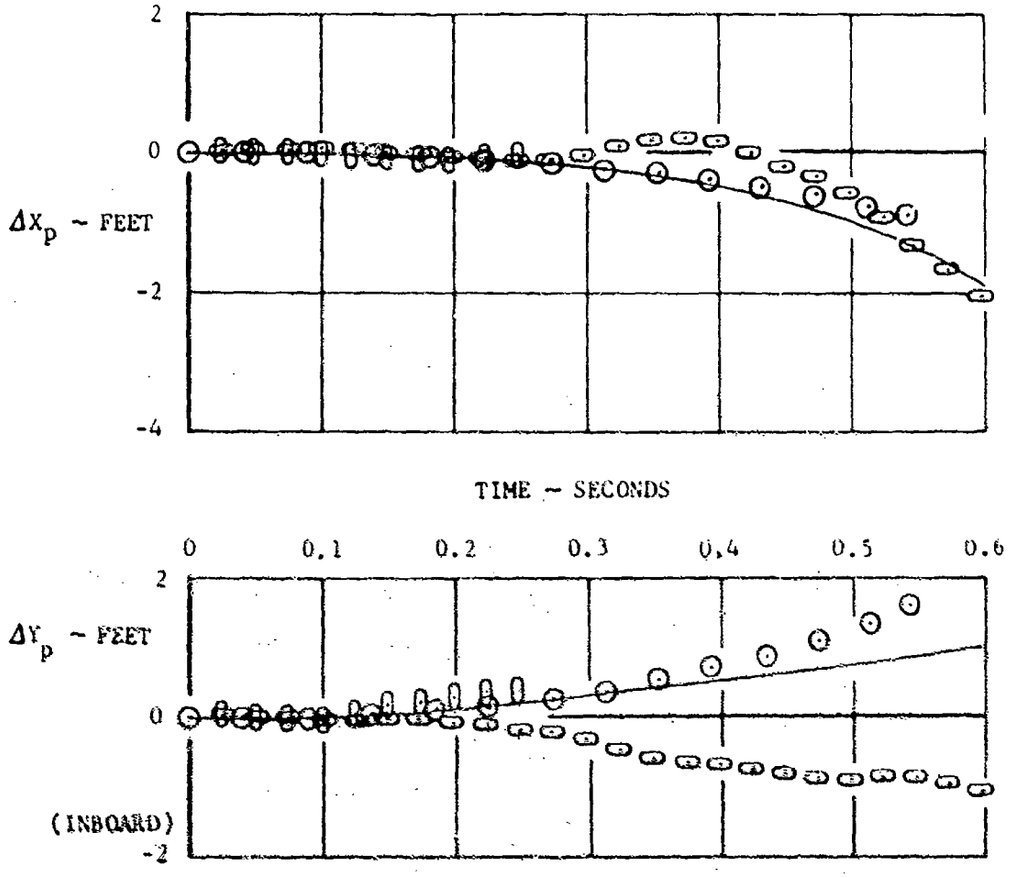


FIGURE 5 CONTINUED

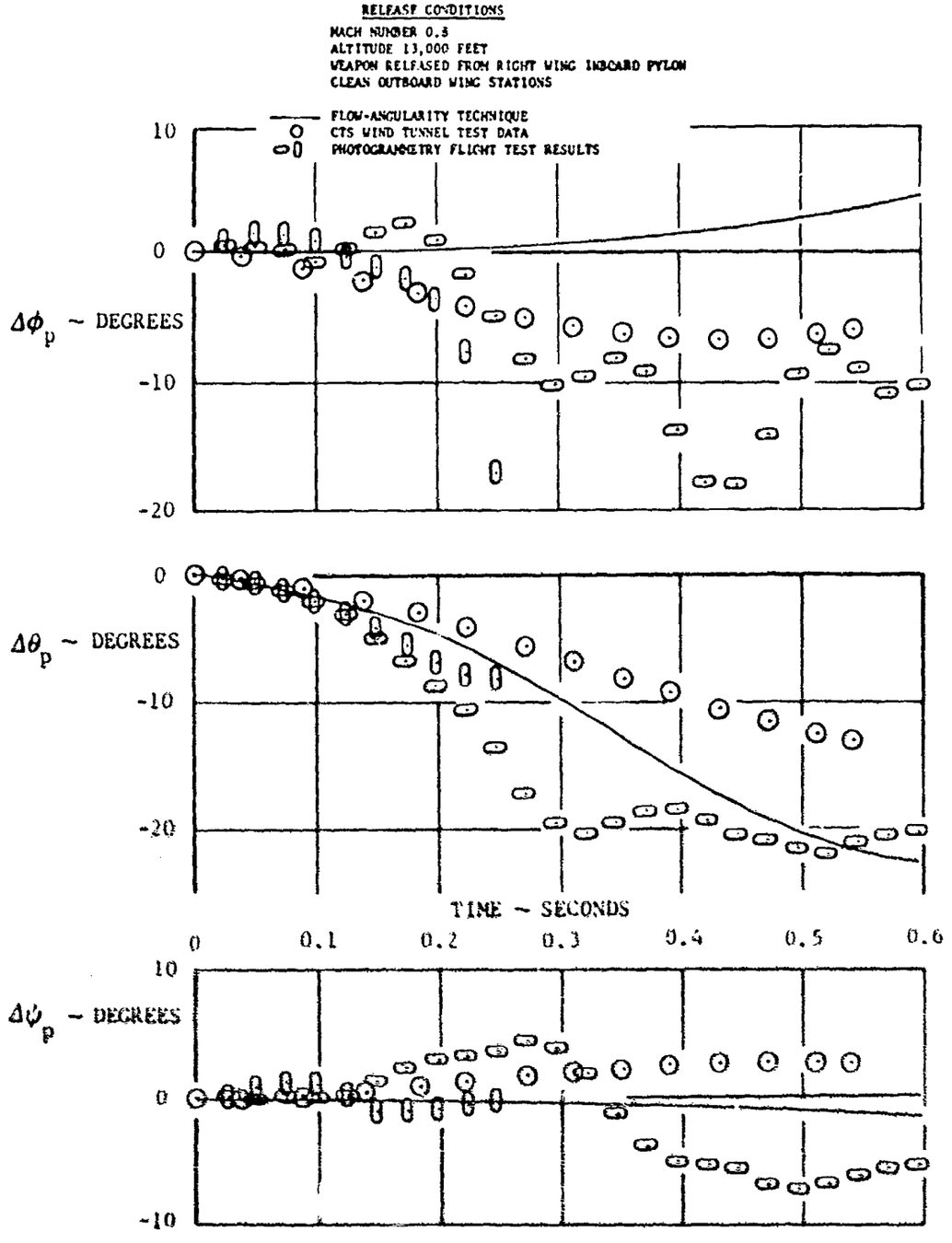


FIGURE 5 CONCLUDED

RELEASE CONDITIONS
MACH NUMBER 0.9
ALTITUDE 40,000 FEET
WEAPON RELEASED FROM LEFT WING INBOARD PYLON
OUTBOARD EXTERNAL FUEL TANKS

——— FLOW-ANGULARITY TECHNIQUE
CTS WIND TUNNEL TEST DATA
PHOTOGRAMMETRY FLIGHT TEST RESULTS
– – – INTERFERENCE COEFFICIENT PROGRAM

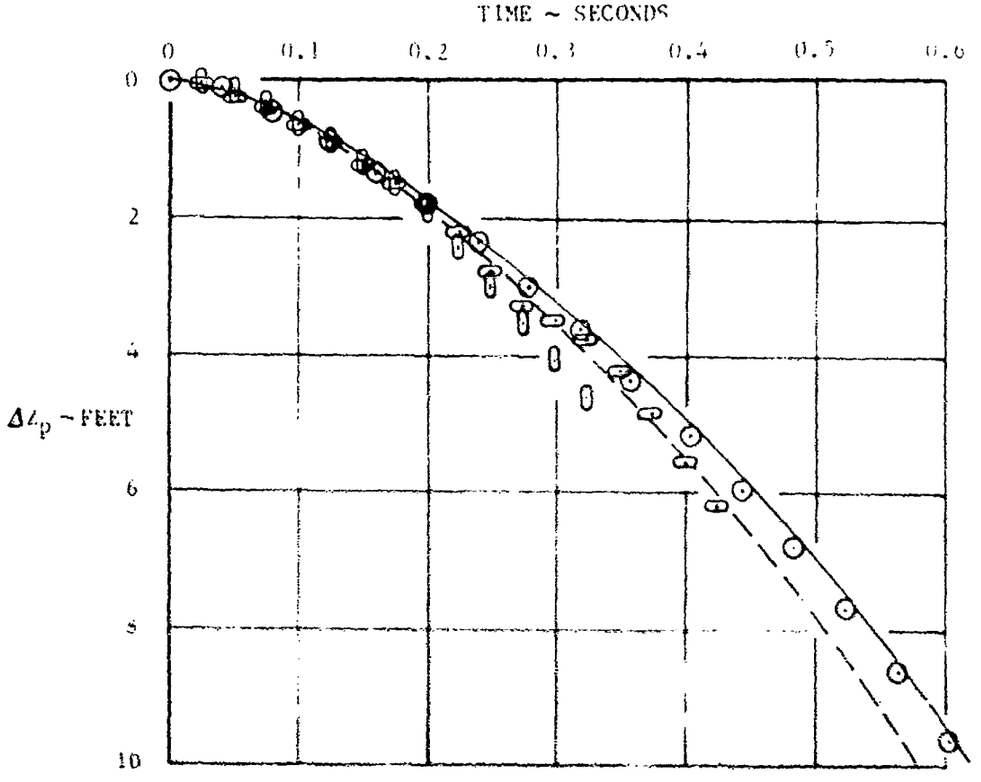


FIGURE 6 CORRELATION OF JETTISON CHARACTERISTICS – SUBSONIC, HIGH ALTITUDE, WITH OUTBOARD EXTERNAL FUEL TANKS

RELEASE CONDITIONS
MACH NUMBER 0.9
ALTITUDE 40,000 FEET
WEAPON RELEASED FROM LEFT WING INBOARD PYLON
OUTBOARD EXTERNAL FUEL TANKS

——— FLOW-ANGULARITY TECHNIQUE
CTS WIND TUNNEL TEST DATA
PHOTOGRAMMETRY FLIGHT TEST RESULTS
– – – INTERFERENCE COEFFICIENT PROGRAM

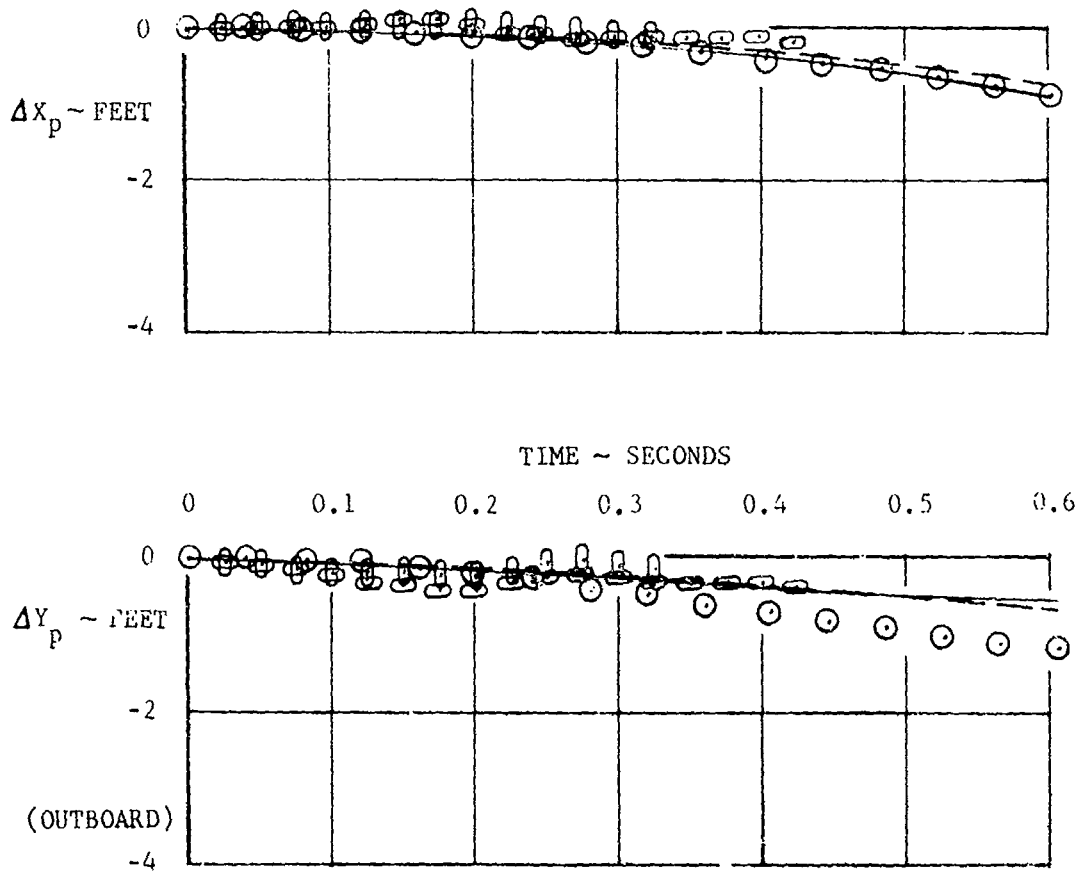


FIGURE 6 CONTINUED

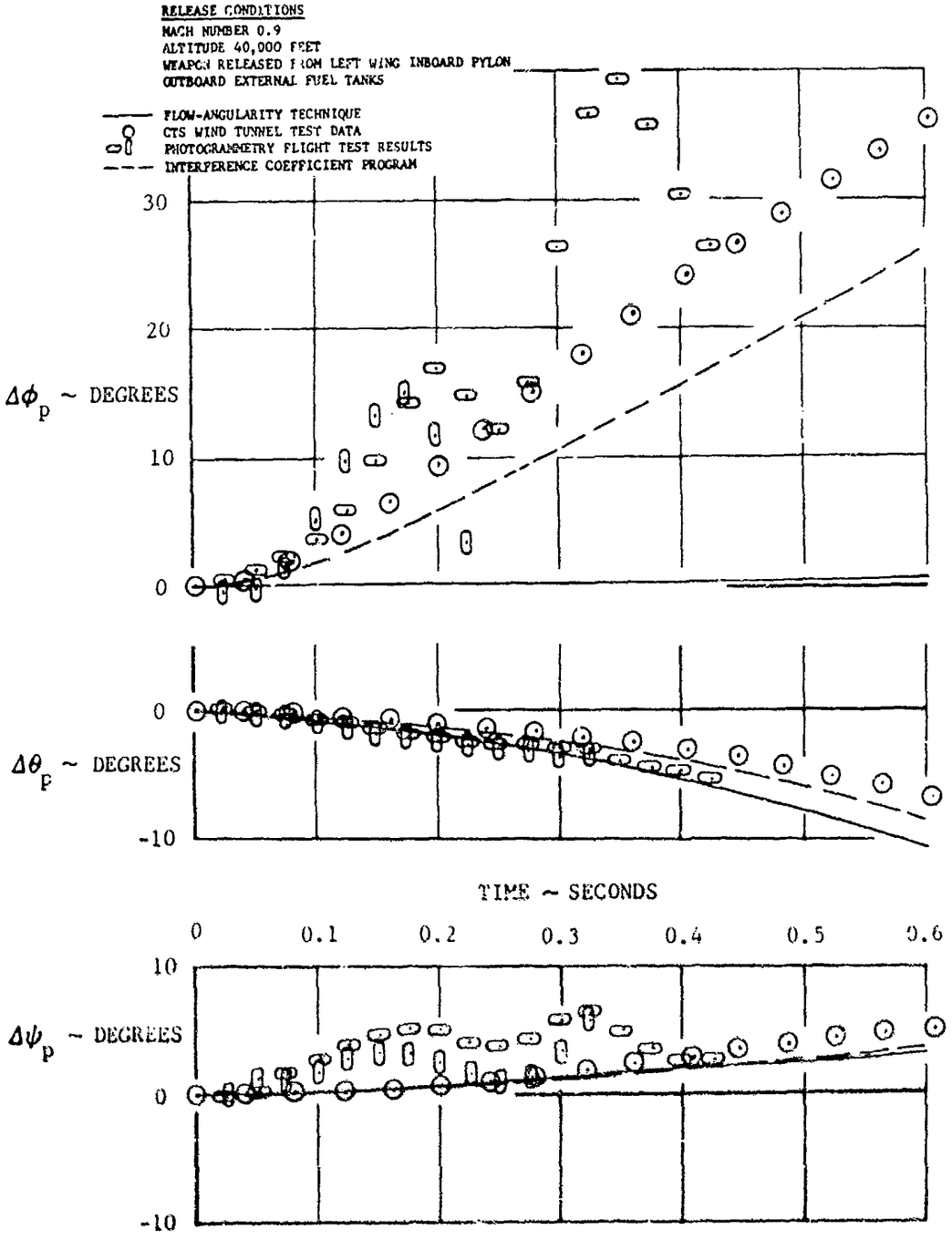


FIGURE 6 CONCLUDED

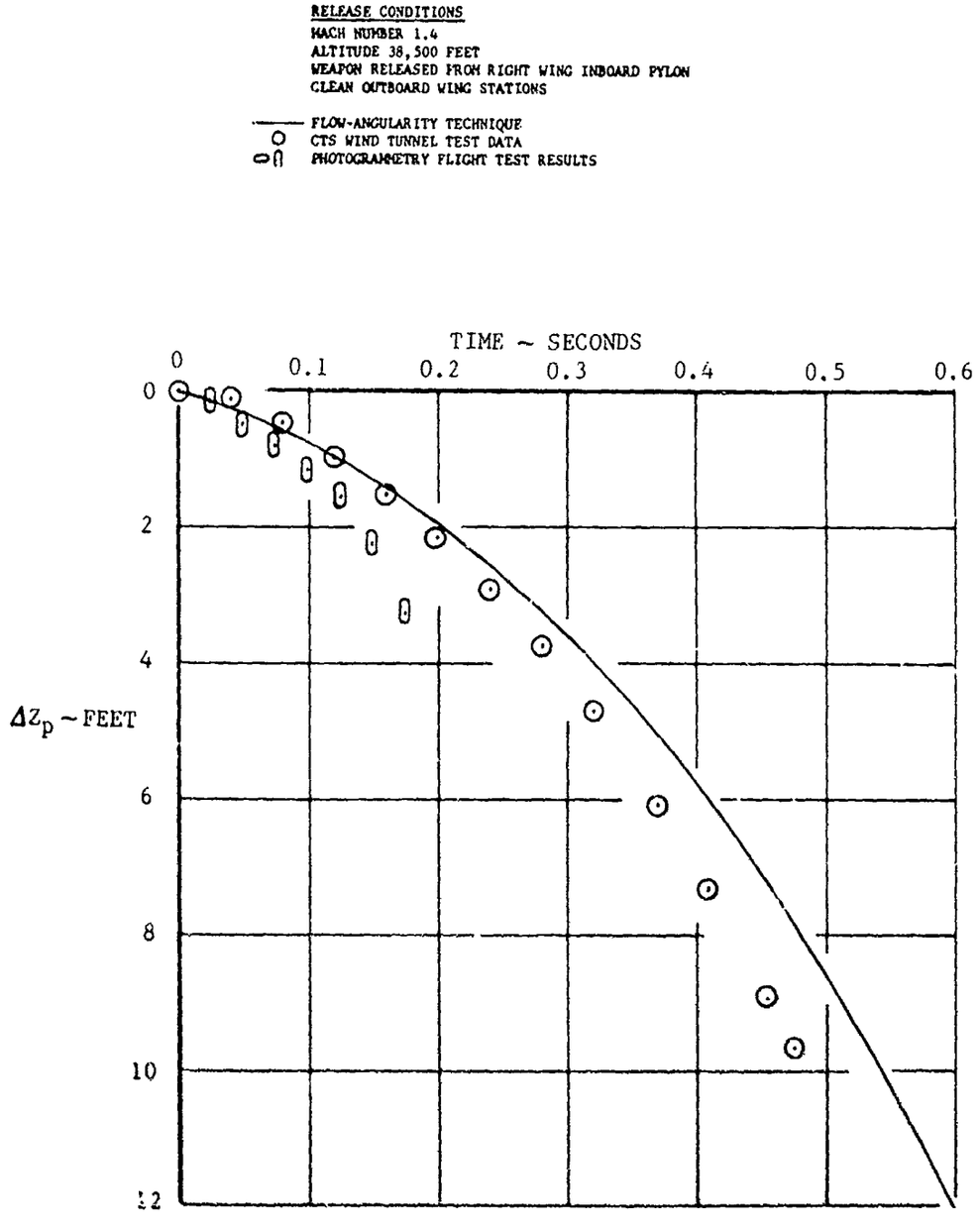


FIGURE 7 CORRELATION OF JETTISON CHARACTERISTICS ~ SUPERSONIC, HIGH ALTITUDE, CLEAN OUTBOARD WING STATIONS

RELEASE CONDITIONS
MACH NUMBER 1.4
ALTITUDE 36,500 FEET
WEAPON RELEASED FROM RIGHT WING INBOARD PYLON
CLEAN OUTBOARD WING STATIONS

——— FLOW-ANGULARITY TECHNIQUE
○ CTS WIND TUNNEL TEST DATA
⊙ PHOTOGRAMMETRY FLIGHT TEST RESULTS

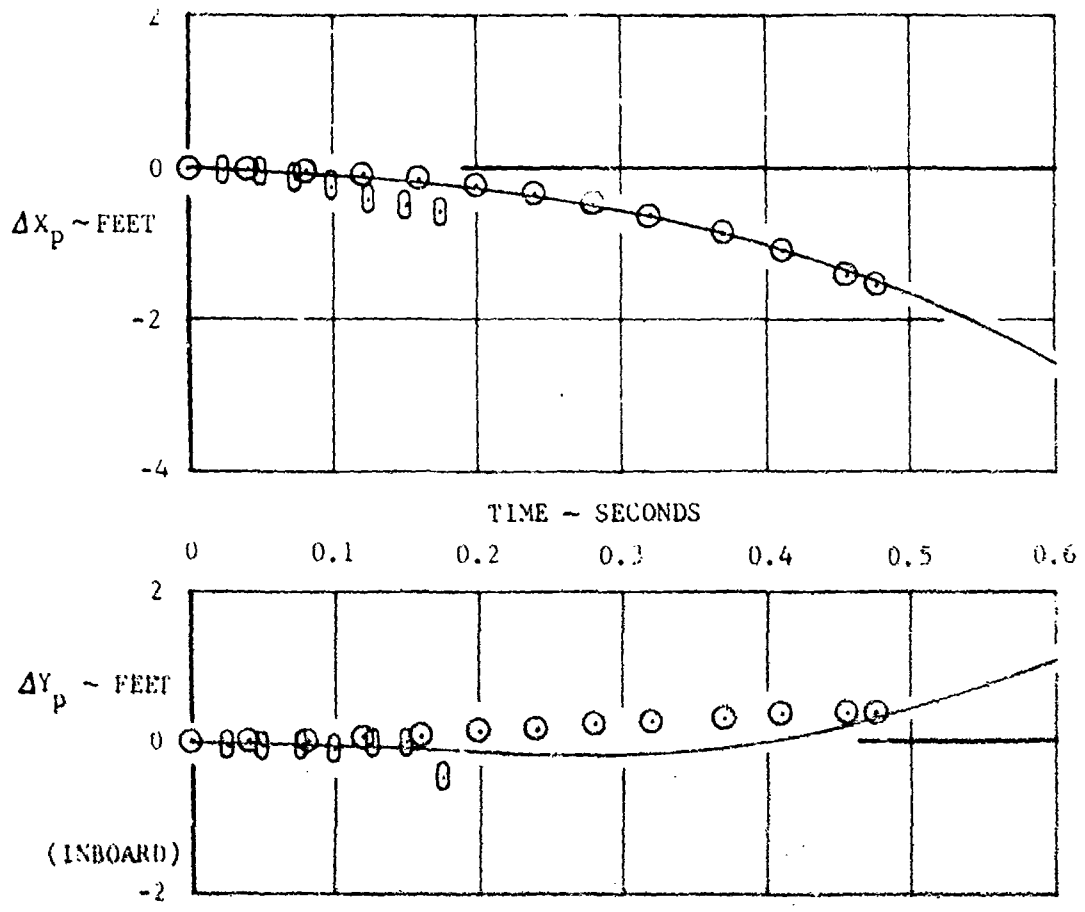


FIGURE 7 CONTINUED

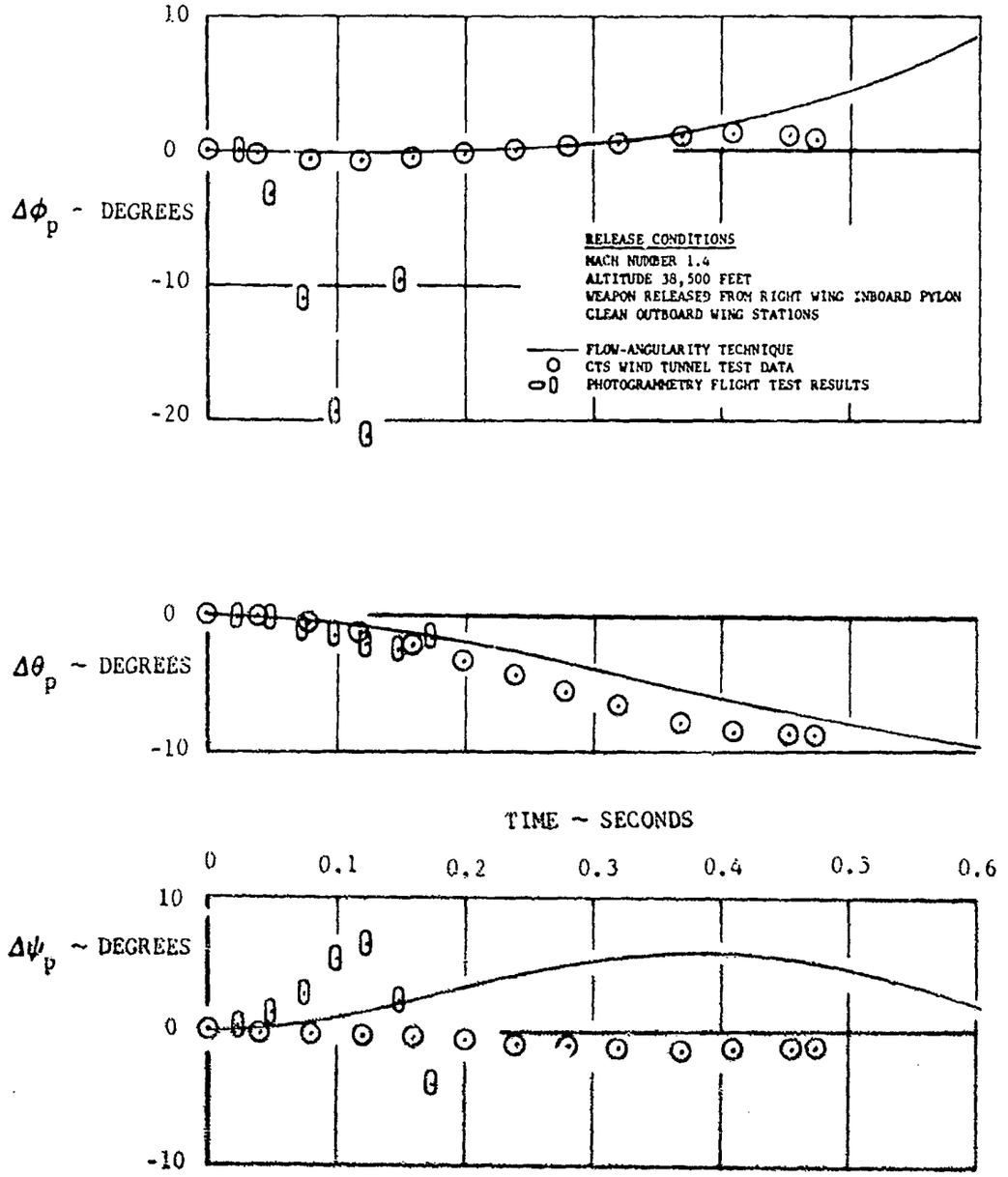


FIGURE 7 CONCLUDED

The initial interference rolling moment coefficient (ΔC_{l_i}) could be calculated based on applying the spanwise flow to the lower lifting surfaces only.

Comparison of the predicted trajectories using the flow-angularity technique with the separation trajectories determined using the DLJC interference coefficient program are shown in Figures 6, 8, and 9. The comparison shows excellent agreement, except in roll angle, at both subsonic and supersonic release conditions.

It is of significance to note that the flight test photogrammetry data are least reliable in roll, and the chase film did not exhibit the magnitude of roll that is indicated by the photogrammetry data. Also, the CTS trajectory and interference coefficient data are subject to small weapon model asymmetries which produce induced rolling moments which were not indicated in the 0.25-scale wind tunnel tests. Therefore, due to these considerations, the discrepancy in roll attitude correlation is expected to be less than shown.

RELEASE CONDITIONS
MACH NUMBER 0.8
ALTITUDE 13,000 FEET
WEAPON RELEASED FROM LEFT WING INBOARD PYLON
OUTBOARD EXTERNAL FUEL TANKS

——— FLOW-ANGULARITY TECHNIQUE
O CTS WIND TUNNEL TEST DATA
– – – INTERFERENCE COEFFICIENT PROGRAM

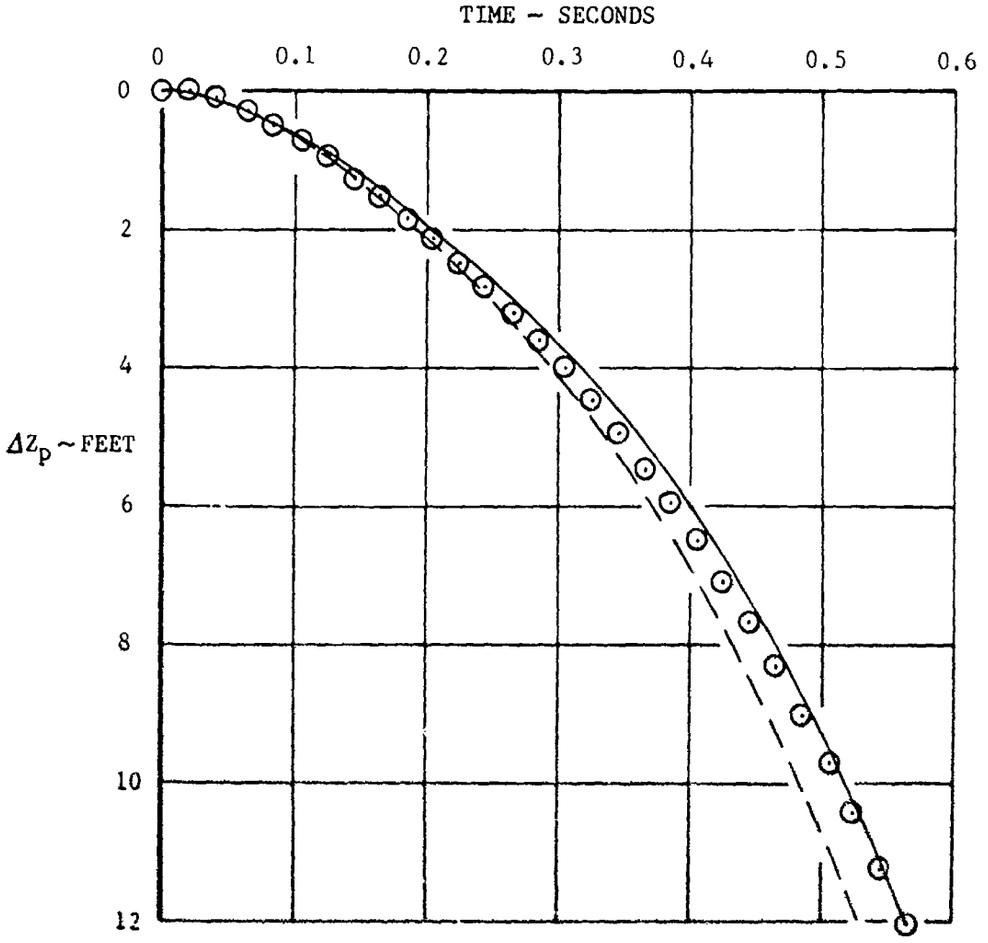


FIGURE 8 COMPARISON OF JETTISON CHARACTERISTICS – SUBSONIC, LOW ALTITUDE, WITH OUTBOARD EXTERNAL FUEL TANKS

RELEASE CONDITIONS
MACH NUMBER 0.8
ALTITUDE 13,000 FEET
WEAPON RELEASED FROM LEFT WING INBOARD PYLON
OUTBOARD EXTERNAL FUEL TANKS

——— FLOW-ANGULARITY TECHNIQUE
O CTS WIND TUNNEL TEST DATA
– – – INTERFERENCE COEFFICIENT PROGRAM

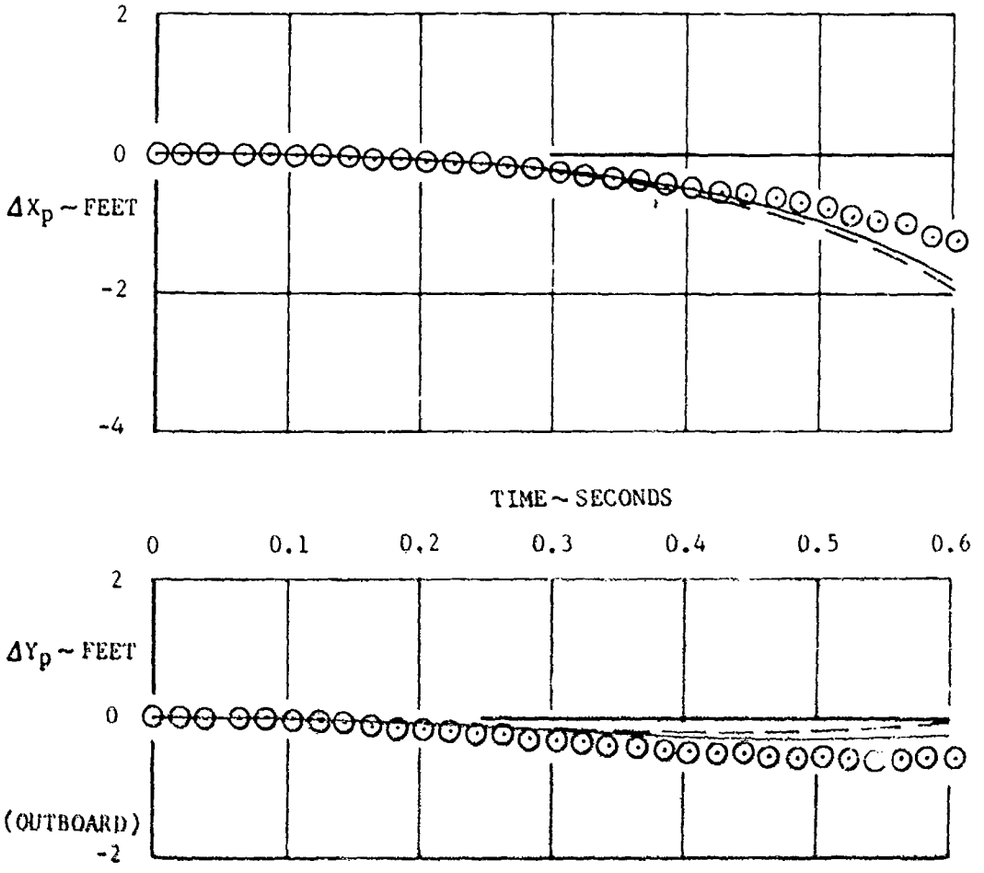


FIGURE 8 CONTINUED

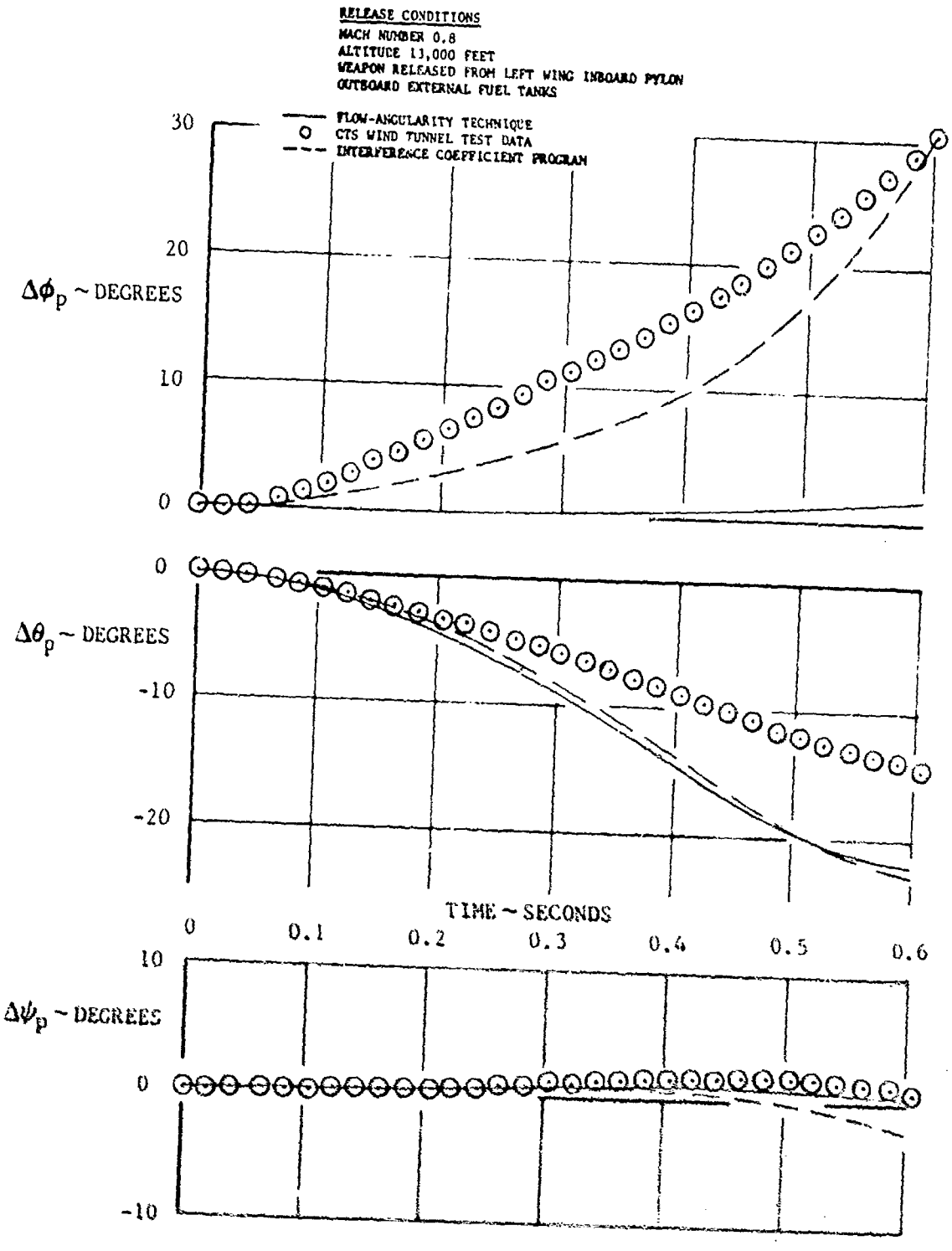


FIGURE 8 CONCLUDED

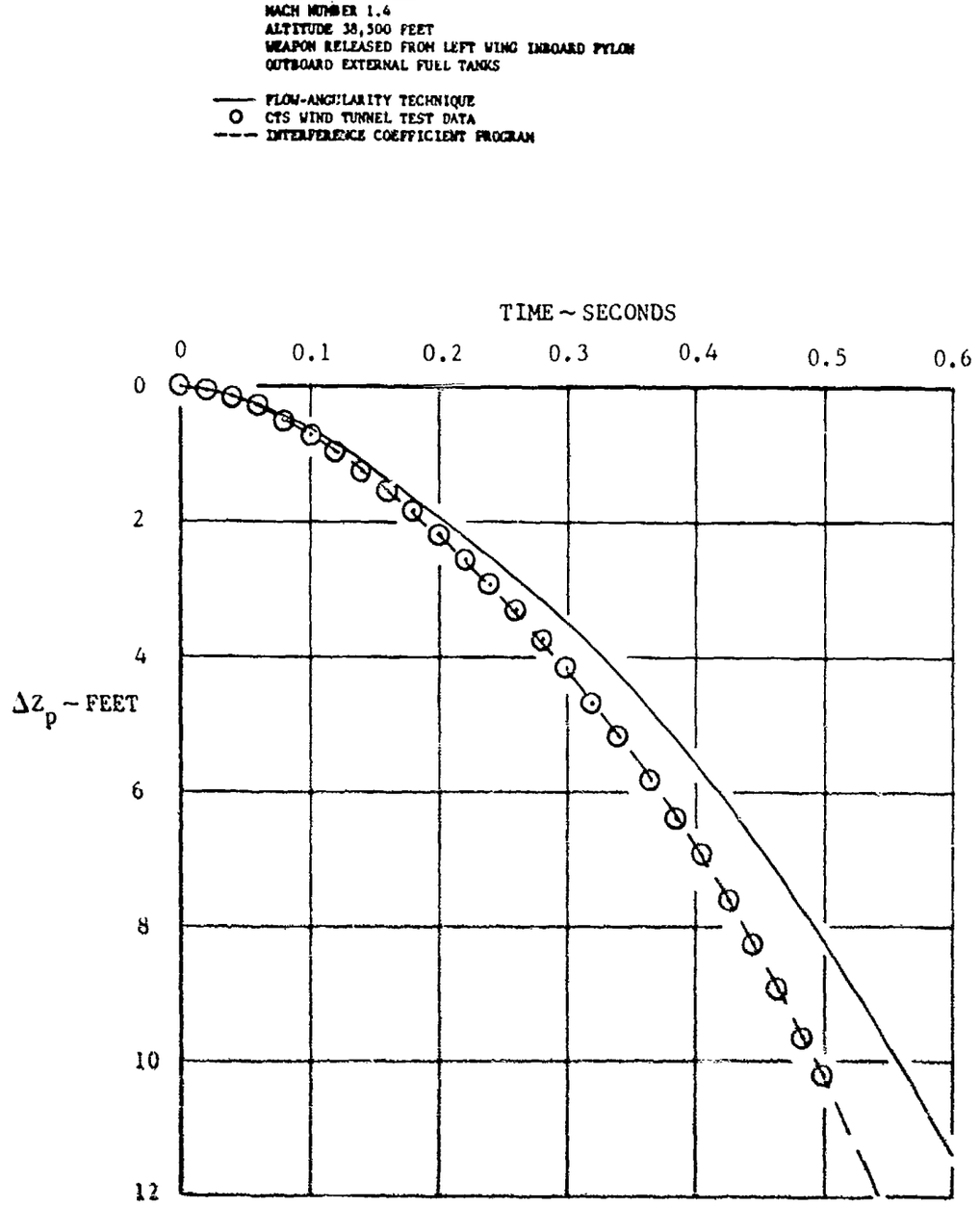


FIGURE 9 COMPARISON OF JETTISON CHARACTERISTICS ~ SUPERSONIC, HIGH ALTITUDE, WITH OUTBOARD EXTERNAL FUEL TANKS

RELEASE CONDITIONS
MACH NUMBER 1.4
ALTITUDE 38,500 FEET
WEAPON RELEASED FROM LEFT WING INBOARD PYLON
OUTBOARD EXTERNAL FUEL TANKS

—— FLOW-ANGULARITY TECHNIQUE
O CTS WIND TUNNEL TEST DATA
--- INTERFERENCE COEFFICIENT PROGRAM

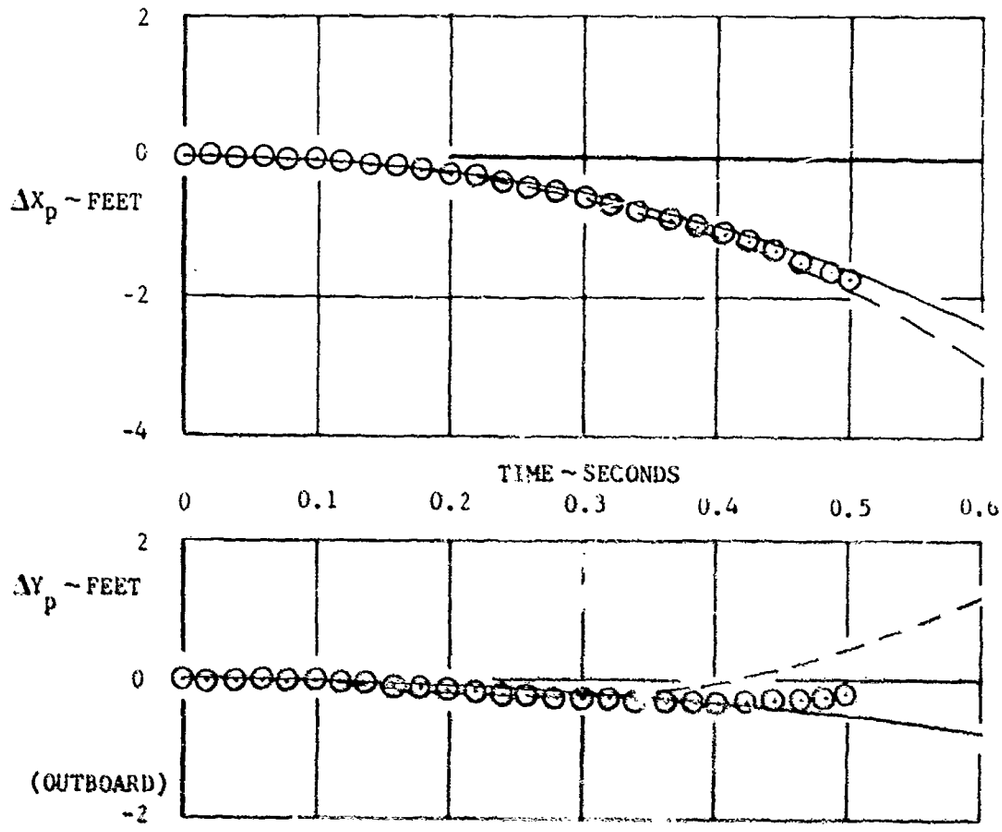


FIGURE 9 CONTINUED

RELEASE CONDITIONS

MACH NUMBER 1.4
ALTITUDE 33,500 FEET
WEAPON RELEASED FROM LEFT WING INBOARD PYLON
OUTBOARD EXTERNAL FUEL TANKS

—— FLOW-ANGULARITY TECHNIQUE
O CTS WIND TUNNEL TEST DATA
– – – INTERFERENCE COEFFICIENT PROGRAM

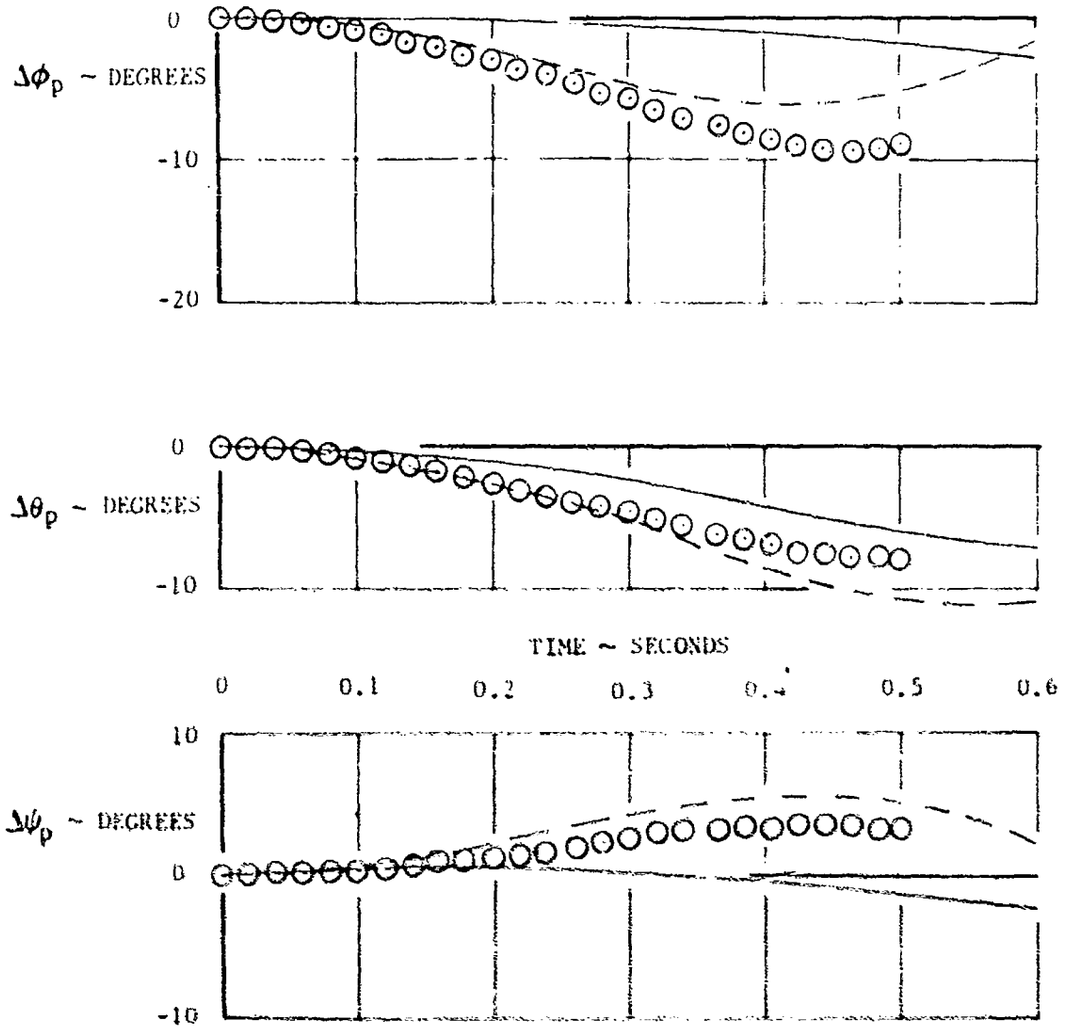


FIGURE 9 CONCLUDED

CONCLUSIONS

1. The flow-angularity technique, as presented herein, provides good prediction of air-launched weapon pitch/yaw separation characteristics. Application of the technique during weapon design and development would need only limited captive trajectory wind tunnel testing at critical conditions, if substantiation is required. The resultant effect would be a considerable reduction in program development costs (tunnel occupancy hours, etc.) associated with extensive CTS separation testing.

2. Comparison of predicted jettison separation characteristics using the flow-angularity technique with those determined using the DLJC force/moment interference program shows excellent agreement.

3. The flow-angularity technique provides analysis flexibility during configuration development of air-launched weapons. Since the technique is based on the use of aircraft flow field angularity data, determined experimentally or from empirical/theoretical methods, numerous weapon configuration designs may be evaluated.

4. For the weapon configuration concepts evaluated in the analyses, satisfactory jettison characteristics at nominal release conditions are indicated with unstable longitudinal/directional static margins. During jettison, the weapon pitch/yaw dynamics are minimized with moderately unstable static margins.

5. The analysis illustrates and supports the concept that detailed separation or launch transient analyses are an essential element of high-lift air-launched weapon configuration development.

RECOMMENDATION

It is recommended that flow-angularity surveys be performed on all future (or current, where necessary) aircraft configurations to provide a data base for air-launched weapon configuration development.

REFERENCES

(1) Carmen, J. B., "Flow-Field, Aerodynamic Loads, and Separation Trajectory Tests on the MK-84 and SUU-54 Super HOBOS Guided Weapons with the F-4C and A-7D Parent Aircraft at Mach Numbers 0.65 to 1.60", AEDC-TR-74-103, October, 1974 (U).

(2) Carmen, J. B. and Kaupp, H., "Aerodynamic and Aircraft Separation Characteristics of the Electro-Optical Guided Bomb (EOGB II)", AEDC-TR-75-66, June, 1975 (U).

(3) Mathews, Charles B., et al, "A Technique for Investigating the Launch and Separation of Guided Weapons", JTCG Aircraft/Stores Compatibility Symposium, September, 1975 (U).

ACKNOWLEDGEMENT

The authors wish to acknowledge the contributions of C. D. Bogart of Rockwell International Corporation, for assistance in programming and developing the analytical six degree-of-freedom digital program.

The authors also wish to acknowledge Mr. Charles B. Mathews and Captain Robert D. Cason of the Air Force Armament Laboratory (AFATL), Aircraft Compatibility Branch (DLJC), for their cooperation and assistance, and for providing a description of the AFATL interference coefficient program and the jettison characteristics presented in Figures 6, 8, and 9.

AUTOBIOGRAPHY

Terry G. Blose graduated from the Georgia Institute of Technology in 1968 with a Bachelor Degree in Aeronautical Engineering, and performed graduate work at Ohio State University. He is presently a Member of the Technical Staff of the Vehicle Engineering Group at Rockwell International, Missile Systems Division. He has conducted theoretical and experimental aerodynamic configuration design studies, and performed pre- and post-flight launch/jettison store separation analyses for the GBU-8/B MK 84 and GBU-9/B M118 Guided Bombs, and the AGM-53A CONDOR Weapon System. For the past two years, he has been responsible for the Launch Transient Analysis of an Electro-Optical Guided Bomb, and has implemented numerous improvements in the area of Analytical Store Separation Prediction Techniques.

Ralph M. Barnes graduated from the University of Cincinnati in 1957 receiving the degree of Aeronautical Engineer. He is presently Lead Aerodynamicist for HOBOS Programs (Homing Bomb Systems). He has been responsible for the aerodynamic configuration development of the MK 84 EOGB I and the M118 EOGB, in addition to the current GBU-15 Program. He participated in the LASRM Air Breathing Propulsion configuration development program and the HORNET Air-to-Ground EO Seeker Development Program. He is a registered Professional Engineer in the State of Ohio and a member of the AIAA. He served as Columbus Section Chairman of AIAA during 1971 and 1972.

CHASE

The Optimum Photoanalysis System

Alan Aden
McDonnell Aircraft Company
Edwards AFB, California

ABSTRACT

The acquisition of accurate, reliable, stores trajectory data at reasonable cost and minimum delay has been an elusive goal. Each of these objectives and more have been achieved in CHASE.

CHASE was developed and used concurrently during the F-15 Development Testing and Evaluation. It became fully operational in the closing months of testing, and contributed heavily to MCAIR's success in this area. Trajectory data in 24 hours became routine.

All this is possible in any facility having a film reader and general purpose computer. The beauty of CHASE is that it requires very little preparation, stores need no markings, uses no special equipment, and is absolutely conservative in the manpower required. A separation requires, on the average, only one hour on a film reader and two minutes on an average computer.

CHASE is an analytical and software technique that yields 6 degrees of freedom data within an accuracy equal to, if not better than, any existing system. This is exemplified through its formal presentation of the unconditioned results. The output is final data including diagrams and a full diagnostic if problems arise. The system has been proven operationally and has been qualified by various means, including a staged test case. Success of CHASE is the result of some innovative math, elimination of all assumptions, and precise optical calibrations. Its reliability is built in with a complete data file and the extreme simplicity of its application.

CHASE has been effective under all adverse conditions including the typical "lousy" coverage. It adjusts for variations encountered. No limitations have been exhibited from the shape of the stores or the location of the cameras.

"Approved for Public Release; Distribution Unlimited"

PRECEDING PAGE BLANK-NOT FILMED

1.0 INTRODUCTION

The CHASE Photoanalysis System is a very recent McDonnell Aircraft Company (MCAIR) development. It is the ultimate evolution of MCAIR photoanalysis techniques into a responsive, accurate and yet economical approach to gathering stores trajectory data from aircraft separations. Hence, the title "Optimum". This efficiency is maintained in the preparation, testing, as well as in the processing and presentation of the data. It is our opinion that any further improvement must result from some approach other than the use of photography. TV of course is one consideration. But, there are other resources that can and probably will be used.

The acquisition of engineering data from cine camera coverage has been an art at MCAIR for many years. This science got its wings, if you wish, in 1957, when movies were used to monitor the wing loads of an F101 Voodoo in operation Redwing. This was a peripheral flight of a nuclear explosion. A substitute aircraft was needed for the fully instrumented loads airplane that was lost in an accident shortly before the test. The camera was a quick and simple successor to the instrumentation and did its thing well.

35mm cameras were used in 1958 on Voodoos to determine the clearing-distance of ordanance launches. Later 16mm gun cameras were used on the F3H Demon to establish the Sparrow III trajectories from rail launchers. CHASE's parent system was developed in 1959 and used to present the fuselage missile trajectories being launched from the F4H-1 Phantom. Two approaches were used then to analyse the Sparrows photo coverage for displacements, pitch, and yaw relative to the launch aircraft. Both of these were multi-camera solutions and the system that evolved, which has been used for years, has been accordingly called "Multi". At one time early in this application a single camera "quick look" method was also introduced. This did yield results overnight, but they were truly cursory since it was assumed that the missile had no yaw or side displacement. This was an applied graphical technique which was used only in absolute necessity because it required a special talent and effort. This approach was mentioned here only because it was MCAIR's first in a series of attempts at the single camera solution.

Multi went through three evolutionary phases culturing it into a system used by MCAIR for the last decade covering all sorts of stores. It was the system proposed to be used in the F-15 test program for which two aircraft were instrumented. We initiated the F-15 stores compatibility testing with the 600 gallon centerline tank and recognized immediately that the multi camera solution could not keep pace with the program. Coverage was limited. Too much dependence was on the camera reliability. But primarily, there was simply too much film to read. To use the resources allocated, the camera installations and staff lines, and yet provide analysis of each separation, the single camera solution dominated the possibilities.

On a number of occassions prior to this decision the single camera solution was attempted. Some met success under lab conditions but failed to produce with actual data. And those that did work were still unacceptable for flight operations because they were sophisticated and required considerable computer time. With our backs to the wall we did achieve an operable single camera solution for the F-15 Eagle. This breakthrough is simply attributed to our disregard of higher mathematics, to our dependence upon fundamental principles, some innovative handling, and the imagination of several individuals. The grand achievements which were made somewhat later are attributed to the attainment of an exceptional optical precision.

2.0 ENTER CHASE

The prototype system was called Single and was a very basic implementation which could be used for research and testing. The input formats for Single were computer card and the same as those used for Multi. Both Single and Multi were used concurrently during the Eagles testing. Since it was an added burden to an already over-loaded effort, we didn't devote near as much time to its development that we would have liked to and needed to. As a result we did not have the confidence nor did we put full dependence on Single till well into the test program; at the point where we began to drop as many as 6 stores per flight. It's introduction still paid off handsomely. We kept pace with testing on both planes.

When time permitted, improvements were added as we continued to use Single. A new name was adopted when a routine was added that located the camera rather than using some fixed, known location. From this point on the Single solution has been referred to as the CHASE solution. This name CHASE does not infer pursuit or anything second rate, but represents the ultimate objective to use real "chase" photo coverage for separation data. By Fall 1974 the uprated CHASE system was being used exclusively to support the weapons testing. It's responsiveness contributed immeasurably to meeting the milestone commitments. Flights needing previous results for go-ahead were flown on successive days. Some reservations were expressed when such data appeared so promptly.

Before continuing, our definition of Photoanalysis is: The art of taking linear information from photographic coverage, converting that into angular representations, combining those angles with measurements of the aircraft and/or of a store, to convert all of that information into trajectory data of the store relative to the airplane.

Basically CHASE is a simple concept. However, its computer program is very large and complex. Much of this is to maintain absolute precision in the analysis, to assume all possible human duties, to simplify the operation, and to provide check and balances wherever possible. From years of experience we've

learned that there is no room for assumptions in photoanalysis. Many times these will work. But, there is always that condition that prohibits a solution under such constraints. Too often this is on a critical test when the analyst is under pressure to produce results, simply compounding the problem.

3.0 THE CHASE CONCEPT

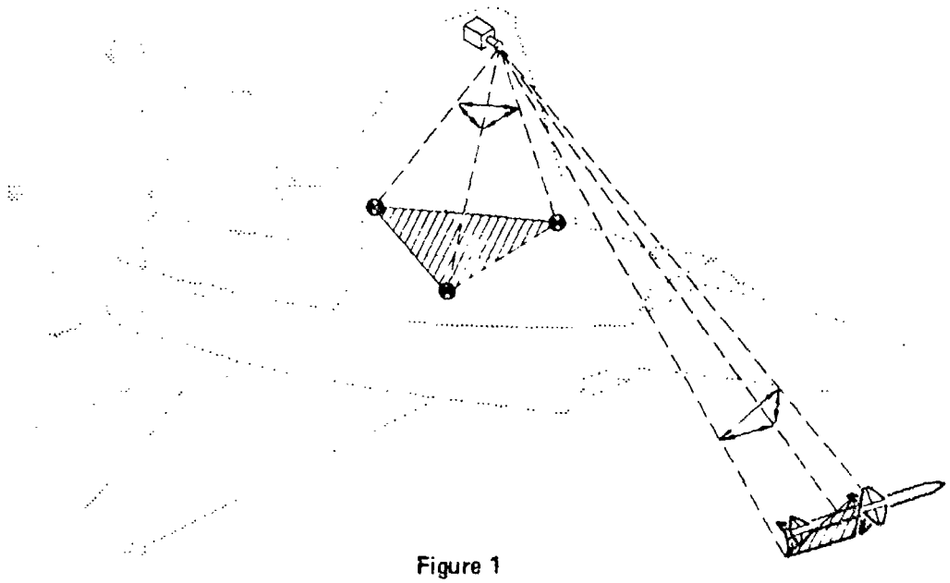


Figure 1
"CHASE CONCEPT"

The concept of CHASE is illustrated in Figure 1. The principal used is:

(1) In the field of view information of three targets on the airplane is read from the film. These three targets are referred to as Boresite Targets. Their readings are converted into included angles between the line of sights from the camera. This forms a tetrahedron, a rigid structure. The baseline dimensions of this tetrahedron are established using the aircraft stations of the boresight points. Then math that fundamentally applies an iteration of the Law-of-Cosines is used to locate the camera such that the projected radials make a best fit of the targets. When the coordinate sum of the successive radial errors is less than one inch, a solution has been established that is used to obtain the camera location. The orientation or look angle of the camera is computed using this camera location and the optical transfer functions. The camera location and orientation is computed for every frame that is processed. Each frame then is in itself a complete solution, and is not dependent upon another camera nor is it time dependent. It adjusts for the conditions that exist at that very precise moment.

(2) Using that same frame, three points are read on the store. Various features of the store having distinct outlines are used for these three points. Again the included angles to those points define another tetrahedron. Using the location of these points for the baseline of that tetrahedron, the base is shifted around in the same manner until there is a best fit for the radials. When the sum of the differences here is less than one tenth of an inch, the location of the plane (the stores coordinate system in space) is established.

(3) At this point the store is numerically reconstructed. From this numerical representation the data, as requested by the user, is precisely furnished. Discrete points on, in or outside of the store and attitudes of a preferred coordinate system are presented rather than the traditional nose, CG, tail. The analyst can now observe clearances of critical points. This is particularly beneficial for non-symmetrical stores or those having protrusions.

The rule of thumb that was developed in choosing targets to be read and which has proven faithful is very simple. You select and read three targets that give you the largest included area between those three points. It does not matter if the plane is horizontal, vertical or oblique. Boresite targets are located throughout the aircraft such that a suitable choice of targets can be found even as masking occurs. The same applies to targets on the store. Normally about a dozen targets are designated for a store to facilitate film reading. Any three targets may be read on any frame, with no limitations.

4.0 CHASE REFINEMENTS

Over a period of a year many refinements were incorporated in Single and/or CHASE. Some of these were small but yet contributed to the precision we sought. Others were benefits to its operational use.

4.1 Optical Improvements

Initially with Single we experienced some unacceptable errors. We looked for problem areas and the first and most obvious was the optics. Assessing the lens calibrations we found three major errors. The first was relatively easy to detect although it did require the preparation and use of a digital optical system simulation. The calibration geometry was handled incorrectly. The second was found after a series of lab and shop tests where we recognized that the optics were changing every time a camera was repaired. With the same lens and the same camera, the optics would change. Why? This was prevalent with the 5.9mm lens and probably was due to their telescopic structure which could flex. The older 5.7mm lens which we were also using did not have as pronounced a problem probably because they were cast and

conical in shape. We then realized that the lens holder itself was noticeably altering the distortions when its set screws were tightened. This and the third error required that we combine the camera and lens for calibration. Quite astonishingly we found that the third source was an offset between the optical and physical centers inadvertently manufactured into the cameras. The fix for these aberrations resulted in; (1) a new calibration board with a jig to precisely locate and point the cameras, (2) new computer logic, and (3) a procedure requiring that each camera and lens be calibrated together and as released for flight. Now the physical and optical centers could be separated and measured. This was not the end, there were more optical findings that are discussed later.

4.2 Information Files

One of the more beneficial gains was the minimization of the human factor. Any photoanalysis system that operates in the software domain does require a lot of information. We doubled this requirement when we went to the single camera solution. Single received these inputs manually by computer cards. CHASE was uprated so that these inputs were on recall from a computer file.

There are four different files. The first file contains all of the boresite information. In particular, it holds the aircraft stations of each boresite target assigned to the airplane. A second file is for the optical calibrations. Contents of this file are shown in Figure 4 and discussed later. A third file is the Aircraft File, and it has the instrumentation configurations for each airplane. It contains information of the cameras, their designations, and their locations if defaults are ever used. The fourth and newest file is called the "W" file or Weapon File. It is the file that numerically describes the shape and size of each of the stores. Figure 2 is an example of an AIM-7F in this file. These files are called up for processing by key words. The key words are entered into one computer card which is called the Control Card.

4.3 Camera Positioning

As mentioned, CHASE locates and points its camera. This is done each frame to maintain its independent integrity. The program does offer options and defaults if other choices are desired or required. Should a camera see fewer or no boresite targets, CHASE will default to the lesser solutions or at worst use the file information. All too frequently we experienced a reorientation of a camera due to turbulence, G loads, mislocation, etc. This corrected such a variable. Bending and/or flexing is especially prevelent under heavy load factors and when heavy store or ordinance loads are jettisoned. We have evaluated data showing that such an effect does induce a noticeable error.

CHASE PHOTOMETRICS WEAPON .STORE) DEFINITION

WEAPON DESCRIPTION:	AIRCRAFT STATIONS, INCH/DEG F.S.	B.L.	W.L.	WEAPON STATIONS, INCHES X(+AFT)	Y(+RT)	Z(+UP)
WEAPON TYPE.....AIM-7F, FIXED WINGS						
WEAPON LOCATION...MISSILE STA 3, L/H FORWARD MISSILE WELL	498.81	-58.50	84.91	0.0	0.0	0.0
WEAPON ROTATION FROM ACFT COORDINATES	0.0 RU	0.0 RR	0.0 CM			
WEAPON PRESENTATION DESCRIPTION:						
POINT 1 (O).....NOSE	415.2	-58.5	84.9	-83.64	0.0	0.0
POINT 2 (▷).....UPPER WING TIP (AFT)	494.9	-58.5	105.0	-4.02	0.0	20.10
POINT 3 (+).....TAIL	559.1	-58.5	84.9	60.36	0.0	0.0
WEAPON PROCESSING DESCRIPTION:						
WEAPON ORGIN.....WEAPON SPEC CENTROID				0.	0.	0.
POINT A.....NOSE POINT				-83.64	0.0	0.0
POINT B.....TAIL CENTER				60.36	0.0	0.0
POINT C.....UPPER WING TIP (AFT)				-4.02	0.0	20.10
POINT D.....RT WING TIP (AFT)				-4.02	20.10	0.0
POINT E.....BOTTOM WING TIP (AFT)				-4.02	0.0	-20.10
POINT F.....LT WING TIP (AFT)				-4.02	-20.10	0.0
POINT G.....UPPER FIN TIP				60.60	0.0	15.63
POINT H.....RT FIN TIP				60.60	15.63	0.0
POINT I.....BOTTOM FIN TIP				60.60	0.0	-15.63
POINT J.....LT FIN TIP				60.60	-15.63	0.0
POINT K.....						
POINT L.....						
POINT M.....						
POINT N.....						
POINT R.....						
POINT T.....						
POINT U.....						
POINT X.....						
POINT Y.....						
POINT Z.....						

Figure 2
"WEAPON FILE LISTING"

4.4 Optical Finesse

After a series of refinements, we found ourselves investigating the optics again. A ground simulation that is discussed later indicated a need to further search this area. The accuracy of the transfer function was still relatively poor and contributed much too large an error to the system. Putting much more effort and depth into the study this time we really made some breakthroughs. To eliminate any optical influence of the calibration, a three-dimensional (3D) grid matrix was fabricated. Our prototype grid board is shown in Figure 3. The first finding and a rather startling one was that the optical center was not related to the physical center of the aperature (which we had expected), nor was it related to the images center, or to the aimed center of the lenses. It was random and varied as much as 10% from these references.

Figure 4 illustrates this offset, the magnitude, and pattern of its variation. Shown is the exactness of the transfer function as a function of selected optical centers. It appears insignificant. But, the use of this center has improved the calibration accuracies by a factor of 2 to 3. The table shows the random nature of this offset as represented by the Y and Z Biases. This gain has penetrated accuracies where we are now able to see and evaluate

subtle effects in an optical system. We found that the mere removal and replacement of a lens on a camera (same lens, same camera) changes its characteristics. Recently we exhibited where closing of the "f" stop (increasing the setting) improved the calibration accuracy by better than 50%. This exemplified the fact that the more area of the lens that is used, the more distortion one can experience. The replacement of safety wires, the tightening of lens holders, the mere tampering with the installation noticeably affect the calibration. Each affects the photogrammetric results under the proper conditions. We now expect one sigma accuracies of +0.05° where before accuracies of +0.2° were considered good.

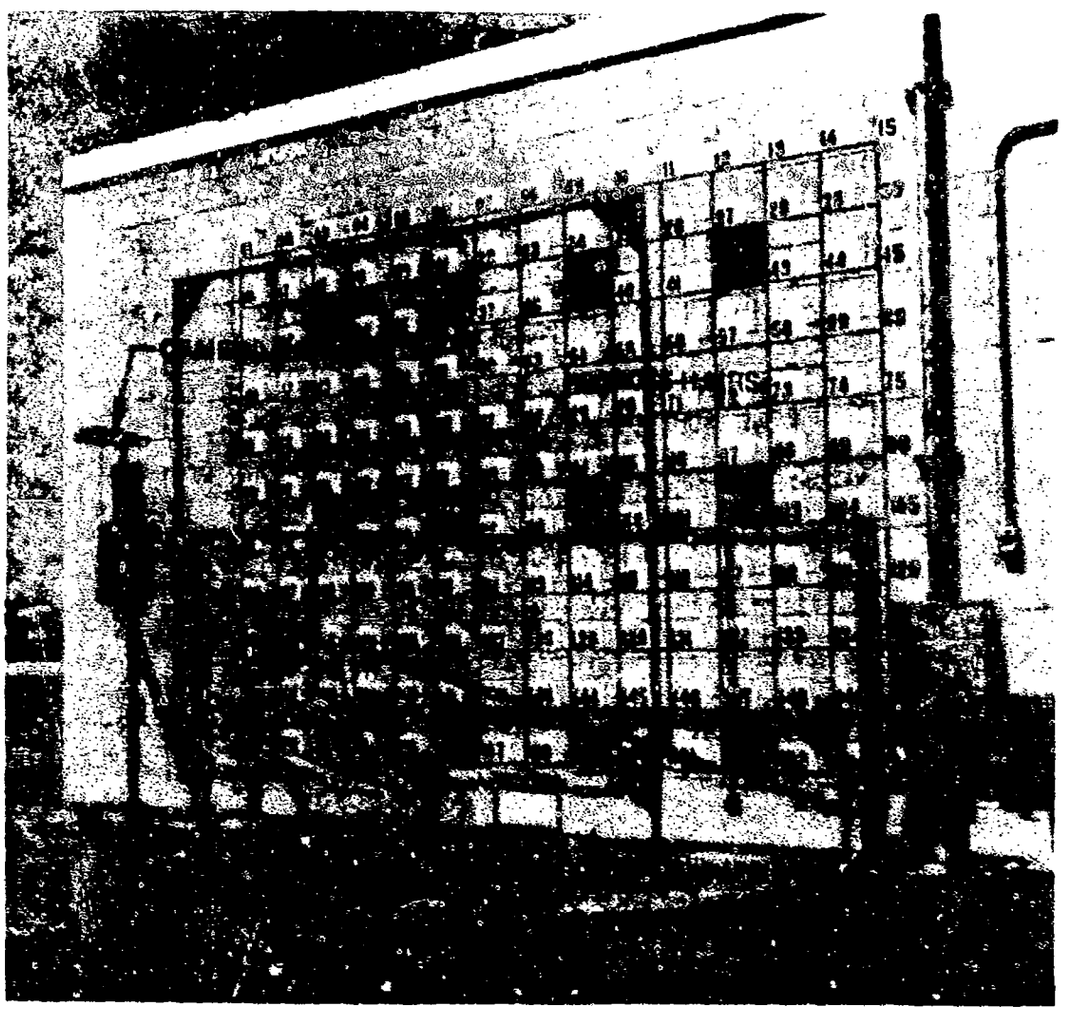
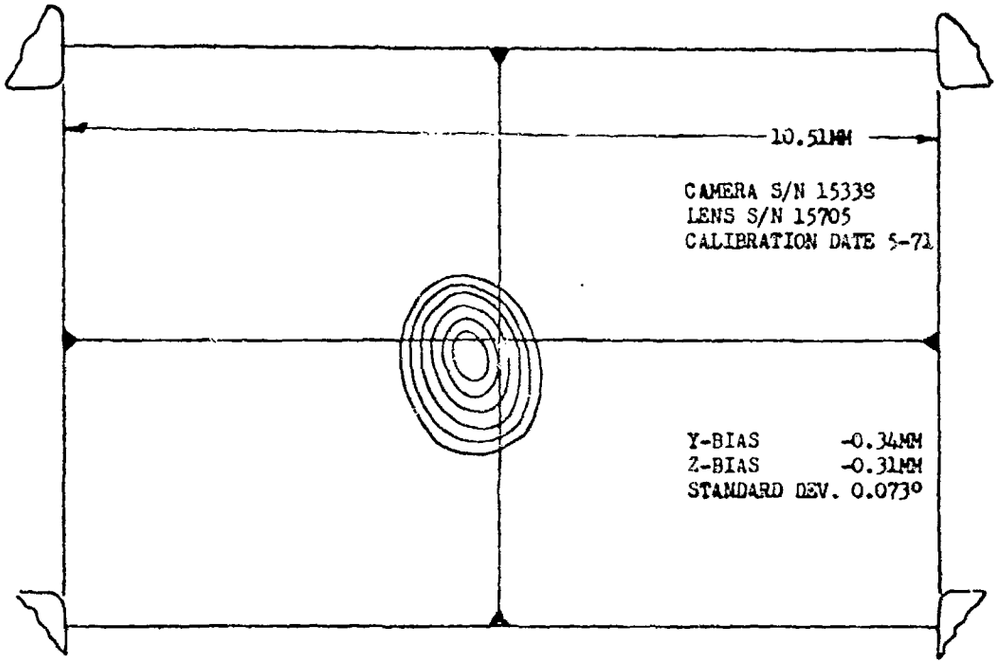


Figure 3
"3D CALIBRATION BOARD"



CROSS PHOTOGRAPHIC REFERENCE FILE "L"
[illegible] CALIBRATIONS

DATE 04/29/71

CAMERA SERIAL NUMBER	LENS SERIAL NUMBER	LENS CHP TO NODAL POINT DIST. (INCHES)	LENS (C1) FOCAL LENGTH COEFFICIENT-MM	LENS (C2) DISTORTION COEFFICIENT	LENS OFFSET Y-BIAS (MM)	LENS OFFSET Z-BIAS (MM)	CARD YEAR DAY NO
15330	15721	0.0	6.4[illegible]	0.001[illegible]	0.35	0.0	5- 57
15329	15701	0.0	6.4003	0.00[illegible]01	0.21	+0.12	5- 54
15330	15734	0.0	6.3[illegible]74	0.00[illegible]36	0.31	0.06	5- 57
15331	15705	0.0	6.4375	0.002204	0.16	0.02	5- 52
15334	15723	0.0	6.4[illegible]46	0.00[illegible]58	0.35	+0.16	5- 51
15336	15727	0.0	6.3952	0.00[illegible]02	0.09	+0.02	5- 71
15337	15[illegible]16	0.0	6.4164	0.00[illegible]03	0.19	+0.31	5-[illegible]28
15338	15[illegible]02	0.0	6.4[illegible]21	0.00[illegible]03	0.34	0.31	5- 71
15339	15[illegible]13	0.0	6.4[illegible]5	0.00[illegible]03	0.11	0.25	5- 71
15340	15[illegible]19	0.0	6.4279	0.00[illegible]89	0.35	0.03	5- 71
15349	15703	0.0	6.4563	0.00[illegible]04	0.30	0.26	5- 52
15342	15732	0.0	6.3922	0.00[illegible]5	0.03	+0.16	5- 54
15343	15[illegible]36	0.0	6.4[illegible]82	0.00[illegible]03	-0.04	+0.12	5- 54
[illegible]	15[illegible]32	0.0	6.3829	0.00[illegible]93	0.07	+0.31	5- 55
15345	15[illegible]28	0.0	6.3948	0.00[illegible]05	-0.01	0.21	5- 45
15346	15[illegible]19	0.0	6.3979	0.00[illegible]07	-0.03	0.15	5- 52
15347	15[illegible]40	0.0	6.3910	0.00[illegible]95	0.00	+0.42	5- 45
15348	15[illegible]43	0.0	6.4183	0.00[illegible]68	0.15	+0.09	5- 52
15349	15[illegible]41	0.0	6.4167	0.00[illegible]83	-0.05	0.24	5- 52
15350	15[illegible]42	0.0	6.4410	0.00[illegible]32	0.14	0.24	5- 51
15351	15[illegible]47	0.0	6.4444	0.00[illegible]98	0.28	+0.31	5- 55
15352	15[illegible]44	0.0	6.4552	0.00[illegible]89	+0.33	0.12	5- 57
15353	15[illegible]47	0.0	6.3933	0.00[illegible]01	0.01	+0.42	5- 43
15354	15[illegible]45	0.0	6.3973	0.00[illegible]38	0.24	+0.32	5- 38
15355	15[illegible]46	0.0	6.3[illegible]59	0.00[illegible]26	+0.03	+0.33	5- 1
15356	15[illegible]48	0.0	6.3[illegible]28	0.00[illegible]35	+0.03	0.33	5- 16
15357	15[illegible]46	0.0	6.3[illegible]50	0.00[illegible]30	0.31	+0.33	5- 29
15358	15[illegible]46	0.0	6.3[illegible]56	0.00[illegible]34	0.28	+0.35	5- 28
15359	15[illegible]46	0.0	6.3[illegible]58	0.00[illegible]34	0.30	+0.26	5- 43
15360	15[illegible]46	0.0	6.4010	0.00[illegible]26	0.31	+0.33	5- 52
15361	15[illegible]47	0.0	6.4[illegible]72	0.00[illegible]34	0.39	+0.37	5- 52
15362	15[illegible]48	0.0	6.3[illegible]54	0.00[illegible]32	0.4	+0.12	5- 52
15363	15[illegible]49	0.0	6.4[illegible]58	0.00[illegible]41	0.31	+0.37	5- 54
15364	15[illegible]28	0.0	6.5117	0.00[illegible]28	0.04	+0.48	5- 55
15365	15[illegible]31	0.0	6.4[illegible]26	0.00[illegible]67	0.0	+0.21	5- 52
15366	15[illegible]32	0.0	6.3[illegible]63	0.00[illegible]36	0.17	+0.21	5- 54
15367	15[illegible]43	0.0	6.4332	0.00[illegible]24	0.00	+0.49	5- 57
15368	15731	0.0	6.3[illegible]74	0.00[illegible]93	0.13	+0.31	5- 54
15369	15761	0.0	6.4001	0.00[illegible]87	0.27	+0.02	5- 55
15367	15716	0.0	6.3[illegible]76	0.00[illegible]68	0.42	+0.19	5- 52

Figure 4
"OPTICAL DECENTRALIZATION" OF A 5.9MM LENS,
16MM CAMERA

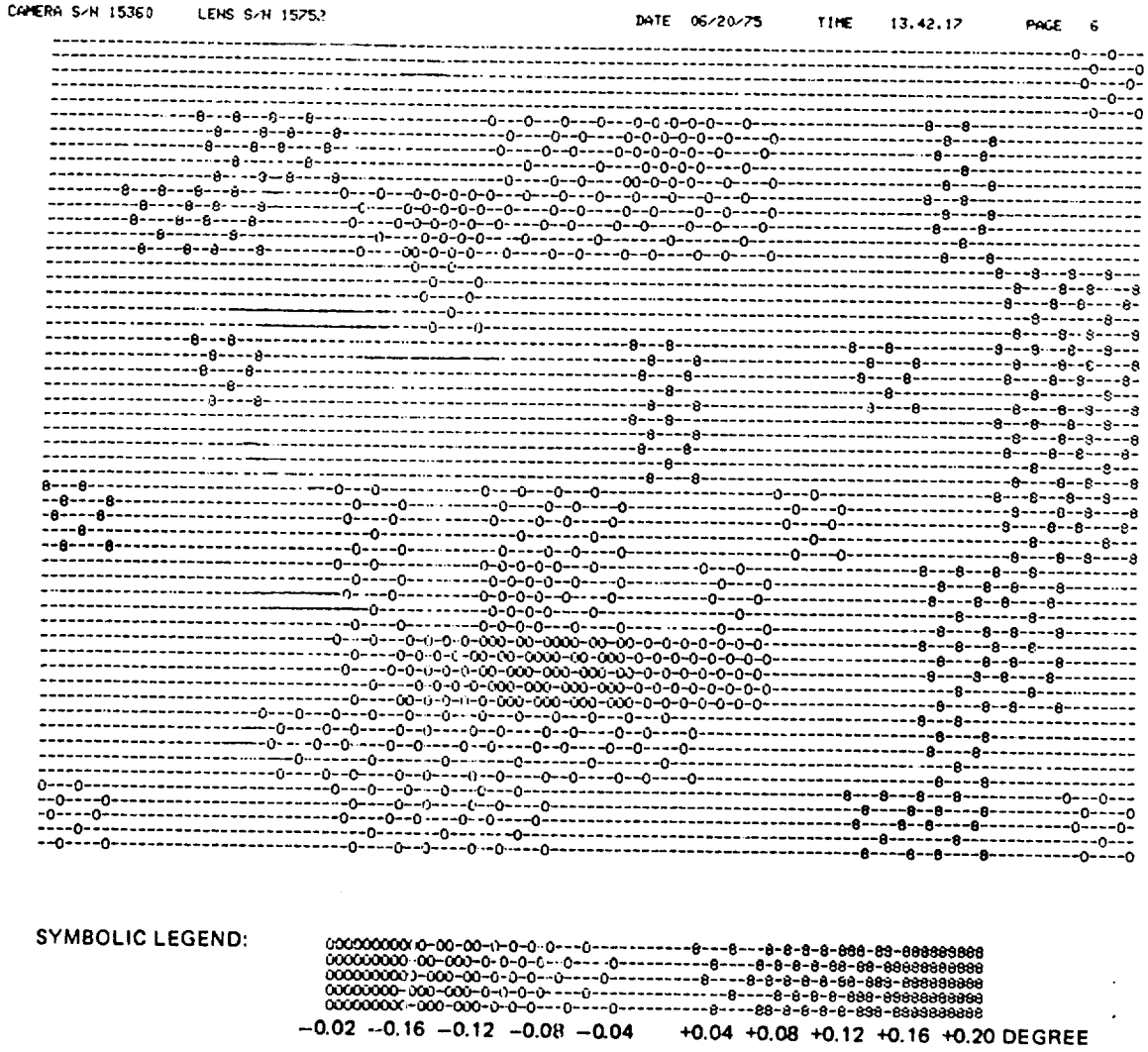


Figure 5
"CALIBRATION CURVE FIT ERRORS"

A second order curve is used to represent the transfer of the film dimensions to their angular representation. Presently the achieved accuracies are compatible and acceptable for CHASE. Figure 5 shows a typical pattern of the curve fit errors. The greater the density, the larger the error with polarities symbolically indicated. Some of these patterns are systematic and if future gains are needed the errors can be reduced. As time permits, the effects of the thermal, inertial and aerodynamic loads will be investigated. Also the precision and thus the preferred choice of image coordinate references, the repeatability of the film advance, and the film types will be looked at. By tradition and for economy, MCAIR has used the perforations (sprocket holes) for the coordinate reference. This may be changed.

The optical revelations have netted real gains and have opened new fields for photoanalysis. With the "3D Calibration Board" the camera/lens calibration process is an ultra simple one. On an average, a minute on a computer and 10 total minutes of the lab tech, analyst, and operator are needed. This is swift, cheap, and should never influence a decision not to calibrate. It yields much for so little.

The production calibration board is small, rugged, and easily portable. This makes the technique highly desirable for field operation. As far as is known it is the only such application with its degree of accuracy. With it one inherently calibrates an optical system "as is", as a whole which few systems can do. The cameras do not have to be brought to the lab, the board can be taken to the cameras.

5.0 BORESITING

Recently our boresite practices were investigated. Our ground simulation indicated improvements were needed here. However, it has been long recognized that better accuracies were needed from the boresites. No successor could be conceived. Now the excellent accuracies in our conversion of camera data opened new possibilities for a better method.

Boresiting originally was the pointing and measuring of the cameras' look angles and their locations. This same term has been retained but the scope hardly remains the same or appropriate. With CHASE where this data need not be known, boresiting is the practice of precisely locating the targets on the aircraft. Even methods to do just this have changed considerably over the years. Originally a grid system under the aircraft was laid out and measurements were made within it. Then to lessen the layup these measurements were made from known aircraft points and some temporary points on the ground. Instead of the rectalinear measurements, slant measurements were used in a computer routine. Even with this update, "boresiting" has been an extremely tedious job. Loft line information is gathered of identifiable locations on the airplane. Then measurements are made between these and other targets so that new target coordinates could be established and computed. Finally a set of numbers are compiled which are considered acceptable, at least representative of the points.

These aren't accurate points. Absolute accuracies of $\pm 0.5^{\circ}$ are the goal of the new technique, 3 to 4 times better than the current method. In a normal operation there is not the convenient layup nor sufficient time and facilities for good results. Good plans can be made, but they never materialize. Every airplane seems to have different dimensions for common points and even repeat measurements differ. We have also found that the camera location calculations yield considerable

variation in their results. This is quite natural because of the poor boresite accuracies. Quite possibly the cameras see an apparent motion from airloads etc. Regardless it is not detrimental for weapons testing as validity tests under all conditions have shown that the magnitude of variation does not aggravate the results. We, of course, plan to improve this.

A radical approach for "boresiting" is now planned and in development. This is expected to be rapid, precise, and will uniquely establish the boresite target coordinates for each separate aircraft. Representative tests have shown that it is feasible and should yield acceptable accuracies. The concept is depicted, in Figure 6. After cameras have been pointed, boresite targets are placed on the aircraft for each camera where they will give the best visibility and math geometry. These locations will no longer have to be a compromise. With loft data we use physical features such as rivets, corners, etc. which permit locating the points. Next a series of still photographs will be taken in which a group of the targets (not necessarily all) and three Coordinate Reference Points are included in the views. These Coordinate Reference Points are three distinct points of the airplane that are visible from all quadrants, and for which their static locations are accurately known. For some views, one or two substitute points may be required.

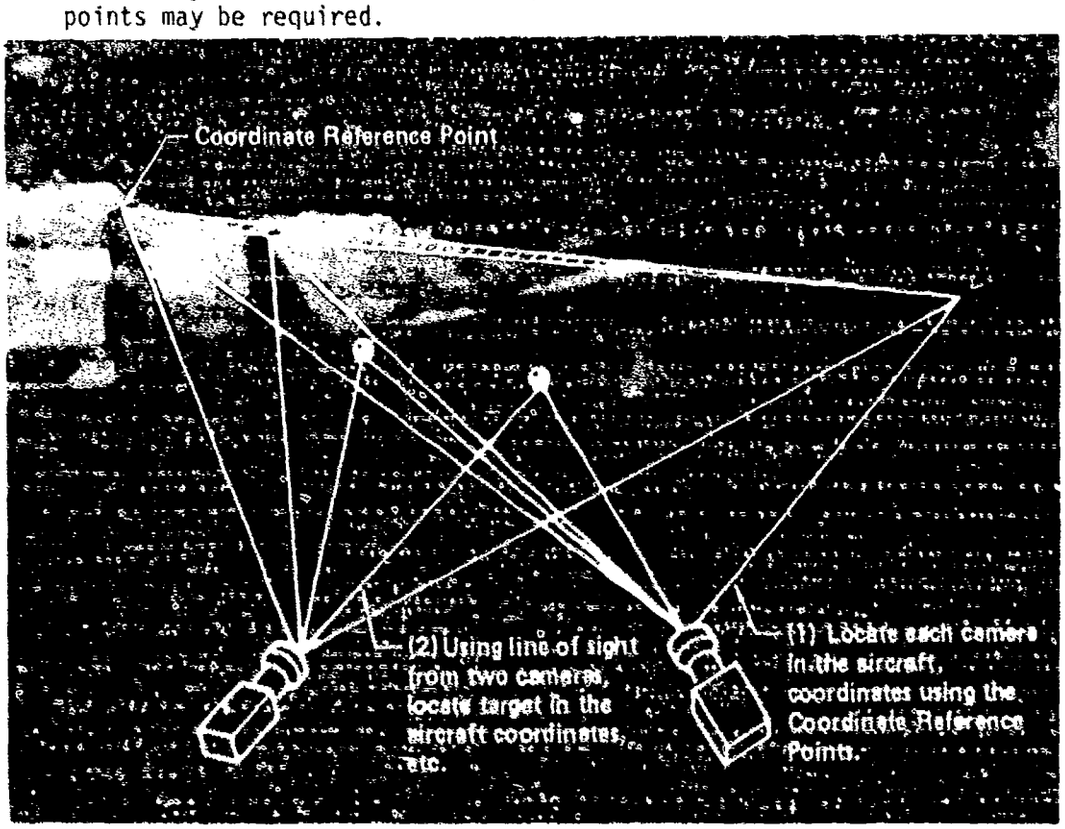


Figure 6
"OPTICAL BORESITE TECHNIQUE"

Applying portions of the Multi and CHASE analyses to these photographs, each camera is located and in turn the targets are located. Since many calculations for each target are obtained from the pairing of photographs, a statistical selection is made of each location further improving accuracies. If far greater precision is required, the substitution of transit measurements for the camera data may be made.

In addition to having strategic target locations and improved accuracies, this approach:

(a) Does not require that the aircraft be in layup. Photographs can be taken individually and at any time, wherever, and in any configuration; even with people working on the aircraft.

(b) Is cheap. The analysis is done by the computer and all other tasks are token.

(c) Is quick. If need be it can be accomplished in a day. Any new airplane whatever the type can be readied for flight with very little lead time.

(d) Any errors in the Coordinate Reference Points are normalized. All "jig" and "config" variations from aircraft to aircraft are routinely accepted. It is surprising how much one airplane varies from another when tight accuracies are sought.

6.0 OPERATIONAL HANDLING

Aside from the technical enrichments CHASE was also experiencing general cleanup, efficiency and novelty mods, standardization, etc. With most of these incorporated, CHASE has proven to be functionally an excellent and easy system to use. Having used all of the MCAIR photometric systems, and having appraised some used by others, we report that CHASE is a "real charm" to use. Its ease has been facilitated in the operational design considerations. There is no engineering judgement or participation required in the set-up, the film reading, or the verification of the data. The rules are few, simple, and straightforward.

The operator reads only those frames that capture the dynamics. He chooses the targets that need to be read. He picks three store targets and three or fewer boresite targets, applies the rule to get the largest area, and proceeds to read the film. The X and Y cartesian coordinates are read from the image coordinate reference to each of the six points. These, the frame number, and an ID are entered into a card and used for processing. The system is designed so that he can switch targets at random, both the store and the boresite targets. When he makes these switches he records them on a coding sheet. This coding sheet is punched and that card is added to the data deck. We require that he make both boresite and store

target switches on a drop whether they are needed or not. This is for data verification purposes which is explained later.

The control card having the Data File key words is added to the film deck and if desired, cards containing the launch conditions are added. The job is then submitted to the computer for processing. It is a "one shot" process. The output is formal, final data. The functions and formats of this data are shown later. The final data also includes cover sheets, one which is similar to Figure 2 that describes the store that was processed and the references used to present the data. Also included are diagnostic data for the job. If there is a problem often it can be detected by referral to the diagnostics. One does not have to refer back to raw data.

CHASE is a very efficient system. One drop takes maybe two minutes on an average size computer. It takes on an average of only four to six hours of labor to handle a drop. For those who have not worked separation data, a good portion of that labor is spent editing, titling it, and splicing the coverage together.

7.0 VALIDATION

CHASE results have been verified in a number of ways. One means being used to obtain a quantitative measure of its accuracy is the ground simulation mentioned earlier. This test, aside from the flight loads, realistically represents an actual flight. The simulation examined all aspects of flight data plus extreme attitudes, multiple store and boresite combinations, and obstructed or degraded coverage. But we could not simulate the normal to extreme vertical displacements. An AIM-7F launch and jettison were simulated from an F-15 chocked on the ramp. Each simulated location was measured and translated into the aircraft coordinate system for comparison with results from each camera normally carried. The processing also was operationally the same as that of flight coverage. Results of this test are being compiled the same as that of flight coverage. Results of this test are being compiled and will be reported. As a preliminary observation the accuracies appear to be well within the expected ±2" and ±2° (5° for roll angle). With special editing and care these accuracies could be several orders better.

Inherently and intentionally CHASE results each time are explicitly verified. This is the most distinguished yet salient feature of the CHASE system. Unlike any other known technique, a subjective test is made and if errors exist, they are visibly and prominently shown in the formal data. A quick look at the results reveals the integrity. For acceptable data one observation is to insure that the stowed results are at zero or their appropriate location. The other and most reliable test is the insurance that there are no transients in the results as target switches are made. The basis for this test is simply

that each frame and each target combination is, and again we repeat, an autonomus solution which is geometrically different. This is why the switching of targets is a mandatory procedure. Obvious errors produce scatter accentuated by the line fairings while subtle errors induce biases. Figure 7 shows both of these errors.

In this presentation the format and functions are now seen. Figure 8 of the same test shows the attitude data. The line fairing associated with each function is included to (1) show what a bias to a stowed position represents if offset is experienced, but primarily (2) to accentuate the transients. An option eliminates the bias. Generally the attitudes are insensitive to judgement or system errors which lends credence to those functions when they are used as critical or key parameters in the evaluations. Worthy of comment are the electrostatic printer/plotters we've used with the computer system. In over three years of use we've found them to be extremely efficient, reliable, flexible, accurate, functional, and legible. They have been ideal for the variety of CHASE formats.

Another very hardy test but one requiring extra effort is the comparison of results from cameras having different vantage points. Again, each of these is an independent solution of its own. Shown in Figure 9 are views of an AIM-7F Missile as seen from seven different cameras. The coverage from each camera was read in its entirety. The photo quality is good to poor and representative of that used. Figures 10 through 16 show their photoanalysis displacement results. An extrodinarily large number of target switching was used in reading this data to exhibit the effectiveness of CHASE in achieving continuity of the data. The AIM-7F targets used in reading this data are noted on the presentation and are as identified back in Figure 2. Figure 17 shows the fine comparison of these data. Note (1) that this data was processed for a severe, 5 G load factor and with the AIM-7F as much as 80 ft. from the camera, (2) that the errors of Figure 7 have been removed and (3) the degree of accuracy in which nose data is extrapolated from the fins in Figure 15. Only the fin tips were used in reading the images. This was done intentionally to demonstrate the extrapolation abilities of CHASE. An error amplification of around five exists in this case. Extrapolations of this type are a common practice as stores exit the bottom or edge of a frame or when the entire store is not captured as was the case for camera stations 10 and 12 (see Figure 9).

Several comparisons have been made with data from other systems, particularly the NCAIR Multi solution. Each comparison showed good agreement except where results were discrepent or suspect.

With the above cursory knowledge the analyst can now, himself, easily sense the quality. We had such confidence in the answers that we programmed the raw results into the presentations. He gets what we sees!

8.0 RESPONSIVENESS

CHASE gives the ultimate response for an emulsion imaging system. Black and white coverage is preferred for film reading and of course it can be developed on site, immediately. Separation data has been processed with presentations at both St. Louis and Edwards AFB within 8 hours after the landing. On one occasion the data from four bombs were presented in 12 hours after landing. As an even greater credit to CHASE these accomplishments were made by personnel who at the time were novices to the system which in itself was still a research tool. These were just two of a series of separations made from F-15 No. 5 during the concluding weeks of the "Essentially Complete" Milestone when results were required for continuing tests. In any case, CHASE routinely will provide 24 hour data. Exemplary of CHASE's speed, rejection of an automatic, image matching, film reader is in order because, among other reasons, it simply would delay the processing.

Now <u>any</u> aircraft with <u>any</u> store can be readied for testing in hours rather than weeks or months. In fact, they can be readied in minutes with most of the preliminaries being handled on post-flight. Stores do not have to be marked. Roughly 80% of the stores inventory have sufficient distinct features for processing. For the remaining 20%, pressure sensitive, quadrature targets are quickly and easily positioned with the store in place. Occasionally a splotch of paint from an aerosol can adds contrast to weak features. Views in shaded areas or of similar colors need some help. Again this is done with the store installed so that only the problem stores and/or areas are enhanced. No joke, Figure 16 represents a situation on a turn-around when the data pre-flight was sacrificed.

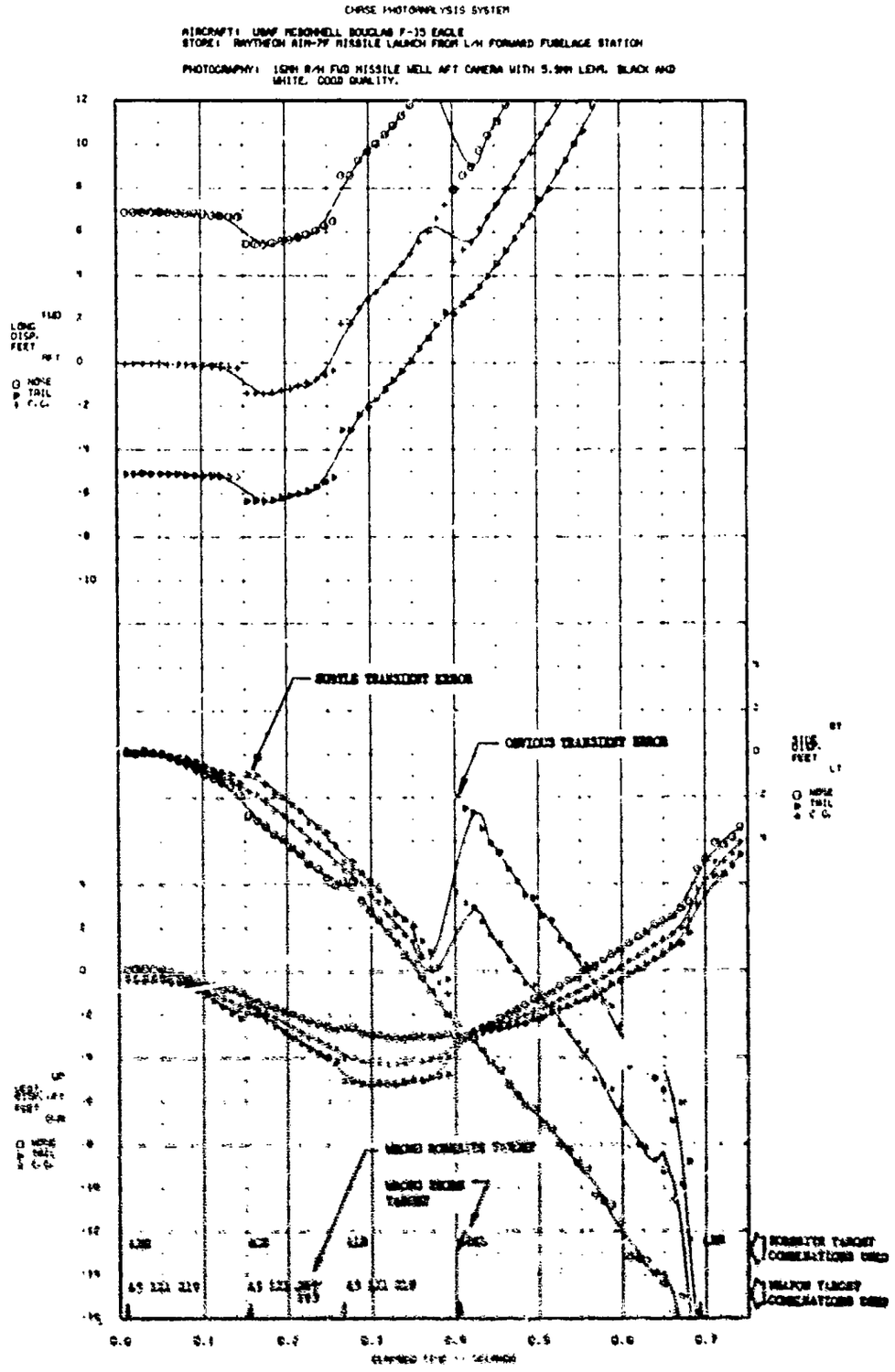


Figure 7
"VERIFICATION WITH TRANSITION ERRORS"
Position Data

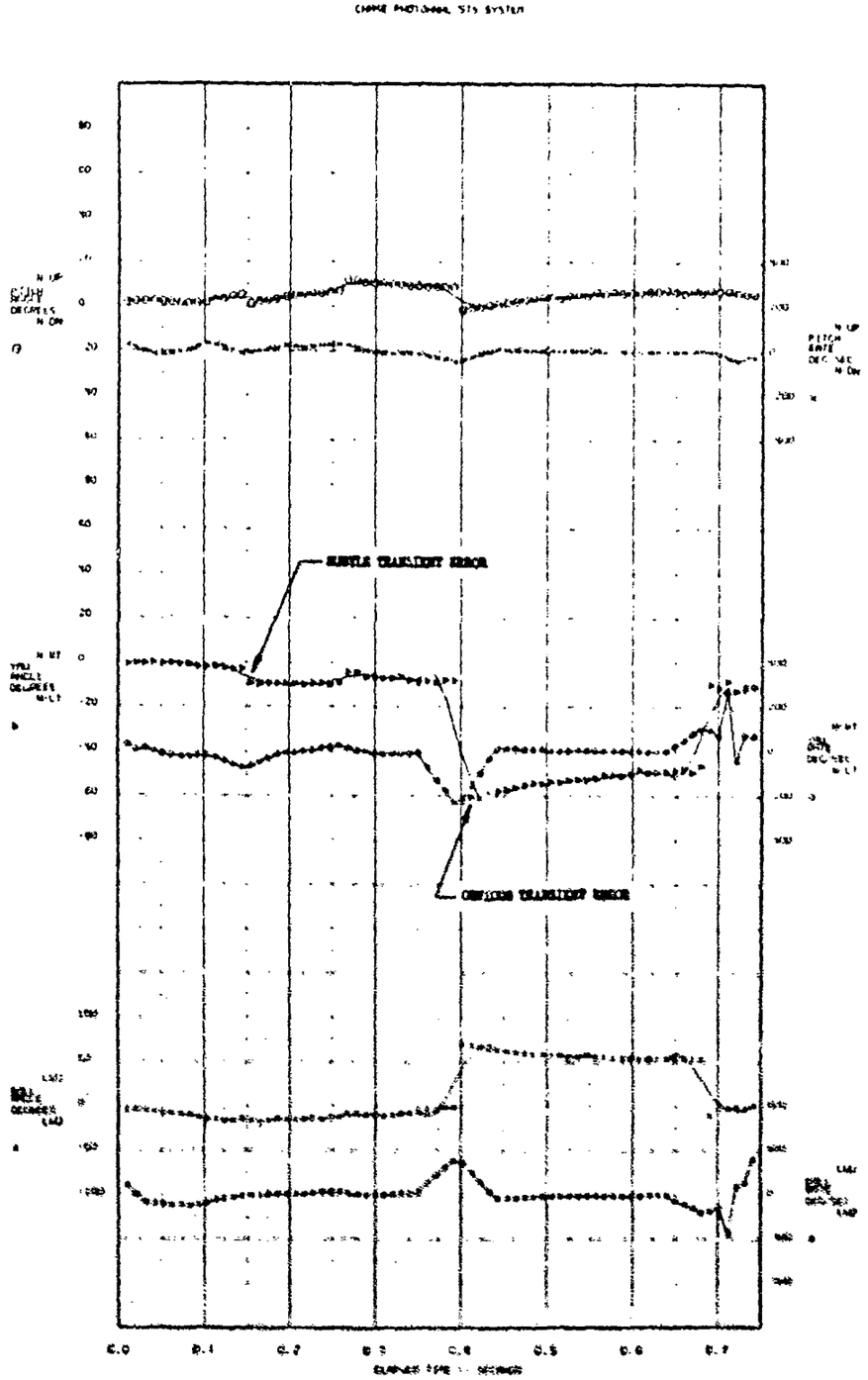
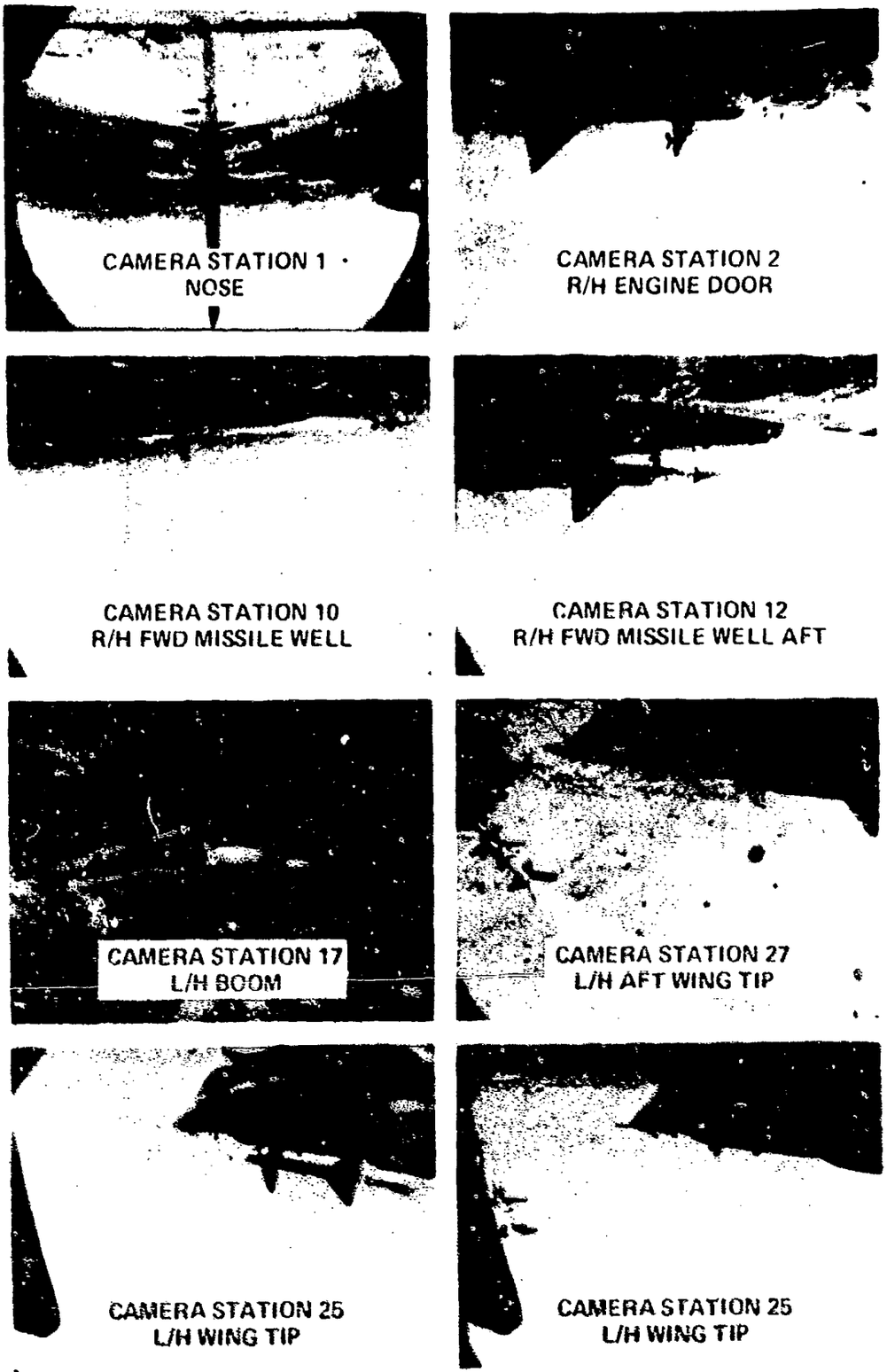


Figure 8
"VERIFICATION WITH TRANSITION ERRORS"
Attitude Data



Note: Each camera was fixed until last three AIM 7F targets left field of view

Figure 9
PHOTOGRAPHY ASPECTS OF AIM-7F LAUNCH

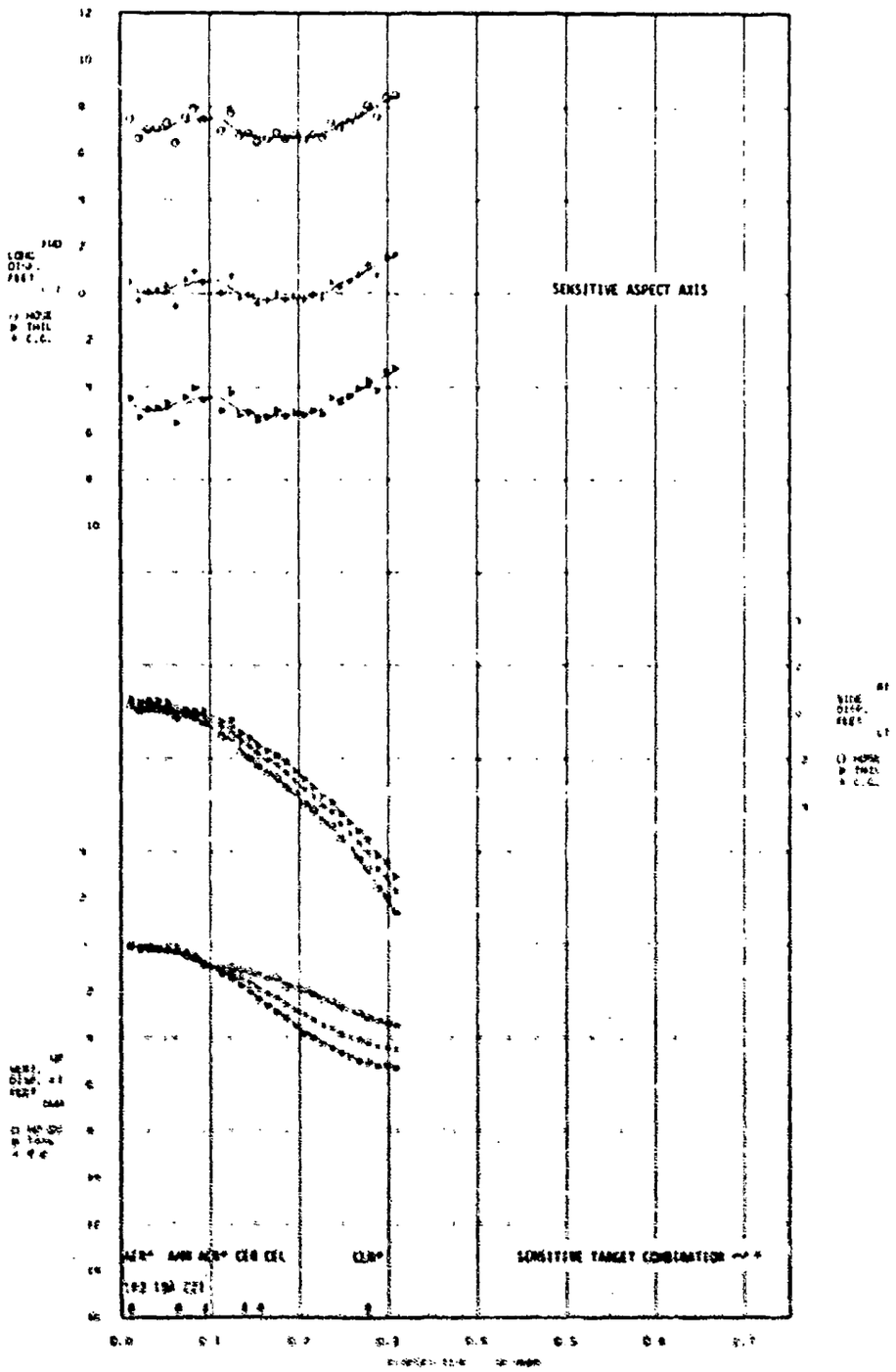


Figure 10
"CHASE RESULTS OF AIM-7F LAUNCH"
Camera Station 1

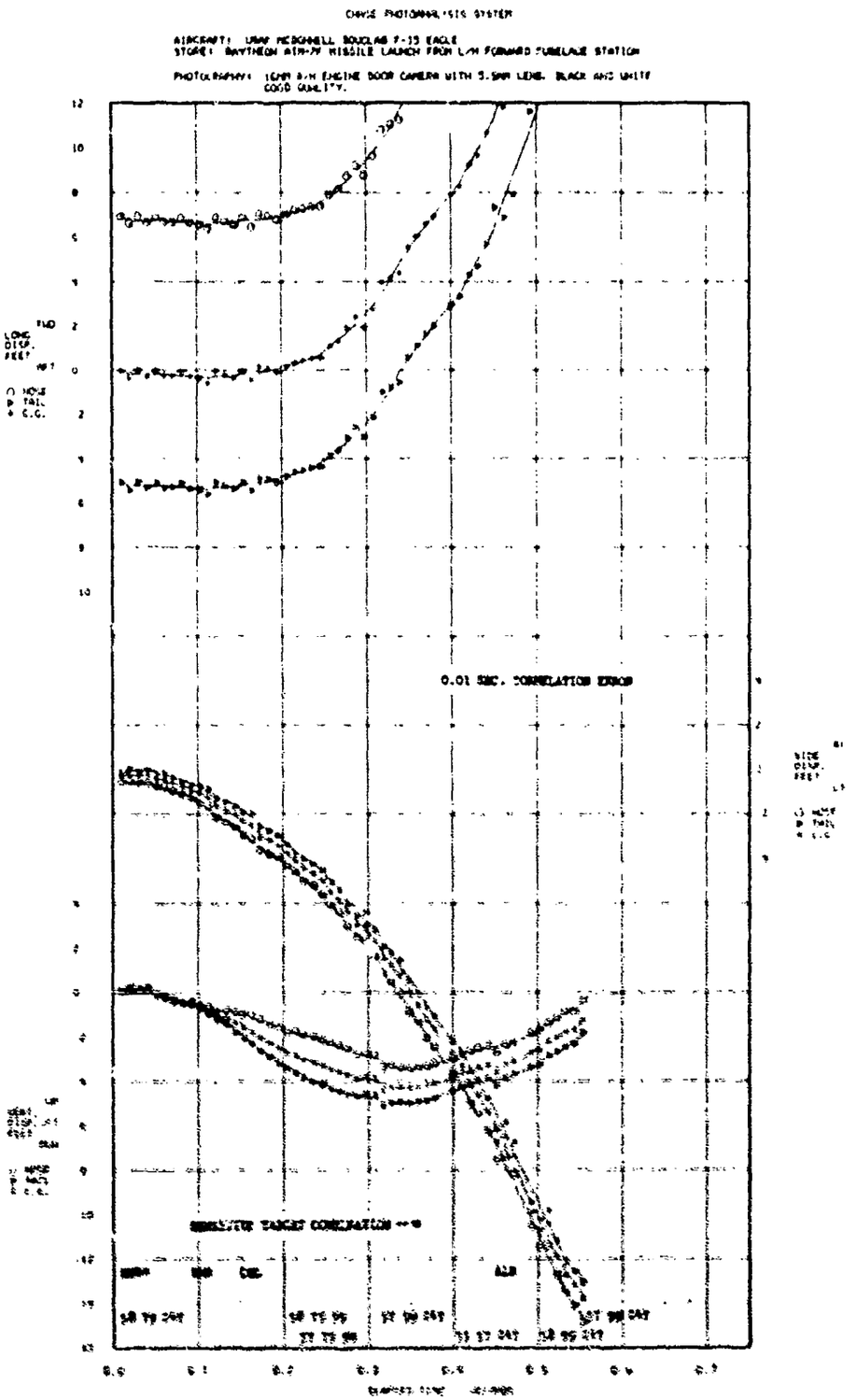


Figure 11
"CHASE RESULTS OF AIM-7F LAUNCH"
Camera Station 8

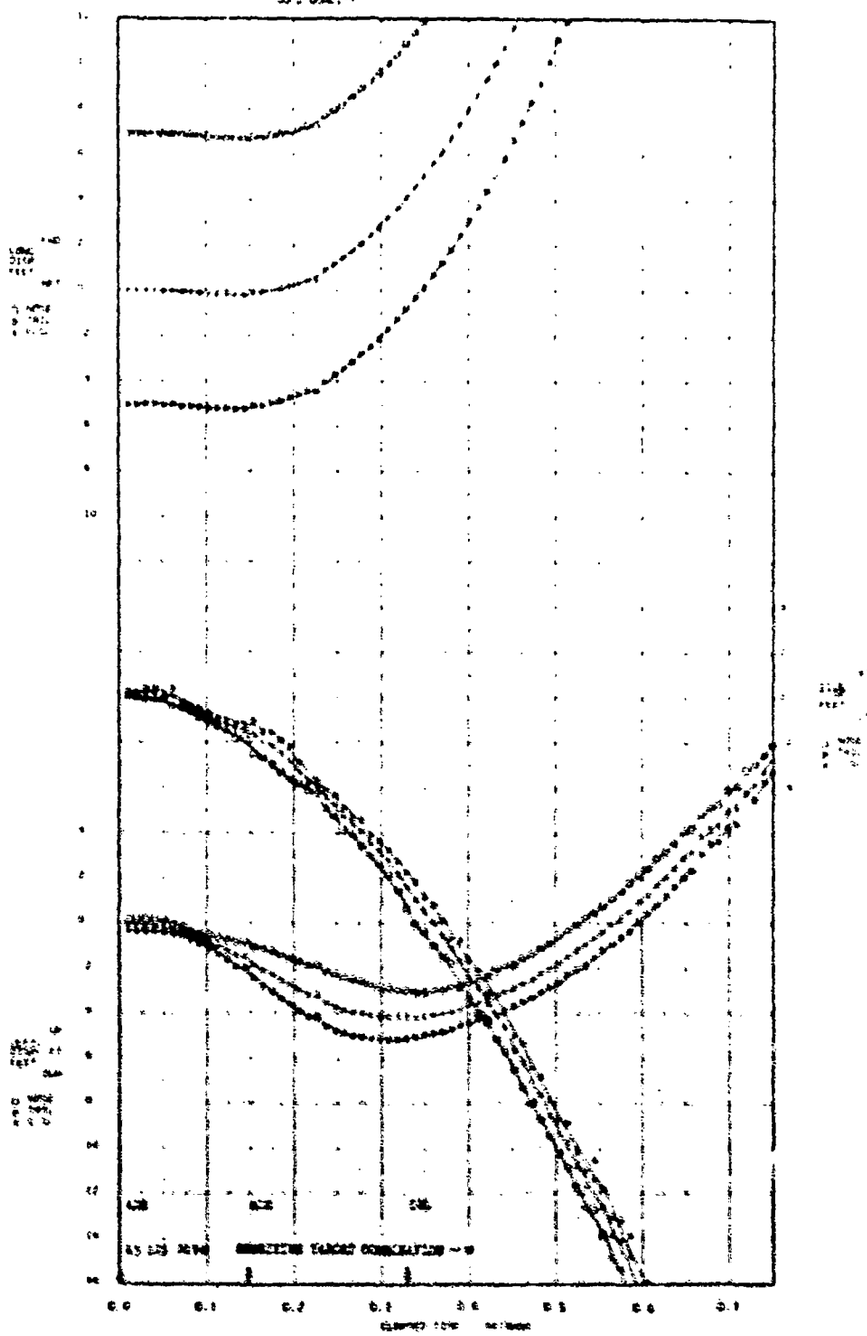


Figure 12
"CHASE RESULTS OF AIM-7F LAUNCH"
Camera Station 10

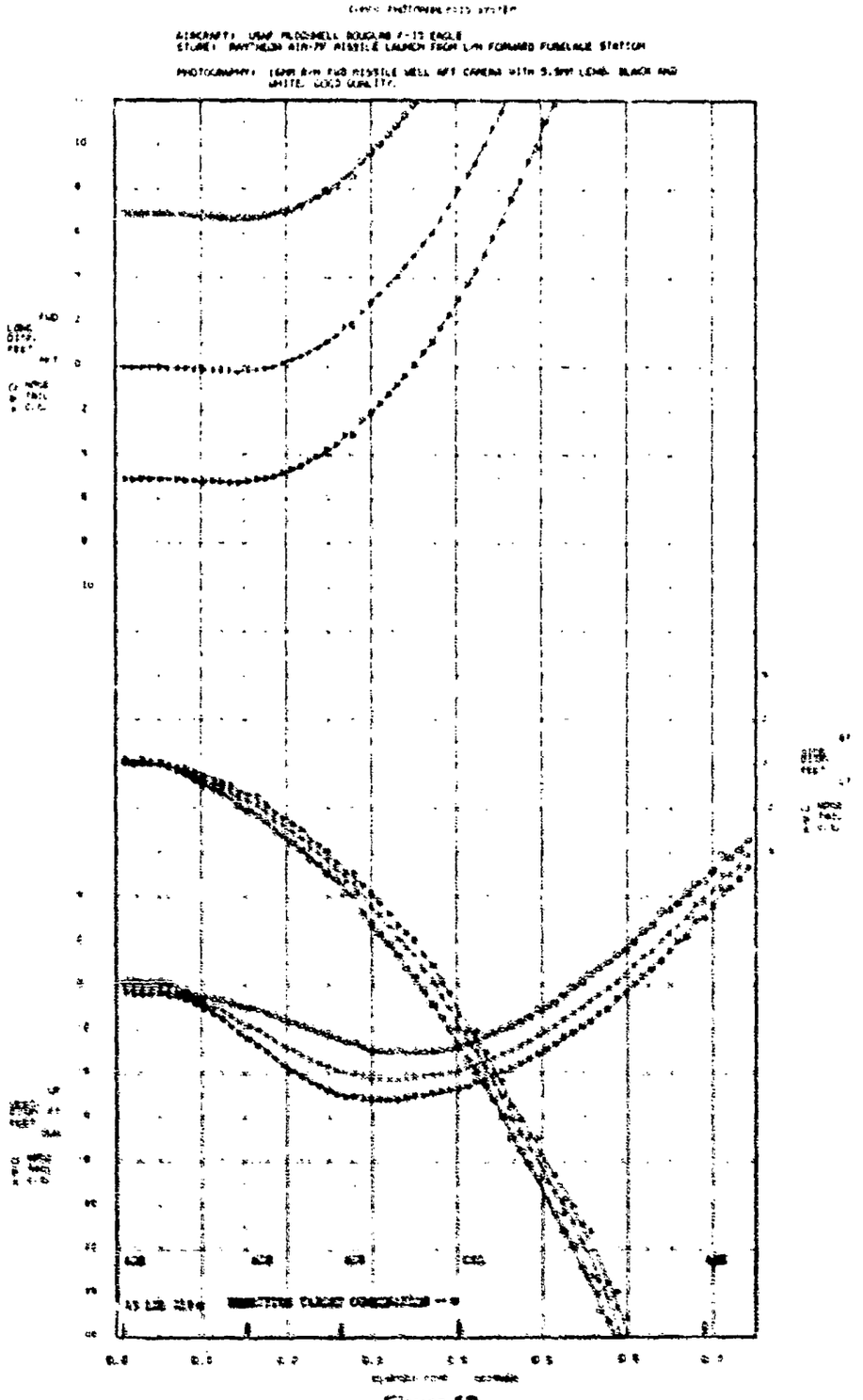


Figure 13
"CHASE RESULTS OF AIM-7F LAUNCH"
Camera Station 12

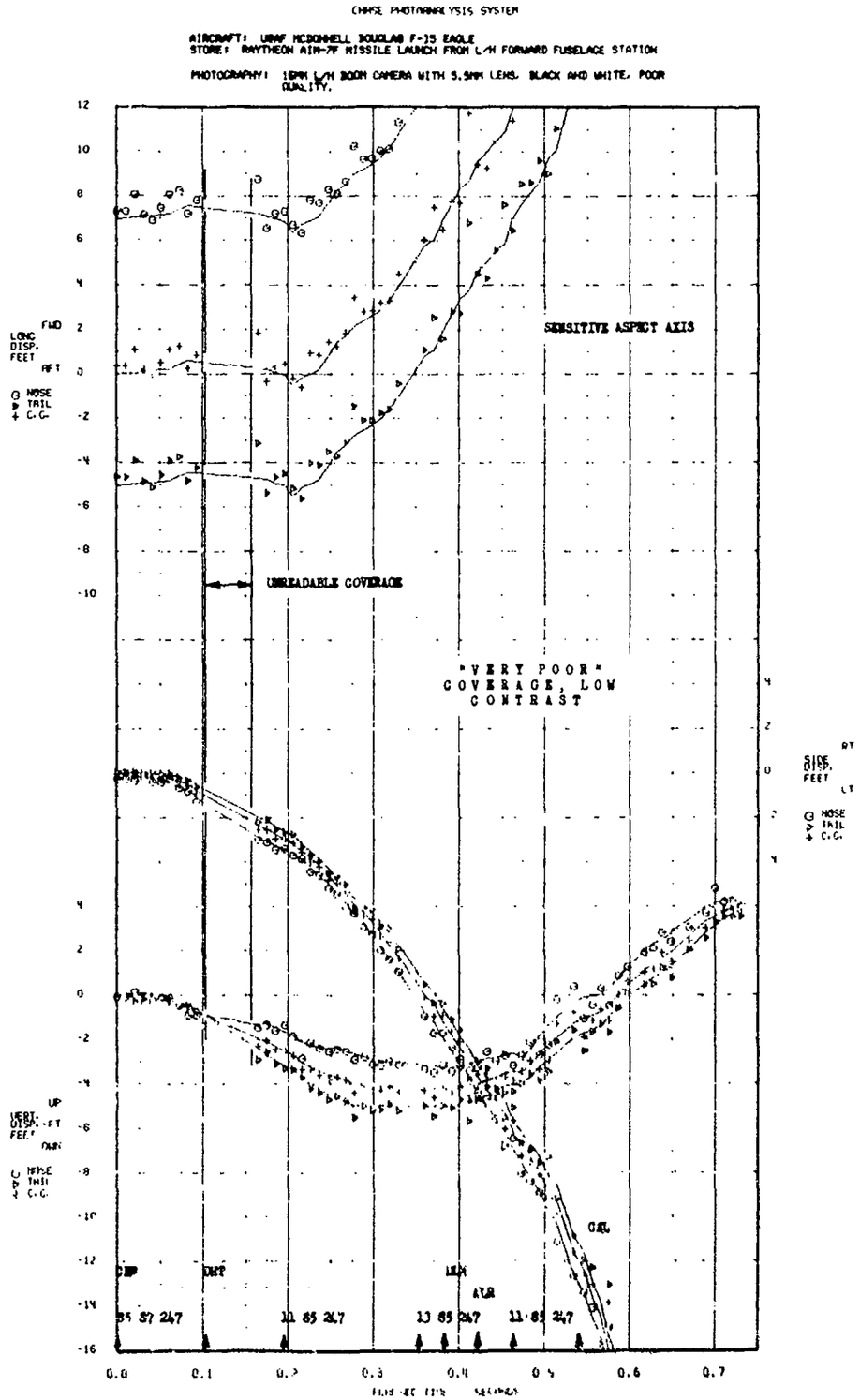


Figure 14
"CHASE RESULTS OF AIM-7F LAUNCH"
Camera Station 17

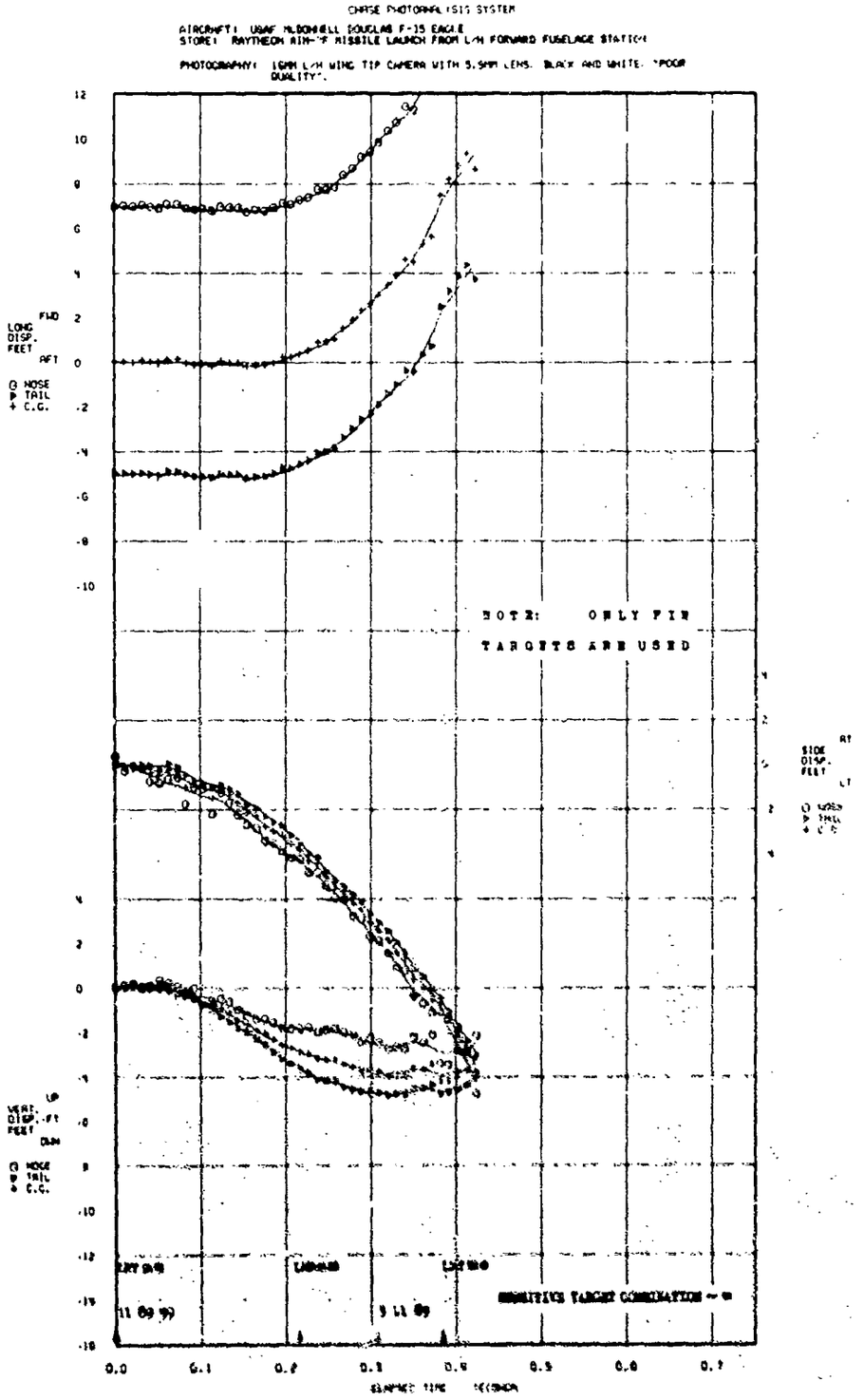


Figure 15
"CHASE RESULTS OF AIM-7F LAUNCH"
Camera Station 25

AIRCRAFT: USAF MCDONNELL DOUGLAS F-15 EAGLE
STORE: RAYTHEON AIM-7F MISSILE LAUNCH FROM L/H FORWARD FUSELAGE STATION

PHOTOGRAPHY: 16MM L/H AFT WING TIP CAMERA WITH 5.9MM LENS. BLACK AND WHITE. GOOD QUALITY.

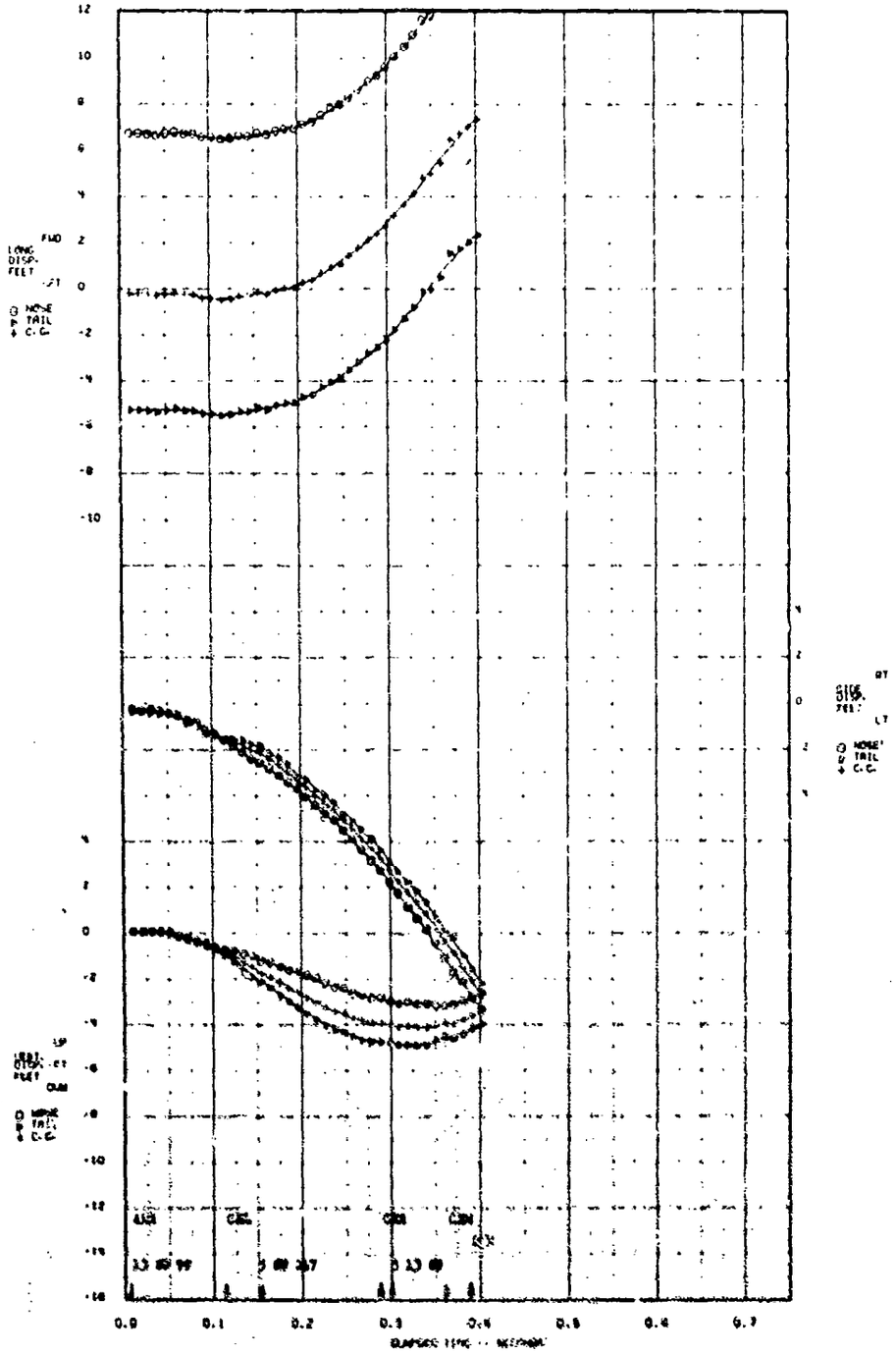


Figure 16
"CHASE RESULTS OF AIM-7F LAUNCH"
Camera Station 27

CHASE PHOTOANALYSIS SYSTEM

AIRCRAFT: USAF McDonnell Douglas F-15 Eagle
STORE: Raytheon AIM-7F Missile Launch From L/H Forward Fuselage Station

PRESENTATION: Results comparison from different camera stations.

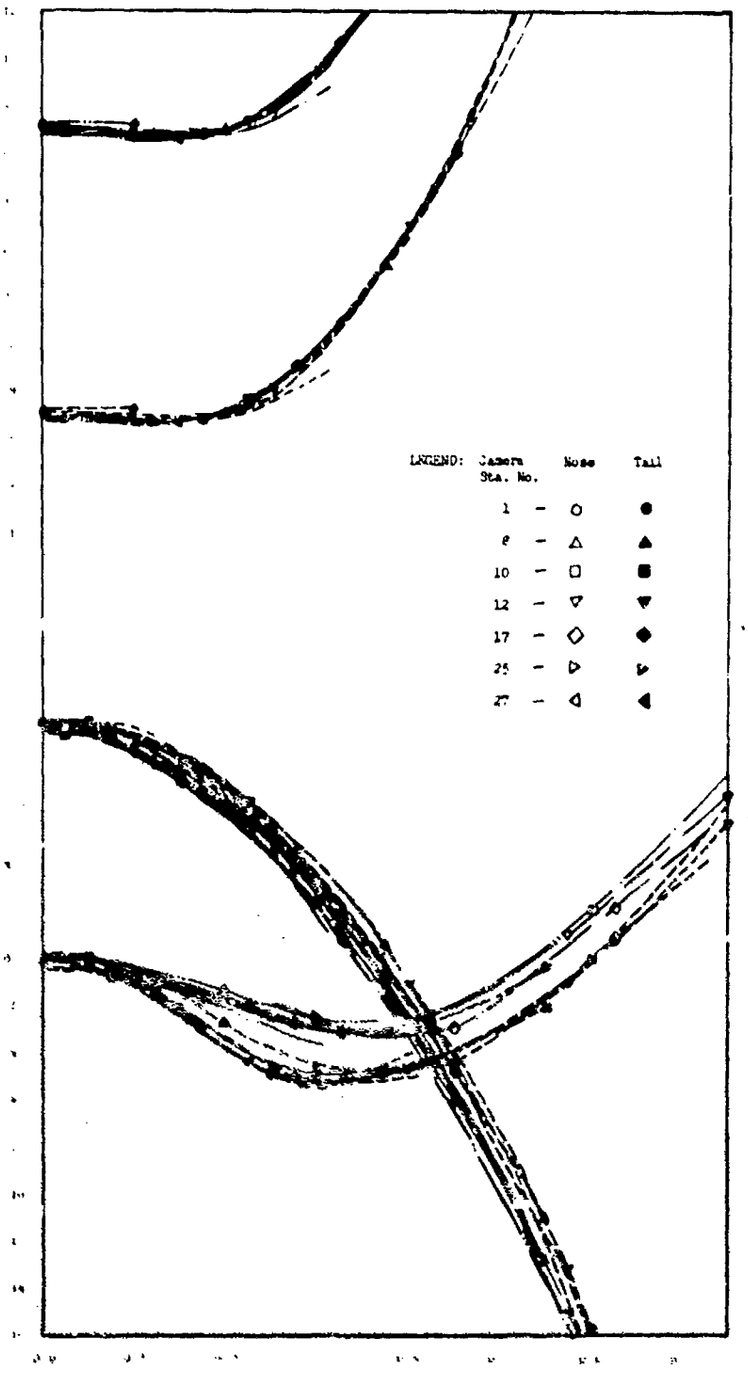


Figure 17A
"CHASE COMPARISONS FROM SEVERAL CAMERA SOLUTIONS"

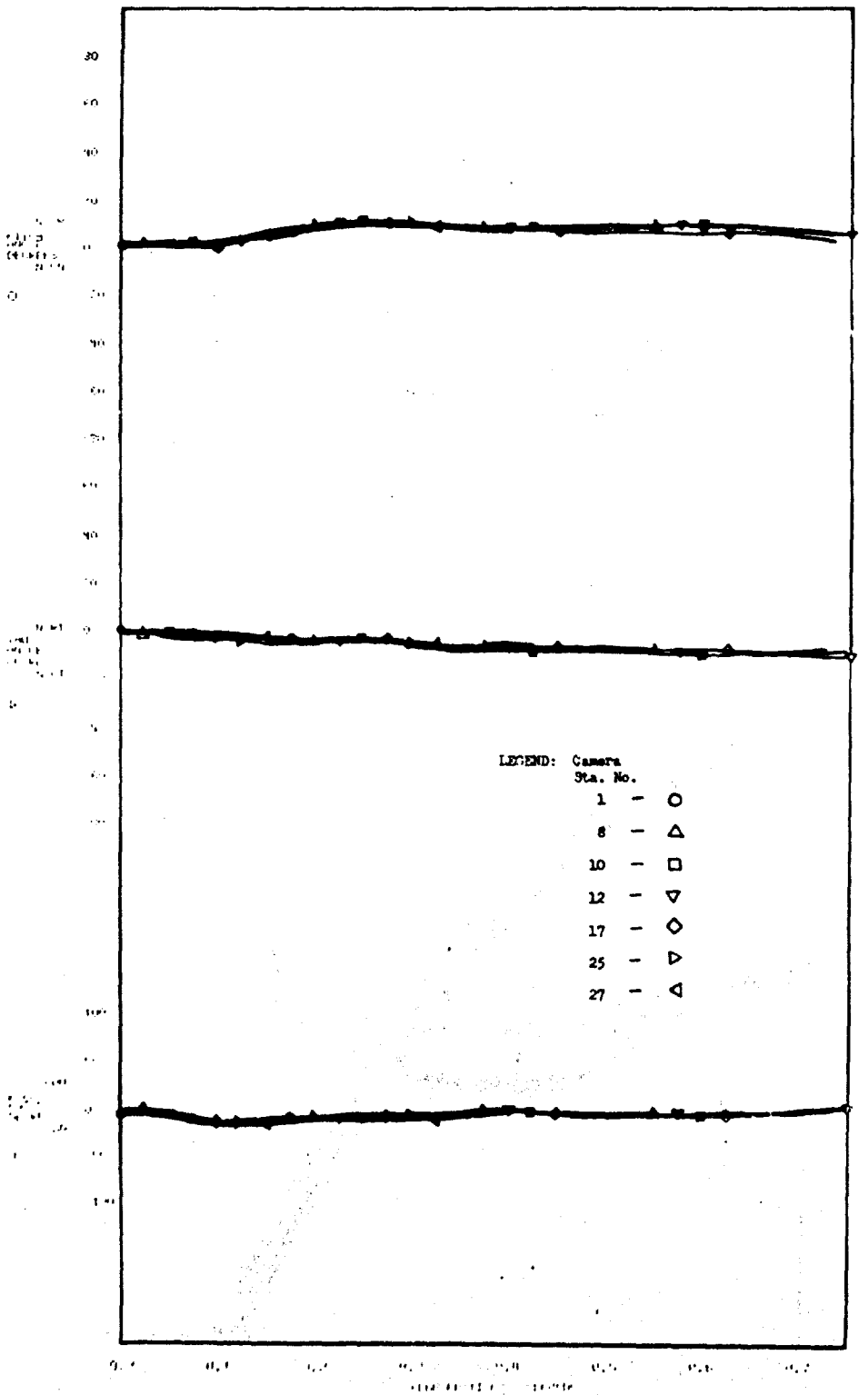


Figure 17B
"CHASE COMPARISONS FROM SEVERAL CAMERA SOLUTIONS"



Figure 18
"MARKING STORES IN A HASTE"

9.0 COST EFFECTIVENESS

Foremost, CHASE is a very cost effective approach. Its implementation merely involves the fabrication of a calibration board and the incorporation of the software into a general purpose computer or if desired into a mini-computer. It uses existing facilities! Any X/Y film reader with a computer compatible output, cards, tape etc., is adequate. Little training is required. This training really amounts to nothing more than an indoctrination of the System. An individual with an elementary geometric perception can read the film with good

results. Since standard and simple equipment is involved, little time is spent maintaining the system, nor are the recurring alignment or calibration costs seen. To increase the processing capacity of CHASE, you simple use more film readers to cover the loading. Not only are the installation costs token but the recurring or operating costs are minimum. We could not find anymore "corners to cut".

10.0 TEST COMPATIBILITY

CHASE is compatible with any store, large and small, symmetrical and odd, or clean and dirty. If a new store is introduced, its specs can be used for the file build-up. But preferrably, tape measurements, made in 15 minutes, are used. The Weapon File is created in less than an hour for each and every station on the aircraft.

The location or aspect angle of the camera is insignificant. Views, regardless of the vantage point, are processed equally well. The quality of the data remains the same, but its character will change some. Depending on the view angle, one axis or a pair of axes will have the more sensitive results. For beam coverage, the side displacements are sensitive, etc. It is desired or preferred that we have part of the aircraft in the field of view. Here we can calculate the camera locations from the boresite points. We like to have the camera in a position where features of the store will stand out. Lastly we don't have to see the entire store, only a portion of it. It appears that solutions should be improved with the wider fields of view or "fisheye lens". This seemed contrary, but when investigated had meaning. The main reason we found was that the CHASE concept is convergence dependent. In using the wider fields, closer observations are obtained. This in turn establishes greater angles on which CHASE thrives. Other systems are more dependent upon angular accuracies and resolution which discourage the use of the wider fields. Data is being gathered and processed from a 3.5mm (160°) lens to substantiate these observations.

11.0 RELIABILITY

CHASE is reliable. Since standard and simple equipment are involved there is little opportunity for breakdown. We've stated that it's a "charm" to use. It's simplicity in use, its internal auditing and defaults, and its verification aspects promote a high degree of success. Photometric data inherently requires some re-runs. We have experienced a reduction of these and have found that their re-starts are quickened. CHASE has developed into a very sensitive system where it is now tolerant of many interpretation and judgement errors. To exemplify this, we took a 16mm frame and printed it on a microfilm viewer/printer. This was then read with a ruler. Scaling these measurements into units of the reader system, results were obtained for every frame. The data was a little noisier than normal but would have been use-

ful if the engineer needed it. On one occasion we encountered absolutely the worst conditions: an unmarked, low contrast olive drab MK-82 (which in itself is a nasty configuration), under an overcast near sunset, and mind you with an improper f-stop. It was dark! The data was obtained and was usable. CHASE also allows a reduction in the number of cameras required. This likewise decreases their dependence and increases the success of a mission.

12.0 GROWTH AND APPLICATIONS

CHASE or its derivatives have many applications. One that was avoided in earlier discussions does offer proof of its accomplishment and validity. This is the use of actual chase coverage for engineering results. Figure 19 is a 600 gallon tank recently dropped from a Phantom as photographed with a 16mm camera in a chase plane. The sequence was filmed at a range of better than 300 feet abeam. Figure 20 is a CHASE diagnostic page of this drop illustrating the limited degree of convergence available for solution. In this case it is so small that it is even difficult to detect. Figure 21 shows the chase CHASE results along with the data from a wing tip camera. There are noticeable but rational variations in the sensitive side displacement, otherwise there is good agreement. Some view this application simply as an expression of CHASES' ability. However, the Systems Specialist recognize this as a very suitable backup to those occasions when onboard coverage is lost, events occur beyond their field of view, or simply to clean-up the aircraft cameras were not carried. Regardless, it has justified further investigation. The chase plane in the above case was another Phantom whose rear canopy could introduce distortion. No compensation was made for this.

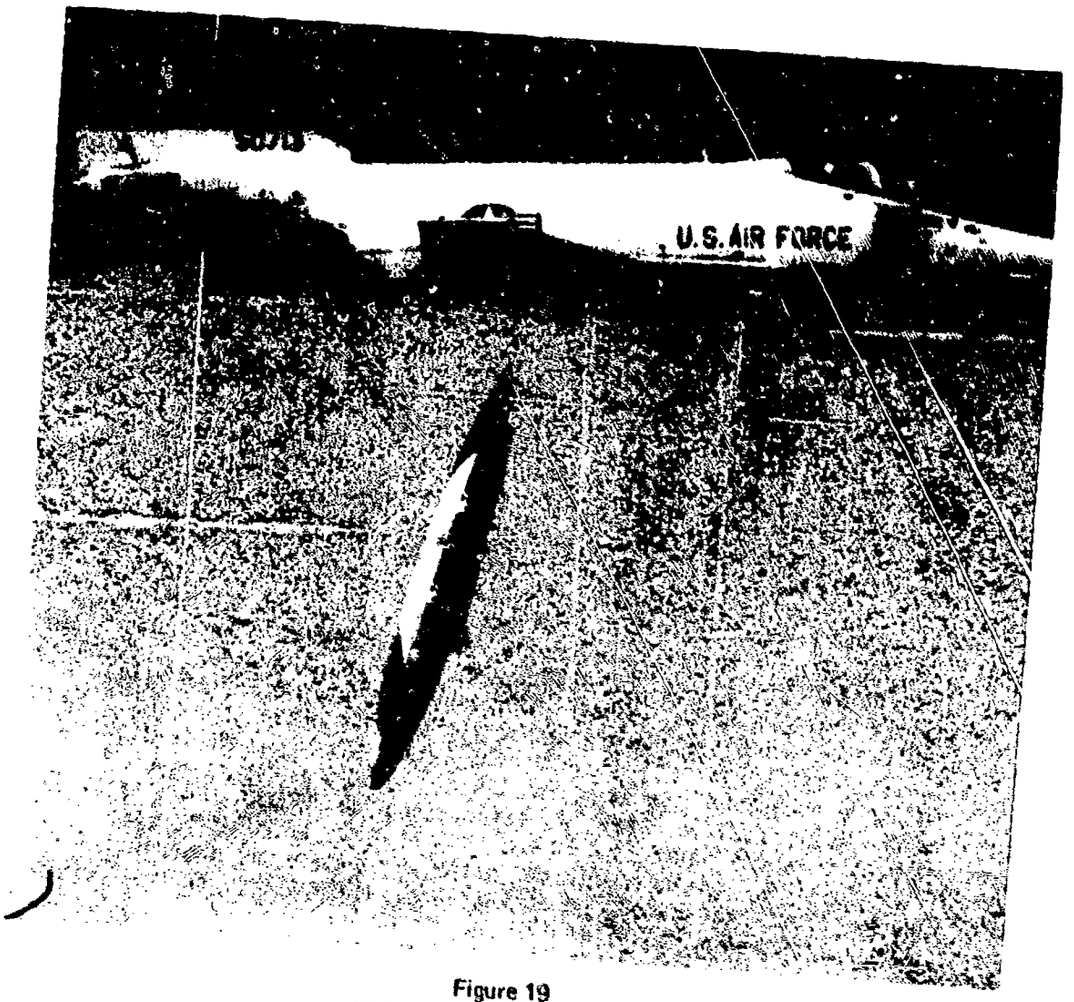


Figure 19
"CHASE PHOTOGRAPHY"

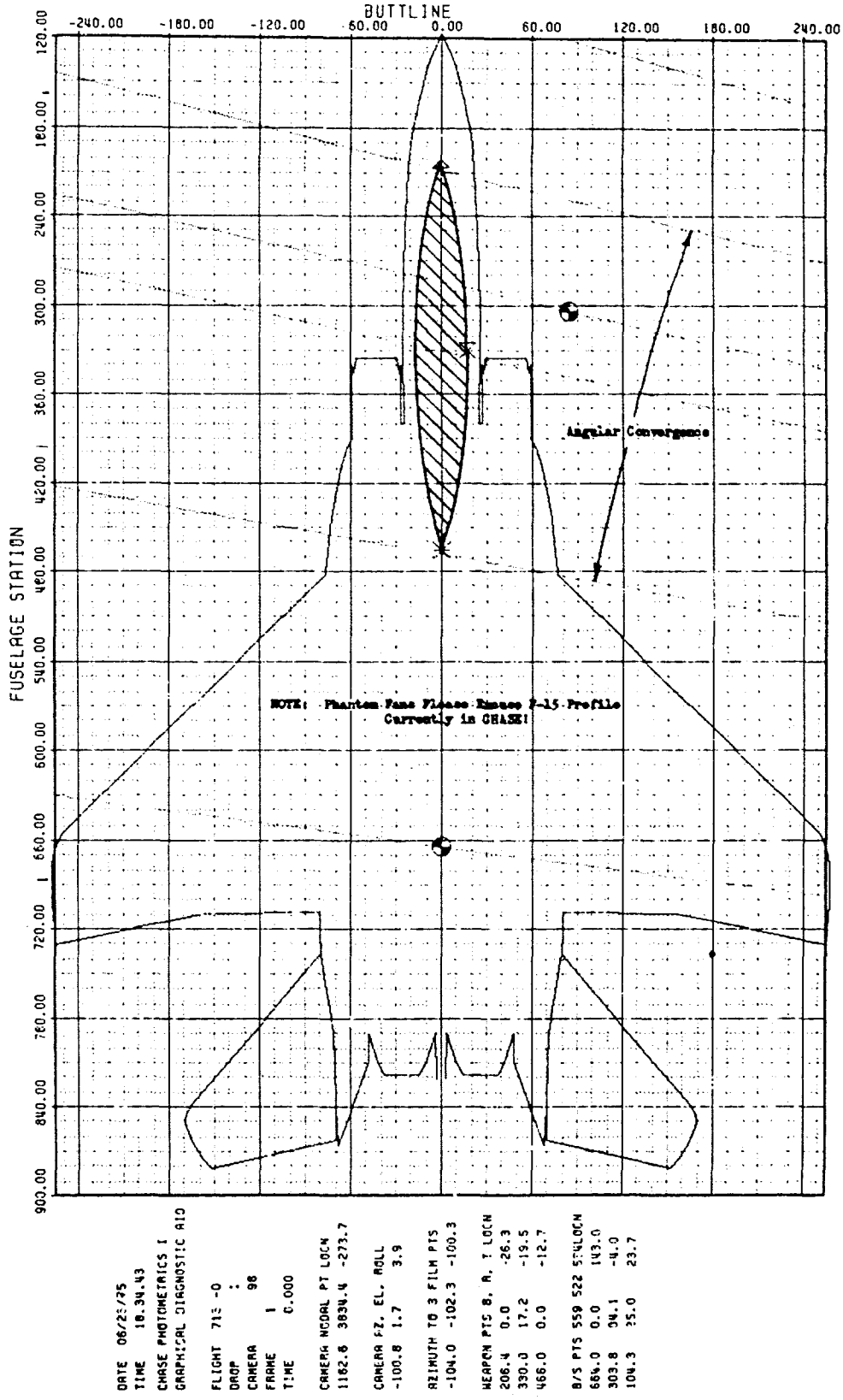


Figure 20
"ANGULAR CONVERGENCE FROM PHOTO CHASE"

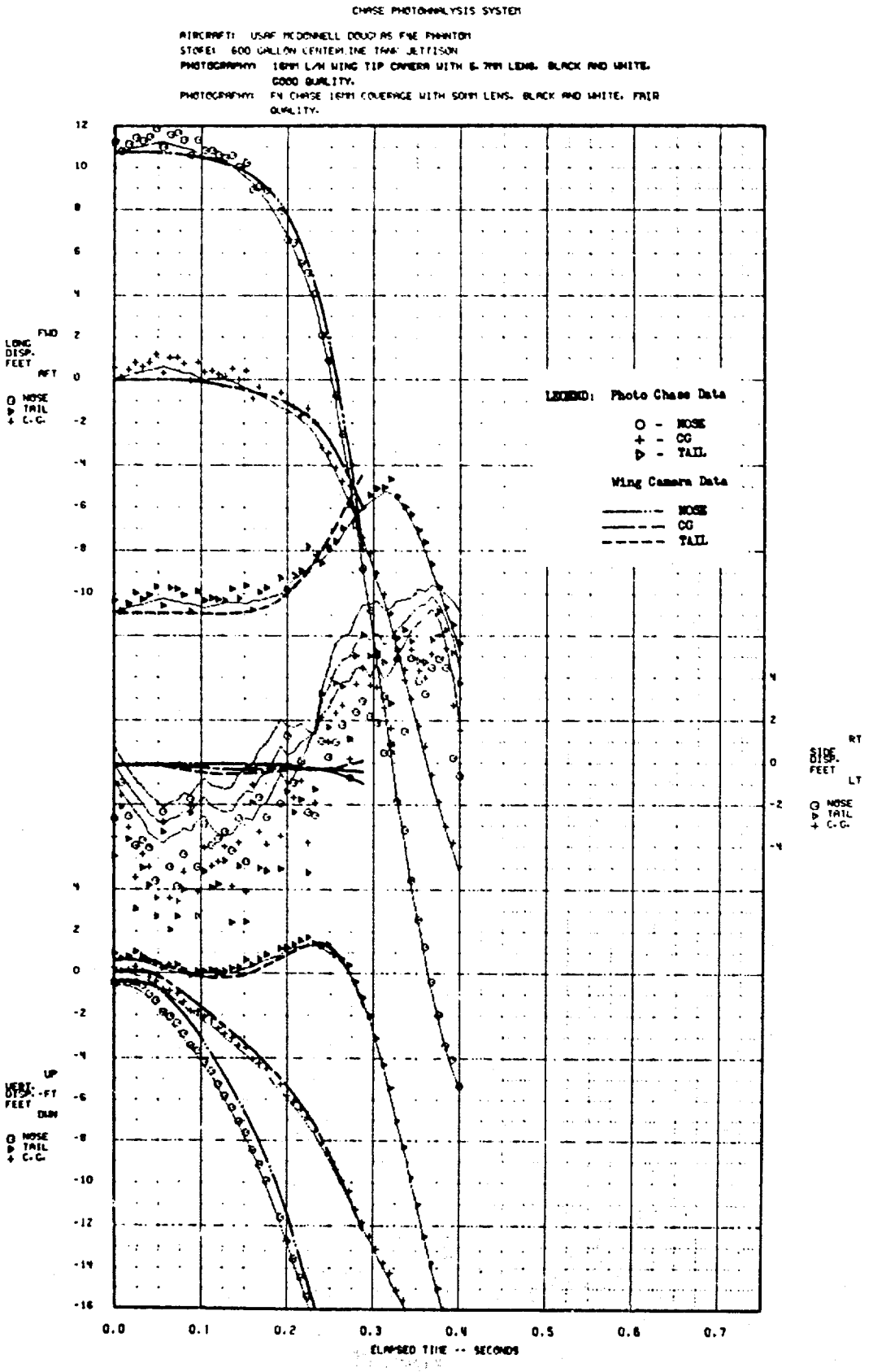


Figure 21A
"CHASE RESULTS"

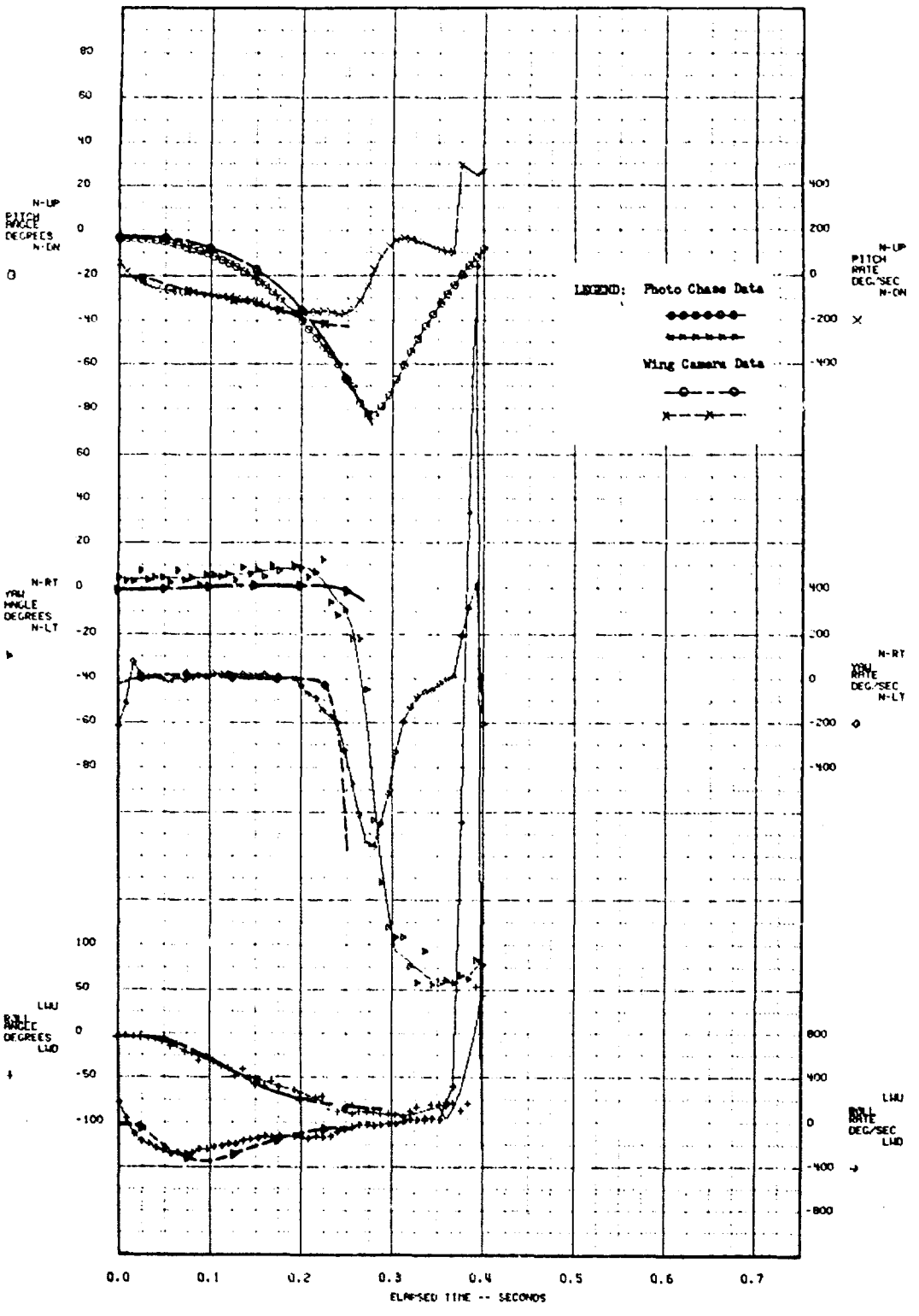


Figure 21B
"CHASE RESULTS"

13.0 CONCLUSION

CHASE conveniently and quickly provides space position data. A camera may also be used, actively or passively, i.e. airborne or fixed, for takeoff and landing performance, or other similar uses. MCAIR is in pursuit of these other CHASE applications that we are not at liberty to presently reveal. Some of these will be a marked improvement over existing techniques. MCAIR is pleased to announce that the marketing of CHASE installations has been approved and will permit others to enjoy its merits.

AUTOBIOGRAPHY

Alan Aden is a Sr. Group Data Engineer in the Data Analysis Department of the Flight Test Section, Laboratory and Flight Division (Phone (805) 277-3456). He has been with McDonnell for 17 years and has been associated with all flight test photoanalysis efforts, including spacecraft.

The concepts and engineering of CHASE were done by Alan Aden, Dean Gonzalez, Joe Lobacz, and Dennis O'Keefe with development support from the Data Analysis Department Engineering, Programming and Operations Groups.